



Tailored Collaboration

Optimization of UV Disinfection

Subject Area:
High-Quality Water



Optimization of UV Disinfection

About the Awwa Research Foundation

The Awwa Research Foundation (AwwaRF) is a member-supported, international, nonprofit organization that sponsors research to enable water utilities, public health agencies, and other professionals to provide safe and affordable drinking water to consumers.

The Foundation's mission is to advance the science of water to improve the quality of life. To achieve this mission, the Foundation sponsors studies on all aspects of drinking water, including supply and resources, treatment, monitoring and analysis, distribution, management, and health effects. Funding for research is provided primarily by subscription payments from approximately 1,000 utilities, consulting firms, and manufacturers in North America and abroad. Additional funding comes from collaborative partnerships with other national and international organizations, allowing for resources to be leveraged, expertise to be shared, and broad-based knowledge to be developed and disseminated. Government funding serves as a third source of research dollars.

From its headquarters in Denver, Colorado, the Foundation's staff directs and supports the efforts of more than 800 volunteers who serve on the board of trustees and various committees. These volunteers represent many facets of the water industry, and contribute their expertise to select and monitor research studies that benefit the entire drinking water community.

The results of research are disseminated through a number of channels, including reports, the Web site, conferences, and periodicals.

For subscribers, the Foundation serves as a cooperative program in which water suppliers unite to pool their resources. By applying Foundation research findings, these water suppliers can save substantial costs and stay on the leading edge of drinking water science and technology. Since its inception, AwwaRF has supplied the water community with more than \$300 million in applied research.

More information about the Foundation and how to become a subscriber is available on the Web at **www.awwarf.org**.

Optimization of UV Disinfection

Prepared by:

**Harold Wright, Erin D. Mackey, David Gaithuma, Cristina Fonseca,
Laura Baumberger, and Trinia Dzurny**
Carollo Engineers, P.C., Boise, Idaho 83713

Jennifer Clancy, Thomas Hargy, and Kristen Fallon
Clancy Environmental Consultants, Inc., St. Albans, Vermont 05478

Alexander Cabaj and Alois Schmalweiser
Inst. für Medizinische Physik und Biostatistik, Veterinärmedizinische Universität Wien, Austria
and

Andrew Bierman and Chris Gribbin
Rensselaer Polytechnic Institute, Troy, New York 12180

Jointly sponsored by:

Awwa Research Foundation
6666 West Quincy Avenue, Denver, CO 80235-3098
and

New York State Energy Research and Development Authority
17 Columbia Circle, Albany, NY 12203-6399

And the Tailored Collaboration partners:

City of Phoenix
City of Tacoma
New York City Department of Environmental Protection

Published by:

DISCLAIMER

This study was jointly funded by the Awwa Research Foundation (AwwaRF), New York State Energy Research and Development Authority (NYSERDA), and the following Tailored Collaboration (TC) partners: City of Phoenix, City of Tacoma, and New York City Department of Environmental Protection. AwwaRF, NYSERDA, and the TC partners assume no responsibility for the content of the research study reported in this publication or for the opinions or statements of fact expressed in the report. The mention of trade names for commercial products does not represent or imply the approval or endorsement of AwwaRF, NYSERDA, or the TC partners. This report is presented solely for informational purposes.

Copyright © 2007
by Awwa Research Foundation and New York State Energy Research and Development Authority

All Rights Reserved

Printed in the U.S.A.



Printed on recycled paper

CONTENTS

LIST OF TABLES	xi
LIST OF FIGURES	xv
FOREWORD	xxix
ACKNOWLEDGMENTS	xxxix
EXECUTIVE SUMMARY	xxxiii
CHAPTER 1: PROJECT IMPETUS AND GOALS	1
Part 1: Optimization of Validation.....	1
Application of UV Disinfection to Drinking Water	1
Problems Posed By Current Validation Methods	2
Challenge Microbe.....	2
UV Light-Absorbing Compounds.....	5
Impact of Non-Uniform Lamp Aging.....	7
Part 1: Objectives and Approach	7
Part 2: Optimization of Design and Operation	8
Part 2: Objectives and Approach.....	8
CHAPTER 2: NEW MICROBIAL SURROGATES	9
Literature Review.....	10
Materials and Methods.....	11
Microorganisms Selected for Study.....	11
Propagation and Enumeration.....	12
Results.....	14
φX174	14
PRD1	14
T4	15
fr, R17, PP7 and M13	15
Qβ	18
T7	20
SP8	22
Comparison of LP and MP Dose Response.....	23
Summary and Conclusions	23
CHAPTER 3: IDENTIFICATION OF NEW SURROGATE UV-ABSORBING COMPOUNDS	25
Introduction.....	25
Approach.....	26

Materials and Methods.....	27
NOM Sources.....	27
UV Absorbance Measurements	27
Polychromatic Bias and RED Calculation Using the UVDGM Workbook	28
Results and Discussion	30
Characteristics and Availability of UV-Absorbers.....	30
NOM Source Absorption Spectra.....	31
Impact of UV-Absorbers on Dose Delivery and the Polychromatic Bias	35
Feasibility for Full-Scale Validation Using New NOM Surrogates	46
Summary and Conclusions	49
CHAPTER 4: IMPACT OF LAMP AGING ON UV DOSE DELIVERY AND MONITORING	51
Introduction.....	51
Approach.....	52
Materials and Methods.....	53
Lamp Operation	53
UV Irradiance Measurements	54
Calculation of Germicidal Output and Lamp Aging Factor	58
Results and Discussion	59
Visual Observations.....	59
Low Pressure-High Output Lamps	62
Medium Pressure LampS - Type 1	74
Medium Pressure LampS - Type 2	88
Summary and Conclusions	105
Visual Signs of Lamp Aging	105
Low-Pressure High-Output Amalgam Lamps	106
Medium Pressure UV Lamps.....	106
General Conclusions	106
CHAPTER 5: FIELD-TESTING OF NEW VALIDATION TOOLS.....	107
Materials and Methods.....	107
Test Train Location and Set-up.....	107
UV Reactor	109
UV-Absorbing Chemical	111
Challenge Microorganisms	111
Aged UV Lamp.....	112
Test Protocol	112
Results and Discussion	114
Spectral Absorbance	114
UV Sensor Calibration Check.....	115
Biodosimetry.....	115
Challenge Microbe UV Dose-Reponse.....	117
Controls and Blanks.....	119
Bacteriophage Samples Stability	120
Biodosimetry Testing Results.....	120

RED Bias Assessment.....	121
Impact of Lamp Aging on UV Dose Delivery.....	124
Conclusions.....	125
CHAPTER 6: ANALYSIS USING COMPUTATIONAL DISINFECTION MODELS.....	127
Approach.....	127
Results.....	130
RED Bias	130
Spectral Shifts with MP Lamps	136
Spectral Shifts with LPHO Lamps.....	145
Non-Uniform Lamp Aging	147
Non-Uniform Lamp Aging with the MP Reactor	148
Non-Uniform Lamp Aging with the LPHO Reactor	153
Conclusions.....	157
Impact of Microbe Inactivation Kinetics on RED	158
Relation Between RED and UV Sensor Readings.....	158
Impact of Spectral Shifts in UV Output from LPHO and MP Lamps	159
Impact of Non-Uniform Lamp Output on Dose Delivery and Monitoring	159
CHAPTER 7: DEVELOPMENT OF UV COST ANALYSIS TOOL (UVCAT).....	161
Standard Life-Cycle Cost Analysis.....	161
Lamp Replacement Interval Cost Analysis.....	161
Advanced Life-Cycle Cost Analysis.....	161
UVCAT Inputs.....	169
UV System Sizing Criteria.....	170
Reactor Configuration.....	170
Redundancy.....	170
Lamp Data.....	171
Sleeve Data	171
Ballast Data.....	172
UV Sensor Data	172
UV Dose Pacing.....	172
Power Failure Data	173
WTP Inputs	174
Capital Cost Inputs.....	174
UV Dose Delivery.....	175
Ballast Power Settings	175
Water Quality Data	175
RED Model	175
Risk Model.....	176
UVCAT Algorithms.....	176
UVCAT Outputs	176
Quality Assurance/Quality Control.....	178

CHAPTER 8: EXPERIMENTAL LAMP-AGING STUDIES.....	179
Methods.....	179
UV Reactor Pilot System.....	179
Method of Measurement.....	182
Measurement Chamber.....	182
UV Detector.....	184
System Calibration.....	184
Measurement Uncertainty.....	186
Measurement Procedure.....	187
Results and Analysis.....	188
8-kW Medium-Pressure Lamps.....	188
6-kW Medium Pressure lamps.....	195
Amalgam LPHO Lamps.....	202
Non-Amalgam LPHO Lamps.....	205
Sources of Error with Measurements of Lamp Output.....	206
Sleeve Transmittance Measurements.....	206
UV Sensor Port Irradiance Measurements.....	208
LPHO Ballast Starting Measurements.....	209
Power Measurements.....	209
Conclusions and Recommendations.....	214
CHAPTER 9: LAMP AGING FACTOR ANALYSIS.....	215
Industry UV System Cost and Lamp Aging Data.....	215
Lamp Aging Factor Analysis Using UVCAT.....	221
CHAPTER 10: UV DOSE MONITORING AND CONTROL ANALYSIS.....	235
UV Dose Monitoring and Control by Commercial UV Reactors.....	235
UV Intensity Setpoint Approach.....	236
UV Intensity and UVT Setpoint Approach.....	236
Calculated Dose Approach.....	237
UVT and Flow Rate Variability Data.....	237
Dose-Pacing Analysis.....	241
Case 1. Using UVCAT to Evaluate UV System Sizing.....	241
Case 2. Impact of Ballast Power Settings on Dose Pacing.....	249
Case 3. Comparison of Dose Pacing Options.....	252
Case 4. Impact of Lamp Configuration on Dose Pacing.....	260
Conclusions and Recommendations.....	261
CHAPTER 11: PEAK LOAD REDUCTION.....	265
New York State Energy Pricing Structures.....	265
Peak Load Reduction Strategies for UV Disinfection.....	266
NAS Battery Energy Storage Systems.....	267
Peak Load Reduction Case Studies.....	267
Conclusions.....	269

CHAPTER 12: UV SYSTEM FAILURE AND RISK ANALYSIS	271
Industry UV System Failure Data.....	271
Utility 1, Vendor 1	271
Utility 2, Vendor 2	273
Utility 3, Vendor 1	274
Utility 4, Vendor 3	276
Power Quality Events	277
UV System Failure and Risk Analysis Using UVCAT	279
UVCAT Risk Analysis Case Studies	281
Conclusions and Recommendations	293
 APPENDIX A: UVCAT USER MANUAL	 295
 REFERENCES	 319
 ABBREVIATIONS	 323

TABLES

2.1	UV dose requirements for virus inactivation credit.....	10
2.2	Bacteriophages and their corresponding bacterial hosts selected for further study.....	11
3.1	UV-absorbing sources tested for similarity to WTP waters	27
3.2	UV absorbance and production volume of identified NOM sources.....	30
3.3	UV dose as a function of UVT 254 for different spectra UVA	35
3.4	Delta UV dose as a function of UVT 254 for different spectra UVA	36
3.5	Polychromatic Bias for germicidal and SiC UV sensors located with a 10 cm water layer between UV sensor and lamp.....	44
3.6	Volume of UV-absorbing surrogates required for a 10-mgd UV reactor validation.....	47
3.7	Characteristics of undiluted WC-IX brine	48
4.1	Summary of UV lamps collected from full-scale treatment plants.....	59
4.2	UV output of LPHO lamps at 254 nm measured at the middle and at the ends of the lamps	65
4.3	Summary of UVA, UVB, UVC and germicidal UV output from the new and aged Type 2 MP lamps.....	100
5.1	Properties of the duty and reference UV sensors.....	111
5.2	Estimation of the measurement uncertainty of the UV intensity sensor.....	111
5.3	Biodosimetry test plan	116
5.4	T7 and MS2 phage UV dose-response regression analysis	117
5.5	Controls collected during validation testing.....	119
5.6	Blanks collected during validation testing.....	119
5.7	Bacteriophage sample stability	120
5.8	Biodosimetry test results.....	120

5.9	RED bias calculations	122
5.10	RED bias uncertainty factors for demonstrating <i>Cryptosporidium</i> inactivation	123
5.11	Impact of lamp aging on UV dose delivery	124
6.1	Polychromatic bias with Aged LPHO lamps	145
7.1	UVCAT worksheets used for input.....	169
7.2	Data inputs into UVCAT	169
7.3	UVCAT worksheets used for output.....	177
8.1	Lamp operating characteristics used in the lamp-aging study	182
8.2	Coefficients of Equation 8.1 fitted to the lamp aging data for the UV reactor equipped with four 8.0 kW MP lamps	191
8.3	Coefficients of Equation 8.2 fitted to the lamp aging data for the UV reactor equipped with four 8.0 kW MP lamps	194
8.4	Coefficients for Equation 8.3 fitted to the lamp aging data for the UV reactor equipped with six 6-kW MP lamps.....	198
8.5	Empirical coefficients for Equation 8.4 fit to the lamp aging data for the UV reactor equipped with eight 300-W amalgam LPHO lamps	202
8.6	Empirical coefficients for Equation 8.5 fit to the lamp aging data for the UV reactor equipped with eight 130-W non-amalgam LPHO high-output lamps	205
8.7	UV irradiance measured at the UV sensor ports of the LPHO reactors.	208
8.8	Electrical power measurements for medium pressure reactors.....	211
8.9	Electrical power measurements for LPHO reactor 1	212
8.10	Electrical power measurements for LPHO reactor 2	213
9.1	Performance data on UV lamps provided by lamp manufacturers.....	219
9.2	UV system component performance data	220
9.3	Inputs to UVCAT for three UV system case studies	221

9.4	UV dose model coefficients used to predict UV dose delivery for the three hypothetical UV system case studies.....	223
9.5	Lamp aging equations used with the three hypothetical UV system case studies	224
10.1	Model coefficients for Equations 10.1 and 10.2.....	242
10.2	Model coefficients for Equations 10.4 and 10.5.....	252
10.3	Comparison of O&M costs and public health risk with different dose pacing strategies.....	260
11.1	Example of New York State energy price structures.....	266
11.2	Cost analysis comparing the NaS battery system to conventional UPS for a 100 kW power consumption.....	268
12.1	UV system information for Utility 1, Vendor 1.....	272
12.2	Summary of UV system component failure events for Utility 1, Vendor 1	272
12.3	UV system information for Utility 2, Vendor 2.....	273
12.4	Summary of UV system component failure events for Utility 2, Vendor 2	273
12.5	UV system information for Utility 3, Vendor 1.....	274
12.6	Summary of UV system component failure events for Utility 3, Vendor 1	275
12.7	UV system information for Utility 4, Vendor 3.....	276
12.8	Summary of UV system component failure events for Utility 4, Vendor 3	276
12.9	IEEE classification of power quality events by voltage	277
12.10	IEEE classification of power quality events by duration.....	277
12.11	Coefficients for the pathogen UV dose-response model	280
12.12	Model coefficients for Equations 12.5 and 12.6.....	281
12.13	Summary of conditions for risk analysis examples	282

FIGURES

1.1	The dose distribution in real systems is not ideal	4
1.2	Impact of the dose distribution in Figure 1.1 on inactivation	4
2.1	T4 bandpass filter UV transmittance	14
2.2	T4 UV dose-response.....	15
2.3	UV dose-response of fr	16
2.4	UV dose-response of R17	16
2.5	UV dose-response of PP7	17
2.6	UV dose-response of M13	17
2.7	UV dose-response of Q β	18
2.8	Response of Q β to a range of UV wavelengths	19
2.9	Response of MS2 to a range of UV wavelengths	19
2.10	Response of Q β and MS2 to selected UV wavelengths relative to 254 nm	20
2.11	T7 UV dose-response.....	21
2.12	Response of T7 to a range of UV wavelengths.....	21
2.13	Response of T7 and MS2 to selected UV wavelengths relative to 254 nm	22
2.14	UV dose-response of SP8	23
3.1	UV output of an MP lamp and absorbance spectra of a natural WTP water and UVA surrogates commonly used during UV reactor validation (coffee and LSA).....	25
3.2	Comparison between a spectrophotometer scan and holmium standard peaks	28
3.3	Comparison of the UVA measured with WTP finished waters. Data is normalized to give a UVA at 254 nm of 0.039 cm ⁻¹ . Legend shows the UVT at 254 nm before normalization	31

3.4	Comparison of the UVA spectra from 200 to 400 nm of membrane and electro dialysis concentrates with the UVA spectra of LSA, coffee, and WTP waters.....	32
3.5	Comparison of the UVA spectra from 200 to 400 nm of MIEX [®] and IX brine concentrates with the UVA spectra of LSA, coffee, and WTP waters.....	32
3.6	Comparison of the UVA spectra from 240 to 300 nm of membrane and electro dialysis concentrates with the UVA spectra of LSA, coffee, and WTP waters.....	33
3.7	Comparison of the UVA spectra from 240 to 300 nm of MIEX [®] and IX brine concentrates with the UVA spectra of LSA, coffee, and WTP waters.....	34
3.8	Lamp output, UV sensor spectral response, and microbial action data used as inputs to the Polychromatic Bias worksheet.....	34
3.9	Dose delivery as a function of UVT for the annular reactor for different UVA spectra.....	36
3.10	Impact of UVT and UV sensor-to-lamp water layer on B _{Poly} with VG-RO concentrate	38
3.11	Impact of UVT and UV sensor-to-lamp water layer on B _{Poly} with LC-MIEX [®]	39
3.12	Impact of UVT and UV sensor-to-lamp water layer on B _{Poly} with Super Hume [™]	40
3.13	Impact of UVT and UV sensor-to-lamp water layer on B _{Poly} with LSA	41
3.14	Impact of UVT and UV sensor-to-lamp water layer on B _{Poly} with coffee.....	42
3.15	UV dose and UV sensor readings as a function of UVT at 254 nm calculated using the UVA spectra of Super Hume [™]	45
3.16	UV dose and relative UV sensor readings as a function of UVT at 254 nm calculated using the UVA spectra of Super Hume [™]	45
4.1	Discoloration observed with aged MP lamps after approximately 4000 hours of operation compared to a relatively new lamp (third down from top).....	51
4.2	Schematic of the LPHO lamp power supply and ballast	53
4.3	LPHO ballast and igniter	54

4.4	Apparatus used to measure spectral UV irradiance	55
4.5	Mounting of the spectroradiometer sensor used to measure spectral irradiance with the LPHO lamp	55
4.6	Axial and radial locations for spectral irradiance measurements with LPHO and MP lamps	56
4.7	Mounting of SED 240 sensor used to measure UV lamp output at 254 nm along length of lamp	57
4.8	SED 240 sensor is located 2 mm from surface of lamp envelope using a spacer.....	57
4.9	Location of SED 240 sensor relative to the lamp at the beginning of measurements of UV output along the length of the lamp	58
4.10	End darkening in LPHO lamps (top photo) and MP lamps (middle and bottom photos).....	60
4.11	Random discoloration with a MP lamp	60
4.12	Discoloration along lamp length but around only 180° of the circumference.....	60
4.13	Lamp end distortion with a MP lamp with lamp end darkening.....	61
4.14	Resonant darkening with a MP lamp	61
4.15	Resonant distortion and darkening with a MP lamp.....	61
4.16	End darkening with LPHO lamps after 940 and 6,696 hours of operation.....	63
4.17	Close up of lamp end darkening with LPHO lamps	63
4.18	Unusual coloration of lamp #3 (6,188 hours) during operation, before it finally became defective (no color enhancement to photo)	63
4.19	Spectral irradiance of the LPHO lamp (432 hours) normalized to 254 nm on a linear scale.....	64
4.20	Spectral irradiance LPHO lamp #8 (432 hours) normalized to 254 nm on a semi-logarithmic scale	64
4.21	Relative cumulative spectral irradiance of LPHO lamp #8 (432 hours).....	65
4.22	Spectral irradiance of five LPHO lamps measured at the lamp end.....	66

4.23	Spectral irradiance of five LPHO lamps measured at the lamp middle.....	66
4.24	Spectral output of LPHO lamps relative to the output of lamp # 2 at the lamp end (upper graph) and middle (lower graph).....	67
4.25	UV output at 254 nm of a new amalgam LPHO lamp as a function of position along the length of the lamp.....	68
4.26	LPHO lamp #2 (432 hours) viewed from four locations about its circumference.....	69
4.27	UV output at 254 nm of LPHO lamp #2 (432 hours) as a function of position along the length and around the circumference of the lamp.....	69
4.28	LPHO lamp #1 (940 hours) viewed from four locations about its circumference.....	70
4.29	UV output at 254 nm of LPHO lamp #1 (940 hours) as a function of position along the length and around the circumference of the lamp.....	70
4.30	LPHO lamp #8 (1,472 hours) viewed from four locations about its circumference.....	71
4.31	UV output at 254 nm of LPHO lamp #8 (1,472 hours) as a function of position along the length and around the circumference	71
4.32	LPHO lamp #9 (6,696 hours) viewed from four locations about its circumference.....	72
4.33	UV output at 254 nm of LPHO lamp #9 (6,696 hours) as a function of position along the length and around the circumference	72
4.34	Relative integrated irradiance along the length of the lamp as a function of lamp hours	74
4.35	Type 1 MP lamps analyzed: full view (top photo) and close-up (bottom photo). Lamp ages are, from top to bottom: 0, 3,266, and 4,098 hours, respectively	75
4.36	Spectral irradiance of the new Type 1 MP lamp as a function of location along the lamp length at location C2	75
4.37	Integrated and germicidal irradiance of the new Type 1 MP lamp as a function of position along the lamp length for location C2	76
4.38	Photographs of the Type 1 MP lamp #10	77
4.39	Close up of the “powder” spot.....	77

4.40	Spectral irradiance of Type 1 MP lamp #10 as a function of location along the lamp length and around the circumference (C1 - top, C2 - bottom).....	78
4.41	Integrated and germicidal irradiance of the aged Type 1 MP lamp #10 as a function of position along the lamp length at location C1.....	80
4.42	Germicidal irradiance of the aged Type 1 MP lamp #10 as a function of position along the lamp length.....	80
4.43	Germicidal irradiance of the aged Type 1 MP lamp #10 as a function of position about the circumference.....	81
4.44	Photographs of the Type 1 MP lamp #8.....	82
4.45	Close up on the most fouled section of Type 1 MP lamp #8 (Position C1).....	82
4.46	Close up of the coated end of Type 1 MP lamp #8 on the power supply side.....	82
4.47	Spectral irradiance of Type 1 MP lamp #8 as a function of location along the lamp length and around the circumference (C1 - top, C2 - bottom).....	83
4.48	Integrated and germicidal irradiance of the aged Type 1 MP lamp #8 as a function of position along the lamp length at location C1.....	85
4.49	Germicidal irradiance of the aged Type 1 MP lamp #8 as a function of position along the lamp length.....	86
4.50	Germicidal irradiance of the aged Type 1 MP lamp #8 as a function of position about the circumference.....	86
4.51	Ratio of UV irradiance measured with old Type 1 MP lamps to that measured with new lamps as a function of wavelength.....	87
4.52	Germicidal irradiance as a function of operating hours with Type 1 MP lamps.....	88
4.53	New Type 2 MP lamp.....	89
4.54	Spectral irradiance of the new Type 2 MP lamp as a function of location along the lamp length at location C1.....	89
4.55	Integrated and germicidal irradiance of the new Type 2 MP lamp as a function of position along the lamp length for location C1.....	90
4.56	Type 2 MP lamp aged 2,292 hours (SR4) photographed from location C2 (top) and C3 (bottom).....	91

4.57	Type 2 MP lamp aged 2,361 hours (SR3) photographed from location C4 (top) and C3 (bottom)	91
4.58	Type 2 MP lamp aged 4,001 hours (BP4) photographed from location C1 (top) and C2 (bottom)	92
4.59	Spectral irradiance of Type 2 MP lamp SR4 aged 2,292 hours as a function of location along the lamp length and around the circumference (C1 - top, C2 - bottom)	93
4.60	Spectral irradiance of Type 2 MP lamp SR3 aged 2,361 hours as a function of location along the lamp length and around the circumference (C1 - top, C2 - bottom)	95
4.61	Spectral irradiance of Type 2 MP lamp BP4 aged 4,001 hours as a function of location along the lamp length and around the circumference (C1 - top, C2 - bottom)	97
4.62	Integrated and germicidal irradiance of the aged Type 2 MP lamp SR4 as a function of position along the lamp length for location C1	99
4.63	Integrated and germicidal irradiance of the aged Type 2 MP lamp SR3 as a function of position along the lamp length for location C1	99
4.64	Integrated and germicidal irradiance of the aged Type 2 MP lamp BP4 as a function of position along the lamp length for location C1	100
4.65	Germicidal irradiance of the aged Type 2 MP lamp SR4 as a function of position along the lamp length.....	101
4.66	Germicidal irradiance of the aged Type 2 MP lamp SR3 as a function of position along the lamp length.....	101
4.67	Germicidal irradiance of the aged Type 2 MP lamp BP4 as a function of position along the lamp length.....	102
4.68	Germicidal irradiance of the aged Type 2 MP lamp SR4 as a function of position about the circumference.....	102
4.69	Germicidal irradiance of the aged Type 2 MP lamp SR3 as a function of position about the circumference.....	103
4.70	Germicidal irradiance of the aged Type 2 MP lamp BP4 as a function of position about the circumference.....	103

4.71	Ratio of UV irradiance measured with old Type 2 MP lamps to that measured with new lamps as a function of wavelength.....	104
4.72	Germicidal irradiance as a function of operating hours with Type 2 MP lamps	105
5.1	Test train schematic	108
5.2	Spectral output of a new lamp for the Sentinel UV reactor.....	110
5.3	UV transmittance of a 1.5 mm thick lamp sleeve for a 90° of incidence angle and air-quartz interfaces.....	110
5.4	New lamp with 100-hour burnin (top) and the aged lamp (bottom) used during field-testing.....	112
5.5	Spectral UV absorbance coefficients of raw test water and test water with Super Hume™	115
5.6	Relationship between reference and duty UV sensors obtained during reactor validation	116
5.7	UV dose-response of MS2 phage measured during testing.....	118
5.8	UV dose-response of T7 phage measured during testing	118
5.9	MS2 dose delivery predictions versus measured dose for MS2 field-testing conditions.....	121
5.10	Comparison of MS2 and T7 UV dose-response with <i>Cryptosporidium</i> UV dose requirements.....	123
6.1	Schematic of the LPHO UV system	127
6.2	Schematic of the MP UV system.....	128
6.3	UV intensity algorithm accounts for non-uniform UV output along length and about the circumference of the lamp using weighting functions	128
6.4	RED delivered by the MP reactor as a function of relative lamp output (S/S_0) and microbe inactivation kinetics (D10) for 98 % UVT (top) and 80% UVT bottom.....	131
6.5	RED delivered by the 6-row LPHO reactor as a function of relative lamp output (S/S_0) and microbe inactivation kinetics (D10) for 98 % UVT (top) and 80% UVT bottom.....	132

6.6	RED bias relative to $D_{10} = 4 \text{ mJ/cm}^2$ of the MP reactor as a function of relative lamp output (S/S_0) and microbe inactivation kinetics (D_{10}) for 98 % UVT (top) and 80% UVT bottom.....	133
6.7	RED bias relative to $D_{10} = 4 \text{ mJ/cm}^2$ of the LPHO reactor with 6 rows of operating lamps as a function of relative lamp output (S/S_0) and microbe inactivation kinetics (D_{10}) for 98 % UVT (top) and 80% UVT bottom.....	134
6.8	RED bias with the MP reactor as a function of RED based on $D_{10} = 4 \text{ mJ/cm}^2$. RED bias is calculated as the ratio of REDs for $D_{10} = 18$ and 4 mJ/cm^2	135
6.9	RED bias with the 6-row LPHO reactor as a function of RED based on $D_{10} = 4 \text{ mJ/cm}^2$. RED bias is calculated as the ratio of REDs for $D_{10} = 18$ and 4 mJ/cm^2	135
6.10	Log inactivation as a function of $S/S_0/D_{10}$ and UVT for the MP reactor	137
6.11	Log inactivation as a function of $S/S_0/D_{10}$ and UVT for the LPHO reactor operating with 6 rows of lamps.....	137
6.12	Spectral response of DVGW and SiC UV sensors	138
6.13	Angular response of DVGW and SiC UV sensors	138
6.14	MS2 RED ($D_{10} = 18 \text{ mJ/cm}^2$) as a function of DVGW UV sensor readings and UVT for water layers of 2, 5, 10, 15, and 20 cm	139
6.15	MS2 RED ($D_{10} = 18 \text{ mJ/cm}^2$) as a function of SiC UV sensor readings and UVT for water layers of 2, 10, and 20 cm	142
6.16	MS2 RED ($D_{10} = 18 \text{ mJ/cm}^2$) delivered by new and aged Type 1 MP lamps as a function of SiC UV sensor readings for water layers of 2 and 20 cm and UVTs of 98 and 75%.....	143
6.17	MS2 RED ($D_{10} = 18 \text{ mJ/cm}^2$) delivered by new and aged Type 1 MP lamps as a function of DVGW UV sensor readings for water layers of 2 and 20 cm and UVTs of 98 and 75%.....	144
6.18	MS2 RED ($D_{10} = 18 \text{ mJ/cm}^2$) delivered by new and aged Type 2 MP lamps as a function of SiC UV sensor readings for water layers of 2 and 20 cm and UVTs of 98 and 75%	146
6.19	UV output along the length of the lamp used in the MP system analysis	147
6.20	UV output about the circumference of the lamp used in the MP system analysis.....	147

6.21	UV output along the length of the lamp used in the LPHO system analysis.....	148
6.22	Impact of non-uniform MP lamp output along the lamp length on UV sensor readings (location S1 - center of the lamp, location S7 - lamp end, spacing between UV sensors - 5 cm).....	149
6.23	Relation between MS2 RED (D10 = 18 mJ/cm ²) and DVGW UV sensor readings at 98% UVT for different cases of non-uniform MP lamp aging along the lamp length.....	150
6.24	Dose monitoring bias caused by non-uniform MP lamp aging along the lamp length as a function of axial UV sensor location (0 cm - lamp end, 30 cm - lamp middle).....	151
6.25	Impact of non-uniform MP lamp output about the circumference of the lamp on UV sensor readings (location S90° -UV sensor views lamp #1 from above, location S°0 - UV sensor views lamp from the right hand side).....	152
6.26	Relation between MS2 RED (D10 = 18 mJ/cm ²) and DVGW UV sensor readings at 80% UVT for different cases of non-uniform MP lamp aging about the lamp circumference.....	154
6.27	Dose monitoring bias caused by non-uniform lamp aging about the MP lamp's circumference as a function of angular UV sensor location (°0 - UV sensor views lamp from the right hand side, 90° - UV sensor views lamp from above).....	155
6.28	Impact of non-uniform LPHO lamp output along the lamp length on UV sensor readings (location S1 - lamp end, location S6 - center of the lamp, spacing between UV sensors - 15 cm).....	156
6.29	Relation between MS2 RED (D10 = 18 mJ/cm ²) and DVGW UV sensor readings at 98% UVT for different cases of non-uniform LPHO lamp aging along the lamp length.....	157
7.1	Flow rate, UVT, raw water pathogen concentration, and power quality data used as inputs to the Advanced LCA UVCAT tool.....	162
7.2	Number of operating reactor trains and banks per reactor predicted by the Advanced LCA UVCAT tool.....	163
7.3	Power consumption by a UV system predicted by the Advanced LCA UVCAT tool under ideal and actual dose-pacing strategies.....	164

7.4	Ratio of actual to ideal power consumption predicted by the Advanced LCA UVCAT tool.....	164
7.5	Lamp-aging simulated by the Advanced LCA UVCAT tool	165
7.6	Daily and accumulated power costs predicted by UVCAT	166
7.7	Off-specification performance over time predicted by the Advanced LCA UVCAT tool.....	166
7.8	UV dose delivery over time predicted by the Advanced LCA UVCAT tool	167
7.9	Pathogen log inactivation over time predicted by the Advanced LCA UVCAT tool.....	168
7.10	Public health risk over time predicted by the Advanced LCA UVCAT tool	168
8.1	Schematic of the test process train installed at the John P. Buckley WTP.....	179
8.2	Photograph of the R-Can amalgam and non-amalgam LPHO reactors.....	180
8.3	Photograph of the IDI reactor equipped with six 6 kW MP lamps.....	180
8.4	Photograph of the IDI reactor equipped with four 4 kW MP lamps.....	181
8.5	Spectral measurement positions.....	181
8.6	Schematic of the measurement chamber.....	183
8.7	Photograph of the measurement chamber.....	183
8.8	Monochromator system	185
8.9	Input optics to the fiber-coupled monochromator. Integrating sphere optics provided cosine response for proper irradiance measurements.	185
8.10	Spectrometer calibration curves.....	186
8.11	Lamp aging data for the UV reactor equipped with four 8.0 kW MP lamps - Lamps 1, 2, 3, and 4 were operated at 8.0, 6.5, 5.5, and 5.0 kW, respectively	189
8.12	Coefficients a, b, and c of Equation 8.1 plotted as a function of ballast power for the UV reactor equipped with four 8.0 kW MP lamps	192
8.13	Comparison of UV irradiance predicted by Equation 8.2 to measured data	194

8.14	Lamp aging data for the UV reactor equipped with six 6.0-kW MP lamps - Lamps 1, 2, 3, 4, 5 and 6 were operated at 6.0, 6.0, 5.5, 5.0, 4.0, and 3.5 kW, respectively; Average excludes lamp 5.....	196
8.15	Coefficients b and c of Equation 8.3 as a function of ballast power for the UV reactor equipped with six 6.0-kW MP lamps.....	199
8.16	Spectral irradiance for medium pressure lamp #2, reactor #2 recorded at different operating times over the course of the study.....	201
8.17	Expanded wavelength axis (zoom) of 8.16 in the wavelength vicinity of the principle Hg emission line at 254 nm	201
8.18	Lamp aging data for the UV reactor equipped with eight 300-W amalgam LPHO lamps. Lamps 1 through 4 operated at 100% power; Lamps 5 through 8 operated at 80% power.....	203
8.19	Lamp aging data for the UV reactor equipped with eight 130-W non-amalgam LPHO amps. Lamps 1 through 4 operated at 100% power; Lamps 5 through 8 operated at 80% power	204
8.20	UV transmittance of quartz sleeve samples taken from the medium pressure reactors (MP) and the LPHO reactors (LP). The transmittance curves shown are the average of three samples.....	207
8.21	Transmittance of new quartz sleeve samples taken from replacement sleeves that were never used, and the transmittance of the two sleeve samples after cleaning with mild phosphoric acid bathroom cleaner	207
8.22	Oscilloscope traces of lamp current (C2, pink trace) and electrode heating voltage (C3, blue trace) for a stable operating lamp.....	210
8.23	Oscilloscope traces of lamp current (C2, pink trace) and electrode heating voltage (C3, blue trace) during the starting of the lamp	210
9.1	Lamp aging curves for LPHO and MP lamp technologies.....	215
9.2	Lamp aging data for three lamp types.....	216
9.3	Model fits (curves) to lamp aging data (symbols)	217
9.4	Lamp aging curves used in the UVCAT analysis of Lamp Aging Factors	225

9.5	Present worth costs for the three hypothetical UV systems assuming no dose pacing and lamp aging curves based on industry data; Electricity assumed \$0.05/kW-hr.....	227
9.6	Impact of dose pacing strategies on O&M costs for the three hypothetical UV systems using lamp aging curves based on industry data; Electricity assumed \$0.05/kW-hr	228
9.7	Impact of power costs and dose pacing strategies on O&M costs for UV System 1 using lamp aging curves based on MP lamp aging data measured in this project.....	230
9.8	Impact of power costs and dose pacing strategies on O&M costs for UV System 3 using lamp aging curves based on amalgam lamp aging data measured in this project	231
9.9	Impact of lamp replacement interval on life-cycle costs for the three hypothetical UV systems; Analysis uses lamp-aging curves from industry data, power costs of \$0.15/kW-hr, no dose pacing, and reactor capital costs varying with Lamp Aging Factor.....	232
9.10	Impact of lamp replacement interval on life-cycle costs for the modeled UV systems, Analysis uses lamp-aging curves from data measured in this project, power costs of \$0.15/kW-hr, no dose pacing, and reactor capital costs varying with Lamp Aging Factor	233
10.1	Poughkeepsie WTP filter effluent UV absorbance.....	238
10.2	Flow rate data for an eastern U.S. WTP	238
10.3	UVT data of an eastern U.S. WTP.....	239
10.4	Scott's Valley effluent flow rate and UVT	239
10.5	Flow rate and UVT at a California WWTP	240
10.6	UVT at a California WWTP	240
10.7	Case 1/three 1-bank reactors: reactors on (top left), banks on (top right), power consumption (bottom left), and ratio of ideal-to-actual power (bottom right).....	243
10.8	Case 1: UV system consisting of three 2-bank reactors: reactors on (top left), banks on (top right), power consumption (bottom left), and ratio of ideal-to-actual power (bottom right).....	245

10.9	Case 1/three 3-bank reactors: reactors on (top left), banks on (top right), power consumption (bottom left), and ratio of ideal-to-actual power (bottom right).....	247
10.10	Case 2/four-train UV system with electronic ballasts: power consumption (top left), power costs (top right), log inactivation (bottom left), public health protection (bottom right).....	250
10.11	Case 2/four-train UV system with electromagnetic ballasts; power consumption (top left), power costs (top right); log inactivation (bottom left); public health (bottom right).....	251
10.12	Case 3 reactors operating over time with no dose pacing (top left), flow pacing (top right), flow and UVT pacing (bottom left), and full dose pacing (bottom right).....	254
10.13	Case 3 banks operating over time with no dose pacing (top left), flow pacing (top right), flow and UVT pacing (bottom left), and full dose pacing (bottom right).....	255
10.14	Case 3 power costs with no dose pacing (top left), flow pacing (top right), flow and UVT pacing (bottom left), and full dose pacing (bottom right).....	256
10.15	Case 3 off spec performance with no dose pacing (top left), flow pacing (top right), flow and UVT pacing (bottom left), and full dose pacing (bottom right).....	257
10.16	Case 3 <i>Cryptosporidium</i> inactivation with no dose pacing (top left), flow pacing (top right), flow and UVT pacing (bottom left), and full dose pacing (bottom right).....	258
10.17	Case 3 public health protection with no dose pacing (top left), flow pacing (top right), flow and UVT pacing (bottom left), and full dose pacing (bottom right).....	259
10.18	Case 4/1-bank UV system with full dose pacing: power consumption (top left), power costs (top left), UV system log kill (bottom left), health impact (bottom right).....	262
12.1	Monthly summary of power quality events from i-grid monitoring sites in New York State.....	278
12.2	Summary of power quality events by weekday from i-grid monitoring sites in New York State.....	278
12.3	Hourly summary of power quality events from i-grid monitoring sites in New York State.....	279

12.4	Flow rate and UVT profiles	282
12.5	Raw water <i>Cryptosporidium</i> concentrations.....	283
12.6	Line voltage data showing power quality events.....	283
12.7	Number of reactors (top) and banks (bottom) of lamps predicted for the Case 1 LPHO system.....	284
12.8	Power consumption (top) and costs (bottom) over time for the Case 1 LPHO system.....	285
12.9	UV dose delivery by the first reactor (top) and UV system log inactivation (bottom) over time for the Case 1 LPHO system	286
12.10	Annual health risk and accumulated <i>Cryptosporidium</i> infections in a population of 1,000,000 people for the Case 1 LPHO system.....	287
12.11	UV system log inactivation (top), and annual infection risk, and accumulated infection for the Case 2 LPHO system (bottom)	288
12.12	UV system log inactivation (top), and annual infection risk and accumulated infection (bottom) for the Case 3 LPHO system	289
12.13	UV system log inactivation (top), and annual infection risk and accumulated infection (bottom) for the Case 4 LPHO system	290
12.14	Annual infection risk and accumulated infection for the Case 5 LPHO system	291
12.15	UV system log inactivation (top), and annual infection risk and accumulated infection (bottom) for the Case 6 LPHO system	292

FOREWORD

The Awwa Research Foundation (AwwaRF) is a nonprofit corporation that is dedicated to the implementation of a research effort to help utilities respond to regulatory requirements and traditional high-priority concerns of the industry. The research agenda is developed through a process of consultation with subscribers and drinking water professionals. Under the umbrella of a Strategic Research Plan, the Research Advisory Council prioritizes the suggested projects based upon current and future needs, applicability, and past work; the recommendations are forwarded to the Board of Trustees for final selection. The foundation also sponsors research projects through the unsolicited proposal process; the Collaborative Research, Research Applications, and Tailored Collaboration programs; and various joint research efforts with organizations such as the U.S. Environmental Protection Agency, the U.S. Bureau of Reclamation, and the Association of California Water Agencies.

This publication is a result of one of these sponsored studies, and it is hoped that its findings will be applied in communities throughout the world. The following report serves not only as a means of communicating the results of the water industry's centralized research program but also as a tool to enlist the further support of the nonmember utilities and individuals.

Projects are managed closely from their inception to the final report by the foundation's staff and large cadre of volunteers who willingly contribute their time and expertise. The foundation serves a planning and management function and awards contracts to other institutions such as water utilities, universities, and engineering firms. The funding for this research effort comes primarily from the Subscription Program, through which water utilities subscribe to the research program and make an annual payment proportionate to the volume of water they deliver and consultants and manufacturers subscribe based on their annual billings. The program offers a cost-effective and fair method for funding research in the public interest.

A broad spectrum of water supply issues is addressed by the foundation's research agenda: resources, treatment and operations, distribution and storage, water quality and analysis, toxicology, economics, and management. The ultimate purpose of the coordinated effort is to assist water suppliers to provide the highest possible quality of water economically and reliably. The true benefits are realized when the results are implemented at the utility level. The foundation's trustees are pleased to offer this publication as a contribution toward that end.

David E. Rager
Chair, Board of Trustees
Awwa Research Foundation

Robert C. Renner, P.E.
Executive Director
Awwa Research Foundation

ACKNOWLEDGMENTS

The authors would like to thank the following water utilities for co-funding this research effort:

- The City of New York Department of Environmental Protection (Debbie Keesler)
- The City of Phoenix Water Services Department (Laxman Devkota)
- Tacoma Water (Khis Suravallop)

The authors would also like to thank the following water utilities for their participation and their staff for their cooperation and kind assistance with the on-site testing:

- The Big Bend Water District (Thom Reilly)
- The City of Bowling Green Water Treatment Division (Bill Ash, Norman Langenderfer)
- The City of Daytona Beach Dept. of Water and Wastewater Services (Bill Banks, James Thurston)
- The City of Helsinki Pitkääkoski Water Treatment Plant (Eira Toivanen)
- The City of Santa Rosa Dept. of Utilities (Joseph Schwall)
- The City of Troy (Neil Bonesteel and Chris Wheland)

The authors would like to thank R-Can Environmental Inc. (R-Can) and Infilco Degremont, Inc (IDI) for providing the UV reactors and technical assistant for the lamp aging studies conducted at the City of Troy. In particular, we would like to recognize the assistance of Mike Sarchase of R-Can Environmental of Guelph, Ontario and Bruno Ferran of the Degremont North American Research Development Center in Richmond, Virginia.

The authors would like to acknowledge the participation and helpful review comments of the AwwaRF PAC, consisting of Joel Ducoste (University of North Carolina at Chapel Hill), Mehrdad Morabbi (City of Austin Water and Wastewater Utility), Margaret Rodgers (City of Cleveland Division of Water), and Curtis B. Skouby (Saint Louis Water Division), and the AwwaRF Project Manager, Kenan Ozekin.

Finally, the authors would also like to acknowledge Galina Vasaros at the Veterinärmedizinische Universität Wien for assisting with the UV lamp analysis, Dennis Greene for his assistance with the Troy lamp aging study, and Stacy Fuller and Matthew Parrott of Carollo Engineers for preparing the manuscript.

EXECUTIVE SUMMARY

Many U.S. water treatment utilities recognize the great potential benefits of UV disinfection for improving public health protection, while complying with Stage 2 of the Microbial/Disinfection By-Products (M/DBP) Rules. UV disinfection is named in the Long Term 2 Enhanced Surface Water Treatment Rule (LT2ESWTR) as a disinfection technology alternative for earning *Cryptosporidium*, *Giardia*, and virus inactivation credits (USEPA, 2006a).

The inclusion of UV disinfection in the draft and final versions of the LT2ESWTR has led to its swift and widespread implementation in drinking water utilities across North America. However, UV disinfection in drinking water applications remains a comparatively new technology in the medium-to-large-scale drinking water systems, particularly in North America. This was especially true at the inception of this work. This joint “validation and design” project was sought to address some of the big inefficiencies and unknowns in drinking water disinfection validation and design. These issues and their solutions are summarized below.

PROBLEM STATEMENT

For inactivation credit to be earned, the UV reactor must be validated to prove that the reactor will meet the required UV dose delivery and that the on-line compliance monitoring system can provide valid measurements of UV dose delivery. Validation protocols (typically based on the guidance provided in the USEPA *UV Disinfection Guidance Manual*, USEPA 2006b) focus on:

1. The use of challenge microorganisms to measure UV dose delivery,
2. The addition of UV light-absorbing compounds to simulate lowered water UV transmittance, and
3. The use of new lamps operated at low power to simulate end-of-lamp-life, or “aged lamp” conditions.

Current implementation of the first two methods (challenge microorganisms and absorbing chemicals) have limitations that will result in the need of large safety factors, potentially underrating equipment performance in many applications. The underlying assumptions of the third method (that the output of an aged lamp is equivalent to a new lamp operated at low power) may lead to over-estimation of UV dose delivery by the on-line monitoring system and thus a loss of public health protection.

UV disinfection is also a relatively new technology in drinking water. And while UV disinfection has been used in wastewater applications for 20 years, the technology in both drinking water and wastewater has rapidly evolved in terms of lamp technologies, reactor configurations, and dose monitoring and control algorithms. Because of these characteristics, there are opportunities for technology optimization through improved system selection, sizing, and operation. For example, optimization of dose monitoring and control has a significant impact on the electrical power consumption and lamp replacement, the two most significant operating costs of UV disinfection.

PROJECT OBJECTIVES AND APPROACH

The overall goal of this project was to develop practical tools for optimizing the validation, design, and operation of UV disinfection systems. The optimization of UV validation was achieved by addressing the three key issues: identification of better challenge microbes, identification of improved UV-absorbing compounds, and the generation of comparative data on non-uniform UV lamp aging and its impact on UV dose delivery and monitoring. These issues were addressed by the following five tasks:

1. Identify challenge microbes that have a UV dose-response similar to target pathogens (*e.g.*, *Cryptosporidium*) (discussed in Chapter 2);
2. Identify a UV absorbing chemical that appropriately mimics WTP water (discussed in Chapter 3);
3. Characterize the spectral UV output from aged lamps (discussed in Chapter 4);
4. Conduct validation testing to demonstrate the use of new UV absorbers and surrogate organisms (discussed in Chapter 5).
5. Evaluate the impact of surrogate microorganisms, UV absorbers, and non-uniform lamp aging on dose delivery and monitoring using Computational Disinfection Modeling (discussed in Chapters 3 and 6).

The optimization of UV design and operation was achieved by developing a software tool for analyzing UV system operation, sizing, and costs, conducting lamp aging studies on low-pressure high-output and MP lamps, and evaluating alternative approaches for providing energy to UV systems. Specific objectives of the analysis were to:

1. Quantify the impact of operational factors such as on/off cycling and operating power level on the efficiency and performance of UV lamp/ballast assemblies over their useful life;
2. Develop rational approaches for selecting lamp aging factors for sizing UV systems and dose pacing strategies for operating UV systems;
3. Develop rational approaches for selecting UV system redundancy and backup power in response to system failure;
4. Evaluate the performance of commercial UV lamp/ballast assemblies by lighting experts providing utilities with a benchmark on which to base the selection of lamp/ballast technologies and UV system operating strategies with the goal of reducing electrical power costs.

SUMMARY OF FINDINGS

New Microbial Surrogates

Ten bacteriophages were evaluated as possible target pathogen surrogates that more effectively mimic the behavior of *Cryptosporidium* and *Giardia* than MS2 and *Bacillus subtilis*. Essential characteristics of a useful surrogate include: non-pathogenic to humans and the environment, ease of handling, simple and inexpensive culturing requirements, ease of propagation to high titers ($>10^{11}$ /mL) and stability. The following is a summary of the findings:

- Bacteriophage ϕ X174 and PRD1 can only be propagated to 1×10^8 PFU/mL, a concentration that is too low for practical UV validation.
- While bacteriophage fr, R17, PP7 and M13 can be propagated to titers of 3×10^{11} PFU/mL or higher, they have a UV dose-response at 254 nm very similar to MS2 phage and hence would no advantage over MS2 phage as a test microbe.
- While bacteriophage T4 can be propagated to 6×10^{10} PFU/mL, it is inactivated by 4 log with a UV dose of 5 mJ/cm^2 and is too UV sensitive for validating UV reactors for *Cryptosporidium* inactivation credit.
- Q β was successfully propagated in large (6 L) batches with titers of 3×10^{11} pfu/mL with a highly reproducible UV dose-response through 4-log inactivation at 50 mJ/cm^2 . This suggests that Q β phage has great potential as an alternative to MS2 in UV validation of reactors for *Cryptosporidium* inactivation credit. For UV reactors with very narrow dose distributions, the use of Q β could reduce UV reactor capital and O&M costs by a factor of 4 to 30 percent, depending on the UVT of the water.
- Bacteriophage T7 has a UV dose response at 254 nm very similar to the *Cryptosporidium* UV dose requirements in the LT2ESWTR. For UV reactors with very narrow dose distributions, the use of T7 could reduce UV reactor capital and O&M costs by a factor of 16 to 62 percent, depending on the UVT of the water. However, T7 could only be propagated to a titer of 5×10^{10} PFU/mL, which limits its use for large-scale validation. Furthermore, T7 appears to have an action spectrum that provides greater inactivation at wavelengths above 254 nm than does the action of MS2. Hence, the T7 Reduction Equivalent Doses (REDs) measured with a MP UV reactor would be higher than expected based on a test microbe with an action spectrum similar to MS2 phage. This polychromatic bias is estimated at 1.15.
- While bacteriophage SP8 has a UV dose-response similar to *Cryptosporidium*, it could only be propagated to 3×10^9 PFU/mL, less than the titer of T7.
- Action spectra were measured in this work using UV light from a MP lamp filtered using ~ 10 nm bandpass filters. Because UV light was not monochromatic, the dose-response measured using MP light filtered through a 254 nm bandpass filter was significantly different from that measured using monochromatic 254 nm light from a LP lamp. To avoid these errors, further work measuring the action spectra of microbes should use monochromators or optical filters with a narrow bandpass $\ll 10$ nm.

New NOM Surrogates

Eleven NOM sources were identified and evaluated as possible UV-absorbing surrogates that more closely approximate the interaction between water and UV light than coffee or lignin sulphonic acid (LSA). Additionally, the application of these sources for large-scale UV reactor validation was also investigated. The following is a summary of the findings:

- The UVA spectra of the UV absorber used during validation impacts dose delivery and dose monitoring with UV system equipped with polychromatic UV lamps (e.g. MP lamps). Ideally, the UVA spectra used during validation matches that of the water over the germicidal wavelength range (200 to 300 nm) and the wavelength range detected by the sensor (up to 400 nm with SiC UV sensors).
- The UVA spectra of membrane and electro dialysis concentrates closely matched the UVA spectra of WTP waters at wavelengths from 200 to 400 nm. The UVA spectra of the MIEX® and IX brine concentrates matched the UVA spectra of WTP waters at wavelengths above 240 nm but had lower UV absorbance at wavelengths below 240nm. The UVA spectra of all of these concentrates did a better job matching the UVA spectra of WTP waters than did coffee or LSA. The UVA spectra of Super Hume™ matched WTP waters at wavelengths below 260 nm but had higher UV absorbance at wavelengths above 260 nm. While the UVA spectra of Super Hume™ matched WTP waters better than the UVA spectra of coffee, no obvious advantage of Super Hume™ over LSA was apparent.
- For a given flow, UVT 254, and lamp output, the RED measured during validation using the UVA spectra of coffee, LSA, or Super Hume will be typically lower than the RED delivered at the WTP. This level of conservatism is minor at high UVT and significant at low UVT (as much as 30%), is greatest with coffee, least with Super Hume, and varies depending on the UVA spectra at the WTP. The RED measured using the UVA spectra of MIEX® and IX brine concentrates will also be lower than the RED delivered at the WTP at UVTs from 75 to 90 percent but will be greater by as much as 8% at UVTs above that range. The RED measured using the UVA spectra of membrane and electro dialysis concentrates will on average match the RED at the WTP. However, because the UVA spectra of the concentrates and WTP waters vary, the RED measured using membrane and electro dialysis concentrates can be higher or lower than at the WTP by as much as 14 percent.
- The over prediction of RED for a given flow, UVT at 254 nm, and UV lamp output caused by the UV absorber used during validation will impact UV system sizing but not the dose monitoring if the Polychromatic Bias has a value of one or less.
- For a given flow, UVT, and UV sensor reading, differences in the UVA spectra of the UV absorber used during validation and the UVA spectra of the water can cause bias errors in dose monitoring. This Polychromatic Bias depends on the UVA spectra of the validation and WTP waters, the UVT 254 value, the spectral response of the UV sensor, and the location of the UV sensor relative to the lamps.
- The bias error is small at high UVT but increases exponentially as UVT decreases. The bias error is greater with SiC sensors that measure UV light above 300 nm compared to germicidal UV sensors that measure UV light from 200 to 300 nm. Whether the bias error leads to over or under predictions of dose delivery depends on

- the UV sensor-to-lamp water layer distance and differences in the UVA spectra during validation and at the WTP. For coffee, LSA, and Super Hume, the bias error leads to under predictions of dose delivery at the WTP if the UV sensor is located relatively close to the lamp and over predictions if the UV sensor is located relatively far from the lamp. With some membrane concentrates, the opposite occurs.
- While the 2006 UVDGM indicates that the Polychromatic Bias is only an issue with non-germicidal UV sensors, the bias can be large with germicidal UV sensors if they are placed far enough from the lamps and the UVT is low.
 - The magnitude of the bias error follows the order Coffee > Super Hume ~ LSA > MIEX® and IX brine concentrates > membrane and electro dialysis concentrates.
 - An ideal sensor location exists that minimizes the magnitude of the error. That ideal sensor location is equivalent to the ideal sensor location used for dose monitoring using the UV intensity setpoint method described in the USEPA UV Disinfection Guidance Manual (UVDGM). Using a germicidal UV sensor located relatively close to the lamps is the best approach for minimizing the bias error.
 - Utilities considering on site validation should use UVA absorbers whose UVA spectra best matches that of their water. UV vendors conducting broad based validation of their products should use UVA absorbers whose UVA spectra provides somewhat conservative estimations of dose delivery to provide UV system sizing data that is broadly applicable to a wide range of WTP waters. Super Hume™ appears to provide a reasonable compromise by ensuring UV systems are appropriately sized for most WTP UVA spectra without undue conservatism. Super Hume improves the stability of test microbes and is available in large volumes. It is now used at the Portland UV Validation Test Facility.
 - Validation using membrane concentrates is not practical because of the large volumes needed.
 - The use of IX and MIEX® brines as UV-absorbing surrogates during UV reactor validation could be feasible depending on volume requirements and availability. During this study, no source was identified that could provide enough volume for a large-scale validation.

Demonstration of New Microbes and UV Absorbers

A UV reactor equipped with medium pressure lamps was validated at the Portland UV Validation Test Facility. The validation used Super Hume as a UV absorber and compared dose delivery measured using MS2 and T7 phage with new and aged lamps. The following conclusions were made:

- The concentrations of microbial samples with Super Hume™ remained stable over an 8-day period of analysis. This was consistent with previous studies, which indicated that Super Hume™ enhanced microbial stability (Hargy *et al.* 2004).
- For a given UV dose, the uncertainty of the UV dose-response of T7 was less than that of MS2, especially at low UV doses. As such, if both MS2 and T7 were used to validate a reactor for similar *Cryptosporidium* inactivation credit, the T7 analysis would have greater confidence associated with the UV dose-response analysis and the REDs determined using that UV dose-response.

- The ratio of RED measured using MS2 and T7 phage with the reactor evaluated in this study was notably less than the RED bias uncertainty factors listed in the UVDGM. This indicates that the reactor's dose distributions are not as wide as the dose distributions used by USEPA to define the RED bias uncertainty factors.
- Validation of the UV reactor using T7 bacteriophage as opposed to MS2 significantly reduces the RED bias uncertainty factors needed for *Cryptosporidium* inactivation credit. For example, the RED bias uncertainty factors in the UVDGM for 3-log *Cryptosporidium* credit are 1.0 with T7 phage but range from 1.18 to 2.45 with MS2.
- Dose delivery for the test reactor was not significantly impacted by use of an aged lamp compared to a new lamp. This observation indicates either that the UV sensor was appropriately located within the reactor to account for non-uniform lamp aging, that the reactor baffle ensured non-uniform lamp aging did not significantly impact the relation between RED and UV sensor readings, or that non-uniform lamp aging was not significant with the aged lamp tested. This result is specific to this reactor and the lamp tested and further evaluation of the impact of lamp aging on dose delivery and monitoring with different commercial UV reactors is recommended.

Non-Uniform Lamp Aging

One type of LPHO lamp and two types of MP lamps were collected from U.S. and European utilities. These lamps and sleeves had been operated in the field under normal process conditions, including variations in flow rate and water UV transmittance, while maintaining a specific target delivered UV dose. The spectral outputs of four LPHO and eight MP lamps were evaluated along the length and about the circumference of the lamps. The output of aged lamps was compared to that of new lamps. The following is a summary of the findings:

- Visual affects of lamp aging could be classified into five types as follows:
 - Darkening of the quartz envelope at each end of the lamp
 - Random discoloration along the length of the lamp
 - Discoloration along the length of the lamp but only 180° about the circumference
 - Lamp end distortion
 - Resonant darkening
 - Resonant distortion
- Lamp envelope distortion, resonant darkening, and 180 degree darkening only occurred with MP lamps. Resonant darkening occurred on the opposite side of the resonant distortion. Likely, distortion is occurring along the topside of the lamp due to arc deflection.
- Low-Pressure High-Output Amalgam Lamps

Amalgam UV lamps have five UV peaks between 300 and 400 nm that have a UV output 5 percent or greater than the UV output at 254 nm. UV output at 254nm showed a greater reduction as lamps aged than did the peaks from 300 to 400 nm.

Amalgam lamps showed a reduction in UV output at 254 nm that correlated with lamp age and was greater at the lamp ends as compared to the middles.

The UV output at 254 nm of a new amalgam lamp varies along the length of the lamp with greater UV output at locations 12 cm from the electrodes and lower output at the middle of the lamps compared to this location. The UV output also showed a sharp drop at the locations of the amalgams.

The aged LPHO lamps showed greater non-uniformity along their length compared to the new lamp

In general, the UV output of new and aged amalgam lamps did not vary significantly around the lamp circumference.

- **Medium Pressure UV Lamps**

UV output with aged MP lamps was lower than UV output with new lamps.

Some of the aged MP lamps exhibited UV outputs that varied around the circumferences of the lamps. Non-uniform aging of MP lamps about their circumference is likely related to arc deflection.

One MP lamp type did not show a significant non-uniformity in lamp output along the length of the lamp with new and aged lamps. The other MP lamp type showed lower output at the ends compared to the middle of the lamp.

Both MP lamp types showed “spectral shifts” in UV output as a function of wavelengths as the lamps aged. In general, the UV output at lower wavelengths aged faster than higher wavelengths. However, one lamp showed greater aging at 260 nm compared to 245 nm and the other showed greater aging at 400 nm compared to 340 nm.

Computational Disinfection Modeling

UV intensity modeling and CFD-based dose delivery modeling were used to understand dose delivery and monitoring with two hypothetical UV reactors equipped with LPHO and MP lamps. Conclusions are as follows:

- **Impact of Microbe Inactivation Kinetics on RED**

The RED delivered by a reactor depends on the reactor’s dose distribution and the microbe’s UV inactivation kinetics. The RED of a UV resistant microbe, like MS2 phage, will be greater in value than that of a UV sensitive microbe, like *Cryptosporidium*. The difference will be greater with a reactor with a wider dose distribution. Because the dose distribution is wider at lower UVT, the difference with a given reactor will be greater at low UVT. For a given flow and UVT, the difference also depends on the relative lamp output.

The impacts of microbe kinetics on RED impacts how validation data should be interpreted for a given target pathogen. If the validation microbe is more resistant to UV light than the target pathogen, the REDs measured during validation for a given flow, UVT, and lamp output will be greater than the REDs delivered to the pathogen. This bias is eliminated if the validation microbe has the same inactivation kinetics as the target pathogen.

A single relation between microbe log inactivation and S/S₀/D₁₀ can be defined for a given reactor at a given UVT, where S/S₀ represents the relative UV output from the lamps and D₁₀ is the UV dose required to inactivate microbe with first order inactivation kinetics by one log. The relation suggests that validation data

measured as a function of S/S_0 with one microbe can be used to predict log inactivation and RED of another microbe with a different D10. Hence, RED Bias values can be estimated with validation data obtained using one microbe. The relation also provides a rationale for analyzing validation data obtained with two microbes with different UV sensitivities.

- Relation Between RED and UV Sensor Readings

The relation between RED and UV sensor reading at a given flow and UVT depends on UV sensor position relative to the lamps. If the UV sensor is located relatively close to the lamps, the RED for a given UV sensor reading decreases as UVT decreases. If the UV sensor is located relatively far from the lamps, the RED for a given UV sensor reading increases as UVT decreases.

In theory, an optimal UV sensor reading can be defined where the relations between RED and UV sensor readings for different UVT values overlap and can be described by a single relation. Model data for the MP reactor shows there was not one UV sensor location where RED as a function of UV sensor reading overlapped for a wide range of UVTs. Instead, a location could be defined where RED for a given UV sensor reading has a minimum value at some intermediate UVT. Above and below that UVT, the RED increased for a given UV sensor reading. The relation between RED and UV sensor reading at this intermediate UVT and UV sensor location could be used for UV intensity setpoint dose monitoring.

The German DVGW and Austrian ONORM specify dose monitoring using the UV intensity setpoint approach where the UV reactor delivers a validated UV dose value when the UV sensor reads above an alarm level. The DVGW and ONORM standards state that the dose delivery at the alarm UV intensity setpoint is validated using two test conditions. Test 1 involves high UVT and lamp power lowered to give a UV sensor reading at the alarm level. Test 2 involves maximum lamp power and UVT lowered to give a UV sensor reading at the same alarm level. The validated dose is defined as the lower of the REDs measured with the two test conditions. This work shows that a third test condition at an intermediate UVT is needed when the minimum RED for a given UV sensor reading occurs at an intermediate UVT.

- Impact of Spectral Shifts in UV output from LPHO and MP Lamps

The reduction in UV output due to lamp aging varies as a function of wavelength with lower wavelengths aging faster than higher wavelengths.

SiC UV sensors measure UV light at wavelengths from 200 to 400 nm. Microbes are inactivated by UV light at wavelengths from 200 to 300 nm. Because SiC sensors measure non-germicidal light above 300 nm, dose-monitoring algorithms that use SiC sensors can over estimate dose delivery as MP and LPHO lamps age because the germicidal wavelengths age faster than wavelengths from 300 to 400 nm. These dose-monitoring errors are negligible if the UV sensor has a germicidal spectral response.

- Impact of Non-Uniform Lamp Output on Dose Delivery and Monitoring

UV intensity models and CFD-based dose delivery models were developed that account for non-uniform output along the length and about the circumference of UV lamps that occurs as lamps age.

Non-uniform lamp output along the length of the lamp and about the circumference impacts dose monitoring and dose delivery.

With the MP reactor modeled, the dose-monitoring algorithm over predicted UV dose by as much as 45% if the UV sensor viewed a location along the lamp length and about the circumference that aged the least. The algorithm under predicted UV dose by as much as a factor of 5 if the UV sensor viewed a location that aged the most.

With the LPHO reactor modeled, the dose-monitoring algorithm over predicted UV dose by as much as 20% if the UV sensor viewed a location along the lamp that aged the least and under predicted UV dose by as much as a factor of 2 if the UV sensor viewed a location that aged the most.

To minimize under and over dosing caused by non-uniform lamp output along the length of the lamp, UV sensors used with the modeled MP reactor should monitor locations along the lamp length that are 25% of the arc length away from the electrode and UV sensors used with the modeled LPHO reactor should monitor locations that are 13% of the arc length away from the electrode.

To minimize under and over dosing caused by non-uniform lamp aging about the lamp's circumference, the UV sensor should monitor MP lamps from the side as opposed to the top or bottom.

- The conclusions from the computational modeling are dependent on the hypothetical reactors modeled. Different results would be obtained with different reactor designs. For example, a baffle plate can be used to improve the reactor's dose distribution and reduce the impacts of end darkening on dose delivery. As another example, the impact of lamp end darkening on dose delivery and monitoring may differ depending on whether the lamps were oriented parallel to flow or perpendicular to flow. The results from this work should be used to guide the reader on the potential impact of dose distributions, spectral shifts, and non-uniform lamp output and how to evaluate these impacts with commercial UV reactor technologies.

UVCAT Provides Comprehensive UV System Analysis

A UV system cost-analysis tool, "UVCAT," was developed to provide a comprehensive evaluation of UV disinfection system performance and costs. The tool consists of an Excel™ workbook with embedded Visual Basic™ software. The Excel™ workbook serves as a user interface to enter data, initiate the software algorithms, and view outputs. The software provides three types of analysis:

- Standard Life-Cycle Cost analysis – estimates O&M and life-cycle assuming operation at average flow rate, UVT, and lamp output.
- Lamp Replacement Interval Cost analysis - estimates O&M and life-cycle costs as a function of lamp replacement interval assuming operation under average conditions of flow rate, UVT, and lamp output.
- Advanced Life-Cycle Cost analysis – simulates UV system performance as a function of time for a given dataset on flow, UVT, power quality, and pathogen concentrations.

Optimal Lamp Replacement Interval Depends on Lamp Type and Lamp Aging Curve

The Lamp Replacement Interval Cost Analysis tool was used to analyze UV system life-cycle costs as a function of lamp replacement interval. The following observations were made:

- With UV systems using LPHO lamps, the life-cycle costs decreased with increasing lamp replacement interval. Utilities should realize cost benefits by operating LPHO lamps beyond their recommended lamp life.
- With UV systems using MP lamps, if the lamp-aging curve showed a significant reduction over time, the optimal lamp replacement interval was between 2,000 and 5,000 hours. If the lamp-aging curve did not show a significant reduction over time, the life-cycle costs of the MP system decreased with greater lamp replacement intervals, albeit with diminishing returns.

UV Dose-Pacing Strategies Can Provide Significant Cost Benefits

The Standard and Advanced Life Cycle Cost Analysis tools were used to evaluate dose-pacing strategies used by UV systems. The following observations were made:

- Dose pacing can provide significant cost benefits both in terms of power savings and component replacement. However, those benefits depend on the variability in flow rate, UVT, lamp aging, and fouling occurs with a given UV disinfection application.
- The cost benefits of dose pacing are more significant with MP UV reactors than LPHO UV reactors. Full dose pacing improves the ability of MP systems to compete with LP and LPHO systems, especially in applications with highly variable flow and UVT.
- The efficiency of dose pacing depends on the efficiency of the dose-monitoring algorithm. Algorithms that use flow, UV intensity, and UVT alarm setpoints are less efficient than algorithms that define dose delivery as a function of these variables. The efficiency of setpoint approaches will depend on the variability of flow rate and UVT with the application and the location of the UV sensor relative to the lamps.
- With drinking water applications, the minimum validated flow and the maximum validated UVT are used in the dose-monitoring algorithm whenever flow is below the validated range and UVT above the validated range. This can lead to significant over dosing by the UV system.
- Lamp ballasts with continuous ballast power settings provide more efficient dose pacing than ballasts with discrete ballast power settings.
- The efficiency of dose pacing depends on the efficiency of the lamp ballast assembly. MP lamp-ballast assemblies tend to be less efficient at lower ballast power settings while LPHO lamp-ballast assemblies tend to be less efficient at higher ballast power settings.
- UV systems using lamps oriented perpendicular to flow and configured as multiple banks of lamps in series can provide more efficient dose pacing than UV reactors using lamps oriented parallel to the flow and configured as one bank of lamps.

Risk Analysis Provides a New Approach for UV System Design

The Advanced Life Cycle Cost Analysis tool was used to evaluate the impact of dose-pacing strategies, operational dose, power quality events, and component failure on infection risk. The following observations were made:

- Risk analysis can provide a rational approach for sizing and operating a UV system for a given application.
- Regulators, utilities, and engineers should compare the risk associated with off-specification performance and UV system failure to a baseline level (USEPA's one infection per 10,000 persons per year risk target) in order to rank the importance of these events.
- The cost benefits of dose pacing are offset by an increase in public health risk. Utilities should consider the tradeoffs between cost and risk when assessing UV system operation alternatives.
- Without back-up power, shutdown valves, or some other response measure, sustained voltage sags or power interruptions will have a significant adverse impact on public health protection.
- A UPS system is not always required with a UV disinfection system to provide adequate health protection. A UV system operating at a higher dose with a generator can provide better health protection than a UV system operating at the design dose with a UPS system.
- Component failure will have a minor impact on public health risk if the UV system always has one or more banks of lamps treating the flow. If the UV system operates as one-bank reactors and the number of lamps is low (*e.g.*, 2 or 4 lamps), lamp or ballast failure can lead to significant underdosing.
- There is poor correlation between UV system off-specification performance, as defined by the USEPA *UVDGM*, and public health risk. For example, low UVT events can easily cause off-specification operation that exceeds the 5-percent USEPA requirement, but has a negligible impact on public health risk. However, power quality events that cause UV system shutdown can lead to off-specification operation that meets the 5-percent requirement, but may have a serious adverse impact on public health protection.

Lamp-Aging Depends on Lamp Type, Location, and Power Setting

A lamp aging study was conducted on four types of UV lamps – 300-W amalgam LPHO lamps, 130-W non-amalgam LPHO lamps, and 6.5 and 8-kW MP lamps. The following observations were made:

- Lamp aging observed with the 8-kW lamps depended on time and ballast power setting and could be modeled using:

$$I = A \times P^B \times \exp(-E \times P^F \times t) + C \times P^D \times (1 - \exp(-E \times P^F \times t)) \quad (\text{ES.1})$$

where I is the measured UV intensity, P is the ballast power setting, t is time, and A through F are model coefficients. Model coefficients depended on the location along the lamp length and about the circumference being modeled. The model predicts a faster lamp-aging rate with lower lamp power. The lamp-aging rate also depended on the lamp location, with faster rates at the lamp ends compared to the center.

- Lamp aging observed with the 6.5-kW lamps could be modeled using:

$$I = a \times b^t \times t^{-c} \quad (\text{ES.2})$$

where I is the measured UV intensity, t is time, and a , b and c are model coefficients. Lamp aging depended on time but no dependence on ballast power setting was observed. The lamp-aging rate also depended on the lamp location, with faster rates at the lamp ends compared to the center and at the top end compared to the side end. The lamp aging had an unusual profile as a function of time – the lamp output decreased for the first 3,000 to 4,000 hours and either stabilized or increased for the next 2,000 to 3,000 hours. The increase can be explained by changes in the amount of mercury available within the lamp to form the plasma.

- Lamp aging observed with the amalgam and non-amalgam lamps was modeled using:

$$I = a \times t^{-b} \quad (\text{ES.3})$$

where I is the measured UV intensity, t is time, and a and b are model coefficients. The rate of lamp aging was greater with the 300-W amalgam LPHO lamps compared to the 130-W non-amalgam LPHO lamps. The rate of lamp aging tended to be greater at the lamp ends and did not vary significantly with lamp power settings of 80 and 100 percent.

- Because the capital costs of a UV system depend on the lamp-aging factor used to size the UV system, a UV vendor with a lamp-aging factor higher than their competitors will realize a significant competitive advantage. Hence, UV vendors have a strong economic driver to base their lamp aging factors on the location about the lamp that gives the highest lamp-aging factor. Utilities need to ensure lamp-aging factors used to size a UV system are selected based on the most representative position along the length and about the circumference of the lamp.

Advanced Battery Systems Can Provide Peak Load Reduction

Approaches for reducing peak electrical load reduction strategies for UV disinfection systems were investigated. The following observations were made:

- Utilities can purchase electrical power either at a fixed or variable rate. The cost of electricity purchased at night can be half the cost of electricity purchased during the day. For example, day and night time costs in New York State have been 13.3 and

6.5 ¢/kW-hr. If energy is purchased during off-peak hours, a variable-rate structure can provide significant cost savings.

- Advanced battery systems can be used to reduce UV disinfection power costs by storing energy at night when power costs are low and supplying energy during the day when power costs are high. Advanced power systems also can be used as a UPS to ensure UV disinfection during short-term and sustained power interruptions.
- Sodium-sulfur batteries are a new battery technology recently commercialized in Japan. They have been successfully used at wastewater treatment plants for reducing energy costs through peak load shaving.
- Using the above-mentioned energy pricing structure for New York State, a UV system using a 12-hour sodium-sulfur battery system to take advantage of nighttime power costs has life-cycle costs comparable to a UV system using a 5-minute UPS. The analysis indicates that the sodium-sulfur battery system has potential for providing a cost-effective alternative power supply for UV systems, especially if battery capital costs drop in the future due to more efficient production or increased day time energy costs.

RECOMMENDATIONS

The best UV technology for a drinking water disinfection installation comes from the optimal implementation of all aspects of system application: validation, design and operation.

- UV validation should be conducted with the tools that provide the most accurate measurement of performance. This includes:
 - Using a challenge microbe with a UV dose response that closely matches the target pathogen(s). The microbe T7 provides a very accurate match to the UV dose responses of *Cryptosporidium* and *Giardia* as defined by USEPA (USEPA 2006a)
 - Using a UV-absorbing chemical that will not adversely impact the stability of challenge microbe and may, in some cases, enhance it. To date, Super Hume™ has been found to be the most attractive NOM surrogate identified. It is easy to use and in some cases (in full-scale validation testing at the Portland Validation Facility) has increased challenge microbe stability in test waters. If a non-germicidal sensor is used, IX and MIEX® brines may be better alternatives depending on volume requirements and availability.
- Lamp aging is specific to given lamp technology and its operation. To account for non-uniform lamp aging, UV sensors should be placed to measure the region of the lamp that ages faster. Data collected in this study show the lamps typically age faster near the electrodes and along the top of the lamps. With LPHO and MP lamps, analysis suggests that UV sensors should view a location along the arclength that is located 13 % and 25%, respectively, of the arclength away from the electrodes. With MP lamps, analysis also suggests that UV sensors should view the lamps from the side of the lamp as opposed to from the top or bottom.
- UV systems should be sized using lamp-aging factors that are based on lamp performance data measured with installed UV systems.

- Utilities should consider using UVCAT to analyze UV system performance. UVCAT can provide the following analysis:
 - Evaluate UV system alternatives for a given disinfection application prior to system selection.
 - Identify the best UV dose monitoring and control strategy for each candidate system.
 - Quantify the impacts of the validated range on O&M costs for a given reactor.
 - Justify re-validation if the benefits of an improved dose monitoring and control strategy are greater than the costs of re-validation.
 - Quantify costs and benefits traditionally evaluated using a qualitative ranking system, such as public health protection.
 - Optimize the operation of installed UV systems.
- Utilities should consider the tradeoffs between increased capital and power costs and decreased lamp replacement costs that occur with a longer lamp replacement interval. The lamp replacement interval of energy efficient LP and LPHO lamps can be extended beyond the replacement interval of 8,000 to 12,000 hours typically quoted by UV vendors without increasing life-cycle costs. However, an optimal lamp replacement interval of 3,000 to 5,000 hours can occur with less energy efficient MP lamps, beyond which life-cycle costs increase.
- Utilities should evaluate the operation and maintenance costs of UV system alternatives accounting for the flow rate and UVT profile that occurs with a given UV application, the dose-pacing strategy used by the UV system, and the impacts of the validated range and ballast power settings, and the efficiency of the dose-monitoring algorithm and the lamp-ballast assembly.
- Utilities can use risk analysis to rank options for UV system design and operation and identify practical approaches for specifying off-specification performance requirements. Risk analysis can be used to evaluate UV system sizing for a given flow rate and UVT profile, evaluate the impacts of power quality and off-specification performance, and select an operational UV dose that provides a specified level of public health protection.
- Off-specification performance as defined by the USEPA (2006a) is a poor indicator of public health protection by UV disinfection systems. Instead, Utilities and State regulators should base UV system compliance on a UV system log inactivation defined as:

$$\log I_s = -\log \left(\frac{\sum_{i=1}^L \sum_{n=1}^N Q_{i,n} 10^{-\log I_{i,n}}}{Q_{i,T}} \right) \quad (\text{ES.4})$$

where $\log I_s$ is the UV system log inactivation, $Q_{i,n}$ is the flow rate through reactor n at time i , $\log I_{i,n}$ is the log inactivation credit through reactor n at time i based on the pathogen UV dose indicated by the reactor's UV dose monitoring system, $Q_{i,T}$ is the total flow rate through the UV system at time i , N is the total number of UV reactors in the UV system, and L is the time period over which the UV system log inactivation credit is determined. The UV system log inactivation credit would be calculated over a one-month period to be consistent with the time period used to calculate the

off-specification performance or calculated over a four hour period to be consistent with the 4 hour dose reporting interval recommended by the USEPA UVDGM.

This calculation is no more complex than many of the calculations and functions currently programmed into the PLC of a UV reactor. The UV system log inactivation credit would be reported to the State as a measure of UV system compliance. This metric of UV system performance would considerably simplify reporting to the State; especially with UV systems using multiple reactors in parallel. It would also provide operators with a metric on which to apply an operational UV dose to ensure UV system performance meets public health objectives.

- Utilities should evaluate using sodium-sulfur battery systems to take advantage of energy pricing structures. Sodium-sulfur battery systems would be charged during the night when power costs are low and used to power the UV system during the day when power costs are high.

CHAPTER 1

PROJECT IMPETUS AND GOALS

PART 1: OPTIMIZATION OF VALIDATION

Ultraviolet (UV) disinfection is listed in the Stage 2 Microbial/Disinfection By-products (M/DBP) Rules' Long-Term 2 Enhanced Surface Water Treatment Rule (LT2ESWTR) as a compliance technology for achieving *Cryptosporidium*, *Giardia*, and virus inactivation credits (USEPA 2006a). To qualify for disinfection credit, the UV reactor's performance must be validated. UV reactor validation requires the generation of data that proves that the reactor will meet the required UV dose delivery and that the on-line compliance monitoring system can provide valid measurements of UV dose delivery. Validation protocols are defined in the United States Environmental Protection Agency (USEPA) *UV Disinfection Guidance Manual* (USEPA 2006c), the Austrian Standards *ÖNORM M 5873-1* and *M 5873-2* (ÖNORM 2003), the German Guideline *DVGW W294* (DVGW 2003) and NWRI/AwwaRF *UV Disinfection Guidelines for Drinking Water and Water Reuse* (2003) among others.

Protocols currently used in the United States (U.S.) focus on:

1. The use of challenge microorganisms to measure UV dose delivery.
2. The addition of UV light-absorbing compounds to simulate lowered water UV transmittance.
3. The use of new lamps operated at low power to simulate end-of-lamp-life, or "aged lamp" conditions.

Current implementation of the first two methods (challenge microorganisms and absorbing chemicals) have serious limitations that will result in the need of large safety factors, potentially underrating equipment performance in many applications. The underlying assumptions of the third method (that the output of an aged lamp is equivalent to a new lamp operated at low power) may lead to over-estimation of UV dose delivery by the on-line monitoring system and thus present a public health risk.

APPLICATION OF UV DISINFECTION TO DRINKING WATER

UV disinfection of drinking water is accomplished using closed-vessel reactors equipped with mercury-vapor lamps enclosed in quartz tubes. Four types of mercury lamps are typically used - low-pressure (LP), low-pressure high-output (LPHO), amalgam LPHO, and medium-pressure (MP). LP and LPHO lamps emit germicidal UV light at 254 nanometer (nm) whereas MP lamps emit germicidal light from 200 to 300 nm. Germicidal UV light emitted from the lamps inactivates waterborne pathogens by damaging their nucleic acid. The inactivation is a function of wavelength and peaks near 260 nm. The damage prevents the microbes from being able to replicate and cause infection.

UV dose is a measure of the germicidal energy delivered to microbes. UV dose is typically expressed in units of millijoules per square centimeter (mJ/cm^2) or joules per square meter (J/m^2). The UV dose delivered to the microorganisms depends on the flowrate of water through the reactor, the number and location of the lamps within the reactor, the UV output from

each lamp, the UV transmittance of the water, and the trajectories of the microbes relative to the lamps. Because different microbes follow different trajectories as they pass through a UV reactor, the dose delivery by a UV reactor is best represented by a dose distribution. A dose distribution is a probability plot that a microbe passing through a reactor will receive a given dose.

Dose delivery by a UV reactor and the associated inactivation of waterborne pathogens cannot be directly measured during normal operation of the reactor at a water treatment plant (WTP). Instead, dose delivery is indicated by an on-line dose monitoring system that relates measurements of flowrate, UV intensity, lamp status, and UV transmittance at 254 nm (UVT) to UV dose. Because of the complex relation between dose delivery and these variables, UV regulations and guidance require UV validation testing to prove the dose-monitoring algorithm.

With validation testing, the UV reactor is installed within a test train. Water is passed through the reactor at a controlled flowrate. UV absorbers are injected into the flow upstream of the reactor to adjust the water UVT to a target value. UV lamps are turned on and operated at target power levels. Test microbes are added to the flow upstream of the reactor. Inactivation of the test microbe is measured using water samples collected from the reactor's inlet and outlet. Dose delivery is determined by relating the measured log inactivation of the test microbe to a dose value using the known UV dose-response of the test microbe. The dose thus determined is termed the reduction equivalent dose (RED). Analysis of the relation between RED and measured flowrate, UVT, UV intensity, and lamp on/off status is used to define the dose monitoring algorithm of the reactor.

The RED measured during validation depends on the reactor's UV dose distribution and the test microorganism's inactivation kinetics (Cabaj 1996, Wright and Lawryshyn 2000). The value of the measured RED will be greater with a more UV-resistant test microorganism and lower with a more UV-sensitive test microorganism. The magnitude of the difference will depend on the reactor's dose distribution, being greater with a wider dose distribution. Because the RED value depends on the test microorganism's inactivation kinetics, reference should always be made to the challenge microorganism when specifying the RED. For example, "a Type 2 Male-specific coliphage (MS2) RED of 40 mJ/cm² was measured for the stated operating conditions."

Further discussion of the concepts presented here can be found in the *UV Disinfection Guidance Manual* (USEPA 2006c).

PROBLEMS POSED BY CURRENT VALIDATION METHODS

Challenge Microbe

MS2 coliphage is typically used as challenge microbes for UV validation in the U.S. and *Bacillus subtilis* spores are typically used in Europe. Because these microorganisms are much more resistant to UV light than many waterborne pathogens, they were historically considered conservative indicators of UV reactor performance (NWRI/AwwaRF 2003). This is true if the log inactivation measured using the test microorganism is used to indicate the log inactivation of a more UV-sensitive pathogen.

A typical interpretation of biodosimetry is that the UV dose measured using the challenge microbe is a measure of the UV dose delivered to all other microbes (Qualls and Johnson 1983). In other words, if an MS2 RED of 20 mJ/cm² is measured, then the UV dose delivered to

Cryptosporidium would be 20 mJ/cm². This interpretation is true if the reactor has ideal hydraulics such that each microbe passing through the reactor receives the same UV dose. However, this interpretation is not valid with real reactors because dose delivery is not ideal and measured RED depends on the dose distribution and the inactivation kinetics of the microbe.

A hypothetical example illustrating the limitations of this assumption follows. A UV reactor has a dose distribution whereby 99 percent of the flow uniformly receives an infinite UV dose and 1 percent of the flow receives zero UV dose. All microbes in the 99 percent of the flow that receives infinite dose would be completely inactivated while none of the microbes in the 1 percent of flow that receives zero dose would be inactivated. As such, the reactor achieves 2-log inactivation with all microbes regardless of their UV sensitivity. If MS2 phage were used as a challenge microbe, the net inactivation by the reactor would be 2 log, which corresponds to an MS2 RED of 40 mJ/cm² assuming MS2 has a UV sensitivity of 20 mJ/cm² per log inactivation. On the other hand, if *Cryptosporidium* had been used as a challenge microbe, the net inactivation would have also been 2 log, which corresponds to an *Cryptosporidium* RED of 4 mJ/cm², assuming a *Cryptosporidium* UV sensitivity of 2 mJ/cm² per log inactivation. The hypothetical example clearly illustrates the dependence of RED on both the reactor's dose distribution and the UV sensitivity of the test microbe.

Figure 1.1 is a real-world example of how non-ideal hydraulic conditions of a UV reactor impacts the RED measured using a challenge microbe. The figure is based on a UV dose distribution predicted from laser Doppler velocimetry measurements made on a LP UV system with vertically mounted lamps (Chui *et al.* 1999). The RED was calculated from the UV dose distribution using (Wright and Lawryshyn 2000):

$$RED = -\frac{1}{k} LN \left[\int p e^{-kD} dp \right] \quad (1.1)$$

where k is the first order inactivation coefficient of the microbe, D is a dose value in the dose distribution, and p is the probability of delivering that dose. The RED is plotted as a function of the UV sensitivity of the microbe defined as the UV dose required per log inactivation. The UV dose required per log inactivation used to define the x-axis is related to the first order inactivation coefficient using:

$$D_{10} = -\ln(0.1) / k \quad (1.2)$$

where D₁₀ is UV dose required per log reduction (mJ/cm² per log inactivation) and k is first order inactivation coefficient (cm²/mJ). The x-axis is represented using a UV dose per log reduction as opposed to first-order inactivation because it offers better visualization of the UV sensitivity of the microbe.

Due to the reactor's non-ideal hydraulic behavior, the reactor represented in Figure 1.1 delivers a UV dose distribution with an average value of ~26 mJ/cm². If the reactor had been challenged using MS2, the measured RED would be 18 mJ/cm² (Figure 1.2). Yet, the RED delivered to *Cryptosporidium*, based on a UV sensitivity of 4 mJ/cm² per log inactivation (from the LT2ESWR requirements for 3 log inactivation), would be 12 mJ/cm². In other words, with this reactor, the MS2 RED over-predicts the *Cryptosporidium* RED by a factor of 1.5.

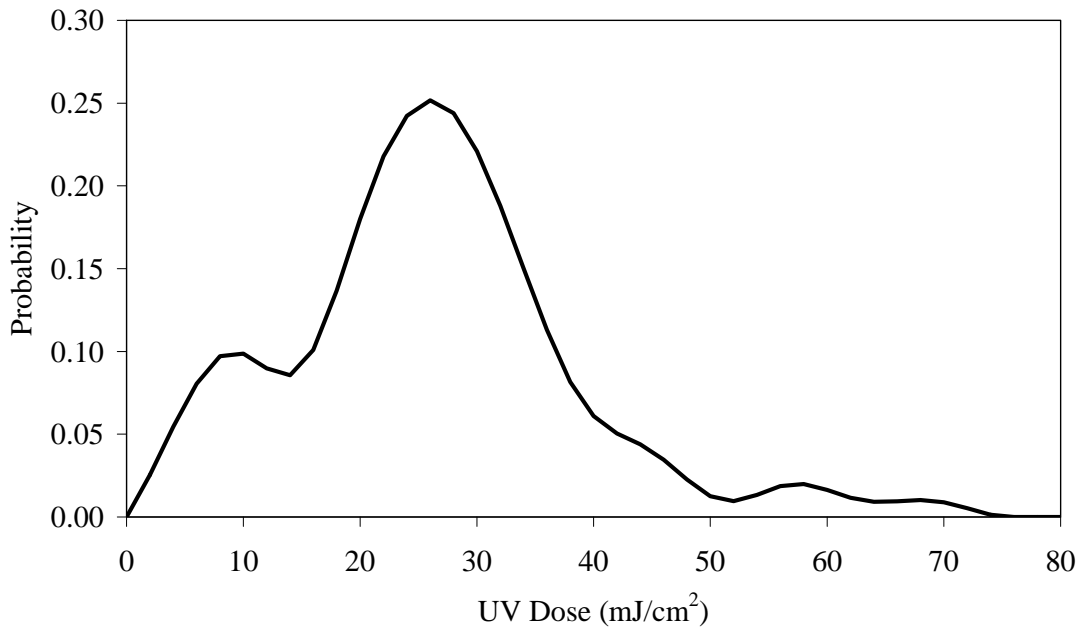


Figure 1.1 The dose distribution in real systems is not ideal

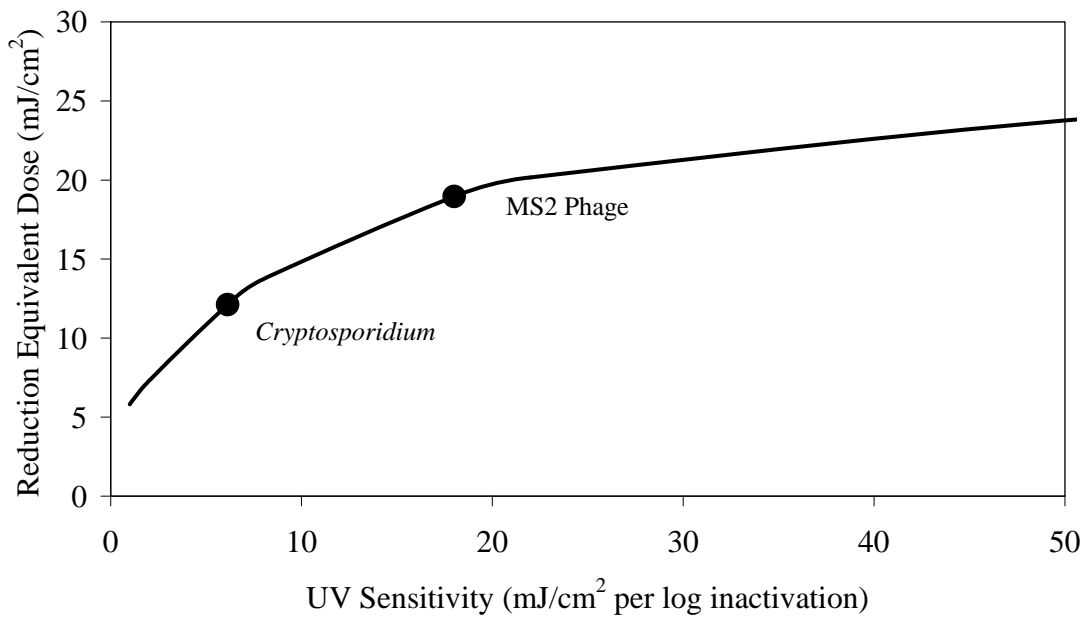


Figure 1.2 Impact of the dose distribution in Figure 1.1 on inactivation

If the dose distribution of a reactor was known, RED values for microbes with different inactivation kinetics could be estimated. Dose distributions can be estimated using UV dose modeling based on Computational Fluid Dynamics (Wright and Lawryshyn 2000) or estimated using fluorescent microspheres. However, the accuracy of these methods to predict different REDs of different microbes has not been demonstrated. If the UV dose distribution of the reactor is not known, an uncertainty factor, termed the RED bias, must be applied to RED values measured using MS2 and *B. subtilis* if the validation data measured using those microbes is used to indicate the inactivation of UV sensitive pathogens such as *Cryptosporidium*. The USEPA UV Disinfection Guidance Manual (UVDGM) (USEPA 2006c) specifies the use of RED bias factors based on dose distributions estimated for commercial reactors. Because commercial reactors have narrow or wide dose distribution based on their design, the RED bias factors specified by the UVDGM were selected based on a reactor with a relatively wide dose distribution to be conservative. Hence the factors will be conservative if the validated UV reactor has a narrow dose distribution and possibly even not conservative enough if the reactor has very inefficient dose delivery.

To provide a more accurate assessment of UV reactor dose delivery and minimize the need to apply conservative RED bias factors, there is a significant need to identify a microbial surrogate that can better mimic the UV dose-response of *Cryptosporidium* and *Giardia*. A better microbial surrogate would significantly reduce over-sizing of hydraulically-efficient UV reactors, resulting in lower capital and operations and maintenance (O&M) costs, and would level the playing field among reactors with narrow and wide dose distributions.

UV Light-Absorbing Compounds

Validation of UV reactors equipped with LP and LPHO lamps is simplified by the monochromatic germicidal UV output of those lamps. LP and LPHO lamps emit germicidal UV light only at 254 nm. As such, only the optical properties at 254 nm need to be considered when validating UV reactors equipped with those lamps. On the other hand, MP UV lamps emit UV light at many wavelengths. As such, the optical properties over a range of wavelengths must be considered during the validation of UV reactors equipped with MP lamps. In particular, the spectral UV absorbance during UV reactor validation must sufficiently mimic the spectral UV absorbance of natural water expected at a WTP over the wavelength range that inactivates microbes and the wavelength range detected by the UV intensity sensor.

During reactor validation, low UVT water conditions are simulated by the addition of UV-absorbing chemicals to the test water. UV absorbers commonly used are coffee (NWRI/AwwaRF 2003, ÖNORM 2003) and lignin sulfonate (DVGW 2003). For a given UV absorbance at 254 nm, the spectral UV absorbance of coffee and lignin sulfonate differs substantially from that of WTP waters. In particular, the absorbance of these compounds at wavelengths higher and lower than 254 nm is greater than WTP waters for a given UV absorbance at 254 nm. As such, the strength of the UV intensity field within the UV reactor at these wavelengths will be lower during validation than with operation in the field. This difference impacts both UV dose delivery and monitoring with UV systems equipped with medium pressure lamps.

Using Computational Fluid Dynamics (CFD) to model UV dose delivery by a UV reactor equipped with MP lamps, Wright *et al.* (2002) reported that using coffee during validation resulted in UV dose delivery being under rated compared to expected performance at a WTP.

This error was greater with lower UV transmittance and varied with the UV spectrum of WTP under consideration. With one surface WTP, the MS2 RED predicted using coffee during validation was 28 percent less than that predicted at a WTP. Using a UV absorber that appropriately mimics the spectral absorbance of WTP waters can minimize this error.

The impact on UV dose monitoring of the differences in the spectral absorbance between validation and the WTP is a complex function of the spectral response and positioning of the UV intensity sensor and the UV dose delivery of the reactor. The spectral response of commercial sensors varies with UV vendors and can differ notably from the response of microorganisms. UV sensor placement also varies with UV vendors with some placing their sensors relatively close to the lamps while other place their sensor on the reactor wall far from the lamps. The water layer between the lamps and the sensor will act as an optical filter impacting the intensity of the wavelengths that reach the microbes and the sensor. Sensors placed too close or too far from the lamp will respond to wavelength intensities that differ from the wavelengths impacting the microbes. If the spectral absorbance of the bioassay test water differs significantly from that of WTP water, the relationship between the sensor value and the delivered UV dose observed during validation will not be the same as at the WTP. This will result in either an under-estimation of UV dose if the sensor is too close or an over-estimation if the sensor is too far from the lamps.

Using polychromatic intensity models to predict UV intensity sensor readings and CFD models to predict UV dose delivery, Wright and Cushing (2002) reported significant errors with UV dose monitoring at a WTP due to differences in spectral absorbance between validation and the WTP. With UV reactors equipped with unfiltered silicon carbide sensors and validated at low UV transmittance using coffee, errors were as large as a factor of two. These errors could be reduced if the sensor spectral response matched the microbial wavelength response to UV light and the sensor was positioned where UV dose delivery was proportional to sensor readings regardless of the water UV transmittance and lamp power. This location, however, varies with the hydraulics through the reactor and is currently determined using expensive iterative validation. An alternative approach to minimizing the error is to use a UV absorber whose spectral response matches that of WTP waters. This would minimize the need to apply correction factors or safety factors to account for this issue.

In summary, the absence of a UV absorber that appropriately mimics the spectral UV absorbance of WTP waters leads to significant errors in the validation results of UV systems equipped with medium-pressure lamps. Arguably, the use of coffee during validation can lead to under estimations of UV dose delivery at the WTP by as much as 28 percent and UV dose monitoring errors with silicon carbide sensors as great as a factor of two. There is a need to identify a UV absorber that mimics WTP waters over the range of wavelengths that impact UV dose delivery and monitoring. With UV reactors using unfiltered silicon carbide UV sensors, that wavelength range extends up to 400 nm. Because low wavelength UV light is strongly absorbed by water, this light does not contribute much to UV dose delivery and UV intensity sensor readings and the lower limit to the range of wavelengths is near 220 nm. The appropriate UV absorber should be selected not based on a similarity to any one UV light absorbing chemical species found in waters such as nitrates or humic compounds but selected based on a comparison to the spectral absorbance data that has been collected from various WTPs.

Impact of Non-Uniform Lamp Aging

New lamps at lowered power are used during UV reactor validation to simulate aged lamps. New lamps operating at lowered power have relatively uniform output along their length and circumference (Phillips 1983). However, UV lamp aging can be very non-uniform. The impact of non-uniform UV lamp aging on UV dose delivery and monitoring is not known. Depending on sensor positioning along the length of the lamp, reactor UV dose monitoring could significantly under or overestimate UV dose delivery. This problem is expected to worsen with lamps oriented perpendicular to flow where the water that flows past the lamp ends will experience low UV doses leading to poor reactor performance.

Spectral shifts in the UV output of medium pressure lamps (Phillips 1983) and the UV transmittance of lamp sleeves (Kawar *et al.* 1998) with aging has been reported. Typically, the lamp output and sleeve UV transmittance at lower wavelengths degrades more than higher wavelengths with aging. While the impact of reported spectral shifts on UV dose delivery is small, the impact on UV dose monitoring is significant with UV sensors whose response includes wavelengths above 300 nm (USEPA 2002). The degree of spectral shifts in lamp output and sleeve UV transmittance with commercial UV reactors used in drinking water applications is not known. If significant, there will be a need to restrict sensor response or use appropriate safety factors to account for these effects.

The issue of lamp and sleeve aging and its impact on UV dose delivery and monitoring represents one of the more significant unknowns regarding UV reactor performance in drinking water applications. For this reason, AwwaRF targeted studies of lamp and sleeve aging on UV reactor performance as a top research priority at a spring 2002 UV disinfection workshop held in the Netherlands.

PART 1: OBJECTIVES AND APPROACH

The goal of this portion of the study was to improve the validation techniques available for use in full-scale performance testing by addressing three key issues: identification of better microbes, identification of improved UV absorbing compounds that can more adequately model the optical behavior of WTP waters, and the generation of comparative data on non-uniform UV lamp and sleeve aging, and its impact on UV dose delivery and monitoring. Part 1 of this project was divided into four tasks:

1. Identify a surrogate organism(s) that has a UV dose-response similar to target pathogens (*e.g.*, *Cryptosporidium*) (discussed in Chapter 2);
2. Identify a UV absorbing chemical that appropriately mimics WTP water (discussed in Chapter 3);
3. Characterize the effects of non-uniform lamp aging on UV dose delivery and monitoring (discussed in Chapter 4); and
4. Assess new validation protocols developed from the first three tasks to prove their benefits (discussed in Chapters 5 and 6).

PART 2: OPTIMIZATION OF DESIGN AND OPERATION

The most significant operating costs of UV disinfection are electrical power consumption and lamp replacement, which are directly related to the design and operation of the UV system's lamp/ballast assembly and the UV system size required to meet dose targets. Because UV disinfection is a relatively new technology in drinking water, there are opportunities for technology optimization through improved system design and operation. For example:

- While the design and operation of UV lamp/ballast assembly varies significantly among UV vendors, there is little performance data available to utilities on which to select one system over another.
- While lamp aging factors can increase the sizing of a UV system by 20 to 30 percent, the values used in design are often based on rule-of-thumb values established over prescribed one-year periods with no consideration of the optimal balance of power, capital, lamp and labor costs.
- While dose-pacing strategies are attractive in concept, there is little data on the costs and benefits of one strategy over another.
- While emergency response systems such as redundant reactors and backup power are specified in UV guidance manuals, no models exist for quantifying the risk to public health due to failure on which one can establish appropriate response systems.

PART 2: OBJECTIVES AND APPROACH

The objective of Part 2 of this project was to develop tools for utilities, consultants, and state regulators that promote energy efficient and cost-effective design and application of UV disinfection systems. This objective was achieved using the following five tasks:

- Develop a software tool for providing a comprehensive simulation and evaluation of UV system performance.
- Evaluate the performance of commercial UV lamp/ballast assemblies using long-term pilot studies.
- Develop approaches for selecting lamp-aging factors for sizing UV systems and dose-pacing strategies for operating UV systems.
- Develop approaches for evaluating and selecting the optimum dose monitoring and control strategy for a UV application
- Identify opportunities for reducing peak load to reduce energy costs with UV system operation.
- Develop approaches for evaluating public health risks associated with UV disinfection systems, and assess the effectiveness of risk-minimization strategies, including system redundancy, back-up power, and failure responses for UV reactors.

CHAPTER 2

NEW MICROBIAL SURROGATES

This chapter describes work conducted to identify new challenge microorganisms for UV validation that have a UV dose-response that matches the dose-response of *Cryptosporidium* and *Giardia* better than MS2 and *Bacillus subtilis* spores. MS2 and *B. subtilis* spores are much more resistant to UV light than *Cryptosporidium* and *Giardia*. For example, 3-log inactivation of MS2 and *B. subtilis* spores requires a UV dose of approximately 60 and 55 mJ/cm², respectively. In comparison, the UV dose required for 3-log *Cryptosporidium* and *Giardia* inactivation credit is 12 and 11 mJ/cm², respectively. If MS2 is used to validate a UV reactor for 3 log *Cryptosporidium* inactivation credit, the USEPA UVDGM recommends application of an RED bias uncertainty factor ranging from 1.19 to 2.65, depending on the UVT of the water (USEPA 2006c). By identifying challenge microbes that better match the dose-response of *Cryptosporidium* and *Giardia*, the uncertainty validating UV reactors for *Cryptosporidium* and *Giardia* credit is reduced, thereby allowing application of lower RED bias uncertainty factors.

Validation of large-scale UV reactors also requires high numbers of challenge microorganisms. As the UV sensitivity of the challenge microorganism increases, the numbers of microorganisms needed to validate the reactor increases logarithmically. For example, consider a UV reactor validated using MS2 phage to show an MS2 RED of 20 mJ/cm². A one-log inactivation of MS2 phage is expected with an MS2 RED of 20 mJ/cm². To ensure the concentration of MS2 phage leaving the reactor produces a countable result and to account for experimental uncertainties conducting the validation, the concentration of MS2 at the reactor influent should be about 1,000 plaque-forming units per milliliter (pfu/mL) or 2 log higher than the expected inactivation. If the reactor is being validated at 40 million gallons per day (mgd), the MS2 would be injected into that flow at a rate of 10¹¹ pfu/min to achieve the required reactor influent concentration. If the MS2 stock solution had a concentration of 10¹¹ pfu/mL, the stock solution would be injected at a rate of 1 milliliter per minute (mL/min). If instead of MS2, the reactor was validated with a challenge microbe with a UV sensitivity of 5 mJ/cm² per log inactivation, the phage injection rate would need to be increased by a factor of 1,000 to account for the increased UV sensitivity of this microbe. This would require a stock solution injection rate of 1 liter per minute (L/min) if the stock solution of this phage had the same 10¹¹ pfu/mL concentration. If the stock solution could only be prepared to a concentration of 10⁹ pfu/mL, the injection rate would need to be increased again by a factor of 100. Therefore, to provide practical UV validation, any new challenge microbe must have the ability to be propagated in large volumes and/or at high titers.

The criteria for challenge microbes for use in full-scale reactor validation include:

- Ease of handling, no extraordinary culturing requirements
- No biohazard issues to humans, animals, or the environment
- Inexpensive
- Ability to grow large volumes (>30 L) of stock solutions to high titers (>10¹¹/mL)
- Able to be purified with no loss of titer (e.g., filtration to remove bacterial contaminants)
- Stability in storage
- Similar UV dose-response to target pathogen

Bacteriophages meet many of the above-mentioned criteria. Based on a literature review, several bacteriophages that varied in structure, morphology, and nucleic acid type were selected for further testing of their viral yield, UV dose-response, and action spectra.

LITERATURE REVIEW

The UV dose-responses of microorganisms vary considerably from species to species. In general, viruses as a group are more resistant to UV light than bacteria and protozoa. For example, 4-log inactivation of protozoa (*Cryptosporidium*) and vegetative bacteria (*Escherichia coli* (*E. coli*), *Staphylococcus aureus*) requires 4 to 10 mJ/cm² (Clancy *et al.* 2000, Sommer *et al.* 1998, Chang *et al.* 1985), while 4-log inactivation of enteric viruses such as Hepatitis A and Rotavirus SA-11 requires 30 to 40 mJ/cm² (Wilson *et al.* 1992). Adenovirus is very resistant to UV light. Gerba *et al.* (2002) reported that the UV dose required to achieve 3-log inactivation of human adenovirus type 2 is 119 mJ/cm². The high UV dose requirements for virus credit in the *Ultraviolet Disinfection Guidance Manual* (USEPA 2006c) are based on inactivation requirements for adenovirus (Table 2.1).

Studies using enteric viruses have demonstrated significant differences in their UV dose-response which have been related to viral morphology, the type of nucleic acid, high guanine and cytosine content, or the complexity of the viral capsid (Lasobras 1997, Meng and Gerba 1996). For example, viruses with double-stranded genomes are more resistant to UV light because the undamaged strand may serve as a template for dark repair of the damaged strand (Thurston-Enriquez *et al.* 2003).

Table 2.1
UV dose requirements for virus inactivation credit

UV dose (mJ/cm ²)	Log inactivation credit
39	0.5
58	1.0
79	1.5
100	2.0
121	2.5
143	3.0
163	3.5
186	4.0

Source: USEPA Office of Water 2006a

Results reported by Wiedenmann *et al.* (1993) indicated that the UV dose required to achieve a 4-log reduction of MS2 is approximately three times higher than that necessary for 4-log inactivation of Hepatitis A Virus (HAV). Meng and Gerba (1996) reported that MS2 is approximately two times more resistant than coliphage PRD-1 (4-log reductions at 65.2 mJ/cm² and 31.6 mJ/cm², respectively). Two coliphages, PRD1 and B40-8, were reported to have UV dose-response profiles that are comparable to that of *Cryptosporidium*, and a third coliphage, ΦX174, is less resistant (Meng and Gerba 1996). Other researchers (Sommer *et al.* 1998) reported similar results, indicating that coliphage ΦX174 is most susceptible to UV (4-log reduction at 10 mJ/cm²), followed by phage B40-8 (4-log reduction at 27 mJ/cm²), then MS2 and *B. subtilis* spores (2-log reduction at 38 and 40 mJ/cm², respectively).

Kamiko and Ohgaki (1989) used the bacteriophage Qβ to bioassay dose delivery by UV reactors and reported a 1-log reduction with a UV dose of 13.6 mJ/cm². Otaki *et al.* (2003) verified the inactivation of Qβ follows first-order reaction kinetics and that bacteriophage T4 is as sensitive to UV light as *E. coli*.

The bacteriophages T4 and T7 have been used extensively in UV irradiation studies to examine DNA repair mechanisms (Hyman 1993); however, only limited UV dose-response information exists for both of these organisms.

MATERIALS AND METHODS

Microorganisms Selected for Study

The research team selected and acquired a total of ten bacteriophages and their corresponding bacterial hosts from American Type Culture Collection (ATCC) for study (Table 2.2). Following acquisition from ATCC, all bacterial strains were cultured and checked for purity. Phages were re-hydrated and working stocks prepared using the general procedures provided by ATCC.

Table 2.2
Bacteriophages and their corresponding bacterial hosts selected for further study

Bacteriophage	Host
φX174 ATCC 13706-B1	<i>E. coli</i> C ATCC 13706
PRD1 ATCC BAA-769-B1	<i>E. coli</i> HER 1221 ATCC BAA-769
T4 ATCC 11303-B4	<i>E. coli</i> B ATCC 11303
fr ATCC 15767-B1	<i>E. coli</i> ATCC 19853
R17 ATCC 25868-B1	<i>E. coli</i> ATCC 25868
PP7 ATCC 15692-B2	<i>Pseudomonas aeruginosa</i> ATCC 15692
M13 ATCC 15669-B1	<i>E. coli</i> ATCC 15669
Qβ ATCC 23631-B1	<i>E. coli</i> 23631 ATCC 23631
T7 ATCC 11303-B7	<i>E. coli</i> B ATCC 11303
SP8 ATCC 15563-B1	<i>B. subtilis</i> ATCC 15563

Phage ϕ X174 belongs to the family *Microviridae* and infects several species of *E. coli*, including *E. coli* C. The virion is approximately 27 nm in diameter, with icosahedral symmetry, a burst size of 100 – 200, and contains one molecule of circular, single-stranded deoxyribonucleic acid (DNA).

Phage PRD1 belongs to the family *Tectiviridae* and infects several species of *E. coli*, including *E. coli* HER 1221. The virion is similar in size to rotavirus and adenovirus (nucleocapsid 63 nm diameter; tail 60 nm long, 10 nm wide), with icosahedral symmetry. It contains one molecule of linear, single-stranded DNA.

Phage T4 belongs to the family *Myoviridae* and infects several species of *E. coli*, including *E. coli* B. The virion is approximately 78 nm in diameter, with a 65 × 80 nm head and a 120 × 20 nm tail, a burst size of approximately 300, and contains one molecule of linear, double-stranded DNA.

Phage T7 is a member of the family *Podoviridae* and like T4, infects *E. coli* including *E. coli* B. The virion has 6 short tail fibers, its symmetry is icosahedral, it is approximately 45 - 60 nm in diameter, and the burst size is approximately 300. T7 contains one molecule of linear double stranded DNA.

Phages fr and R17 are members of the family *Leviviridae* and belong to the same subgroup as MS2. Morphologically, these virions are not enveloped or tailed, their symmetries are icosahedral, they are approximately 26 nm in diameter, and have burst sizes of 10,000. Like MS2, these virions contain one molecule of linear, positive-sense, single-stranded RNA.

Phage PP7 is also a member of the family *Leviviridae*, but it is not classified in a specific subgroup. Its morphology is similar to the phages MS2, fr, and R17, but it infects *Pseudomonas aeruginosa* as its bacterial host and has a burst size of 10,000.

Phage M13 belongs to the family *Inoviridae*. It is a filamentous, male-specific coliphage composed of a single-stranded, circular DNA genome. M13 is not enveloped and measures approximately 900 nm long and 6 - 8 nm in diameter. Although its burst size is not reported in the literature, the data collected during this project indicate a value of approximately 10,000.

Phage Q β belongs to the family *Leviviridae* and belongs to a different subgroup than MS2 (genotype III, MS2 is genotype I). Morphologically, this virion's symmetry is icosahedral, and it is approximately 24 - 26 nm in diameter with a burst size of 10,000. Like MS2, this virion contains one molecule of linear, positive-sense, single-stranded RNA.

Phage SP8 is a member of the family *Myoviridae*, genus "SPO-1-like virus," that infects *Bacillus subtilis*. The virion is approximately 78 nm in diameter, is not enveloped, and has a contractile tail. Phage SP8 contains one molecule of linear, double-stranded DNA, with hydroxymethyluracil replacing thymine.

Propagation and Enumeration

Viral propagations of all phages were accomplished using liquid culture methods. In brief, log phase cultures of bacterial host were grown in appropriate broth and inoculated with phage at multiplicities of infection ranging from 0.01 to 5.0. Several hours post-infection, the lysed bacterial suspension was clarified by centrifugation at 7000×g for 20 minutes. The supernatant containing phages was decanted to sterile containers and stored at 4°C. Viral concentrations were determined via the double agar layer technique. Briefly, top agar overlay tubes were inoculated with 100 μ L of log-phase host bacteria and 100 microliter (μ L) subsamples of phage prepared from serial dilutions. Tubes were poured over appropriate bottom

agar in 100-mm Petri dishes. After the top agar hardened, samples were inverted and incubated at 35°C for up to 24 hours or until lysis was observed. All samples were plated in triplicate. Viral plaque forming units (pfu) were counted and recorded, and the concentration of phages calculated. For UV-irradiated samples, quantitative reductions were computed as the base-10 logarithm of the ratio of the concentration of surviving viruses over the concentration present in the unexposed samples ($\log N_t/N_o$).

UV dose-responses of microbes were measured with a collimated beam apparatus equipped with low-pressure UV lamp (254 nm). The collimated beam apparatus is designed to deliver a known UV dose to a stirred suspension of microbes (Blatchley 1997). The doses delivered were calculated as:

$$D = \frac{I_o P_f (1 - R) t (1 - e^{-\alpha d})}{\alpha d} \quad (2.1)$$

where D is the dose, I_o is the UV intensity incident on the suspension, α is the suspension's UV absorption coefficient at 254 nm, d the suspension's depth, P_f is the Petri factor, R is the suspension's surface UV reflectance, and t is the exposure time. Incident UV intensity was measured using the average reading of two radiometers and sensors (International Light model IL1400A with SEL 240; Gigahertz-Optik X9₁₁ with UV-3718-4). Radiometers and sensors were calibrated at 254 nm, traceable to National Institute of Standards and Technology (NIST) standards, within 12 months of any testing. Varying the exposure time using a manually controlled shutter regulated UV light delivery to the suspension. A non-reflective polyvinyl chloride (PVC) tube (6.4 cm in diameter × 50 cm in length) ensured the UV light incident onto the suspension was collimated. Test solutions were mixed constantly, with care taken to minimize air bubbles and vortices. Prior to irradiating any organisms, the irradiance distribution across the surface of the suspension was measured at 0.5 cm intervals along the x-y axis of an 6 cm diameter grid originating at the center of the UV beam. These readings were used to develop the "Petri factor" used to relate the intensity measured to the radiometer to the average intensity incident on the suspension. The UV reflectance of the suspension's surface was assumed at 2.5 percent.

The microorganism's action spectrum was estimated using UV dose-response data measured with the collimated beam apparatus equipped with a MP UV lamp and optical bandpass filters. The bandpass filters had nominal wavelengths of 254, 265, 280, and 300 nm. [Figure 2.1](#) shows the UV transmittance of the bandpass filters measured using a spectrophotometer and normalized at the nominal wavelengths. The data shows that the bandpass filters have a bandwidth of 11 to 13 nm at 50 percent of the peak transmittance and a bandwidth of 26 to 32 nm at 5 percent of the peak transmittance. UV dose delivered by the filtered UV light was calculated using Equation 2.1 with the exception that I_o was the UV intensity incident on the suspension measured using the radiometer with the calibration factor defined at the bandpass filter's nominal wavelength and α is the suspension's UV absorption coefficient measured at the bandpass filter's nominal wavelength. This approach provides a biased dose calculation because the bandpass filtered light was not monochromatic. However, the approach can be used to provide relative comparison of the wavelength response of two microorganisms, such as QB and MS2 phage.

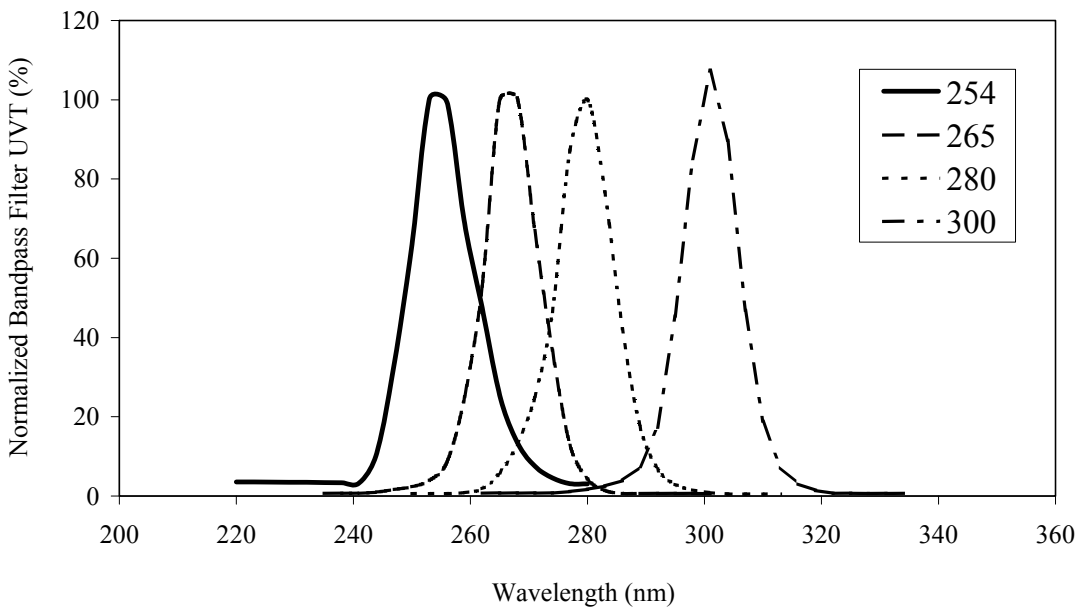


Figure 2.1 T4 bandpass filter UV transmittance

RESULTS

ϕ X174

ϕ X174 was successfully propagated in the laboratory; however, titers did not exceed 1×10^8 pfu/mL, despite several attempts to optimize viral yield. Validation of large-scale UV reactors requires high concentrations of phage ($> 1 \times 10^{11}$ pfu/mL); therefore, ϕ X174 was not further pursued as potential microbial surrogates due to its suboptimal viral yield.

PRD1

PRD1 was successfully propagated in the laboratory; however, titers did not exceed 1×10^8 pfu/mL, despite several attempts to optimize viral yield. Therefore, PRD1 was not further pursued as potential microbial surrogates due to its suboptimal viral yield.

T4

T4 was successfully propagated to 6×10^{10} pfu/mL in 50-mL volumes and a single collimated beam experiment was performed. Results from this experiment are shown in [Figure 2.2](#). These data indicate that T4 is quite susceptible to UV, demonstrating over 4-log inactivation at a UV dose of 5 mJ/cm^2 . Noticeable tailing was observed above 5 mJ/cm^2 , and the precise inactivation kinetics at lower UV doses was not measured. Because T4's demonstrated sensitivity would result in such high inactivation, its utility is limited as a surrogate in UV reactor validations where UV doses of 5 mJ/cm^2 or greater are targeted. Further investigation was not pursued.

fr, R17, PP7 and M13

fr, R17, PP7 and M13 phage were propagated in 50-mL volumes to 3×10^{11} , 1×10^{12} , 3×10^{11} , and 3×10^{11} pfu/mL, respectively. [Figures 2.3 to 2.6](#) gives the UV dose-response curves measured with these solutions. Because the UV dose-response of these phages were similar to that of MS2 phage, they were not considered good replacements for MS2 and further investigation was not pursued.

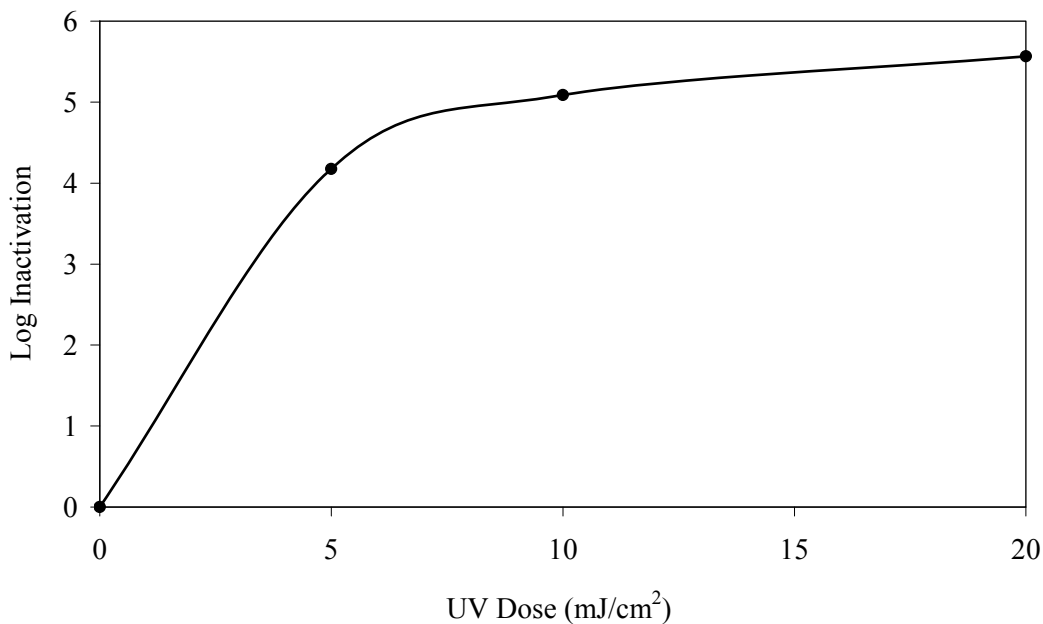


Figure 2.2 T4 UV dose-response

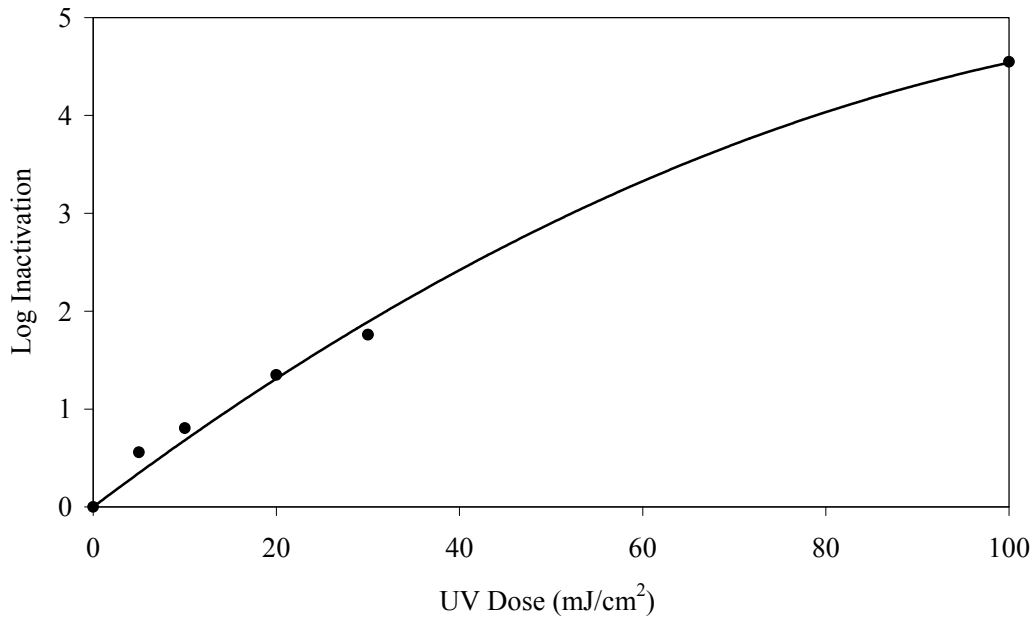


Figure 2.3 UV dose-response of fr

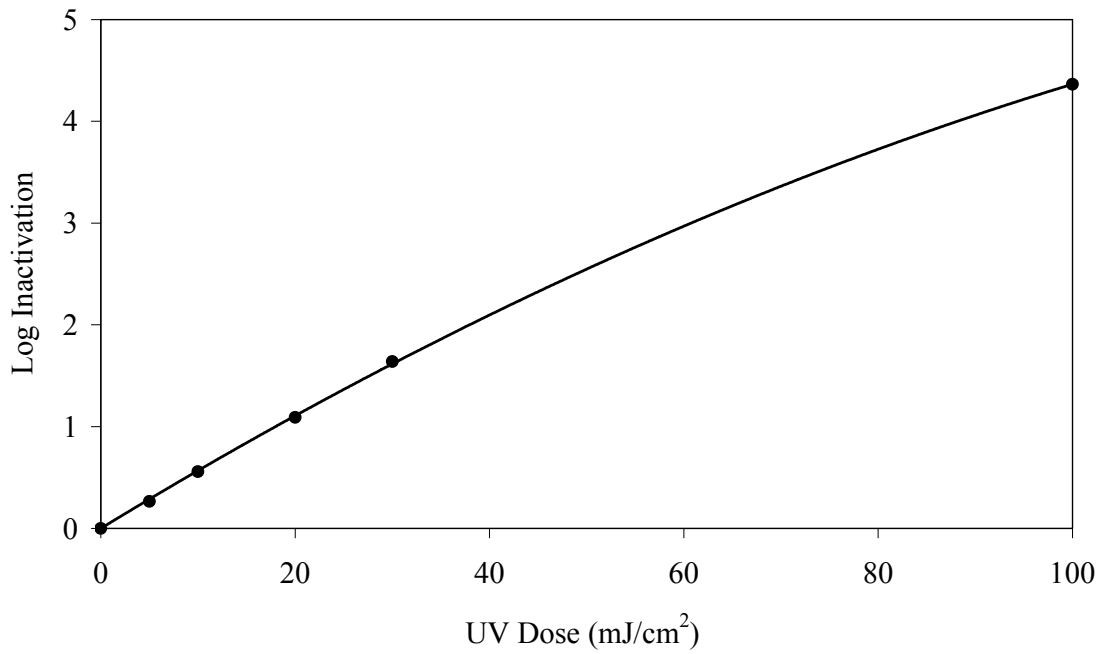


Figure 2.4 UV dose-response of R17

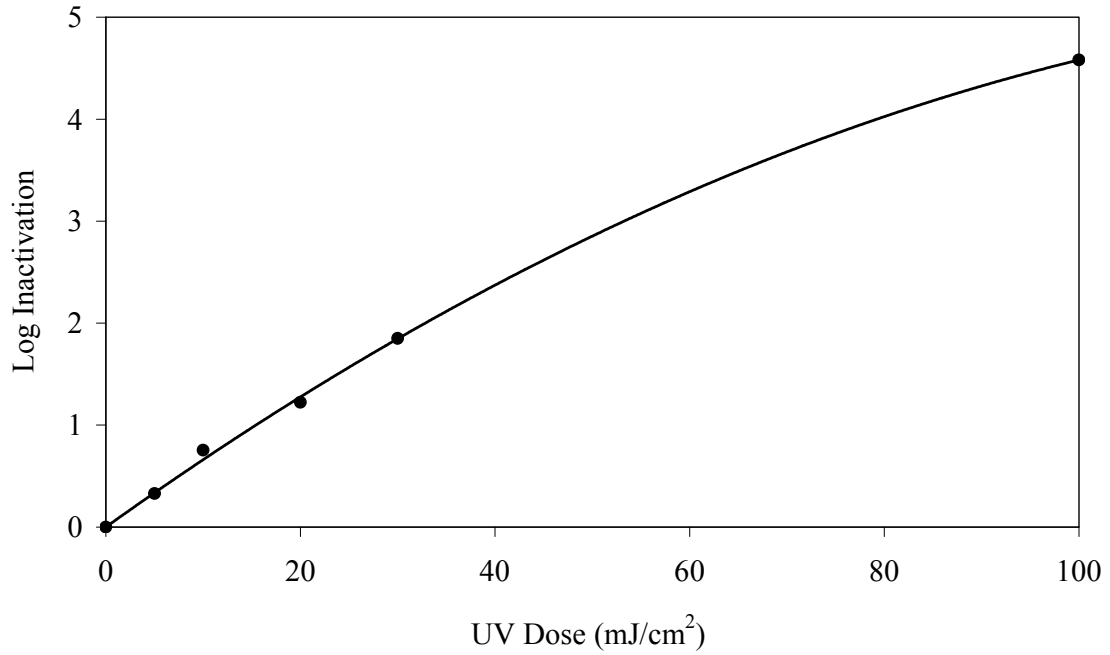


Figure 2.5 UV dose-response of PP7

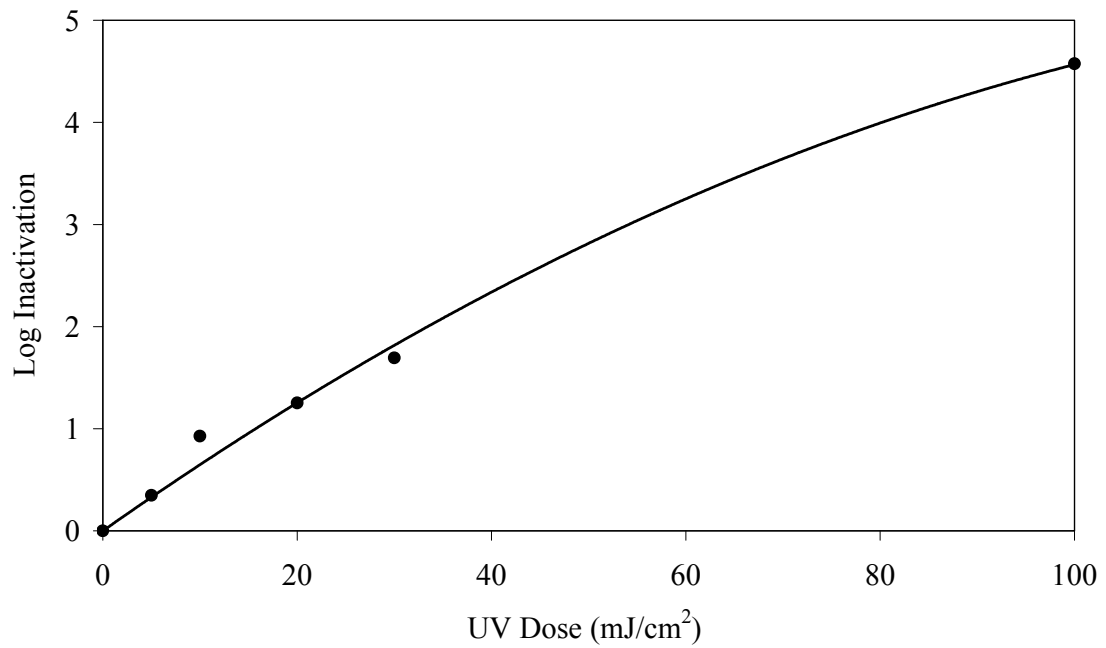


Figure 2.6 UV dose-response of M13

Qβ

Qβ was successfully propagated in large (6 L) batches with titers of 3×10^{11} pfu/mL. Duplicate and identical collimated beam UV dose-response curves were measured and are given in Figure 2.7. The dose-response shows some curvature and was best fitted using a polynomial function. Because of the curvature, the UV sensitivity ranged from 9.8 to 10.4 mJ/cm² per log inactivation. If Qβ was used to validate a UV reactor for 3-log *Cryptosporidium* credit, the RED bias uncertainty factors would range from 1.14 to 1.86, depending on the water UVT (USEPA 2006c). In comparison, if MS2 had been used the range of RED bias uncertainty factors would have been 1.19 to 2.65. Hence, if the reactor has a very narrow dose distribution, the use of Qβ could reduce UV reactor capital and O&M costs by a factor of 4 to 30 percent, depending on the UVT of the water.

The UV dose-response curves of Qβ and MS2 at 254, 265, 280, and 300 nm UV light are given in Figures 2.8 and 2.9, respectively. Figure 2.10 displays the responses normalized to the response observed at 254 nm. For the wavelengths tested, the results show that Qβ has a similar action spectra or wavelength-response to UV light as MS2. Wavelengths lower than 254 nm; however, were not tested. Linden *et al.* (2000) reports that the action spectra of MS2 peaks at lower wavelengths near ~216 nm. A future evaluation of Qβ's response to wavelengths lower than 254 nm is therefore recommended.

In summary, the high propagation titer and highly reproducible UV dose-response through 4-log inactivation at 50 mJ/cm² suggests that Qβ phage has great potential as an alternative to MS2 in UV validation of reactors for *Cryptosporidium* inactivation credit.

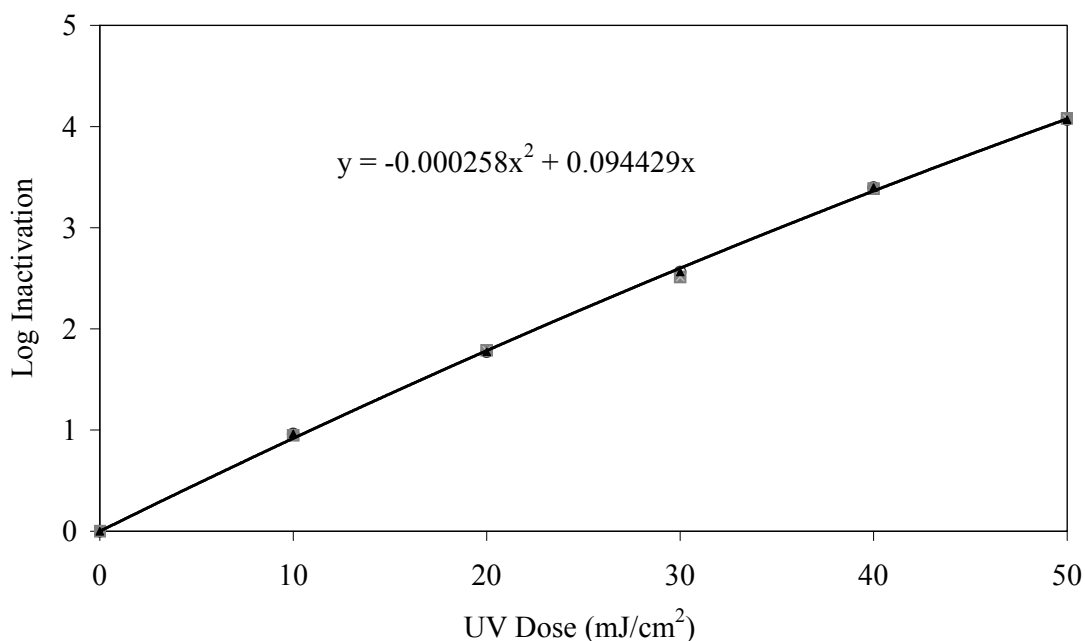


Figure 2.7 UV dose-response of Qβ

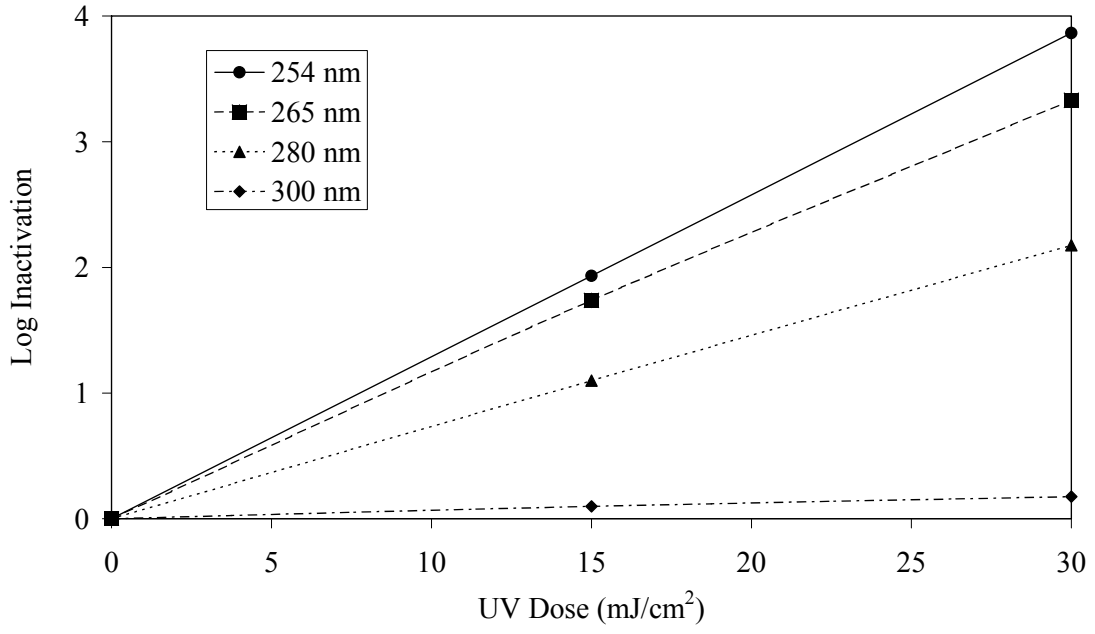


Figure 2.8 Response of QB to a range of UV wavelengths

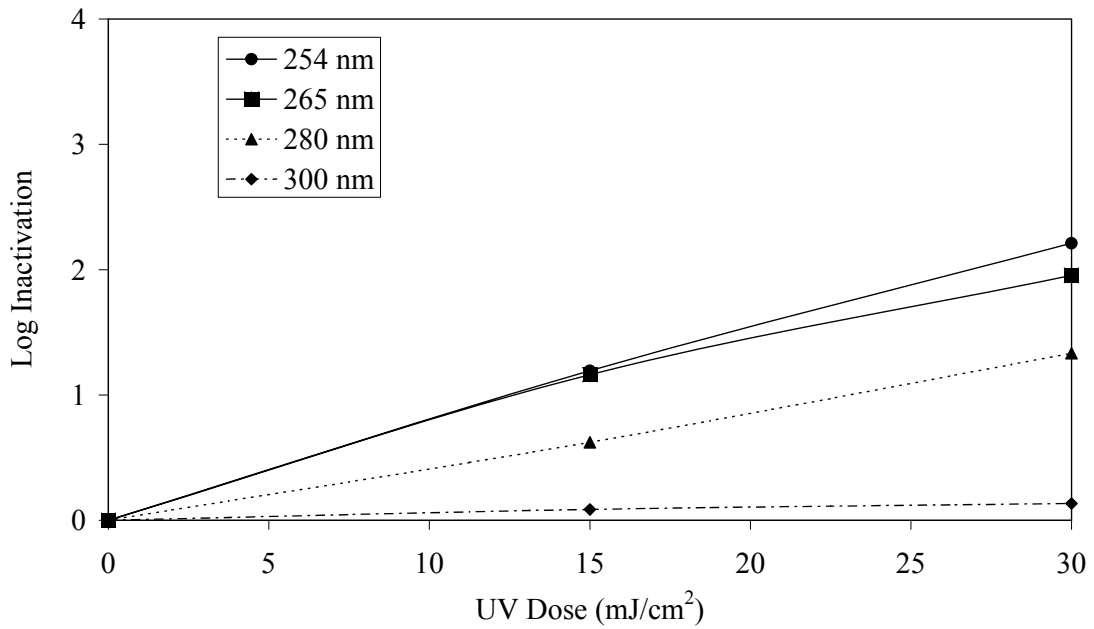


Figure 2.9 Response of MS2 to a range of UV wavelengths

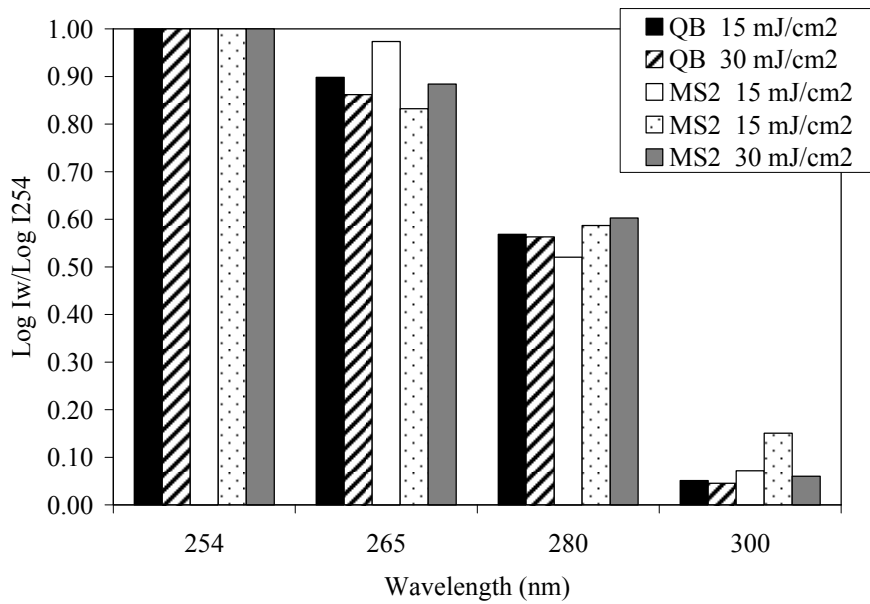


Figure 2.10 Response of QB and MS2 to selected UV wavelengths relative to 254 nm

T7

T7 was propagated to 5×10^{10} pfu/mL in 50-mL volumes and a single collimated beam experiment was performed. The results of exposing T7 to doses of 5 to 30 mJ/cm² are given in Figure 2.11. The dose-response of T7 showed some curvature and was best fitted using a polynomial. Because of the curvature, the UV sensitivity ranged from 3.6 to 4.9 mJ/cm² per log inactivation. If T7 was used to validate a UV reactor for 3 log *Cryptosporidium* credit, the RED bias uncertainty factors would be ~1.0. In comparison, the range of RED bias uncertainty factors is 1.19 to 2.65 if MS2 had been used. Hence, if the reactor has a very narrow dose distribution, the use of T7 could reduce UV reactor capital and O&M costs by a factor of 16 to 62 percent, depending on the UVT of the water.

The UV dose-response curves of T7 to 254, 265, 280, and 300 nm UV light are given in Figure 2.12. The responses relative to that at 254 nm are displayed in Figure 2.13. These results suggest that T7 is more sensitive than MS2 to UV light at wavelengths above 254 nm. This enhanced sensitivity implies that T7 REDs measured with a medium-pressure UV system will be higher than expected based on the action spectra of MS2. Using the average of the action spectra measured, this polychromatic bias is estimated as a factor of 1.15 using:

$$\text{Bias} = \frac{\int_{254\text{nm}}^{300\text{nm}} G_{T7}(\lambda) \times P(\lambda)}{\int_{254\text{nm}}^{300\text{nm}} G_{MS2}(\lambda) \times P(\lambda)} \quad (2.2)$$

where $G(\lambda)$ is the action spectra of the microbe indicated by the subscript and $P(\lambda)$ is the UV output from a standard medium pressure lamp.

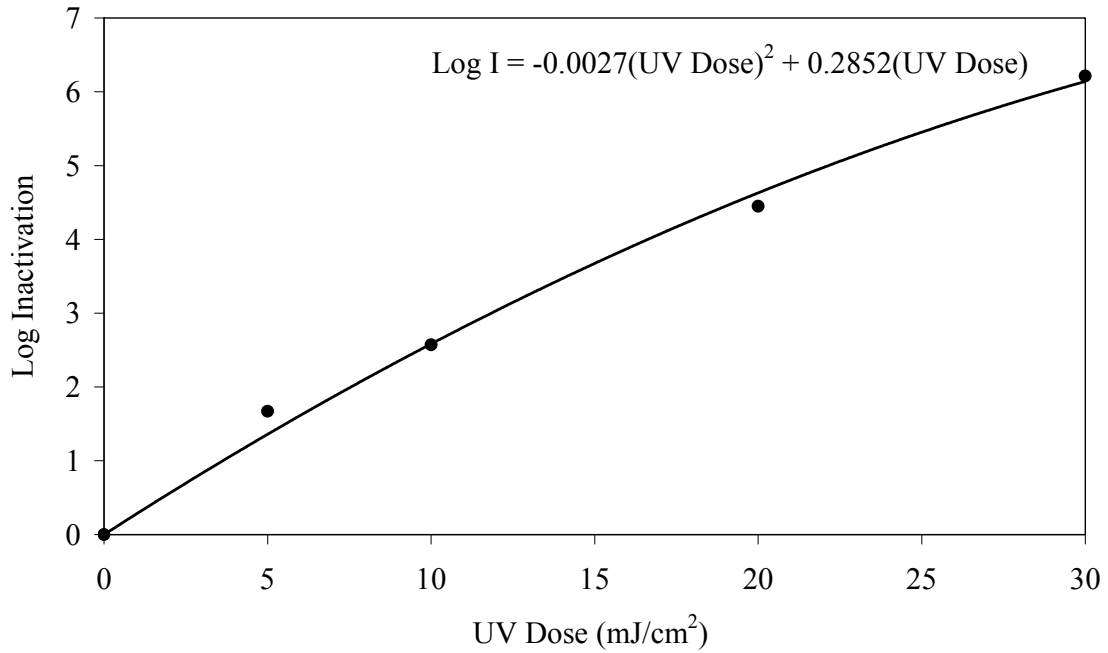


Figure 2.11 T7 UV dose-response

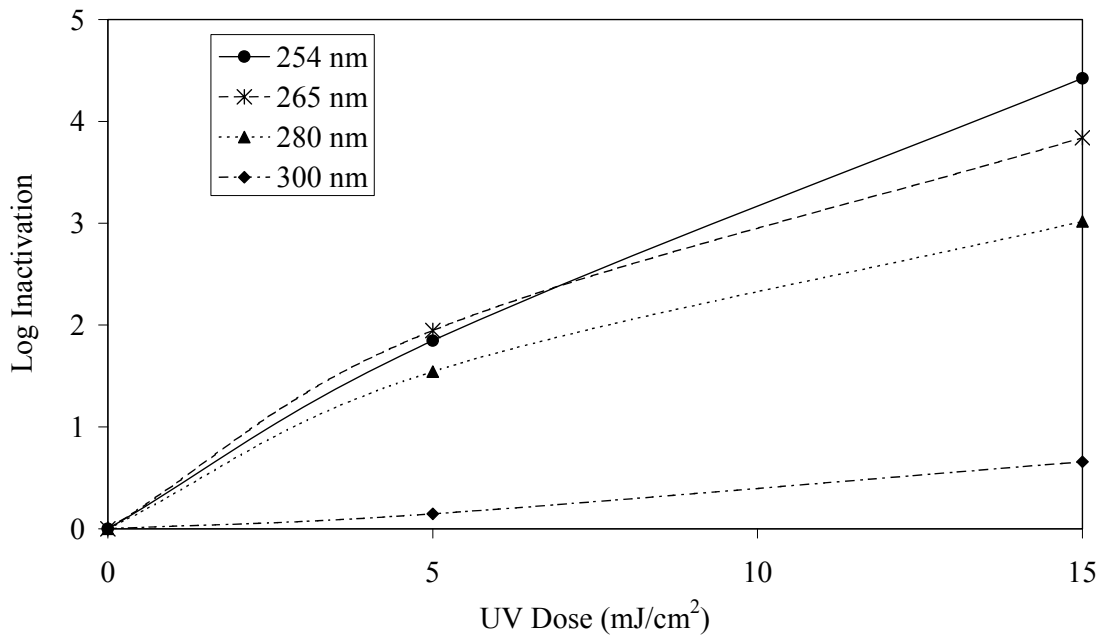


Figure 2.12 Response of T7 to a range of UV wavelengths

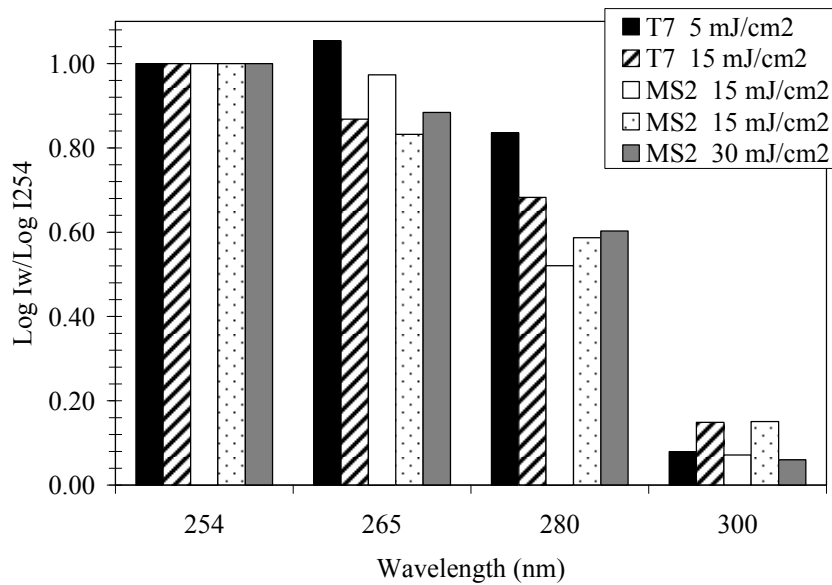


Figure 2.13 Response of T7 and MS2 to selected UV wavelengths relative to 254 nm

Results to date indicate that T7 is a viable candidate as a UV reactor validation test microbe. Validation using T7 will reduce the RED bias uncertainty factor to a value near one with LP UV systems, thereby significantly reducing UV reactor capital and O&M costs and promoting the selection of efficient UV reactors with narrow dose distributions. With MP UV systems, the reduction of the RED bias appears to be countered by a polychromatic bias caused by the action spectra of T7 relative to that of MS2. Because the UV light used to measure the action spectra was not monochromatic, further evaluation of T7's action spectra is recommended. The action spectra for T7 at wavelengths lower than 254 nm should also be analyzed. Last, T7 could only be cultured to titer concentrations of 10^{10} pfu/mL, which may limit validation of UV reactors at high flows.

SP8

SP8 was propagated to 3×10^9 pfu/mL in 50 mL and a single collimated beam experiment was performed. The results of exposing SP8 phages to UV doses of 5 to 20 mJ/cm² are given in [Figure 2.14](#). Its UV dose-response was quite similar to that of *Cryptosporidium*.

Based on the similarities between SP8's and *Cryptosporidium*'s UV dose-responses, several attempts to optimize viral yield of phage SP8 were made. Unfortunately, titers were generally in the range of 10^8 to 10^9 pfu/mL, with the highest titer achieved being 3×10^9 pfu/mL. This falls short of T7, which has a maximum viral yield of 5×10^{10} pfu/mL.

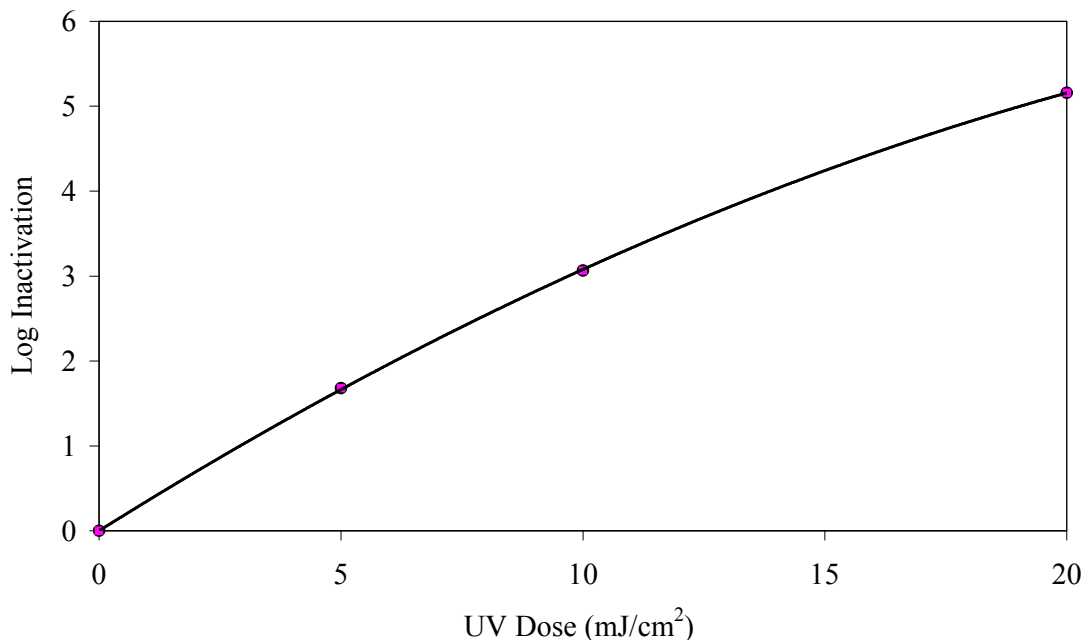


Figure 2.14 UV dose-response of SP8

Comparison of LP and MP Dose Response

The UV dose-response measured using UV light filtered with a 254 nm optical bandpass filter showed lower dose requirements for a given log inactivation than the UV dose response measured at 254 nm using UV light from a LP lamp. For example, the UV dose required to inactivate QB and T7 phage by 3 log was about 23 and 9.5 mJ/cm², respectively, with the 254 nm filtered MP light and 35 and 12 mJ/cm², respectively, with the 254 nm LP light. These differences are likely caused by the dose calculation used with the filtered UV light from the MP lamp. As described in the methods section, the optical filters had a bandpass of ~10 nm at 50 percent of peak transmittance. Yet, the UV dose was calculated assuming monochromatic light with a wavelength at the peak transmittance of the filters. Given this issue, we recommend that further work measuring the action spectra of microbes should use monochromatic light obtained using either a monochromator or an optical filter with a narrow bandpass.

SUMMARY AND CONCLUSIONS

Ten bacteriophage were investigated as replacements for MS2 phage for the validation of UV reactors for *Cryptosporidium* inactivation credit. The following is a summary of the most important findings:

- Bacteriophage ϕ X174 and PRD1 can only be propagated to 1×10^8 PFU/mL, a concentration that is too low for practical UV validation.

- While bacteriophage fr, R17, PP7 and M13 can be propagated to titers of 3×10^{11} PFU/mL or higher, they have a UV dose-response at 254 nm very similar to MS2 phage and hence would have no advantage over MS2 phage as a test microbe.
- While bacteriophage T4 can be propagated to 6×10^{10} PFU/mL, it is inactivated by 4 log with a UV dose of 5 mJ/cm^2 and is too UV sensitive for validating UV reactors for *Cryptosporidium* inactivation credit.
- Q β was successfully propagated in large (6 L) batches with titers of 3×10^{11} pfu/mL with a highly reproducible UV dose-response through 4-log inactivation at 50 mJ/cm^2 . This suggests that Q β phage has great potential as an alternative to MS2 in UV validation of reactors for *Cryptosporidium* inactivation credit. For UV reactors with very narrow dose distributions, the use of Q β could reduce UV reactor capital and O&M costs by a factor of 4 to 30 percent, depending on the UVT of the water.
- Bacteriophage T7 has a UV dose response at 254 nm very similar to the *Cryptosporidium* UV dose requirements in the LT2ESWTR. For UV reactors with very narrow dose distributions, the use of T7 could reduce UV reactor capital and O&M costs by a factor of 16 to 62 percent, depending on the UVT of the water. However, T7 could only be propagated to a titer of 5×10^{10} PFU/mL, which limits its use for large-scale validation. Furthermore, T7 appears to have an action spectrum that provides greater inactivation at wavelengths above 254 nm than does the action of MS2. Hence, the T7 REDs measured with a MP UV reactor would be higher than expected based on a test microbe with an action spectrum similar to MS2 phage. This polychromatic bias is estimated at 1.15.
- While bacteriophage SP8 has a UV dose-response similar to *Cryptosporidium*, it could only be propagated to 3×10^9 PFU/mL, less than the titer of T7.
- Action spectra were measured in this work using UV light from a MP lamp filtered using ~ 10 nm bandpass filters. Because UV light was not monochromatic, the dose-response measured using MP light filtered through a 254 nm bandpass filter was significantly different from that measured using monochromatic 254 nm light from a LP lamp. To avoid these errors, further work measuring the action spectra of microbes should use monochromators or optical filters with a narrow bandpass < 10 nm.

CHAPTER 3

IDENTIFICATION OF NEW SURROGATE UV-ABSORBING COMPOUNDS

INTRODUCTION

Water UV absorbance (UVA), or transmittance¹, particularly at 254 nm, significantly impacts dose delivery by UV reactors. To provide an accurate dose-monitoring algorithm and ensure dose delivery at the WTP meets requirements, UV reactors should be validated with test waters that have a UVA that is representative of the water that will be treated at the water WTP. During validation, the UVT of the test water is lowered by adding a UV-absorbing compound. With UV reactors using MP lamps, the UVA spectrum of the absorbing chemical should match the UVA spectrum of the WTP water.

Coffee and lignin sulfonate (LSA) are commonly used during validation as UV absorbers. As shown in Figure 3.1, the UVA spectra of these compounds do not match the UVA spectra of WTP waters. This mismatch poses a problem when validating reactors equipped with polychromatic MP lamps. For a given flow, UVT at 254 nm, and UV lamp output, differences between the UV-absorbing characteristics of the test and WTP waters will result in different UV doses and UV sensor readings during validation and operation at the WTP. This does not occur with UV systems equipped with LP or LPHO lamps and germicidal UV sensors because these lamps only emit monochromatic UV light at 254 nm.

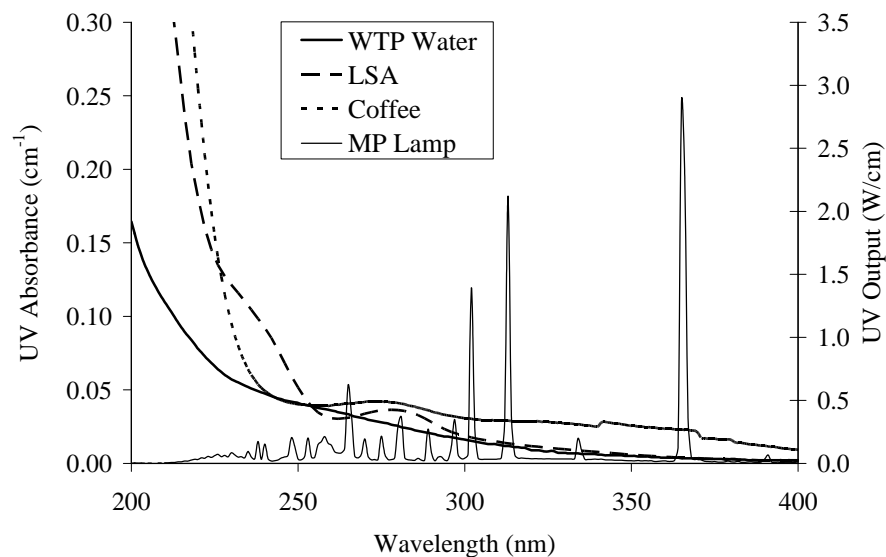


Figure 3.1 UV output of an MP lamp and absorbance spectra of a natural WTP water and UVA surrogates commonly used during UV reactor validation (coffee and LSA)

¹ UVT [%] = 100×10^{-UVA}

The USEPA's *UV Disinfection Guidance Manual* (USEPA 2006b) specifies application of a validation factor (VF) to REDs predicted using the dose-monitoring algorithm as follows:

$$RED_p = \frac{RED_c}{VF} \quad (3.1)$$

where RED_p is the RED predicted for target pathogen, either *Cryptosporidium*, *Giardia*, or virus, and RED_c is the RED predicted for the challenge microbe used during validation. The validation factor accounts for the random uncertainties and measurement bias that occurs with validation. The validation factor is calculated using:

$$VF = B_{RED} \times B_{Poly} \times (1 + U_{Val} / 100) \quad (3.2)$$

where B_{RED} is the RED bias uncertainty factor (described and addressed in Chapter 2), B_{Poly} is the polychromatic bias factor, and U_{Val} is the percent uncertainty of RED_c expressed as a 95 percent prediction interval. The polychromatic bias addresses spectral differences between UV reactor validation and its operation at the WTP and includes differences in the spectral output of the lamps, UVT of the sleeves, UVA of the water, and action spectra of the test microbe and target pathogen. The identification of UV absorbers that more closely mimic the UVA spectra of WTP waters will reduce the polychromatic bias and provide more efficient and accurate application of UV disinfection. This chapter describes work conducted to identify better UV absorbers.

APPROACH

Because the spectral UVA of WTP water depends on the UVA of natural organic matter (NOM) present in those waters, concentrated sources of NOM produced as a waste stream from WTP unit processes were targeted as a potential source of UV absorbers. These unit processes included:

- Reverse osmosis (RO)
- Nanofiltration (NF)
- Ion exchange (IX)
- Magnetic ion exchange (MIEX®)
- Electrodialysis (ED)

Water utilities using these unit processes were asked to provide waste stream samples for evaluation as UV absorbers. Super Hume™ was also evaluated as a candidate UV absorber. Super Hume™ is a soil enhancement product manufactured for agricultural use and is a highly concentrated form of organic carbon comprised of 17 to 20 percent humic and fulvic acids. It is produced from Leonardite shale and is manufactured by United Agricultural Services of America, Inc. It has the advantage of being low-cost (~\$10/gallon) and very easy to procure (shipped within a week directly from the supplier).

NOM sources were compared to LSA and coffee to determine which sources could be potential alternatives for UV reactor validation. Following the selection of the best candidates, a feasibility analysis was conducted to determine which sources could be used cost-effectively.

MATERIALS AND METHODS

NOM Sources

Table 3.1 lists NOM sources evaluated during this study. All sources listed are later referred to in this document by an abbreviated name also given in this table.

UV Absorbance Measurements

UV absorption measurements were performed using a Shimadzu UV-1601 spectrophotometer with a 1-cm quartz cell, both obtained from Shimadzu Scientific Instruments of Columbia, Md. In order to ensure that the UV spectrophotometer was properly calibrated, checks were conducted with a 20 mg/L potassium dichromate standard (RM-02) and a holmium standard (RM-HL) obtained from Starna Cells Inc., Atascadero, Calif. The potassium dichromate standard had a NIST-traceable absorbance of $0.281 \pm 0.002 \text{ cm}^{-1}$ at 257 nm. After zeroing the spectrophotometer with the standard blank, the standard absorbance reading was 0.279 cm^{-1} and within the stated uncertainty of the standard. The holmium standard peaks in the germicidal range (200 - 300 nm) were compared to the spectrophotometer measurements (Figure 3.2). The comparison showed that the wavelength indicated by the spectrophotometer was 0.2 to 0.5 nm higher than the true wavelength.

Table 3.1
UV-absorbing sources tested for similarity to WTP waters

Supplier	NOM source	Source abbreviation
Boynton Beach Utilities, Fla.	NF concentrate	BB-NF
City of Melbourne, Fla.	RO concentrate	Melb-RO
City of Sarasota, Fla.	RO concentrate	Sar-RO
City of Washington, Ill.	IEX regeneration brine	Wash-IX
Lee County, Fla.	MIEX [®] regeneration brine	LC-MIEX [®]
Omaha Public Power District, Neb.	RO concentrate	OPPD-RO
Carlton WTP, Sarasota County, Fla.	EDR brine	Carl-ED
Venice Gardens WTP, Sarasota County, Fla.	RO concentrate	VG-RO
Town of Jupiter, Fla.	RO concentrate	Jup-RO
West Carteret, N.C.	IEX caustic regeneration brine	WC-IX
UAS of America, Hudson, Fla.	Super Hume [™] (humic acid)	SuperHume [™]

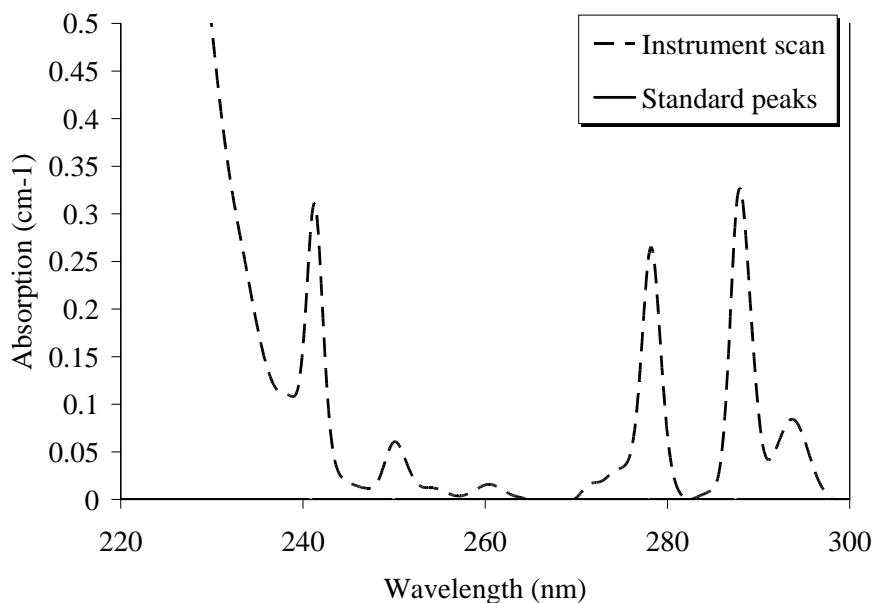


Figure 3.2 Comparison between a spectrophotometer scan and holmium standard peaks

The spectrophotometer was zeroed using de-ionized (DI) water before each measurement of sample UVA. To avoid cross-contamination between samples, the cuvette was rinsed once with 0.1-N potassium dichromate and three times with DI water before the spectrophotometer was zeroed.

UV absorbance of each sample was measured from 200 to 400 nm. Because the Lambert-Beer law defining the relation between UV absorbance and concentration is only valid for weak solutions, some NOM sources had to be diluted. Dilutions were made in Erlenmeyer flasks using DI water. To make sure that no saturation effects were impacting UV measurements, NOM solutions were diluted until there was no difference in the spectral absorption coefficients of two consecutive dilutions.

Polychromatic Bias and RED Calculation Using the UVDGM Workbook

The “Polychromatic Bias” worksheet in the *Ultraviolet Disinfection Guidance Manual Workbook*² that accompanied the June 2003, USEPA Draft *UVDGM* was used to evaluate the UVA spectra of UV absorber candidates. The Polychromatic Bias worksheet estimates dose delivery and UV sensor readings for an annular reactor. The annular reactor consists of a cylinder with an 18.8-cm radius³ that contains a single MP lamp oriented along the central axis

² Excel™ file, <http://www.epa.gov/safewater/lt2/pdfs/guidelt2uvprotocoltooldraft.xls>.

³ With the Polychromatic Bias” worksheet, a lamp-to-lamp distance of x is modeled as an annular reactor with a radius of $x/2$. Hence, a lamp-to-lamp distance of 37.6 cm is entered to simulate an annular reactor with a radius of 18.8 cm.

and housed within a quartz sleeve with a 3.81 cm radius. Water is assumed to flow from one end of the cylinder to the other end. UV intensity is calculated using a polychromatic radial intensity model. Dose delivery is modeled as the product of average intensity within the reactor and residence time defined as reactor volume divided by flowrate. For an annular reactor, dose delivery under these assumptions can be calculated using:

$$D = \sum_{\lambda=200}^{320} P(\lambda) L_{ARC} G(\lambda) T_Q(\lambda) \left(\frac{\exp(-\alpha_e(\lambda) r_{WL}) - 1}{-Q\alpha_e(\lambda)} \right) \quad (3.3)$$

where:

- D = Dose delivered by the UV reactor (mJ/cm²)
- P(λ) = Power output of the lamp per arclength (W/cm per nm)
- λ = Wavelength of UV light (λ)
- G(λ) = Germicidal action spectra of the microbe normalized to a value of one at 254 nm (unitless)
- L_{ARC} = Arc length of the lamp (cm)
- T_Q(λ) = UV transmittance of the sleeve (unitless)
- α_e(λ) = Napierian (Base e) UV absorbance coefficient of the water (cm⁻¹)
- r_{WL} = Reactor water layer defined as the difference between the reactor radius and the sleeve radius (cm)
- Q = Flowrate through the reactor (cm³/s)

UV sensor readings are calculated as the integration of UV intensity weighted by the spectral response of the UV sensor as follows:

$$S = \sum_{\lambda=200}^{400} \frac{P(\lambda) S(\lambda) T_Q(\lambda) \exp(-\alpha_e(\lambda)(r - r_s))}{2\pi r} \quad (3.4)$$

where:

- S = UV intensity measured by the UV sensor (W/cm²)
- S(λ) = UV sensor spectral response normalized to a value of one at 254 nm
- r = Distance from the UV sensor to the lamp
- r_s = Lamp sleeve outer diameter (cm)

The polychromatic bias is calculated as:

$$B_{Poly} = \frac{\left(\frac{D_{Val}}{S_{Val}} \right)}{\left(\frac{D_{WTP}}{S_{WTP}} \right)} \quad (3.5)$$

where D_{val} and D_{WTP} are the UV dose values predicted during validation and at the WTP, respectively, for a given flow, UVT, and lamp output, and S_{val} and S_{WTP} are the UV sensor readings predicted during validation and at the WTP. More information on the different assumptions and equations used can be found in Appendix D (Section D.4.2) of the *UVDGM*.

The Polychromatic Bias worksheet was used to estimate dose delivery, UV sensor readings, and polychromatic bias for UV reactor validation scenarios using NOM surrogates identified in this study. Because the worksheet provided with the UVDGM only provides B_{Poly} as an output, the software embedded within the Poly Bias Calculator was modified to also output estimated values of S and D. The Polychromatic Bias worksheet used as data inputs the lamp output, microbial action spectra, sleeve transmittance, and UV sensor spectral response provided as default data in the worksheet, the spectral UVA of NOM candidates measured in this study, and the spectral UVA of WTP waters obtained from other AwwaRF studies.

RESULTS AND DISCUSSION

Characteristics and Availability of UV-Absorbers

LC-MIEX[®] water was obtained from a pilot-scale MIEX[®] system treating processed water from the Caloosahatchee River and Super Hume[™] was obtained from the manufacturer. All other UV absorber samples were obtained from full-scale WTPs treating groundwater

Table 3.2 shows the undiluted UV absorbance at 254 nm measured with each sample and the volume generated from its source. Such data can be used to determine if the source can produce the UV absorber in sufficient volumes at concentrations that can support full-scale UV reactor validation.

Table 3.2
UV absorbance and production volume of identified NOM sources

Source	Absorbance at 254 nm (cm-1)	Approximate volume produced
BB-NF	2.7231	1.3 mgd
Melb-RO	0.2875	1 mgd
Sar-RO	0.1239	1.5 mgd
Wash-IX	26.18	1,000 gal/day
LC-MIEX [®]	297.2	N/A
OPPD-RO	2.2367	50,000 gal/day
Carl-ED	0.124	1 mgd
VG-RO	0.0824	230,000 gal/day
Jup-RO	0.0856	N/A
WC-IX	337.5	2,100 gal every 2-3 months
Super Hume [™]	3,365	Delivered upon request

NOM Source Absorption Spectra

Figure 3.3 shows the spectral UVA of finished water, normalized to give a UVA of 0.039cm^{-1} at 254 nm. Normalization is done to facilitate comparison of two different UVA spectra. The legend on the graph provides the UVT of the water before normalization. The data was obtained from AwwaRF projects 2623, 2861, and 3004. The UVA spectra represent a range of finished waters with UVT at 254 nm ranging from 81 to 98 percent.

Figures 3.4 and 3.5 compare the UVA spectra of the NOM sources to that of coffee, LSA, and WTP waters. All UVA spectra were also normalized to a UVA of 0.039 cm^{-1} at 254 nm (UVT = 91.4%) to facilitate the comparison. Figure 3.4 shows the spectral UVA of low-concentration sources, such as membrane and electro dialysis concentrates, while Figure 3.5 shows the spectral UVA of high-concentration sources, such as MIEX[®], IX brines, and Super Hume[™]. The UVA spectra of the WTP defined as “WTP min” and “WTP max” are the lower and upper bounds of the range of UVA spectra for WTP waters given in Figure 3.3.

With the exception of the UVA spectra of the BB-NF source below 240 nm, the UVA spectra of the membrane and electro dialysis concentrates closely matched the UVA spectra of WTP waters at wavelengths from 200 to 400 nm. The UVA spectra of the MIEX[®] and IX brine concentrates matched the UVA spectra of WTP waters at wavelengths above 240 nm but had lower UV absorbance at wavelengths below 240nm. The UVA spectra of all of these concentrates did a better job matching the UVA spectra of WTP waters than did coffee or LSA. The UVA spectra of Super Hume[™] matched WTP waters at wavelengths below 260 nm but had higher UV absorbance at wavelengths above 260 nm. While the UVA spectra of Super Hume[™] matched WTP waters better than the UVA spectra of coffee, no obvious advantage of Super Hume[™] over LSA was apparent in Figure 3.5.

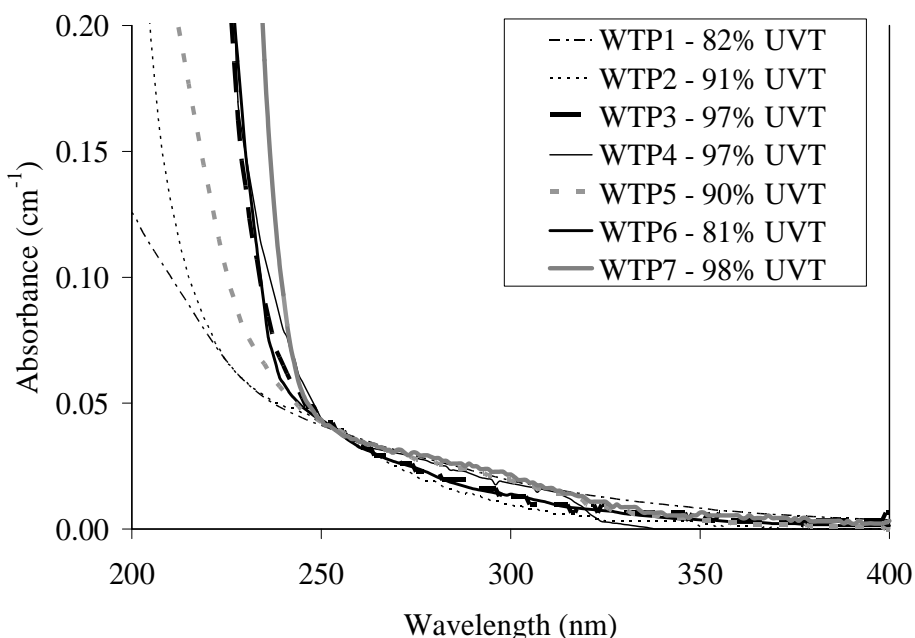


Figure 3.3 Comparison of the UVA measured with WTP finished waters. Data is normalized to give a UVA at 254 nm of 0.039 cm^{-1} . Legend shows the UVT at 254 nm before normalization

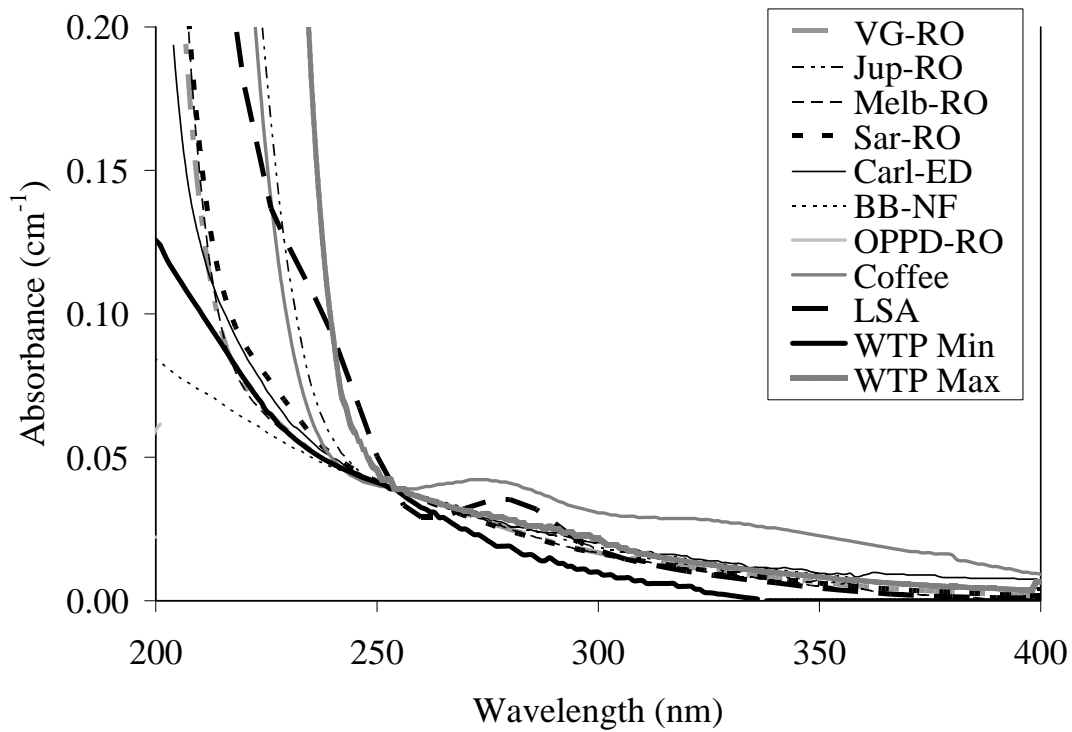


Figure 3.4 Comparison of the UVA spectra from 200 to 400 nm of membrane and electro dialysis concentrates with the UVA spectra of LSA, coffee, and WTP waters

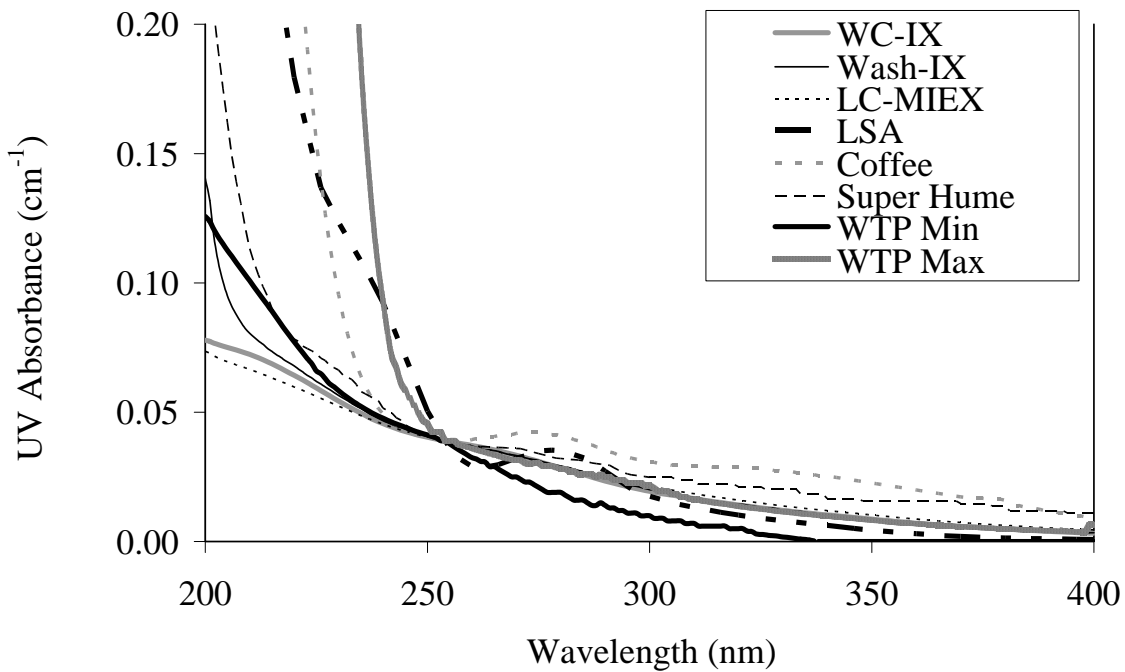


Figure 3.5 Comparison of the UVA spectra from 200 to 400 nm of MIEX[®] and IX brine concentrates with the UVA spectra of LSA, coffee, and WTP waters

MP lamps produce germicidal UV light from 200 to 300 nm. Because the UV absorption of WTP waters increases significantly below 240 nm, the effective germicidal range with a UV reactor is from 240 to 300 nm. If a UV reactor uses germicidal UV sensors that respond from 240 to 300 nm, the UVA spectra of the UV absorber used during validation should match that of the WTP waters from 240 to 300 nm. Figures 3.6 and 3.7 compare the UVA spectra of the NOM surrogates to the UVA spectra of coffee, LSA, and WTP waters over this range.

If the UV reactor uses non-germicidal UV sensors, the UVA spectra of the UV absorber should match over the germicidal wavelength range and the wavelength range detected by the sensor. As shown in Figure 3.8, with an unfiltered silicon carbide (SiC) sensor, the wavelength range extends up to 380 nm.

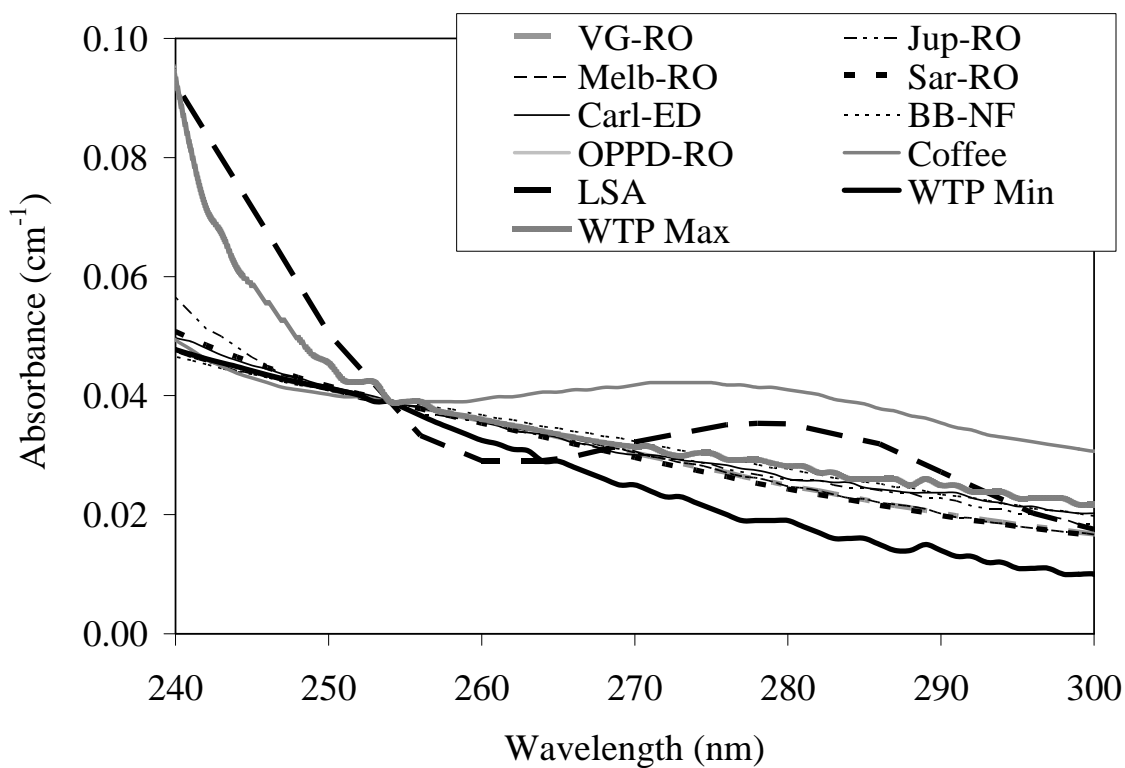


Figure 3.6 Comparison of the UVA spectra from 240 to 300 nm of membrane and electro dialysis concentrates with the UVA spectra of LSA, coffee, and WTP waters

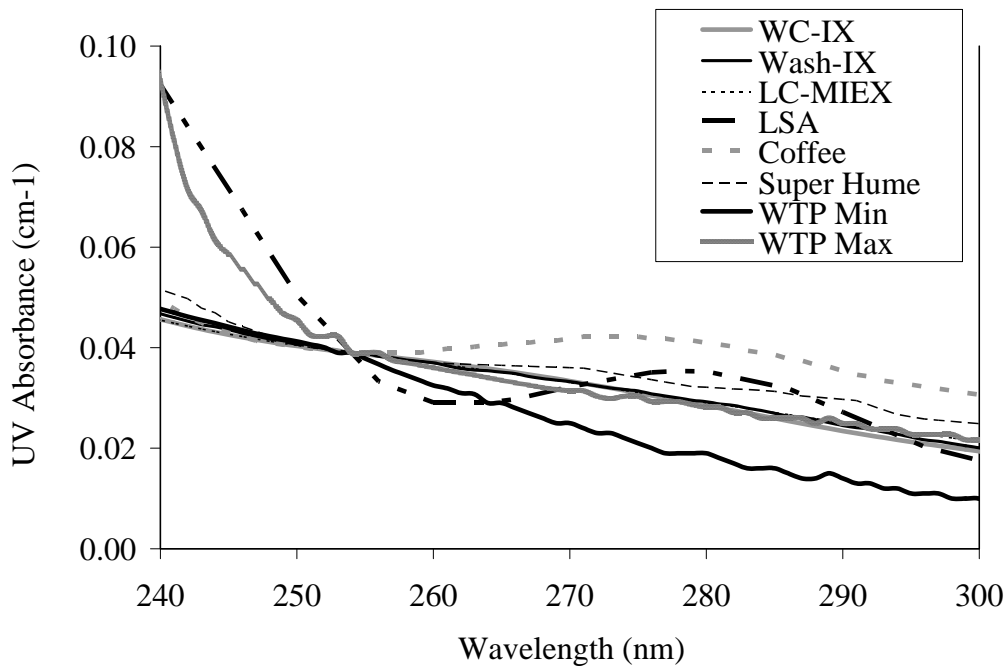


Figure 3.7 Comparison of the UVA spectra from 240 to 300 nm of MIEX[®] and IX brine concentrates with the UVA spectra of LSA, coffee, and WTP waters

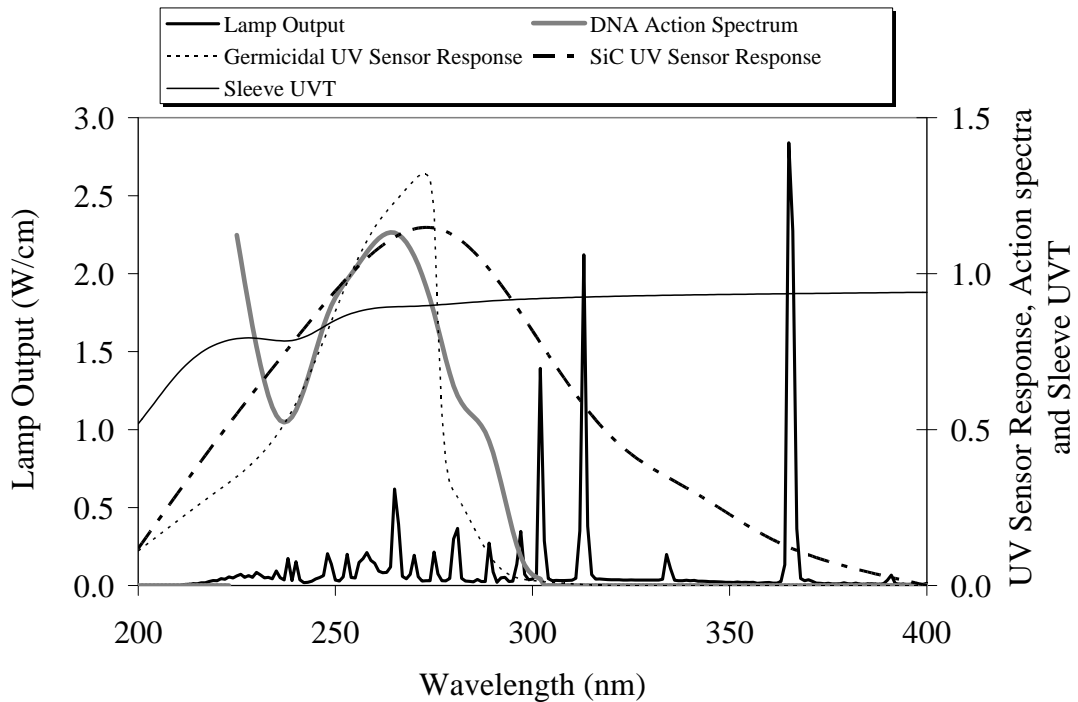


Figure 3.8 Lamp output, UV sensor spectral response, and microbial action data used as inputs to the Polychromatic Bias worksheet

Impact of UV-Absorbers on Dose Delivery and the Polychromatic Bias

Table 3.3 gives UV dose delivered by the annular reactor as a function of UVT at 254 nm and the spectral UVA of WTP waters and UV absorber surrogates. Figure 3.9 presents the UV dose as a function of UVT at 254 nm for WTP waters, VG-RO concentrate, LC-LIEX concentrate, Super Hume, LSA, and coffee. Table 3.4 gives the percent difference between the UV dose predicted using the UVA spectra at the WTP and that using a UV absorber. The percent difference is calculated as:

$$\Delta Dose (\%) = 100 \times \frac{Dose_{UV\ Absorber} - Dose_{WTP}}{Dose_{WTP}} \quad (3.6)$$

The range in $\Delta Dose$ given in Table 3.4 occurs because the difference is calculated using the minimum and maximum WTP UVA spectra.

For a given flow rate, lamp output, and a UVT at 254 nm of 75 percent, the data in Table 3.4 shows that UV dose values predicted using the UVA spectra of coffee was 10 to 30 percent lower than the UV doses delivered at the WTPs, and the UV doses values predicted using the UVA spectra of LSA was 6 to 27 percent lower. This level of conservatism decreases as UVT at 254 nm increases. At 98 percent UVT, the UV dose measured using coffee and LSA are within -5 to +3 percent of the UV dose delivered at the WTP.

Table 3.3
UV dose as a function of UVT 254 for different spectra UVA

UV-absorbing chemical	UV Dose (mJ/cm ²) for UVT 254 of					
	75%	80%	85%	90%	95%	98%
WTP UVA Min	45.4	55.3	68.7	87.1	113.4	134.7
WTP UVA Max	35.5	44.3	56.5	74.1	100.6	124.5
VG-RO	40.6	50.1	63.3	82.2	109.9	133.0
JUP-RO	38.2	47.4	60.3	78.7	106.4	130.5
MELB-RO	39.9	49.5	62.8	81.9	109.9	133.0
SAR-RO	39.8	49.3	62.5	81.4	109.3	132.7
CARL-ED	39.1	48.6	61.9	80.9	109.1	132.6
BB-NN	38.5	48	61.3	80.6	109	132.6
OPPD-RO	35.1	44.2	57.4	76.8	106.4	131.4
WC-IX	37.9	47.4	60.6	79.9	108.5	132.4
WASH-IX	37.7	47.1	60.3	79.5	108.2	132.2
LC-MIEX	37.9	47.3	60.7	79.9	108.6	132.5
Super Hume™	36.2	45.5	58.8	78.3	107.5	131.9
LSA	33.2	41.7	54	72.4	101.6	128.1
Coffee	31.9	40.4	52.7	71.5	101.3	128.3

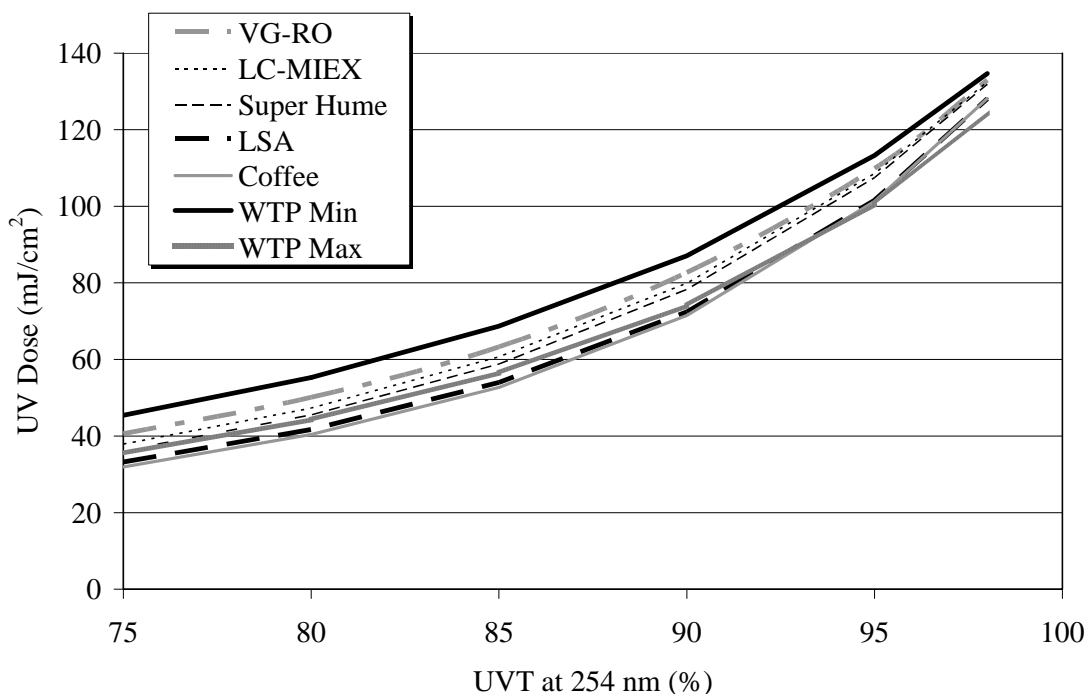


Figure 3.9 Dose delivery as a function of UVT for the annular reactor for different UVA spectra

**Table 3.4
Delta UV dose as a function of UVT 254 for different spectra UVA**

UV-absorbing chemical	Delta UV dose (%) for UVT 254 of					
	75%	80%	85%	90%	95%	98%
VG-RO	-11 to 14	-9 to 13	-8 to 12	-6 to 11	-3 to 9	-1 to 7
JUP-RO	-16 to 8	-14 to 7	-12 to 7	-10 to 6	-6 to 6	-3 to 5
MELB-RO	-12 to 12	-10 to 12	-9 to 11	-6 to 11	-3 to 9	-1 to 7
SAR-RO	-12 to 12	-11 to 11	-9 to 11	-7 to 10	-4 to 9	-1 to 7
CARL-ED	-14 to 10	-12 to 10	-10 to 10	-7 to 9	-4 to 8	-2 to 7
BB-NN	-15 to 8	-13 to 8	-11 to 8	-7 to 9	-4 to 8	-2 to 7
OPPD-RO	-23 to -1	-20 to 0	-16 to 2	-12 to 4	-6 to 6	-2 to 6
WC-IX	-17 to 7	-14 to 7	-12 to 7	-8 to 8	-4 to 8	-2 to 6
WASH-IX	-17 to 6	-15 to 6	-12 to 7	-9 to 7	-5 to 8	-2 to 6
LC-MIEX	-17 to 7	-14 to 7	-12 to 7	-8 to 8	-4 to 8	-2 to 6
Super Hume™	-20 to 2	-18 to 3	-14 to 4	-10 to 6	-5 to 7	-2 to 6
LSA	-27 to -6	-25 to -6	-21 to -4	-17 to -2	-10 to 1	-5 to 3
Coffee	-30 to -10	-27 to -9	-23 to -7	-18 to -4	-11 to 1	-5 to 3

At a UVT of 75 percent, the UV dose values predicted using the UVA spectra of Super Hume™ was within -20 to 2 percent of the dose delivered at the WTP. However, that range was only -2 to 6 percent at a UVT of 98 percent. In general, Super Hume™ provides a conservative estimate of dose delivery for most waters but can lead to an over prediction by about 6 percent.

The UV dose values predicted using the UVA spectra of MIEX® and IX brine concentrates was -17 to 7 percent of the dose delivered at the WTP at a UVT of 75 percent but only -2 to 8 percent at a UVT of 98 percent. MIEX® and IX brine concentrates provides a conservative estimate of dose delivery at most WTPs for UVTs from 75 to 90 percent but can over estimate UV dose by as much as 8 percent at high UVTs from 95 to 98 percent.

With the exception of the OPPD-RO, the UV dose values predicted using the UVA spectra of membrane and electro dialysis concentrates was -14 to +14 percent of the dose delivered at the WTP at a UVT of 254 nm of 75 percent. That range was only -2 to 7 percent at a UVT of 98 percent. On average, membrane and electro dialysis concentrates provide good estimates of the UV dose delivery expected with the average WTP UVA spectra. However, because the UVA spectra of WTP water and these concentrates vary, the dose delivery estimated using membrane and electro dialysis concentrates can lead to under and over predictions by as much as 14 percent.

While the UV absorber used during validation may lead to a UV system being under or over sized for given design conditions of flow, UVT at 254 nm, and UV lamp output, the dose monitoring algorithm used at the WTP will not over predict UV dose delivery if the Polychromatic Bias has a value of one or less. In other words, a UV system validated using VG-RO concentrate may be undersized by 14 percent if the WTP has a UVA spectra similar to “WTP min” used in this study; however, the dose monitoring system used at that WTP will only provide an over estimate of dose delivery if the polychromatic bias is greater than one. If the polychromatic bias is equal to one or less, the UV sensor will measure the impact of the WTP UVA spectra on dose delivery (*i.e.*, read 14 percent less) and public health protection will be maintained.

Which UV absorbers listed in [Tables 3.4](#) and [3.5](#) are best is open to debate. One may argue that coffee is best because it is conservative. One may also argue that membrane and electro dialysis concentrates are best because they are most representative of WTP waters and public health protection can be assured by controlling the Polychromatic Bias. Super Hume™ appears to provide a reasonable compromise by ensuring UV systems are appropriately sized for most WTP UVA spectra without undue conservatism.

For the five UV absorbers in [Figure 3.9](#), [Figures 3.10](#) to [3.14](#) show the polychromatic bias predicted as a function of UVT at 254 nm, WTP UVA spectra, UV sensor spectral response, and UV sensor to lamp water layer. The results show that:

1. The polychromatic bias has a value near one at high UVT. The polychromatic bias increases at lower UVT if the UVA spectrum of the UV absorber surrogate has a greater absorbance at wavelengths above and below 254 nm than the WTP water (*e.g.*, coffee, LSA, Super Hume, and LC-MIEX). The polychromatic bias decreases at lower UVT if the UVA spectrum of the UV absorber surrogate has lower absorbance at wavelengths above and below 254 nm than the WTP water (*e.g.*, VG-RO concentrate, WTP max UVA, [Figure 3.10](#)).

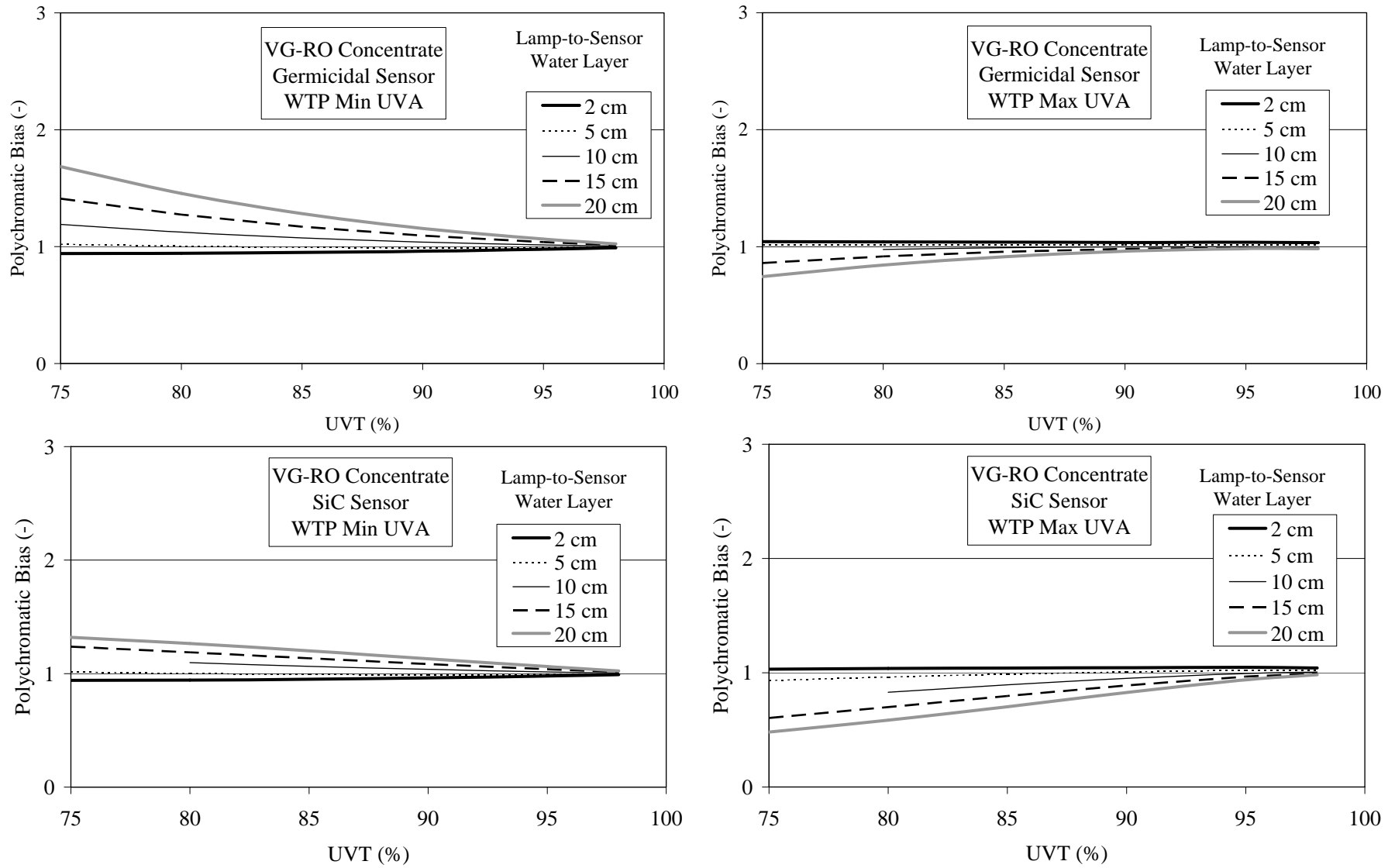


Figure 3.10 Impact of UVT and UV sensor-to-lamp water layer on B_{Poly} with VG-RO concentrate

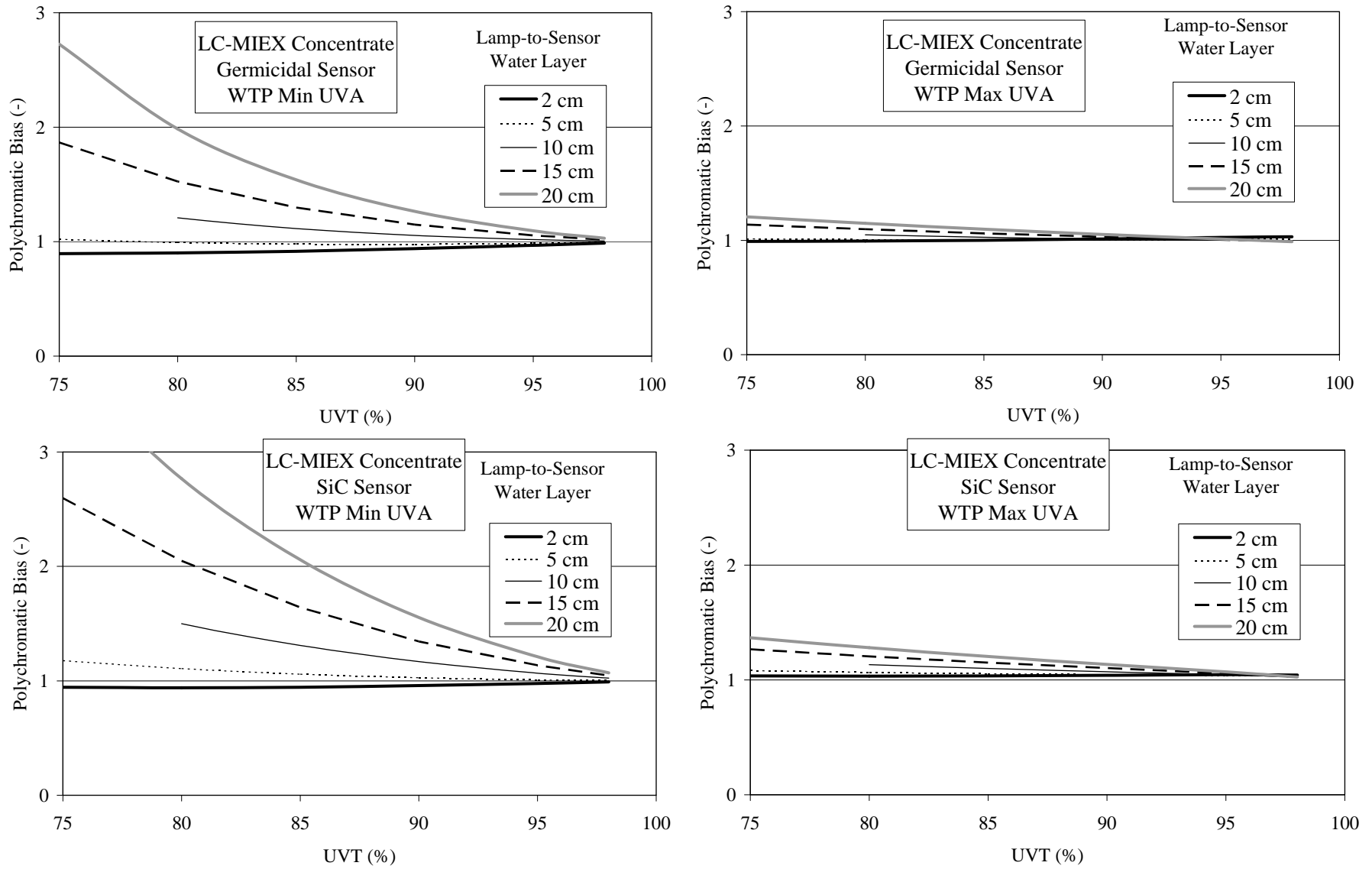


Figure 3.11 Impact of UVT and UV sensor-to-lamp water layer on B_{Poly} with LC-MIEX[®]

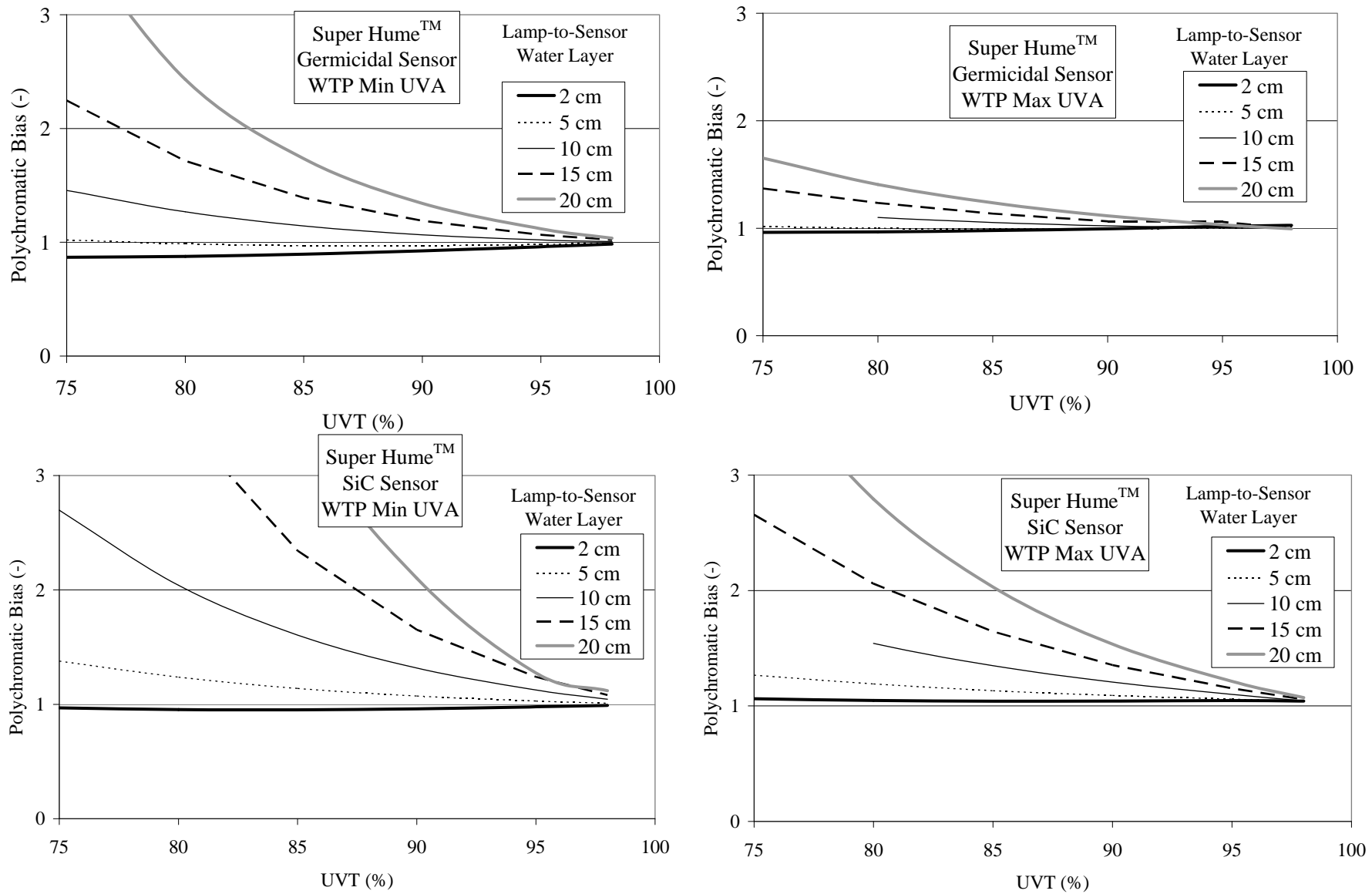


Figure 3.12 Impact of UVT and UV sensor-to-lamp water layer on B_{Poly} with Super Hume™

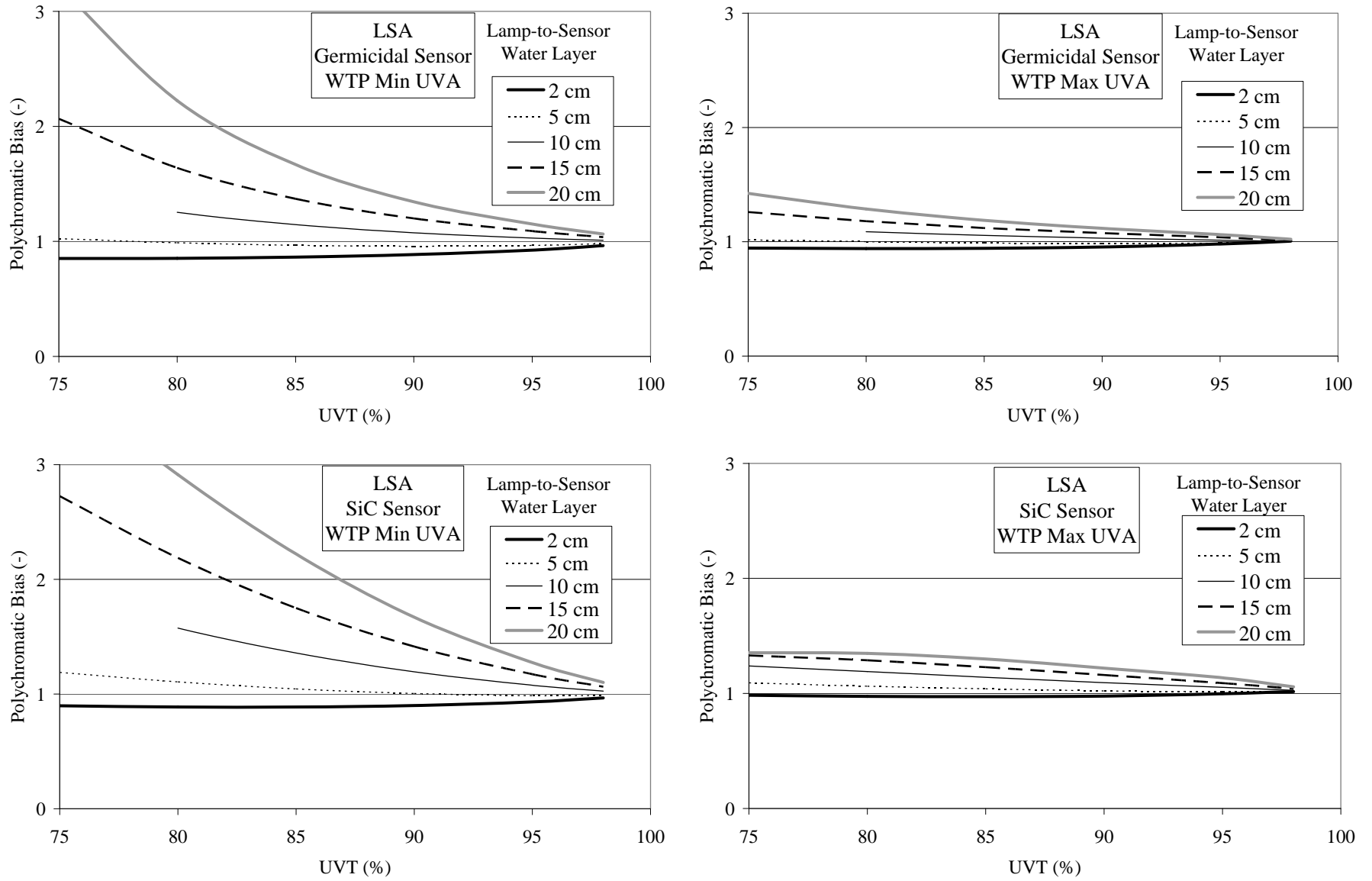


Figure 3.13 Impact of UVT and UV sensor-to-lamp water layer on B_{Poly} with LSA

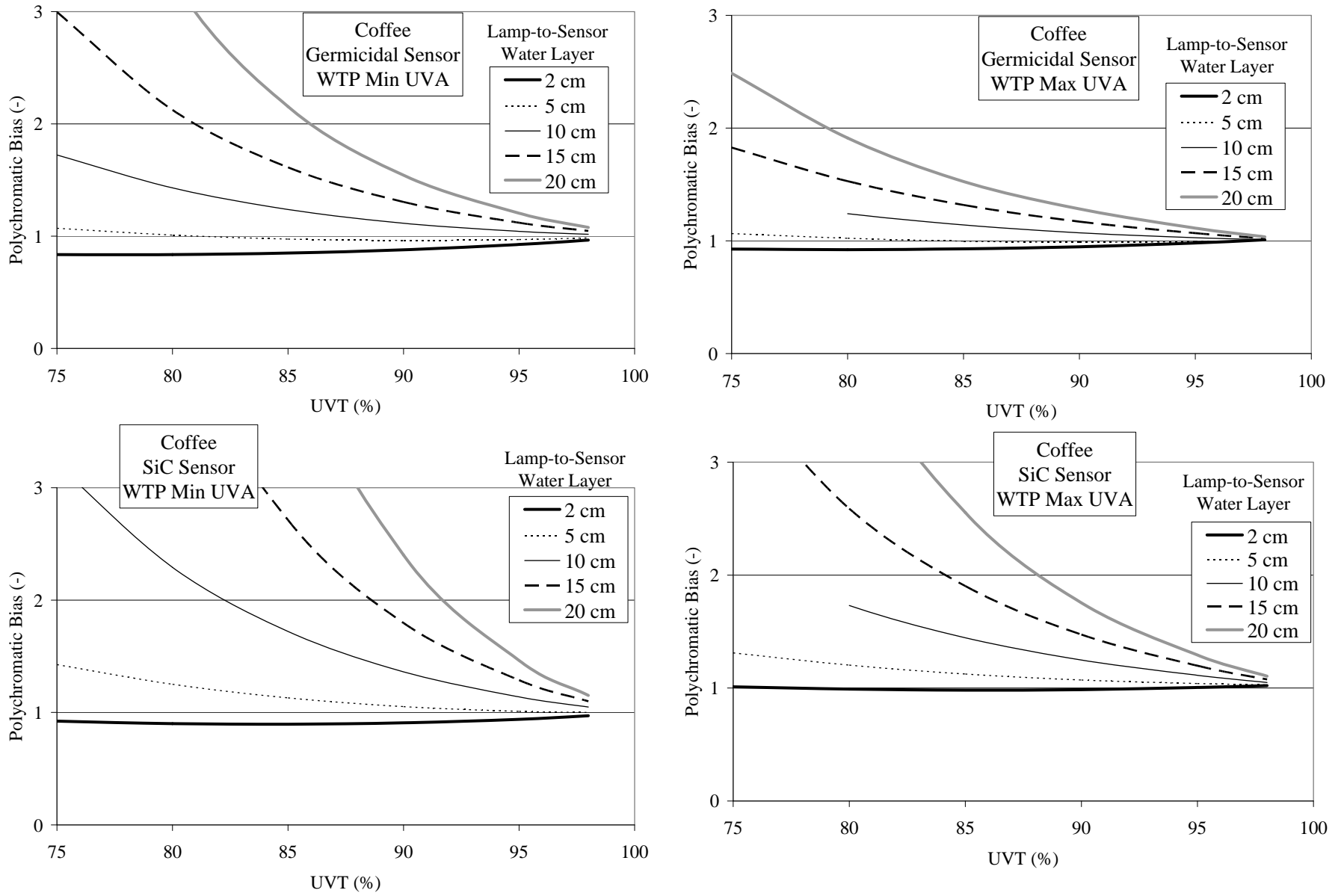


Figure 3.14 Impact of UVT and UV sensor-to-lamp water layer on B_{Poly} with coffee

2. The polychromatic bias has greater values with the minimum WTP UVA spectra compared to the maximum WTP UVA spectra.
3. The polychromatic bias has a value near one when the UV sensor is located close to the lamp (*i.e.*, 2 to 5 cm water layers). The deviation of the polychromatic bias from one increases as the UV sensor is located further from the lamps.
4. With the exception of the polychromatic bias with the VG-RO concentrate relative to the minimum WTP UV spectra, the deviation of the polychromatic bias from one is greater with the SiC UV sensor compared to the germicidal UV sensor.
5. The polychromatic bias has the greatest values with coffee followed by Super Hume, LSA, LC-MIEX concentrate, and VG-RO concentrate.

Table 3.5 gives the Polychromatic Bias for germicidal and SiC UV sensors located with a 10 cm water layer between the UV sensor and the lamp. The Polychromatic Bias is provided for UVTs at 254 nm of 80 and 90 percent and is based on the WTP minimum UVA spectra. In Table 3.5, the Polychromatic Bias is always significantly greater with the SiC UV sensor compared to the germicidal UV sensor, and that difference is greater at lower UVT. With the exception of the OPPD concentrate, the Polychromatic Bias with membrane and electro dialysis concentrates and germicidal UV sensors is relatively low, ranging from 1.04 to 1.05 at 90 percent UVT and from 1.12 to 1.19 at 80 percent UVT. The Polychromatic Bias with MIEX[®] and IX brine concentrates and germicidal UV sensors is somewhat higher, ranging from 1.05 to 1.06 at 90 percent UVT and from 1.21 to 1.22 at 80 percent UVT. The Polychromatic Bias with Super Hume[™] and LSA and germicidal UV sensors are similar, ranging from 1.07 to 1.08 at 90 percent UVT and from 1.25 to 1.27 at 80 percent UVT. The Polychromatic Bias is highest with coffee and germicidal UV sensors being 1.12 at 90 percent UVT and 1.43 at 80 percent UVT.

The results in Table 3.5 are specific to the water layer, UVT at 254 nm, and WTP UVA spectra used. The polychromatic bias would have been lower if a smaller water layer or the maximum WTP UVA spectra had been used. Furthermore, all results in this section depend on the annular reactor model used. The dose delivery and Polychromatic Bias of real reactors depends on the design of the reactor and the hydraulics through the reactor. The dose delivery and Polychromatic Bias of those reactors can be evaluated on a case-by-case basis using polychromatic UV intensity field models and dose delivery models based on CFD.

In summary, no one UV absorber was able keep the Polychromatic Bias near one over a wide range of UVT at 254 nm, UV sensor spectral response, UV sensor location relative to the lamps, and WTP UVA spectra. This objective can only be achieved by a combination of:

1. Using germicidal UV sensors
2. Locating those UV sensors relatively close to the lamps such that the water layer between the UV sensor and lamps is relatively low.
3. Using a UV absorber during validation that mimics the UVA spectra of WTP waters better than coffee

Table 3.5
Polychromatic Bias for germicidal and SiC UV sensors located with a
10 cm water layer between UV sensor and lamp

UVA spectra	Polychromatic bias relative to the minimum WTP UVA spectra			
	Germicidal UV sensor		Si carbide UV sensor	
	UVT = 80%	UVT = 90%	UVT = 80%	UVT = 90%
VG-RO	1.12	1.04	1.10	1.04
JUP-RO	1.13	1.04	1.32	1.11
MELB-RO	1.14	1.04	1.24	1.09
SAR-RO	1.13	1.04	1.27	1.10
CARL-ED	1.14	1.04	1.46	1.16
BB-NN	1.19	1.05	1.41	1.14
OPPD-RO	1.31	1.07	2.78	1.49
WC-IX	1.22	1.06	1.39	1.14
WASH-IX	1.21	1.06	1.41	1.14
LC-MIEX	1.21	1.05	1.50	1.17
Super Hume™	1.27	1.07	2.04	1.32
LSA	1.25	1.08	1.58	1.19
Coffee	1.43	1.12	2.29	1.36

The USEPA UVDGM (2006b) specifies evaluation and application of a Polychromatic Bias uncertainty factor in the VF only if non-germicidal UV sensors are used. However, if a germicidal UV sensor is placed relatively far from the lamps (*e.g.*, mounted on the reactor wall), the polychromatic bias can be large and cause significant under dosing at the WTP if not accounted for. For example, if a germicidal UV sensor was located at the wall of the annular reactor modeled in this study, the degree of under dosing would range up to a factor of three if the reactor was validated using LSA and used to treat water represented by the minimum WTP UVA spectra and up to a factor of 1.4 if the reactor was used to treat water represented by the maximum WTP UVA spectra.

With the germicidal UV sensor, [Figures 3.10 to 3.14](#) show that the Polychromatic Bias has a value slightly less than one with a water layer of 2 cm and progressively increases in value as the water layer increases. At some water layer distance, the Polychromatic Bias has a value near one. Beyond that distance, the value is greater than one.

The UV sensor location where the Polychromatic Bias transitions from negative to positive values can be identified by plotting UV dose and UV sensor readings as a function of UVT. [Figure 3.15](#) shows the UV dose and UV sensor readings plotted as a function of UVT for the annular reactor with Super Hume as the UV absorber. [Figure 3.16](#) shows the same data except UV sensor readings are expressed on a relative scale as $S(UVT)/S(98\%)$ where $S(98\%)$ are the UV sensor readings at 98 percent UVT. Comparing [Figures 3.16 to Figure 3.12](#), the transition from negative to positive Polychromatic Bias values occurs at a UV sensor location

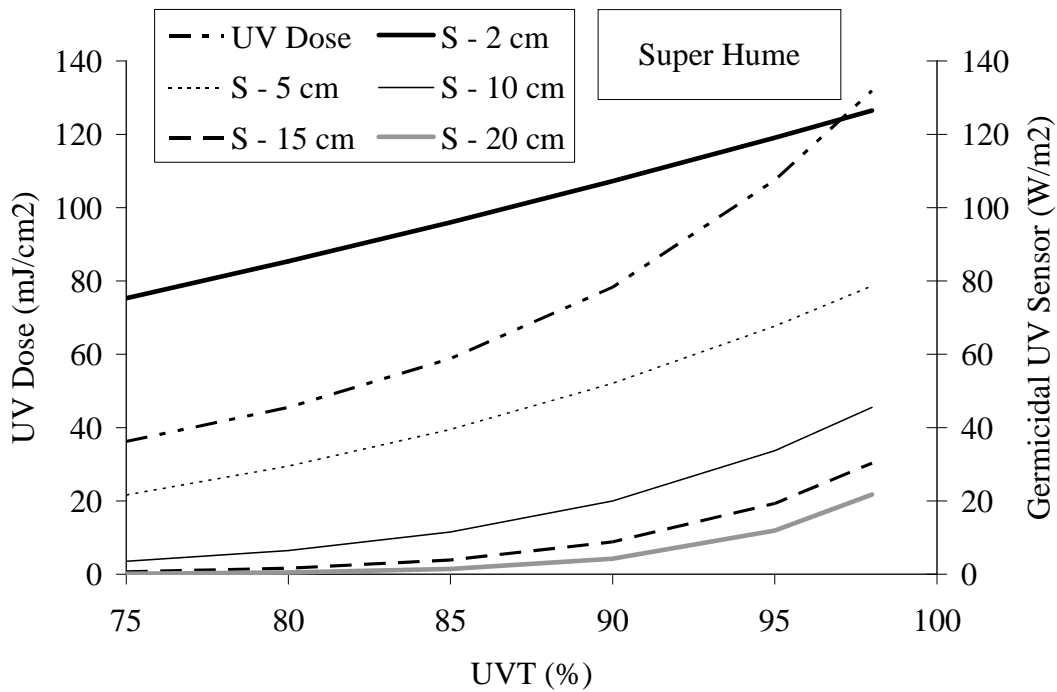


Figure 3.15 UV dose and UV sensor readings as a function of UVT at 254 nm calculated using the UVA spectra of Super Hume™

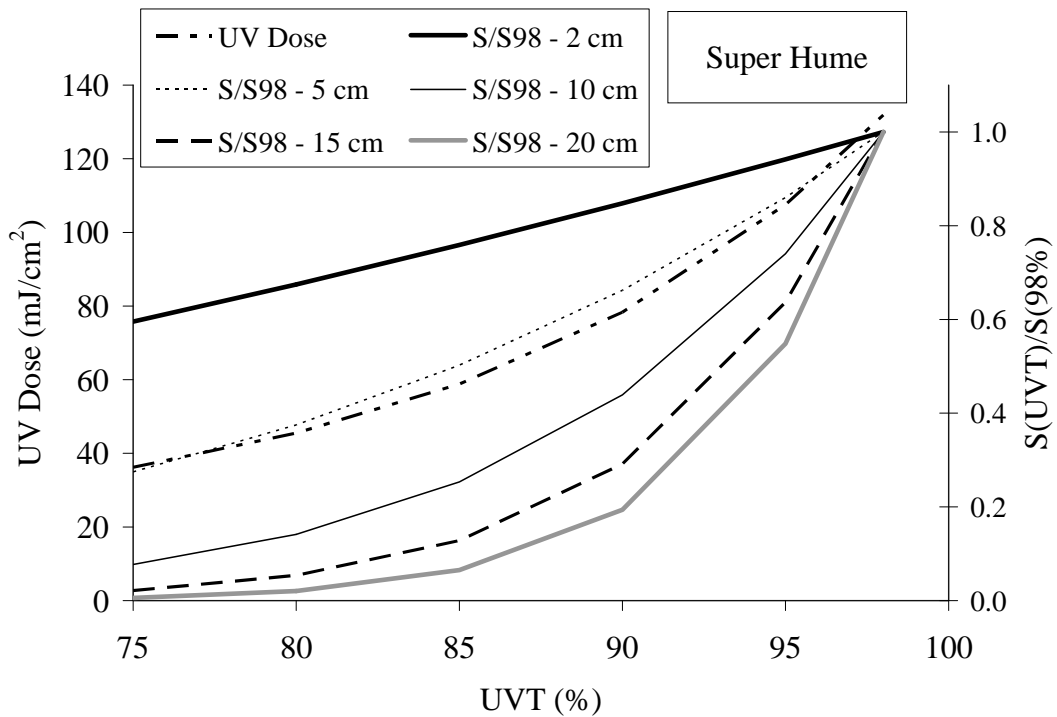


Figure 3.16 UV dose and relative UV sensor readings as a function of UVT at 254 nm calculated using the UVA spectra of Super Hume™

where the relative change in UV dose as a function of UVT is similar to the relative change in UV sensor readings as a function of UVT. With the UV sensors located close to the lamp, the relative change in UV dose as a function of UVT is greater than the relative change in UV sensor readings. Conversely, with the UV sensors located far from the lamp, the relative change in UV dose as a function of UVT is less than the relative change in UV sensor readings. At a water layer of 5 cm, the relative change in UV dose is roughly equal to the relative change in UV sensor reading. At this location, the Polychromatic Bias has value near one.

The location where the change in UV dose as a function of UVT is roughly proportional to the change in UV sensor readings as a function of UVT is referred to as the ideal location for dose monitoring using the UV intensity setpoint approach (Wright *et al.* 2002). At this location, the UV dose values measured at a given flow and UV sensor reading is approximately the same regardless of the combination of UVT and lamp power that gives that sensor reading. If the UV sensor is located closer to the lamp than this location, the UV dose for a given flow and UV sensor reading will be greater with high UVT and lowered lamp power. Conversely, if the UV sensor is located further than this location, the UV dose for a given flow and UV sensor reading will be greater with maximum lamp power and lowered UVT.

The location of the UV sensor relative to the ideal location can be evaluated during validation to determine if the Polychromatic Bias is equal to, less than, or greater than one. If the RED measured at a given flow and UV sensor readings obtained using high UVT and lowered lamp power is equal to or greater than the RED measured at the same flow and UV sensor reading obtained at maximum lamp power and lowered UVT, the polychromatic bias should have a value equal to or less than one.

Feasibility for Full-Scale Validation Using New NOM Surrogates

The feasibility of using any UVA surrogate in validation is strongly influenced by the volumes required for testing. The volume of UV-absorbing surrogate chemical required for a given validation is a function of the number of test conditions, the flow and UVT of those test conditions, and the time required to reach steady state conditions. UV reactors with design capacities in excess of 40 mgd have been validated. In order to support UV reactor validation of this magnitude, the surrogates not only have to mimic WTP waters, but also have to be available in concentrations and volumes that are practical to validate large-scale UV reactors. Because the UVA at 254 nm of the UVA surrogates studies varies by order of magnitude, the volumes that would be required for validation would also vary by orders of magnitude.

Table 3.6 compares the volumes of UV-absorbing surrogates required for a 10-mgd UV reactor validation. The volumes were calculated assuming 24 hours of validation testing, a source water UVT of 96 percent, a target UVT of 80 and 90 percent, and a surrogate stock solution UVA as given in Table 3.2.

In Table 3.6, the volume of LSA estimated for the validation at 80 and 90 percent UVT is 200 and 80 gallons, respectively. In comparison, depending on the source, the volume of membrane and electro dialysis concentrate needed to validate the reactor was between 100,000 and 3,500,000 gallons at 90 percent UVT and 300,000 and 9,600,000 gallons at 80 percent UVT. The volume of MIEX[®] and Ion Exchange Brines required also depending on the source and ranged from 900 to 18,000 gallons at 90 percent UVT and 2,400 to 30,000 gallons at 80 percent UVT. The volume of Super Hume[™] required at 80 and 90 percent UVT was 240 and 90 gallons, respectively. The results suggest that membrane and electro dialysis concentrates are

not practical as UV absorbers unless they could be concentrated. MIEX[®] and IX Brines could be feasible if used for low flow validations or transported using a tanker truck from the source to the site of validation. Super Hume[™], on the other hand, can be obtained in volumes practical for large-scale validation.

RO Concentrates

In this study, RO concentrate sources such as VG-RO and Sar-RO would require approximately 2,700,000 to 10,000,000 gallons to validate a 10-mgd UV reactor at a UVT of 80 percent. Although these volumes were theoretically available from the WTPs, collection and transport would be cost-prohibitive. Moreover, the logistics associated with storing and feeding these large volumes during testing would not be practical.

Therefore, further concentration of the RO concentrates was investigated. Calculations were performed assuming a 10-gpm pilot-scale RO membrane unit with a recovery (permeate flow rate/feed flow rate) of 80 percent. This unit would yield 2 gpm of concentrate for the 10 gpm feed flow. The concentrate would have a UVA approximately five times greater than that of the feed water. To achieve a UVA comparable to the UVA of LSA stock solution, the concentrate would need to be recycled about 7 times through the membrane. Under these conditions, over one million gallons of VG-RO would be required to produce 100 gallons of concentrate with a UV-254 value on the order of 3,500 cm⁻¹. Given these logistics, concentration of RO concentrates using membrane technologies to concentrations comparable to LSA was deemed unfeasible.

Table 3.6
Volume of UV-absorbing surrogates required for a 10-mgd UV reactor validation

Source	UVA at 254 nm (cm ⁻¹)	80% UVT (gal)	90% UVT (gal)
VG-RO	0.0824	9610000	3410000
Jup-RO	0.0856	9250000	3274000
Melb-RO	0.2875	2754000	970000
Sar-RO	0.1239	6390000	2260000
Carl-ED	0.124	6386000	2260000
BB-NF	2.7231	290000	103000
OPPD-RO	2.237	354000	125000
WC-IX	337.5	2400	900
Wash-IX	26.18	30300	17500
LC-MIEX	297.2	2700	950
Super Hume [™]	3365	240	90
Lignin sulfonate	3970	200	80

MIEX[®] and Ion Exchange Brines

Of the IX brines tested, those with the highest application potential were LC-MIEX[®] and WC-IX. These sources would require approximately 900 to 2,700 gallons to validate the 10-mgd UV reactor at UVT values of 90 and 80 percent, respectively.

The WC-IX concentrate was obtained from the West Carteret Water Company. Table 3.7 provides data on the chemical content of WC-IX brine samples. The IX resin regeneration cycle generates approximately 2,000 gallons of brine with a concentration that decreases as the backwash cycle progresses. Because the concentration decreases, the volume of concentrate required for validation would be higher than indicated in Table 3.6. Due to these constraints, WC-IX brine would be better suited for validation of reactors more on the order of 1 mgd or less.

The LC-MIEX[®] concentrate was obtained from a pilot study. While a pilot reactor likely will not produce enough volume of concentrate for large-scale UV validation, full-scale MIEX[®] installation could provide sufficient volumes.

Table 3.7
Characteristics of undiluted WC-IX brine

Parameter	Sample #1	Sample #2	Detection limit
BOD (mg/L)	19.5	5.8	5
COD (mg/L)	23,300	25,000	10
Total phosphorous (mg/L)	0.38	< 0.3	0.3
Orthophosphate phosphorous (mg/L)	< 1.0	-	1.0
Arsenic (mg/L)	< 10	-	10
Silver (mg/L)	< 1.0	-	1.0
Barium (mg/L)	< 2.0	-	2.0
Chromium (mg/L)	< 1.0	-	1.0
Copper (mg/L)	< 1.0	-	1.0
Nickel (mg/L)	< 2.0	-	2.0
Nitrate-N (mg/L)	< 10	-	10
Lead (mg/L)	< 2.0	-	2.0
Antimony (mg/L)	< 5.0	-	5.0
Thallium (mg/L)	< 10	-	10
Zinc (mg/L)	< 2.0	-	2.0

Super Hume™

Super Hume™ was the most promising of the new absorbing surrogates based on its availability. The required volume of Super Hume™ to validate the 10-mgd UV reactor described above would be 90 and 240 gallons for validation at 90 and 80 percent UVT, respectively. This is very similar to the volume of LSA that would be required for such tests. Super Hume™ can be obtained upon request in 55-gallon drums (~\$10/gal⁴) or 275-gallon totes (~\$9/gal¹).

An important added value to using Super Hume™ is that it has been demonstrated to contribute significantly to the stability of test microbes when compared to LSA (Hargy *et al.* 2004). Moreover, Super Hume™ has a lower viscosity than LSA, thereby making it easier to pump during cold temperature conditions. Super Hume™ has been used to validate UV reactors at flows up to 40 mgd and UVT values ranging from 70 to 95 percent. It is now the standard UV-modulating additive used at the Portland Validation Center.

SUMMARY AND CONCLUSIONS

During this study, eleven NOM sources were identified and evaluated as possible UV-absorbing surrogates that better mimic the UVA spectra of WTP waters. Additionally, the application of these sources for large-scale UV reactor validation was also investigated. The following is a summary of the most important findings:

- The UVA spectra of the UV absorber used during validation impacts dose delivery and dose monitoring. Ideally, the UVA spectra used during validation matches that of the water over the germicidal wavelength range (200 to 300 nm) and the wavelength range detected by the sensor (up to 400 nm with SiC UV sensors).
- The UVA spectra of membrane and electro dialysis concentrates closely matched the UVA spectra of WTP waters at wavelengths from 200 to 400 nm. The UVA spectra of the MIEX® and IX brine concentrates matched the UVA spectra of WTP waters at wavelengths above 240 nm but had lower UV absorbance at wavelengths below 240nm. The UVA spectra of all of these concentrates did a better job matching the UVA spectra of WTP waters than did coffee or LSA. The UVA spectra of Super Hume™ matched WTP waters at wavelengths below 260 nm but had higher UV absorbance at wavelengths above 260 nm. While the UVA spectra of Super Hume™ matched WTP waters better than the UVA spectra of coffee, no obvious advantage of Super Hume™ over LSA was apparent.
- For a given flow, UVT 254, and lamp output, the RED measured during validation using the UVA spectra of coffee, LSA, or Super Hume will be typically lower than the RED delivered at the WTP. This level of conservatism is minor at high UVT and significant at low UVT, is greatest with coffee, least with Super Hume, and varies depending on the UVA spectra at the WTP. The RED measured using the UVA spectra of MIEX® and IX brine concentrates will also be lower than the RED delivered at the WTP at UVTs from 75 to 90 percent but will be greater by as much as 8 percent at UVTs above that range. The RED measured using the UVA spectra of

⁴ In Winter 2005 dollars, source: United Agricultural Services, Hudson, Fla., estimate includes shipping.

- membrane and electro dialysis concentrates will on average match the RED at the WTP. However, because the UVA spectra of the concentrates and WTP waters vary, the RED measured using membrane and electro dialysis concentrates can be higher or lower than at the WTP by as much as 14 percent.
- The over prediction of RED for a given flow, UVT at 254 nm, and UV lamp output caused by the UV absorber used during validation will impact UV system sizing but not the dose monitoring if the Polychromatic Bias has a value of one or less.
 - For a given flow, UVT, and UV sensor reading, differences in the UVA spectra of the UV absorber used during validation and the UVA spectra of the water can cause bias errors in dose monitoring. This Polychromatic Bias depends on the UVA spectra of the UV absorbers and the WTP water, the UVT 254 value, the spectral response of the UV sensor, and the location of the UV sensor relative to the lamps.
 - The bias error is small at high UVT but increases exponentially as UVT decreases. The bias error is greater with SiC sensors that measure UV light above 300 nm compared to germicidal UV sensors that measure UV light from 200 to 300 nm. Whether the bias error leads to over or under predictions of dose delivery depends on the UV sensor-to-lamp water layer distance and differences in the UVA spectra during validation and at the WTP. For coffee, LSA, and Super Hume, the bias error leads to under predictions of dose delivery at the WTP if the UV sensor is located relatively close to the lamp and over predictions if the UV sensor is located relatively far from the lamp. With some membrane concentrates, the opposite occurs.
 - While the 2006 UVDGM indicates that the Polychromatic Bias is only an issue with non-germicidal UV sensors, the bias can be large with germicidal UV sensors if they are placed far enough from the lamps and the UVT is low.
 - The magnitude of the bias error follows the order Coffee > Super Hume ~ LSA > MIEX[®] and IX brine concentrates > membrane and electro dialysis concentrates.
 - An ideal sensor location exists that minimizes the magnitude of the error. That ideal sensor location is equivalent to the ideal sensor location used for dose monitoring using the UV intensity setpoint method described in the USEPA UVDGM. Using a germicidal UV sensor located relatively close to the lamps is the best approach for minimizing the bias error.
 - Utilities considering on site validation should use UVA absorbers whose UVA spectra best matches that of their water. UV vendors conducting broad based validation of their products should use UVA absorbers whose UVA spectra provides somewhat conservative estimations of dose delivery to provide UV system sizing data that is broadly applicable to a wide range of WTP waters. Super Hume[™] appears to provide a reasonable compromise by ensuring UV systems are appropriately sized for most WTP UVA spectra without undue conservatism. Super Hume improves the stability of test microbes and is available in large volumes. It is now used at the Portland UV Validation Test Facility.
 - Validation using membrane concentrates is not practical because of the large volumes needed.
 - The use of IX and MIEX[®] brines as UV-absorbing surrogates during UV reactor validation could be feasible depending on volume requirements and availability. During this study, no source was identified that could provide enough volume for a large-scale validation.

CHAPTER 4

IMPACT OF LAMP AGING ON UV DOSE DELIVERY AND MONITORING

INTRODUCTION

UV systems are sized to deliver a required UV dose for design conditions of flowrate, UVT at 254 nm, lamp aging and fouling using dose delivery data obtained through UV reactor validation testing. During validation, the impact of lamp aging is typically simulated using new lamps operating at lowered power. This approach assumes that an aged lamp has the same relative UV output along its length and about its circumference as a new lamp. However, as shown in [Figure 4.1](#), aged lamps can show non-uniform discoloration along their length and about their circumference. The impact of non-uniform discoloration of the lamps on dose delivery by the UV reactor has not been reported in the literature. This non-uniform discoloration raises the question whether operation of a new lamp at lower power is a good representation of the UV output of aged lamps.



Figure 4.1 Discoloration observed with aged MP lamps after approximately 4000 hours of operation compared to a relatively new lamp (third down from top)

Non-uniform lamp aging also impacts UV dose monitoring. For example, if the lamps age more near the lamp ends compared to the center but the UV sensor monitors the UV output from the center, the dose-monitoring algorithm could over estimate dose delivery. Ideally, the UV sensors should be placed to view a location along the lamp where the reduction in output caused by lamp aging is proportional to the reduction in dose delivery caused by lamp aging. However, there is no data published on the magnitude of these impacts or on how to locate the UV sensor to deal with this issue.

The aging of UV lamps (Phillips 1983) and quartz sleeves (Kawar *et al.* 1998) can depend on wavelength with lower wavelengths aging at a faster rate than higher wavelengths. This wavelength dependence appears as a “spectral shift” in lamp output over time. The impact of spectral shifts on dose delivery and dose monitoring was evaluated in Appendix D of the 2003 USEPA UVDGM. Spectral shifts in UV output from the lamps through the sleeves can cause dose-monitoring errors. The magnitude of these errors is greater with SiC UV sensors compared to germicidal UV sensors and increases as UVT decreases and the distance from the UV sensor to the lamp increases. For example, spectral shifts can cause over predictions of dose delivery by as much as 50 percent if a SiC sensor monitors a UV lamp through a 25 cm water layer. While the UVDGM identifies spectral shifts as a potential issue, there is little data published on the magnitude of the issue of spectral shifts with installed UV systems.

The objective of this study was to quantify the impacts of non-uniform lamp aging on the UV output of lamps obtained from operating UV systems, assess how non-uniform lamp aging impacts dose delivery and monitoring, and provide guidance on dose monitoring and validation to account for the issue.

APPROACH

U.S. and European utilities using UV disinfection provided the Research Team with aged lamps and sleeves. The utilities represented different geographical locations, water qualities, treatment processes (water, wastewater and reuse), and lamp technologies (MP and LPHO). These lamps and sleeves had been operated under normal process conditions specific to each utility.

All lamps supplied by US utilities were sent to Carollo Engineers while those collected from European utilities were sent directly to the optics laboratory at the Institute for Medical Physics and Biostatistics, at the University of Veterinary Medicine in Vienna, Austria. Lamps sent to Carollo were inspected for visible signs of lamp aging. Lamps that showed significant darkening of the lamp ends, rippling of the lamp envelope or fouling stains were sent to Vienna for measurement of spectral UV output along the length and about the circumference of the lamp. New lamps or lamps with no visible evidence of lamp aging were also sent for comparison.

MATERIALS AND METHODS

Lamp Operation

Figure 4.2 shows a schematic of the power supply and ballast used to start and operate the LPHO lamps. Figure 4.3 shows photograph of the ignitor and ballast. An isolating transformer and variable transformer (Type R01V7407, Luxor Transformer, Uden, Netherlands) were used to provide a constant AC voltage of 230 ± 0.5 V RMS to the lamps. An inductor (Type VHG, SBA-TrafoTech GmbH, Germany) placed in series with the lamp was used as a ballast to control the lamp current. An ignitor (Type ZRM ND1000 A0002, TridonicAtco GmbH & Co K, Dornbirn, Austria) was connected to the lamp to provide a high voltage to cold start the lamps. Lamp voltage was measured across the lamp using a voltmeter and lamp current was measured using an ammeter in series with the lamp.

The MP lamps were powered by an electronic ballast obtained from NEDAP, Groenlo, Netherlands. Lamp voltage was measured across the lamp using a voltmeter and lamp current was measured using a clamp-on current meter. Voltage and current were also monitored using an oscilloscope.

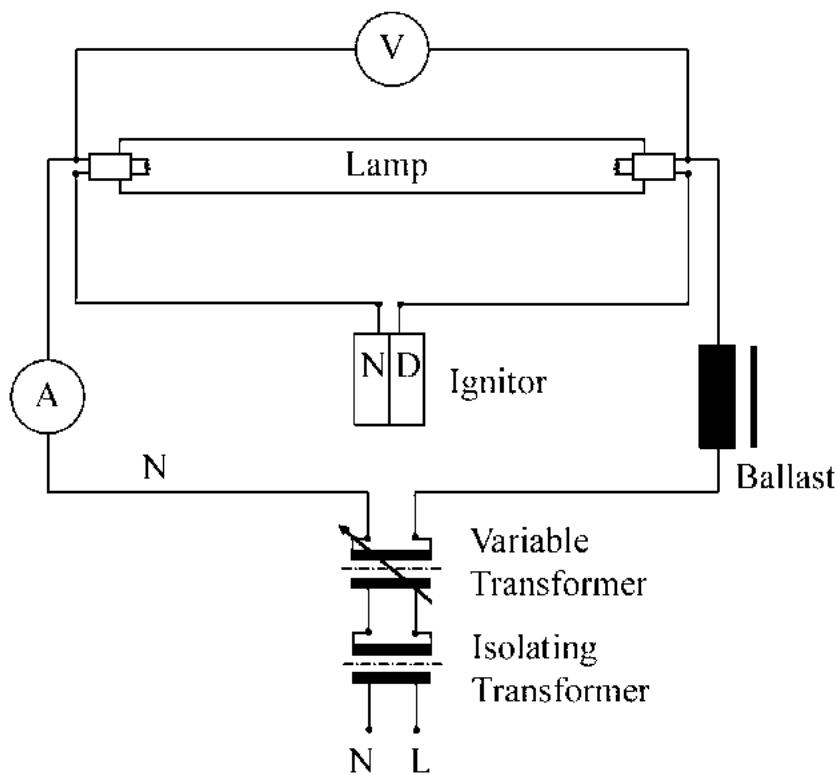


Figure 4.2 Schematic of the LPHO lamp power supply and ballast

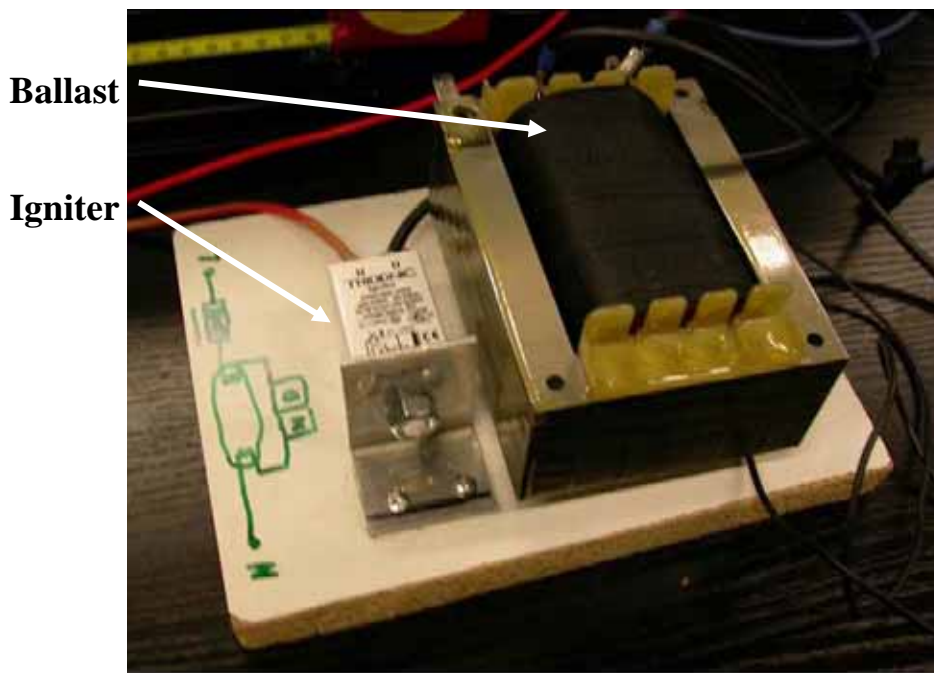


Figure 4.3 LPHO ballast and igniter

UV Irradiance Measurements

Figure 4.4 shows the apparatus used to measure the UV output from the lamps. The lamps were mounted horizontally within a box. The box was ventilated to maintain an internal temperature of approximately 26°C. The box had a rectangular aperture that allowed a radiometer located outside of the box to monitor a 5.0 cm long section of the lamp arc. The radiometer was mounted within a holder that was attached to a rail. The apparatus was designed to allow the aperture and radiometer to be positioned at various locations along the arc length of the lamp.

Spectral irradiance with both LPHO and MP lamps was measured using a Bentham DTM 300 spectroradiometer with PTB-traceable calibration. The spectral radiometer measured irradiance from 200 to 600 nm in steps of 1 nm with a bandwidth of 1 nm. With the LPHO lamps, the distance from the spectral radiometer to the surface of the lamp envelope was set at 20 cm (Figure 4.5). With the MP lamps, the distance from the radiometer to the surface of the lamp envelope was set to 100 cm. A longer distance of 100 cm was selected to ensure the irradiance incident on the radiometer was not excessive, i.e. on the order of 1 W/(m²nm). Figure 4.6 shows the locations along the length and about the circumference of the lamp where spectral irradiance was measured.

All lamps were powered for 30 minutes prior to taking any spectral irradiance measurements to allow the light output to stabilize. Measurement of one irradiance spectrum took approximately 15 minutes. After each measurement, the aperture was moved to the next position. After measuring all locations along the length of the lamp, the power was turned off and the lamp was left to cool for approximately 30 minutes. The lamp was then rotated 90-degrees and the measurements were repeated.

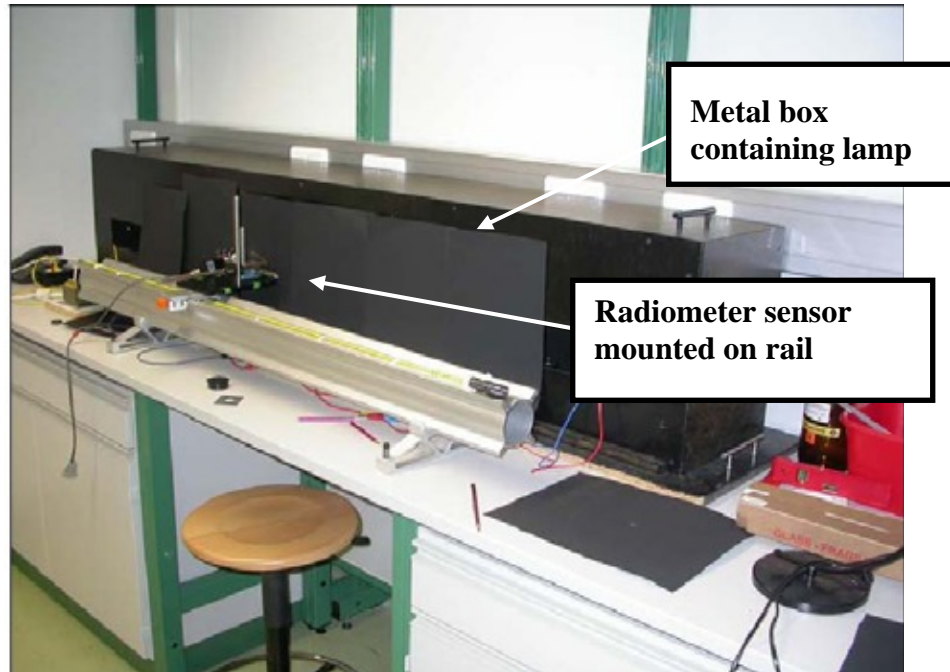


Figure 4.4 Apparatus used to measure spectral UV irradiance

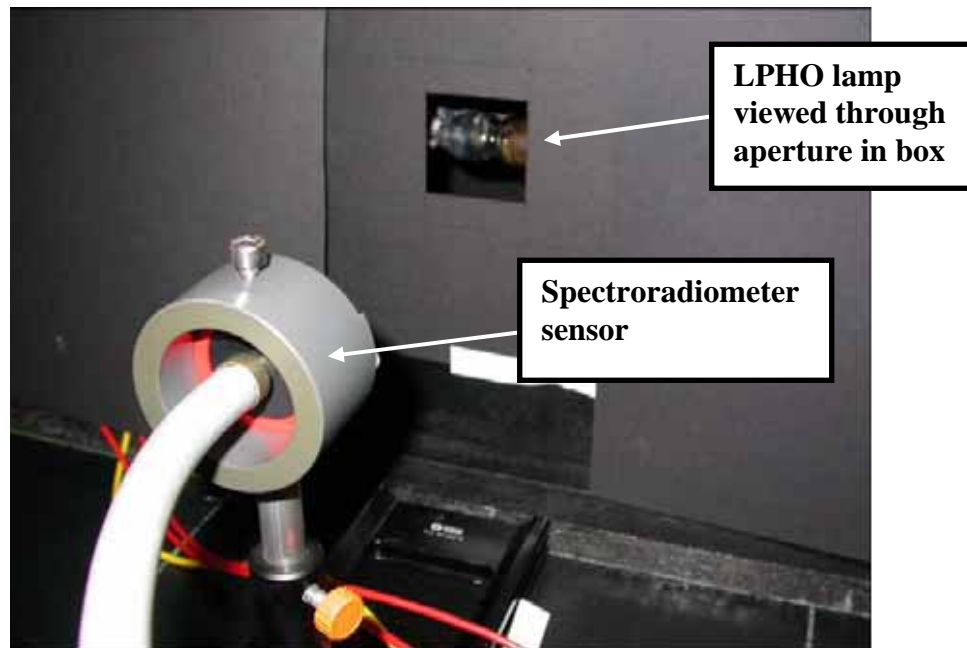
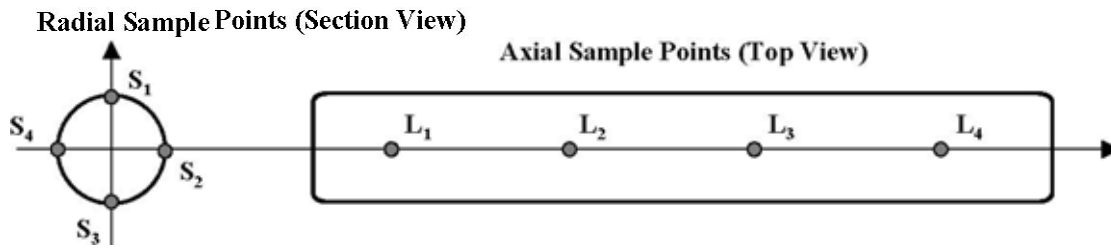


Figure 4.5 Mounting of the spectroradiometer sensor used to measure spectral irradiance with the LPHO lamp

Low-Pressure High-Output Lamps



Medium-Pressure Lamps

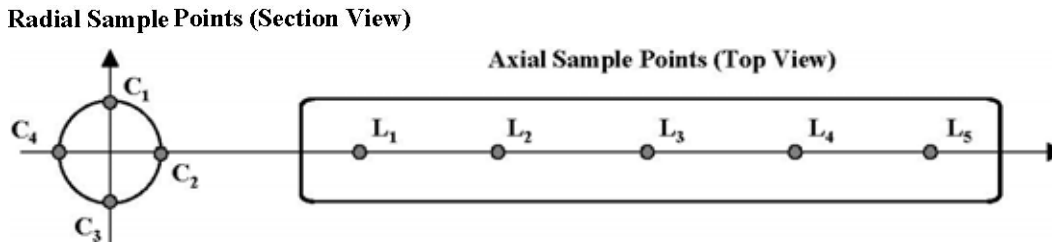


Figure 4.6 Axial and radial locations for spectral irradiance measurements with LPHO and MP lamps

UV irradiance at 254 nm was measured along the length of the LPHO lamps using an IL1700 research radiometer from International Light, Peabody, Mass. The IL1700 used a SED 240 sensor equipped with an NS254 interference filter and diffuser. The IL1700 and SED 240 were calibrated by comparing irradiance readings from a LP lamp with similar readings from the Bentham DM300 spectroradiometer.

To measure UV output along the length of the LPHO lamps, the SED 240 sensor was mounted in an ÖNORM M5372 compliant adaptor and located 2 mm from the surface of the lamp envelope (see Figure 4.7). Alignment of the SED240 relative to the lamp was controlled using a spacer as shown in Figure 4.8. The alignment was set at the each end of the lamp and at the middle prior to conducting a set of measurements. Once the lamp was aligned, measurements along the length of the lamp were obtained by moving the UV sensor and aperture along the length of the lamp in 15 mm increments. Figure 4.9 shows the SED 240 sensor at the starting location for these measurements. Each lamp was scanned 4 times along its length. After each scan, the lamp was rotated by 90-degrees.

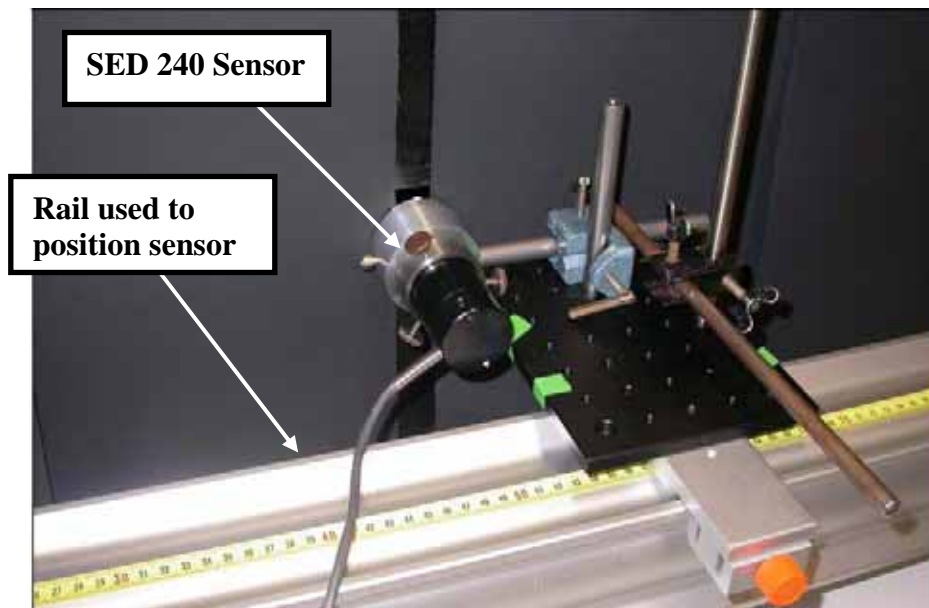


Figure 4.7 Mounting of SED 240 sensor used to measure UV lamp output at 254 nm along length of lamp

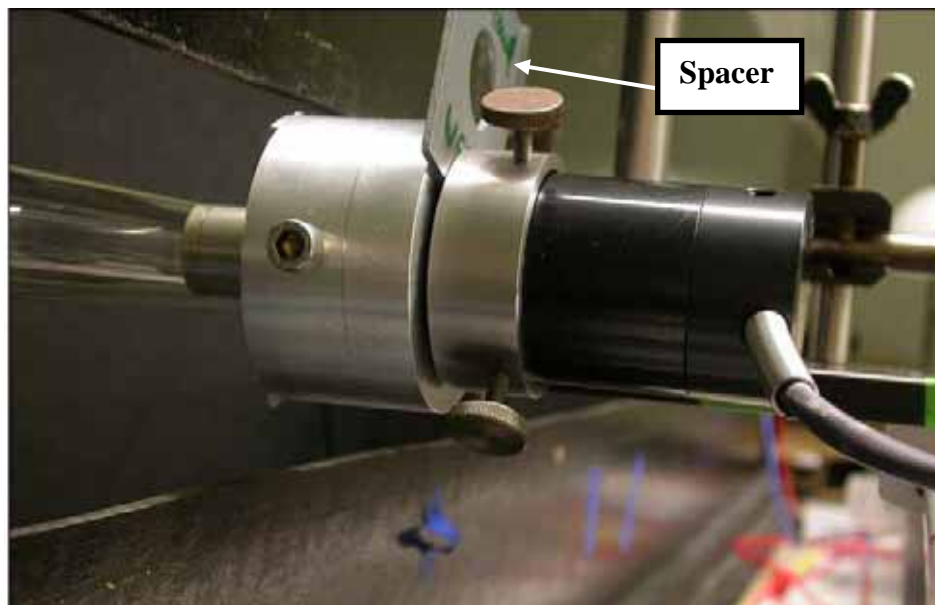


Figure 4.8 SED 240 sensor is located 2 mm from surface of lamp envelope using a spacer

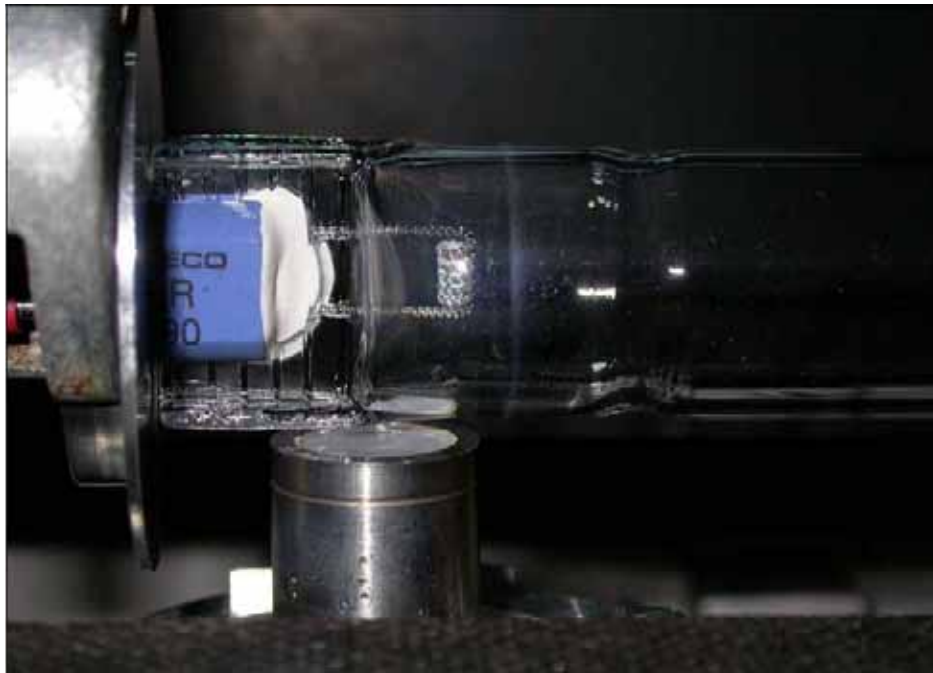


Figure 4.9 Location of SED 240 sensor relative to the lamp at the beginning of measurements of UV output along the length of the lamp

Calculation of Germicidal Output and Lamp Aging Factor

The germicidal output of MP lamps was calculated using the following equation:

$$I_G = \sum_{\lambda=200}^{320} G(\lambda) \times I(\lambda) \quad (4.1)$$

where I_G is the germicidal output of the MP lamp in W/cm, λ is the wavelength in nm, $I(\lambda)$ is the spectral output of the lamp in W/cm measured in 1-nm increments, and $G(\lambda)$ is the UV sensitivity of the microorganism normalized at 254 nm. The lamp-aging factor was calculated using:

$$\text{Lamp Aging Factor (LAF)} = \frac{\text{Germicidal Output (Old Lamp)}}{\text{Germicidal Output (New Lamp)}} \quad (4.2)$$

RESULTS AND DISCUSSION

Table 4.1 provides information on the lamps obtained from utilities for this study. A total of 31 aged lamps and 3 new lamps were obtained from four utilities. The lamps included WEDECO amalgam LPHO lamps, Calgon MP lamps, and Trojan MP lamps. The WEDECO and Calgon lamps were obtained from drinking water UV installations while the Trojan lamps were obtained from wastewater and reuse UV installations. The aged lamps had been operating for between 400 and 7,400 hours

Visual Observations

Visual affects of lamp aging could be classified into five types as follows:

1. Darkening of the quartz envelope at each end of the lamp (Figure 4.10)
2. Random discoloration along the length of the lamp (Figure 4.11)
3. Discoloration along the length of the lamp but only 180 degree about the circumference (Figure 4.12)
4. Lamp end distortion (Figure 4.13)
5. Resonant darkening (Figure 4.14)
6. Resonant distortion (Figure 4.15)

End darkening is likely caused by the sputtering of material off of the electrodes of the lamp during startup and normal operation of the lamp. End darkening was observed with all three lamp technologies evaluated in this study.

Table 4.1
Summary of UV lamps collected from full-scale treatment plants

Utility	Treatment process	UV technology	# aged lamps	Hours of operation
Helsinki, Finland	Drinking water	Wedeco AG, ¹ K Series (LPHO)	10	432-7,390
Bowling Green, Ohio, USA	Drinking water	Calgon Carbon Corp., ² Sentinel™ (MP1)	9 + 1 new	832-5,192
Daytona Beach, Fla., USA	Wastewater	Trojan Technologies Inc., ³ UV4000 (MP2)	8 + 1 new	1,578-4,354
Santa Rosa, Calif., USA	Wastewater Reclamation	Trojan Technologies Inc., UV4000 (MP2)	4 + 1 new	2,292-2,361

¹ Düsseldorf, Germany, lamp type Spektrotherm 2690.

² Pittsburg, Pa., USA lamp type 350287.

³ Ont., Canada, lamp type UV4000.

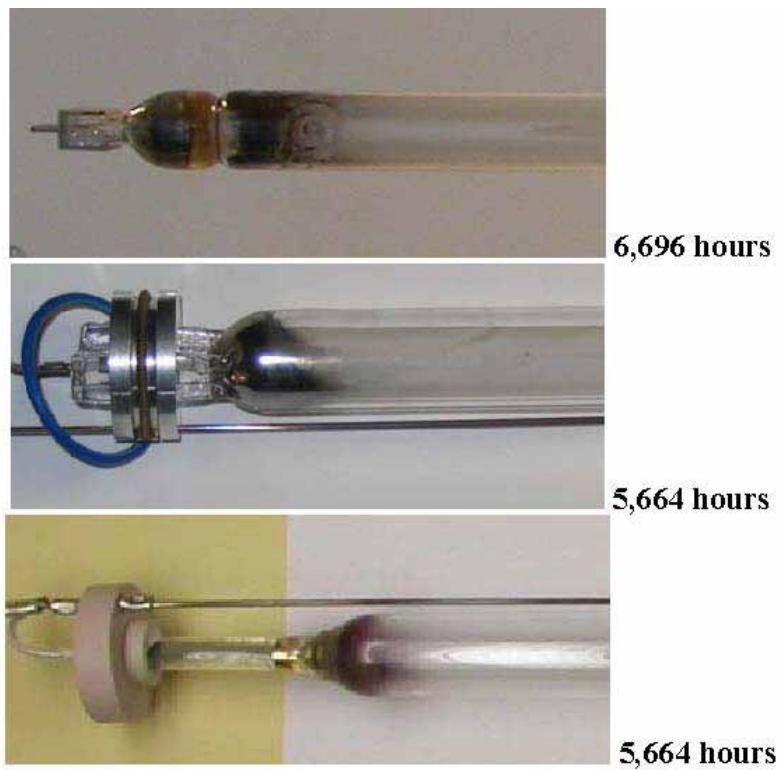


Figure 4.10 End darkening in LPHO lamps (top photo) and MP lamps (middle and bottom photos)



Figure 4.11 Random discoloration with a MP lamp

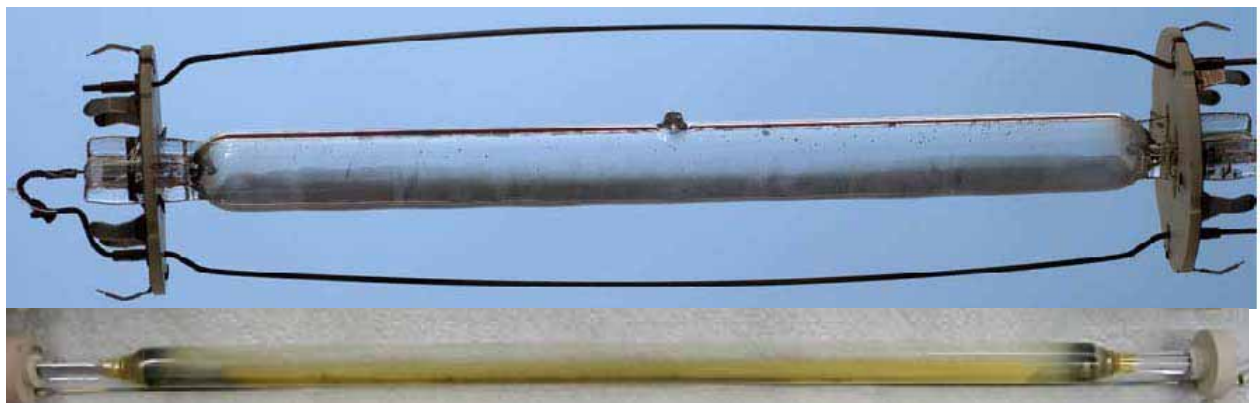


Figure 4.12 Discoloration along lamp length but around only 180° of the circumference

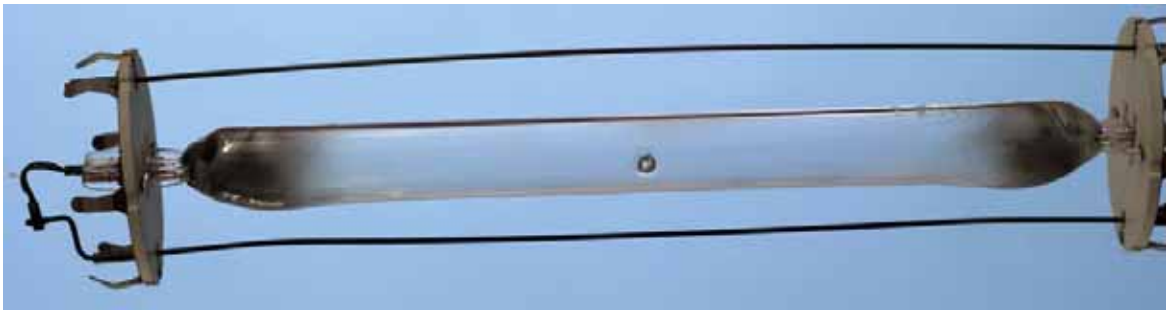


Figure 4.13 Lamp end distortion with a MP lamp with lamp end darkening

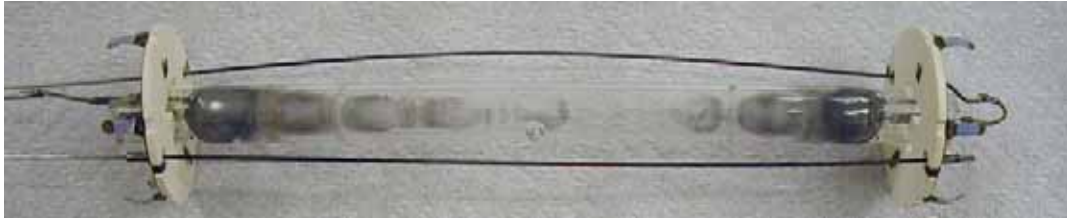


Figure 4.14 Resonant darkening with a MP lamp

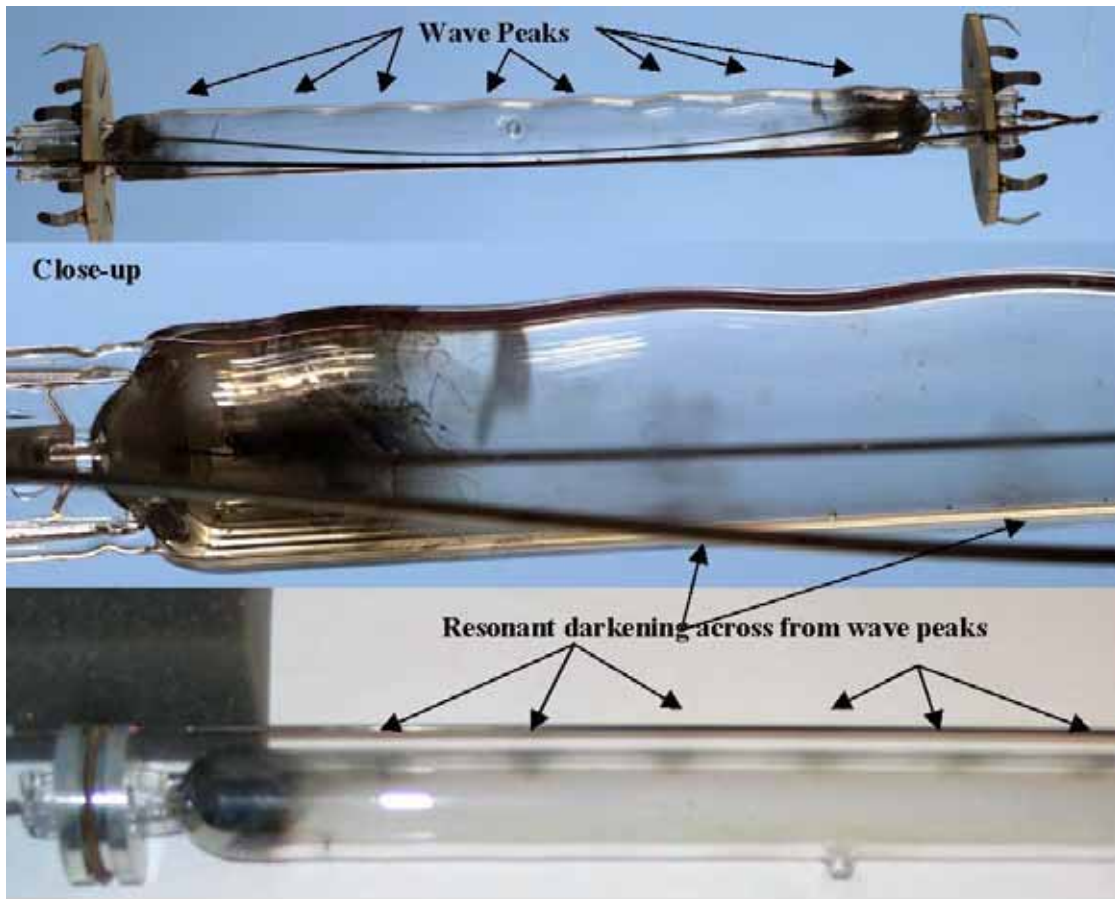


Figure 4.15 Resonant distortion and darkening with a MP lamp

Discoloration along the length of the lamp but only around 180° of the circumference was observed on one sample of each of the two MP lamp types. The discoloration was gray with one MP lamp type and yellow with the other. 180-degree discoloration was not observed with the LPHO lamps. The cause of the 180-degree discoloration was not identified.

A “warping,” or “bulging” of the quartz envelope of the lamp at one or both ends characterizes lamp end distortion. The distortion only occurs on one side of the envelope. The distortion is likely caused by heat generated by the plasma and heat generated by conductive losses at the electrode. The distortion likely occurs on the top of the lamp envelope because of convection effects and deflection of the plasma. With MP lamps, the plasma constricts to a line source and can be deflected by electromagnetic fields and convection flows such that the plasma runs along the topside of the lamp instead of down the middle of the lamp.

Resonant darkening and distortion occurred with one MP lamp technology driven by electronic ballasts. Resonant darkening and distortion with this lamp was characterized by eight evenly spaced distorted and darkened areas along the length of the lamp between the electrodes. The distortion was sinusoidal along one side of the lamp with a peak-to-peak distance equal to one-eighth of the electrode-to-electrode distance of the lamp. The darkening was on the side of the lamp opposite to that of the distortion and consisted of eight alternating regions of dark and clearer areas. The resonant distortion and darkening is likely caused by the formation of standing waves within the plasma due to the operating frequency of the lamp ballast. The distortion along one side of the lamp is likely related to deflection of the plasma along the top of the lamp.

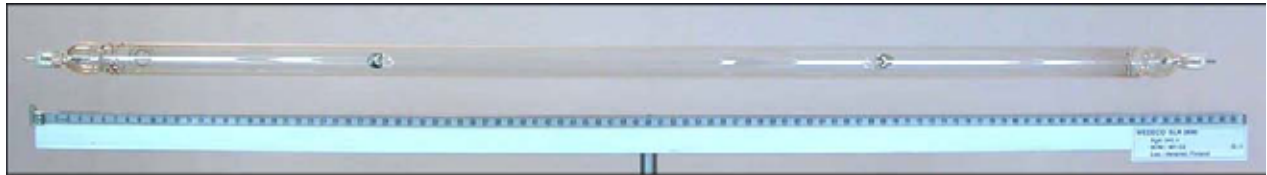
Low Pressure-High Output Lamps

Ten LPHO lamps with lamp age varying from 432 to 7,390 hours were obtained from the Pitkääkoski WTP in Helsinki, Finland. Two new LPHO lamps were also obtained from the manufacturer for comparison. The spectral UV output was measured with five of the aged lamps and the UV output at 254 nm along the lamp length was measured with four aged lamps and one new lamp.

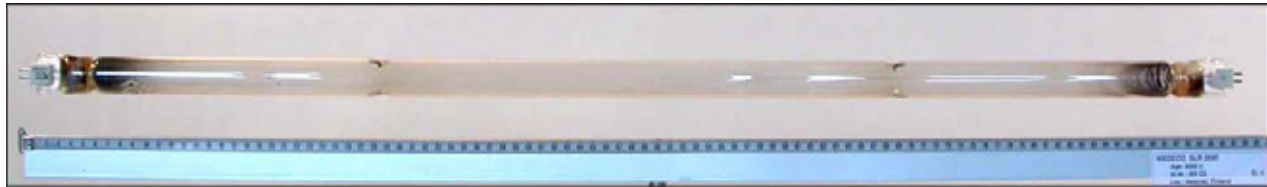
Figures 4.16 to 4.18 shows photographs of the aged lamps. The aged lamps exhibit end darkening that becomes more pronounced as lamp age increases (Figure 4.17). The lamp sleeve also showed a darkening along the length of the lamp as it aged that appeared more pronounced near the amalgams. Figure 4.18 shows unusual coloration near the lamp end of one of the aged LPHO lamps. This lamp could not be re-ignited shortly after this photo was taken.

Figures 4.19 and 4.20 show the spectral irradiance normalized to 254-nm on a linear and a semi logarithmic scale, respectively. The spectral irradiance of the LPHO lamp from 225 to 576 nm has five lines with irradiance greater than 5 percent of the 254 nm line. The spectral irradiance shown on a semi-log scale shows the line outputs of excited mercury in greater detail and also shows continuum that is 10^{-4} of the irradiance at 254 nm.

Figure 4.21 shows the cumulative spectral irradiance from 225 to 576 nm on a relative scale. The data shows that 60 percent of the emitted radiation is at 254 nm, 10 percent is emitted at longer UV wavelengths, and 30 percent is emitted in the visible range.

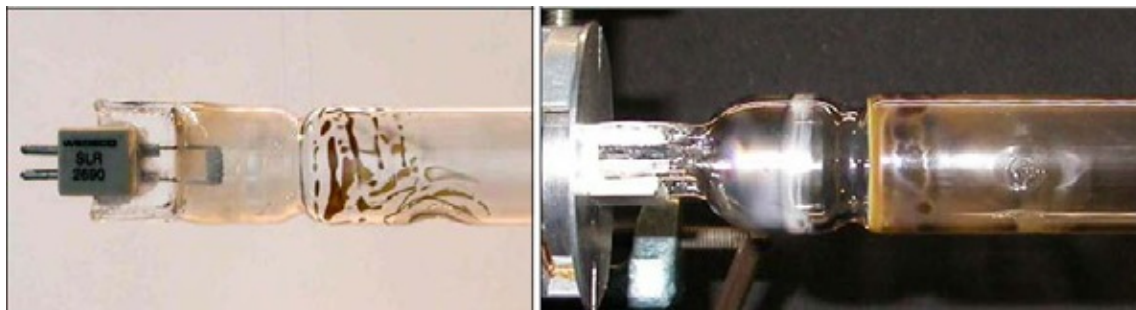


940 hours (lamp #1)



6,696 hours (lamp #9)

Figure 4.16 End darkening with LPHO lamps after 940 and 6,696 hours of operation



940 hours (lamp #1)

6,696 hours (lamp #9)

Figure 4.17 Close up of lamp end darkening with LPHO lamps

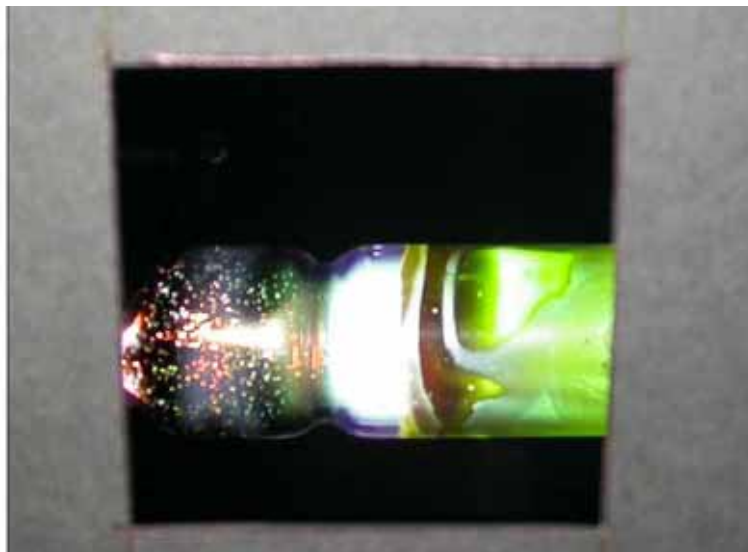


Figure 4.18 Unusual coloration of lamp #3 (6,188 hours) during operation, before it finally became defective (no color enhancement to photo)

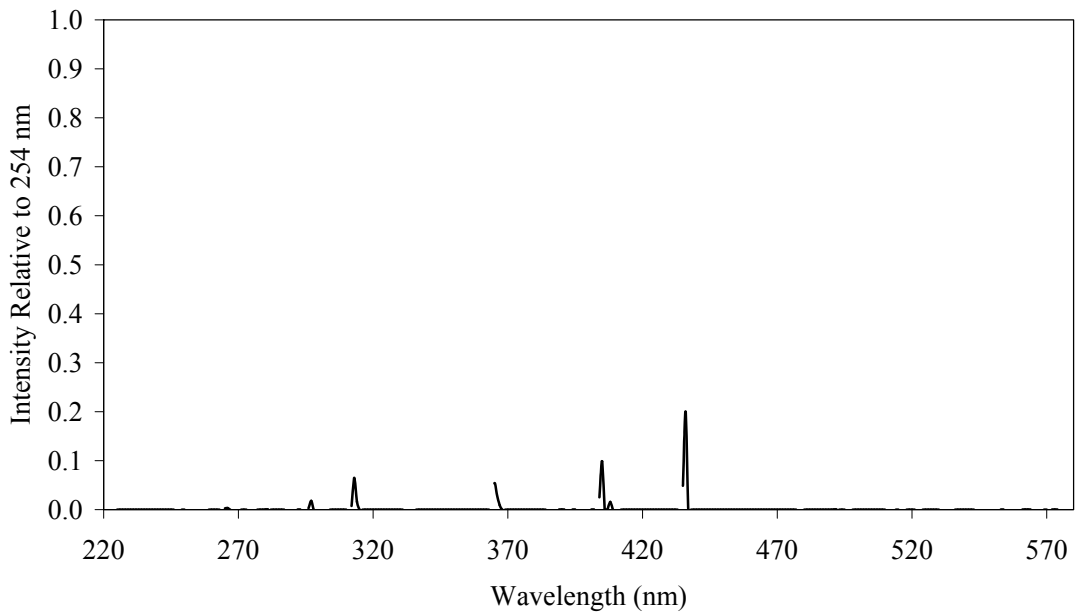


Figure 4.19 Spectral irradiance of the LPHO lamp (432 hours) normalized to 254 nm on a linear scale

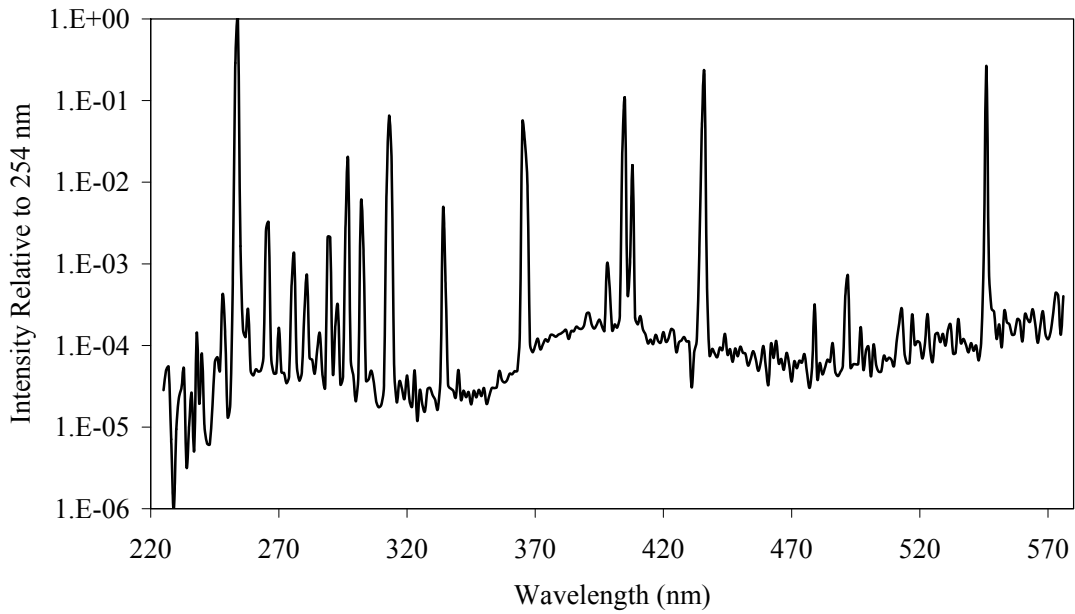


Figure 4.20 Spectral irradiance LPHO lamp #8 (432 hours) normalized to 254 nm on a semi-logarithmic scale

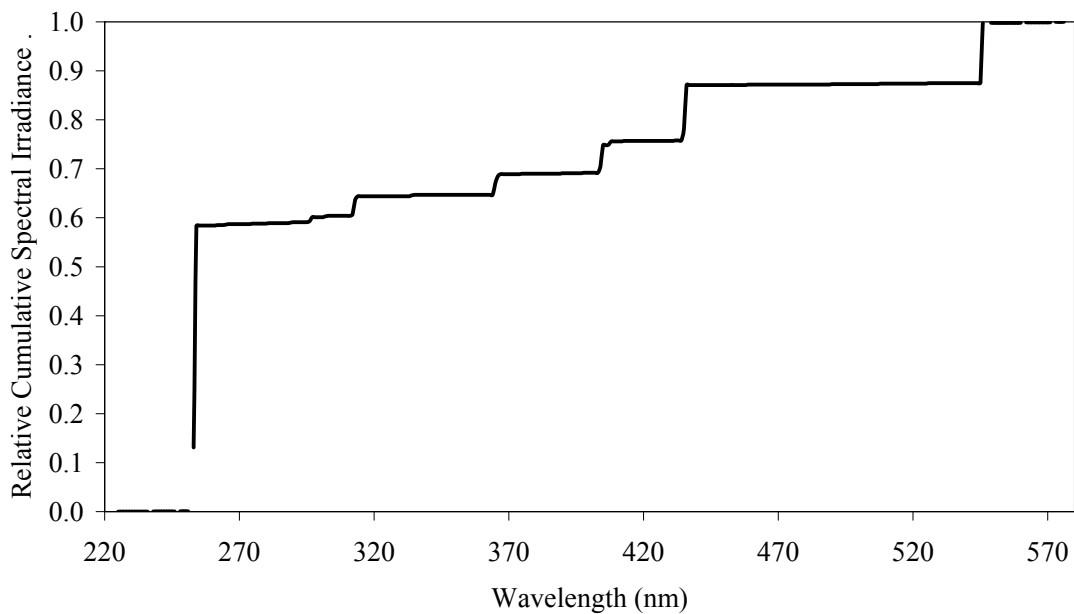


Figure 4.21 Relative cumulative spectral irradiance of LPHO lamp #8 (432 hours)

Figures 4.22 and 4.23 show the spectral irradiance measured at the end and middle of five aged LPHO lamps, respectively. Table 4.2 shows the irradiance at 254 nm measured at the end and middle of the lamps. The data shown in these figures and table shows a reduction in lamp output as operating hours increase. The reduction is notably greater at the lamp ends compared to the middle.

**Table 4.2
UV output of LPHO lamps at 254 nm measured
at the middle and at the ends of the lamps**

Lamp #	Lamp age (hours)	$E_{254 \text{ nm, end}}$ (W/m^2 per nm)	$E_{254 \text{ nm, middle}}$ (W/m^2 per nm)
2	432	1.85	3.24
1	940	2.11	3.06
8	1,472	1.54	2.67
3	6,188	0.0417	2.03
9	6,696	0.383	2.01

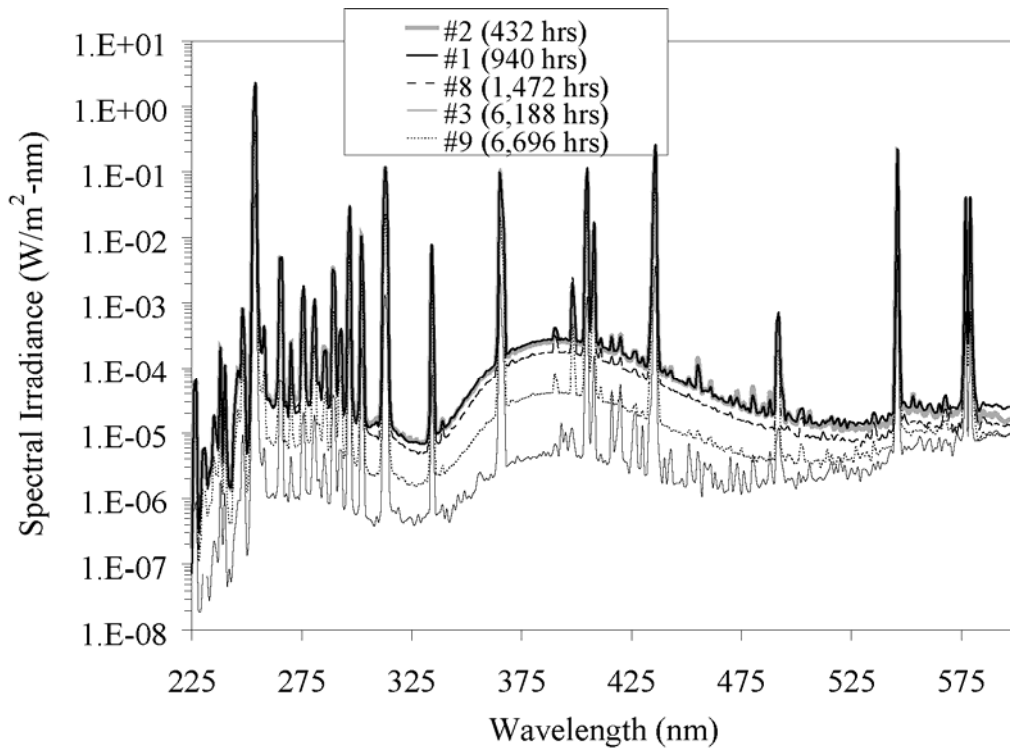


Figure 4.22 Spectral irradiance of five LPHO lamps measured at the lamp end

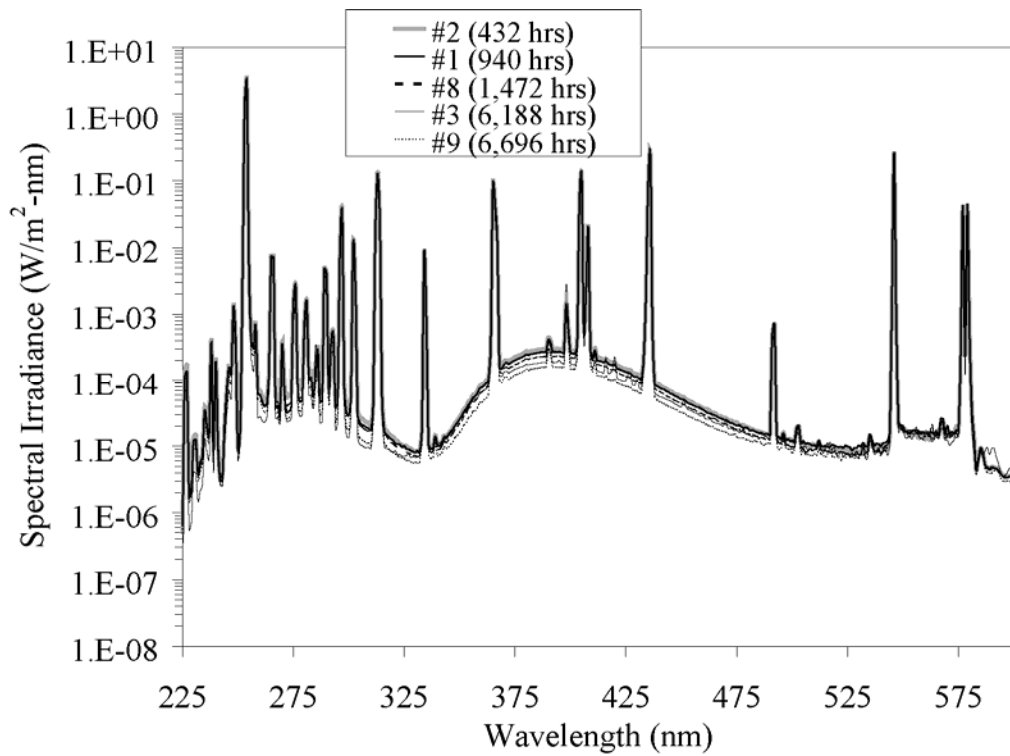


Figure 4.23 Spectral irradiance of five LPHO lamps measured at the lamp middle

Figure 4.24 shows the ratio of the spectral irradiance of each lamp relative to that of lamp # 2. In general, the ratio shows a greater reduction in lamp output at lower wavelengths compared to higher wavelengths.

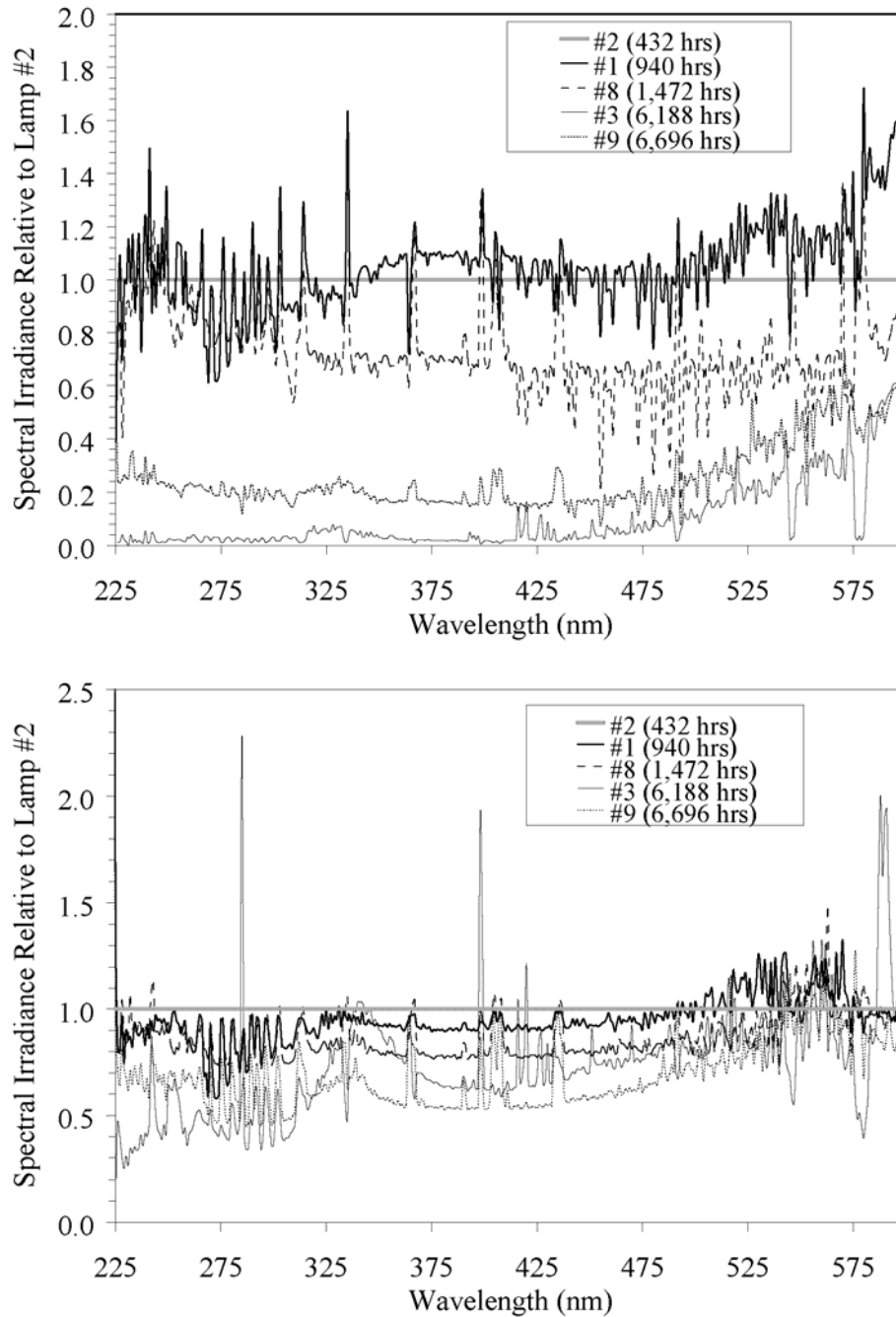


Figure 4.24 Spectral output of LPHO lamps relative to the output of lamp # 2 at the lamp end (upper graph) and middle (lower graph)

Figure 4.25 shows the UV output at 254 nm as a function of location along the length of a new LPHO lamp. Typically, UV irradiance models for UV lamps assume a uniform output along the length of the lamp. However, the data in Figure 4.26 shows that the output of new LPHO lamps is non-uniform along the length. The output peaks at a location approximately 6.0 cm from each lamp end. The output in the middle of the lamp is about 91 percent of the average output of these two peaks. The output also drops significantly at a location 25 cm from the lamp ends due to the mercury amalgams blocking the UV output from the lamp.

Figures 4.26, 4.28, 4.30 and 4.32 show photographs of the aged LPHO lamps viewed from different locations about the lamp's circumference. The photographs show the four mercury amalgams attached to the inside wall of the lamps at locations 25 cm the lamp ends. The photographs also show an increase in lamp end darkening and discoloration along the length of the lamp as the lamps age. With Figure 4.32, the photograph of the lamp with 6,696 operating hours also shows more discoloration near the amalgams.

Figures 4.27, 4.29, 4.31 and 4.33 show the UV output of these lamps at 254 nm as a function of location along the length of the lamp and about the circumference. The UV output along the length of lamps #2 (432 hrs), #1 (940 hrs), and # 8 (1,472 hrs) shows peak UV output at a locations along the length that are 10 to 12 cm from the lamp ends and lower output in the middle. The peak with the aged lamps was further from the lamp ends with the aged lamps compared to the new lamp.

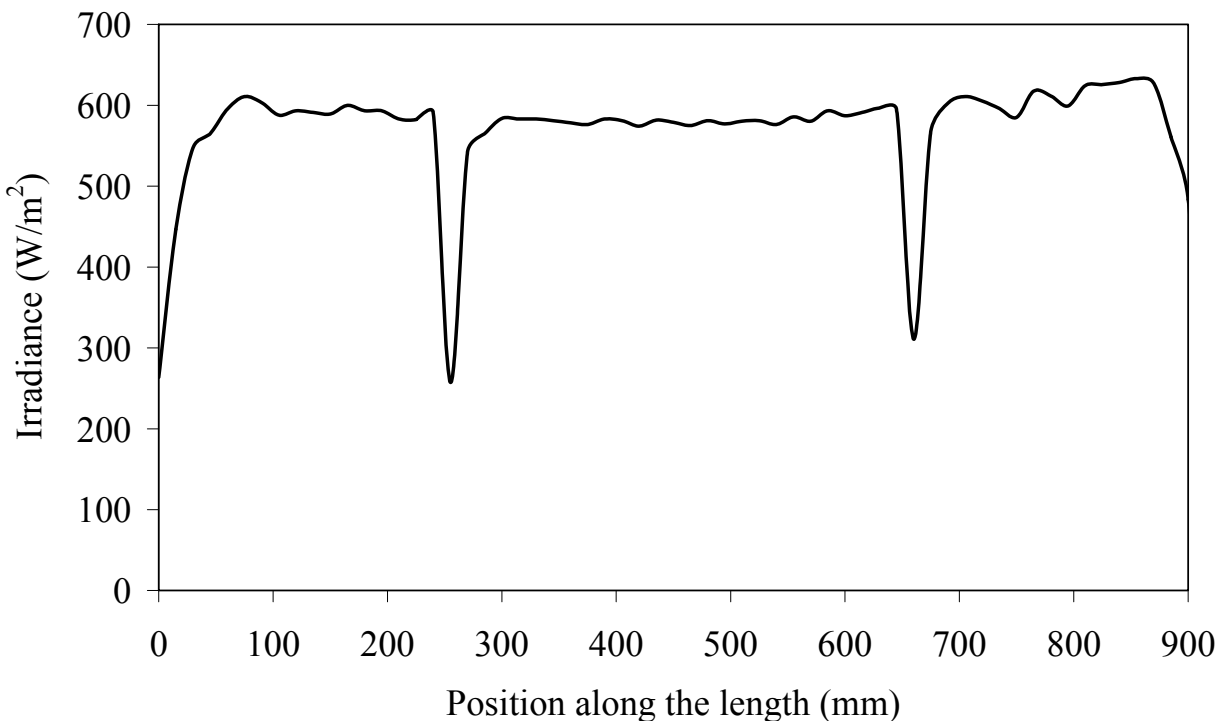


Figure 4.25 UV output at 254 nm of a new amalgam LPHO lamp as a function of position along the length of the lamp

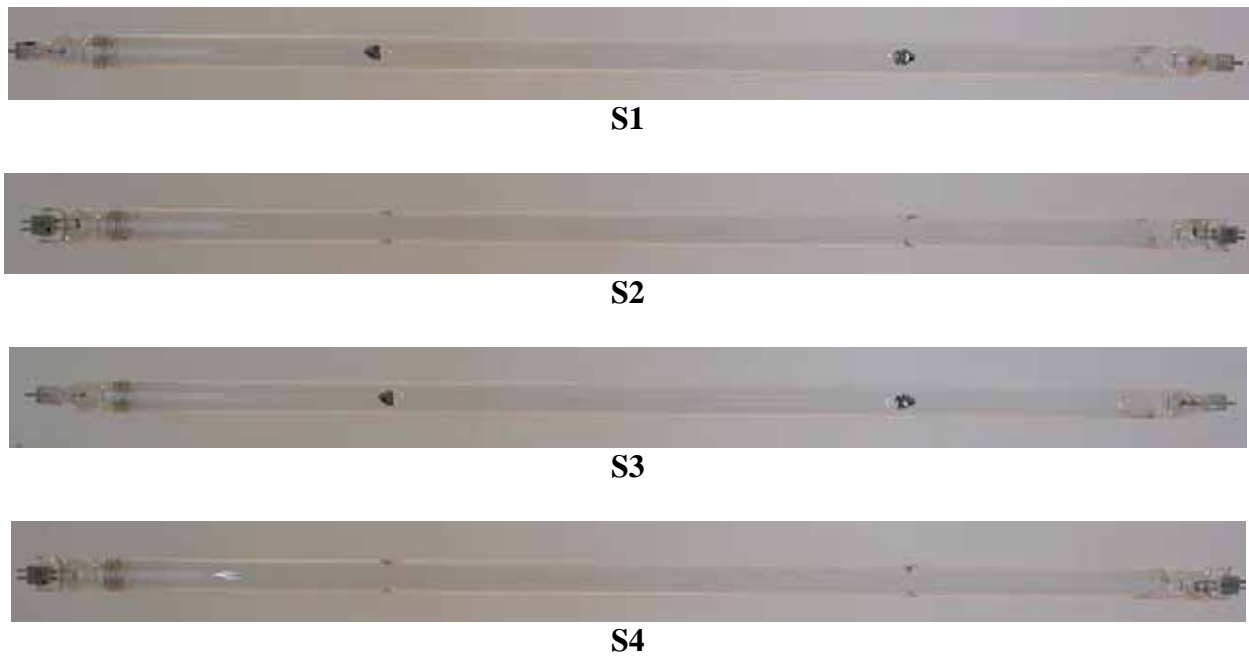


Figure 4.26 LPHO lamp #2 (432 hours) viewed from four locations about its circumference

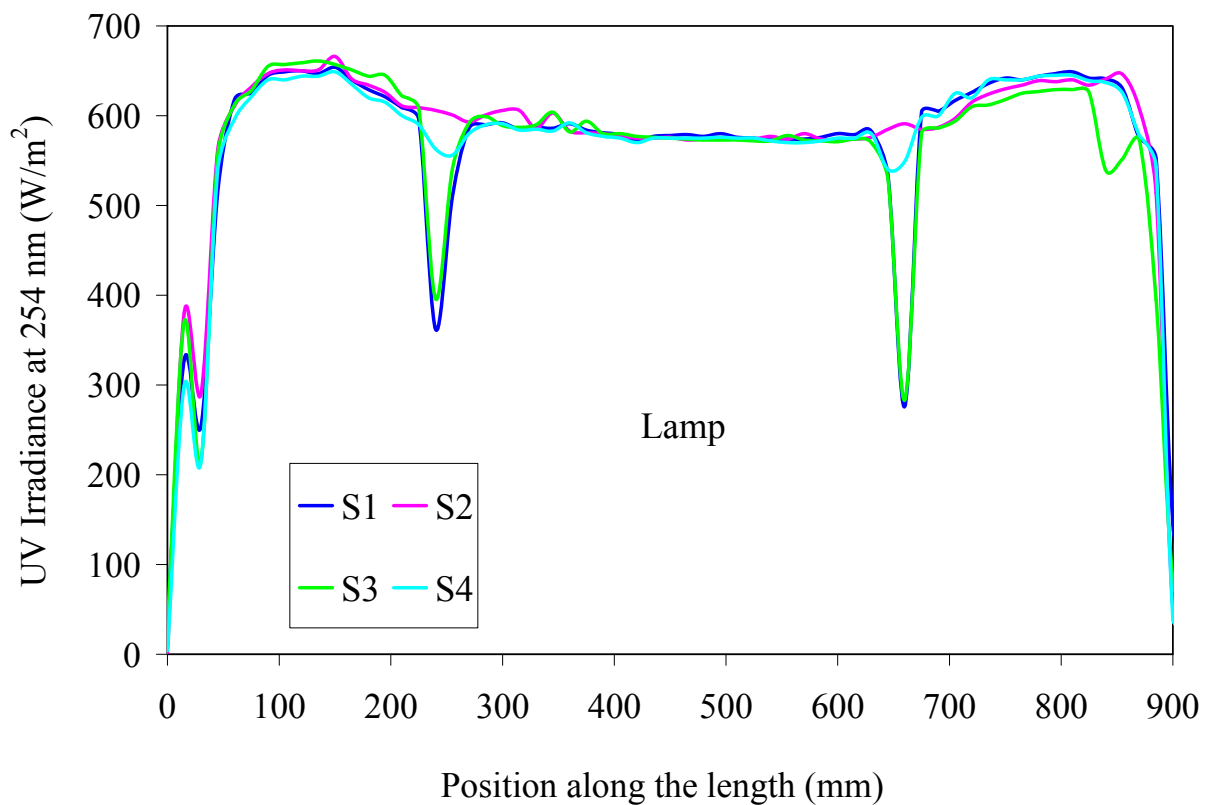


Figure 4.27 UV output at 254 nm of LPHO lamp #2 (432 hours) as a function of position along the length and around the circumference of the lamp

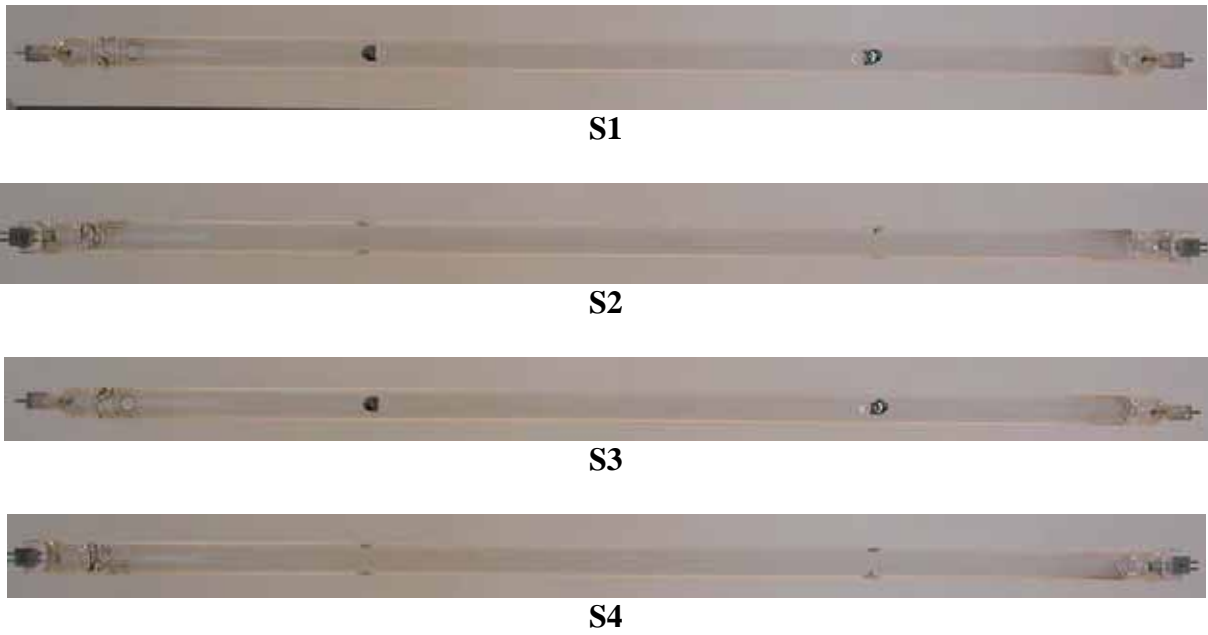


Figure 4.28 LPHO lamp #1 (940 hours) viewed from four locations about its circumference

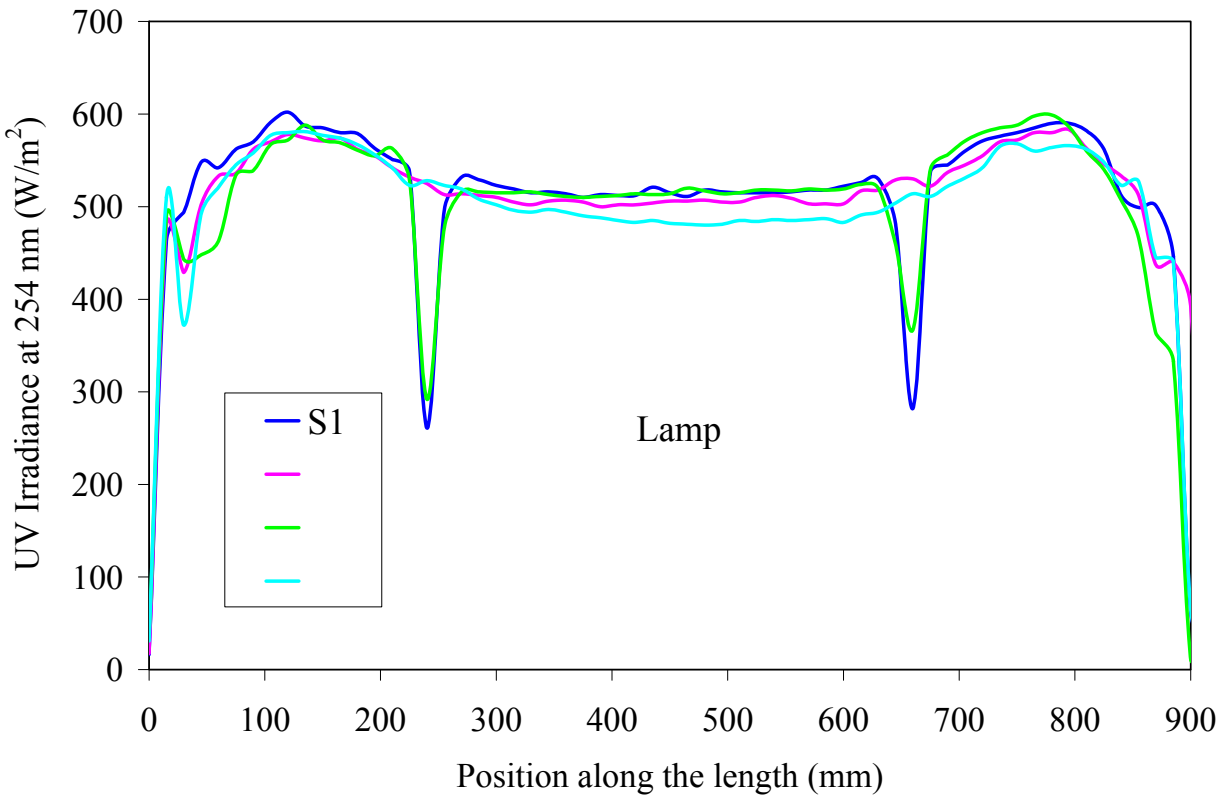


Figure 4.29 UV output at 254 nm of LPHO lamp #1 (940 hours) as a function of position along the length and around the circumference of the lamp

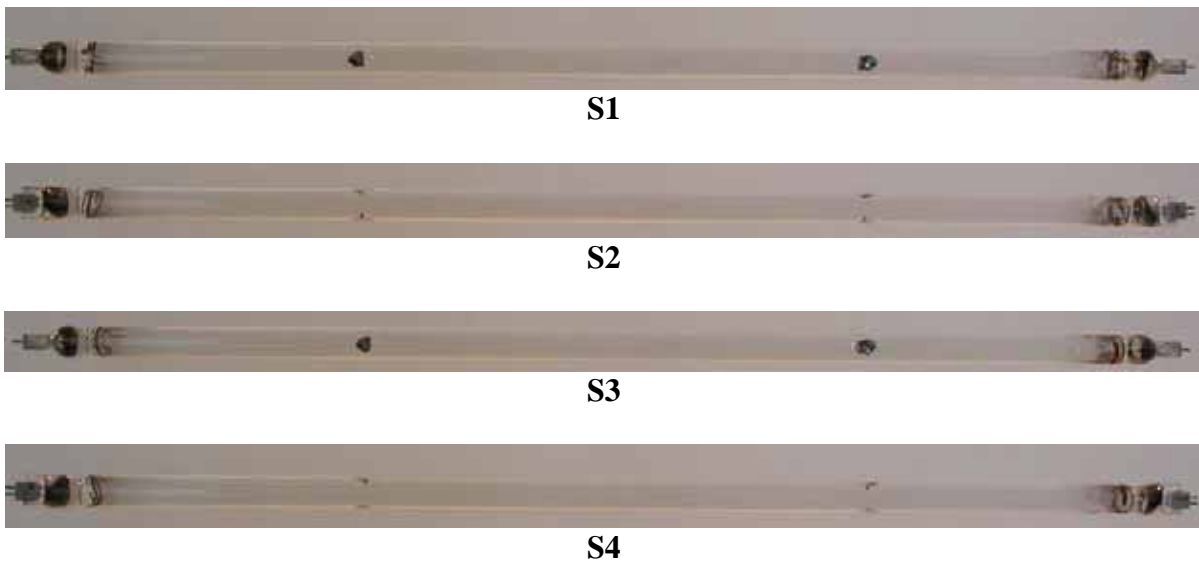


Figure 4.30 LPHO lamp #8 (1,472 hours) viewed from four locations about its circumference

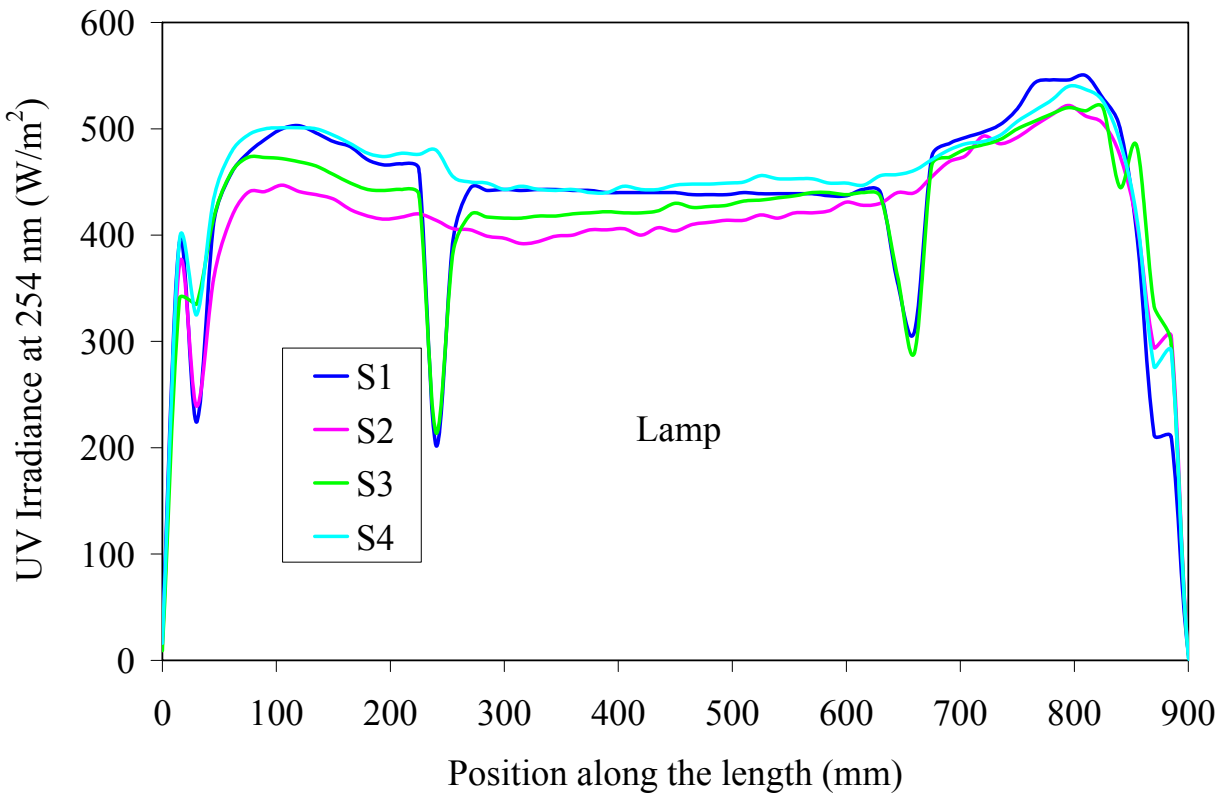


Figure 4.31 UV output at 254 nm of LPHO lamp #8 (1,472 hours) as a function of position along the length and around the circumference

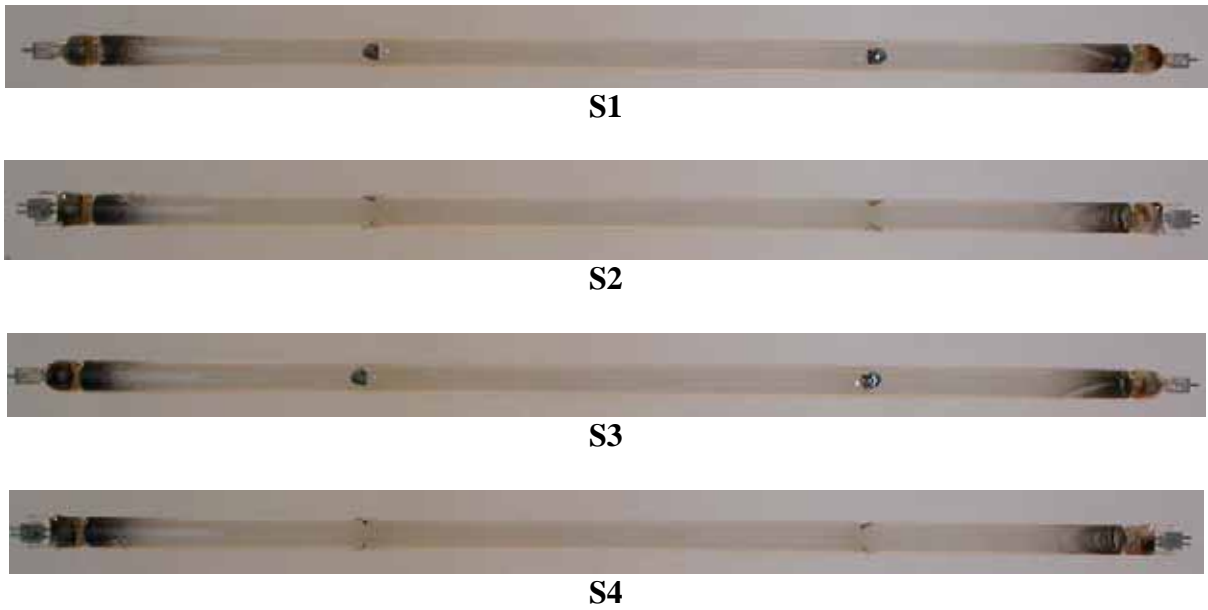


Figure 4.32 LPHO lamp #9 (6,696 hours) viewed from four locations about its circumference

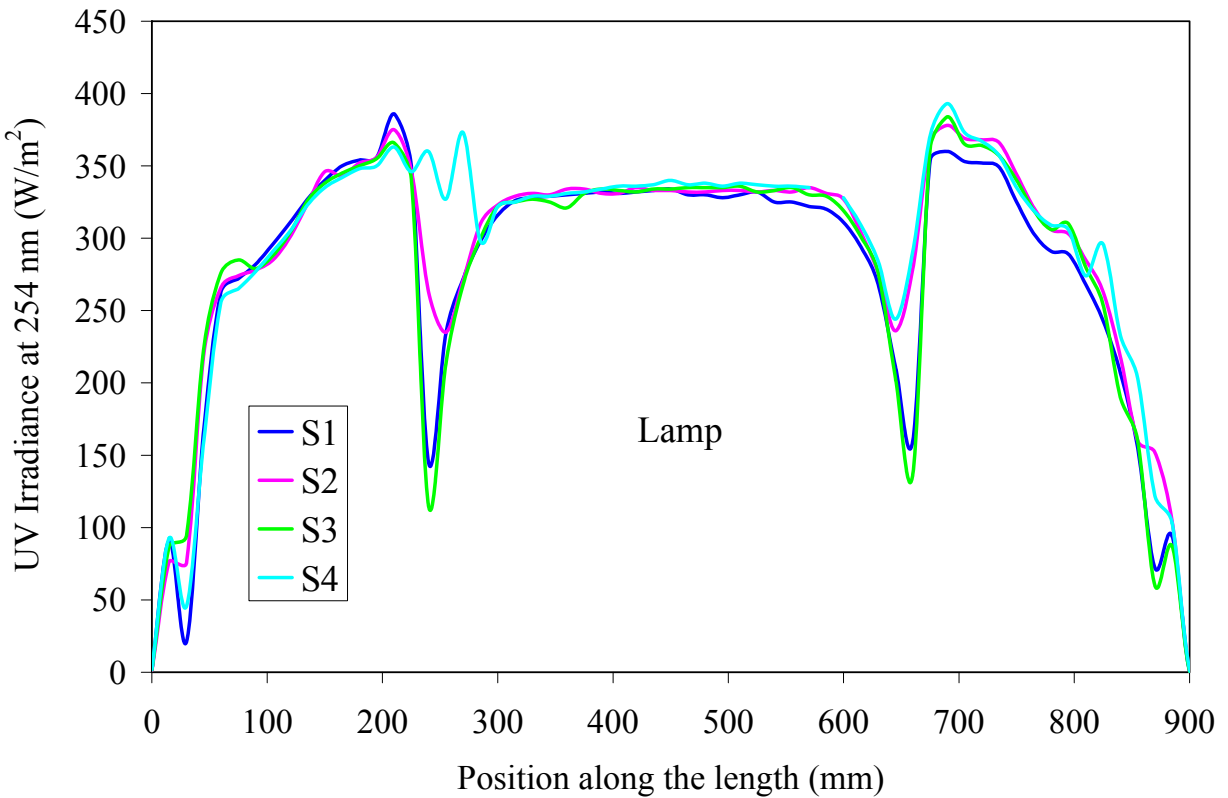


Figure 4.33 UV output at 254 nm of LPHO lamp #9 (6,696 hours) as a function of position along the length and around the circumference

Like the new lamps, the aged lamps also show the reduction in UV output at locations 25 cm from the lamp ends caused by the amalgams. These effects are observed with locations S1 and S3 about the circumference but not with location S2. Location S4 shows a slight reduction with lamps #2, #1 and #8 but a significant reduction with lamp #9. Also, the reduction caused by the amalgam affects a longer section of the lamp length with lamp #9 compared to lamps #2, #1 and #8. These results indicate that the region around the amalgam shows a greater reduction in UV output as lamps age. This observation correlates with the observation of greater discoloration in this region with lamp #9.

The UV output about the circumference of the lamps also changes as the lamps age. With lamp #2, the UV output does not significantly vary as a function of location about the circumference except near the amalgams. However, the UV output of lamps #1 and #8 show significant differences as a function of location about the circumference. For example, the UV output from locations S2 and S3 is notably lower than the UV output from locations S1 and S4 with lamp #8. This impact of lamp aging may be related to the rotational orientation of the lamp when placed within the reactor. However, this orientation was not recorded when the lamps were removed from the reactor.

The UV output from the lamps also shows a significant reduction near the lamp ends as the lamps age. The length of the lamp impacted by end darkening is greater with lamp #9 than lamps #2 and #1. This observation correlates with the increase in lamp end darkening shown in the photographs of these lamps.

Last, the aged lamps show a local peak in lamp output at locations approximately 2 cm from the lamp ends that were not observed with the new lamps. These peaks may be related to the non-uniform nature of the lamp end darkening (see [Figure 4.18](#)).

[Figure 4.34](#) shows the UV irradiance integrated along the length of the lamp as a function of lamp hours. The integrated irradiance is presented relative to the values measured with the new lamp. The integrated irradiance over the full length of lamp (*i.e.*, 0 to 90 cm) decreased as lamp hours increased and was 50 percent of the new lamp integrated irradiance with lamp #9 after 6,696 hrs of operation. The integrated irradiance at the center of the lamp (*i.e.*, 40 to 50 cm) showed a similar reduction with time ending up at 58 percent of the new lamp output with lamp #9 after 6,696 hrs of operation. The integrated irradiance at the peak output (*i.e.*, 7 to 15 cm and 75 to 83 cm) appeared to increase and then decrease with time, ending up at a similar level with lamp #9 as the total integrated irradiance. The integrated irradiance at the lamps ends (*i.e.*, 0 to 5 cm and 85 to 90 cm) shows greater aging over time than all other locations, reflecting the impact of end darkening.

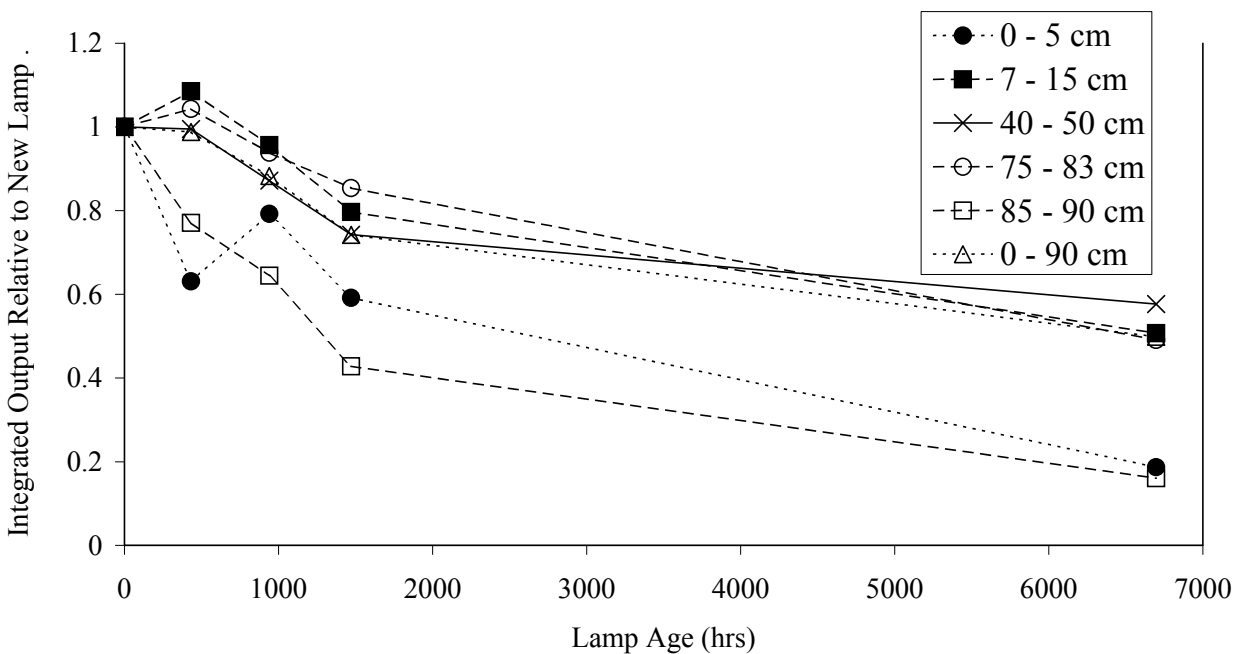


Figure 4.34 Relative integrated irradiance along the length of the lamp as a function of lamp hours

MEDIUM PRESSURE LAMPS - TYPE 1

One new lamp and two aged MP lamps obtained from the UV installation at Bowling Green, Ohio were selected for analysis. The aged lamps had been operating for 3,266 and 4,098 hours, respectively. Figure 4.35 shows photographs of the lamps. The lamp assembly includes two ceramic spacers to control the radial position of the lamp within a quartz sleeve and a lamp wire to allow the lamp to be operated with electrical connections at one end of the lamp assembly. The aged lamps were selected for analysis because they showed darkened ends and lamp envelope fouling.

The new lamp had a clear lamp envelope without any marks or spots, clean metallic contacts, and a straight lamp wire. Figure 4.36 shows the spectral output of the new lamp from 200 to 400 nm measured along the length of the lamp (L1 – L5) for location C2 about the circumference. At location C2, the spectral irradiance showed no dependence on distance along the length of the lamp.

Figure 4.37 shows the integrated irradiance in the UVA, UVB and UVC ranges and the germicidal irradiance from 225 to 400 nm as a function of location along the length of the new lamp for location C2. The germicidal irradiance is based on the action spectra of MS2 phage (Rauth 1965). The UVA range is defined as wavelengths from 315 to 400 nm, the UVB range is defined from 280 to 315 nm, and the UVC range is defined from 200 to 280 nm. The integrated irradiance shows a slight dependence on location along the length of the lamp with lower irradiance at location L1. The dependence may be an artifact of the measurement. The UVA, UVB, UVC, and germicidal UV were 25, 28, 47, and 36 percent of the total UV energy from 200 to 400 nm, respectively.



Figure 4.35 Type 1 MP lamps analyzed: full view (top photo) and close-up (bottom photo). Lamp ages are, from top to bottom: 0, 3,266, and 4,098 hours, respectively

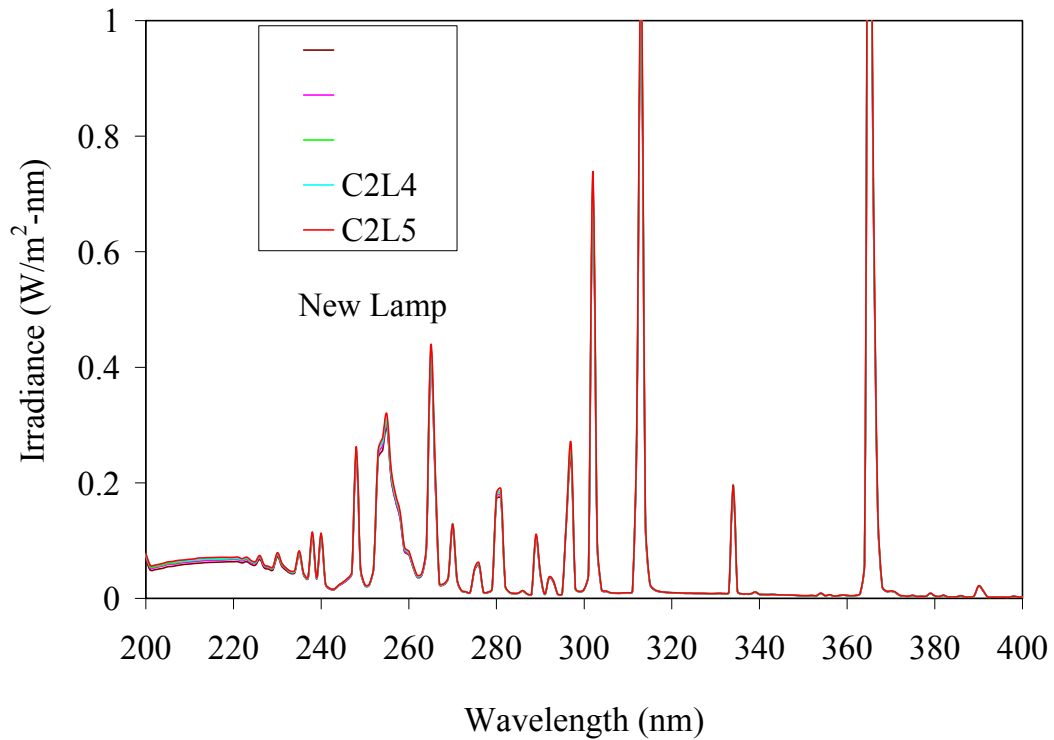


Figure 4.36 Spectral irradiance of the new Type 1 MP lamp as a function of location along the lamp length at location C2

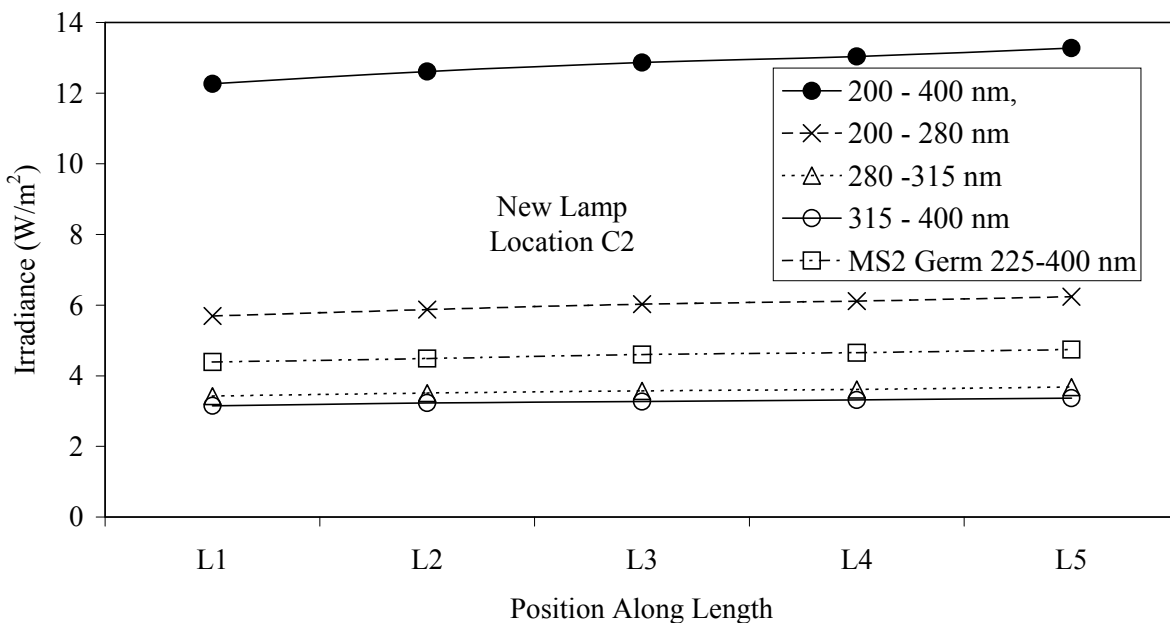


Figure 4.37 Integrated and germicidal irradiance of the new Type 1 MP lamp as a function of position along the lamp length for location C2

Figure 4.38 shows photographs of the aged Type 1 MP lamp #10 with 3,266 hours of operation from different locations about the circumference of the lamp. The lamp showed end darkening at both ends and irregular discoloration at the middle. The end darkening on the power supply side of the lamp showed a distinct transition from the darkened to the clear region while the darkened region on the other side showed a less distinct transition. A white discoloration (“powder” spot) on the lamp envelope about 2.0 cm in size was also observed (Figure 4.39).

Figure 4.40 shows the spectral irradiance of lamp #10 as a function of location along the length of the lamp for locations C1, C2, C3, and C4 about the circumference. The data shows that the aged lamp emits less UV light than the new lamp. The data also shows that the lower wavelengths show greater reduction relative to the new lamp than the higher wavelengths. Last, the spectral output varies as a function of position along the length of the lamp and about the circumference.

Figure 4.41 shows the integrated irradiance in the UVA, UVB and UVC ranges and the germicidal irradiance from 225 to 400 nm as a function of location along the length of lamp #10 for location C1. The UVA, UVB, UVC, and germicidal UV were 31, 31, 38, and 32 percent of the total UV energy from 200 to 400 nm, respectively. Compared to the new lamp, this data indicates a significant spectral shift as the lamp ages.

Figure 4.42 shows the germicidal irradiance as a function of location along the length of lamp #10 for locations C1 to C4. The germicidal UV irradiance does not show any significant dependence on location along the length of the lamp. Figure 4.43 shows the germicidal irradiance as a function of location about the circumference for locations L1 to L5. In this case, the germicidal irradiance shows a strong dependence on the location about the circumference of the lamp with location C4 reading the highest and C2 the lowest. The data indicates that the rate

of lamp aging varies depending on the location about the circumference of the lamp. This may be related to deflection of the arc caused by electromagnetic fields and/or convection current within the lamp.



Position C1



Position C2



Position C3



Position C4

Figure 4.38 Photographs of the Type 1 MP lamp #10

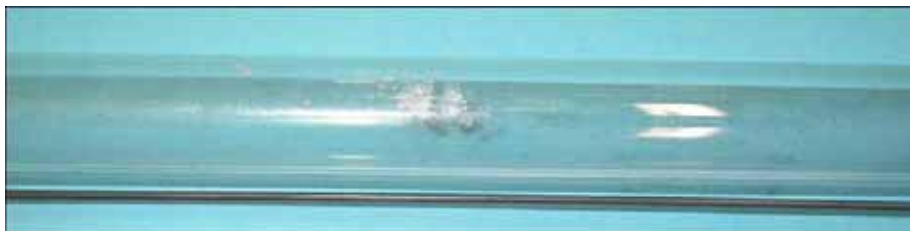


Figure 4.39 Close up of the "powder" spot

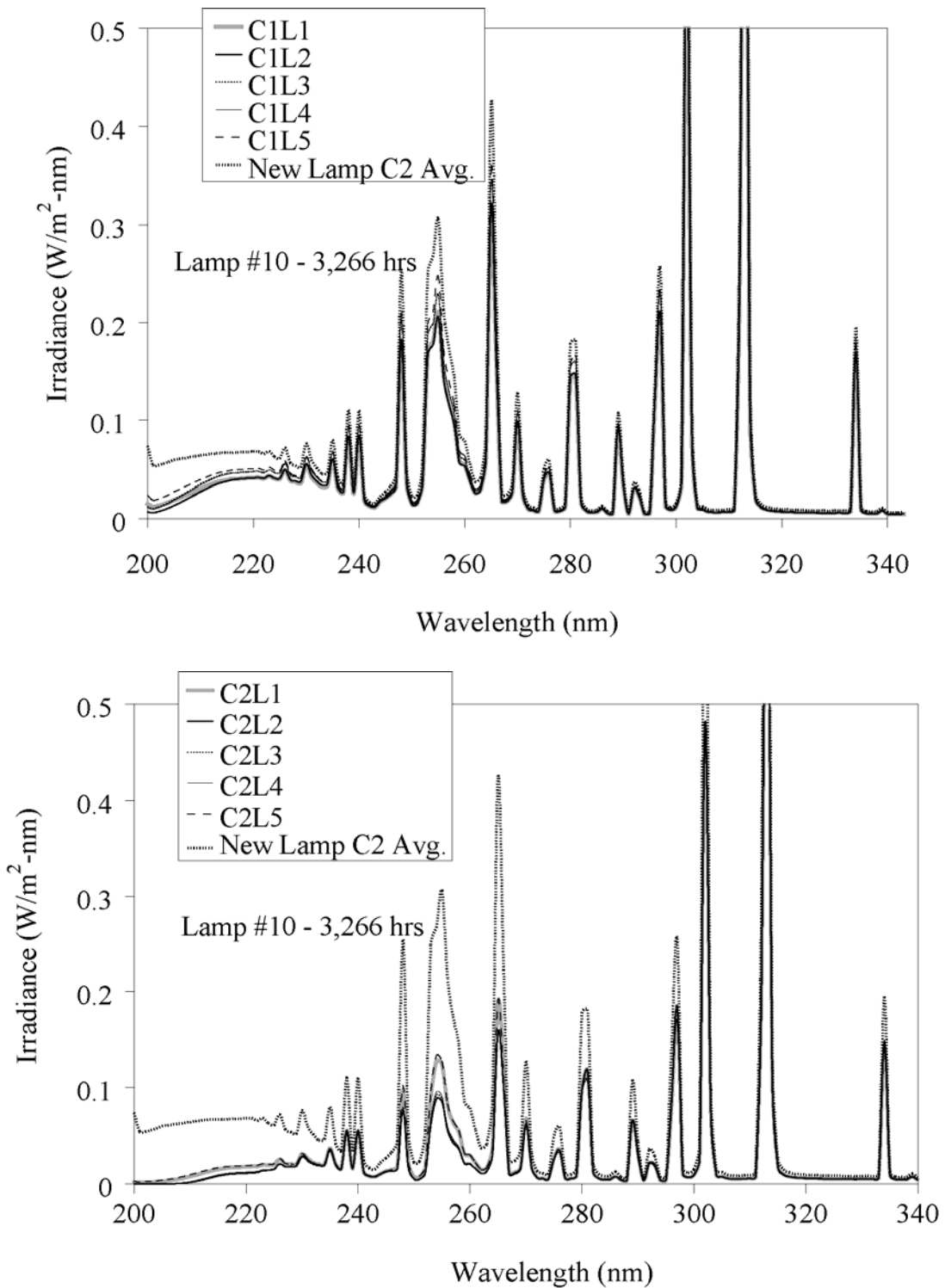


Figure 4.40 Spectral irradiance of Type 1 MP lamp #10 as a function of location along the lamp length and around the circumference (C1 - top, C2 - bottom)

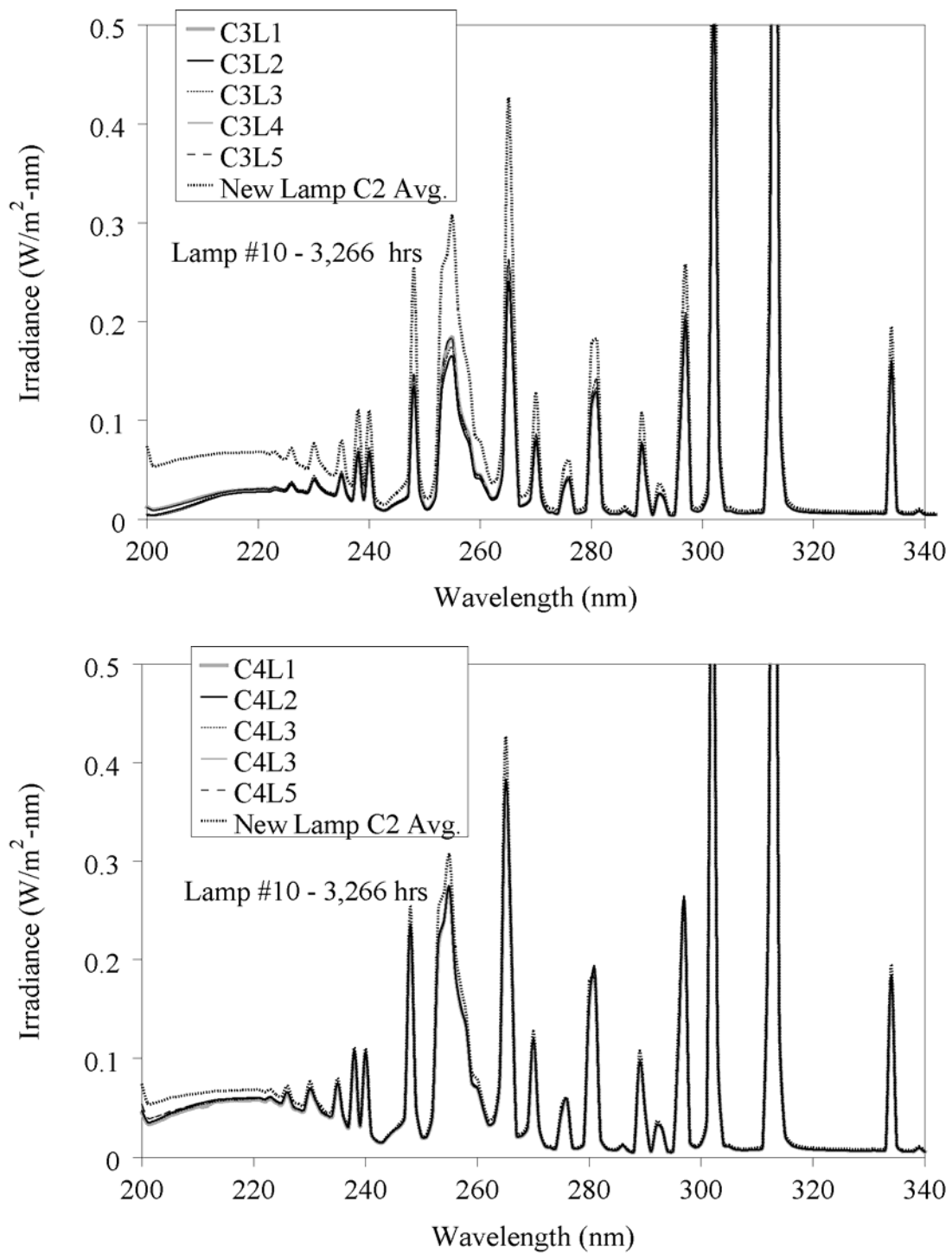


Figure 4.40 (Continued) Spectral irradiance of Type 1 MP lamp #10 as a function of location along the lamp length and around the circumference (C3 - top, C4 - bottom)

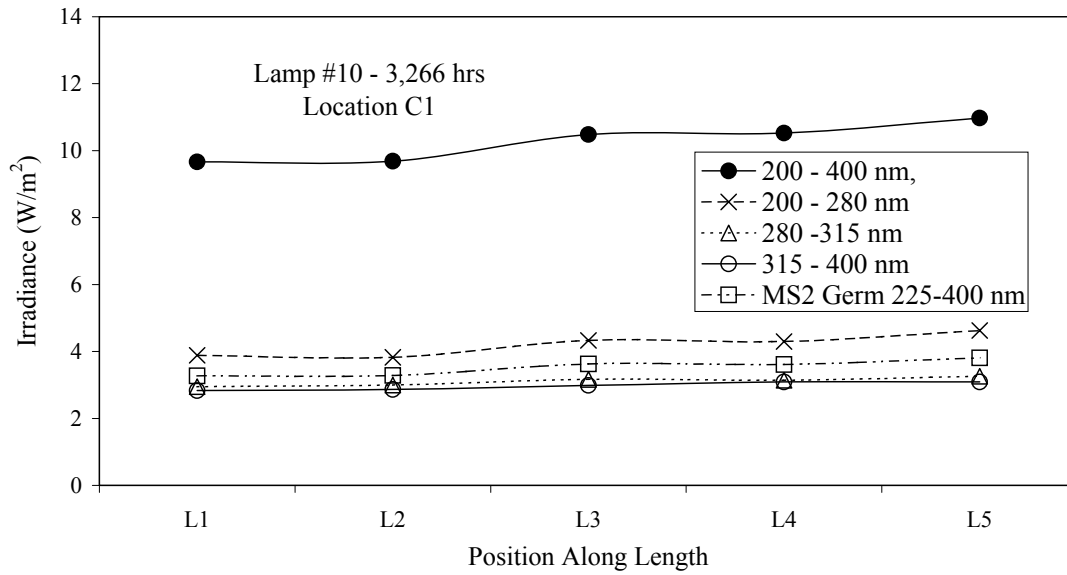


Figure 4.41 Integrated and germicidal irradiance of the aged Type 1 MP lamp #10 as a function of position along the lamp length at location C1

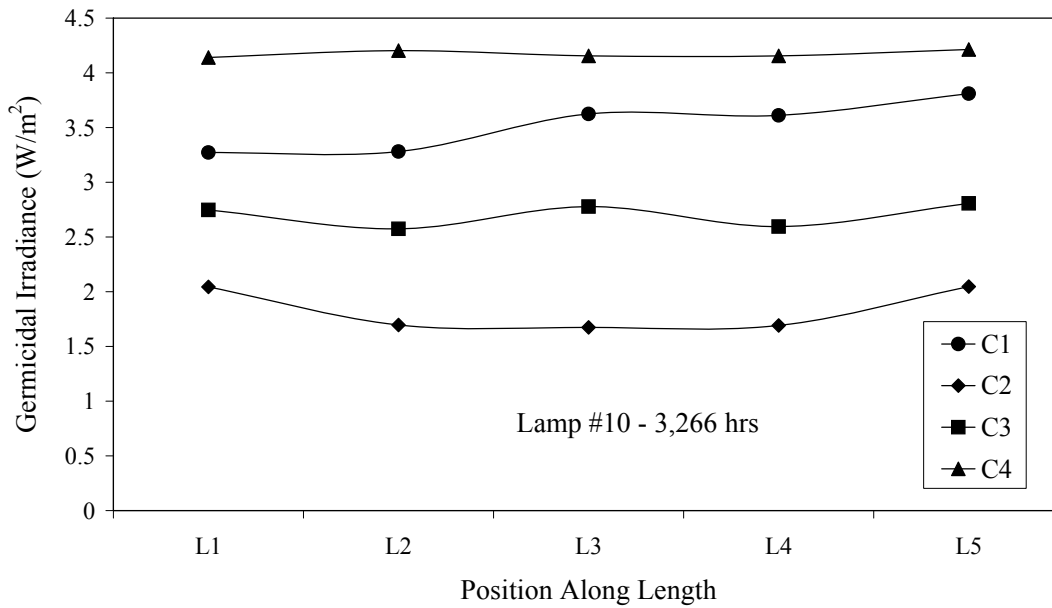


Figure 4.42 Germicidal irradiance of the aged Type 1 MP lamp #10 as a function of position along the lamp length

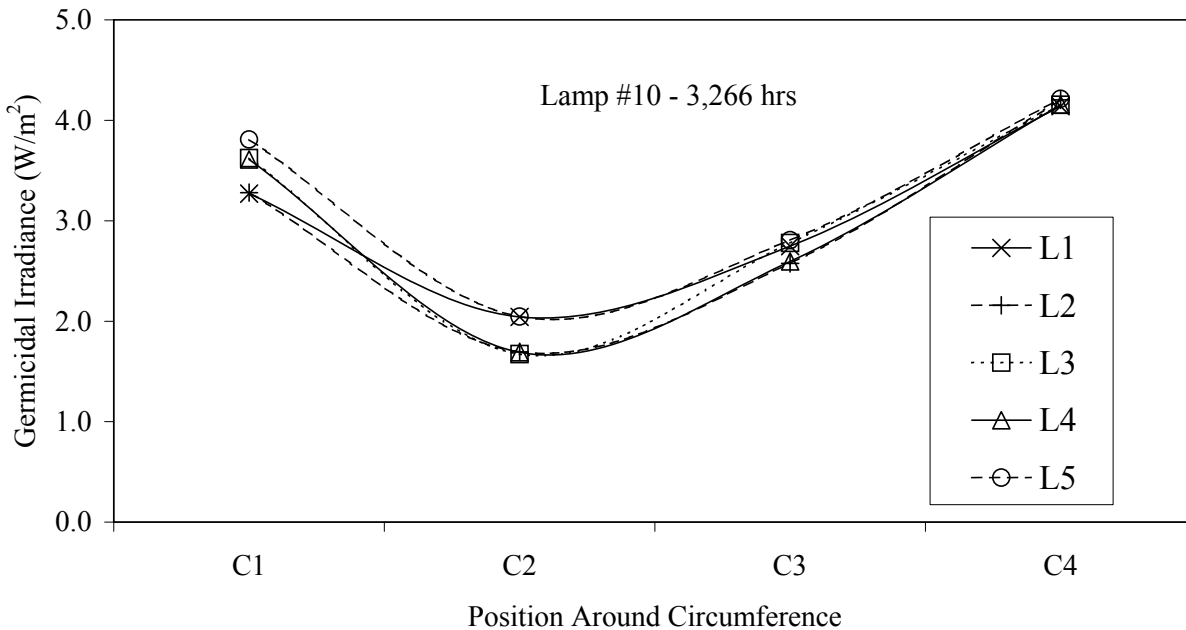
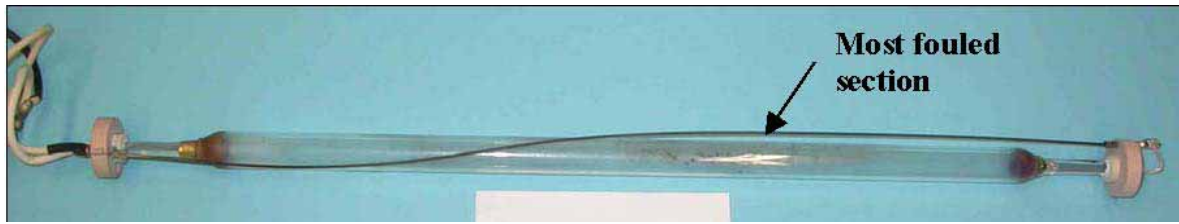


Figure 4.43 Germicidal irradiance of the aged Type 1 MP lamp #10 as a function of position about the circumference

Figure 4.44 shows photographs of the aged Type 1 MP lamp #8 with 4,098 hours of operation from different locations about the circumference of the lamp. The lamp showed end darkening at both ends. The darkened end on the supply side showed a distinct transition from the darkened to clear region while the other side showed a less distinct transition. On the power supply side, the envelope beyond the electrode had a non-transparent discoloration (see Figure 4.46) that covered about 3/4 of circumference (position C3L5 is not affected) and gradually disappeared ~3.5 cm from the end. The middle part of the lamp envelope had an irregular grey discoloration (see Figure 4.45) on the inner side for almost half of the lamp length (L3 - L5) and almost half of the circumference (C1 and C4). The most visibly discolored sections of the lamp were locations C1L3 to C1L5. Three small white “powder” spots were visible on the edge of the darkened part on the power supply side. The outer wire was twisted, so it was not possible to keep it out of sight in all length and circumference positions during measurements of irradiance. In the C1 orientation, the wire crossed in front of the lamp at approximately 1/3 of the lamp length from the power supply side. In the C4 orientation, the wire crossed in front of the lamp at approximately 1/5 of the lamp length from the power supply side (closest to the length position L1).

Figure 4.47 shows the spectral irradiance of lamp #8 as a function of location along the length of the lamp for locations C1, C2, C3, and C4 about the circumference. Similar to lamp #10, lamp #8 emits less UV light than the new lamp, shows greater reduction relative to the new lamps at lower wavelengths, and has a spectral output that varies as a function of position along the length of the lamp and about the circumference.



Position C1



Position C2



Position C3



Position C4

Figure 4.44 Photographs of the Type 1 MP lamp #8



Figure 4.45 Close up on the most fouled section of Type 1 MP lamp #8 (Position C1)



Figure 4.46 Close up of the coated end of Type 1 MP lamp #8 on the power supply side

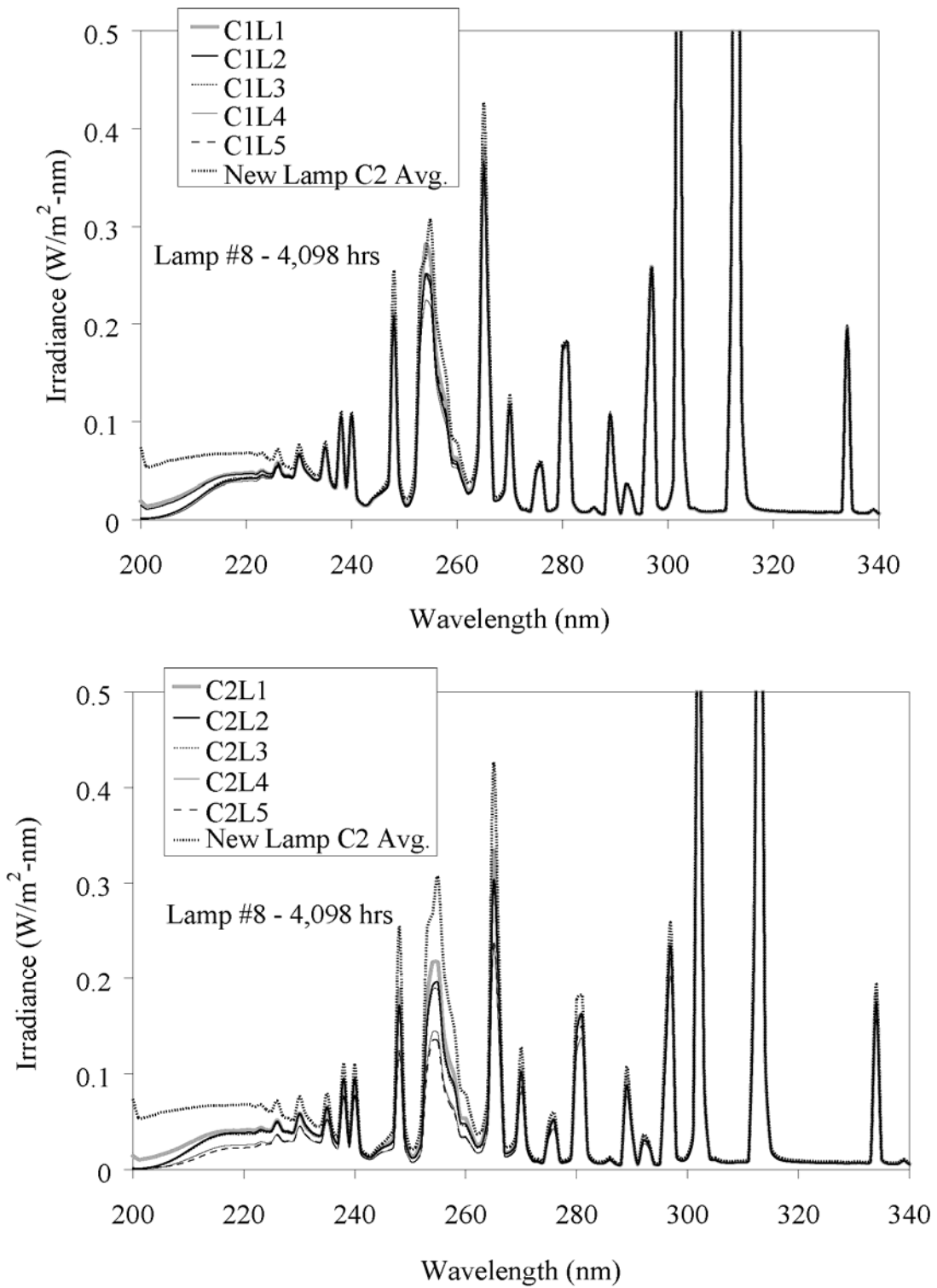


Figure 4.47 Spectral irradiance of Type 1 MP lamp #8 as a function of location along the lamp length and around the circumference (C1 - top, C2 - bottom)

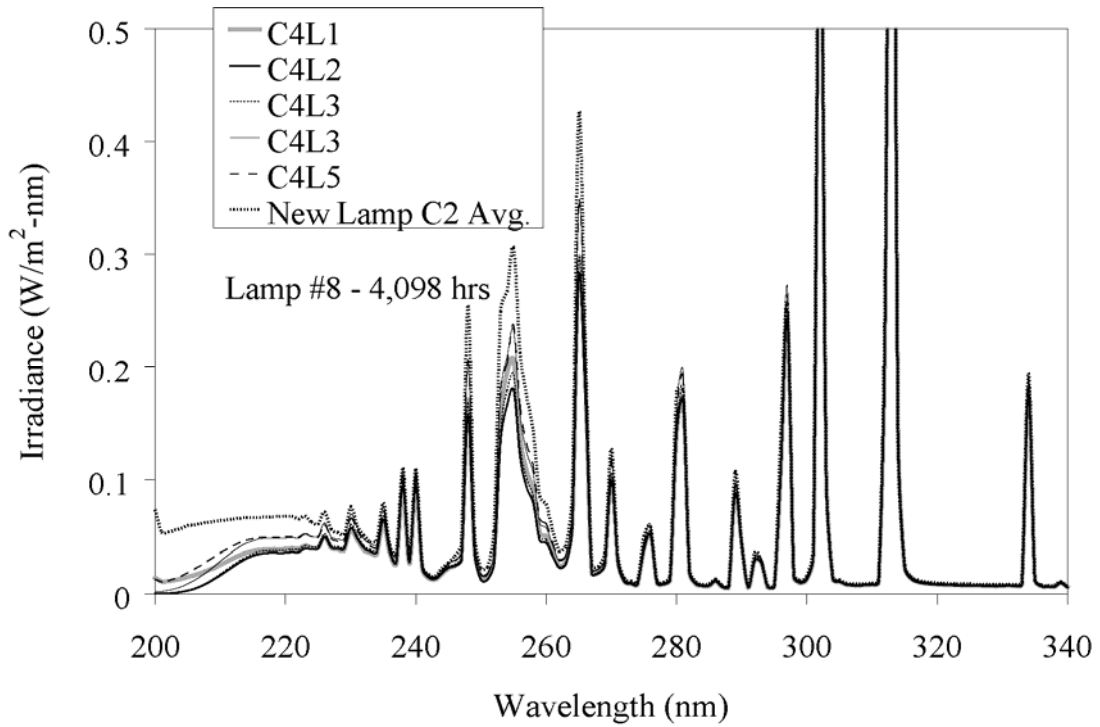
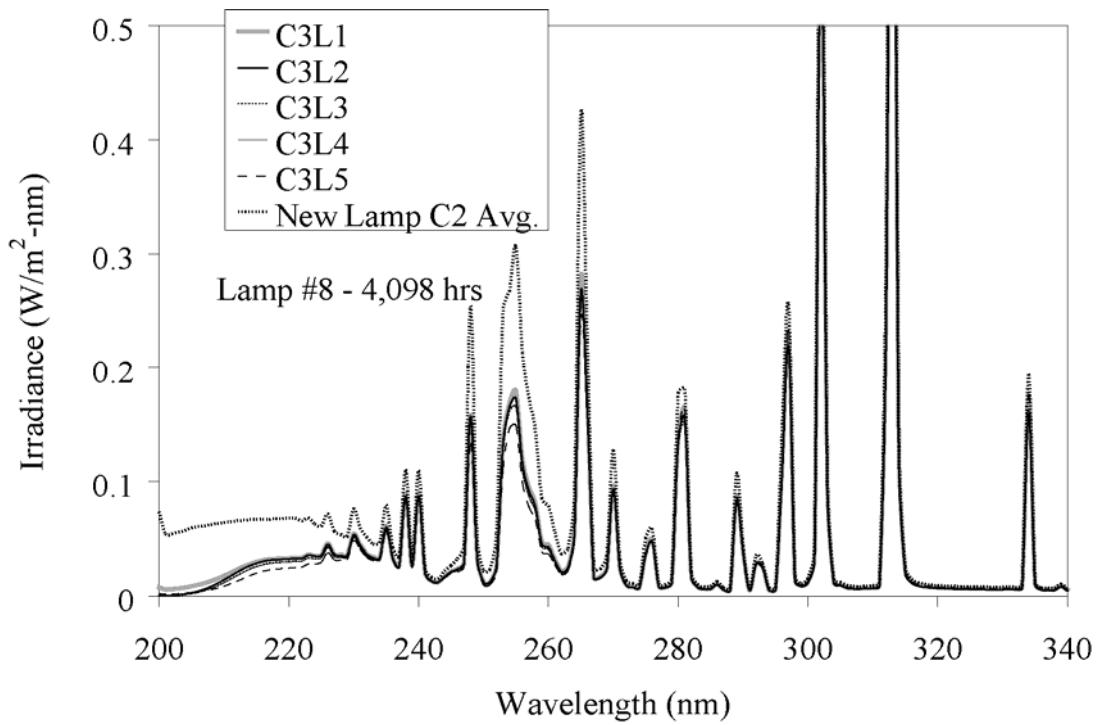


Figure 4.47 (Continued) Spectral irradiance of Type 1 MP lamp #8 as a function of location along the lamp length and around the circumference (C3 - top, C4 - bottom)

Figure 4.48 shows the integrated irradiance in the UVA, UVB and UVC ranges and the germicidal irradiance from 225 to 400 nm as a function of location along the length of lamp #8 for location C1. Similar to lamp #10, the UVA, UVB, UVC, and germicidal UV were 31, 32, 37, and 33 percent of the total UV energy from 200 to 400 nm, respectively. Compared to the new lamp, this data indicates a significant spectral shift as the lamp ages.

Figure 4.49 shows the germicidal irradiance as a function of location along the length of lamp #8 for locations C1 to C4. Unlike lamp #10, the germicidal UV irradiance with lamp #8 at locations C2 and C4 varied along the length of the lamp. Figure 4.50 shows the germicidal irradiance as a function of location about the circumference for locations L1 to L5. The germicidal irradiance shows a strong dependence on the location about the circumference of the lamp with locations C1 and C4 reading the highest and locations C2 and C3 the lowest. Again, the data indicates that the rate of lamp aging varied depending on the location about the circumference of the lamp.

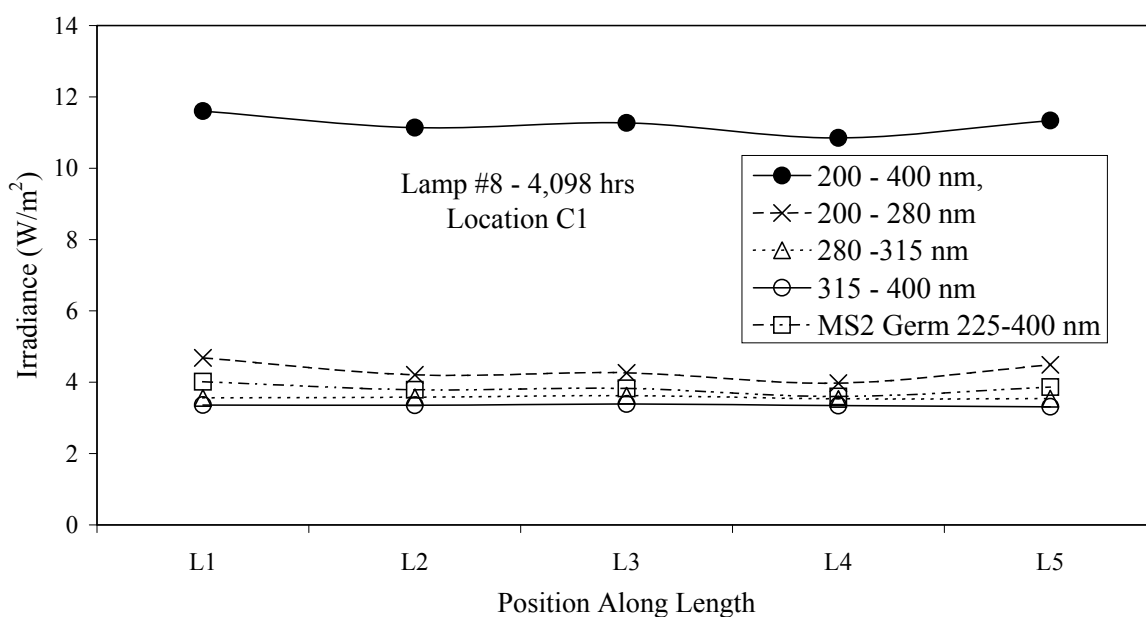


Figure 4.48 Integrated and germicidal irradiance of the aged Type 1 MP lamp #8 as a function of position along the lamp length at location C1

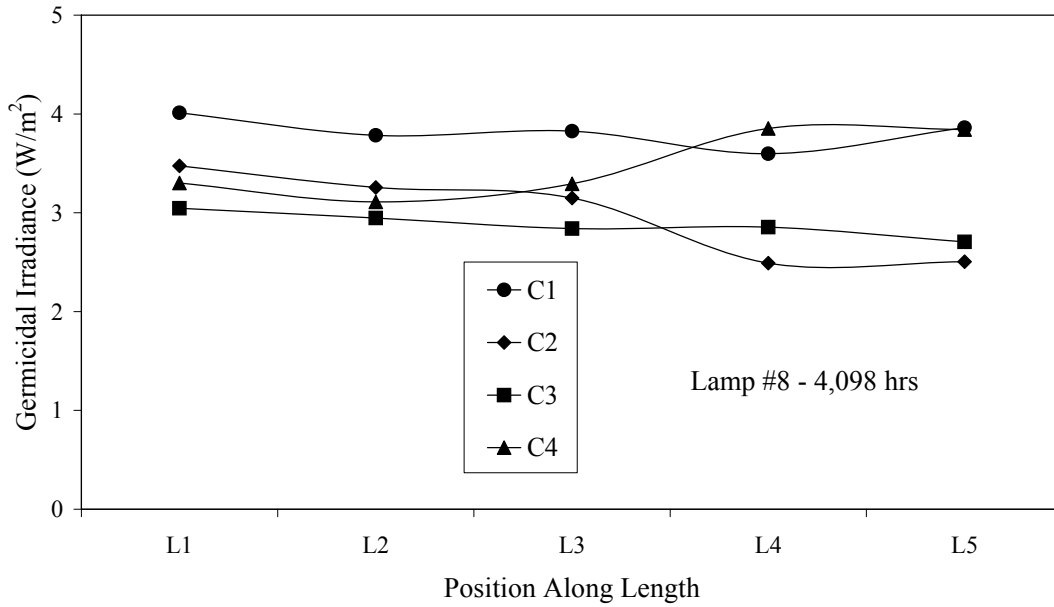


Figure 4.49 Germicidal irradiance of the aged Type 1 MP lamp #8 as a function of position along the lamp length

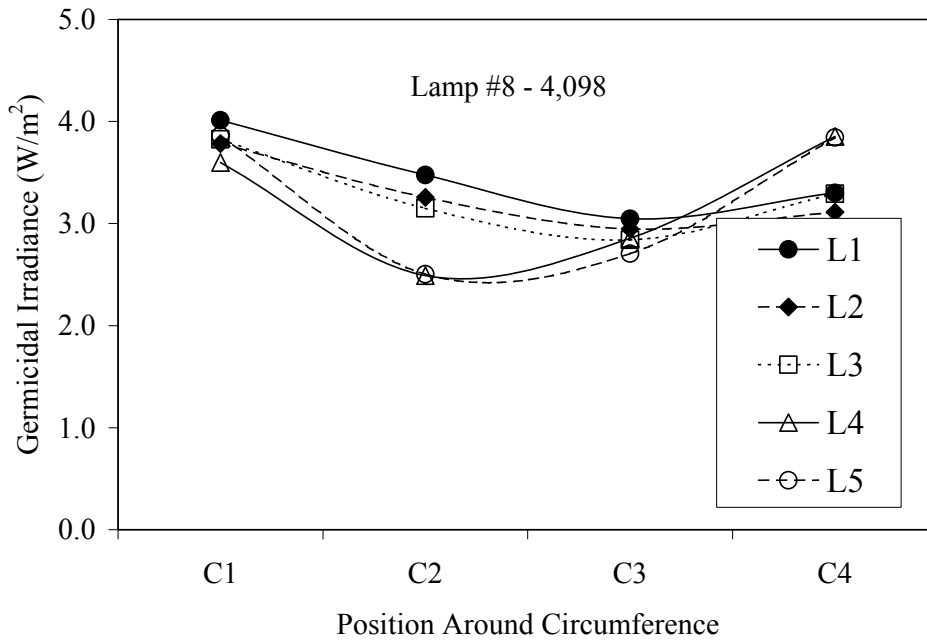


Figure 4.50 Germicidal irradiance of the aged Type 1 MP lamp #8 as a function of position about the circumference

Figure 4.51 shows the ratio of the UV irradiance measured with each aged lamp to that measured with the new lamp as a function of wavelength. The ratio indicates that the UV output of the Type 1 MP lamps experience a significant spectral shift as they age, with lower wavelengths in general aging faster than higher wavelengths. The ratio also shows greater aging from 254 - 265 nm compared to 235 - 245 nm. This observation may be related to the optical characteristics of the discoloration on the lamp envelope.

Figure 4.52 shows the germicidal output of the three Type 1 MP lamps as a function of operating hours. The germicidal output is calculated as the average of all measured positions. The data shows a relative lamp output of 61 percent at 4,000 hours.

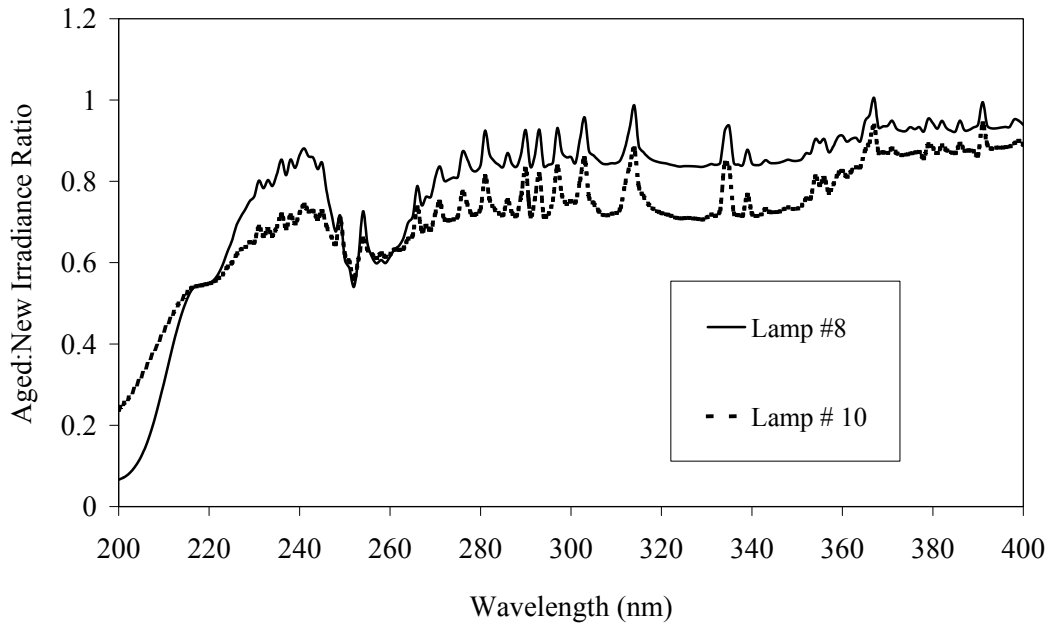


Figure 4.51 Ratio of UV irradiance measured with old Type 1 MP lamps to that measured with new lamps as a function of wavelength

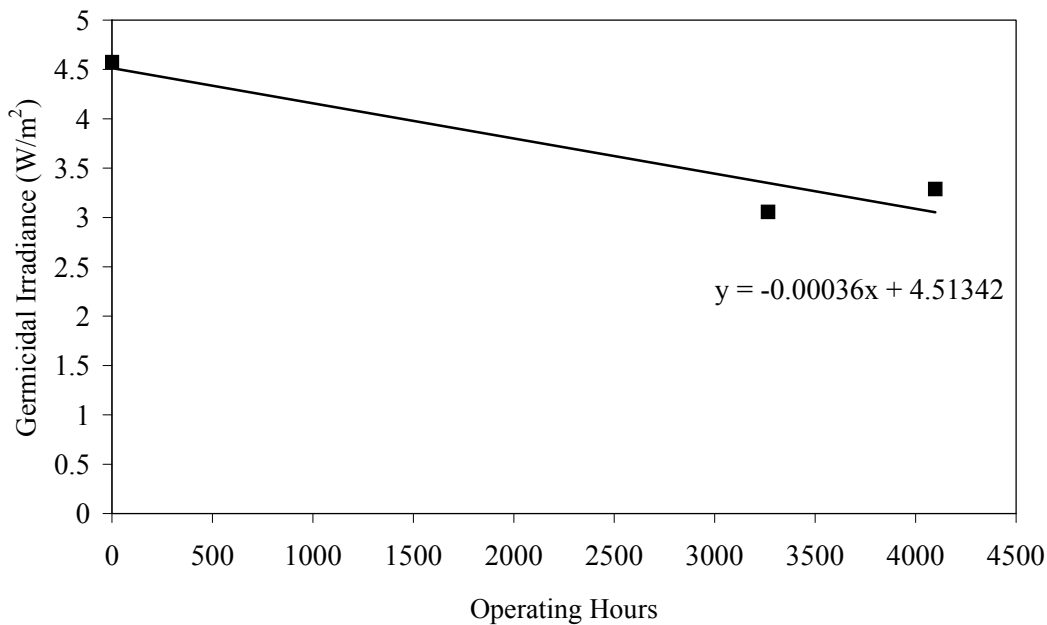


Figure 4.52 Germicidal irradiance as a function of operating hours with Type 1 MP lamps

MEDIUM PRESSURE LAMPS - TYPE 2

Four MP lamps designated as Type 2 lamps were obtained from UV systems used to treat wastewater. One new lamp and one aged lamp with 4,001 hours of operation were obtained from Daytona Beach, Fla. and two aged lamps with 2,361 and 2,292 hours of operation were obtained from Santa Rosa, Calif. The aged lamps were selected for analysis because they showed a combination of end darkening, resonant darkening and distortion, and lamp envelope fouling.

Figure 4.53 shows a photograph of the new lamp. The lamps were rated at ~3 kW at 100 percent power consumption and had an arc length of ~25 cm. The lamp assembly uses two ceramic spacers at each end to control the radial position of the lamp within a quartz sleeve. Two solid wires connect the ceramic spacers, one of which is used to provide electrical energy to one of the lamp electrodes thereby allowing the lamp to be operated with electrical connections at one end of the lamp assembly. The new lamp had a clear envelope without any discoloration or markings.

Figure 4.54 shows the spectral output of the new lamp from 200 to 400 nm measured along the length of the lamp (L1 – L5) for location C2 about the circumference. The spectral irradiance at location L1 was notably lower than the spectral irradiance at the other locations. Figure 4.55 shows the integrated irradiance in the UVA, UVB and UVC ranges and the germicidal irradiance from 225 to 400 nm as a function of location along the length of the lamp for location C1. The integrated irradiance also shows lower irradiance at location L1 in all wavelength ranges. The UVA, UVB, UVC, and germicidal UV were 23, 26, 51, and 37 percent of the total UV energy from 200 to 400 nm, respectively. These ratios are very similar to those observed with the new Type 1 MP lamp.

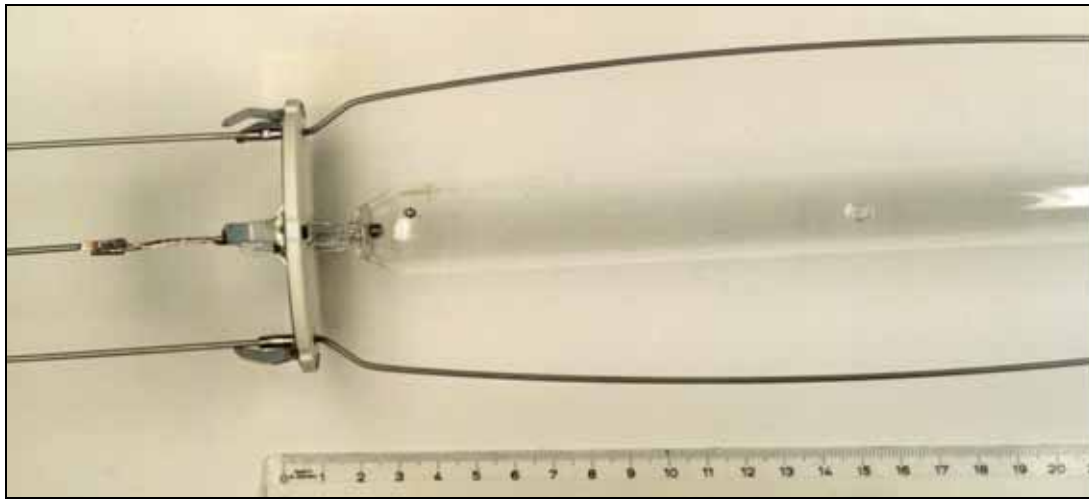


Figure 4.53 New Type 2 MP lamp

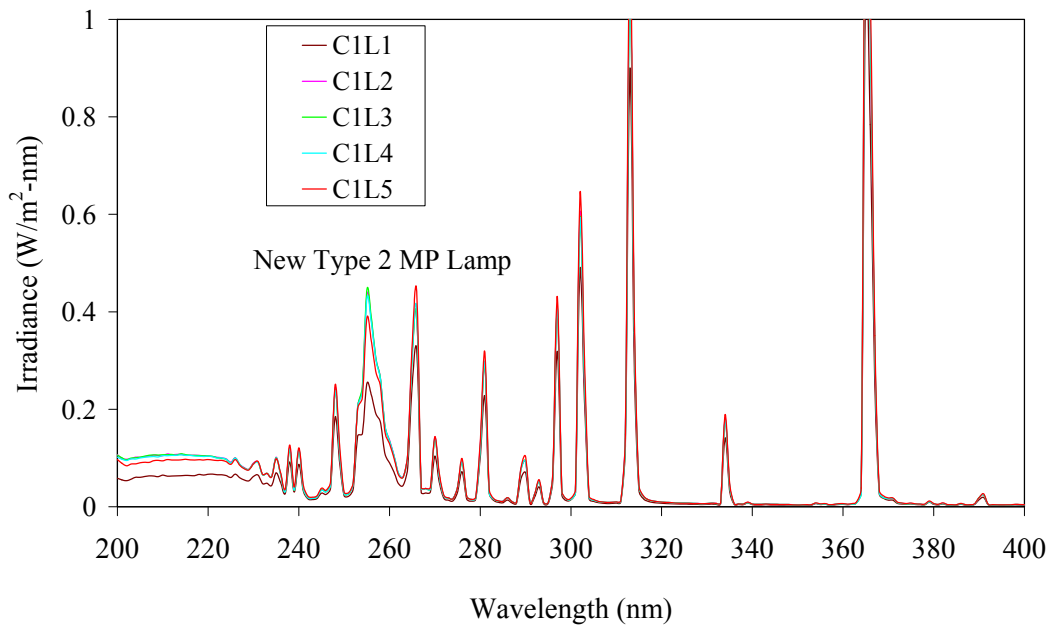


Figure 4.54 Spectral irradiance of the new Type 2 MP lamp as a function of location along the lamp length at location C1

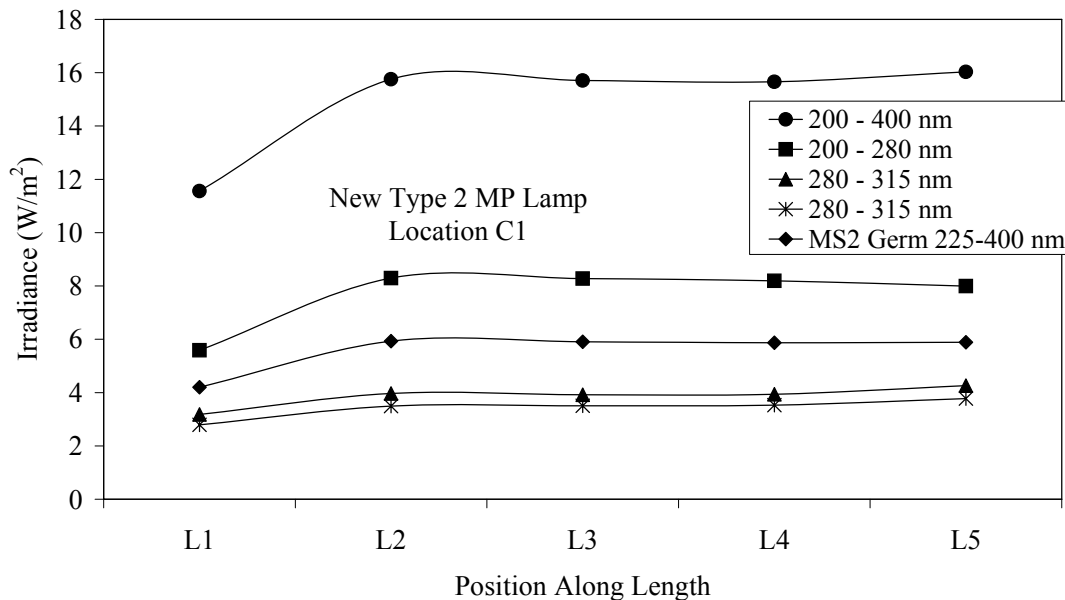


Figure 4.55 Integrated and germicidal irradiance of the new Type 2 MP lamp as a function of position along the lamp length for location C1

Figures 4.56, 4.57, and 4.58 show photographs of the aged Type 2 MP lamps aged 2,292, 2,361, and 4,001 hours, respectively. The visual signs of lamp aging differed significantly from lamp to lamp and did not correlate with the number of lamp hours. The Type 2 MP lamp designated as SR4 and aged 2,292 hours showed the most discoloration. The lamp had significant end darkening that was greater at the power supply side of the lamp and was non-uniform about the circumference. The lamp also showed resonant darkening along the length of the lamp on one side (assumed to be the bottom when located in the UV reactor). However, there was no evidence of resonant distortion. The Type 2 MP lamp designated as SR3 and aged 2,361 hours did not show significant end darkening or resonant darkening but did show resonant distortion along one side (assumed to be the top when placed inside the reactor). The envelope also showed a cloudy white discoloration on half of the lamp opposite the power supply side. The Type 2 MP lamp designated as BP4 and aged 4,001 hours showed slight end darkening but no resonant darkening or distortion.

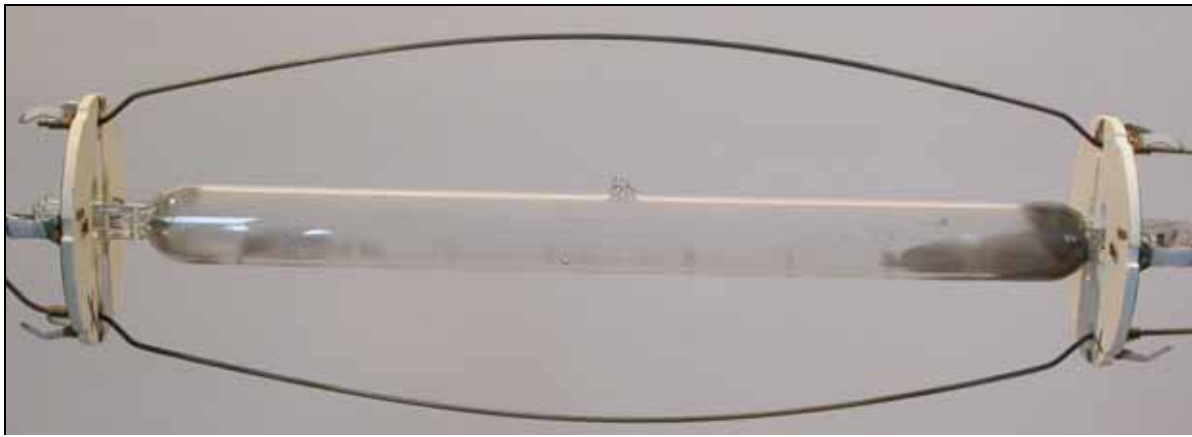


Figure 4.56 Type 2 MP lamp aged 2,292 hours (SR4) photographed from location C2 (top) and C3 (bottom)

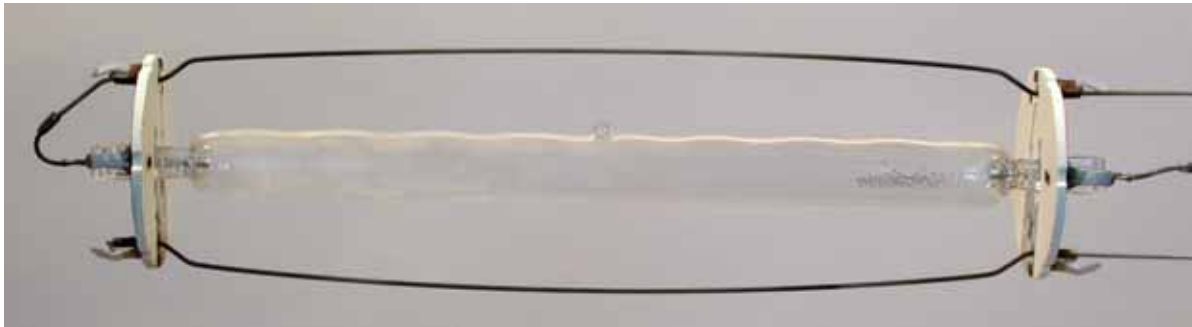


Figure 4.57 Type 2 MP lamp aged 2,361 hours (SR3) photographed from location C4 (top) and C3 (bottom)



Figure 4.58 Type 2 MP lamp aged 4,001 hours (BP4) photographed from location C1 (top) and C2 (bottom)

Figures 4.59, 4.60, and 4.61 show the spectral irradiance of the aged Type 2 MP lamps aged 2,292, 2,361, and 4,001 hours, respectively, as a function of location along the length of the lamps for locations C1 and C2 about the circumference. The spectral output of the new lamp measured at location C1 is shown for comparison. The data shows significant difference in lamp output depending on the location along the length of the lamp and around the circumference. Like the new lamp, location L1 shows a reduced output compared to location L2 to L5. With lamps SR4 and SR3, the UV output from location C1 is much lower than the output with the new lamp. However, with the exception of the L1 position, the UV output from C2 with these lamps is similar to the output from the new lamp. With lamp BP4, the output from location C1 is notably lower than the output from location C2.

Figures 4.62, 4.63, and 4.64 show the integrated irradiance in the UVA, UVB and UVC ranges and the germicidal irradiance from 225 to 400 nm for aged lamps SR4, SR3, and BP4, respectively, as a function of location along the lamp length for location C1. All three lamps show lower integrated irradiance at location L1 compared to L2 to L5. Unlike lamps SR3 and SR4, lamp BP4 also shows lower integrated irradiance at the other end location L5 compared to locations L2 to L4. Table 4.3 compares the ratio of the UVA, UVB, UVC and germicidal output of the aged lamps with the new lamp. Unlike the Type 1 MP lamp, the fraction of UV output in each of the UV ranges with the aged lamps was similar to the output with the new lamp.

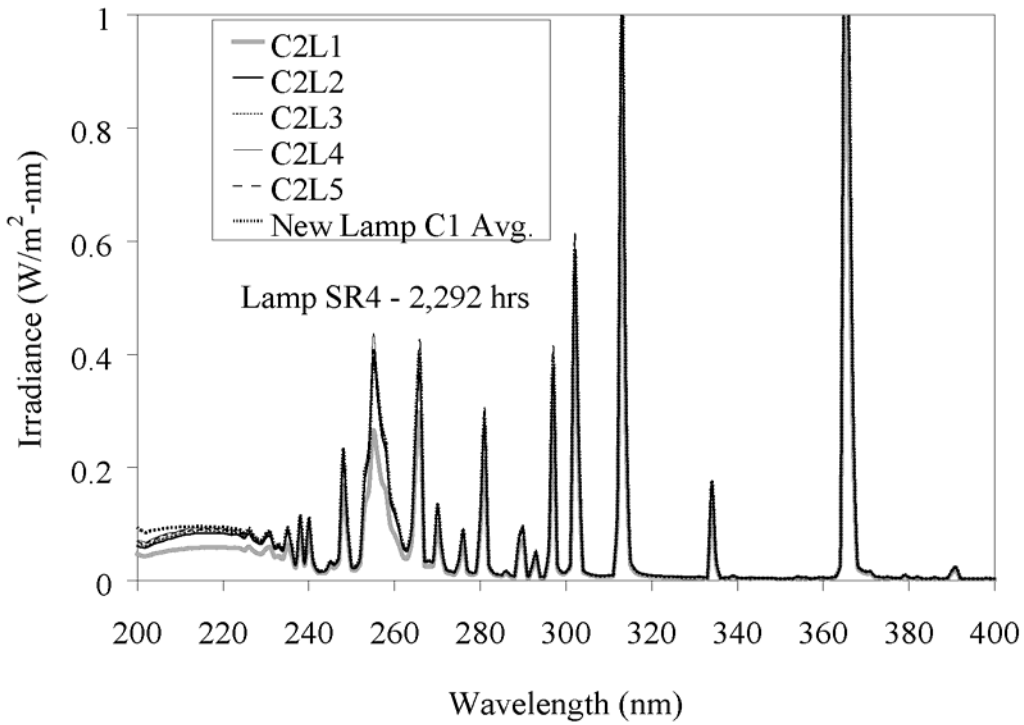
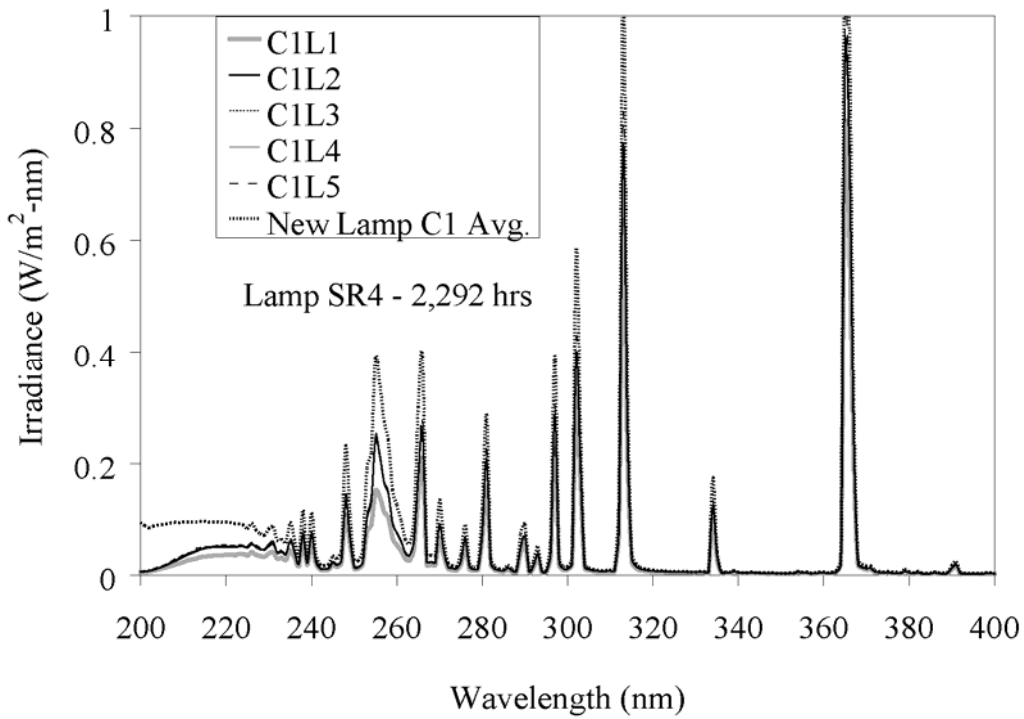


Figure 4.59 Spectral irradiance of Type 2 MP lamp SR4 aged 2,292 hours as a function of location along the lamp length and around the circumference (C1 - top, C2 - bottom)

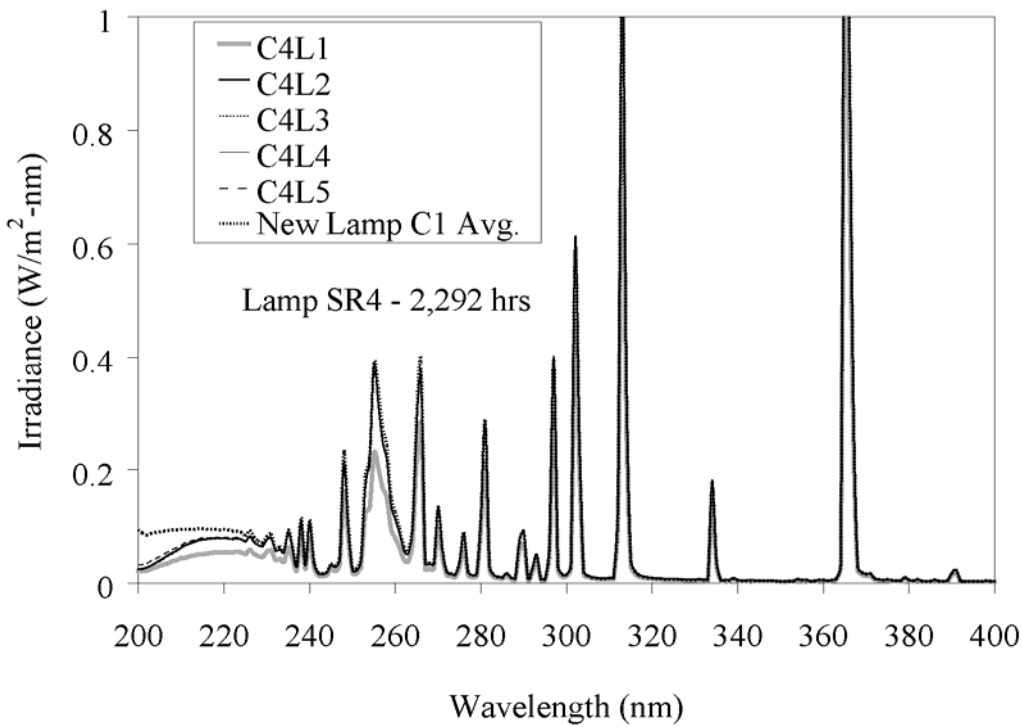
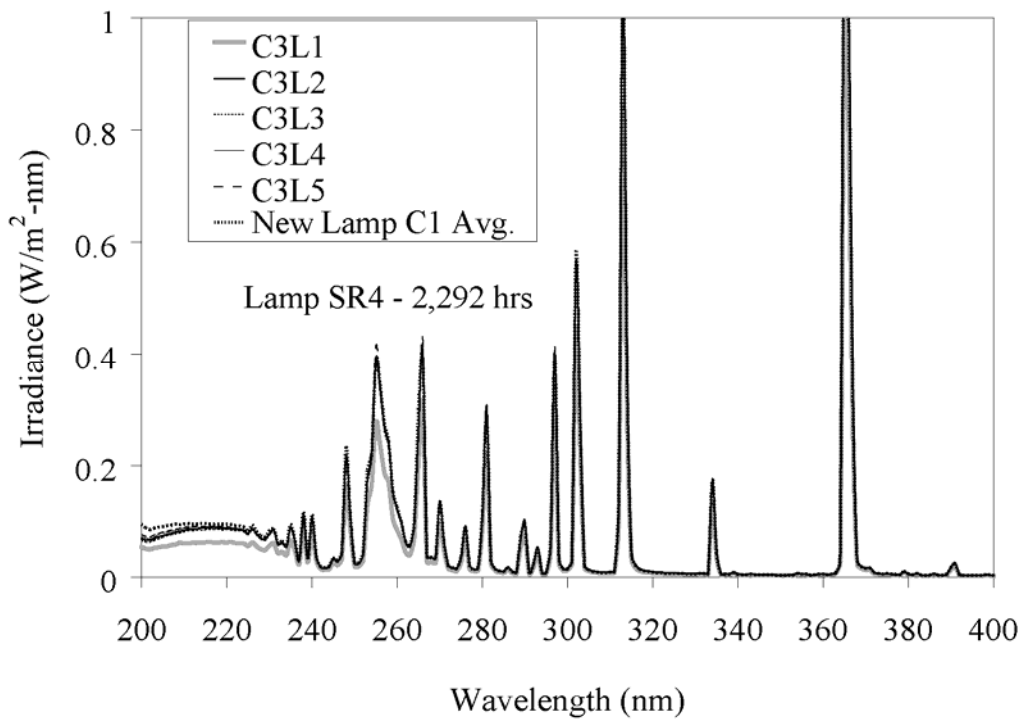


Figure 4.59 (Continued) Spectral irradiance of Type 2 MP lamp SR4 aged 2,292 hours as a function of location along the lamp length and around the circumference (C3 - top, C4 - bottom)

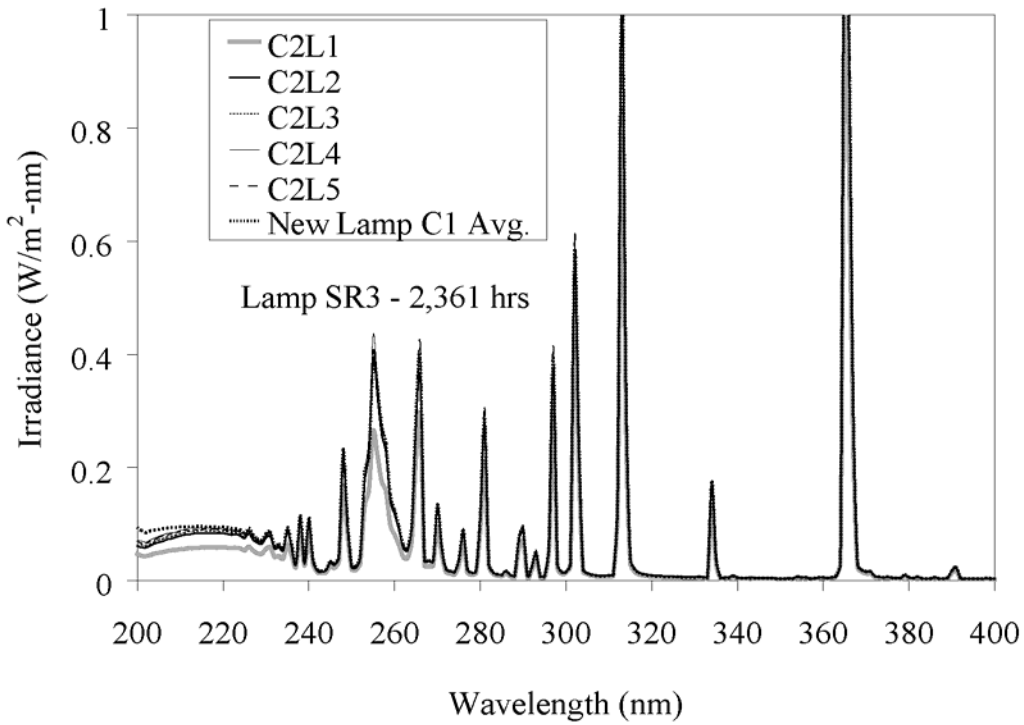
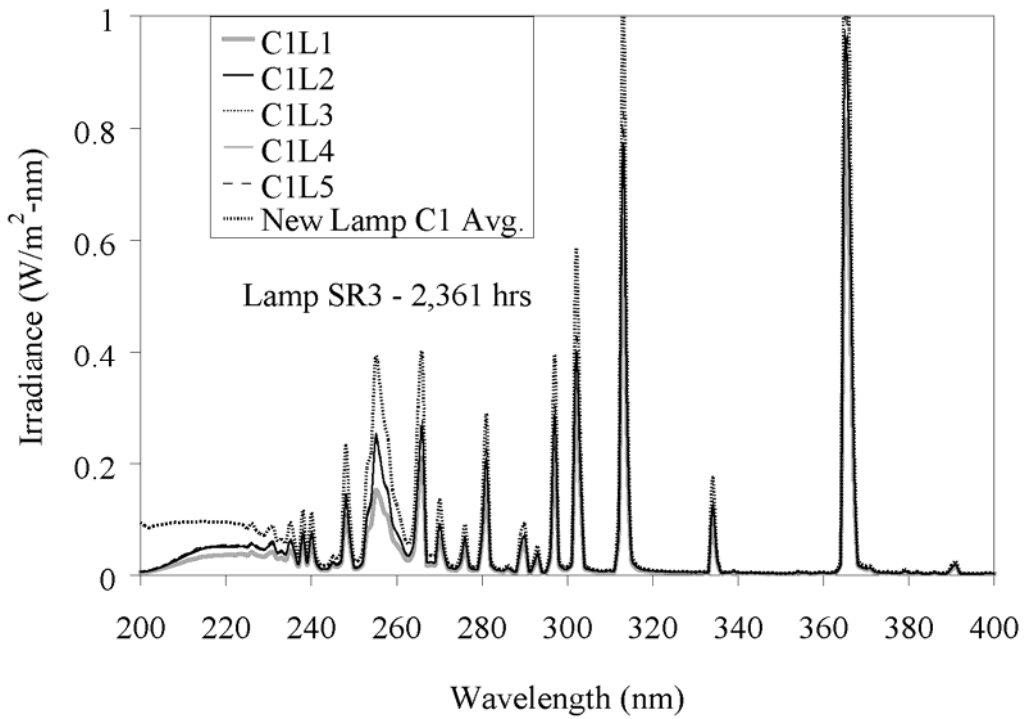


Figure 4.60 Spectral irradiance of Type 2 MP lamp SR3 aged 2,361 hours as a function of location along the lamp length and around the circumference (C1 - top, C2 - bottom)

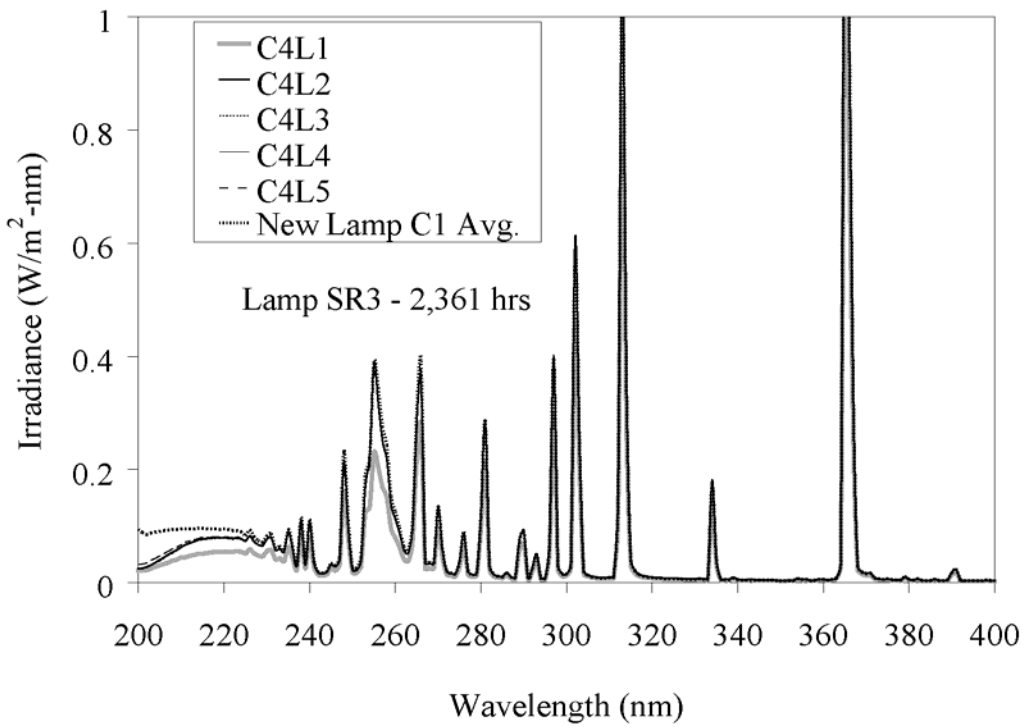
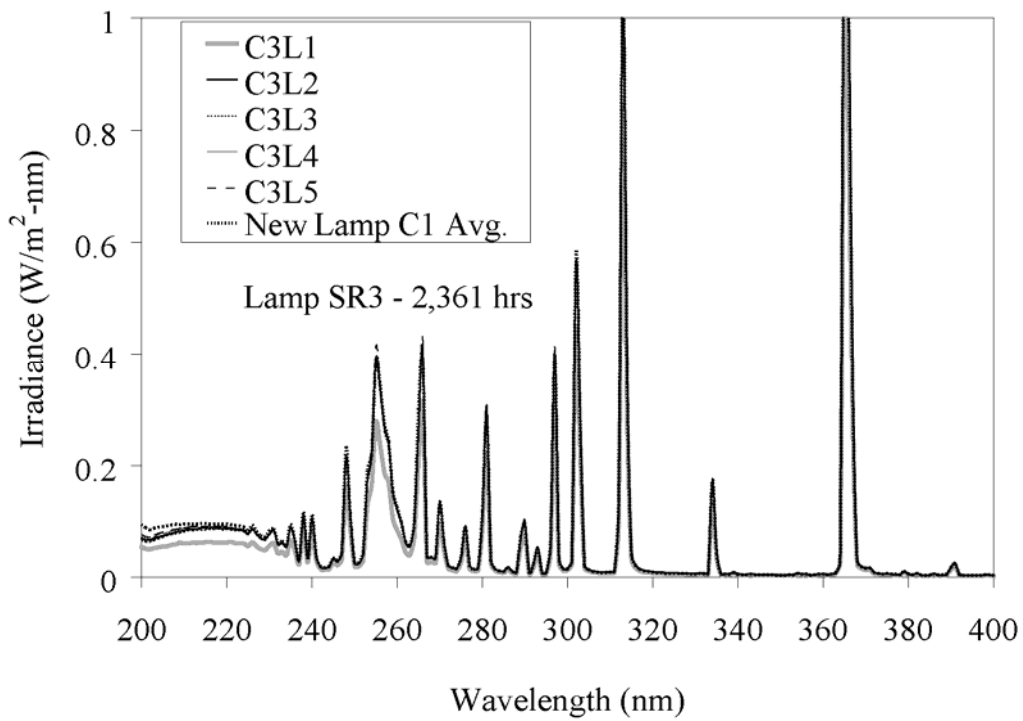


Figure 4.60 (Continued) Spectral irradiance of Type 2 MP lamp SR3 aged 2,361 hours as a function of location along the lamp length and around the circumference (C3 - top, C4 - bottom)

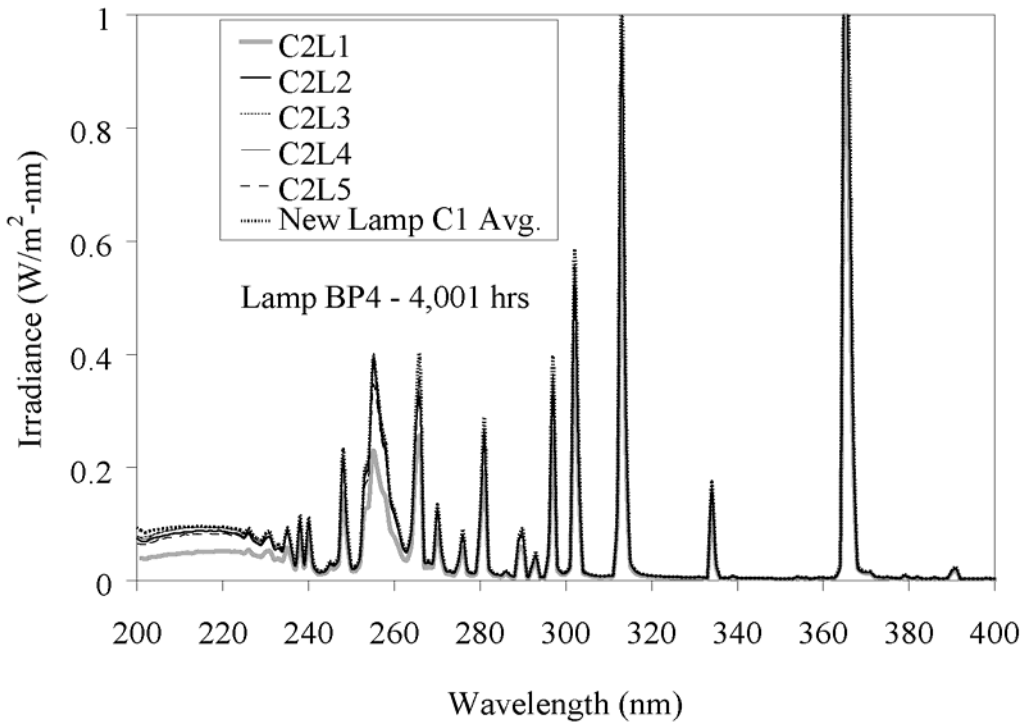
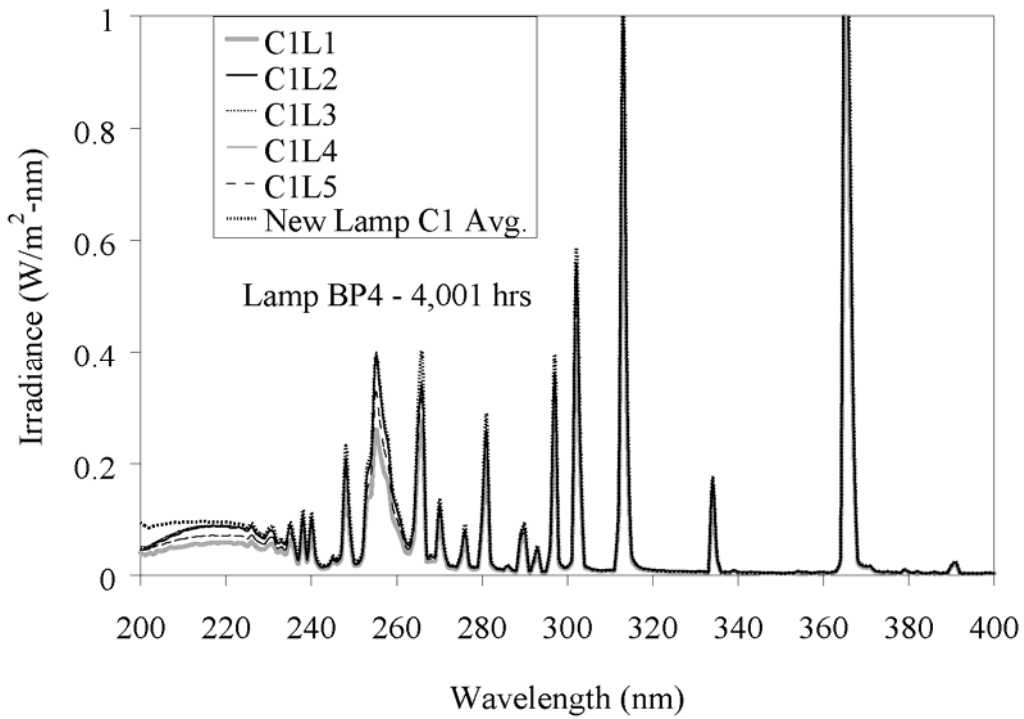


Figure 4.61 Spectral irradiance of Type 2 MP lamp BP4 aged 4,001 hours as a function of location along the lamp length and around the circumference (C1 - top, C2 - bottom)

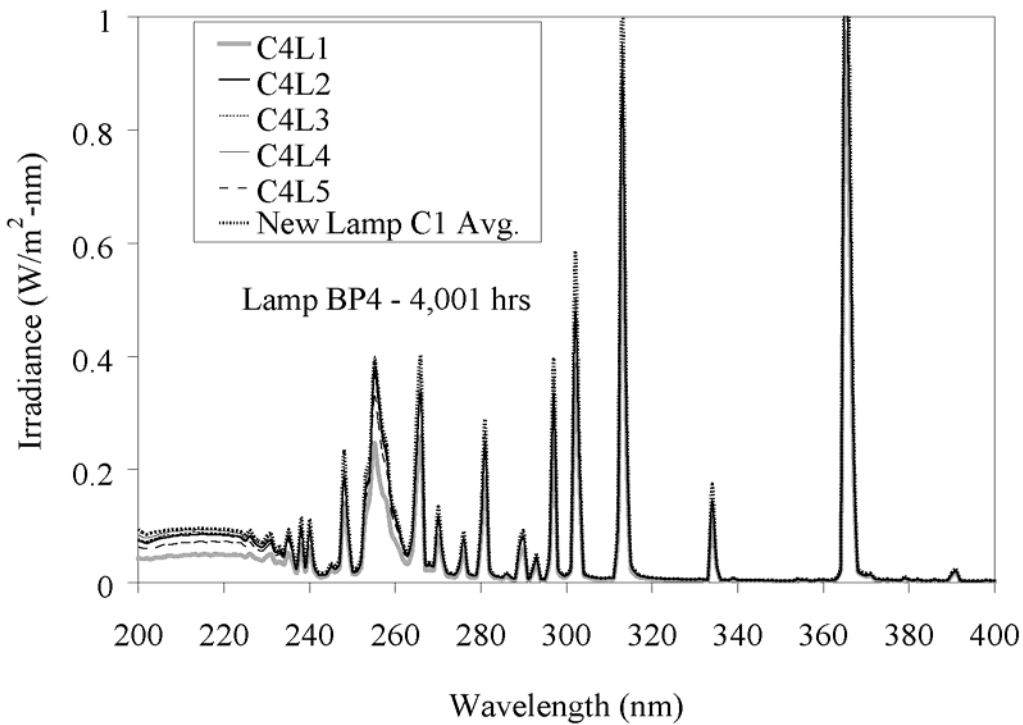
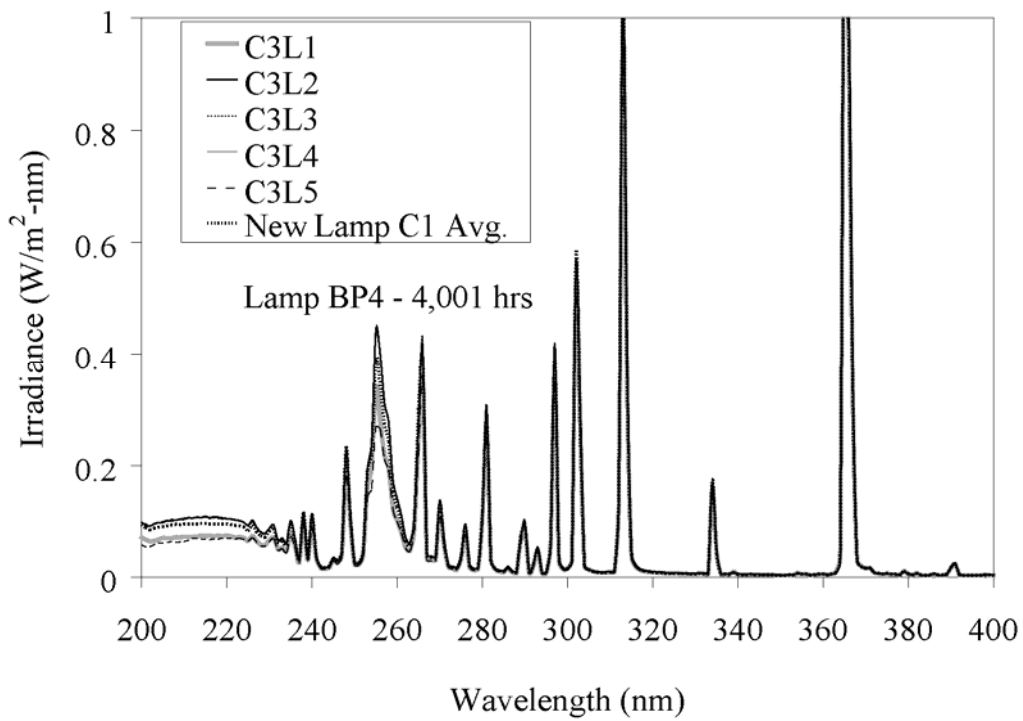


Figure 4.61 (Continued) Spectral irradiance of Type 2 MP lamp BP4 aged 4,001 hours as a function of location along the lamp length and around the circumference (C3 - top, C4 - bottom)

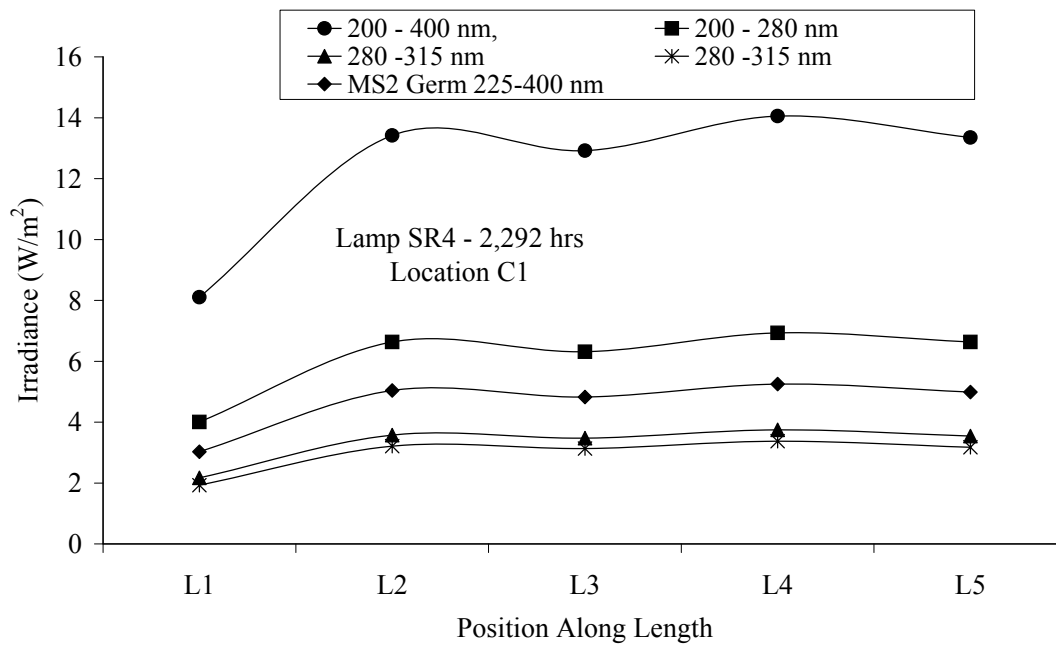


Figure 4.62 Integrated and germicidal irradiance of the aged Type 2 MP lamp SR4 as a function of position along the lamp length for location C1

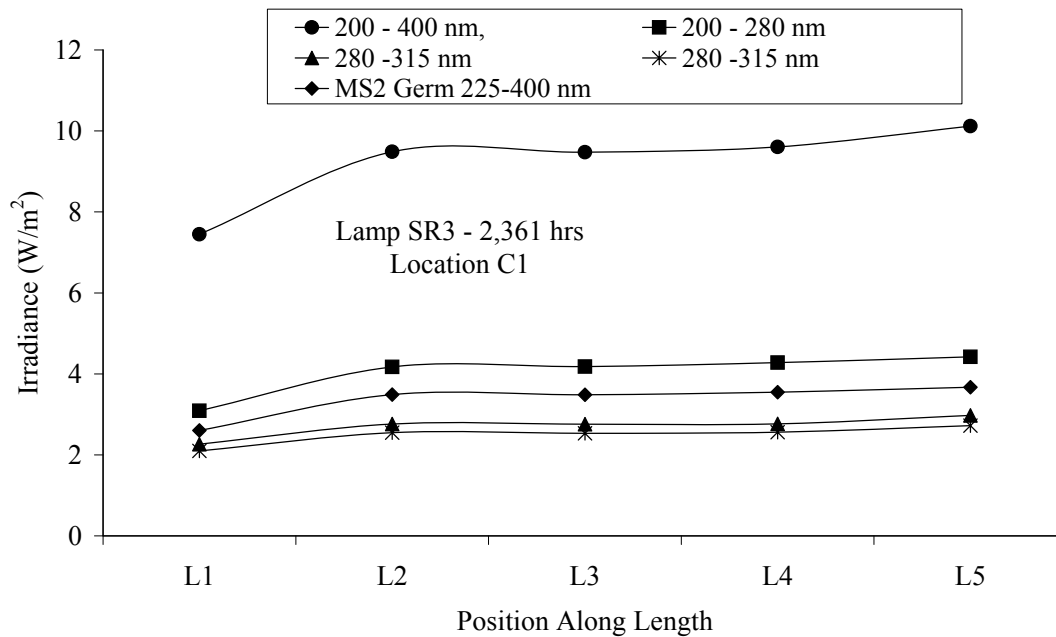


Figure 4.63 Integrated and germicidal irradiance of the aged Type 2 MP lamp SR3 as a function of position along the lamp length for location C1

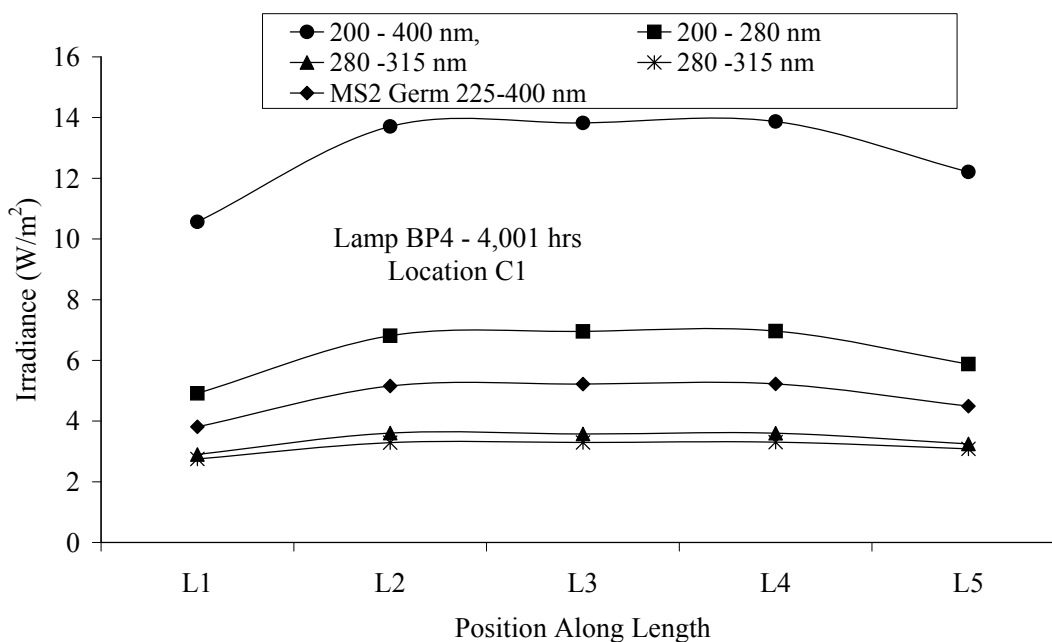


Figure 4.64 Integrated and germicidal irradiance of the aged Type 2 MP lamp BP4 as a function of position along the lamp length for location C1

Table 4.3
Summary of UVA, UVB, UVC and germicidal UV output from the new and aged Type 2 MP lamps

Lamp	Age	Percent of 200 to 400 nm output			
		UVA	UVB	UVC	Germicidal UV
New	0 hrs	23	26	51	37
SR4	2,292 hrs	26	28	47	37
SR3	2,361 hrs	25	28	47	37
BP4	4,001 hrs	24	26	50	37

Figures 4.65, 4.66 and 4.67 show the germicidal irradiance as a function of location along the length of the aged lamps SR3, SR4, and BP4, respectively. Figures 4.68, 4.69, and 4.70 show the germicidal irradiance as a function of location about the circumference. Like the previous figures, the lamps show lower UV output at the lamp end location L1 compared to middle locations L2 to L4 for all positions about the circumference. Lamp SR4 shows a lower UV output at the other end L5 for locations C3 and C4 but not C1 and C2. Lamp BP4 also shows a lower output at end location L5 compared to middle locations L2 to L4 while lamp SR3 has similar UV output from locations L2 to L5. The data also shows that UV output with the aged lamps varies about the circumference of the lamp. In general, one side of the lamp provides the greatest output and one side provides the lowest output. For example, in Figure 4.68, the UV output is greatest at location C2 and lowest at location C3. The dependence of the UV output on the location about the circumference may be related to deflection of the arc within the lamp caused by electromagnetic fields or convection currents.

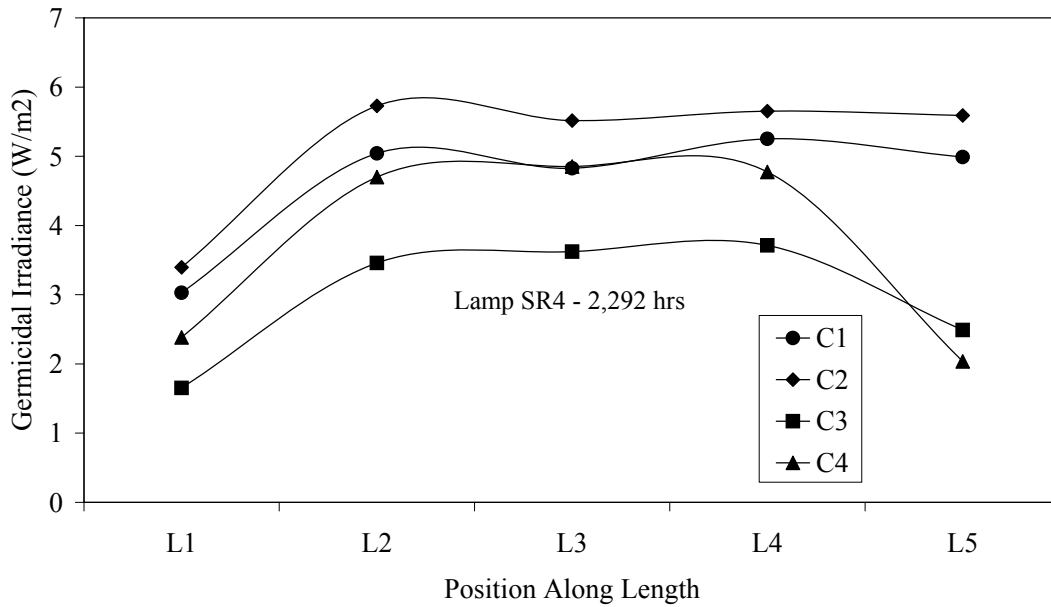


Figure 4.65 Germicidal irradiance of the aged Type 2 MP lamp SR4 as a function of position along the lamp length

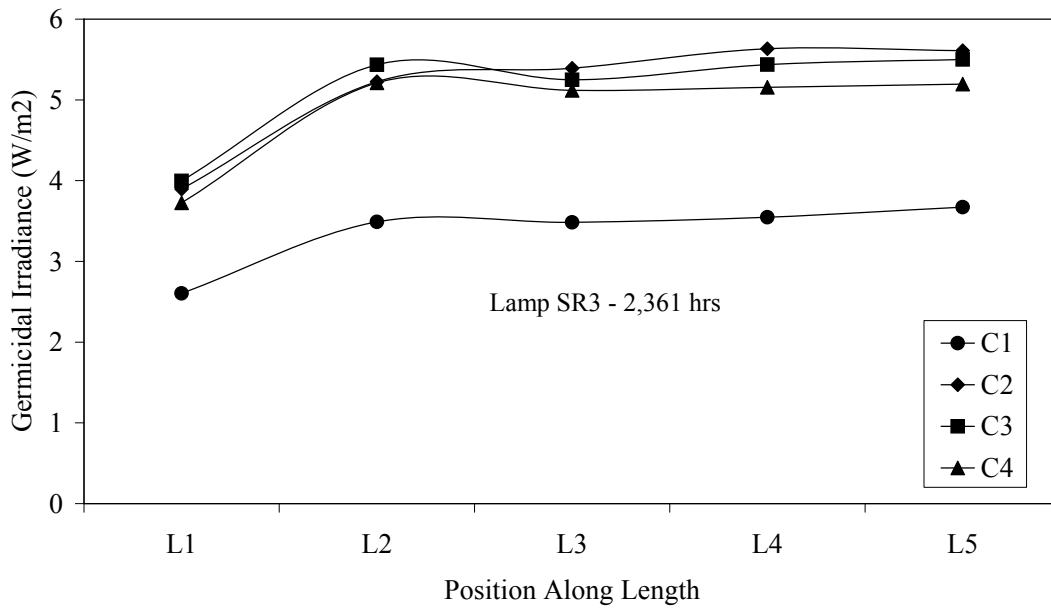


Figure 4.66 Germicidal irradiance of the aged Type 2 MP lamp SR3 as a function of position along the lamp length

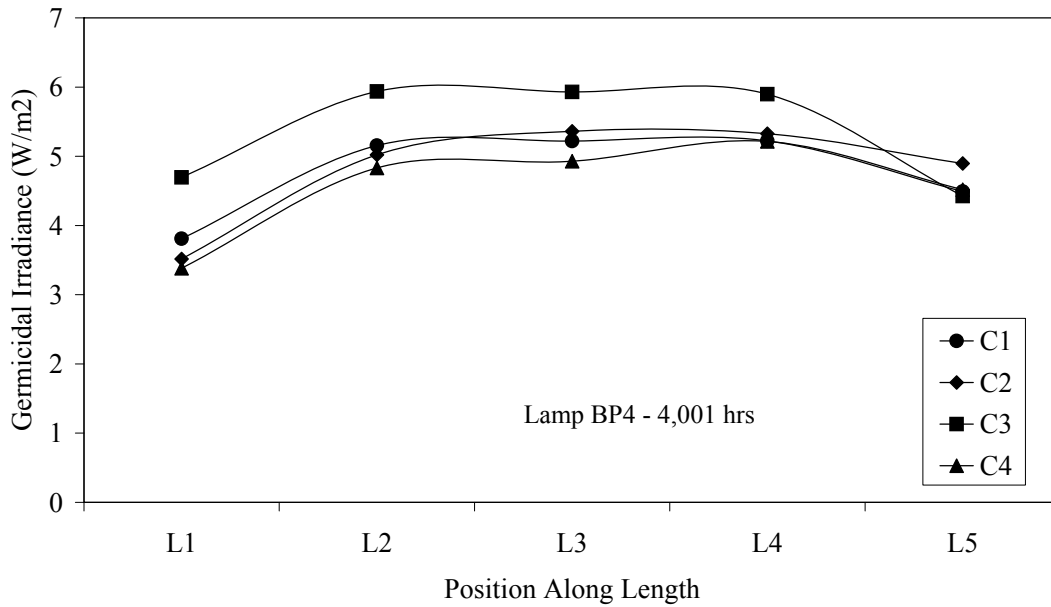


Figure 4.67 Germicidal irradiance of the aged Type 2 MP lamp BP4 as a function of position along the lamp length

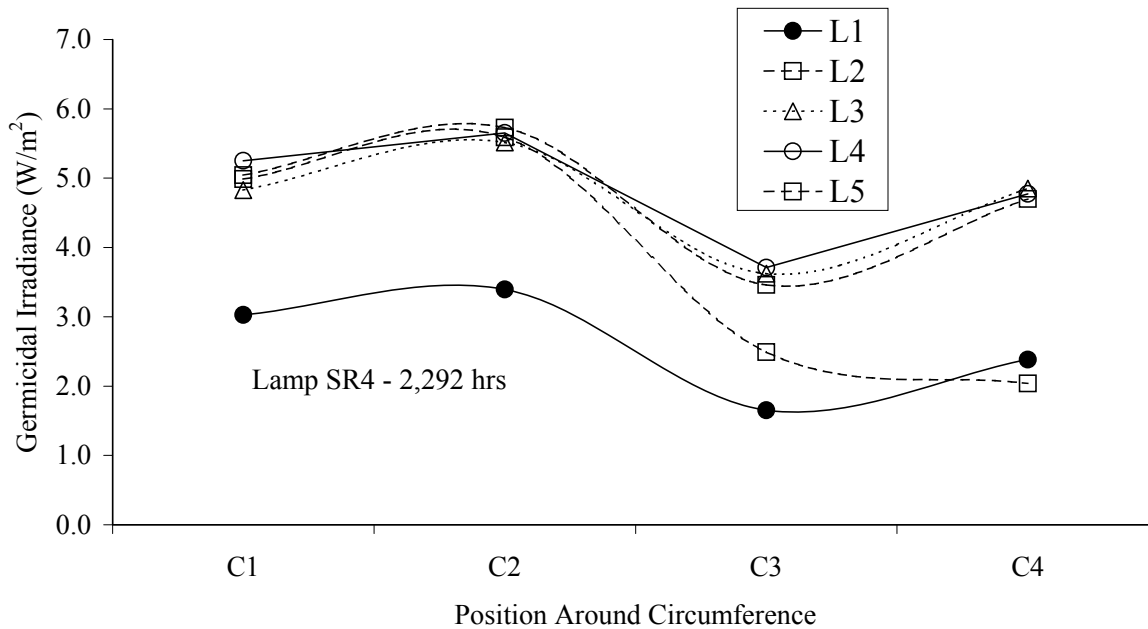


Figure 4.68 Germicidal irradiance of the aged Type 2 MP lamp SR4 as a function of position about the circumference

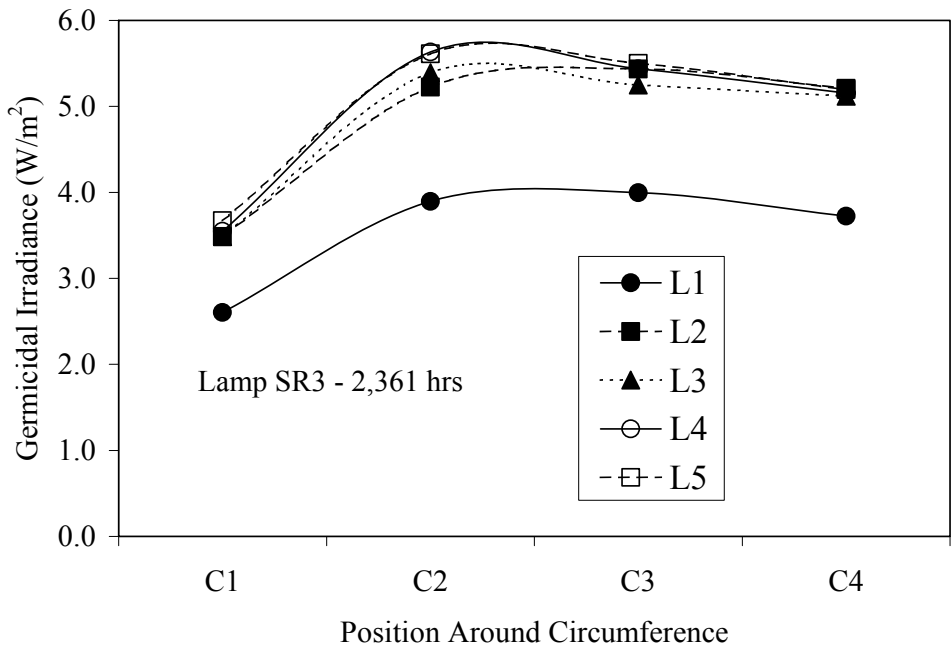


Figure 4.69 Germicidal irradiance of the aged Type 2 MP lamp SR3 as a function of position about the circumference

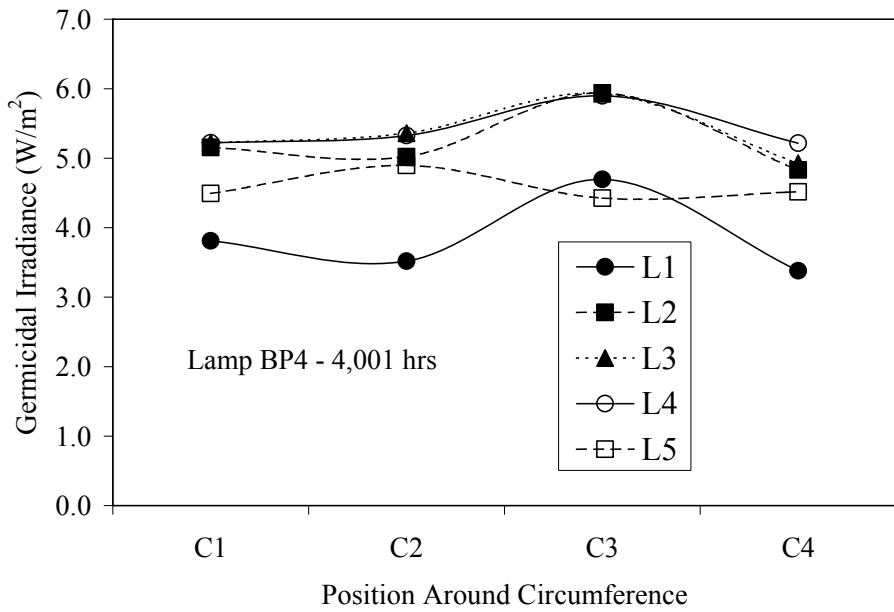


Figure 4.70 Germicidal irradiance of the aged Type 2 MP lamp BP4 as a function of position about the circumference

Figure 4.71 shows the ratio of the UV irradiance measured with each aged lamp to that measured with the new lamp as a function of wavelength. The ratio indicates that the Type 2 MP lamps experience a significant spectral shift as they age, with lower wavelengths in general aging faster than higher wavelengths. The ratio shows no aging at wavelengths from 320 to 360 nm yet aging at higher wavelengths above 360 nm. The extent of spectral shifts appears to correlate with the visual signs of lamp aging.

Figure 4.72 shows the germicidal output of the four Type 2 MP lamps as a function of operating hours. The germicidal output is calculated as the average of all measured positions. A linear fit to the data estimated a UV output of 81 percent after 5,000 hours of operation.

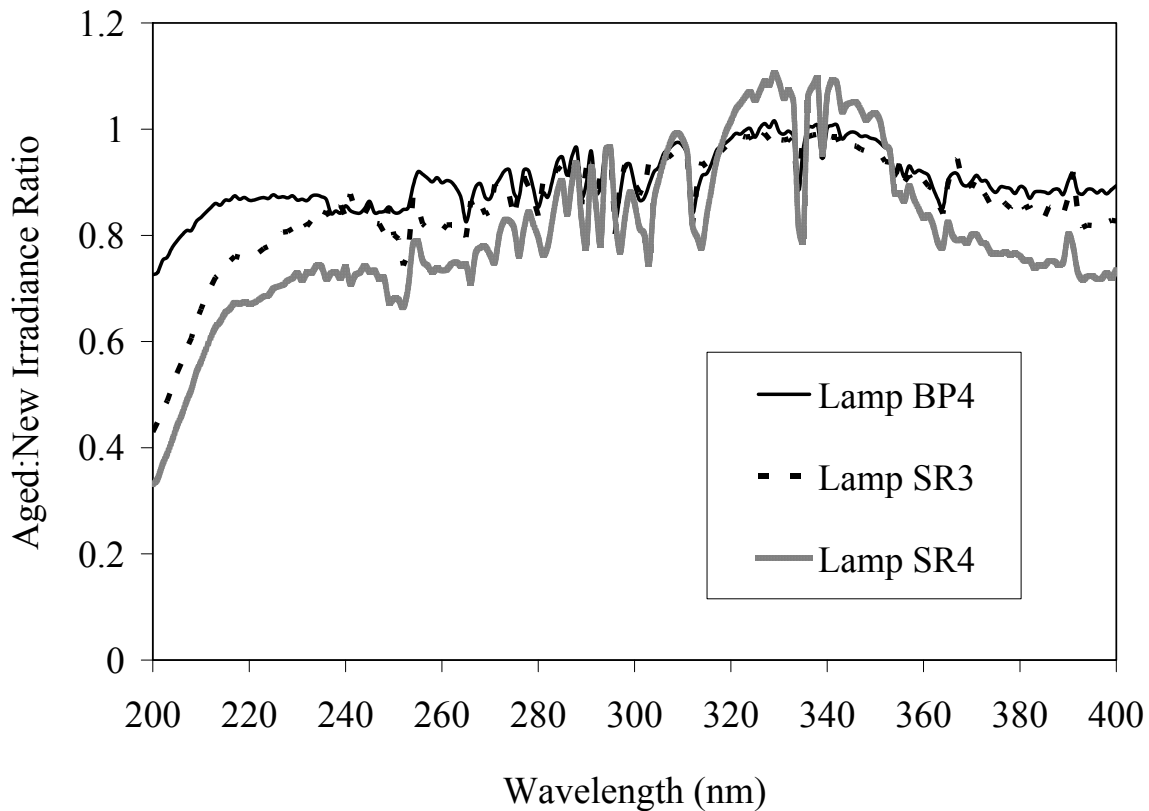


Figure 4.71 Ratio of UV irradiance measured with old Type 2 MP lamps to that measured with new lamps as a function of wavelength

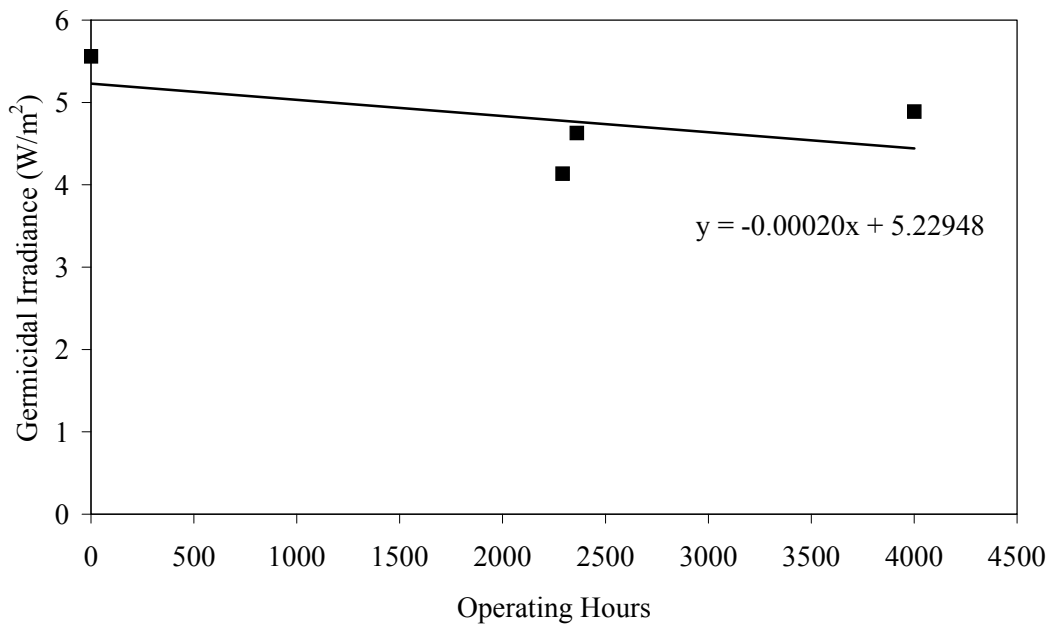


Figure 4.72 Germicidal irradiance as a function of operating hours with Type 2 MP lamps

SUMMARY AND CONCLUSIONS

In this study, LPHO and MP lamps with visual signs of lamp aging were evaluated for UV output along their length and about their circumference. The following is a summary of the most important findings:

Visual Signs of Lamp Aging

- Visual affects of lamp aging could be classified into six types as follows:
 - Darkening of the quartz envelope at each end of the lamp
 - Random discoloration along the length of the lamp
 - Discoloration along the length of the lamp but only 180 degrees about the circumference
 - Lamp end distortion
 - Resonant darkening
 - Resonant distortion
- Lamp envelope distortion, resonant darkening, and 180 degree darkening only occurred with MP lamps. Resonant darkening occurred on the opposite side of the resonant distortion. Likely, distortion is occurring along the topside of the lamp due to arc deflection.

Low-Pressure High-Output Amalgam Lamps

- Amalgam UV lamps have five UV peaks between 300 and 400 nm that have a UV output 5 percent or greater than the UV output at 254 nm. UV output at 254nm showed a greater reduction as lamps aged than did the peaks from 300 to 400 nm.
- Amalgam lamps showed a reduction in UV output at 254 nm that correlated with lamp age and was greater at the lamp ends as compared to the middles.
- The UV output at 254 nm of a new amalgam lamp varies along the length of the lamp with greater UV output at locations 12 cm from the electrodes and lower output at the middle of the lamps compared to this location. The UV output also showed a sharp drop at the locations of the amalgams.
- The aged LPHO lamps showed greater non-uniformity along their length compared to the new lamp
- In general, the UV output of new and aged amalgam lamps did not vary significantly around the lamp circumference.

Medium Pressure UV Lamps

- UV output with aged MP lamps was lower than UV output with new lamps.
- Aged MP lamps exhibited UV outputs that varied around the circumferences of the lamps. Non-uniform aging of MP lamps about their circumference is likely related to arc deflection.
- One MP lamp type did not show a significant non-uniformity in lamp output along the length of the lamp with new and aged lamps. The other MP lamp type showed lower output at the ends compared to the middle of the lamp.
- Both MP lamp types showed “spectral shifts” in UV output as a function of wavelengths as the lamps aged. In general, the UV output at lower wavelengths aged faster than higher wavelengths. However, one lamp showed greater aging at 260 nm compared to 245 nm and the other showed greater aging at 400 nm compared to 340 nm.

General Conclusions

- This data indicates that in some cases UV sensor placement along the length of the lamp will be critical; depending upon its location, germicidal output could be under- or overestimated. It is recommended that this issue be considered in the design of UV dose-monitoring system. This could be accounted for through sensor placement or the application of a safety factor to account for potential over-estimation of the total lamp germicidal output.

CHAPTER 5

FIELD-TESTING OF NEW VALIDATION TOOLS

This chapter describes full-scale testing to demonstrate the use of the new challenge microorganism, and the new UV absorber, and evaluate the impact of non-uniform lamp aging on dose delivery and monitoring. The intent of full-scale testing was to:

1. Evaluate the RED bias of a full-scale UV reactor by comparing REDs measured using T7 and MS2 phage.
2. Use the new UV-absorbing chemical, Super Hume™.
3. Compare dose delivery of new and aged lamps for a given flow, UVT, and UV sensor reading.

The following sections describe the test methodology, present the results, and discuss the implications for future validation testing protocols.

MATERIALS AND METHODS

Test Train Location and Set-up

The field-testing was conducted in October 2005 at the Portland UV Validation Facility, located at the Groundwater Pumping Station of the Columbia Southshore Wellfield in Portland, Ore. The Columbia Wellfield is a 90 mgd supplemental drinking water supply owned and operated by the Portland Water Bureau. The wellfield supplied water with the following characteristics to the test train:

- pH: 6.8 to 7.2
- UVT¹: 97.6 to 98.7 percent
- Free chlorine: 0.00 to 0.02 mg/L as Cl₂

The test train is graphically presented in Figure 5.1. Test train piping and components upstream of the UV reactor included, in order:

- Two check valves installed for backflow prevention.
- An injection loop to facilitate spiking of the UV-absorbing chemical and the microorganisms.
- A static mixer² to disperse the UV-absorbing chemical and spiked microorganisms throughout the influent water.
- 8.7 pipe diameters of straight pipe
- A stab-tube sample port

¹ UV transmittance at 254 nm

² Komax Systems, Inc. of Wilmington, Calif.

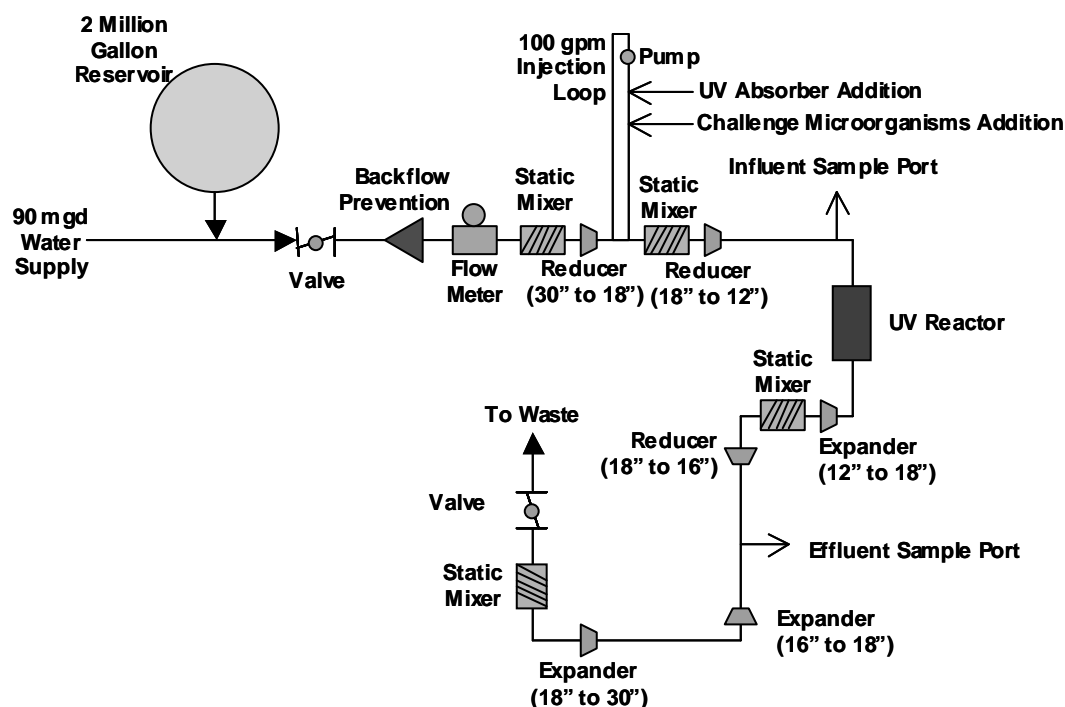


Figure 5.1 Test train schematic

- 1 pipe diameter of straight pipe
- 90° bend
- 3 pipe diameters of straight pipe

Test train piping and components downstream of the UV reactor included, in order:

- Approximately 1 pipe diameter of straight pipe
- 90° bend
- A static mixer to ensure well mixed effluent sampling
- 90° bend
- Approximately 11.5 pipe diameters of straight pipe
- Magnetic flow meter³
- A stab-tube sample port (effluent)
- Effluent piping with control valve prior to discharge

The injection system was designed to meet specifications provided in the German DVGW UV validation guidelines (DVGW 2003). Water for the injection loop was drawn from a location approximately 3 pipe diameters upstream of the inlet static mixer at a flow rate of approximately 100 gpm. The UV-absorbing chemical was added to the injection loop flow using an Allweiler⁴ progressive cavity pump. Challenge microbes were added to the flow using an

³ Endress and Hauser Flowtec AG of Greenwood, Ind.

⁴ Monroe, N.C.

Ismatec digital drive equipped with a Micropump gear pump head⁵. The water was then recirculated back into the bulk flow through a multi-port diffuser located approximately 1.3 pipe diameters upstream of the inlet static mixer.

The inlet sample port was located approximately nine pipe diameters downstream of the inlet static mixer and approximately one pipe diameter upstream of the inlet 90° bend. The use of a 90° bend upstream of the reactor follows the provisions of the German DVGW UV Guidelines, which assume that a 90° bend represents a challenging flow scenario.

The effluent sampling port was located over 14 pipe diameters downstream of the UV reactor, and was preceded by two 90° bends and the effluent static mixer.

UV Reactor

The field-testing was conducted using a Sentinel UV reactor manufactured by Calgon Carbon Corporation (CCC) of Pittsburgh, Pa. The UV reactor was equipped with three medium-pressure UV lamps oriented horizontal and perpendicular to flow. The reactor used baffle plates to direct flow past the lamps and a screw-driven wiper to periodically clean the lamp sleeves and the UV sensor ports. The UV intensity for each lamp was monitored with a DVGW compliant UV sensor. The sensor was mounted within a DVGW compliant sensor port that viewed the lamp from above. The UV reactor was connected to the test train piping with bolted flange joints. Only one of the three lamps within the reactor was operated for this evaluation.

Lamps

The UV lamps were standard MP mercury-arc lamps controlled by electro-magnetic ballasts. [Figure 5.2](#) provides the typical spectral UV output of the lamp. Lamps and ballasts had a nominal power consumption of 4.0 kW at 9.5 Amps.

Sleeves

The UV lamps were housed within commercial-grade 214A quartz sleeves.⁶ The sleeves had a wall thickness of approximately 1.5 mm. [Figure 5.3](#) presents spectral UV transmittance data for the lamp sleeves.

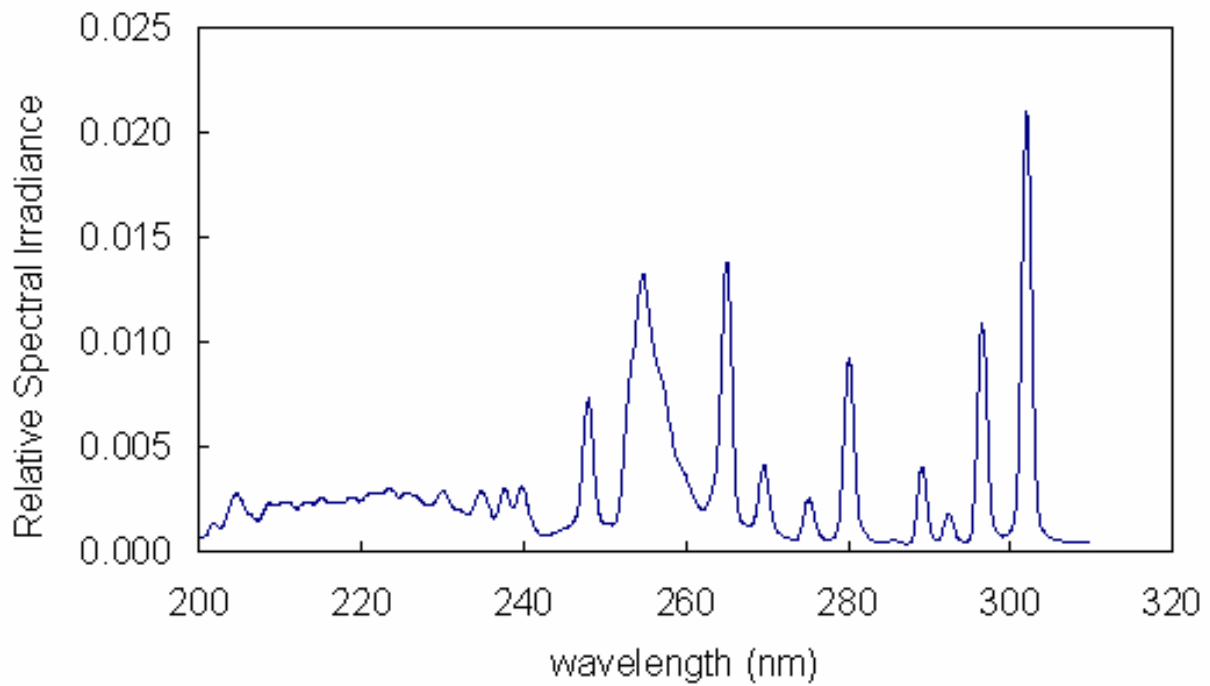
UV Intensity Sensors

The duty and reference UV sensors⁷ used during field-testing were designed to measure UV light in accordance with the German DVGW W294 Rules for UV disinfection (DVGW 2003). [Table 5.1](#) describes the properties of the duty and reference UV sensors. [Table 5.2](#) provides estimates of the measurement uncertainty related to those properties. The uncertainty associated with angular and spectral response was estimated using data obtained from AwwaRF project 2977, *Design and Performance Guidelines for UV Sensor Systems*. All other data was obtained from CCC. Using the sum of variances approach, the total measurement uncertainty was estimated as 17 percent.

⁵ Cole-Parmer of Vernon Hills, Ill.

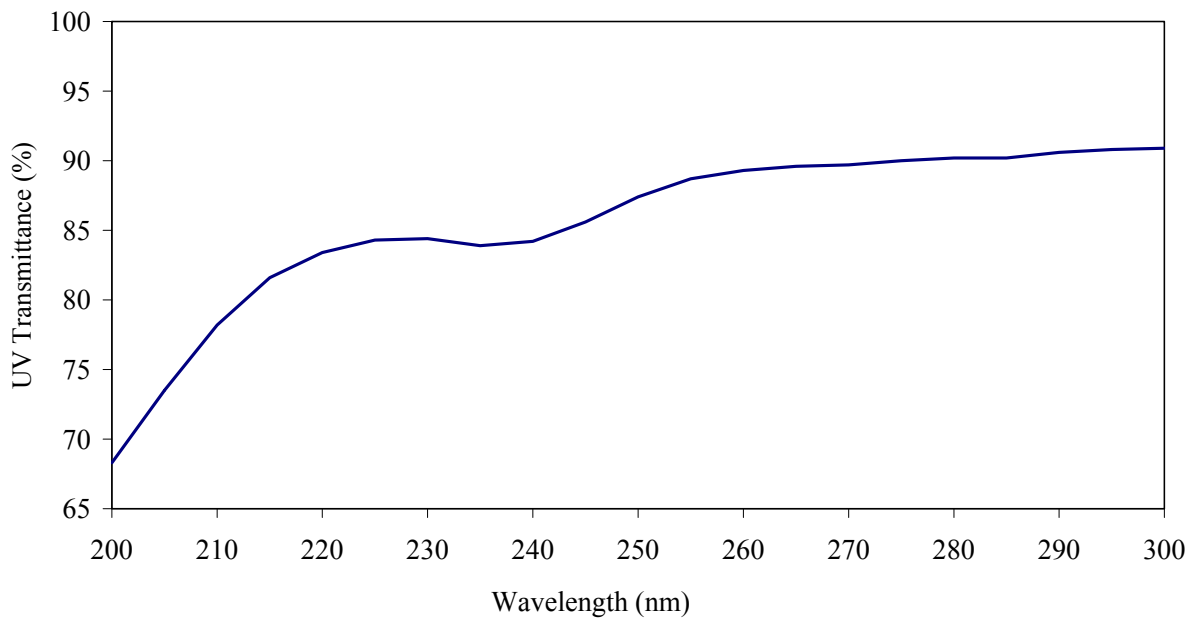
⁶ GE Quartz, Inc., Willoughby, Ohio

⁷ IL Metronic Sensortechnik GmbH, Germany



Source: CCC

Figure 5.2 Spectral output of a new lamp for the Sentinel UV reactor



Source: CCC

Figure 5.3 UV transmittance of a 1.5 mm thick lamp sleeve for a 90° of incidence angle and air-quartz interfaces

Table 5.1
Properties of the duty and reference UV sensors

	Duty	Reference
Output	4 - 20 mA	Not provided
Measurement range	10 – 1,000 W/m ²	Not provided
Linearity	≤1%	≤1%
Spectral selectivity	≤1% (> 300 nm)	≤1% (> 300 nm)
Acceptance angle	30°	30°
Temperature drift	≤2.5% from 5 - 30°C	≤2.5% from 5 - 30°C
Long-term stability	≤1.0% per 1,000 operating hours	≤1.0% per 1,000 operating hours
Calibration uncertainty	5%	5%
Recalibration interval	4,500 operating hrs	9,000 operating hrs

Source: CCC

Table 5.2
Estimation of the measurement uncertainty of the UV intensity sensor

UV sensor property	Uncertainty (%)
Calibration	5
Linearity	1
Spectral response	10
Acceptance angle	12
Temperature drift	2.5
Long-term stability over 4,500 hrs	4.5

UV-Absorbing Chemical

The UV absorbing chemical used for this testing was Super Hume™, acquired from United Agricultural Services of America, Inc.⁸ Super Hume™ is a highly concentrated form of humic acids manufactured from leonardite shale mined in the North Central U.S. Because of its high humic content, Super Hume™ has a UVA spectrum similar to that of WTP water (see Chapter 3). Super Hume™ also enhances the stability of the test microbes used for validation testing (Hargy *et al.* 2004).

Challenge Microorganisms

The challenge microorganisms used for this testing were MS2 and T7 bacteriophage. The preparation of test microbe stock solutions, the enumeration of test microbe concentrations in water samples, and the measurement of test microbe UV dose-response were conducted by Clancy Environmental Consultant's (CEC) of St. Albans, Vermont using the methods described in Chapter 2.

⁸ Hudson, Fla.

The concentrations of MS2 and T1 phage in the stock solutions were approximately 1.5×10^{11} and 1.4×10^{10} pfu/mL, respectively. Stock solutions were stored in 1-L sterile polypropylene bottles labeled to indicate date of preparation, batch number, titer, and technician ID. Stock solutions were stored in a dedicated refrigerator at 4°C prior to testing.

Aged UV Lamp

Figure 5.4 shows photographs of the new lamp with 100-hour burn in (top) and the aged lamp (bottom) used during field-testing. The aged lamp had more lamp end darkening and approximately 15.3 percent less UVC (200 to 280 nm) output than the new lamp (*Source: CCC*). Because the spectral UV output of this lamp was not measured along its length or about its circumference, the degree of UV output non-uniformity was not known.

Test Protocol

Water Quality Measurements

Water quality measurements conducted on-site included UVT at 254 nm, spectral UVT scans from 200 to 400 nm, and total chlorine. Measured data, sample collection time, and information relating the measurements to test conditions were manually recorded in a dedicated logbook.

The UVT of the test water was measured using a DR/4000 UV VIS spectrophotometer equipped with a 5-cm quartz cuvette.⁹ Prior to the measurement, the spectrophotometer was zeroed using distilled water and the cuvette was rinsed three times with the test water. The spectral UVA of the test water was measured from 200 to 400 nm in 1-nm increments.

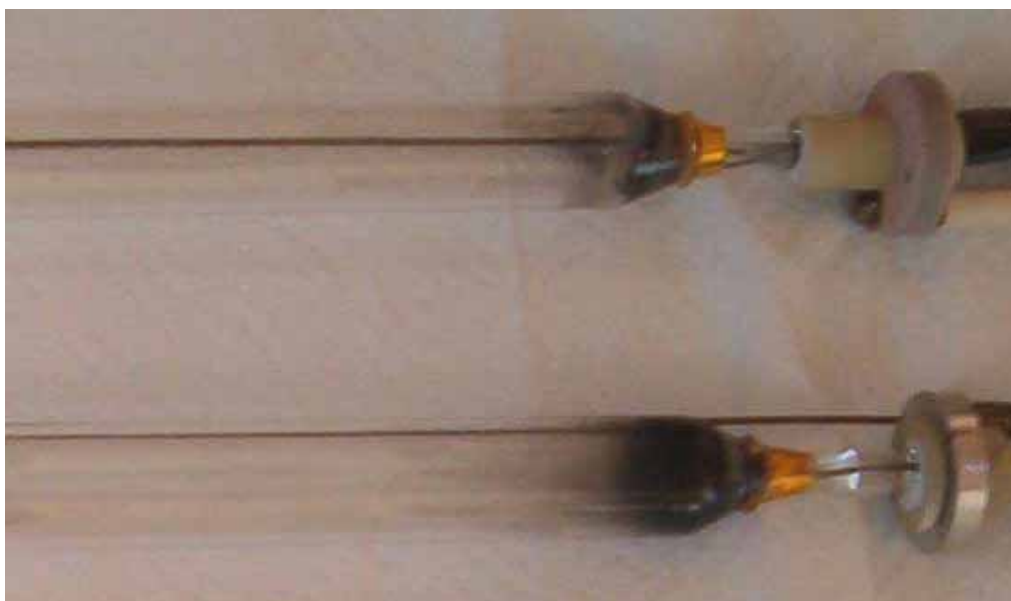


Figure 5.4 New lamp with 100-hour burnin (top) and the aged lamp (bottom) used during field-testing

⁹ Hach Company, Loveland, Colo.

Spectrophotometer accuracy was verified using a NIST¹⁰-traceable holmium oxide UV wavelength and potassium dichromate UV absorbance standards (Starna Cells¹¹). The wavelength accuracy of the instrument was within 0.1 nm of the holmium oxide standard. The distilled water used to zero the spectrophotometer was regularly checked against reagent grade organic-free water purchased from Hach.

The UVT of the water was set by the pumping rate of the Super Hume™ pump. Typically, the target UVT was reached after two to four iterative settings of the pump. Steady-state was confirmed when the measured UVT of three effluent water samples taken one minute apart were within 0.3 percent of the target value. Once the target UVT was reached, the value typically remained stable over multiple test conditions without the need for readjustment.

If the replicate UVT samples measured with a test condition were not within 0.3 percent of the target UVT, the pumping rate was readjusted until the UVT was within the acceptable tolerance and the testing was repeated.

To confirm there was no chlorine in the test water, test water samples were analyzed multiple times throughout the testing period for chlorine concentrations using N,n-diethyl-p-phenylenedramine (DPD) colorimetry. Samples were collected in plastic sample vials and analyzed within two minutes of collection using a Hach pocket colorimeter. The method used was equivalent to USEPA method 330.5 and Standard Method 4500-Cl G for drinking water and wastewater.

UV Sensor Performance

The intensity measurements made by the duty UV sensors were checked using three calibrated reference UV sensors (CCC Serial Numbers NN32, NN33, NN34) with the following procedure:

1. Record time, flow rate, water UVT, and lamp power.
2. Record five (5) duty UV sensor measurements, timed one (1) second apart.
3. For each duty sensor:
 - a. Replace the duty sensor with each of the reference UV sensors and record at least five (5) reference UV sensor measurements, timed one (1) second apart, after the measurement has stabilized.
 - b. Return the duty sensor and repeat step 2 above.
4. Record time, flow rate, water UVT, and lamp power.
5. For each duty UV sensor, calculate the average of the before and after duty sensor readings and the average of the readings recorded with the three reference UV sensors.
6. Compare by plotting average duty UV sensor readings versus average reference UV sensor readings.

The uncertainty of the average reference UV sensor measurement was estimated as $17/\sqrt{3} = 10\%$.

¹⁰ National Institute of Standards and Technology, Boulder, Colo.

¹¹ Atascadero, Calif.

Biodosimetry

Biodosimetry was conducted with water from the Columbia Southshore Wellfield using the following procedure:

1. Initiate data logging of power, UV sensor readings, and flow rate measurements.
2. Set the flow rate to the target value by adjusting the flow-control valve.
3. Set the water UVT to the target value by adjusting the feed rate of the Super Hume™ pump.
4. Set the UV intensity setpoint of the reactor to the target value by adjusting lamp power.
5. Initiate injection of MS2 or T7 bacteriophage.
6. Confirm steady-state conditions. Steady-state conditions were assumed to occur after five residence times from the injection point to the reactor outlet sampling point.
7. Record date and time to synchronize the data recorded by the data logger with the manually recorded data. Record flow rate, UV intensity and dose targets, and UV intensity measurements.
8. Record date and time. Collect five influent and five effluent challenge microbe samples spaced one minute apart. Sample volumes ranged from 9 - 13 mL. Collect separate effluent samples for measurement of UVT in parallel with microbial sampling.
9. Collect the collimated beam sample from the influent sampling port as required.
10. Record date and time, flow rate, UV intensity and dose targets, and UV intensity measurements.

All sample vials were pre-labeled before testing. At the end of each test day, microbiological samples were shipped by overnight courier in coolers with ice packs, for analysis by CEC. Analysis began on the day of receipt.

Collimated Beam Testing

The UV dose-responses of the MS2 and T7 bacteriophage in the seeded reactor inlet samples were measured by CEC using a collimated beam apparatus equipped with a LP mercury-arc lamp. Irradiations were conducted in duplicate on 10 mL sub-samples taken from the inlet sample. MS2 sub-samples were irradiated at UV dose values of 0, 6, 12, 18, 24, 32, and 40 mJ/cm². T7 sub-samples were irradiated at UV dose values of 0, 3, 6, 9, 12, 15, and 18 mJ/cm².

RESULTS AND DISCUSSION

Spectral Absorbance

Figure 5.5 shows the spectral UV absorbance coefficient of the test water with and without Super Hume™. Because the same well was used throughout the testing, the spectral UV absorbance of the raw water did not vary significantly over the duration of the tests.

— Raw Test Water - 98.5% UVT — Test Water with Super Hume - 81.5% UVT

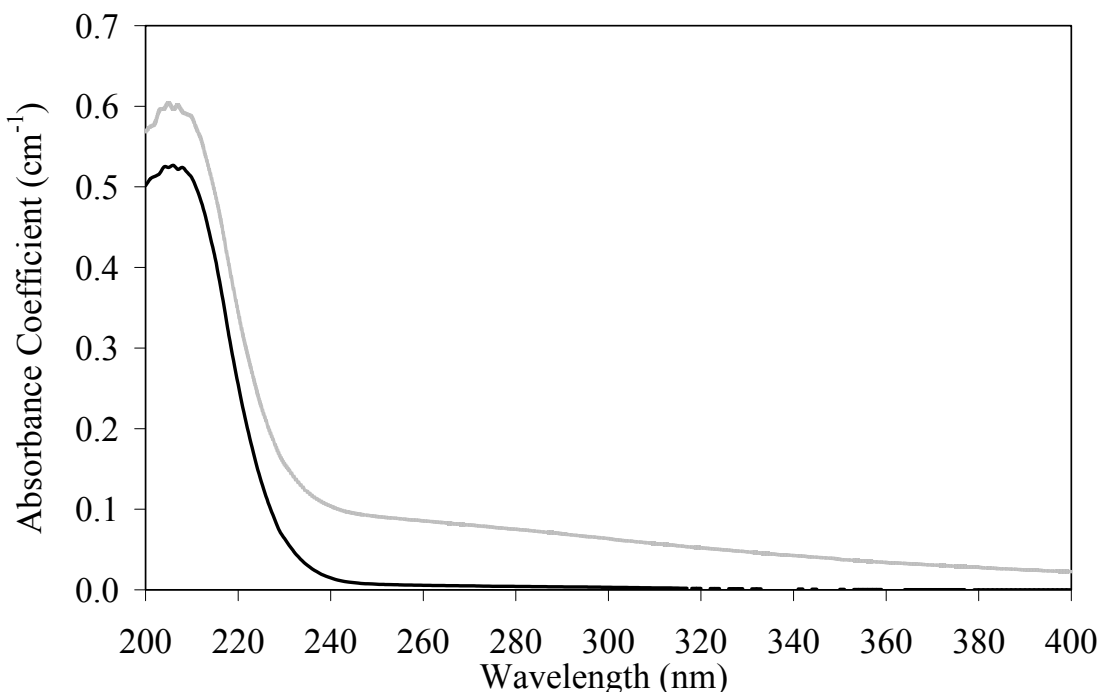


Figure 5.5 Spectral UV absorbance coefficients of raw test water and test water with Super Hume™

UV Sensor Calibration Check

The accuracy of the duty sensors was checked against three calibrated reference UV sensors multiple times over the course of the testing period. The reference UV sensor checks were performed with raw water (~98 % UVT) and water adjusted to 94 percent and 89 percent UVT using Super Hume™. Figure 5.6 compares the reference and duty UV sensor readings measured during testing. The residuals (the percent difference between duty and reference sensor readings) ranged from 1.1 to -3.0 percent. The average and standard deviation of the residuals were -0.4 and 1.2 percent, respectively. This indicated that there was no significant difference between the UV intensity as measured by the duty UV sensors and the reference UV sensors.

Biodosimetry

The biodosimetry test protocol was designed to quantify the difference in dose delivery measured using T7 and MS2 bacteriophage and measured using new and aged lamps. The test matrix, illustrated in Table 5.3, comprised of 12 test conditions plus controls (C1 – C3) and blanks (B1 – B3).

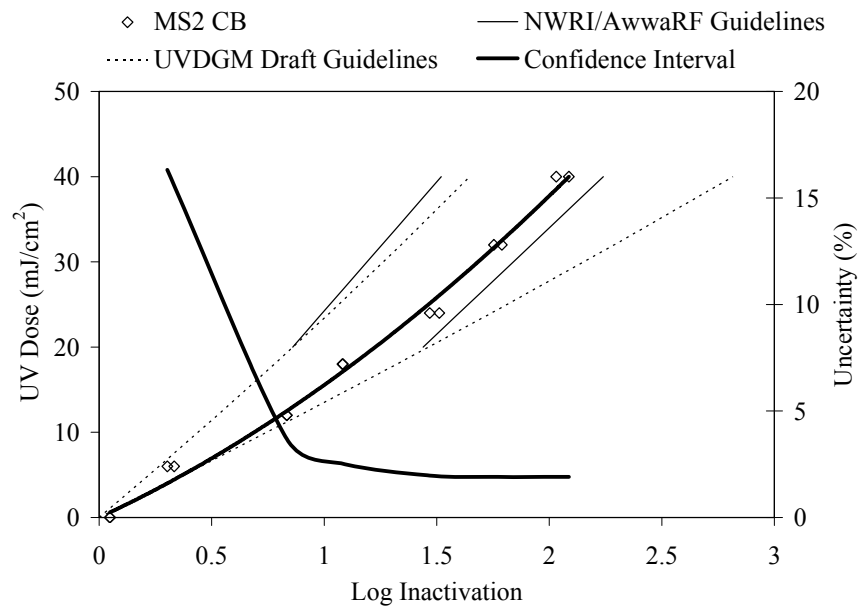


Figure 5.6 Relationship between reference and duty UV sensors obtained during reactor validation

**Table 5.3
Biodosimetry test plan**

Test ID	Microbe	Lamp type	# of lamps on	UVT (%)	UV intensity target (W/m ²)	Target dose (mJ/cm ²)
C1	MS2	N/A	0	76	N/A	N/A
C2	T7	N/A	0	76	N/A	N/A
C3	MS2	N/A	0	89	N/A	N/A
B1	-	New	1	76	N/A	N/A
B2	-	New	1	76	N/A	N/A
B3	-	Aged	1	89	N/A	N/A
1	MS2	New	1	89	162	19.7
2	MS2	New	1	83	99	12.3
3	MS2	New	1	76	58	8.5
4	T7	New	1	89	97	13.4
5	T7	New	1	83	59	8.9
6	T7	New	1	76	32	6.3
7	T7	Aged	1	89	97	13.4
8	T7	Aged	1	83	59	8.9
9	T7	Aged	1	76	32	6.3
10	MS2	Aged	1	89	162	19.7
11	MS2	Aged	1	83	99	12.3
12	MS2	Aged	1	76	58	8.5

Duplicate test runs comparing Super Hume™, the new UV absorber developed in this project, with the more commonly used lignin sulfonate (LSA) were not conducted because Super Hume™ has been used at the Portland Validation Facility since 2003, and its benefits over LSA are well documented (Hargy *et al.* 2004). As discussed in Chapter 3, for a given flow, UVT, and relative lamp output, the RED of a MP UV system measured with Super Hume and LSA is typically less than the RED that would be delivered with WTP waters. This conservatism is less with Super Hume. Super Hume™ also has a similar polychromatic bias as LSA.

The test conditions were conducted over two days. Test conditions 1-3, control C1 and blank B1 were done on October 19th 2005. Test conditions 4-12, controls C2 and C3, and blanks B2 and B3 were done on October 20th 2005. For each test condition, 5 inlet and 5 outlet replicate samples were collected.

Challenge Microbe UV Dose-Response

Figures 5.7 and 5.8 show the UV dose-response of MS2 and T7 phage measured using influent samples collected during tests ID 4 and ID 10, respectively. The dose-response data was analyzed to identify a regression equation that best fit the data with coefficients significant at a 95-percent confidence level (p-statistic <0.05). Both UV dose-response curves were best fit by a quadratic function forced through the origin (0,0):

$$UV \text{ Dose} = A \times (\log \text{ inactivation})^2 + B \times (\log \text{ inactivation}) \quad (5.1)$$

Table 5.4 summarizes the results of the regression analysis.

Both dose-response curves demonstrated curvature as opposed to first order kinetics. The MS2 phage dose-response fell within the recommended bounds provided in both the *USEPA UV Disinfection Guidance Manual* draft (USEPA 2003a) and the *NWRI/AwwaRF UV Guidelines* (NWRI 2003). The T7 UV dose-response curve showed no significant shoulder or tailing in the UV dose range analyzed.

Figures 5.7 and 5.8 also show the uncertainty of the UV dose predicted using each regression equation. The uncertainty was calculated as an 80-percent confidence interval and expressed as a percentage of the predicted UV dose. The uncertainty of the predicted dose with MS2 ranged from 2 to 17 percent as UV dose decreased from 40 to 6 mJ/cm². On the other hand, the uncertainty with T1 ranged from 1 to 4 percent as the UV dose decreased from 18 to 4 mJ/cm². For a given UV dose, especially at low dose values, the uncertainty of the predicted dose was less with T7.

Table 5.4
T7 and MS2 phage UV dose-response regression analysis

Microbe	Sample test ID	UVT (%)	A			B		
			Value	Standard error	p-statistic	Value	Standard error	p-statistic
T7	4	89	0.3577	0.04	5x10 ⁻⁰⁷	3.0293	0.12	1x10 ⁻¹¹
MS2	10	89	3.3257	0.63	2x10 ⁻⁴	12.222	1.08	1x10 ⁻⁷

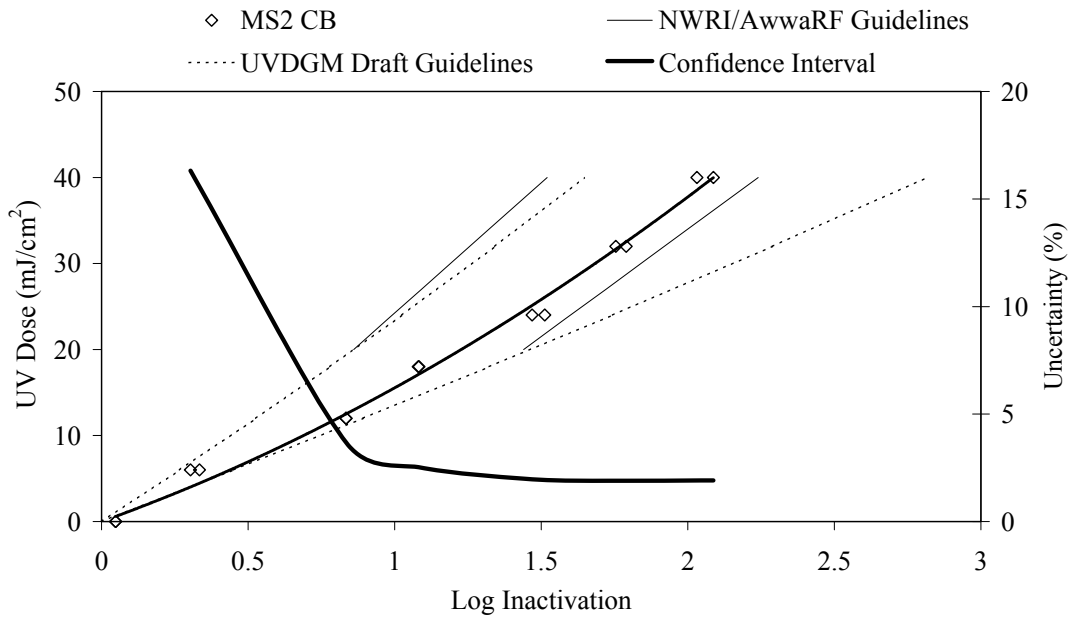


Figure 5.7 UV dose-response of MS2 phage measured during testing

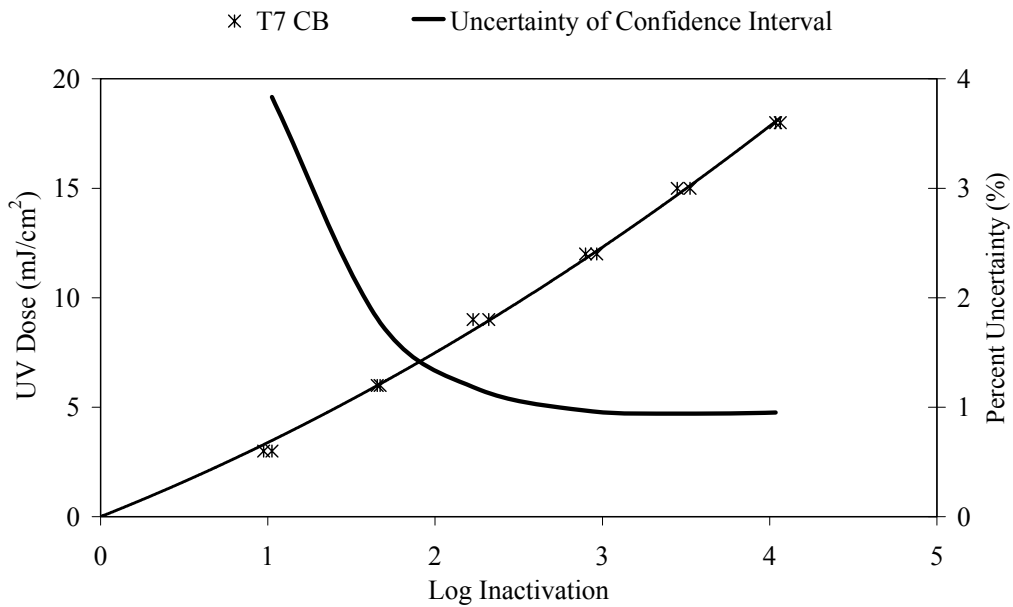


Figure 5.8 UV dose-response of T7 phage measured during testing

Controls and Blanks

Control samples were influent and effluent samples collected with MS2 injection on and the UV reactor off. [Table 5.5](#) presents data on the control samples collected during reactor validation. The mean difference between the log influent and effluent counts observed through the reactor was 0.01 ± 0.05 log. (mean \pm standard deviation). This corresponded to a maximum RED error of 0.16 and 0.04 mJ/cm² for the MS2 and T7, respectively. The data demonstrated that there was no significant change in phage concentration through the UV reactor when the lamps were off.

Blank samples were influent and effluent samples collected with the UV reactor on, halting phage injection, and flushing the system with groundwater for a period corresponding to five residence times of the system (injection loop, inlet piping, reactor and outlet piping). [Table 5.6](#) presents data on the blank samples. Ideally, the blanks should have no microbes present. The maximum phage concentrations in the influent and effluent blanks were 3.1 pfu/mL and 10 pfu/mL, respectively. These levels correspond to approximately 2 and 6 percent of the lowest measured phage concentration in the influent and effluent samples, respectively, during testing. Thus, the background phage concentration had no significant impact on the measured phage concentrations with each test condition.

Table 5.5
Controls collected during validation testing
(Reported as mean \pm standard deviation)

Control ID	Log influent concentration	Log effluent concentration	Log difference
C1	4.51 ± 0.03	4.55 ± 0.02	0.04
C2	4.11 ± 0.05	4.15 ± 0.02	0.04
C3	4.55 ± 0.03	4.51 ± 0.10	-0.04

Table 5.6
Blanks collected during validation testing
(Reported as mean \pm standard deviation)

Blank ID	Blank (pfu/mL)*	
	Influent	Effluent
B1	3.1 ± 2.0	0.4 ± 0.4
B2	0.0 ± 0.0	10.0 ± 3.0
B3	2.4 ± 1.7	0.2 ± 0.4

*Plaque forming units per milliliter

Bacteriophage Samples Stability

The temporal stability of MS2 and T7 phage was analyzed using water samples collected with test conditions 8 and 12. The water samples with test conditions 8 and 12 contained Super Hume™ for UVT adjustment to 83.2 and 75.9 percent UVT, respectively. The samples were stored at 4°C and the phage concentration was monitored over eight days. The results of stability tests, shown in Table 5.7, indicate that phage concentrations were stable. The relative standard deviations of log inactivation over the 8-day period were 2.2 and 1.5 percent for Test ID 8 and 12, respectively.

Biodosimetry Testing Results

Table 5.8 shows the results of the biodosimetry testing.

Table 5.7
Bacteriophage sample stability

Test ID	Log inactivation			RED (mJ/cm ²)		
	Day 1	Day 4	Day 8	Day 1	Day 4	Day 8
8	1.667	1.734	1.672	6.05	6.33	6.07
12	0.422	0.414	0.426	5.75	5.63	5.80

Table 5.8
Biodosimetry test results

Test ID	Microbe	Lamp type	UVT (%)	UV intensity (W/m ²)	Flow (mgd)	Log N ₀	Log N	Log I [*]	Measured	Calculated
									RED (mJ/cm ²)	MS2 RED [†] (mJ/cm ²)
1	MS2	New	89.0	155.3	1.19	4.50	3.48	1.02	15.9	17.4
2	MS2	New	83.0	95.2	1.19	4.47	3.78	0.69	10.0	10.1
3	MS2	New	76.0	56.9	1.19	4.51	4.09	0.42	5.8	6.5
4	T7	New	88.8	91.5	1.20	4.98	2.51	2.47	9.7	11.3
5	T7	New	83.0	57.1	1.20	4.20	2.5	1.70	6.2	6.6
6	T7	New	75.9	30.9	1.20	4.23	3.06	1.17	4.0	4.0
7	T7	Aged	89.1	82.6	1.20	5.01	2.72	2.29	8.8	10.5
8	T7	Aged	83.2	57.3	1.20	4.15	2.48	1.67	6.0	6.7
9	T7	Aged	76.0	31.0	1.20	4.24	2.33	1.91	4.2	4.0
10	MS2	Aged	89.1	148.0	1.20	4.53	3.52	1.01	15.8	16.7
11	MS2	Aged	82.9	91.0	1.20	4.52	3.86	0.66	9.6	9.6
12	MS2	Aged	75.9	49.6	1.20	4.51	4.09	0.42	5.7	5.8

* Log I = Log N₀ - Log N, † Calculated using the UV reactor's MS2 validated calculated dose algorithm

RED Bias Assessment

Because the T7 and MS2 REDs were not measured under identical conditions of flow, UVT, and lamp output, the RED bias could not be directly determined. Instead, the calculated dose algorithm for the Calgon Carbon Sentinel UV reactor, determined from prior MS2 validation, was used to predict the MS2 RED delivered with each test condition. The RED bias was then determined by calculating the ratio of the MS2 RED predicted using the UV dose-monitoring algorithm to the T7 RED measured in this work.

Figure 5.9 shows the relation between the measured and predicted RED values for the MS2 field-testing conditions (Test ID's 1-3 and 10-12). Figure 5.9 shows that the calculated dose algorithm predicts the measured MS2 RED on average within 6 percent. This error is within the uncertainty of the dose-monitoring algorithm provided in the UV reactor's validation report.

Table 5.9 summarizes the RED bias calculations. The RED bias values ranged from 0.95 to 1.19, values notably less than the RED bias uncertainty factors provided in the *UVDGM* (USEPA 2006c). The value of RED bias was greater with higher MS2 REDs. The test conditions only evaluated MS2 REDs up to 11.3 mJ/cm², notably less than the MS2 needed to show compliance to 3-log *Cryptosporidium* inactivation at a UV dose of 12 mJ/cm². Greater RED bias values would be expected with MS2 REDs needed to show 3-log *Cryptosporidium* inactivation (see Chapter 6).

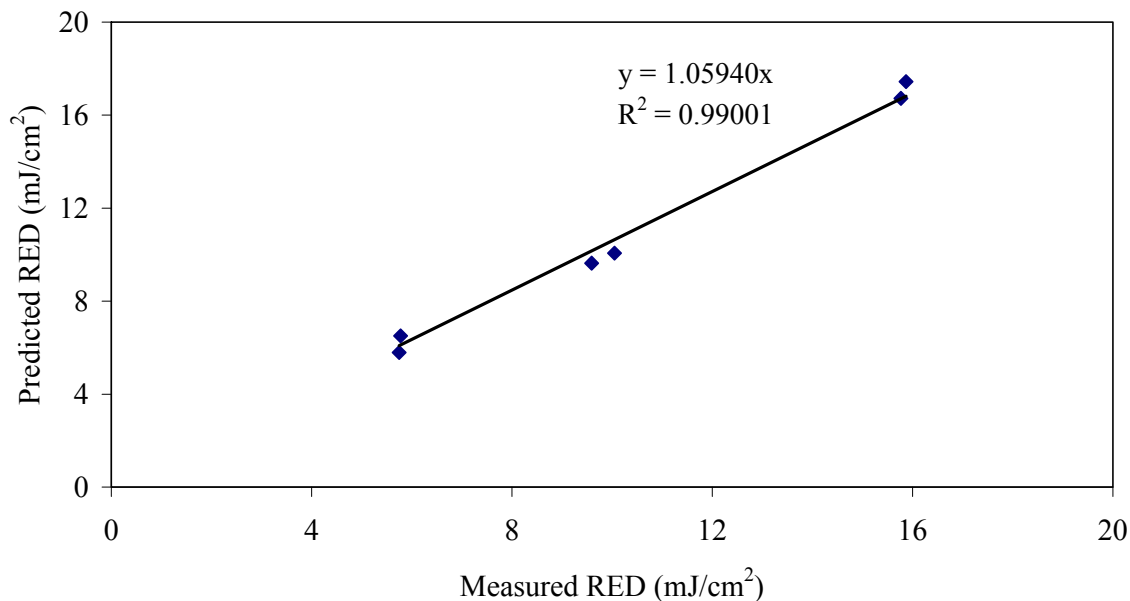


Figure 5.9 MS2 dose delivery predictions versus measured dose for MS2 field-testing conditions

Table 5.9
RED bias calculations

Test ID	T7 RED (mJ/cm ²)	T7 log inactivation	Calculated MS2 RED (mJ/cm ²)*	Calculated MS2 log inactivation†	UVT (%)	RED bias
4	9.7	2.5	11.3	0.76	89	1.16
5	6.2	1.7	6.6	0.48	83	1.07
6	4.0	1.2	4.0	0.30	76	0.99
7	8.8	2.3	10.5	0.72	89	1.19
8	6.0	1.7	6.7	0.48	83	1.10
9	4.2	1.9	4.0	0.30	76	0.95

* Calculated using the UV reactor's MS2 validated calculated dose algorithm

† Determined from MS2 UV dose-response (Figure 5.7) using calculated MS2 RED

The observation that the RED bias values measured with MS2 and T7 are less than the RED bias uncertainty factors in the UVDGM indicates that the test reactor had a narrower dose distribution than that used by USEPA to determine the RED bias uncertainty factors. However, because of differences in the action spectra of T7 and MS2, described in Chapter 2, a polychromatic bias of 1.15 should be applied to the measured RED bias to compare the difference between MS2 and T7 to the RED bias uncertainty factors listed in the UVDGM. The combined bias was estimated as 1.09 to 1.37.

Figure 5.10 compares the UV dose-response of T7 and MS2 phage with the UV dose requirements for *Cryptosporidium* provided in the LT2ESWTR (USEPA 2006a). The comparison shows that the UV dose-response of T7 matches the UV dose-requirements of *Cryptosporidium* provided in the LT2ESSWTR better than MS2. However, T7 is more resistant to UV light than *Cryptosporidium* for UV doses less than 14 mJ/cm². Hence, an RED bias uncertainty factor, albeit small in value, would still be applied to T7 REDs less than 14 mJ/cm².

Table 5.10 gives the RED bias uncertainty factors determined using the USEPA UVDGM for the measured T7 REDs and the calculated MS2 REDs determined for a subset of the test conditions evaluated in this work. The RED bias uncertainty factors for 3-log *Cryptosporidium* credit range from 1.49 to 1.53 with MS2. That range increases to 2.13 to 2.89 for 1-log *Cryptosporidium* credit. The RED bias uncertainty factors with T7 are notably lower being 1.0 for 3-log *Cryptosporidium* credit and ranging from 1.24 to 1.32 for 1-log *Cryptosporidium* credit.

Because the RED bias of the reactor determined using the measured MS2 and T7 REDs is less than the RED bias uncertainty factors given in the UVDGM for MS2 phage, validation using T7 will provide capital and O&M costs savings because the applied RED bias uncertainty factors with T7 will not be overly conservative.

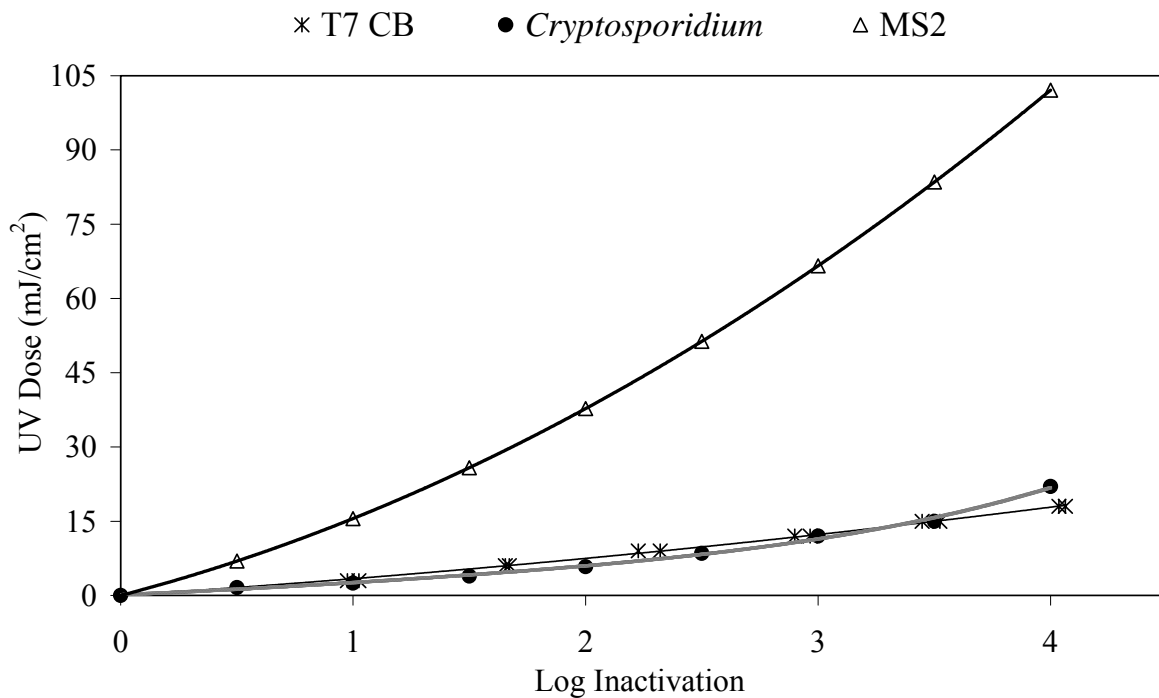


Figure 5.10 Comparison of MS2 and T7 UV dose-response with *Cryptosporidium* UV dose requirements

**Table 5.10
RED bias uncertainty factors for demonstrating *Cryptosporidium* inactivation
with MS2 and T7 REDs**

Test ID	UVT	Test Microbe	Calculated UV sensitivity (mJ/cm ² / log)*	RED bias uncertainty factors for demonstrating a <i>Cryptosporidium</i> inactivation of:							
				0.5- log	1.0- log	1.5- log	2.0- log	2.5- log	3.0- log	3.5- log	4.0- log
4	89	MS2	14.8	1.74	2.13	2.18	2.12	1.98	1.82	1.73	1.53
		T7	3.9	1.10	1.24	1.21	1.14	1.07	1.00	1.00	1.00
5	83	MS2	13.8	2.04	2.47	2.43	2.26	2.03	1.82	1.71	1.49
		T7	3.6	1.13	1.28	1.24	1.16	1.07	1.00	1.00	1.00
6	76	MS2	13.2	2.43	2.89	2.74	2.48	2.18	1.92	1.79	1.53
		T7	3.4	1.15	1.32	1.26	1.18	1.08	1.00	1.00	1.00

* Ratio of calculated MS2 RED and log inactivation given reactor operating conditions (Table 5.9)

This conclusion is specific to the reactor tested. The RED bias of a reactor technology will depend on the reactor's dose distribution, which in turn will depend on its design. If a reactor has a wide enough distribution, the reactor's RED bias may be similar in value to the RED bias uncertainty factors tabulated in the UVDGM, and there will be no advantage testing with T7 compared to MS2 phage. If the dose distribution of the reactor is wider than the dose distribution used to determine the RED bias uncertainty factors, then those factors will not be sufficient to ensure the reactor delivers the required UV dose for *Cryptosporidium* and *Giardia* inactivation. In that case, validation with T7, with appropriate corrections for the action spectra if the UV system uses MP lamps, will ensure better public health protection than MS2 validation.

Impact of Lamp Aging on UV Dose Delivery

Table 5.11 compares the dose delivery by the reactor equipped with the new and aged lamp. For a given flow and UVT, the ballast power setting with the new lamp was lowered to give a UV sensor reading comparable to that measured with the aged lamp. The data shows no significant difference in dose delivery between new and aged lamp for a given UV sensor reading, UVT, and flow. These results indicate either that the UV sensor was appropriately located within the reactor to account for non-uniform lamp aging, that the reactor baffle ensured non-uniform lamp aging did not significantly impact the relation between RED and UV sensor readings, or that non-uniform lamp aging was not significant with the aged lamp tested. As discussed in Chapter 6, models shows that non-uniform lamp aging can have significant impacts on dose delivery monitoring. Therefore, further evaluation of the impact of lamp aging on dose delivery and monitoring with different commercial UV reactors is recommended.

Table 5.11
Impact of lamp aging on UV dose delivery

Microbe	MS2						T7					
Test ID	1	10	2	11	3	12	4	7	5	8	6	9
Lamp type (N or A)*	N	A	N	A	N	A	N	A	N	A	N	A
S (W/m ²)	155.3	148.0	95.2	91.0	56.9	49.6	91.5	82.6	57.1	57.3	30.9	31.0
RED (mJ/cm ²)	15.9	15.8	10.0	9.6	5.8	5.7	9.7	8.8	6.2	6.0	4.0	4.2
Δ RED (mJ/cm ²)	0.1		0.4		0.1		0.9		0.2		-0.2	

* N - New; A - Aged

CONCLUSIONS

The following is a summary of the most important findings from the field-testing:

- The concentrations of microbial samples with Super Hume™ remained stable over an 8-day period of analysis. This was consistent with previous studies, which indicated that Super Hume™ enhanced microbial stability (Hargy *et al.* 2004).
- For a given UV dose, the uncertainty of the UV dose-response of T7 was less than that of MS2, especially at low UV doses. As such, if both MS2 and T7 were used to validate a reactor for similar *Cryptosporidium* inactivation credit, the T7 analysis would have greater confidence associated with the UV dose-response analysis and the REDs determined using that UV dose-response.
- Validation of the UV reactor using T7 bacteriophage as opposed to MS2 significantly reduces the RED bias uncertainty factors needed for *Cryptosporidium* inactivation credit. For example, the RED bias uncertainty factors provided in the UVDGM for 3-log *Cryptosporidium* inactivation are 1.0 with T7 phage but range from 1.18 to 2.45 with MS2 depending on the UVT of the water.
- The ratio of RED measured using MS2 and T7 phage with the reactor evaluated in this study was notably less than the RED bias uncertainty factors listed in the UVDGM. This indicates that the reactor's dose distributions are not as wide as the dose distributions used by USEPA to define the RED bias uncertainty factors.
- The difference in the action spectra of T7 and MS2 phage should be considered when validating UV reactors equipped with MP lamps. In this study, a factor of 1.15 was applied to the T7 REDs measured using the MP reactor to account for the difference in the action of MS2 and T7.
- If UV systems have narrow dose distributions, validation with T7 as opposed to MS2 will reduce the under estimation of dose delivery that occurs when applying the RED bias uncertainty factors provided in the UVDGM. This would provide capital and O&M costs savings when applying the reactor at a WTP.
- If the UV systems have dose distributions wider than those used to develop the RED bias uncertainty factors, validation of the reactor with T7 as opposed to MS2 will prevent overestimation of dose delivery to *Cryptosporidium* and *Giardia*, thereby ensuring the reactors provide the appropriate level of public health protection with application at the WTP.
- Dose delivery for the test reactor was not significantly impacted by use of an aged lamp compared to a new lamp. This observation indicates either that the UV sensor was appropriately located within the reactor to account for non-uniform lamp aging, that the reactor baffle ensured non-uniform lamp aging did not significantly impact the relation between RED and UV sensor readings, or that non-uniform lamp aging was not significant with the aged lamp tested. This result is specific to this reactor and the lamp tested and further evaluation of the impact of lamp aging on dose delivery and monitoring with different commercial UV reactors is recommended.

CHAPTER 6

ANALYSIS USING COMPUTATIONAL DISINFECTION MODELS

This chapter describes work conducted using UV intensity and dose delivery modeling to understand the impact of test microbe inactivation kinetics, UVA spectra, and non-uniform lamp aging on dose delivery and monitoring by commercial UV reactors used in drinking water applications.

APPROACH

Two UV reactors, representing commercial technologies, were modeled as part of two AwwaRF projects - Bridging Pilot-Scale Testing to Full-Scale Design of UV Disinfection Systems (Mackey et al. 2004) and Design and Performance Guidelines for UV Sensor Systems (Wright et al. 2005). Figures 6.1 and 6.2 show schematic illustrations of the two reactors. The UV system shown in Figure 6.1 was equipped with 6 staggered rows of 12 LPHO lamps oriented perpendicular to flow. The lamps had an arc length of 150 cm and were housed within quartz sleeves with a radius of 1.7 cm. The UV system shown in Figure 6.2 was equipped with eight MP lamps oriented perpendicular to flow. The lamps had an arc length of 61 cm and were housed within quartz sleeves with a radius of 3.9 cm.

UV intensity fields within each reactor were modeled using UVXPT software developed by Carollo Engineers (Wright and Reddy 2003). For this work, the software was modified to account for non-uniform UV output along the length and about the circumference of the lamp. Figure 6.3 describes the UV intensity calculation algorithm. The algorithm treats a UV lamp as 199-point sources. The algorithm first calculates the UV intensity as a function of radial and axial distance from a single point source, accounting for UV absorbance of the water and refraction through the air-quartz and quartz/water interfaces of the lamp sleeve (Bolton 2000). The UV intensity about a lamp is then predicted by summing the contribution of each point source along the length of the lamp, weighted by a function that accounts for non-uniform UV output along the arc length and a function that accounts for non-uniform lamp output about the lamp circumference.

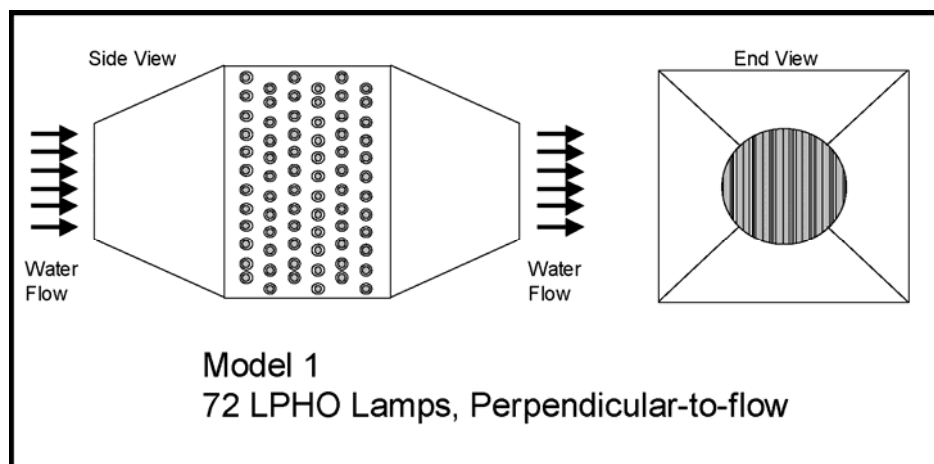


Figure 6.1 Schematic of the LPHO UV system

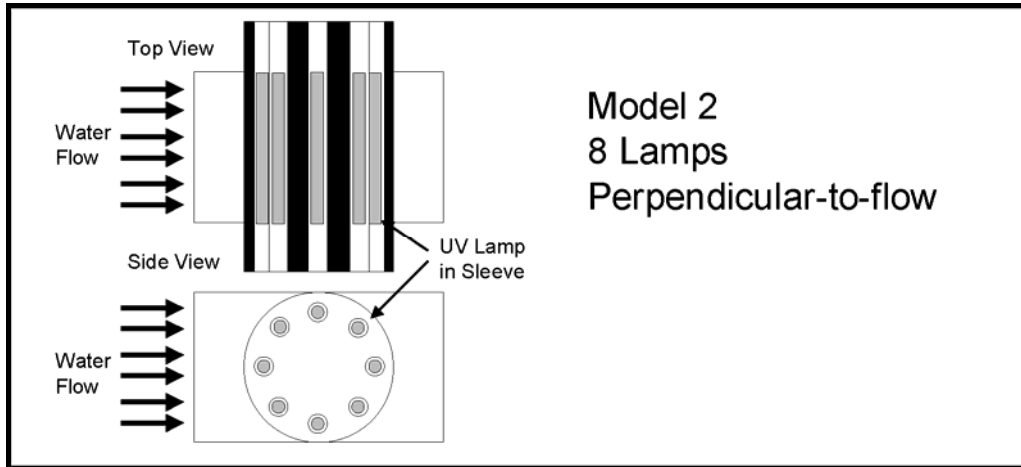


Figure 6.2 Schematic of the MP UV system

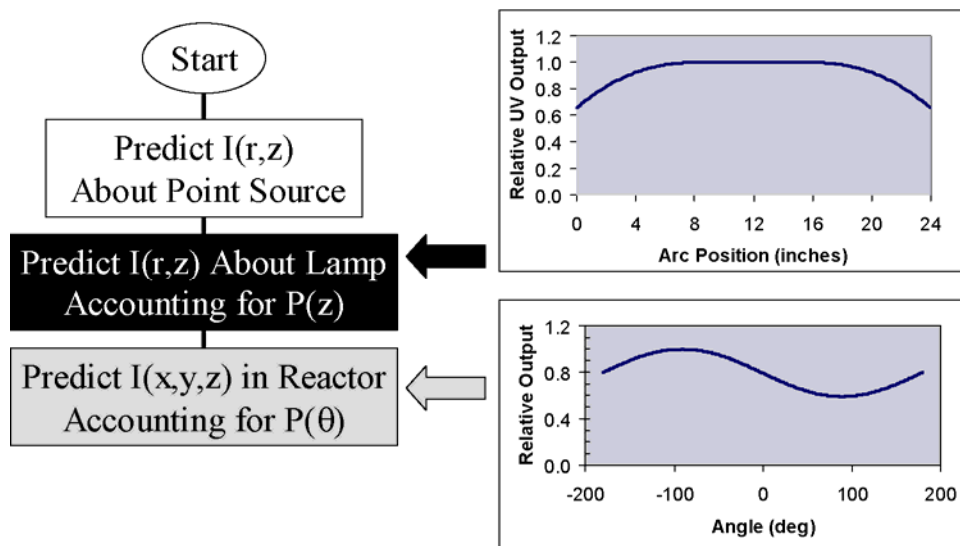


Figure 6.3 UV intensity algorithm accounts for non-uniform UV output along length and about the circumference of the lamp using weighting functions

The software calculates UV intensity for both LP and MP UV lamps. Polychromatic dose calculations are performed over 1 nm intervals from 200 to 320 nm, and account for the spectral output of the lamp, the spectral UV absorbance of the lamps sleeves and the water, reflection and refraction at the lamp sleeve air-quartz and quartz-water interfaces, and the spectral response of the microbes. UV sensor readings are calculated by integrating the UV intensity at the location of the UV sensor, accounting for the angular and spectral response of the UV sensor. Polychromatic sensor calculations are done over 1 nm intervals from 200 to 400 nm. The range extends past 320 nm to 400 nm to provide UV sensor calculations for SiC sensor types used by some commercial UV systems.

The CFD software FLUENT was used to model fluid flow through the reactors and predict the paths taken by microbes as they traveled through the UV reactor. FLUENT software solved the Navier-Stokes equations describing fluid flow over a three-dimensional grid generated using Gambit software. The output from the CFD-modeling was a data file giving the position (x,y,z) and time coordinates describing the trajectories of approximately 3000 virtual microbes through the UV reactors. The starting coordinates of the trajectories were uniformly distributed across the inlet pipe upstream of the reactor.

The UVXPT software was used to determine the UV dose delivered to each virtual microbe by integrating the germicidal UV intensity as a function of time over the trajectory through the UV reactor. The net inactivation of a microbe was determined using:

$$f = \frac{1}{n} \sum_i \exp(-k \times D_i) \quad (6.1)$$

where f is the fractional of microbes remaining, n is the number of microbe trajectories simulated, k is the first order inactivation coefficient of the microbe of interest, and D_i is the UV dose deliver to the trajectory. The Reduction Equivalent Dose (RED) was using:

$$\exp(-k \times RED) = \frac{1}{n} \sum_i \exp(-k \times D_i) \quad (6.2)$$

which can be written:

$$RED = -\frac{1}{k} LN \left[\frac{1}{n} \sum_i \exp(-k \times D_i) \right] \quad (6.3)$$

UVXPT uses Microsoft Excel as a user interface. The user specifies input parameters such as the microbe trajectory data file, the location of the lamps and sensors within the UV reactor, the germicidal output of the lamps, the dimensional and optical properties of the lamp sleeves, the UV absorbance and flowrate of the water, and the action spectra and inactivation kinetics of the microbes. The output from the software included dose per microbe, the dose distribution, net inactivation by the reactor, delivered RED, and UV sensor readings.

RESULTS

RED Bias

Figure 6.4 shows the RED predicted using the MP reactor as a function of relative lamp output S/S_0 and microbe D10 for UVTs of 80 and 98 percent. Figure 6.5 shows similar data for the LPHO reactor with 6 operating rows of lamps. With the term S/S_0 , S represents the UV sensor reading at the power setting of the simulation and S_0 represents the UV sensor readings expected at 100 percent power. Lamp output is defined as S/S_0 instead of lamp power because the relation between power setting and lamp output is often not linear with commercial UV systems and ballast power does not indicate lamp aging or fouling. The term D10 is the UV dose required to inactivate a microbe with first order inactivation kinetics by one log. D10 is related to the microbe's first order inactivation constant, k , by:

$$D10 = - \frac{\text{LN}(0.1)}{k} \quad (6.4)$$

The bias in dose monitoring that occurs if the validation microbe has different inactivation kinetics compared to the target pathogen can be defined as:

$$B_{\text{RED}} = \frac{\text{RED}_V}{\text{RED}_P} \quad (6.5)$$

where RED_V is the validation microbe RED and RED_P is the target pathogen RED for a given flow, UVT, and S/S_0 . Figure 6.6 shows the MP reactor's RED bias as a function of relative lamp output and validation microbe D10. The RED bias is calculated relative to a target pathogen D10 = 4 mJ/cm². Figure 6.7 shows similar data for the LPHO reactor. The RED bias is greater than one for those validation microbes with D10 greater than 4 mJ/cm² and less than one for those validation microbes with D10 less than 4 mJ/cm². The RED bias varies in a complex manner with UVT and S/S_0 . For a given S/S_0 value, the RED bias is greater at low UVT with the MP reactor but greater at high UVT with the LPHO reactor. The RED Bias also varies with S/S_0 , in some cases increasing as S/S_0 increases and in some cases decreasing.

Figure 6.8 shows the RED bias for the MP reactor as a function of pathogen RED (D10 = 4 mJ/cm²). The RED bias is calculated using a validation microbe D10 = 18 mJ/cm² and a pathogen D10 = 4 mJ/cm². Figure 6.9 shows similar data for the LPHO reactor. The figures show that for a constant RED, the RED bias increases with lower UVT for both reactors. For a constant UVT, the RED bias increases with the RED to a maximum and then decreases.

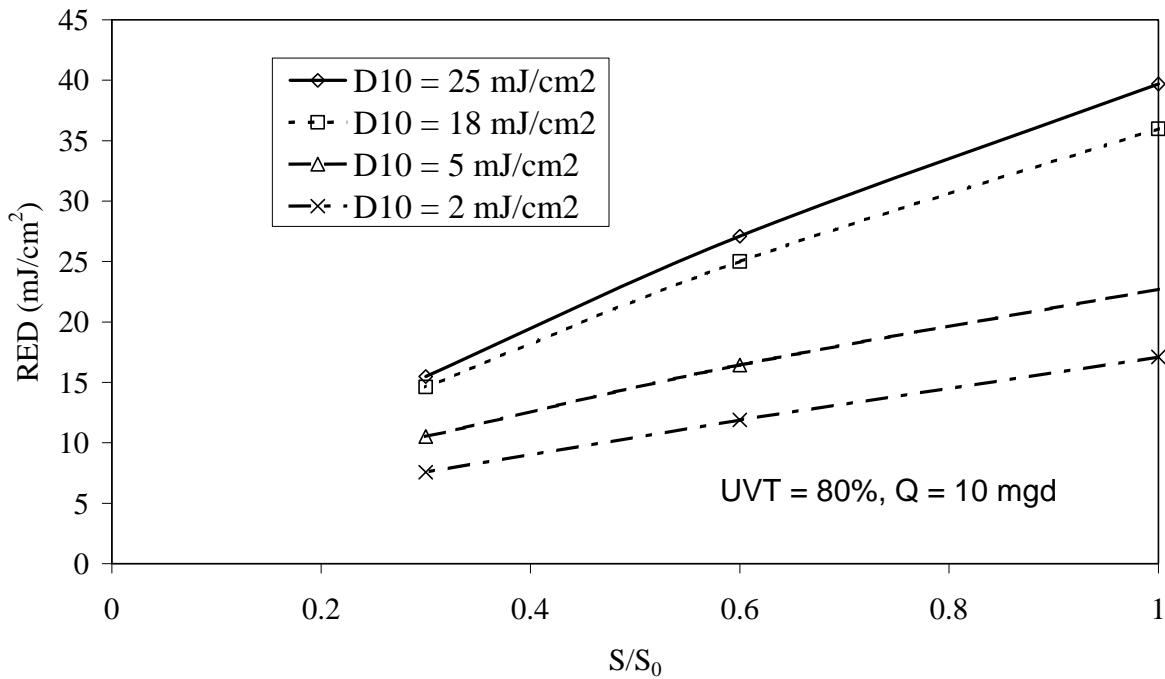
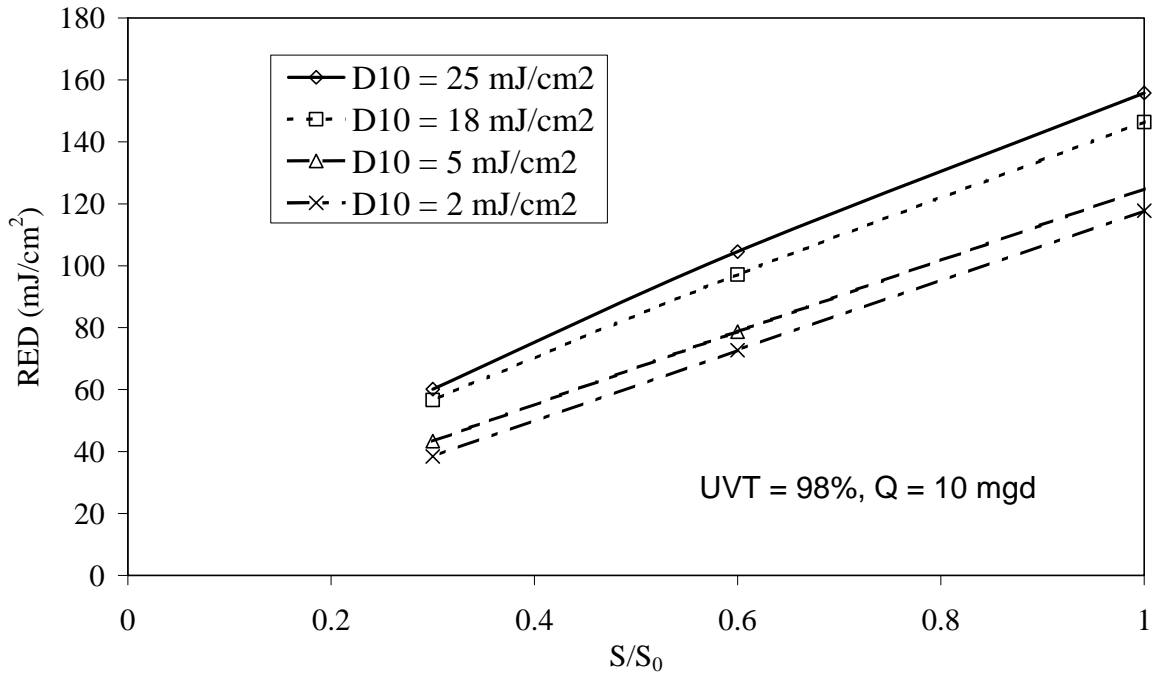


Figure 6.4 RED delivered by the MP reactor as a function of relative lamp output (S/S_0) and microbe inactivation kinetics (D_{10}) for 98 % UVT (top) and 80% UVT bottom

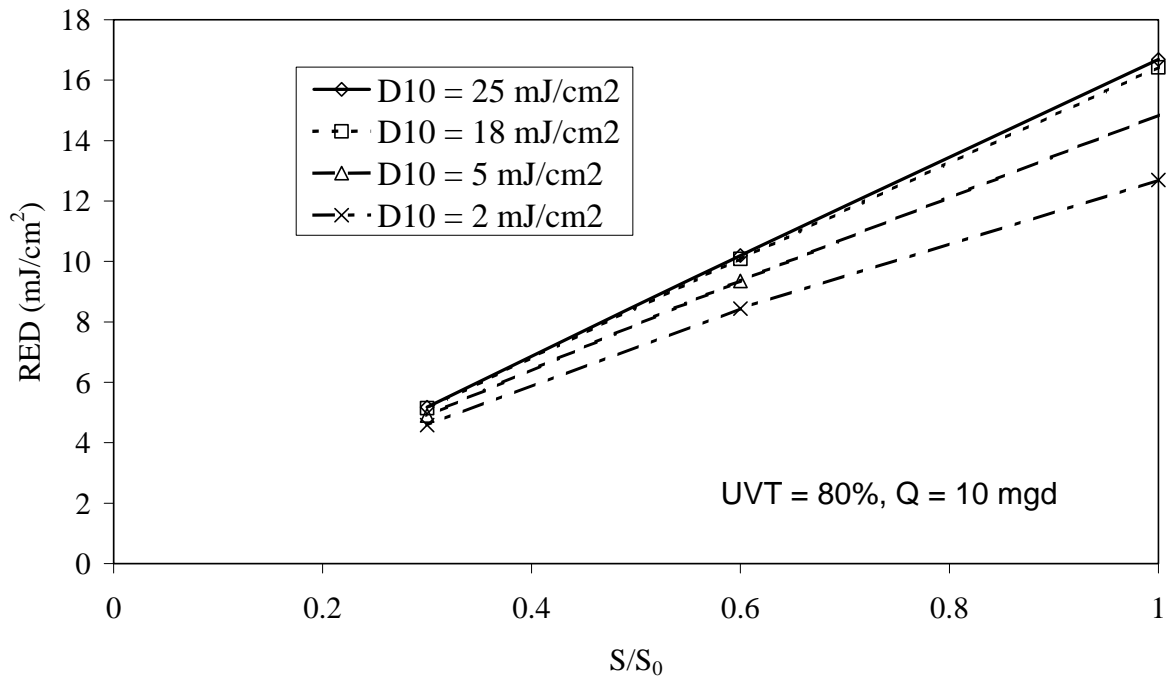
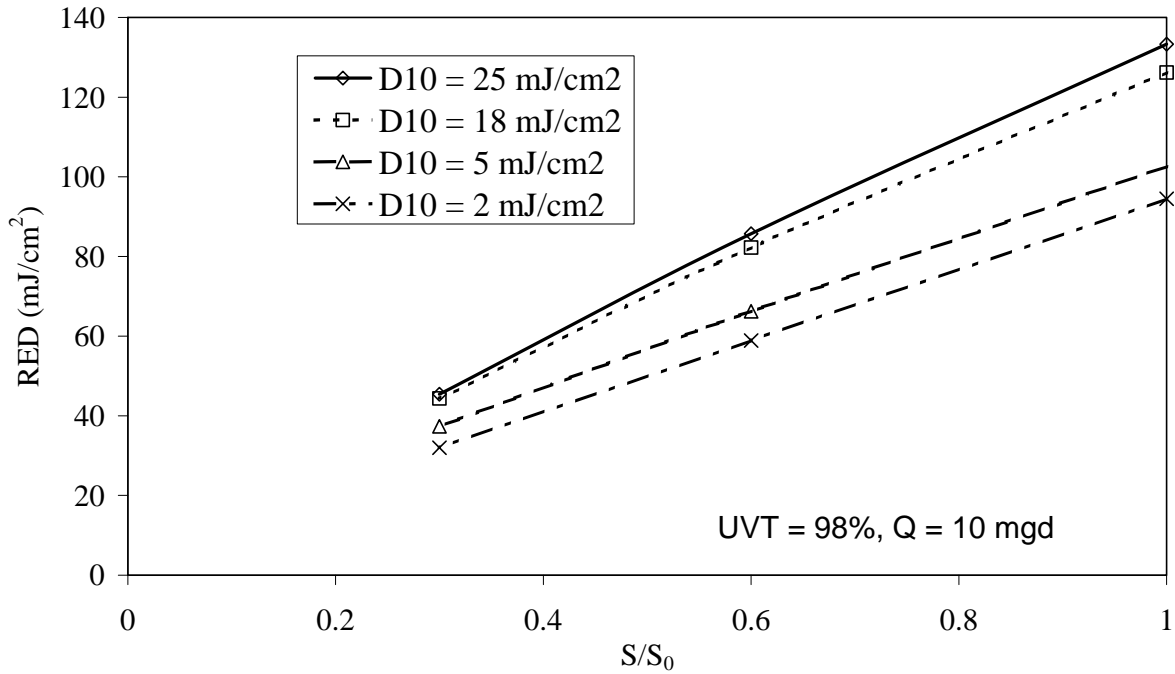


Figure 6.5 RED delivered by the 6-row LPHO reactor as a function of relative lamp output (S/S_0) and microbe inactivation kinetics (D10) for 98 % UVT (top) and 80% UVT bottom

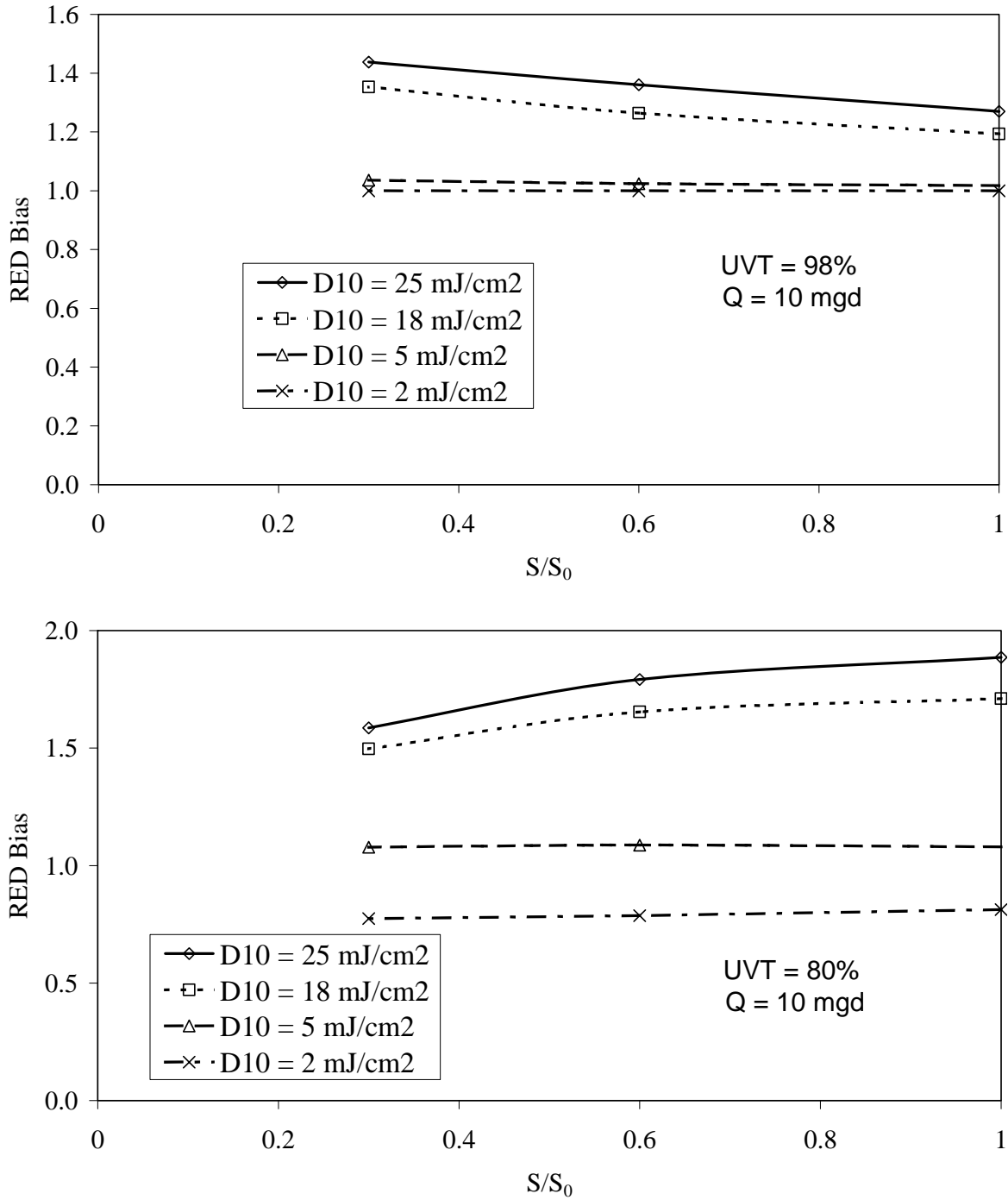


Figure 6.6 RED bias relative to D10 = 4 mJ/cm² of the MP reactor as a function of relative lamp output (S/S_0) and microbe inactivation kinetics (D10) for 98 % UVT (top) and 80% UVT bottom

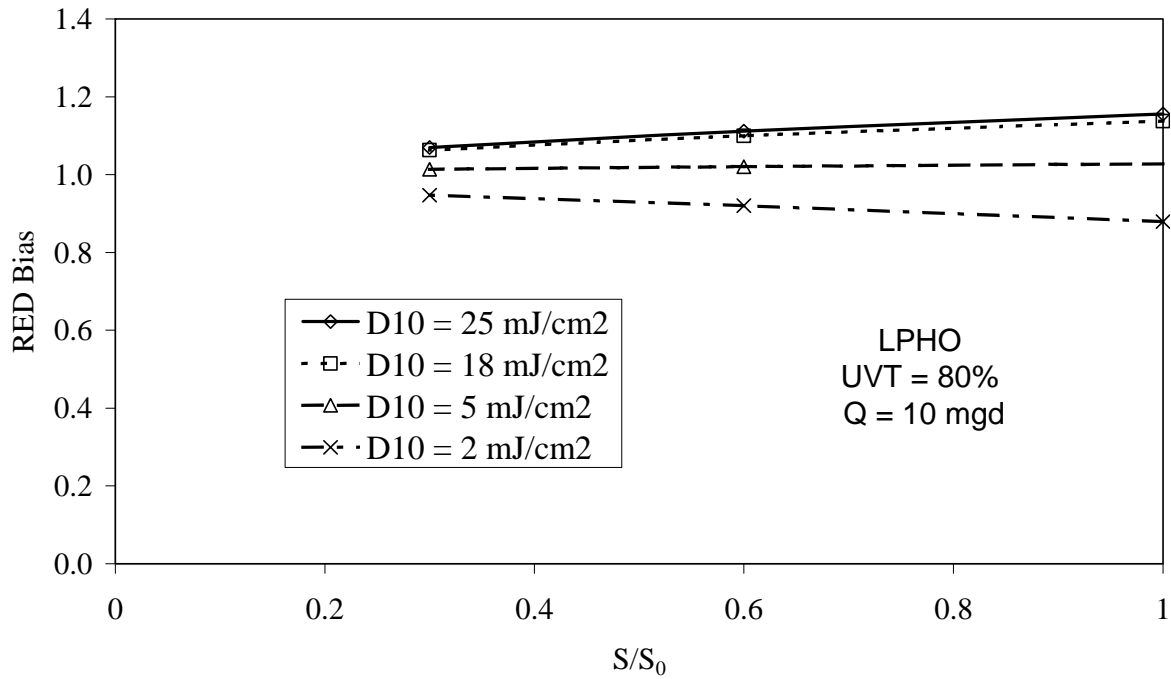
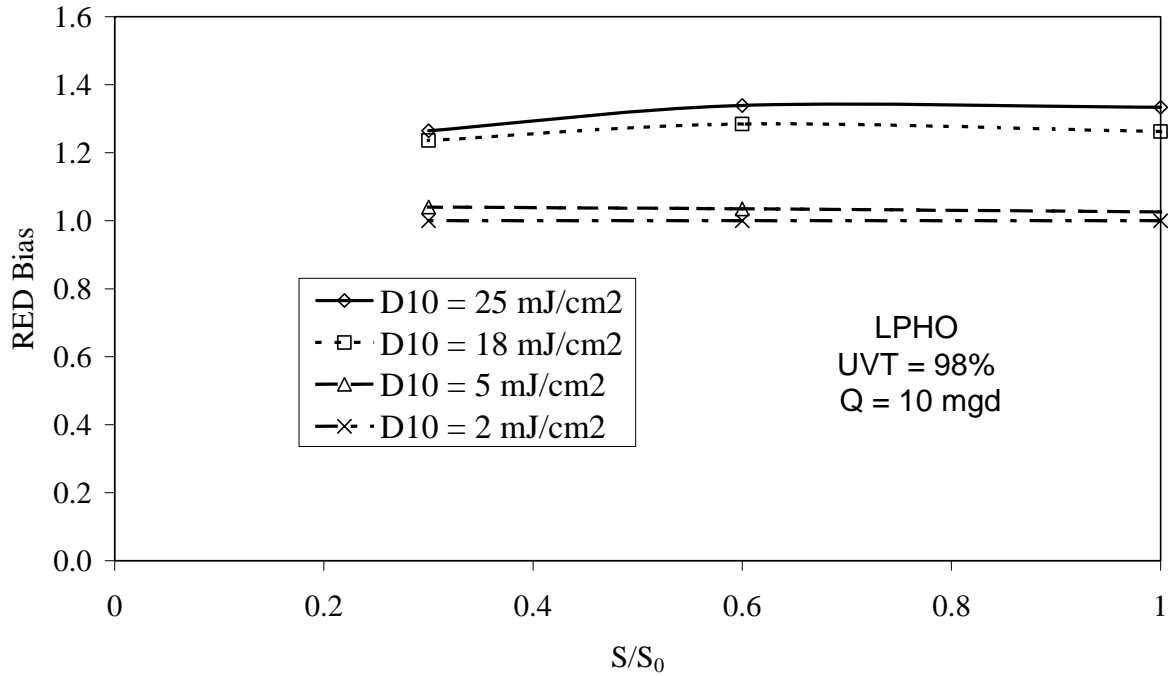


Figure 6.7 RED bias relative to D10 = 4 mJ/cm² of the LPHO reactor with 6 rows of operating lamps as a function of relative lamp output (S/S₀) and microbe inactivation kinetics (D10) for 98 % UVT (top) and 80% UVT bottom

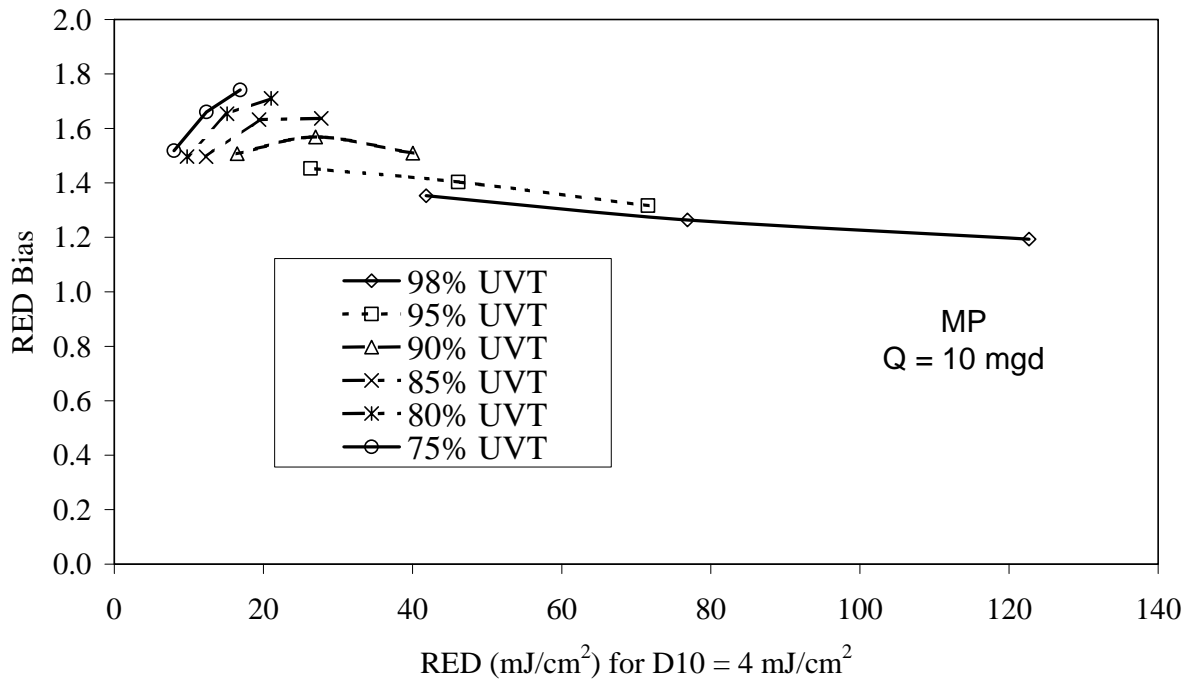


Figure 6.8 RED bias with the MP reactor as a function of RED based on $D_{10} = 4 \text{ mJ/cm}^2$. RED bias is calculated as the ratio of REDs for $D_{10} = 18$ and 4 mJ/cm^2 .

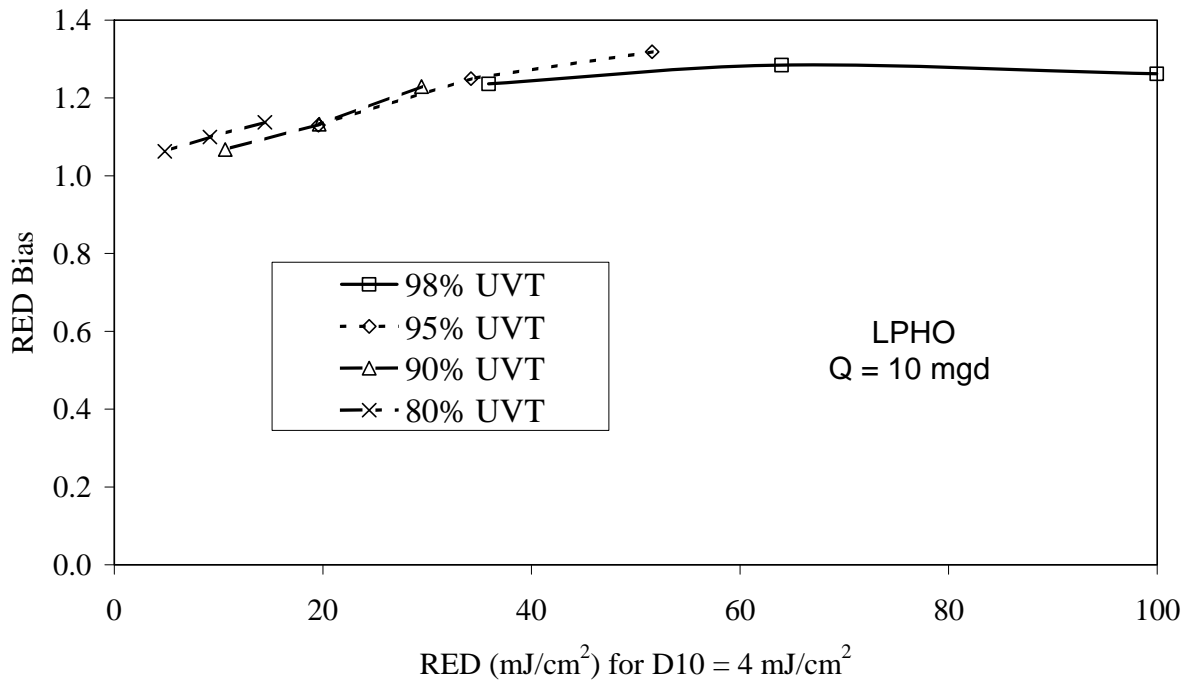


Figure 6.9 RED bias with the 6-row LPHO reactor as a function of RED based on $D_{10} = 4 \text{ mJ/cm}^2$. RED bias is calculated as the ratio of REDs for $D_{10} = 18$ and 4 mJ/cm^2 .

To understand the relations between RED and S/S_0 , D_{10} , and UVT, Equation 6.1 can be written as:

$$\begin{aligned} \log I &= -\log \left[\frac{1}{n} \sum_i \exp \left(-k \times D_i \times \frac{S}{S_0} \right) \right] \\ &= \log \left[\frac{1}{n} \sum_i 10^{\left(-D_i/D_{10} \times S/S_0 \right)} \right] \end{aligned} \quad (6.6)$$

where $\log I$ is the log inactivation of the microbe with first order inactivation kinetics characterized by D_{10} and D_i is the dose delivered to the i th particle with $S/S_0 = 1$ (i.e. 100 % lamp output). The equation assumes that UV dose distribution of the reactor at a relative lamp output of S/S_0 equals the dose distribution at $S/S_0 = 1$ scaled by the ratio S/S_0 . The equation indicates that $\log I$ can be defined as a function of $S/S_0/D_{10}$ using a single relation

Figures 6.10 and 6.11 present $\log I$ as a function of $S/S_0/D_{10}$ for the MP and LPHO reactors, respectively. As expected from equation 6.6, the predicted relation between $\log I$ and $S/S_0/D_{10}$ for a given UVT is described using a single relation. This function can be used to predict the log inactivation and RED of different microbes for a given UVT and relative lamp output. For example, at 90% UVT and a relative lamp output of 0.3, the log inactivation of microbes with $D_{10} = 4$ and 18 mJ/cm^2 is 4.10 and 1.43 log, respectively, which corresponds to REDs of 25.8 and 16 mJ/cm^2 , respectively. The RED bias is calculated as $25.8/16 = 1.57$.

Spectral Shifts with MP Lamps

The impact of changes in the spectral output of MP lamps (i.e. spectral shifts) on dose delivery and monitoring were investigated using the MP reactor model with lamp data given in Chapter 4 for the Type 1 and Type 2 MP lamps. The Type 1 MP lamps modeled were the new lamp and aged lamp #10 and the Type 2 MP lamps modeled were the new lamp and the aged lamp SR4. The UV output data of the new lamp was normalized to give a germicidal output of 12.9 W/cm based on the action spectra of MS2 (Rauth, 1966). The UV output of the aged lamp in W/cm was then calculated by multiplying the normalized new lamp output by the ratio of the aged to new lamp output given in chapter 4 (Figures 4.51 and 4.71). The UV sensor readings were modeled using the spectral responses given in Figure 6.12 and the angular response given in Figure 6.13. The data presented in Figures 6.12 and 6.13 were obtained from the AwwaRF Project Design and Performance Guidelines for UV Sensor Systems. The UV sensor readings were predicted for UV sensor-to-lamp water layers ranging from 2 to 20 cm.

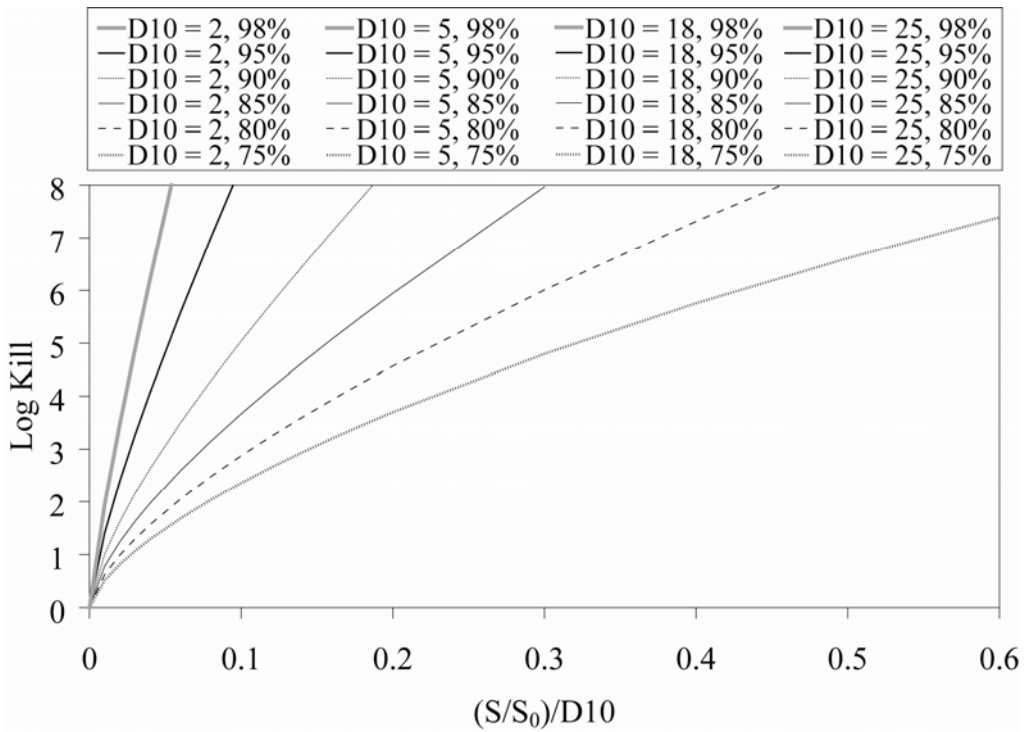


Figure 6.10 Log inactivation as a function of $S/S_0/D_{10}$ and UVT for the MP reactor

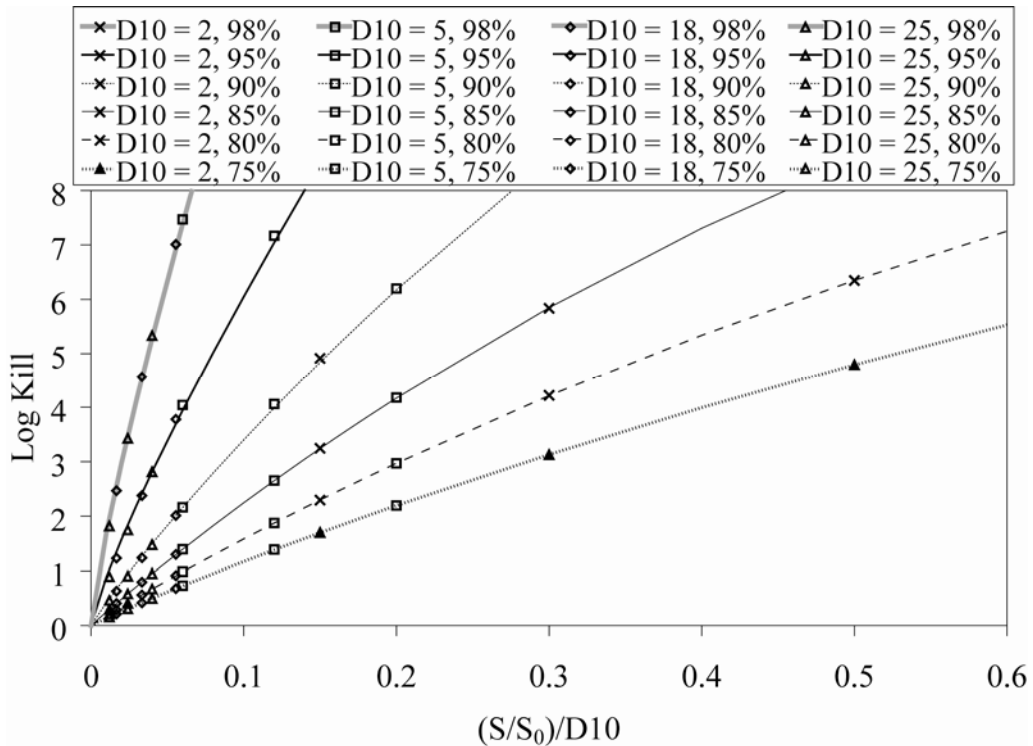


Figure 6.11 Log inactivation as a function of $S/S_0/D_{10}$ and UVT for the LPHO reactor operating with 6 rows of lamps

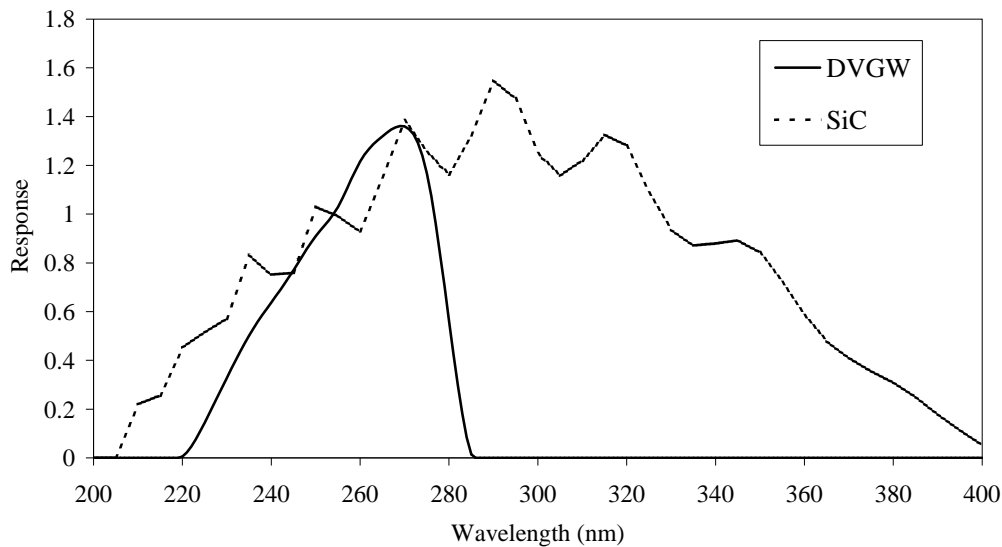


Figure 6.12 Spectral response of DVGW and SiC UV sensors

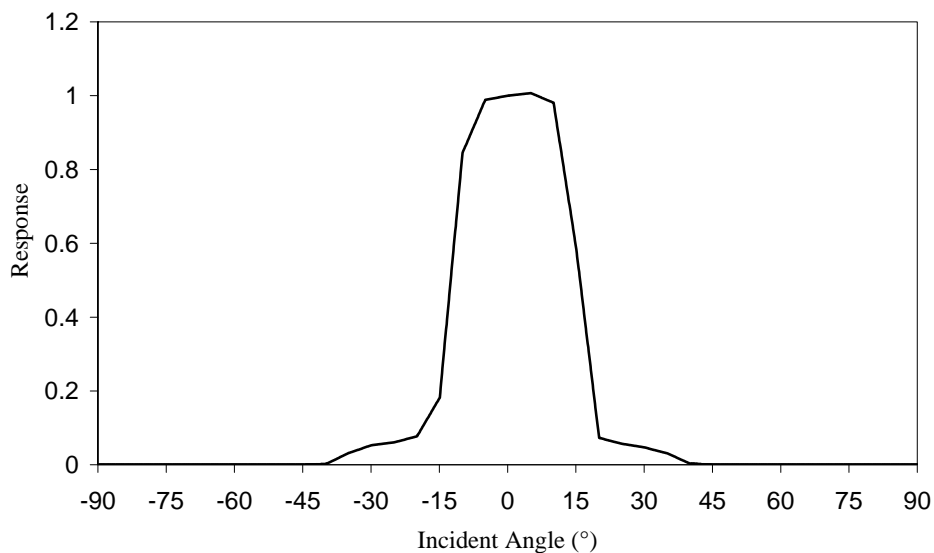


Figure 6.13 Angular response of DVGW and SiC UV sensors

Figure 6.14 presents the MS2 RED ($D_{10} = 18 \text{ mJ/cm}^2$) as a function of UV sensor readings and UVT for different water layers. The UV sensor modeled was the DVGW sensor. With a 2 cm water layer, the RED for given UV sensor reading decreases with lower UVT. However, with a 20 cm water layer, the RED for a given UV sensor reading decreases with higher UVT. At intermediate positions of 5, 10 and 15 cm, the relation between RED and UVT for a given UV sensor reading has a minima at some UVT value. For example, at a water layer of 10 cm, the RED for a given sensor reading has a minimum value at a UVT of 90%. The UVT associated with the minimum RED is higher as the water layer increases. For example, at a water layer of 15 cm, the RED for a given sensor reading has a minimum value at 95% UVT.

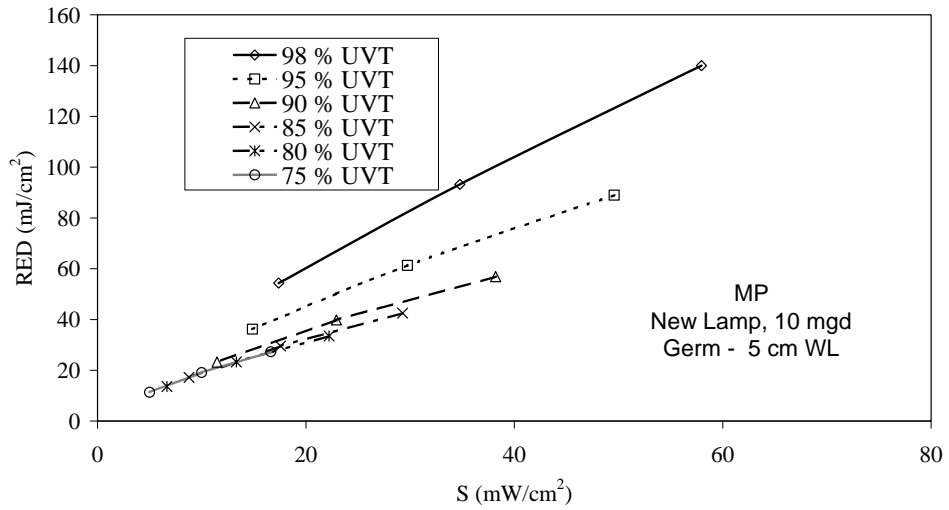
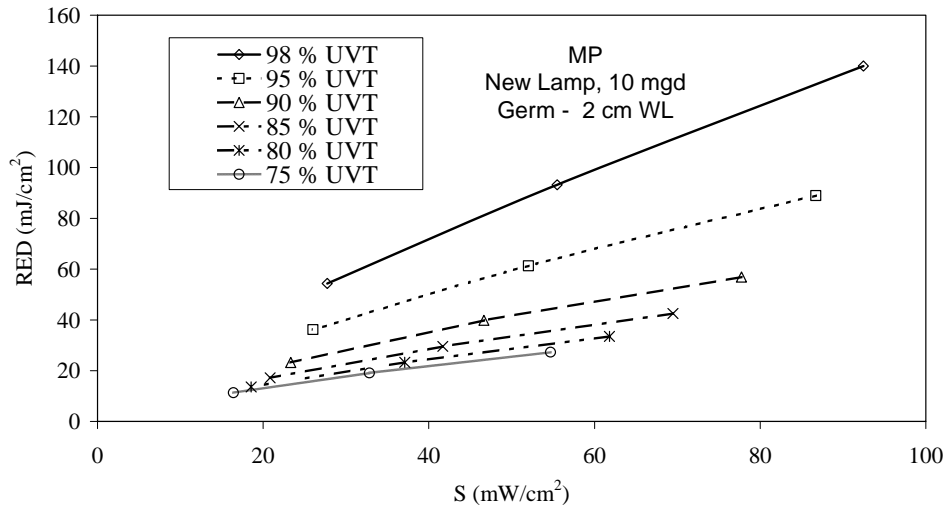


Figure 6.14 MS2 RED ($D_{10} = 18 \text{ mJ/cm}^2$) as a function of DVGW UV sensor readings and UVT for water layers of 2, 5, 10, 15, and 20 cm

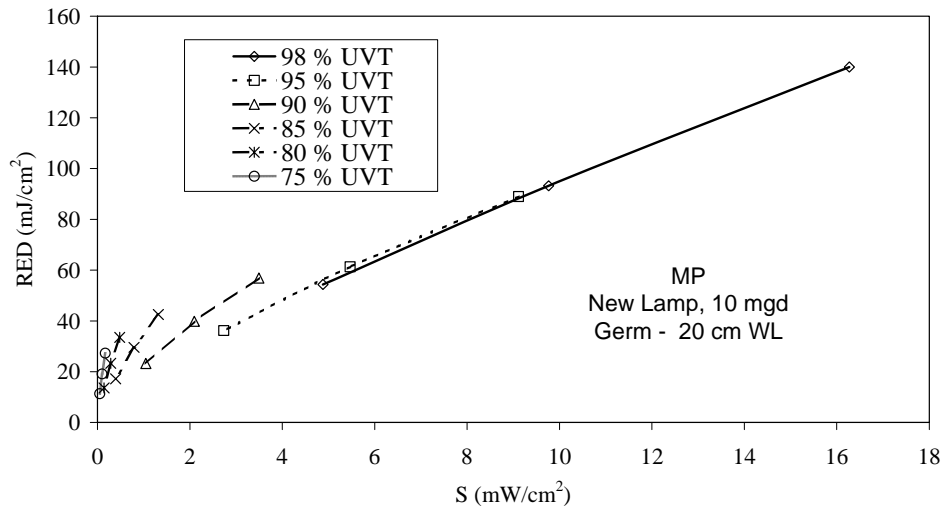
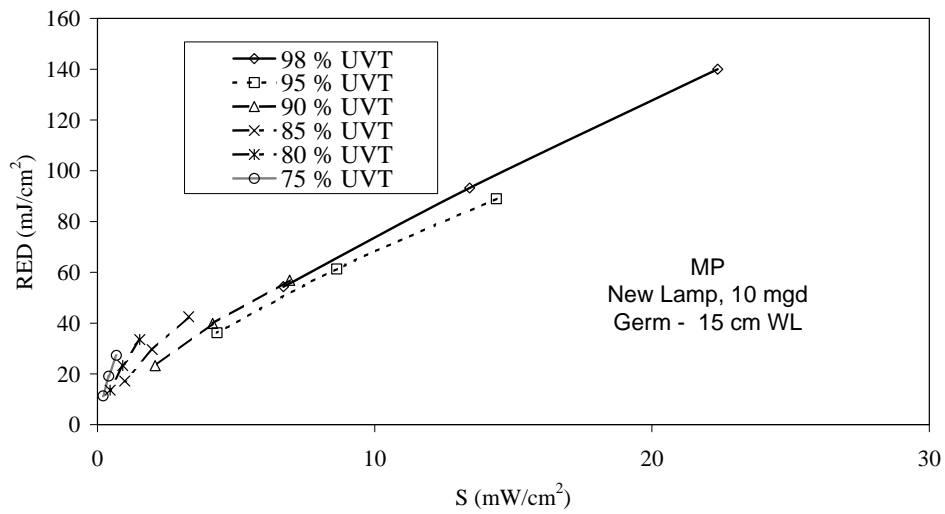
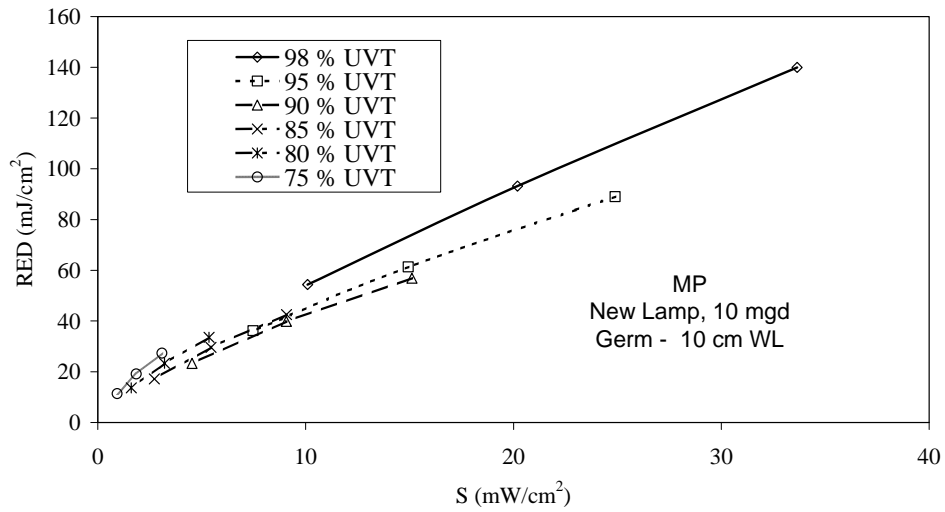


Figure 6.14 (Continued). MS2 RED ($D_{10} = 18 \text{ mJ/cm}^2$) as a function of DVGW UV sensor readings and UVT for water layers of 2, 5, 10, 15, and 20 cm

These observations have profound impact on how dose monitoring using the UV intensity setpoint approach and the validation of that monitoring approach is done. With the UV intensity setpoint dose monitoring approach, the UV reactor delivers a validated dose when the UV sensor reads above an alarm level. The German DVGW, Austrian ONORM, and USEPA UV Guidance Manuals specify dose monitoring using the UV intensity setpoint approach. They also specify that UV reactors that use the UV intensity setpoint approach are validated using two test conditions. The first test condition involves operating the reactor at high UVT (e.g., 98%) and lowering the lamp power until the UV sensor reads at the alarm setpoint value. The second condition involves operating the reactor at maximum lamp power and lowering the UVT until the UV sensor reads at the alarm setpoint value. If the UV sensor is located too far from the lamp, the first test condition will give a lower RED. If the UV sensor is located too close to the lamp, the second condition will give a lower RED. In theory (Wright et al 2005), if the UV sensor is located at some optimal intermediate condition, the relation between RED and UV sensor readings for different UVTs will overlap and can be described by a single relation. This location is described as the ideal location for monitoring using the UV intensity setpoint approach.

In [Figure 6.14](#), there is no one UV sensor location where the relations between RED and UV sensor readings for different UVTs overlap. Instead, at an intermediate UV sensor location, the minimum RED occurs at an intermediate UVT. This observation shows that the test conditions currently used to validate UV reactors using the UV intensity setpoint approach for dose monitoring are not sufficient to prevent underdosing if the UV sensor is located at an intermediate position. For example, at a 10 cm water layer, the RED delivered with a UV sensor reading of 5 mW/cm² is 30 mJ/cm² at 98% UVT and 31 mJ/cm² at 75% UVT but only 25 mJ/cm² at 90% UVT. The results suggest that a third test condition using at intermediate UVT value is needed to validate UV reactors using the UV intensity setpoint approach.

[Figure 6.15](#) presents the MS2 RED (D10 = 18 mJ/cm²) as a function of UV sensor readings and UVT for different water layers with the SiC sensor. The relation between RED and UV sensor readings with the SiC sensor shows similar relations as with the DVGW sensor with the exception that the UVT associated with the minimum RED has a lower value for a given water layer. For example, at a water layer of 10 cm, the minimum RED occurred at a UVT of 90% with the DVGW sensor and 85% with the SiC sensor.

[Figure 6.16](#) shows the relation between RED and SiC UV sensor readings with new and aged Type 1 lamps for water layers of 2 and 20 cm and UVTs of 98 and 75%. The data shows that for a given SiC UV sensor reading, the RED with the aged lamps is less than the RED with the new lamps. The difference is greater at lower UVT and with a larger water layer. The difference between the REDs with new and aged lamps for a given UV sensor readings occurs because the aged lamp has a different spectral output compared to the new lamp. As shown in [Figure 4.51](#), Type 1 lamp #10 appears to have aged more at lower wavelengths than at higher wavelengths. Because the SiC sensor responds to wavelengths well above the germicidal range, the relative reduction in the SiC sensor readings with the aged lamp is less than the impact on dose delivery. This difference would lead to over estimates of dose delivery as the lamp ages.

[Figure 6.17](#) shows the relation between RED and DVGW UV sensor readings with new and aged Type 1 lamps. In this case, the data shows that the REDs with aged and new lamps are the same for a given UV sensor reading. In this case, the relative change in the UV sensor reading accurately mimics the relative change in dose delivery as the lamp ages. These results provide a rationale for using UV sensors whose spectral response mimics the wavelength

response of microbes and not using UV sensors that measure significant quantities of light above the germicidal range (i.e. 300 nm).

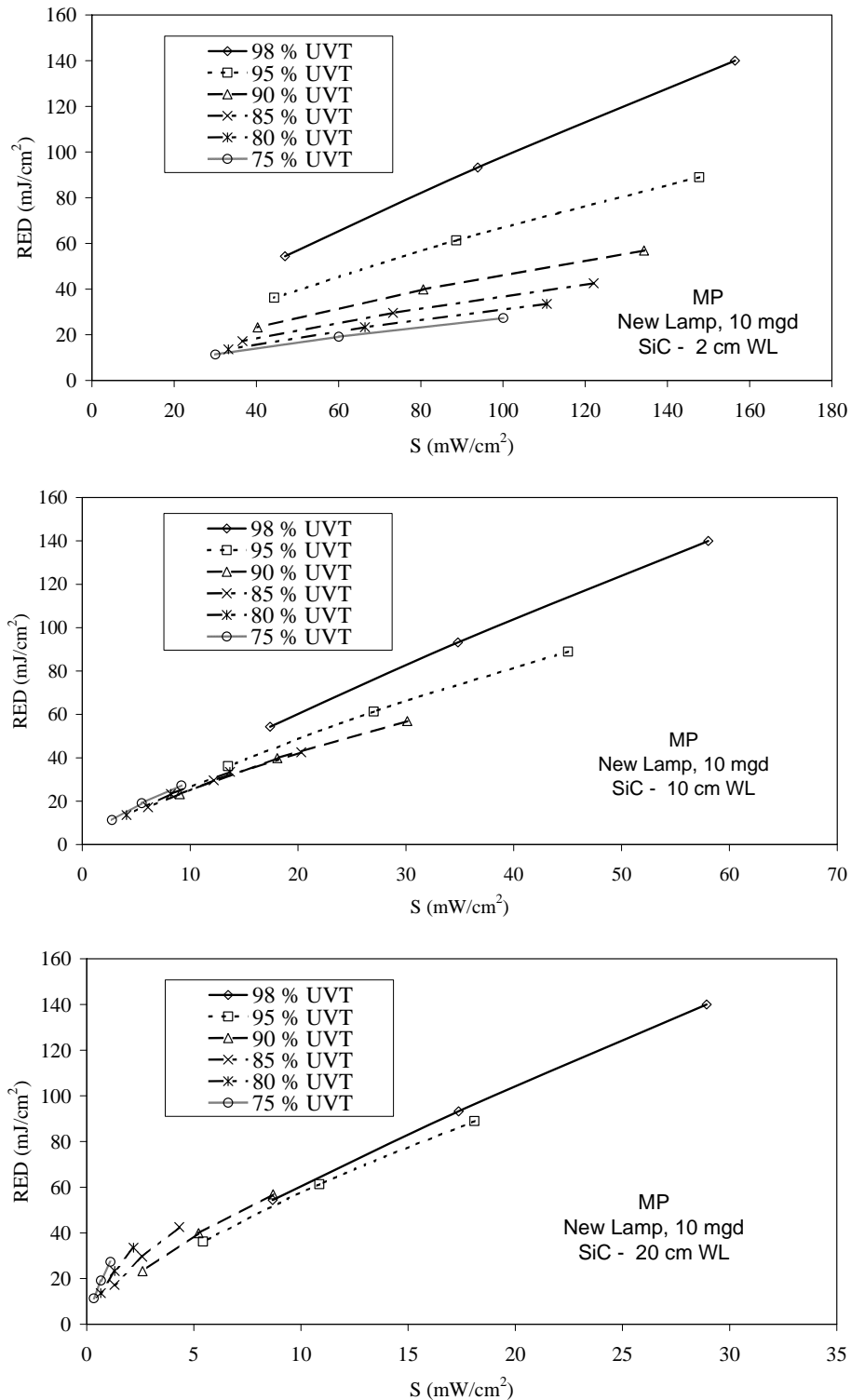


Figure 6.15 MS2 RED ($D_{10} = 18 \text{ mJ/cm}^2$) as a function of SiC UV sensor readings and UVT for water layers of 2, 10, and 20 cm

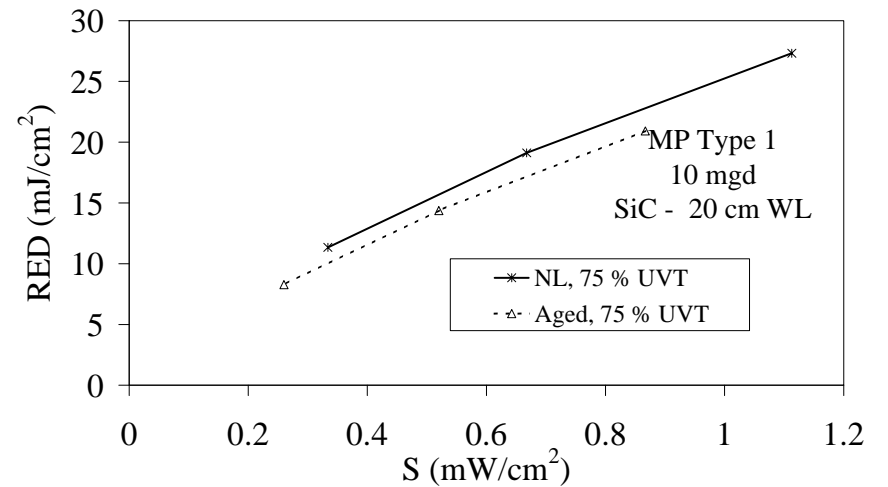
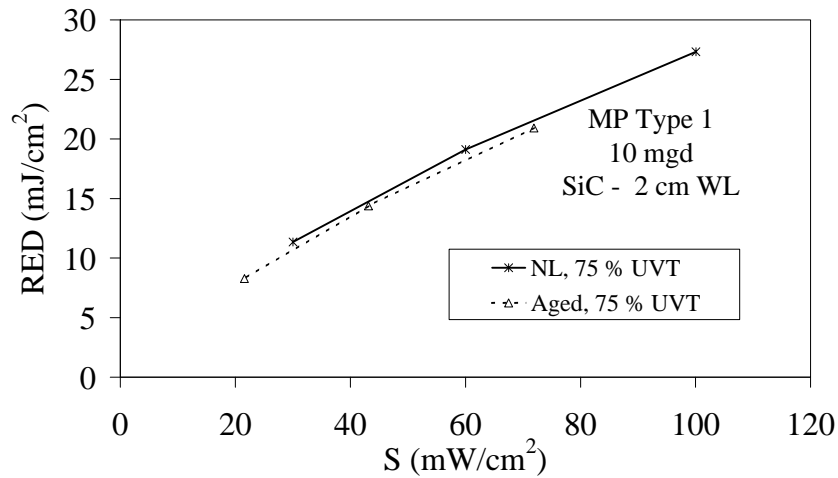
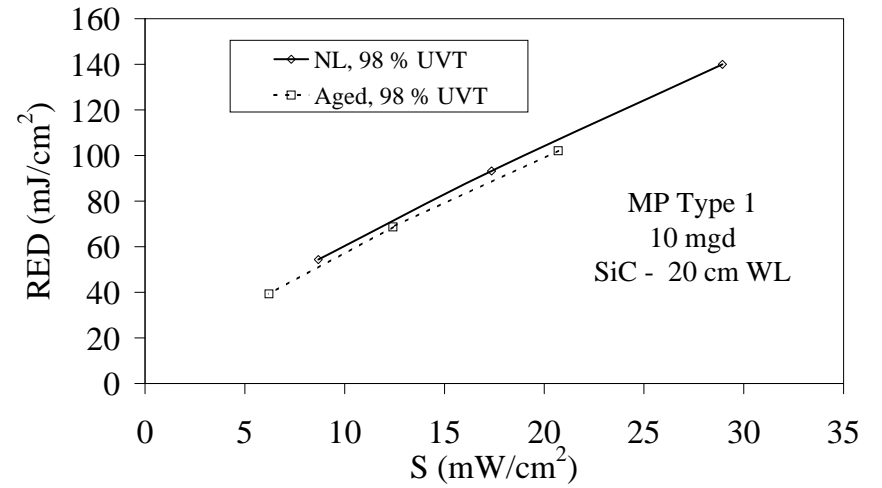
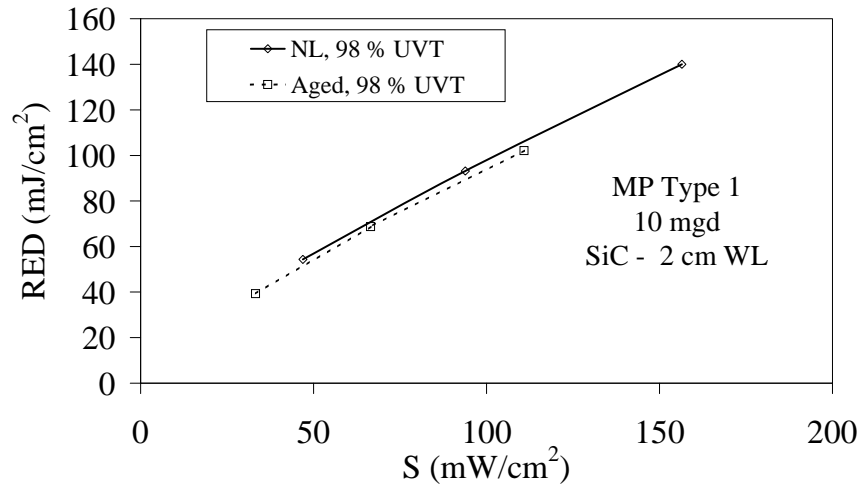


Figure 6.16 MS2 RED ($D_{10} = 18 \text{ mJ/cm}^2$) delivered by new and aged Type 1 MP lamps as a function of SiC UV sensor readings for water layers of 2 and 20 cm and UVTs of 98 and 75%

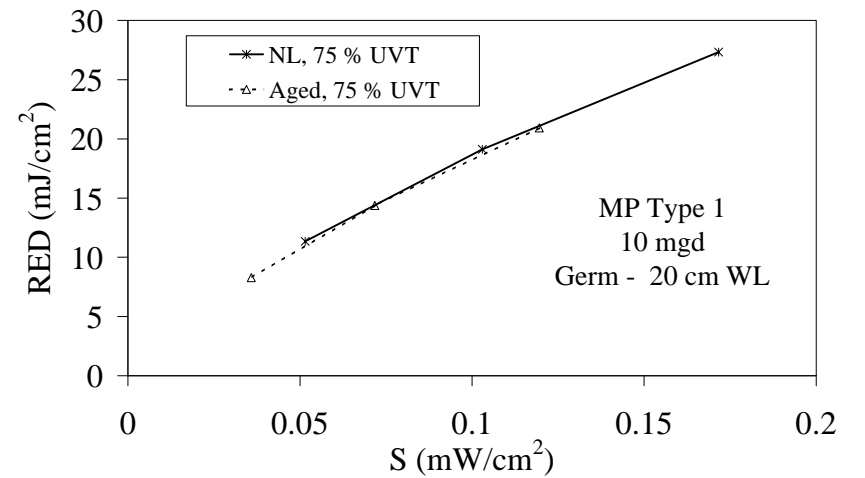
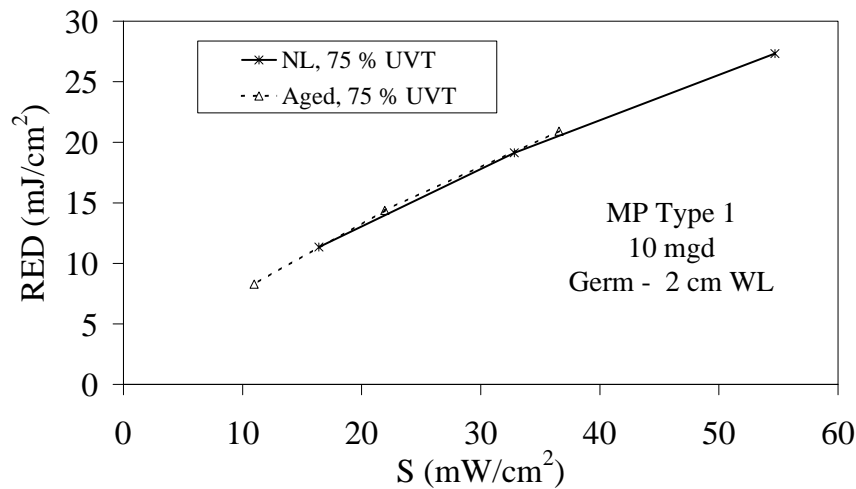
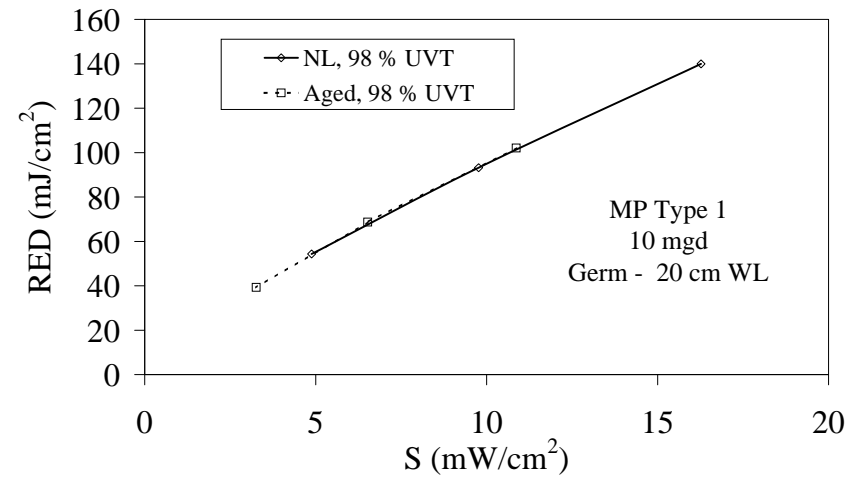
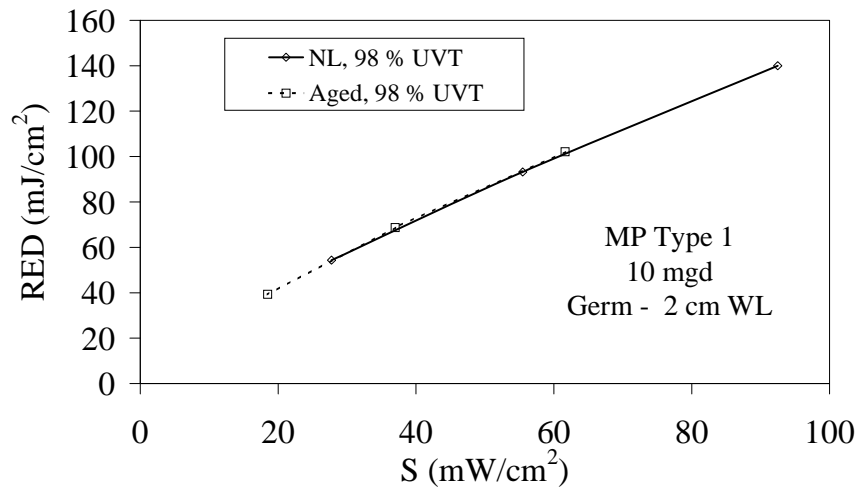


Figure 6.17 MS2 RED ($D_{10} = 18 \text{ mJ/cm}^2$) delivered by new and aged Type 1 MP lamps as a function of DVGW UV sensor readings for water layers of 2 and 20 cm and UVTs of 98 and 75%

Figure 6.18 shows the relation between RED and SiC UV sensor readings with new and aged Type 2 lamps for water layers of 2 and 20 cm and UVTs of 98 and 75%. Unlike the case with the Type 1 lamps, the REDs delivered with the new and aged Type 2 lamps for a given SiC UV sensor reading are very similar. Slightly lower REDs occurred with the aged lamp at 75% UVT with the 20 cm water layer. While the UV output of the Type 2 lamps in general aged faster at lower wavelengths (see Figure 4.71), the wavelengths from 360 to 400 nm aged at a similar rate allowing the SiC UV sensor readings to track dose delivery.

Spectral Shifts with LPHO Lamps

LPHO lamps emit UV light at 254, 297, 313, 334 and 366 nm. The data in Chapter 4 shows that the 254 nm output of the LPHO lamp ages more than the higher wavelengths. To evaluate the impact of these aging effects on dose monitoring, the Polychromatic Bias calculator tool described in Chapter 3 was used to calculate polychromatic bias values with DVGW and SiC sensors. Table 6.1 provides polychromatic bias as a function of UVT and UV sensor water layer for the DVGW and SiC sensors described in Figure 6.12. The data shows that a polychromatic bias can occur with LPHO lamps monitored by a SiC sensor. This polychromatic bias could lead to over dosing by as much as 16 to 20% for a SiC sensor monitoring the lamps through a 20 cm water layer with 75% UVT water. No polychromatic bias occurs with the DVGW sensor monitoring the LPHO lamps.

Table 6.1
Polychromatic bias with Aged LPHO lamps

UV sensor	WTP UVA spectra	UVT (%)	Water layer (cm)			
			2 cm	5 cm	10 cm	20 cm
SiC	WTP Min	75	1.01	1.03	1.08	1.21
		85	1.01	1.02	1.03	1.09
		95	1.01	1.01	1.01	1.02
	WTP Max	75	1.01	1.02	1.05	1.16
		85	1.01	1.02	1.02	1.06
		95	1.01	1.01	1.01	1.02
DVGW	WTP Max	75	1.00	1.00	1.00	1.00
		85	1.00	1.00	1.00	1.00
		95	1.00	1.00	1.00	1.00

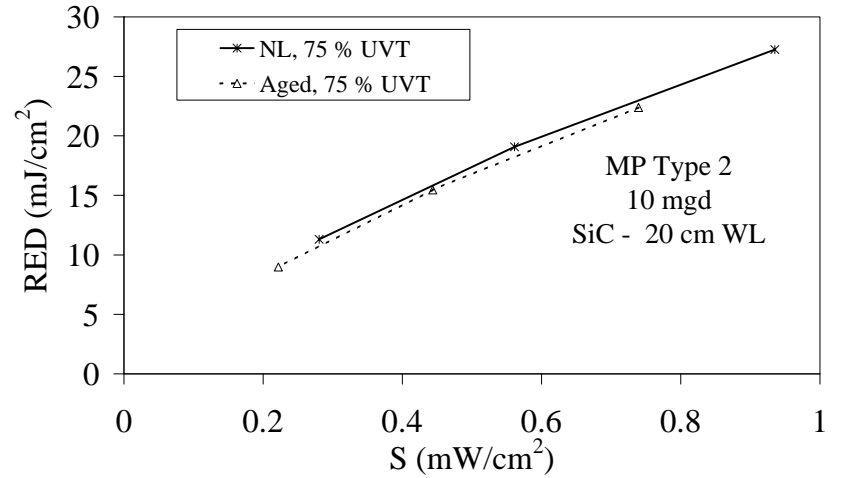
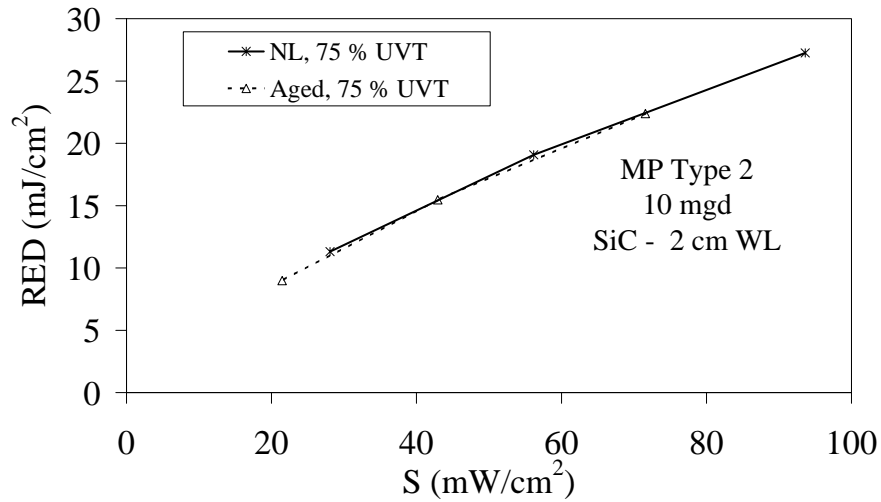
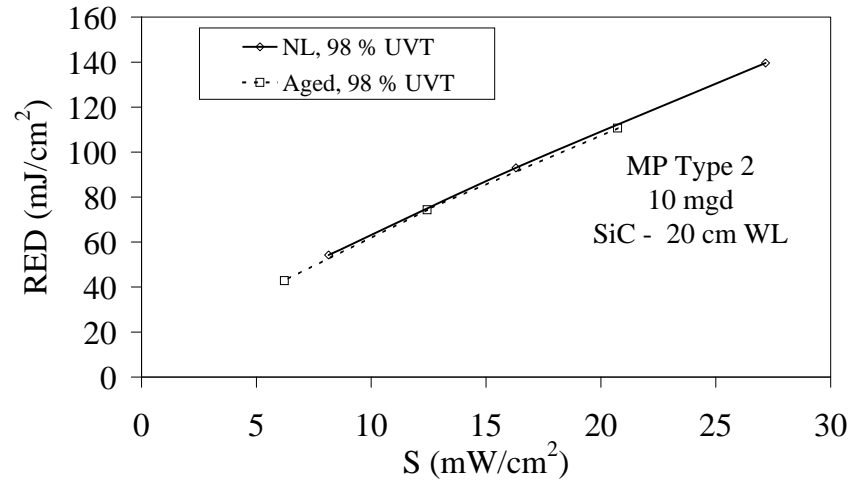
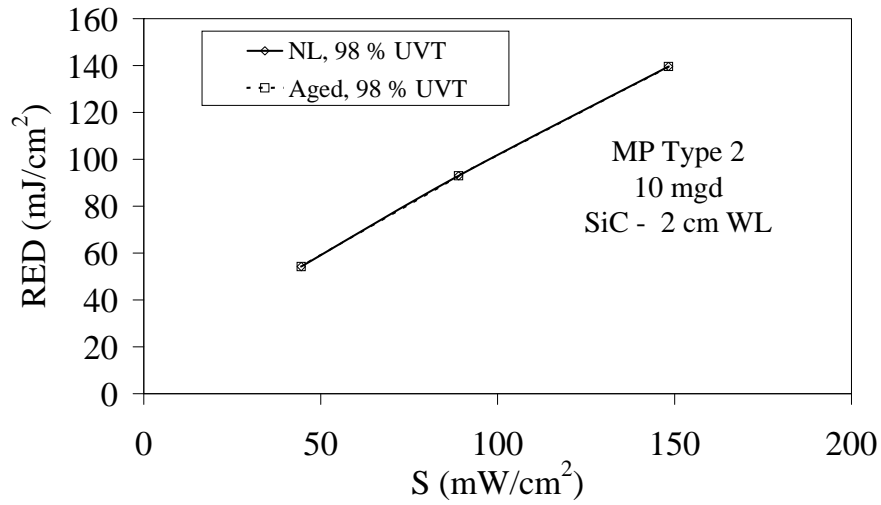


Figure 6.18 MS2 RED (D10 = 18 mJ/cm²) delivered by new and aged Type 2 MP lamps as a function of SiC UV sensor readings for water layers of 2 and 20 cm and UVTs of 98 and 75%

Non-Uniform Lamp Aging

The impact of non-uniform lamp aging along the length and about the circumference of the lamps was investigated using models for the MP and LPHO reactors with lamp data measured in Chapter 4. Figures 6.19 and 6.20 present the UV output profile along the length and about the circumference used in the analysis of the MP system and Figure 6.21 presents the UV output along the length of the lamp used in the analysis of the LPHO system. With the MP lamps, the modeled reactor uses a 61 cm lamp while the Type 2 lamps measured in Chapter 4 were 25 cm long. The Type 1 lamps were 61 cm long. With the LPHO lamps, the modeled reactor uses a 150 cm lamp but the lamps measured in chapter 4 were 90 cm long. To account for the difference in the arc length of the modeled and measured lamps, the measured data was scale by the ratio of the arc lengths.

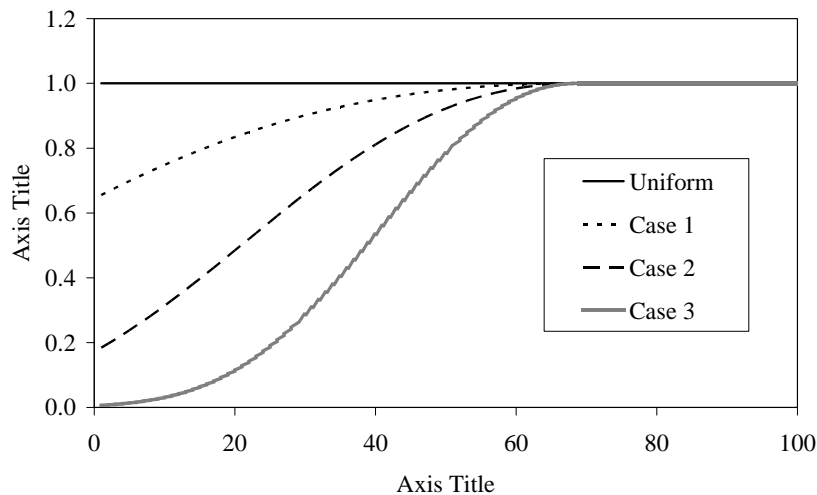


Figure 6.19 UV output along the length of the lamp used in the MP system analysis

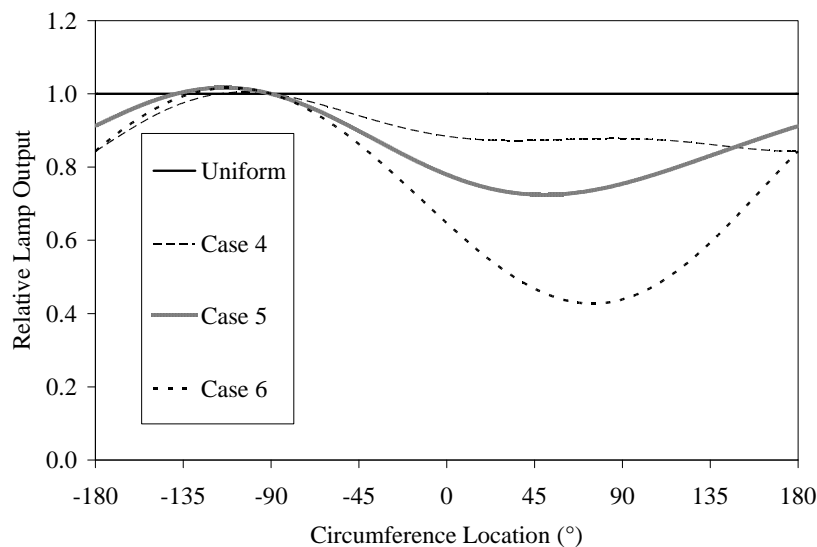


Figure 6.20 UV output about the circumference of the lamp used in the MP system analysis

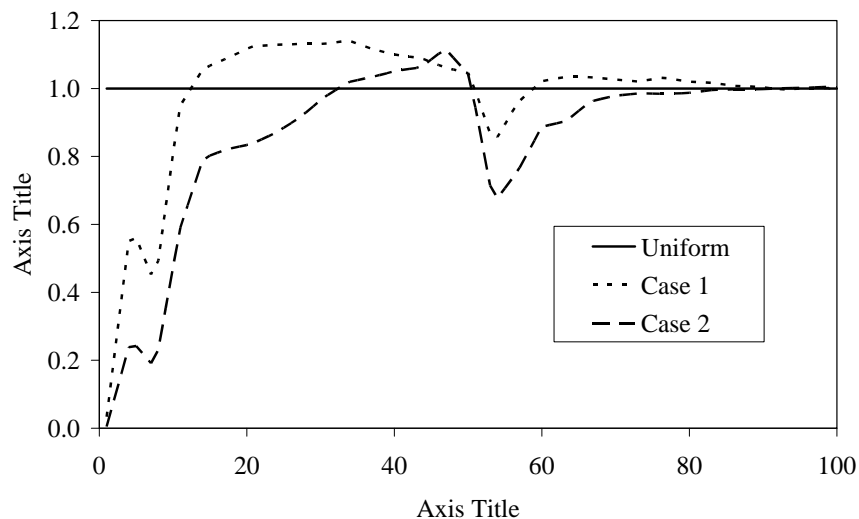


Figure 6.21 UV output along the length of the lamp used in the LPHO system analysis

Non-Uniform Lamp Aging with the MP Reactor

Figure 6.22 shows the UV sensor readings with the MP reactor as a function of location along the length of the lamp for UVTs of 98 and 80%. The UV sensors had a DVGW spectral response as defined in Figure 6.12 and an angular response as defined in Figure 6.13. The UV sensors were located with an 8.7 cm water layer and viewed the lamp from the same location about the circumference. The spacing between adjacent UV sensor locations along the arc length is 5 cm. The data shows that the sensor readings decrease as the sensor location moves closer to the lamp end (position S7), even with the uniform lamp output. The decrease is more pronounced with the aged lamps.

Figure 6.23 shows the relation between RED and UV sensor reading at 98% UVT for UV sensors viewing the middle of the lamp, 25% along the lamp length, and the lamp end. The data shows that the RED delivered with a given UV sensor reading decreases as the lamp ages if the sensor views the middle of the lamp, increases as the lamp ages if the UV sensor views the lamp end, but tracks well with dose delivery if the sensor views a location 25% from the lamp end. This means that a dose monitoring system will over predict dose delivery as the lamp ages if the sensor views the middle of the lamp but significantly under predict dose delivery if the UV sensor views a lamp location near the lamp end. The under prediction of dose delivery will significantly increase the O&M costs of a UV system while the over prediction will reduce the public health protection provided by UV.

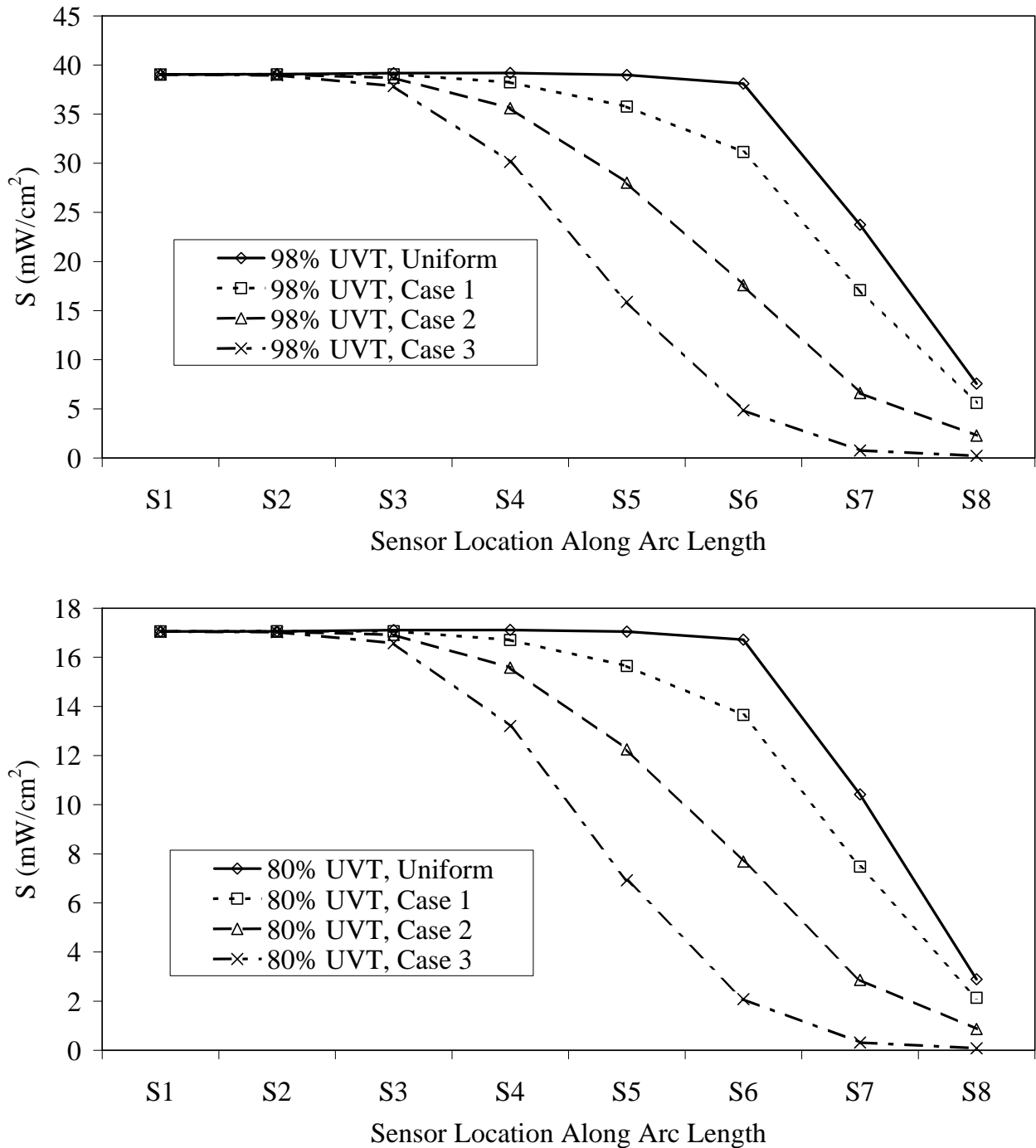


Figure 6.22 Impact of non-uniform MP lamp output along the lamp length on UV sensor readings (location S1 - center of the lamp, location S7 - lamp end, spacing between UV sensors - 5 cm)

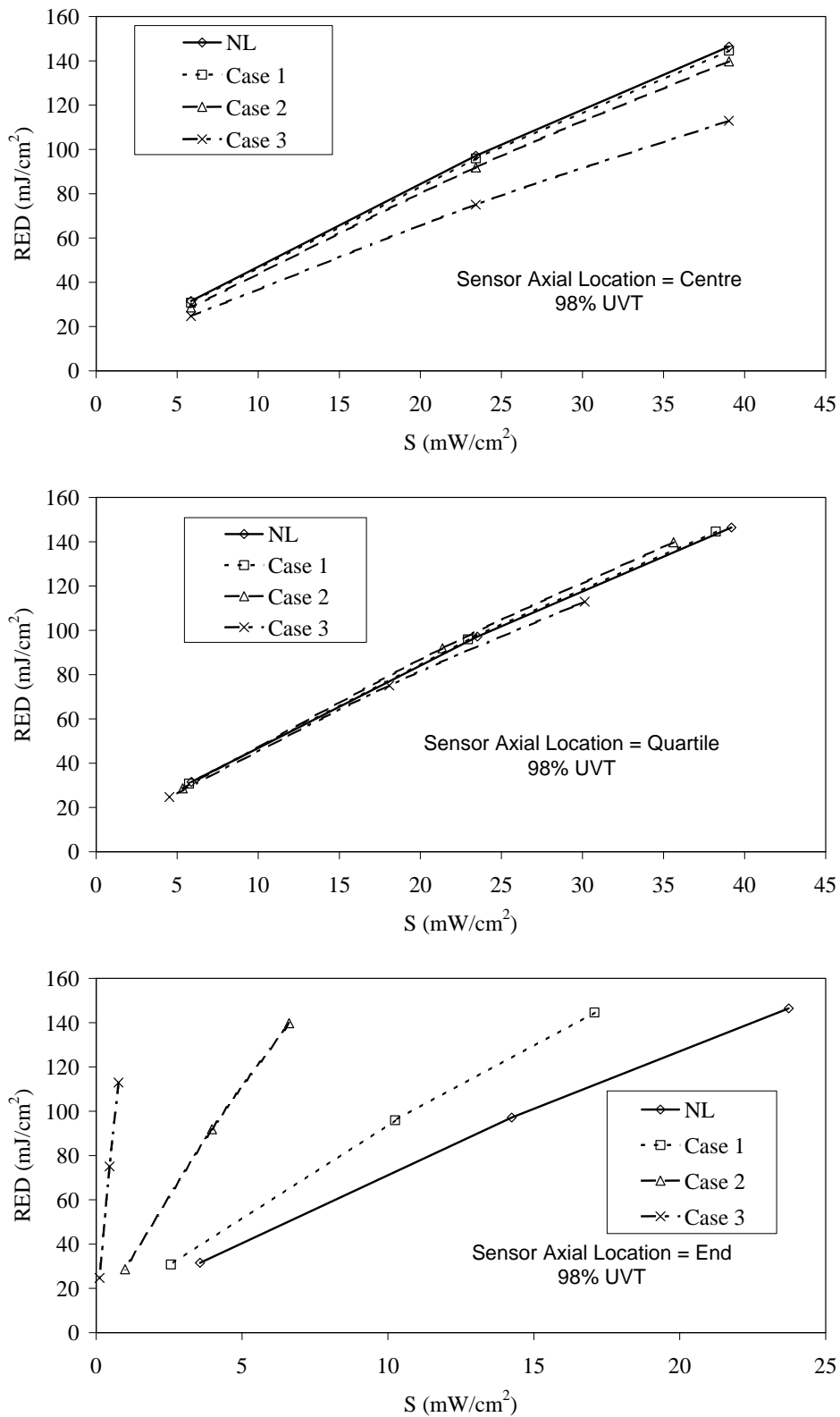


Figure 6.23 Relation between MS2 RED (D10 = 18 mJ/cm²) and DVGW UV sensor readings at 98% UVT for different cases of non-uniform MP lamp aging along the lamp length

The bias in dose monitoring associated with non-uniform lamp aging can be defined as:

$$B_{Lamp\ Aging} = \frac{RED_{New}}{RED_{Aged}} \quad (6.7)$$

where RED_{New} and RED_{Aged} are the REDs delivered with the new and aged lamps, respectively, at a given flow, UVT, and UV sensor reading. Figure 6.24 presented the dose monitoring bias caused by non-uniform lamp aging along the length of the lamp as a function of UV sensor axial location for UVTs of 80 and 98 %. The data shows that a dose-monitoring algorithm could over predict dose delivery by a factor of 1.4 if the UV sensor views the middle of the lamp but under predict dose delivery by a factor of 5 if the UV sensor views the lamp end. The UV sensor readings track well with dose delivery if the sensor views a location approximately 25% of the arclength from the lamp end.

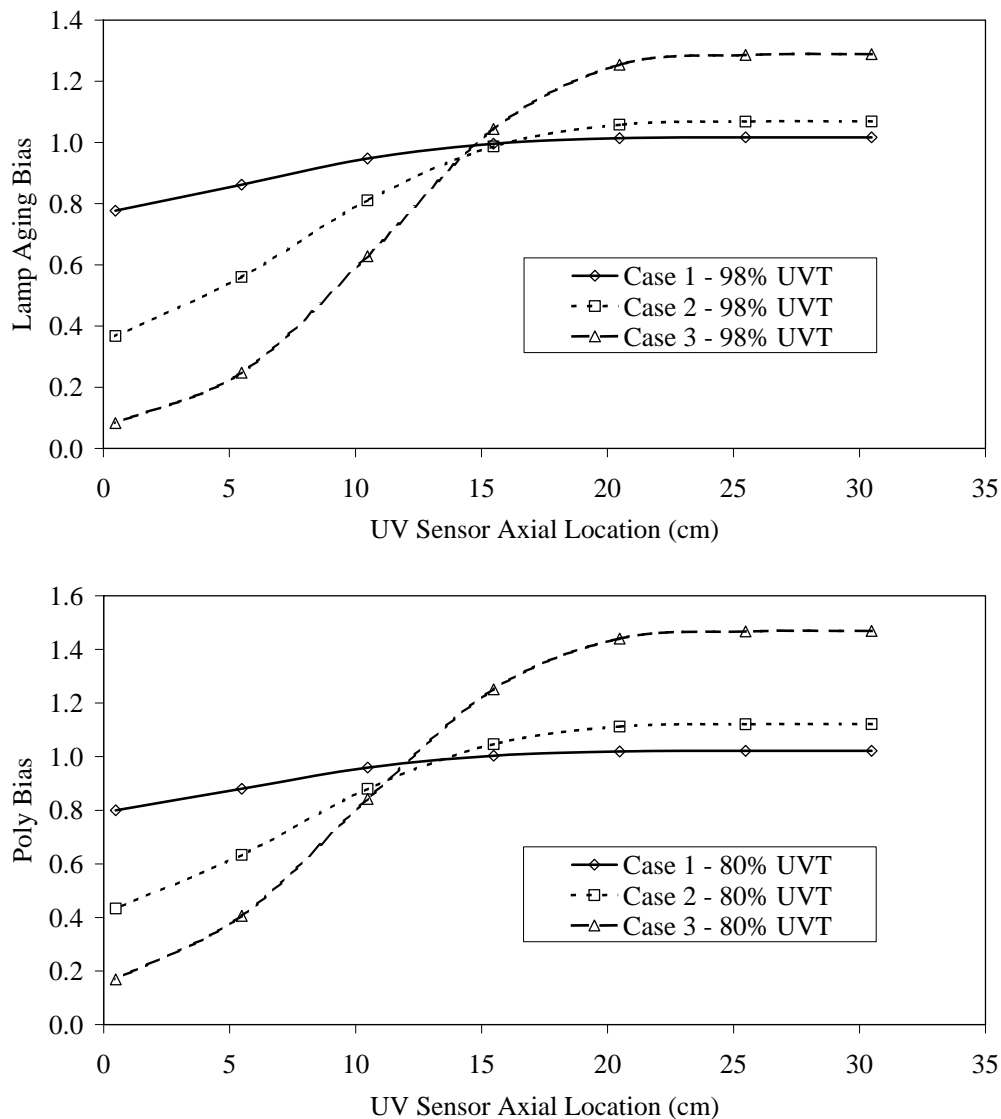


Figure 6.24 Dose monitoring bias caused by non-uniform MP lamp aging along the lamp length as a function of axial UV sensor location (0 cm - lamp end, 30 cm - lamp middle)

Figure 6.25 shows the UV sensor readings of the MP reactor as a function of location about the circumference of lamp #1 for water UVTs of 98 and 80%. Lamp #1 is identified as the lamp at the nine o'clock position in Figure 6.2. The UV sensors are identified using the notation Sx° where x° represents the viewing angle of the sensor. The UV sensor designated as $S90^\circ$ views the lamp from above while the UV sensor designated as $S0^\circ$ views the lamp from the right hand side. All UV sensors were located with an 8.7 cm water layer.

At 98 percent UVT, the data in Figure 6.25 shows that the UV sensor readings vary about the circumference with both new and aged lamps. However, at 80 percent UVT, the UV sensor readings only vary about the circumference with the aged lamp. The UV sensor readings vary about the circumference with the new lamp at high UVT because the UV sensor, depending on viewing angle, reads UV light from more than one lamp. At low UVT, other lamps do not contribute to the UV sensor reading. The UV sensor readings vary about the circumference with the aged lamp at low UVT because of non-uniform lamp aging and at high UVT because of a combination of lamp aging and UV output from different lamps.

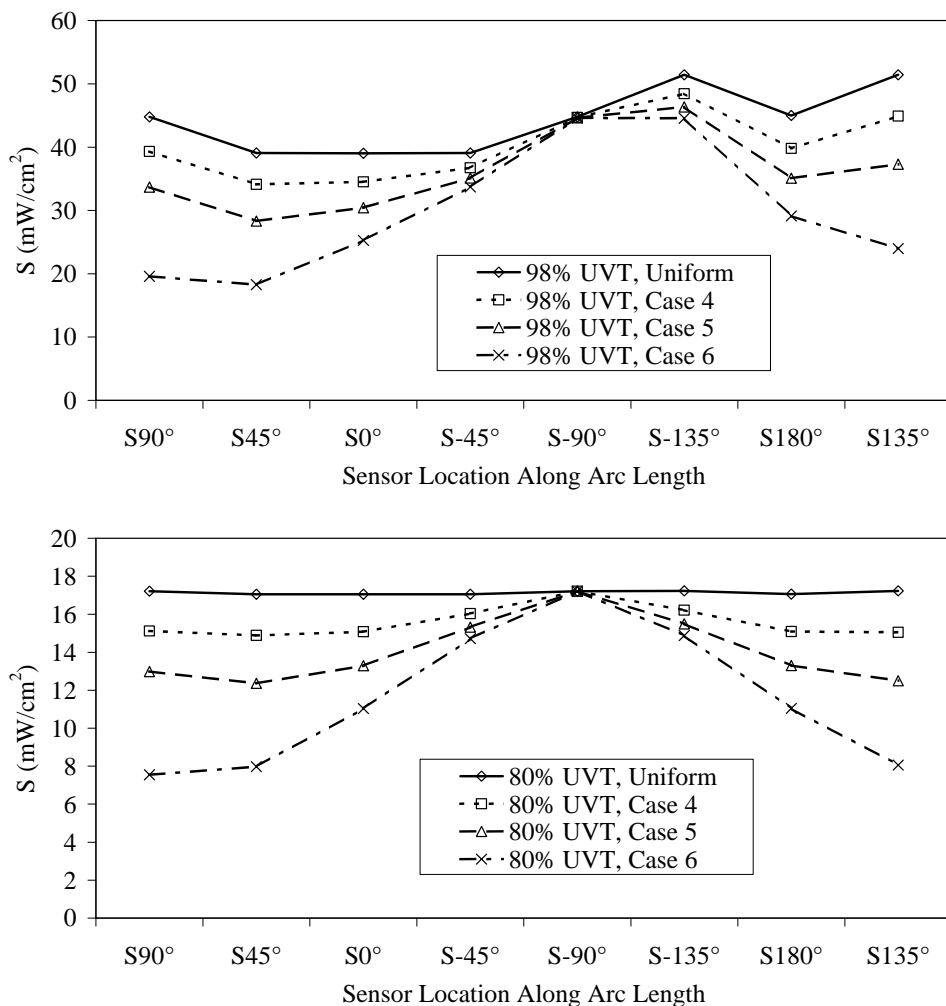


Figure 6.25 Impact of non-uniform MP lamp output about the circumference of the lamp on UV sensor readings (location $S90^\circ$ -UV sensor views lamp #1 from above, location $S0^\circ$ - UV sensor views lamp from the right hand side)

Figure 6.26 shows the relation between RED and UV sensor reading at 80% UVT for UV sensors viewing the lamp from the top, right side, and bottom. The data shows that the RED delivered with a given UV sensor reading decreases as the lamp ages if the sensor views the lamp from the bottom, increases as the lamp ages if the UV sensor views the lamp from the top, but tracks well with dose delivery if the sensor views the lamp from the side. This means that a dose monitoring system will over predict dose delivery as the lamp ages if the sensor views the lamp from the top and under predict dose delivery if the UV sensor views the lamp from below. The under prediction of dose delivery will significantly increase the O&M costs of a UV system while the over prediction will reduce the public health protection provided by UV.

Figure 6.27 shows the dose monitoring bias caused by non-uniform lamp aging about the circumference of the lamp as a function of UV sensor angular location for UVTs of 80 and 98%. The data shows that a dose-monitoring algorithm could under predict dose delivery by a factor of 1.4 if the UV sensor views the lamp from above but over predict dose delivery by a factor of 1.3 if the UV sensor views the lamp from below. The UV sensor readings track well with dose delivery if the UV sensor views the lamps from the side.

Non-Uniform Lamp Aging with the LPHO Reactor

Figure 6.28 shows the UV sensor readings with the LPHO reactor as a function of location along the lamp length for UVTs of 98 and 80%. The UV sensors have an angular response as defined in Figure 6.13 and were located with a 5.0 cm water layer. The spacing between UV sensors located along the arc length is 15 cm. Case 1 represents the new lamp output from the LPHO lamp and Case 2 represents the aged lamp output. As shown, the UV sensor response along the length of the new lamp represented by Case 1 differs from that of the uniform lamp output. In particular, the UV sensor readings with the new amalgam lamp are higher than the uniform case at locations S2 and S3, similar at locations S5 and S6 (middle), and lower at location S1 (lamp end). The UV sensors readings with the aged LPHO lamp are similar to the new lamp at location S6, but become increasingly lower at locations nearer to the lamp end.

Figure 6.29 presents the dose monitoring bias caused by non-uniform lamp aging along the length of the LPHO lamp. The bias is provided as a function of UV sensor axial location for UVTs of 80 and 98 percent. The data shows that a dose-monitoring algorithm could over predict dose delivery by a factor of 1.2 if the UV sensor views the middle of the lamp but under predict dose delivery by a factor of 1.2 to 1.5 if the UV sensor views the lamp end. The UV sensor readings track well with dose delivery if the sensor views a location approximately 13 percent of the arc length from the lamp end.

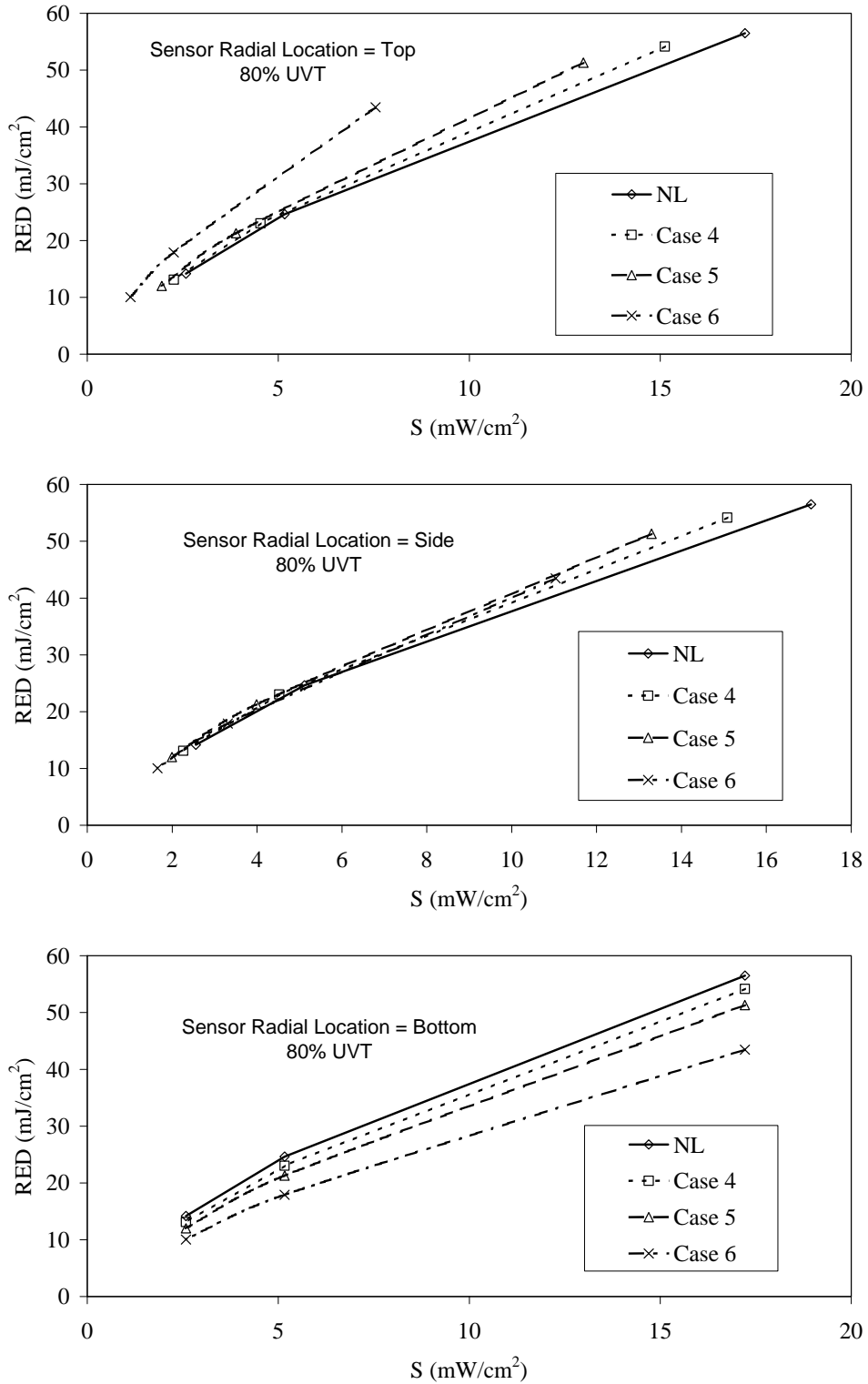


Figure 6.26 Relation between MS2 RED (D10 = 18 mJ/cm²) and DVGW UV sensor readings at 80% UVT for different cases of non-uniform MP lamp aging about the lamp circumference

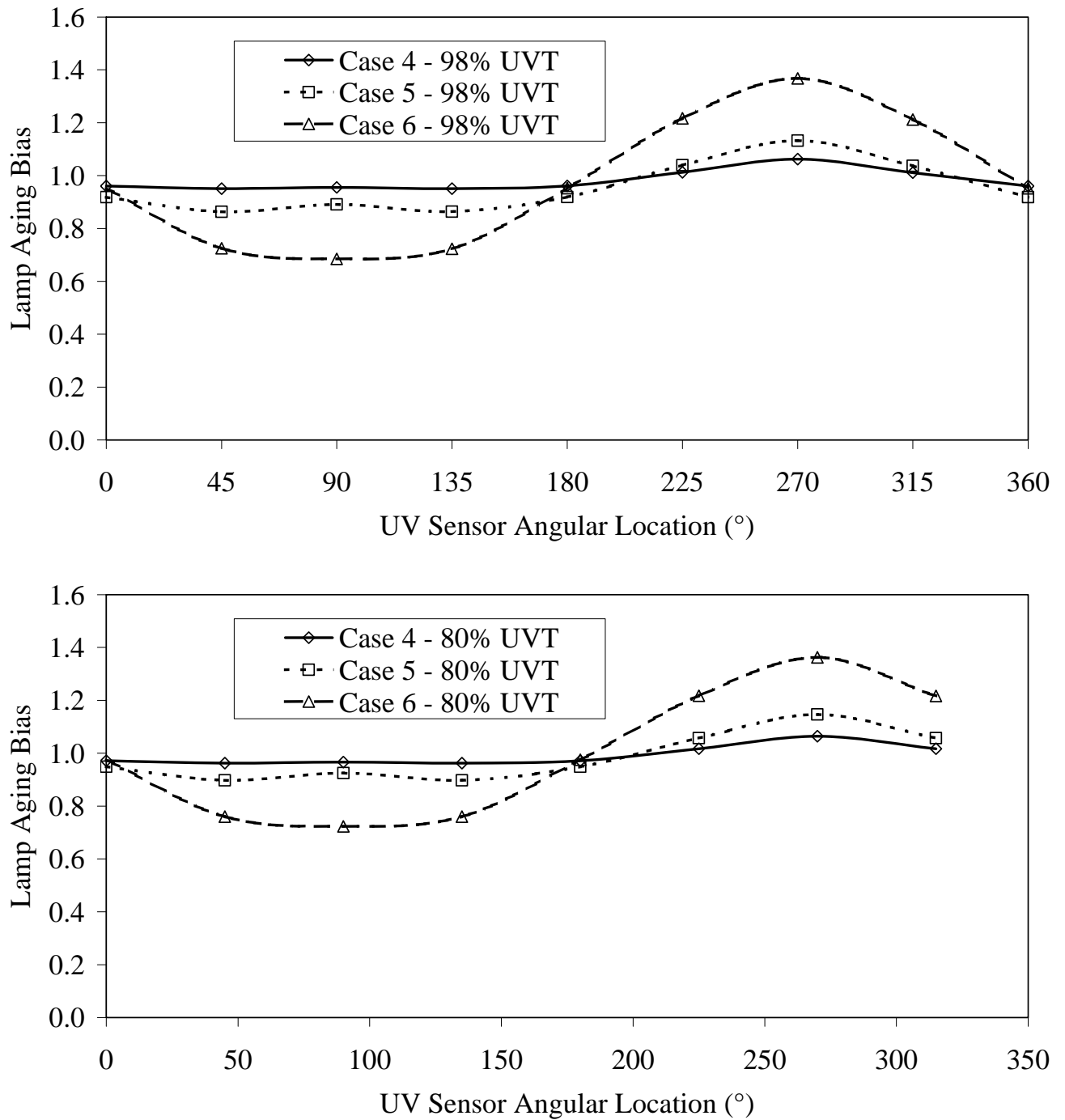


Figure 6.27 Dose monitoring bias caused by non-uniform lamp aging about the MP lamp's circumference as a function of angular UV sensor location (°0 - UV sensor views lamp from the right hand side, 90° - UV sensor views lamp from above)

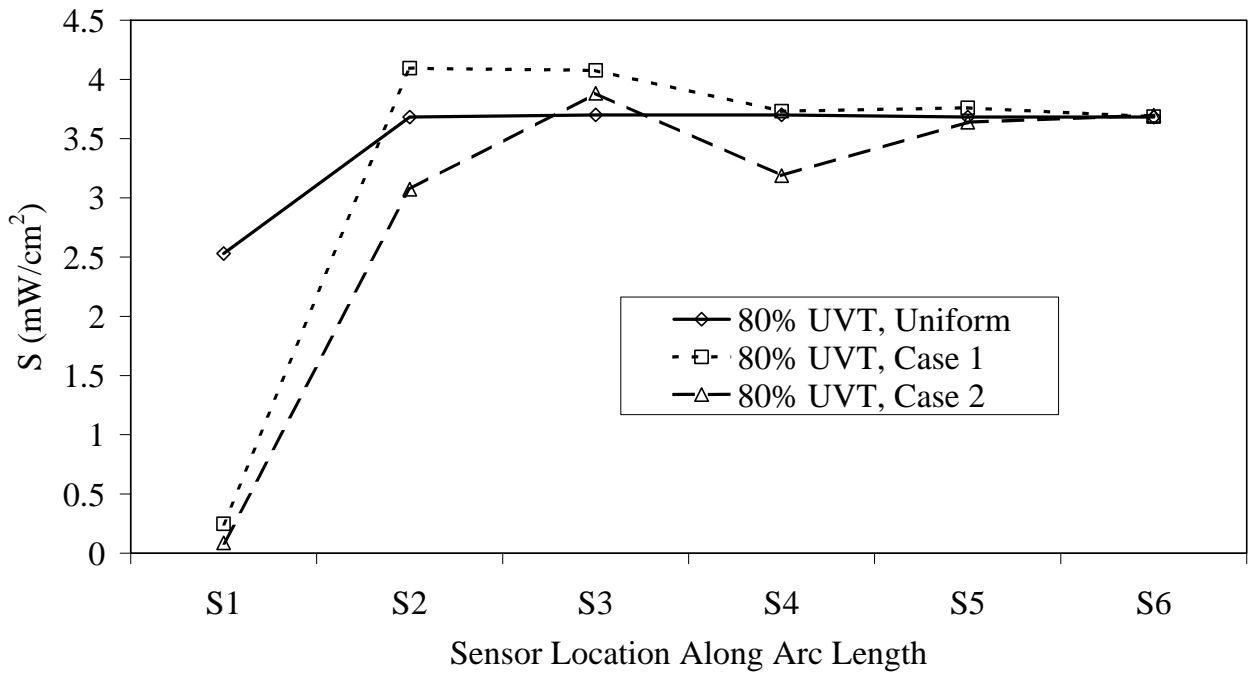
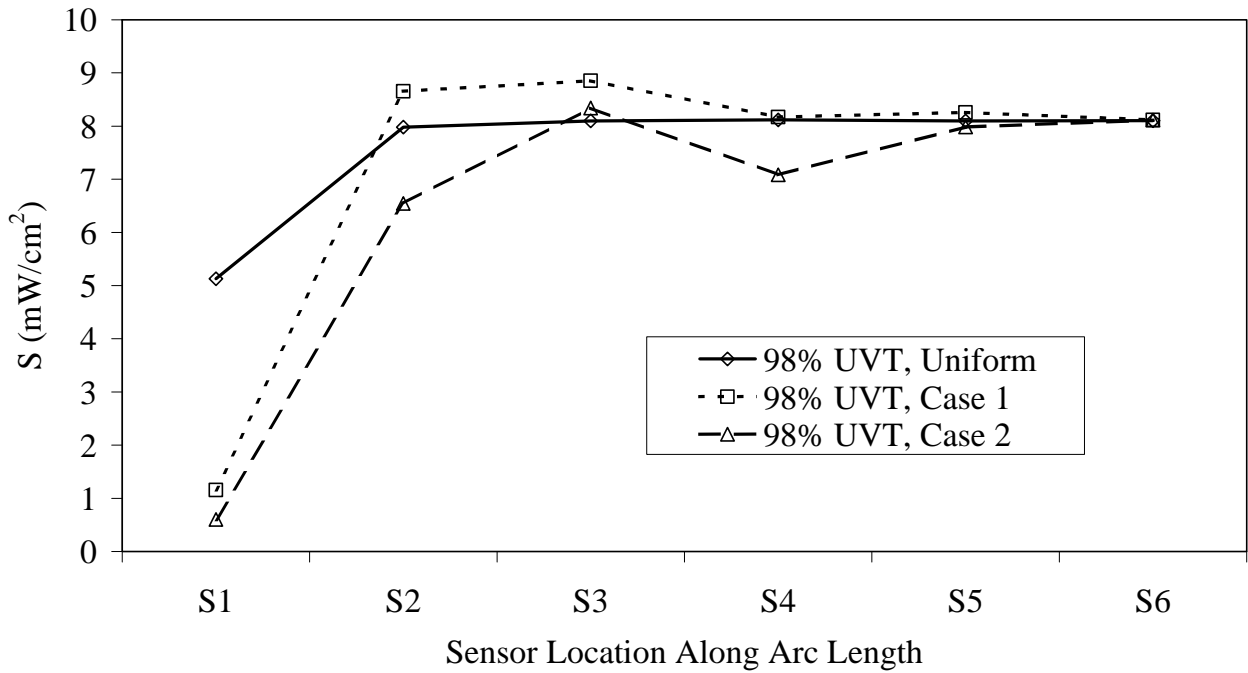


Figure 6.28 Impact of non-uniform LPHO lamp output along the lamp length on UV sensor readings (location S1 - lamp end, location S6 - center of the lamp, spacing between UV sensors - 15 cm)

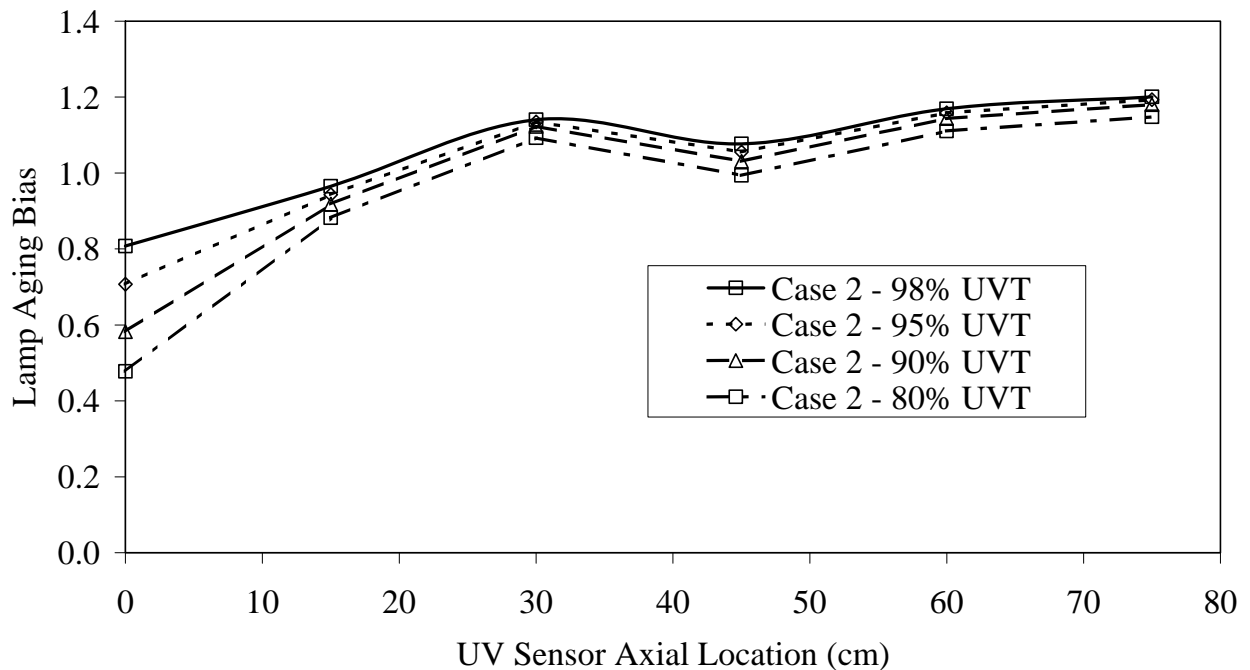


Figure 6.29 Relation between MS2 RED ($D_{10} = 18 \text{ mJ/cm}^2$) and DVGW UV sensor readings at 98% UVT for different cases of non-uniform LPHO lamp aging along the lamp length

CONCLUSIONS

UV intensity modeling and CFD-based dose delivery modeling were used to understand dose delivery and monitoring with two hypothetical UV reactors equipped with LPHO and MP lamps. The models were used to understand:

1. The impact of the reactor's dose distribution and microbe inactivation kinetics on log inactivation and RED for that microbe
2. The impact of UV sensor-to-lamp water layer on the relations between RED and UV sensor readings for different UVTs
3. The impact of "spectral shifts" in UV lamp output on dose delivery monitoring
4. The impact of non-uniform lamp aging along the length of the lamp and about the circumference on dose delivery and monitoring

All conclusions from this work are dependent on the reactor designs modeled. Different results would be obtained with different reactor designs. For example, a baffle plate can be used to improve the reactor's dose distribution and reduce the impacts of end darkening on dose delivery. As another example, the impact of lamp end darkening on dose delivery and monitoring may differ depending on whether the lamps were oriented parallel to flow or perpendicular to flow. The results from this work should be used to guide the reader on the potential impact of

dose distributions, spectral shifts, and non-uniform lamp output and how to evaluate these impacts with commercial UV reactor technologies. Conclusions are as follows:

Impact of Microbe Inactivation Kinetics on RED

- The RED delivered by a reactor depends on the reactor's dose distribution and the microbe's UV inactivation kinetics. The RED of a UV resistant microbe, like MS2 phage, will be greater in value than that of a UV sensitive microbe, like *Cryptosporidium*. The difference will be greater with a reactor with a wider dose distribution. Because the dose distribution is wider at lower UVT, the difference with a given reactor will be greater at low UVT. For a given flow and UVT, the difference also depends on the UV output from the lamps.
- The impacts of microbe kinetics on RED impacts how validation data should be interpreted for a given target pathogen. If the validation microbe is more resistant to UV light than the target pathogen, the REDs measured during validation for a given flow, UVT, and lamp output will be greater than the REDs delivered to the pathogen. This bias is eliminated if the validation microbe has the same inactivation kinetics as the target pathogen.
- A single relation between microbe log inactivation and $S/S_0/D10$ can be defined for a given reactor at a given UVT, where S/S_0 represents the relative UV output from the lamps and D10 is the UV dose required to inactivate a microbe with first order inactivation kinetics by one log. The relation suggests that validation data measured as a function of S/S_0 with one microbe can be used to predict log inactivation and RED of another microbe with a different D10. Hence, RED Bias values can be estimated with validation data obtained using one microbe. The relation also provides a rational for analyzing validation data obtained with two microbes with different UV sensitivities.

Relation Between RED and UV Sensor Readings

- The relation between RED and UV sensor reading at a given flow and UVT depends on UV sensor position relative to the lamps. If the UV sensor is located relatively close to the lamps, the RED for a given UV sensor reading decreases as UVT decreases. If the UV sensor is located relatively far from the lamps, the RED for a given UV sensor reading increases as UVT decreases.
- In theory, an optimal UV sensor reading can be defined where the relations between RED and UV sensor reading at different UVTs overlap and can be described by a single relation. Model data for the MP reactor shows there was not one UV sensor location where RED as a function of UV sensor reading overlapped for a wide range of UVTs. Instead, a location could be defined where RED for a given UV sensor reading has a minimum value at some intermediate UVT. Above and below that UVT, the RED increased for a given UV sensor reading. The relation between RED and UV sensor reading at this intermediate UVT and UV sensor location could be used for UV intensity setpoint dose monitoring.
- The German DVGW and Austrian ONORM specify dose monitoring using the UV intensity setpoint approach where the UV reactor delivers a validated UV dose value

when the UV sensor reads above an alarm level. The DVGW and ONORM standards state that the dose delivery at the alarm UV intensity setpoint is validated using two test conditions. Test 1 involves high UVT and lamp power lowered to give a UV sensor reading at the alarm level. Test 2 involves maximum lamp power and UVT lowered to give a UV sensor reading at the same alarm level. The validated dose is defined as the lower of the REDs measured with the two test conditions. The data from this work shows that a third test condition at an intermediate UVT is needed when the minimum RED for a given UV sensor reading occurs at an intermediate UVT.

Impact of Spectral Shifts in UV Output from LPHO and MP Lamps

- That reduction in UV output due to lamp aging varies as a function of wavelength with lower wavelengths aging faster than higher wavelengths.
- SiC UV sensors measure UV light at wavelengths from 200 to 400 nm. Microbes are inactivated by UV light at wavelengths from 200 to 300 nm. Because SiC sensors measure non-germicidal light above 300 nm, dose-monitoring algorithms that use SiC sensors can over estimate dose delivery as MP and LPHO lamps age because the germicidal wavelengths age faster than wavelengths from 300 to 400 nm. These dose-monitoring errors are negligible if the UV sensor has a germicidal spectral response.

Impact of Non-Uniform Lamp Output on Dose Delivery and Monitoring

- UV intensity models and CFD-based dose delivery models were developed that account for non-uniform output along the length and about the circumference of UV lamps that occurs as lamps age.
- Non-uniform lamp output along the length of the lamp and about the circumference impacts dose monitoring and dose delivery.
- With the MP reactor modeled, the dose-monitoring algorithm over predicted UV dose by as much as 45% if the UV sensor viewed a location along the lamp and about the circumference that aged the least. The algorithm under predicted UV dose by as much as a factor of 5 if the UV sensor viewed a location that aged the most.
- With the LPHO reactor modeled, the dose-monitoring algorithm could over predict UV dose by as much as 20% if the UV sensor viewed a location along the lamp and about the circumference that aged the least and under predicted UV dose by as much as a factor of 2 if the UV sensor viewed a location that aged the most.
- To minimize under and over dosing caused by non-uniform lamp output along the length of the lamp, UV sensors used with the modeled MP reactor should monitor locations along the lamp length that are 25% of the arc length away from the electrode and UV sensors used with the modeled LPHO reactor should monitor locations along the lamp length that are 13% of the arc length away from the electrode.
- To minimize under and over dosing caused by non-uniform lamp aging about the lamp's circumference, the UV sensor should monitor MP lamps from the side as opposed to the top or bottom.

CHAPTER 7

DEVELOPMENT OF UV COST ANALYSIS TOOL (UVCAT)

The UV System Cost Analysis Tool (UVCAT) is a software tool developed through this project to provide a comprehensive evaluation of UV disinfection system performance and operating cost. UVCAT is an Excel™ spreadsheet with embedded Visual Basic™ software. The spreadsheet has a user interface to enter data, initiate the software algorithms, and view outputs. This chapter provides an overview of UVCAT applications, data inputs and model outputs.

UVCAT is designed to conduct the following analyses:

- Standard Life-Cycle Cost (LCA) Analysis
- Lamp Replacement Interval Cost Analysis
- Advanced LCA

STANDARD LIFE-CYCLE COST ANALYSIS

The Standard LCA tool estimates UV system O&M and present worth costs based on UV system operation under average conditions of flow rate, water UVT, lamp aging, and fouling.

LAMP REPLACEMENT INTERVAL COST ANALYSIS

The Lamp Replacement Interval Cost Analysis tool estimates O&M and present-worth costs for a UV system as a function of the lamp replacement interval. The O&M costs are estimated based on UV system operation under defined “average” conditions of flow rate, UVT, lamp-aging, and fouling rate.

ADVANCED LIFE-CYCLE COST ANALYSIS

The Advanced LCA tool simulates UV system operation over time as a function of flow rate, UVT, lamp-aging, fouling rate, power quality, and UV system component failure. UV system operation is estimated using the specific UV dose-monitoring and control algorithm for that reactor. The tool predicts the number of reactors and lamps, their power setting, UV dose delivery by each reactor, log inactivation of a target pathogen, and the associated public health protection. The tool predicts O&M costs by integrating power consumption, labor, and UV system component replacement over the time.

[Figure 7.1](#) provides an example of the flow rate, UVT, pathogen, and power quality data that can be used as an input to the Advanced LCA tool. Ideally, the data should cover a one-year period to capture seasonal impacts on water quality and have sufficient resolution to capture any significant variability, such as diurnal cycles.

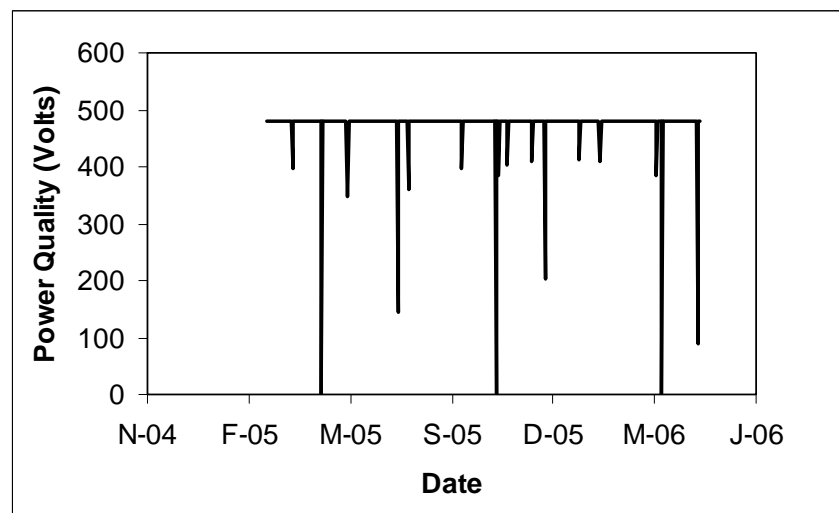
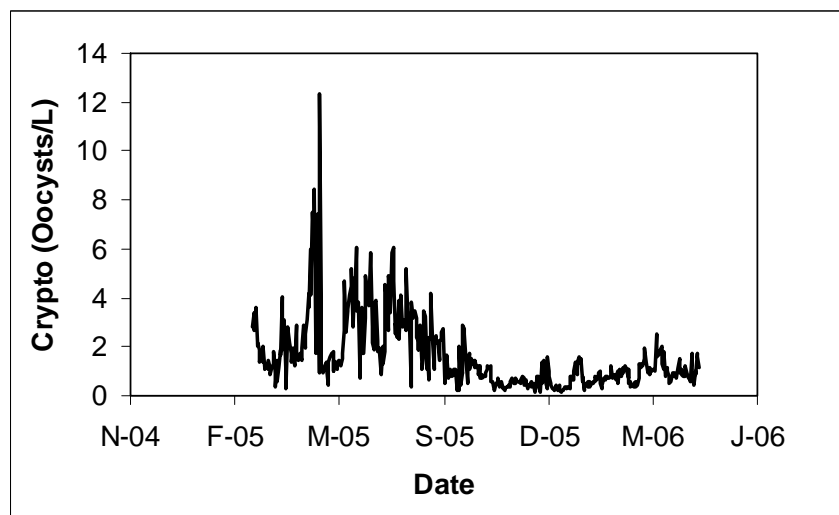
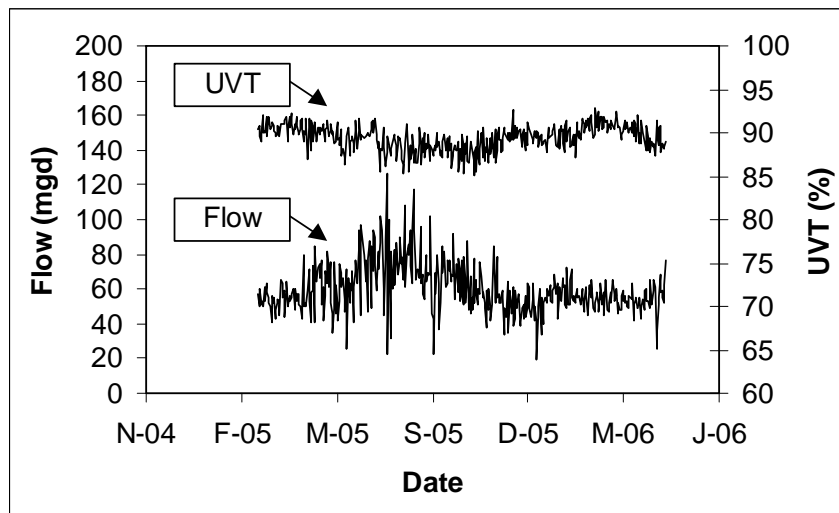


Figure 7.1 Flow rate, UVT, raw water pathogen concentration, and power quality data used as inputs to the Advanced LCA UVCAT tool

For a given flow rate and UVT profile over time, the Advanced LCA tool simulates the number of reactors and banks of lamps within a UV system required to deliver the target UV dose. If the UV system does not have the capacity to deliver the required UV dose under given conditions of flow rate and UVT, the UVCAT algorithm assumes that the UV system is operating with all reactors and banks of lamps on, including any redundant reactors, at 100 percent power.

Figure 7.2 presents the number of operating trains of reactors and banks of lamps for an example UV system predicted over time by UVCAT. The predictions can be used by engineers and utilities to understand how frequently UV reactors and banks of lamps will be turned on and off in response to changes in operating conditions (*e.g.*, flow rate and UVT) over time. Such data can be used to identify the level of automation needed to best control the UV system. It can also be used to identify whether or not the given UV reactor is “oversized” for the application (*i.e.*, the number of banks of lamps being used to deliver the design UV dose will be less than total number of banks in the reactor). Recognizing that extra banks of lamps do provide redundancy, the utility and engineer can evaluate whether or not the number of banks proposed for a given UV application by a UV vendor is appropriate, does not provide adequate redundancy, or provides too much.

The Advanced LCA tool also predicts the operating power setting of each bank of lamps and the total power consumption of the UV system over time, accounting for predicted lamp-aging and fouling and available ballast power settings. Figure 7.3 presents the total power consumed by a UV system for two different scenarios. The first scenario assumes ideal reactor turndown – the lamp ballast power settings are not limited to discrete levels, but rather can operate below and above the minimum and maximum levels entered into the simulation.

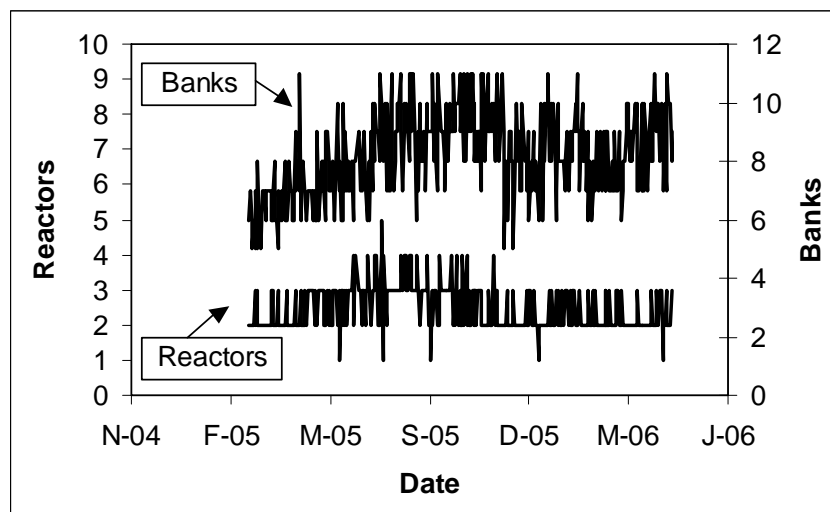


Figure 7.2 Number of operating reactor trains and banks per reactor predicted by the Advanced LCA UVCAT tool

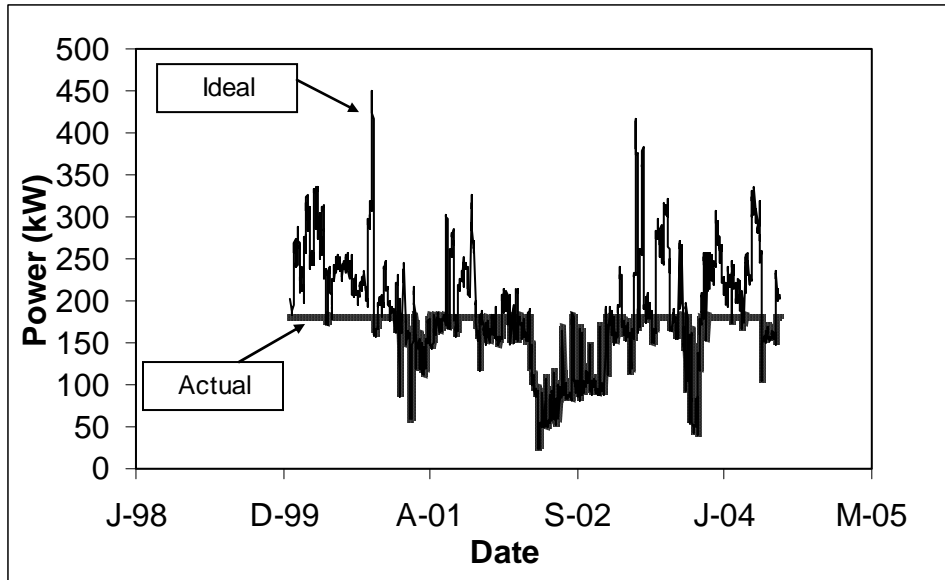


Figure 7.3 Power consumption by a UV system predicted by the Advanced LCA UVCAT tool under ideal and actual dose-pacing strategies

The second scenario assumed that the power settings are restricted to those levels entered into the simulation. The ratio of the actual to ideal power consumption (see [Figure 7.4](#)) provides a measure of the dose-pacing efficiency. The UV system is underdosing when the ratio is less than one, and overdosing when the ratio is greater than one. Such data allows engineers and utilities to assess if a UV system is undersized or has sufficient turndown capacity for a given application.

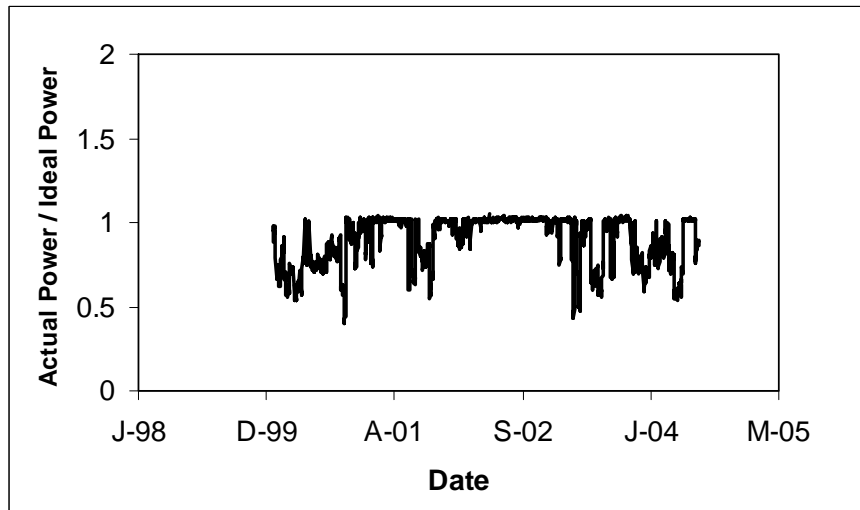


Figure 7.4 Ratio of actual to ideal power consumption predicted by the Advanced LCA UVCAT tool

Figure 7.5 presents the lamp-aging factor for a multi-bank UV reactor predicted over time. The UVCAT algorithm assumes the lamps only age when they are operating. As such, the lamp aging factor for a given bank stays constant over time if the UVCAT simulation predicts the bank of lamps are not being used. UVCAT includes lamp replacement when the lamp hours reach the defined “end-of-lamp-life.” The predicted lamp-aging data allows the user to better understand the schedule and labor associated with lamp replacement for a given system.

Figure 7.6 presents predictions of daily and accumulated power costs over time, which UVCAT also uses to provide annualized and present worth costs. In estimating UV system performance and costs, UVCAT includes the impact of factors such as the UV output efficiency of the lamp and ballast, turndown limitations of the UV system, hydraulic limitations of each reactor, the discrete operation of the UV system (e.g., a UV system may have four ballast power settings), and the off-specification¹ limitations of validation data. This provides the user a significantly more accurate estimate of UV system O&M costs than rule-of-thumb approaches.

Figure 7.7 presents a simulation of off-specification performance by a UV system. Off-specification performance is calculated as a sliding monthly value based on time. With the UV system presented in Figure 7.7, off-specification performance was significant both in terms of magnitude (as much as 100 percent in one month) and duration (greater than 5 percent over several months). In this case, the UV system being simulated was undersized for the application. Using UVCAT, the UV system size can be modified iteratively until the appropriate level of off-specification performance is achieved for a given application. Sizing a UV system based on a target “off-specification” performance goal represents a significant paradigm shift compared to sizing UV systems for a design flow rate, UVT, and lamp-aging and fouling factor.

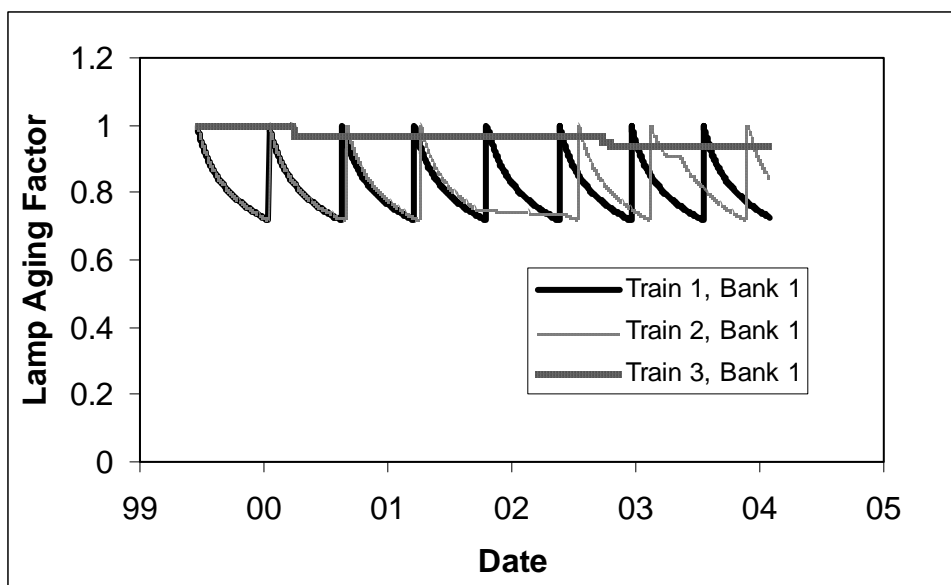


Figure 7.5 Lamp-aging simulated by the Advanced LCA UVCAT tool

¹ UV dose delivery is below the minimum dose required to earn the desired level of log inactivation credit.

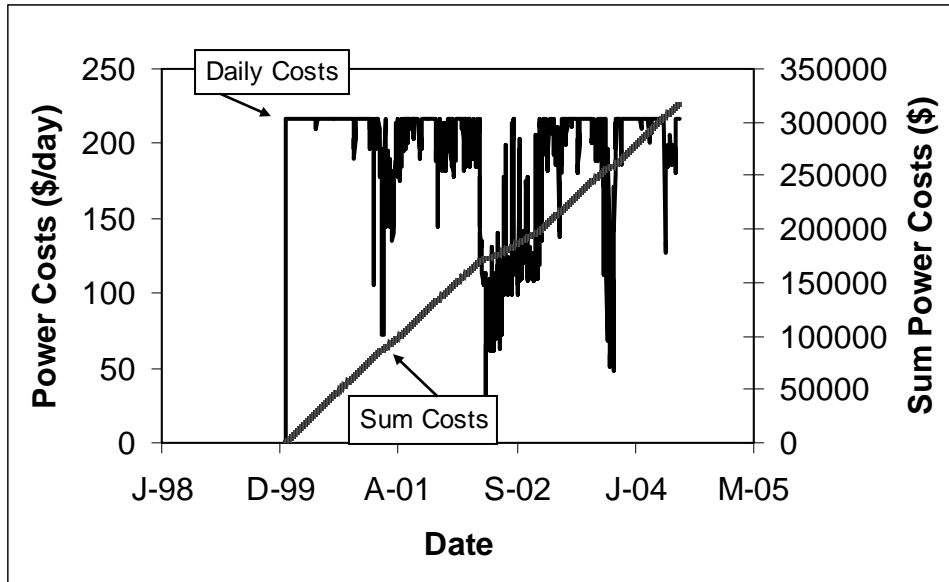


Figure 7.6 Daily and accumulated power costs predicted by UVCAT

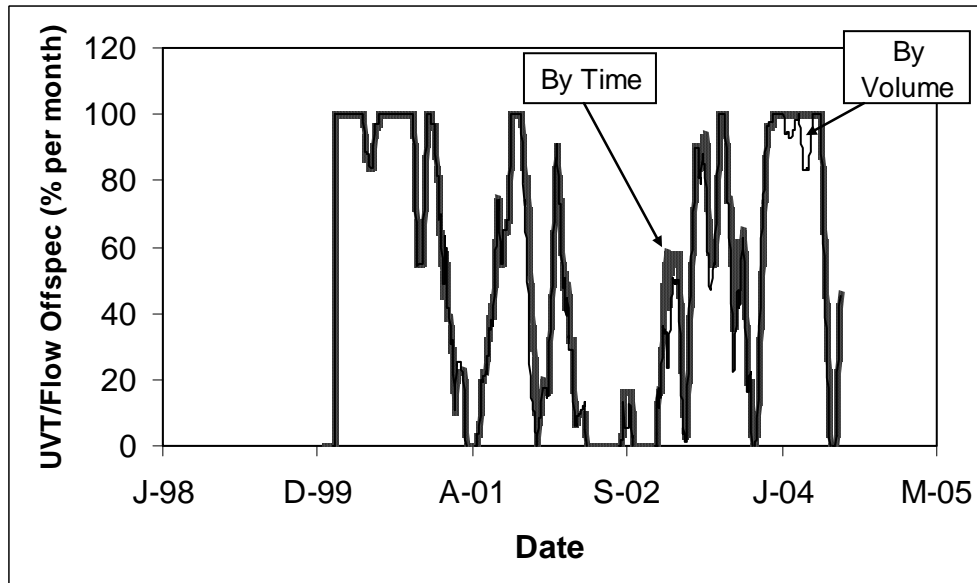


Figure 7.7 Off-specification performance over time predicted by the Advanced LCA UVCAT tool

Figure 7.8 presents the results of a simulation of UV dose delivery over time. UVCAT determines the UV dose delivered by each reactor in the UV system. The UV dose delivered by each train of reactors in the UV system is an output. UV dose delivery by reactors in series is assumed to be additive. The objective of UV dose pacing is to maintain as close to a constant delivered dose (typically the design dose plus some defined safety factor) as possible. Data such as that provided in Figure 7.8 can be used to assess how well different UV systems meet this goal.

Figure 7.9 presents the results of a simulation of the log inactivation of a target pathogen achieved over time for a defined UV system. UVCAT calculates the log inactivation for each reactor train using a UV dose-response relationship defined by the user. The log inactivation achieved by the UV system is calculated as the log of the average pathogen concentration in the UV system effluent, factoring in the contribution by each train. Plots of log inactivation over time are useful for assessing the impact of under- and overdosing and off-specification performance on meeting target pathogen inactivation objectives.

Figure 7.10 presents the results of a simulation of the instantaneous and accumulated infection risk for a UV system. The instantaneous risk is calculated as risk per year using a risk model defined by the user. The instantaneous risk predicted by UVCAT varies over time due to the variability in raw water pathogen concentration, response to power quality events and component failure, and fluctuations in UV dose delivery. The instantaneous risk is used to estimate the accumulated risk over time based on a population size entered by the user. The accumulated risk over time provides the user an integrated assessment of risk that can be used to compare various operating scenarios with a UV system and/or different UV system designs.

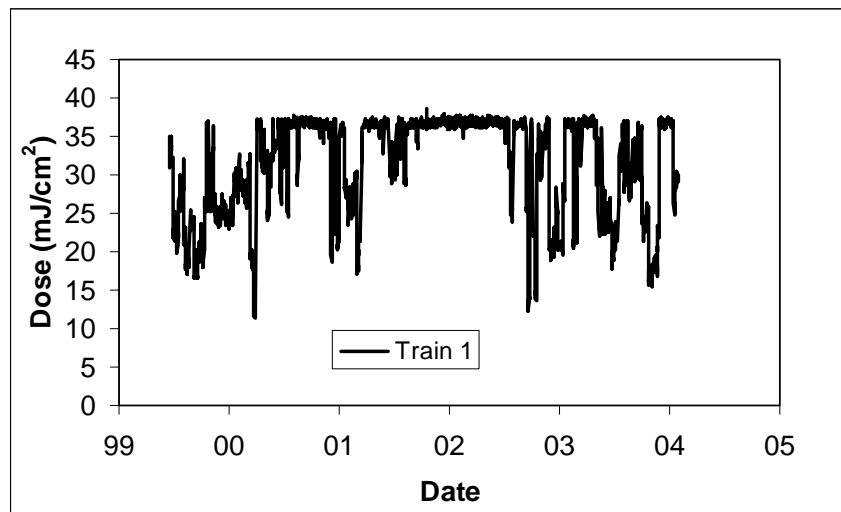


Figure 7.8 UV dose delivery over time predicted by the Advanced LCA UVCAT tool

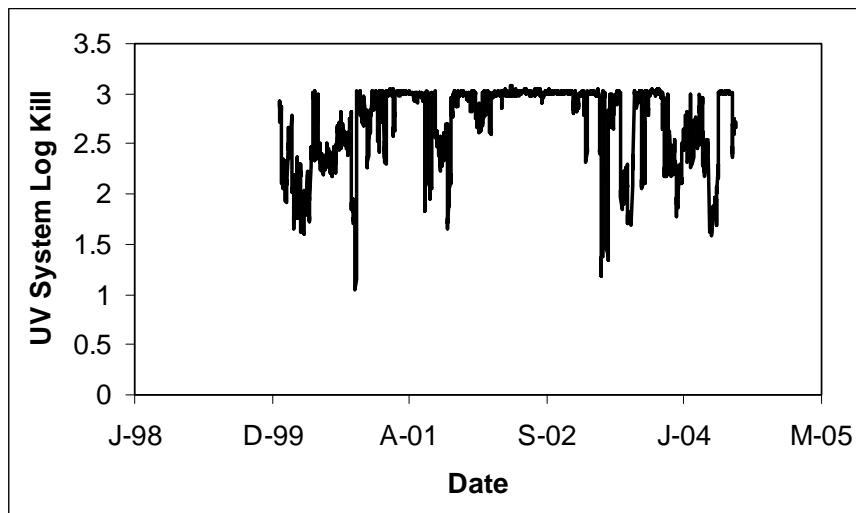


Figure 7.9 Pathogen log inactivation over time predicted by the Advanced LCA UVCAT tool

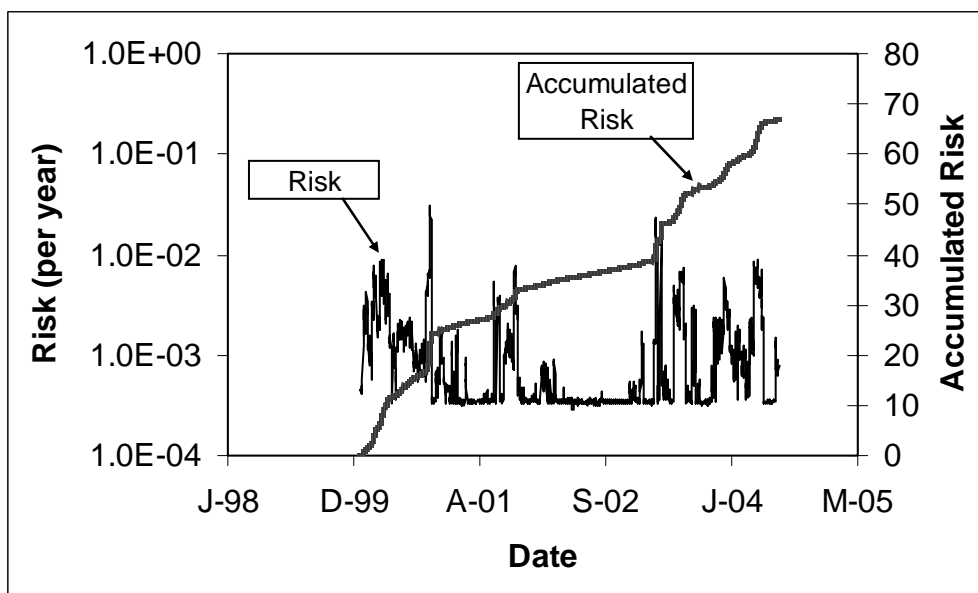


Figure 7.10 Public health risk over time predicted by the Advanced LCA UVCAT tool

UVCAT INPUTS

Table 7.1 lists the titles of the worksheets within UVCAT that are used to input data used for the Standard Life-Cycle Cost Analysis, Lamp Replacement Interval Cost Analysis and Advanced LCA. Table 7.2 summarizes the type of information entered in these worksheets. A detailed description of data input methods is included in the UVCAT User Manual (Appendix A). The data inputs for each parameter in Table 7.2 are described in the following sections.

Table 7.1
UVCAT worksheets used for input

Analysis	Input worksheets
Standard life-cycle cost analysis	STANDARD LCA
Lamp replacement interval cost analysis	LAMP AGE LCA TOOL
Advanced life-cycle cost analysis	ADVANCED LCA WQ RED MODEL RISK MODEL

Table 7.2
Data inputs into UVCAT

Parameter	Data usage for analysis type		
	STANDARD LCA	LAMP AGE LCA TOOL	ADVANCED LCA
UV system sizing criteria	√	√	√
Reactor configuration	√	√	√
Redundancy	√	√	√
Lamp data	√	√	√
Sleeve data	√	√	√
Ballast data	√	√	√
UV sensor data	√	√	√
Dose pacing	√	√	√
Failure data			√
WTP inputs	√	√	√
Capital cost inputs	√	√	√
Dose delivery	√	√	
Ballast power settings			√
Water quality data			√
RED model data			√
Risk data			√

UV System Sizing Criteria

UV systems are sized to deliver the target UV dose under design conditions of flow rate and water UVT. This section of the worksheet is used to enter the following data:

- Design flow rate - flow rate used to size the UV system
- Average flow rate - average flow rate treated by the UV system
- Average UVT - average UVT of the water passed through the UV system
- Design UVT - water UVT used to size the UV system
- Design UV dose - required minimum UV dose delivery value

Reactor Configuration

This section of the spreadsheet is used to enter the following information on the UV reactor configuration.

- Trains - number of UV reactor trains, including redundant reactor trains, installed in parallel and used to treat the total flow through the UV system
- Reactors/train - number of UV reactors in series in each treatment train
- Banks/reactor - number of banks of UV lamps in each reactor. A bank of lamps is defined as a group of lamps oriented across the reactor cross-section perpendicular to the flow through the UV reactor. In a multi-bank reactor, this configuration of lamps is repeated in the direction of flow
- Lamps/bank - number of lamps in each bank
- Lamps/ballast - number of lamps operated by each ballast assembly. A ballast assembly, the power supply of the lamp, is classified as either electronic or electromagnetic. Electromagnetic ballasts typically consist of a transformer to adjust the operating voltage and a network of capacitors to control lamp current. Electronic ballasts typically consist of solid-state power supplies capable of starting lamps and controlling lamp current. Ballast assemblies typically drive either one or two lamps.
- Duty UV sensors/bank - number of duty UV sensors used per bank of lamps to monitor the UV lamps. LPHO and amalgam UV systems often use one UV sensor per bank of lamps. MP UV systems used in drinking water systems often use one UV sensor per lamp. MP UV systems used in wastewater systems use either one sensor per bank of lamps or do not use UV sensors.

Redundancy

Redundant UV reactors or trains are used to ensure the UV system provides the required UV dose when a UV reactor or train is out of service for maintenance or service. This section of the spreadsheet is used to enter the number of redundant trains and reactors per train used by the UV system.

Lamp Data

The most significant operating costs of a UV system are due to lamp replacement and power consumption. UV systems are sized to deliver the required UV dose with the degree of lamp-aging that occurs when the lamps are replaced. This section of the spreadsheet is used to enter the following information on the lamps.

- Lamp 100% power - electrical consumption of the UV lamp and ballast assembly when the UV lamp is operating at the 100% ballast power setting. The value can be estimated as the total power of the UV system operating at 100% power divided by the total number of UV lamps.
- Lamp life - the average operating life of the lamp.
- Lamp-aging Factor - the relative UV output of the lamp at the end of its operating life as compared to a new lamp.
- Lamp cost - purchase price of a new UV lamp
- Lamp replacement time - operator time required to replace one lamp.
- Lamp-aging equation - a mathematical formula that describes relative lamp output as a function of operating time. The equation must predict a relative lamp output equal to the Lamp-aging Factor at an operating time equal to the End-of-Lamp-Life.

Sleeve Data

UV lamps used within UV reactors are housed within quartz sleeves. The quartz sleeves protect the lamp from the water flow rate through the reactor and control heat transfer from the lamp to the water. With operation of the UV system, the UV transmittance of the quartz sleeve will decrease due to external and internal fouling of the sleeve surfaces and aging of the quartz material. UV systems are equipped with cleaning mechanisms that remove foulant from the external surfaces of the sleeves. This section of the spreadsheet is used to enter the following information on the lamp sleeves and cleaning systems.

- Sleeve life - the average operating life of the lamp sleeves
- Sleeve cost - purchase price of a new lamp sleeve
- Sleeve replacement time - operator time required to replace one lamp sleeve
- Sleeve cleaning type - the type of cleaning mechanism used by the UV system (rinse, wiper)
- Sleeve cleaning period - the time period between lamp sleeve cleanings
- Sleeve cleaning time/reactor - the operator time required to clean the lamp sleeves of one UV reactor in the system
- Fouling Factor - the ratio of the UV transmittance of an aged and fouled lamp sleeve to that of a new and clean sleeve; this is often termed the design “Fouling Factor” and is used in sizing the UV system

Ballast Data

Many UV systems use electronic ballasts that power and control one or two UV lamps. Some UV systems use electromagnetic ballasts that consist of transformers to adjust the operating voltage and a network of capacitors to control lamp current. This section of the spreadsheet is used to enter the following information on the lamp ballasts:

- Ballast life - the average operating life of the ballast
- Ballast cost - purchase price of a new ballast
- Ballast replacement time - operator time required to replace a ballast

UV Sensor Data

Drinking water UV systems are all equipped with duty UV sensors for performance monitoring. Often, the duty UV sensors are regularly checked using an independent reference UV sensor. The duty sensors are either calibrated by a certified calibration laboratory or calibrated on-site by the operator through comparison with a calibrated reference UV sensor. This section of the spreadsheet is used to enter the following information on the UV sensors:

- Sensor life - the average operating life of the duty UV sensor
- Sensor cost - purchase price of a new duty UV sensor
- Sensor replacement time - operator time required to replace one duty UV sensor
- Sensor calibration period - the average time period between calibrations of the duty UV sensors
- Sensor calibration cost - cost to calibrate a duty UV sensor excluding operator labor
- Sensor calibration time - operator time required to calibrate one duty UV sensor

UV Dose Pacing

While UV systems are sized to deliver the required UV dose under design conditions of flow rate, water UVT, lamp-aging, and sleeve fouling, they typically operate at lower flow rates and higher water UVTs with lamps and sleeves that are less aged and fouled than the design conditions. In these situations, if the UV system operated with all lamps on at 100% power, the UV system would overdose. To prevent overdosing and minimize unnecessary costs, UV systems turn banks of lamps on and off and/or reduce ballast power to deliver the required UV dose delivery with minimal over dosing. The UV system can turn on and off banks of lamps or adjust lamp power in response to changes in one or more of the following measured parameters:

- Flow rate
- UVT
- UV intensity
- Lamp output predicted using a defined lamp-aging curve and the simulated lamp operating hours

Dose-pacing strategies vary from UV reactor-to-reactor and from installation-to-installation. When measured intensity is used for dose pacing, it accounts for lamp and sleeve

aging and fouling. In some cases, the UV dose-monitoring system is only dependant upon flow rate and measured intensity, so a UVT monitor is not required.

With the STANDARD LCA and LAMP AGE LCA tools, the “Dose Pacing” section of the worksheet is used to indicate which factors impacting dose delivery are accounted for by the dose-pacing strategy used by the UV system. This section is also used to input the Peak UV Dose, defined as the UV dose delivered by the duty UV reactors operating under design conditions of flow rate, water UVT, lamp-aging, and sleeve fouling with all lamps on at 100 percent power.

With the ADVANCED LCA tool, the “Dose Pacing” section of the worksheet is used to indicate the dose monitoring and control algorithm used by the UV system by entering a numeric reference to a dose-pacing model defined in the Input Worksheet “RED Model.” Detailed information on this type of data input is described in the UVCAT User Manual (Appendix A).

Power Failure Data

Dose delivery over time by a UV system is affected by power quality and UV system component reliability. Power quality events that cause the UV lamps to extinguish include voltage sags and interruptions. Typically, the lamps extinguish when the voltage drops below a threshold voltage value for some duration. A generator is often used to provide power to the UV system during a power interruption. However, a generator does not prevent the lamps from extinguishing during a power quality event. As an alternate, an uninterruptible power source (UPS) can be used to provide continuous power supply to the UV system during power quality events. The time required to startup a UV system following a power quality event will depend on the lamp cool-down and warm-up times, the duration of the power quality event, and the time required to startup a generator if used. Dose delivery is also impacted by failure of UV lamps and ballasts. Dose monitoring is impacted by failure of UV sensor and UVT monitors. This section of the worksheet is used to enter the following information on UV system failure and response to failure:

- Supply voltage lower limit - the percentage of nominal voltage that causes lamps to extinguish
- PQ event duration lower limit - the duration of power quality event that causes lamps to extinguish
- UPS - is an uninterruptible power supply used to provide backup power?
- Generator - is a generator used to provide backup power?
- Generator start-up time - time required to start up the generator following the power quality event
- Lamp cool-down time - time required to cool down the lamps before they can be restarted
- Lamp warm-up time - time required to startup a UV lamp after cool down
- Lamp failure probability - probability a single UV lamp will fail over a one-day period
- Ballast failure probability - probability a single lamp ballast will fail over a one-day period

- UV sensor failure probability - probability a single UV intensity sensor will fail over a one-day period
- UVT monitor failure probability - probability a single UVT monitor will fail over a one-day period

WTP Inputs

This section of the spreadsheet is used to enter the following site-specific data that impacts system O&M costs and performance:

- Labor rate - the average labor rate including overhead of the personnel operating and maintaining the UV system
- Electricity cost - the cost of electricity paid by the utility
- Patent fees - patent royalties paid by the utility for using the UV system. CCC has requested patent royalties of \$0.015 per 1,000 gallons treated from utilities using UV for *Cryptosporidium* and *Giardia* inactivation
- Interest rate - the annual interest rate on money borrowed by the utility
- Period - the period over which the utility pays back money borrowed to pay for the UV system. The life-cycle costs are calculated over that period.
- Supply Voltage - the nominal supply voltage to the UV system
- Population - the population served by the UV system

Capital Cost Inputs

This section of the spreadsheet is used to enter UV system capital cost information:

- Reactor - the total capital costs of the UV reactors including the control panels
- Install factor - the cost of installing the UV equipment
- Validation - the cost for validating the UV reactor
- Inlet/outlet piping - the capital cost including installation of all inlet and outlet piping needed for the UV system including flowmeters, valves, pipes, and channels
- Power supply - capital cost of providing power to the UV system including switchgear, transformers, distribution panels, generators, and UPS systems
- Other - other costs include yard piping, chlorine contactors, and low lift pumps
- UV building - capital costs for demolition, civil/site work, building, and heating, ventilation, and air conditioning (HVAC)
- Instrumentation - capital cost of all instrumentation including SCADA and on-line UVT monitors
- HVAC - an alternate field for entering HVAC
- Miscellaneous Electrical - a field for entering cost of any miscellaneous electrical work
- Civil/site work - an alternate field for entering civil site work
- Contingency - capital cost contingency typically set as a percent of all capital costs
- General conditions - includes mobilization/demobilization, major equipment, site preparation such as fences, temporary facilities for contractors, bonds/insurance,

- permits, supervision and engineering salaries, support systems (e.g., water), and general expense items
- Contractor O&P - contractor overhead and profit typically set as a percent of all the above costs
- Engineering, legal, and administration - the engineering costs of the UV project typically set as a percent of all the above costs
- Total - total of all capital costs

UV Dose Delivery

For the Standard LCA and Lamp Age LCA tools, this section of the spreadsheet is used to enter data on dose delivery by a UV reactor as a function of specified values of water UVT. UV dose delivery by the reactor should be entered for one UV reactor operating at the design flow rate with new lamps all on and operating at 100% power within new clean sleeves.

Ballast Power Settings

Ballasts typically operate at discrete power settings. For the Advanced LCA, this section of the spreadsheet is used to specify discrete power settings in ascending order starting with the minimum power setting.

Water Quality Data

The Advanced LCA can be used to simulate UV system performance over any time period (historical or forecasted). The Advanced LCA uses the worksheet entitled "WQ" to enter the following historical or forecasted water and power quality data:

- Date/time
- Flow rate
- UVT
- Raw water pathogen concentration
- Supply voltage
- Power quality event duration

RED Model

The Advanced LCA algorithm of UVCAT uses UV dose delivery models located in the "REDMODEL" worksheet to calculate UV reactor operation as a function of target UV dose, flow rate, UVT, and lamp-aging and fouling factors. This equation is often of the form:

$$RED = 10^A \times UVA^B \times Q^C \times \left[\frac{S}{S_o} \right]^D \times Banks^E \quad (7.1)$$

where UVA is the UV absorbance of the water calculated from the UVT, Q is the flow rate through the reactor, Banks is the number of banks of operating lamps, S/S_o is the relative output

from the lamps accounting for ballast power setting, lamp-aging, and fouling, A, B, C, D, and E are fitted constants. The value of S/S_o can be determined from the equation describing the UV sensor readings as a function UVT and ballast power setting. This equation is often of the form:

$$S = 10^{A'} \times \exp(B' \times UVT) \times P^{C'} \times f_L \times f_f \quad (7.2)$$

where f_L is the lamp-aging factor, f_f is the fouling factors, and A' , B' , and C' are constants. Using this equation, the relative lamp output is expressed as:

$$\frac{S}{S_o} = \frac{P^{C'} \times f_L \times f_f}{P_{\max}^{C'}} \quad (7.3)$$

where P_{\max} is the maximum power setting of the lamps. With MP UV lamps, the relationship between S and P can depend on the orientation of the sensor relative to the lamp. To account for different relations, the RED Model is structured to predict the ballast power setting for two S versus P relations. Lamps with the first relation are termed “Type 1 lamps” while lamps with the second relation are termed “Type 2 lamps”. Further details on the RED Model worksheet is described in the UVCAT User Manual (Appendix A).

Risk Model

The worksheet “RISKMODEL” is used to enter the UV dose-response of the target pathogen and the risk model for human infection (USEPA 2006b). The Advanced LCA algorithm uses these models as a calculator tool to determine log inactivation credit and public health impact of a given UV dose and a raw water pathogen concentration. The tool allows the user to enter site-specific pathogen risk information. Detailed information on this type of data input is described in Chapter 12 and the UVCAT User Manual (Appendix A).

UVCAT ALGORITHMS

Detailed information on UVCAT calculation algorithms is described in the UVCAT User Manual (Appendix A).

UVCAT OUTPUTS

The input worksheets entitled STANDARD LCA, LAMP AGE LCA TOOL, and ADVANCED LCA are structured to enter information UV systems as columns of data, where each column describes a UV system. The user can then specify which columns of data to analyze when running the UVCAT software. This feature allows the user to analyze multiple UV system scenarios with a single execution of the software. The output data generated by UVCAT for each UV system analyzed is placed into the worksheets described in [Table 7.3](#).

Table 7.3
UVCAT worksheets used for output

Analysis	Output worksheets
Standard life-cycle cost analysis	STANDARD LCA
Lamp replacement interval cost analysis	LAMP AGE LCA TOOL
Advanced life-cycle cost analysis	ADVANCED LCA WQ REACTOR DOSE TARGET POWER 1 TARGET POWER 2 POWER 1 POWER 2 LAMP HOURS LAMP-AGING FACTOR

The outputs for the Standard LCA are:

- Number and power setting of the lamps required to deliver the design UV dose under average conditions of flow rate, UVT, lamp-aging, and sleeve fouling.
- Annual power costs
- Annual lamp, sleeve, ballast, and duty UV sensor replacement costs
- Annual UV sensor calibration costs
- Total annual consumable costs, patent costs, and O&M costs
- Total capital costs
- Total present worth costs and present worth of O&M

These outputs are placed in the STANDARD LCA worksheet in the columns associated with the input data for the UV systems analyzed.

The output from the Lamp Replacement Interval Cost Analysis is a table containing the following fields as a function of the lamp replacement interval:

- Lamp Life - from 1,000 to 20,000 hours in 1,000 hour increments
- Age Factor - lamp-aging factor associated with each lamp life
- Average Lamps - number of lamps that would operate under average conditions of flow rate, UVT, lamp age, and sleeve fouling
- Power Setting - power setting of those lamps
- Power - annual power costs
- Consumables - annual consumable costs
- Labor - annual labor costs
- Patent - annual patent costs
- Total O&M - total annual O&M costs

- Capital - total capital costs
- NPV - net present value of O&M and capital costs

The outputs from the Advanced LCA tool are placed in the following worksheets:

- LAMP-AGING FACTOR - relative output of the UV lamps of each bank as a function of time
- LAMP HOURS - age of the lamps of each bank as a function of time based on accumulated operating hours and accounting for lamp replacement
- TARGET POWER 1 and TARGET POWER 2 - target power of the type 1 and 2 lamps of each bank predicted by the RED model as a function of time
- POWER 1 and POWER 2 - operating power of the type 1 and 2 lamps of each bank as a function of time based on the entered ballast power settings achievable
- REACTOR DOSE - UV dose delivered by each reactor in the UV system as a function of time with operation not impacted by power quality events and component failure
- WQ - various measures of UV system performance as a function of time including:
 - Target RED
 - Trains
 - Reactors per train
 - Banks per reactor
 - Flow rate per reactor
 - Fouling Factor
 - Total power based on Power 1 and Power 2 data
 - Ideal total power based on Target Power 1 and Target Power 2 data
 - Ratio of total power and ideal total power
 - Daily power costs
 - Power costs
 - Sum power costs
 - Off-specification flag
 - Percent off-specification time
 - Percent off-specification volume
 - UV system log kill
 - Risk
 - Annual risk
 - Accumulated risk

The UVCAT software saves the information outputted to the worksheet WQ with each UV system analyzed. However, information outputted to the other worksheets is not saved.

QUALITY ASSURANCE/QUALITY CONTROL

The UVCAT software checks the inputs to the software and flags the user if those inputs do not meet defined QA/QC criteria. UVCAT QA/QC criteria are described in the UVCAT User Manual (Appendix A).

CHAPTER 8

EXPERIMENTAL LAMP-AGING STUDIES

This chapter describes experimental lamp-aging studies conducted from March 2004 to March 2006 by the Lighting Research Center of Rensselaer Polytechnic Institute in Troy, N.Y. The purpose of these studies was to:

- Investigate the degradation of UV output of LPHO lamps (amalgam and non-amalgam) and MP lamps over time at different power levels
- Evaluate the efficiency of lamp operation including startup characteristics
- Evaluate the impact of sleeve and sensor window fouling

METHODS

UV Reactor Pilot System

Life testing of UV lamps was performed at the John P. Buckley Water Treatment Plant, Troy, N.Y. Four UV pilot reactors were installed at the water plant. Two of the UV reactors used MP lamps, four 8-kW lamps in one and six 6-kW lamps in the other. The other two UV reactors used LPHO lamps, each having eight lamps. One of the LPHO reactors used mercury amalgam-type lamps, while the other used non-amalgam mercury lamps. Figure 8.1 illustrates the UV pilot reactor system. Figures 8.2, 8.3 and 8.4 show photographs of the UV reactors. Table 8.1 summarizes the lamp characteristics of each UV pilot reactor. Reactors were arranged in series and were operated at a flow rate of approximately 50 gpm for the duration of the lamp aging study.

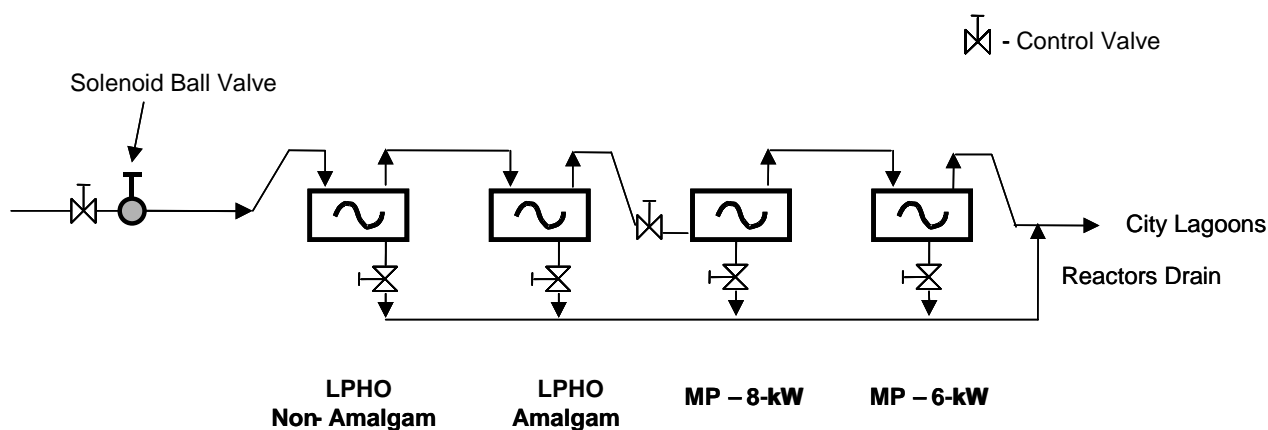


Figure 8.1 Schematic of the test process train installed at the John P. Buckley WTP



Figure 8.2 Photograph of the R-Can amalgam and non-amalgam LPHO reactors



Figure 8.3 Photograph of the IDI reactor equipped with six 6 kW MP lamps



Figure 8.4 Photograph of the IDI reactor equipped with four 4 kW MP lamps

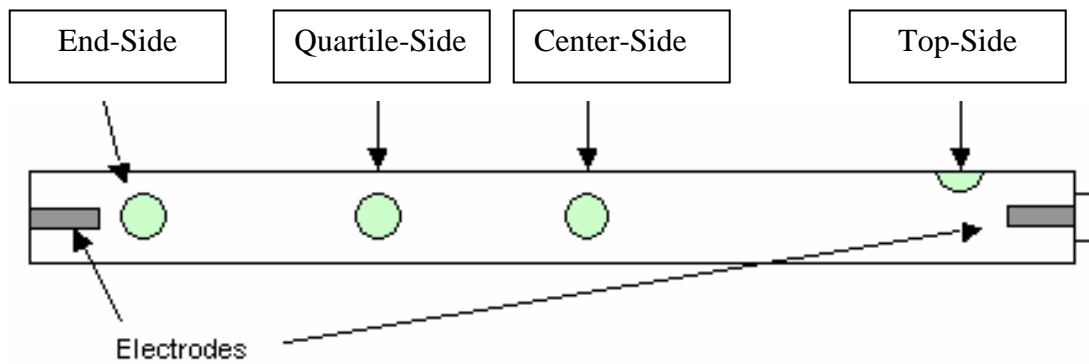


Figure 8.5 Spectral measurement positions

Table 8.1
Lamp operating characteristics used in the lamp-aging study

UV system manufacturer	R-Can	R-Can	ODI	ODI
Technology	LPHO	LPHO	MP	MP
Type	Amalgam	Non-amalgam	-	-
N ^o . of lamps	8	8	6	4
Total power (kW)	0.35	0.15	6	8
Hg/lamp (mg)	60	60	450	660
Power levels tested (%)	70 and 100 %	70 and 100 %	60, 70, 80, 90, and 100%	60, 70, 80 and 100%
Daily on/off cycles	1	1	1	1

Method of Measurement

The UV output of the lamps was measured over the course of the life test after 350, 650, 1,000, 2,000, 4,000 and 6,000 or 7,000 hours of operation. The hours of operation of the lamps did not coincide with calendar time, as there were long periods of time when the reactors were shut down due to problems with their operation, mainly concerning the MP reactors. Lamps were removed from the UV reactor vessels for measurement and operated individually in a specially built measurement chamber. Each LPHO lamp was operated in the measurement chamber using its corresponding ballast from the reactor. However, each MP lamp was driven by a dedicated ballast selected from the corresponding reactor. During measurement, the lamps were operated at the same power setting at which it was operated during the life test.

As indicated in [Figure 8.5](#), the UV output from the lamp was measured at four locations along the length and around the circumference of each lamp. These locations were designated center-side, quartile-side, end-side, and end-top. Irradiance measurements were taken at a distance of 16.5 cm from the lamp envelope. Spectral irradiance was measured using a double-grating monochromator. With the MP lamps, UV irradiance was measured from 200 to 350 nm. With the LPHO lamps, UV irradiance was measured from 240 to 400 nm at the center-side position and 245 to 300 nm at the other positions.

Measurement Chamber

The lamp measurement chamber, illustrated in [Figures 8.6](#) and [8.7](#), served three purposes: 1) to provide a means of supporting the lamp and repeatedly positioning the irradiance detector, 2) to provide a proper thermal environment for operating the lamp, and 3) to shield the operator and room from the intense UV radiation produced by the lamps. The inside of the chamber was painted with heat-resistant, flat black paint to reduce reflectance of UV light from contributing to the measured UV output. Four-inch wide baffles that ran along the length of the chamber also reduced scattered and reflected UV light. A fan located at each end of the chamber, one blowing

in and one blowing out, were used to dissipate heat generated by the lamps. Each fan was rated at 600 ft³/min. (17 m³/min), although the exact resulting airflow inside the chamber was not measured.

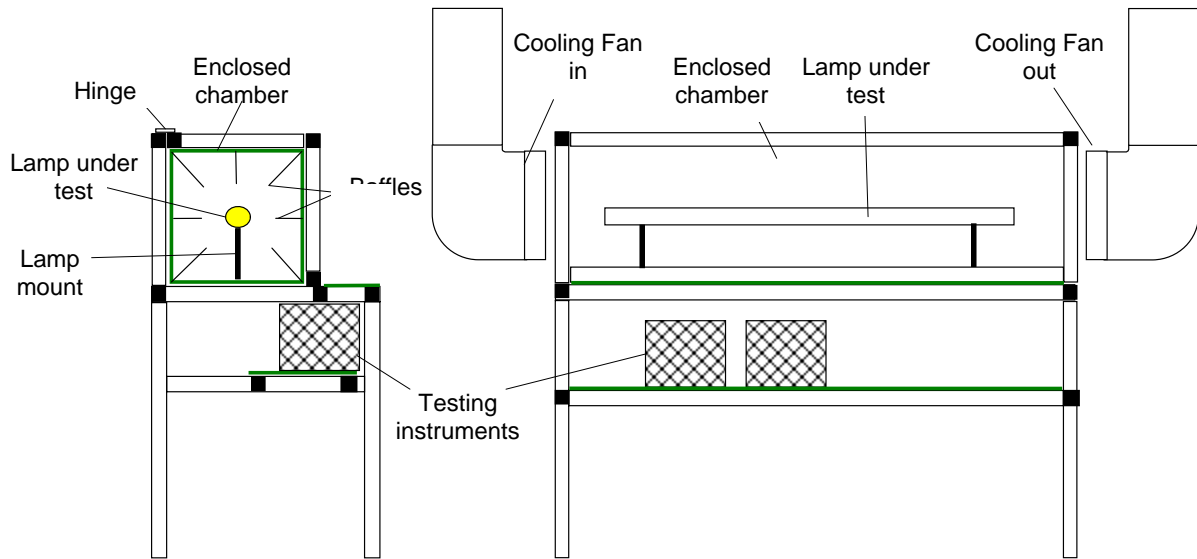


Figure 8.6 Schematic of the measurement chamber

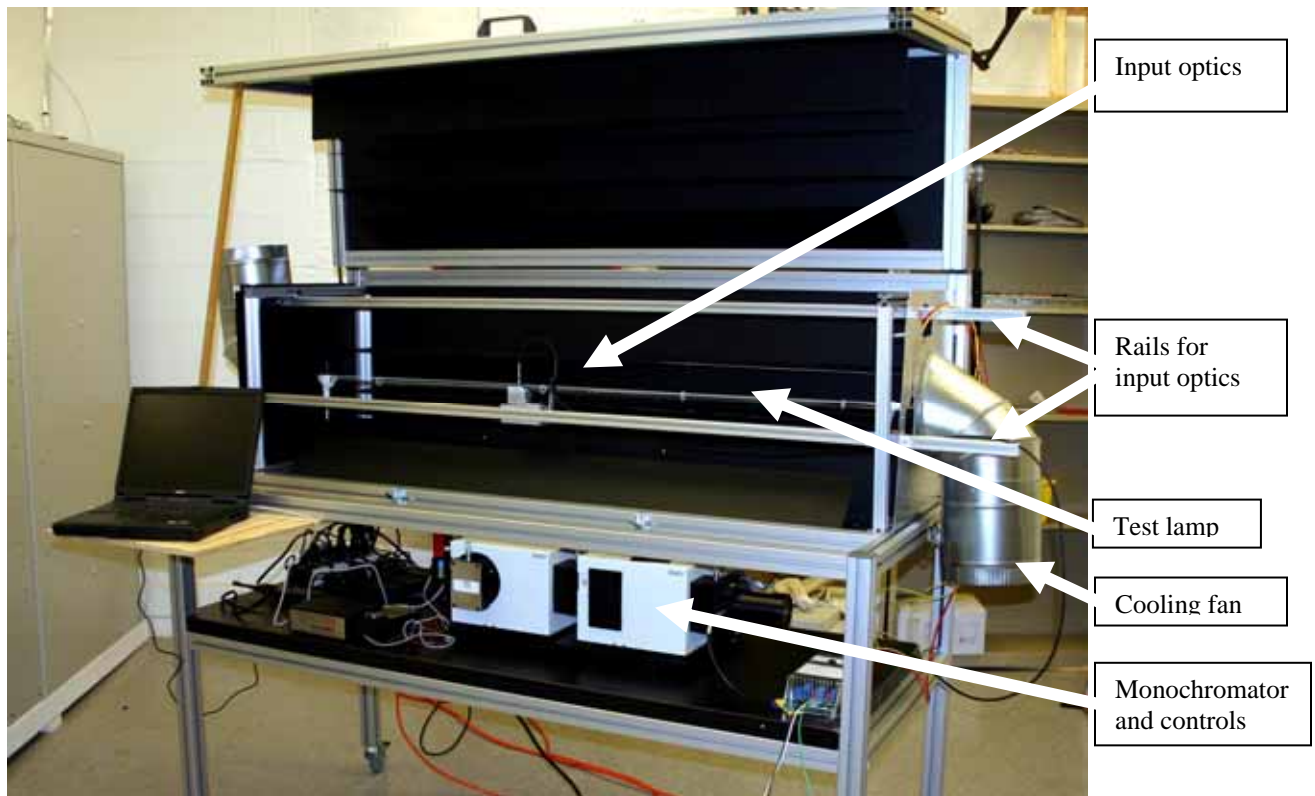


Figure 8.7 Photograph of the measurement chamber

The inside of the chamber contained two rails that carried the optical detector along the length of the lamp. One rail was located 16.5 cm to the side of the lamp, and the other was located 14.0 cm above the lamp. The detector could be placed on either rail from outside the chamber and slid on a trolley along the length of the lamp without opening the chamber or disturbing the lamp. Measurements taken from the top rail were adjusted to correspond to the side rail measurement distance by treating the lamp as a line source where the irradiance was inversely proportional to the measurement distance.

UV Detector

Spectral irradiance was measured using a double grating monochromator, as illustrated in [Figure 8.8](#). The input optics for the monochromator consisted of a small integrating sphere and a 3-meter UV-transmitting fiber-optic cable. The sphere with attached fiber optic cable is shown in [Figure 8.9](#). The fiber-optic cable was made of high-purity fused silica to transmit UV light at wavelengths down to 200 nm. Tests were done to ensure that UV light throughput of the fiber bundle remained constant with movement of the cable that occurred during the course of measurements. The integrating sphere acted as a cosine collector for the irradiance measurements. The fiber-optic cable was connected to the integrating sphere at a 90-degree angle to the input port of the sphere. The sphere was 1 inch (25.4 mm) in diameter and was coated internally with special high-purity barium sulfate paint for diffuse UV reflectivity. The fiber-optic cable was supported on a guide so that the cable was not bent in a way that would attenuate the throughput or damage the optical fibers. The cable was wrapped in white Teflon tape to prevent overheating when exposed to the intense radiation from the MP lamps. The input aperture of the sphere was 5 mm in diameter. An aperture holder at the input port allowed a smaller aperture to be used as a means of reducing the input signal.

The monochromator was an Acton Research SpectraPro 300i double monochromator with a holographic UV grating (2400 lines/mm). A photomultiplier tube (PMT) module served as the detector (Hamamatsu model H7710-12). The monochromator system had a bandpass of approximately 0.5 nm. Spectral scans were done at 0.25-nm increments to ensure complete coverage of the spectral range scanned.

System Calibration

The primary calibration sources for the monochromator system were a 1,000-W FEL-type incandescent lamp acquired directly from NIST (NIST Test No. 844/269247-03), and a 30-W deuterium arc lamp purchased from Oriel Corporation with NIST-traceable calibration (Oriel model 66145, Oriel Lamp Serial No. CB93580). The FEL lamp provided calibrated spectral irradiance output over the range from 250 to 2,500 nm, and the deuterium lamp was spectrally calibrated over the range 200 to 400 nm (see [Figure 8.10](#)). Because the FEL lamp was a more stable source and calibrated to a higher degree of accuracy than the deuterium lamp, it was used to set the magnitude of the overall calibration and the relative shape of the calibration curve for wavelengths greater than 300 nm. The deuterium arc lamp was used to set the relative response of the system for wavelengths less than 300 nm. The two relative calibration curves had a considerable range of overlap (250 to 400 nm) showing agreement better than 3 percent for wavelengths between 280 and 350 nm. The combined calibration curve was smoothed using a 3-point average and had no discernible discontinuities.

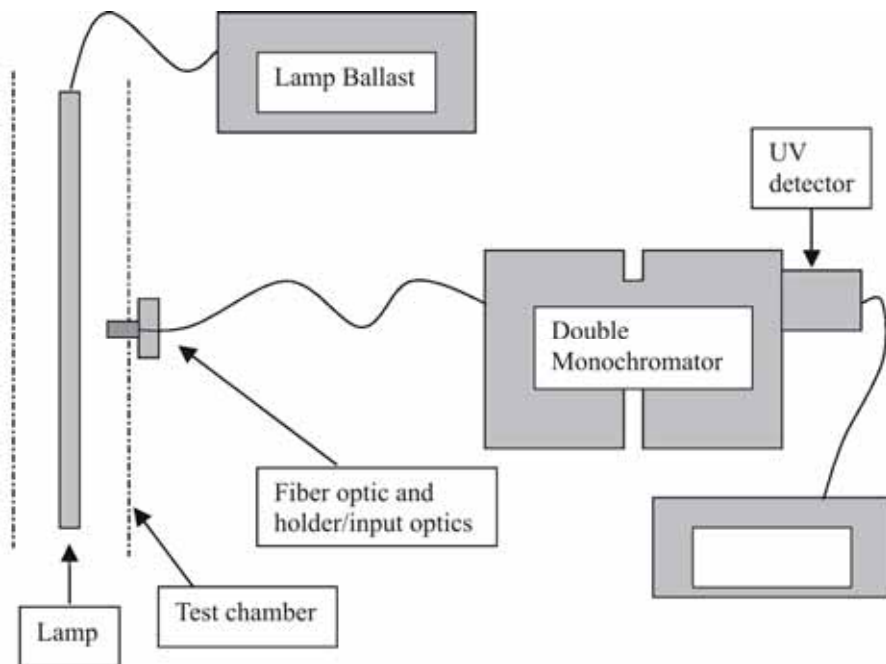
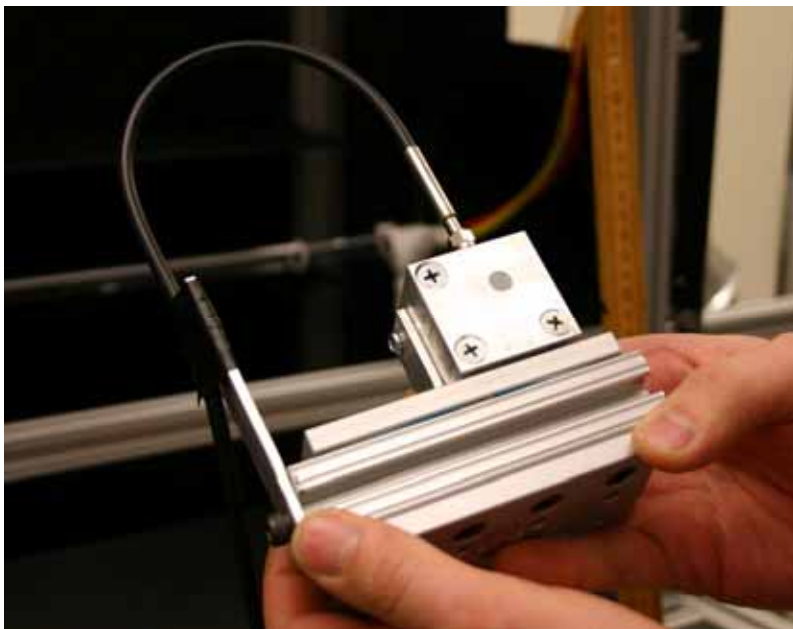


Figure 8.8 Monochromator system



Fiber-optic cable

Integrating sphere

Rail mount

Figure 8.9 Input optics to the fiber-coupled monochromator. Integrating sphere optics provided cosine response for proper irradiance measurements.

Two 750-watt FEL type incandescent lamps, calibrated as secondary standards, were used for calibration of the measurement system at the water plant. Each day when irradiance measurements were taken, the system would be calibrated by measuring one 750-W FEL lamp and the deuterium lamp and calculating a new calibration curve from the combined responses as described above. The lamp standards were mounted on a rail attached to the outside of the measurement chamber. Because of the low UV output of the lamp standards relative to that of the LPHO and MP lamps, calibration was done with the full 5 mm aperture open on the 1-inch sphere. A smaller aperture, made from a thin sheet of stainless steel with an area approximately 5 percent of the full aperture was then placed over the sphere aperture when measuring the LPHO and MP lamps. The attenuation factor for the aperture was determined optically from UV readings taken with and without the aperture in place.

Measurement Uncertainty

The measurement system minimized stray light effects by using a double monochromator and filters. The wavelength accuracy of the monochromator was stated by the manufacturer to be ± 0.2 nm. The accuracy was easily verified by noting the positions of the Hg emission lines within the spectrum recording of the lamps. The precision of the monochromator for wavelength was reported as ± 0.05 nm.

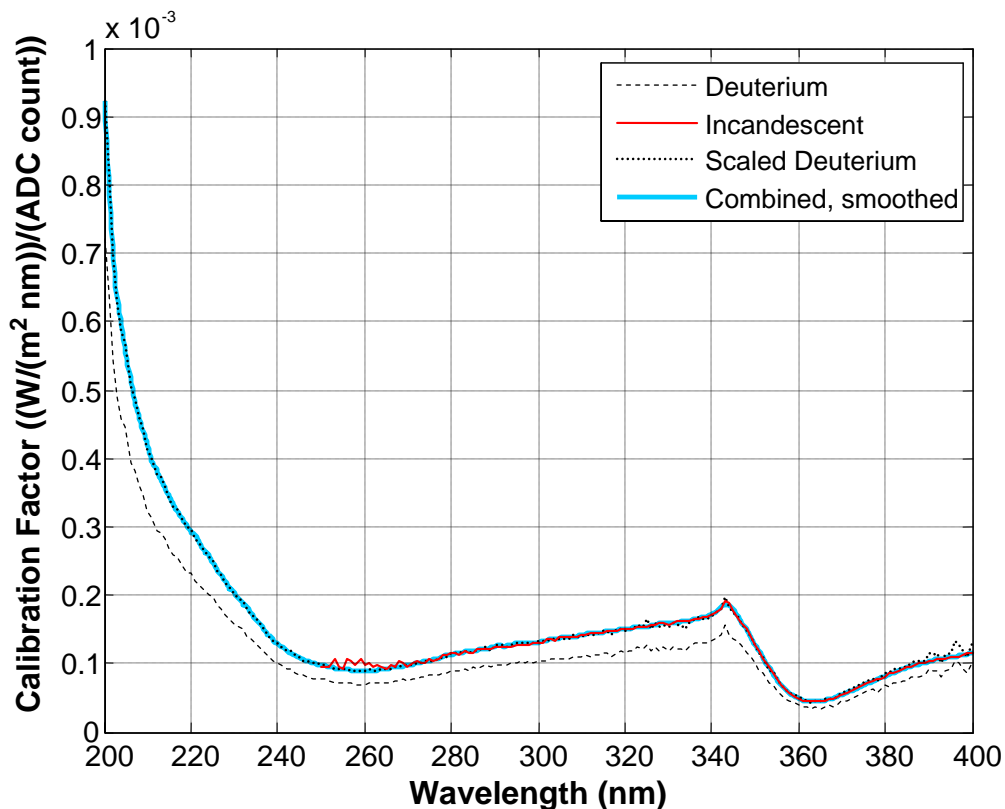


Figure 8.10 Spectrometer calibration curves

The 30-W deuterium lamp has an uncertainty of 8 percent in the wavelength range of 200-250 nm and 6 percent in the wavelength range of 250-400 nm. The quartz-halogen lamp used as a primary standard was NIST calibrated with an uncertainty of 1.6 percent at 250 nm and 1.1 percent at 350 nm (coverage factor $k=2$).

Error transferring the primary calibration to the working standards increased the overall measurement uncertainty. The major sources of error included uncertainties in the distance from lamps to detector, the operating current of the lamps, and stray light. Taken together these uncertainties were estimated to add an additional 3 percent to the absolute calibration of the working standard.

Calibration of the spectrometer system and the measurement of the lamps also introduced additional uncertainties. These uncertainties affected both the absolute and relative determination of UV irradiance from the lamps. Factors contributing to this uncertainty included cosine correction for UV input (sphere optic), signal read-out equipment errors (linearity), detector noise and stability, lamp stability for both standard lamps and test lamps, the distance of the detector from the emission source, and scattered/stray light. The combined uncertainty for these factors, based on calculations of distance and lamp current uncertainties and a review of the calibration curves, is estimated to be 10 percent (coverage factor of 2, or 95 percent confidence interval). The total absolute uncertainty of the UV irradiance measurements is dominated by the relatively large uncertainty of daily calibration and lamp measurements.

Measurement Procedure

At the start of a measurement period, the UV reactor was shut down and the lamps were allowed to cool. A variable amount of time elapsed between when the reactor was shut down and when the lamps were measured, ranging from a few hours to over a week. During this time, the lamps were not disturbed inside the reactor vessel.

When ready for measurement, a single lamp would be removed from the reactor and placed in the measurement chamber. Care was taken not to shake or tip the lamp from its horizontal position so as not to disturb the condensed mercury in the lamp. For the MP lamps, each lamp under test was electrically connected to one of the ballasts powering the reactor using the existing lamp leads. For the LPHO lamps, the lamp under test was electrically connected to its corresponding ballast on the reactor using four 18 AWG wires approximately 2 meters in length, to which a current monitor (Pearson Electronics, Model 411) and differential voltage probe (LeCroy, model P532) were attached to measure lamp current and lamp arc voltage. The chamber was then closed and the lamp switched on.

The MP lamps were switched on and allowed to stabilize, as judged by monitoring the UV output at 260 nm measured by the spectrometer system. Once stable, a spectral scan was recorded at each measurement position using the sphere-detector. A long metal rod was used to move the sphere-detector into each measurement position, thereby allowing the lamp to remain lit throughout the series of measurements.

For the LPHO lamps, a UV sensor located at the top-center of the lamp (Hamamatsu Model No. S2684-254) monitored relative UV (254 nm) output. Over approximately 10 minutes, the UV output would reach a peak value and then decline. The peak value was recorded. The lamp was allowed to stabilize, judged by monitoring the UV sensor reading. If the UV output dropped considerably (more than 30 percent), the fans on the testing chamber were switched on to cool the lamps and bring the UV output closer to its peak value. When the

lamp was stable, the irradiance was measured at the specified locations using the calibrated spectrometer system. The irradiance measured by the UV sensor was recorded. The ratio of the peak to steady state UV sensor readings was used to adjust the UV irradiance measured by the spectrophotometer to the value expected with peak output. The intended purpose of this procedure was to ensure that the irradiance spectrum always represented the output at the optimum operating temperature. This method was necessary to account for the range of ambient temperatures encountered at the water plant due to measurements occurring during different seasons.

RESULTS AND ANALYSIS

8-kW Medium-Pressure Lamps

Figure 8.11 presents the UV irradiance from 240 to 300 nm (not weighted by an action spectra) as a function of lamp operating hours for the UV reactor equipped with four 8-kW MP lamps. The four lamps were operated at the following power settings both for the long-term aging and for the measurements of UV irradiance:

- Lamp 1 - 8.0-kW
- Lamp 2 - 6.5-kW
- Lamp 3 - 5.5-kW
- Lamp 4 - 5.0-kW

Figure 8.11 also presents the average UV irradiance measured with the four lamps as a function of time. Except for the values collected at 350 hours, the data showed a monotonic reduction in UV irradiance as a function of time that was best fit using the modified exponential function:

$$I = (a - b) \times \exp(-c \times t) + b \quad (8.1)$$

where I is the UV irradiance, t is time, and a , b , and c are model coefficients. Table 8.2 presents the model coefficients obtained when the data was fit to Equation 8.1 using non-linear regression. Because the UV irradiance data at 350 hours was biased low, especially with the plot of average UV irradiance as a function of time, that data was not used when fitting Equation 8.1 to the dataset.

Functionally, Equation 8.1 describes an exponential reduction in UV irradiance from a level “ a ” to level “ b ”. The UV irradiance asymptotically approaches the value “ b ” as the lamp age increases, but never falls below that value. While this may not be a valid representation of the true lamp aging relationship, Equation 8.1 does fit the average irradiances as a function of time with very high R^2 values (*e.g.*, 0.999996 for the middle side position data). Other mathematical functions investigated did not fit the dataset as well as Equation 8.1.

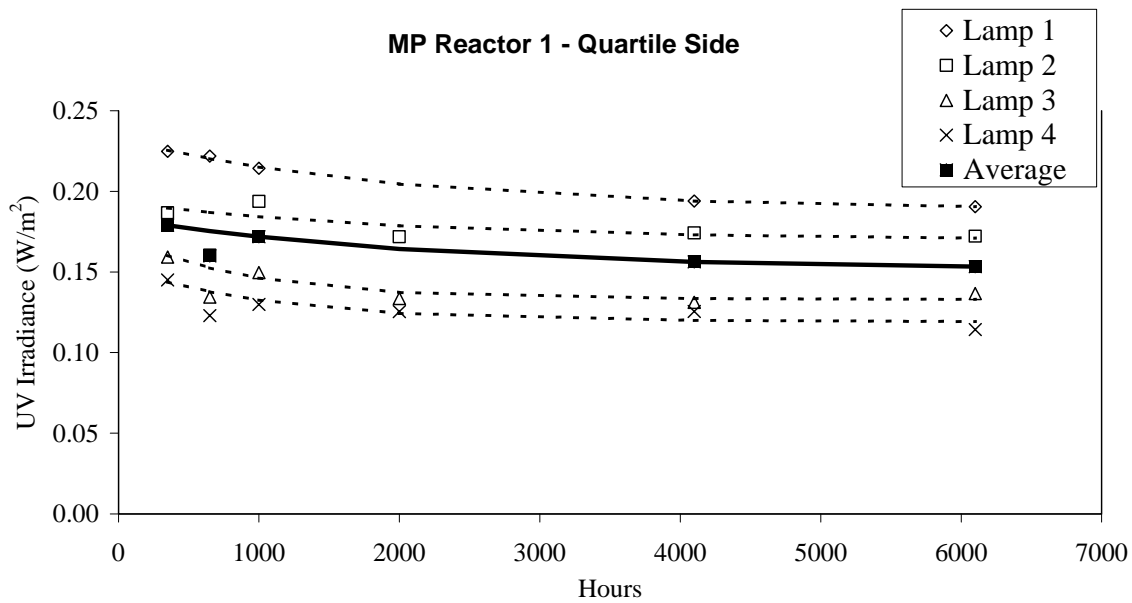
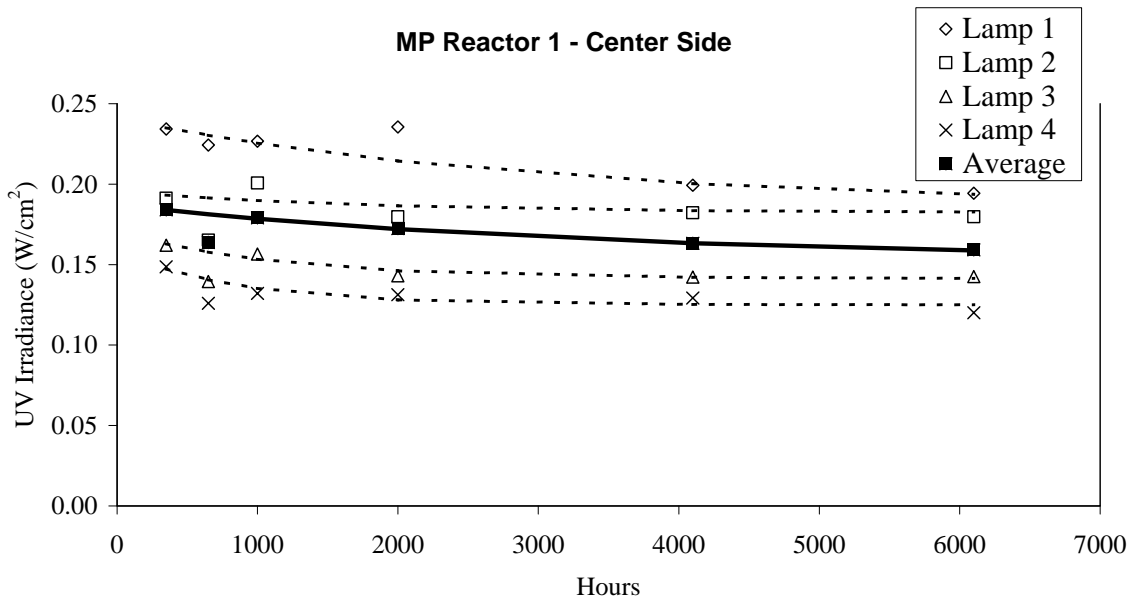


Figure 8.11 Lamp aging data for the UV reactor equipped with four 8.0 kW MP lamps - Lamps 1, 2, 3, and 4 were operated at 8.0, 6.5, 5.5, and 5.0 kW, respectively

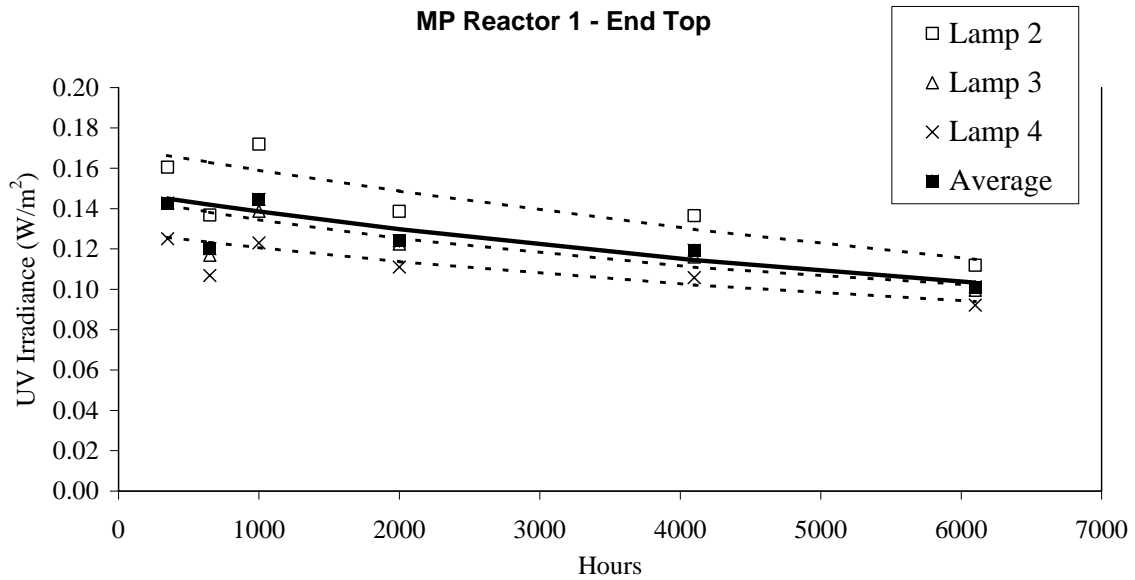
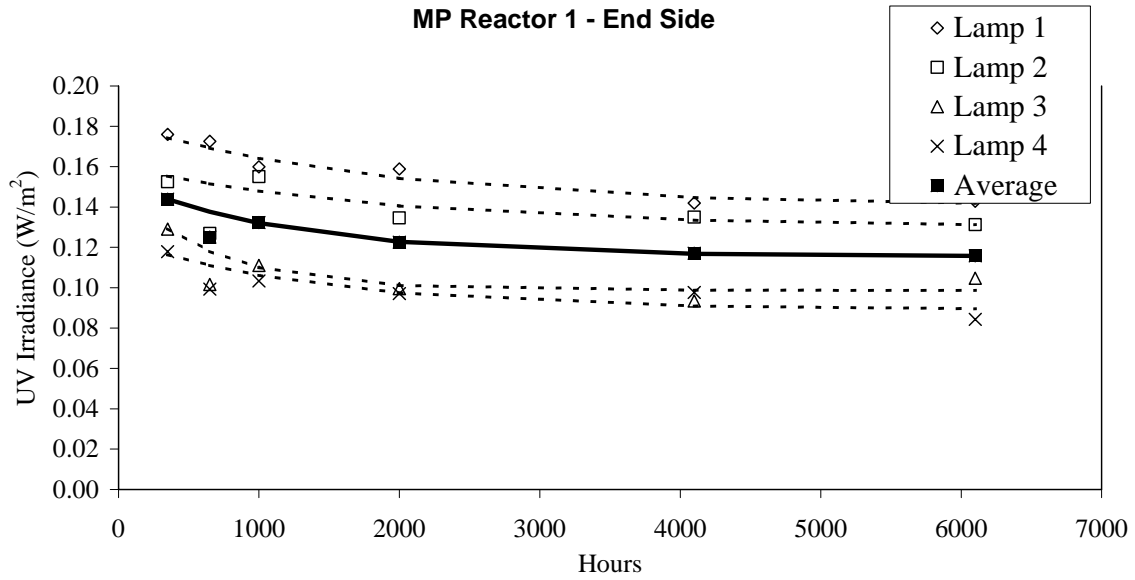


Figure 8.11 (Continued) Lamp aging data for the UV reactor equipped with four 8.0 kW MP lamps - Lamps 1, 2, 3, and 4 were operated at 8.0, 6.5, 5.5, and 5.0 kW, respectively

Table 8.2
Coefficients of Equation 8.1 fitted to the lamp aging data for the
UV reactor equipped with four 8.0 kW MP lamps

Middle side position					
Coefficient	Lamp 1	Lamp 2	Lamp 3	Lamp 4	Average
a	0.2411	0.1956	0.1710	0.1590	0.1872
b	0.1867	0.1822	0.1412	0.1248	0.1533
c	0.000338	0.000580	0.000906	0.001194	0.000298

Quartile side position					
Coefficient	Lamp 1	Lamp 2	Lamp 3	Lamp 4	Average
a	0.2327	0.1933	0.1733	0.1535	0.1838
b	0.1884	0.1697	0.1330	0.1191	0.1514
c	0.000508	0.000485	0.001116	0.000946	0.000463

End side position					
Coefficient	Lamp 1	Lamp 2	Lamp 3	Lamp 4	Average
a	0.1814	0.1604	0.1510	0.1242	0.1534
b	0.1402	0.1300	0.09863	0.08910	0.1155
c	0.000542	0.000531	0.00153	0.000724	0.000831

End top position					
Coefficient	Lamp 1	Lamp 2	Lamp 3	Lamp 4	Average
a	-	0.1704	0.1458	0.1286	0.1486
b	-	0.04288	0.08412	0.06972	0.06463
c	-	9.40E-05	0.000203	0.000146	0.000127

Figure 8.12 presents the coefficients a, b, and c plotted as a function of ballast power setting. The coefficients showed a dependence on ballast power that could be described using a power function (e.g., $y = Ax^B$). Substituting the power function into Equation 8.1 gave the following equation:

$$\begin{aligned}
 I &= (A \times P^B - C \times P^D) \times \exp(-E \times P^F \times t) + C \times P^D \\
 &= A \times P^B \times \exp(-E \times P^F \times t) + C \times P^D \times (1 - \exp(-E \times P^F \times t))
 \end{aligned}
 \tag{8.2}$$

where P is the ballast power setting in units of kW and A, B, C, D, E, and F are model coefficients.

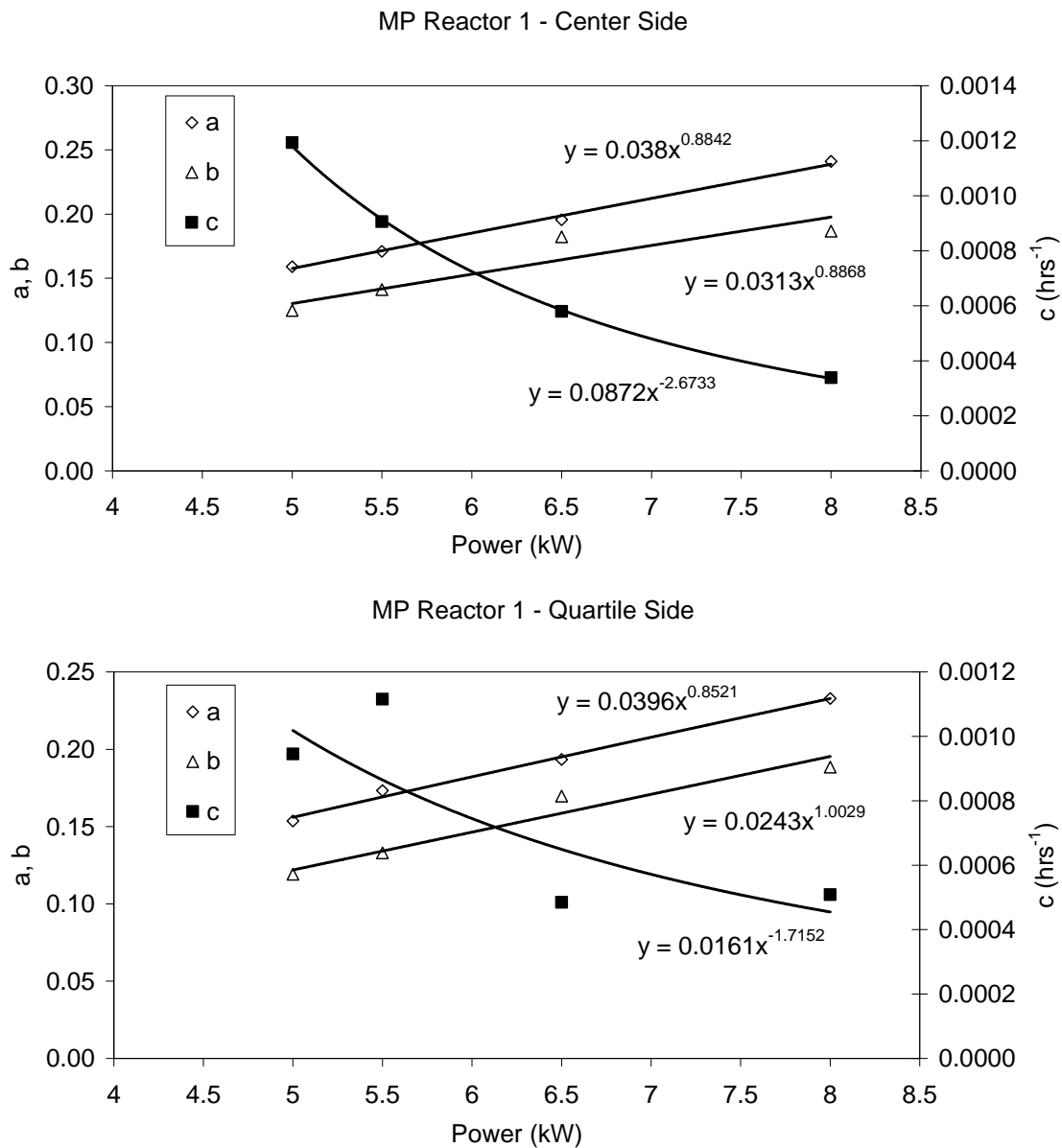


Figure 8.12 Coefficients a, b, and c of Equation 8.1 plotted as a function of ballast power for the UV reactor equipped with four 8.0 kW MP lamps

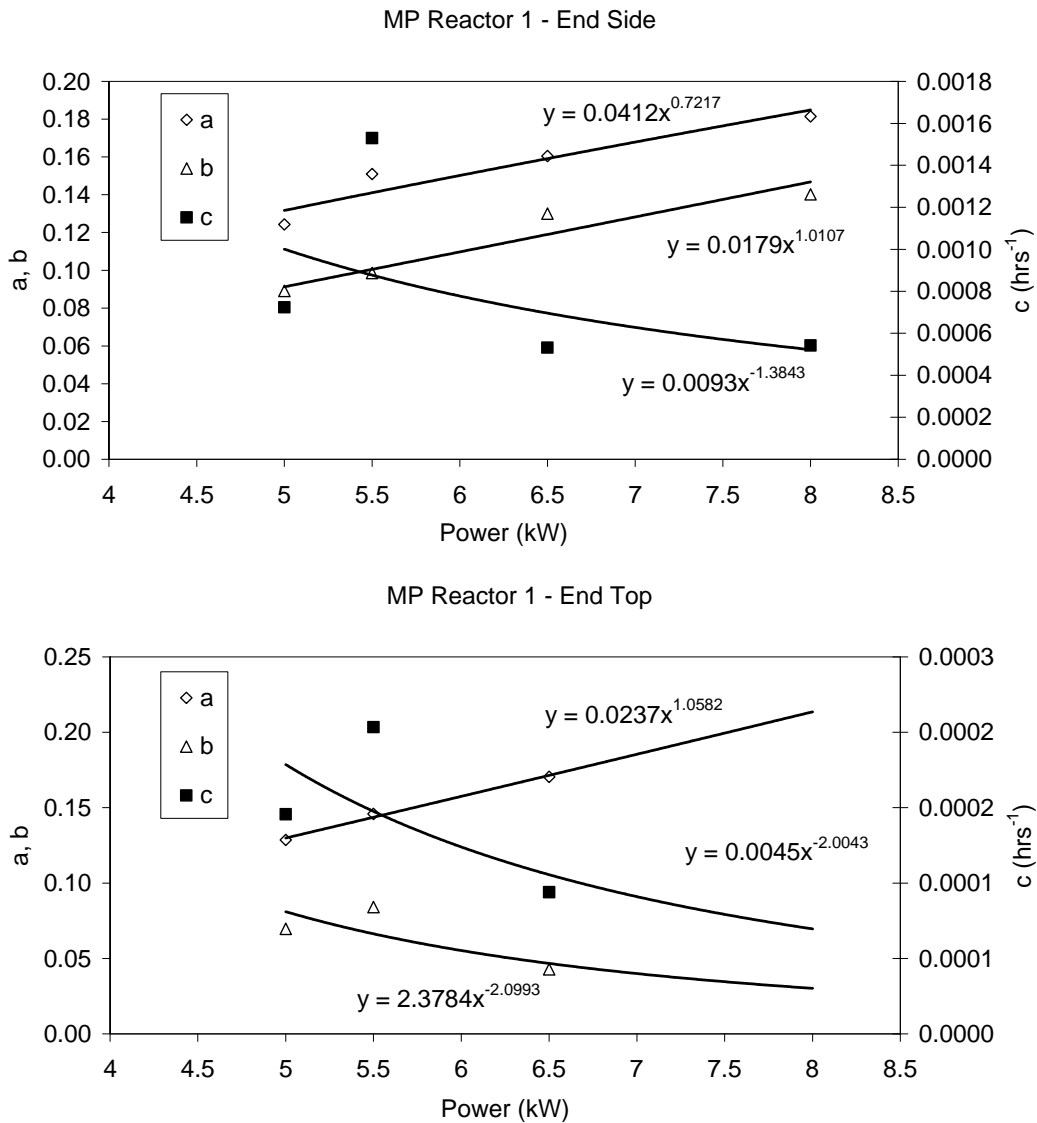


Figure 8.12 (Continued) Coefficients a, b, and c of Equation 8.1 plotted as a function of ballast power for the UV reactor equipped with four 8.0 kW MP lamps

Equation 8.2 was fitted to the lamp aging data using non-linear least-squares regression. Table 8.3 presents the fit coefficients. The model predicts a faster lamp-aging rate with lower lamp power. The lamp-aging rate also depended on the lamp location, with faster rates at the lamp ends compared to the center.

Figure 8.13 compares the UV irradiance predicted using the model to the measured UV irradiance. The R-squared is 0.95 with the middle-side and quartile-side positions and 0.91 and 0.93 with the end-side and end-top positions, respectively. The standard deviation of the residuals is 0.0079, 0.0070, 0.0074, and 0.0056 W/m² with the middle-side, quartile-side positions, end-side and end-top positions, respectively. Overall, the models predict the UV

irradiance over the tested range within 9 percent, a value comparable to the 10 percent measurement uncertainty of the UV irradiance measurement system.

Table 8.3
Coefficients of Equation 8.2 fitted to the lamp aging data for the
UV reactor equipped with four 8.0 kW MP lamps

Coefficient	Position			
	Middle side	Quartile side	End side	End top
a	0.020932	0.0243	0.021632	2.007558
b	0.986533	1.0029	0.913012	-2.81594
c	0.02278	0.0396	0.077712	0.023385
d	1.140259	0.8521	0.391017	1.06174
e	1.24E-05	0.0161	0.695996	4.25E-05
f	1.137082	-1.7152	-3.67115	0.273256

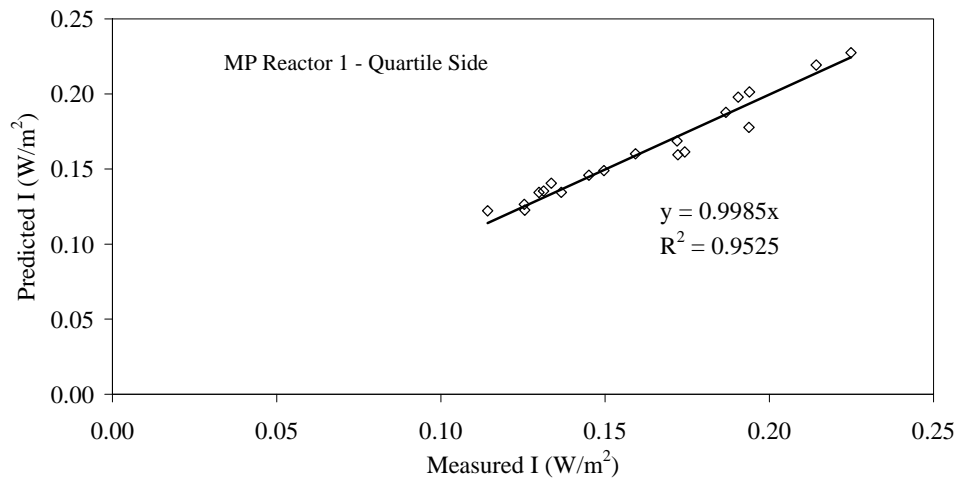
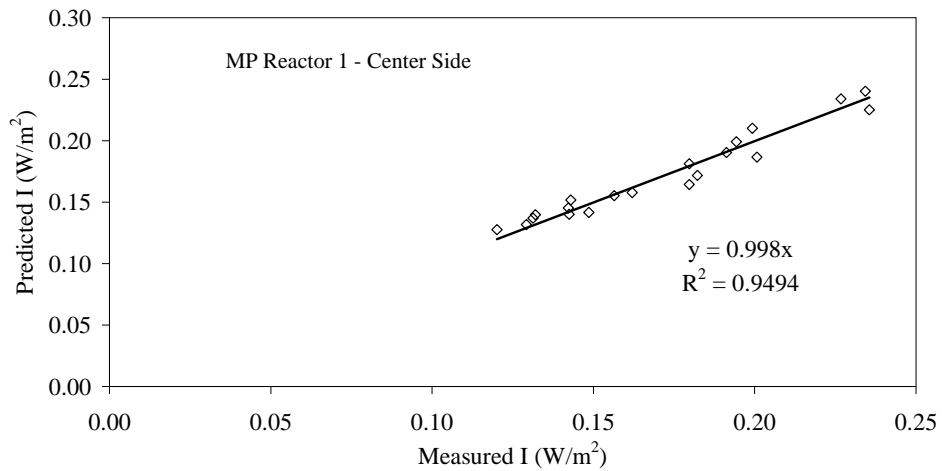


Figure 8.13 Comparison of UV irradiance predicted by Equation 8.2 to measured data

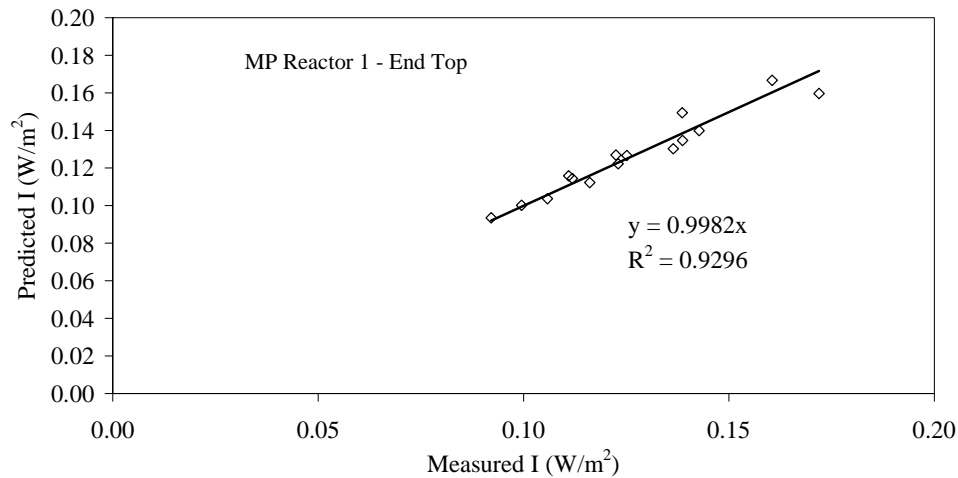
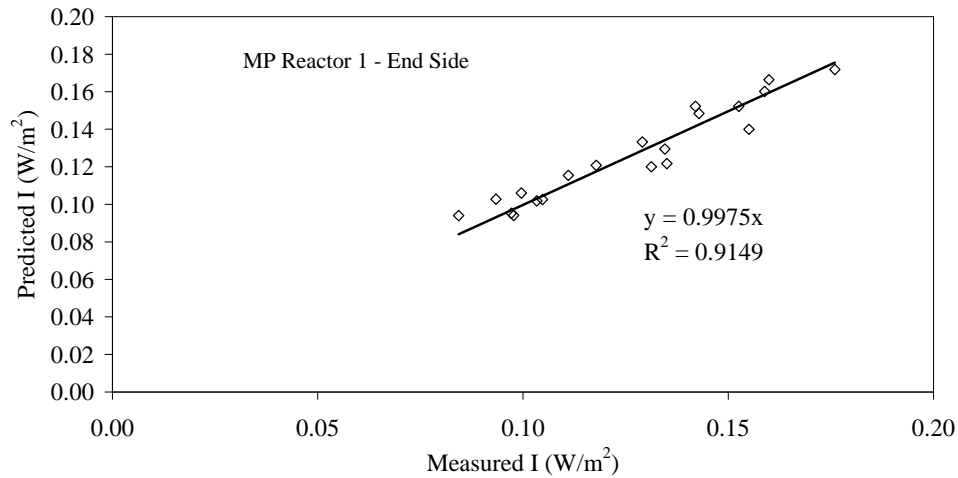


Figure 8.13 (Continued) Comparison of UV intensity predicted by Equation 8.2 to measured data

6-kW Medium Pressure lamps

Figure 8.14 presents UV irradiance as a function of lamp operating hours for the UV reactor equipped with six 6-kW MP lamps. The six lamps were operated at the following power settings both for the long-term aging and for the measurements of UV irradiance:

- Lamp 1 - 6.0 kW
- Lamp 2 - 6.0 kW
- Lamp 3 - 5.5 kW
- Lamp 4 - 5.0 kW
- Lamp 5 - 4.0 kW
- Lamp 6 - 3.5 kW

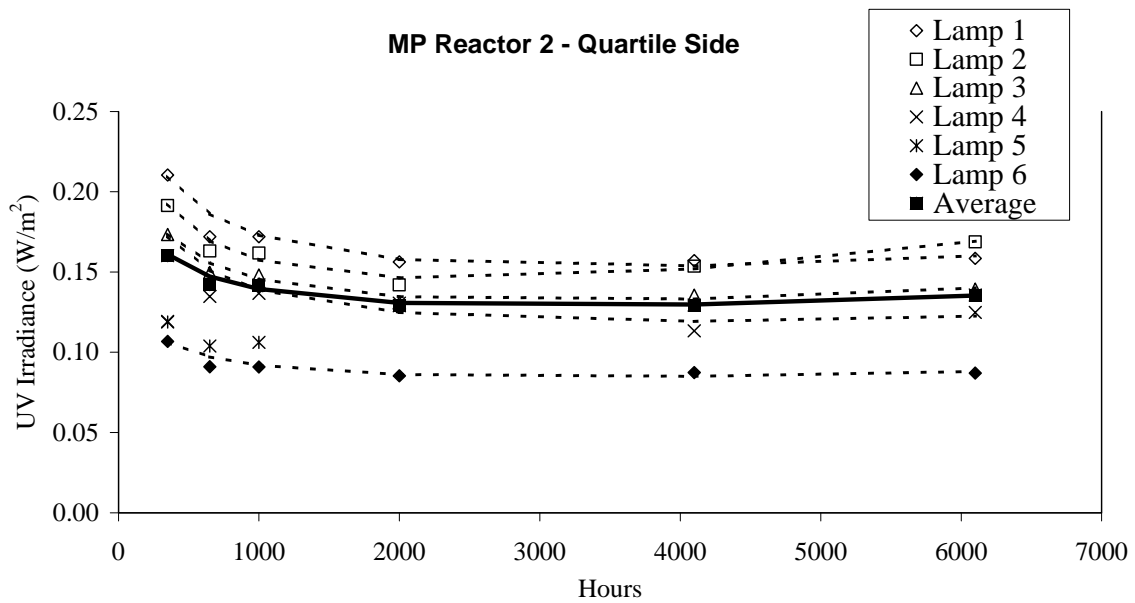
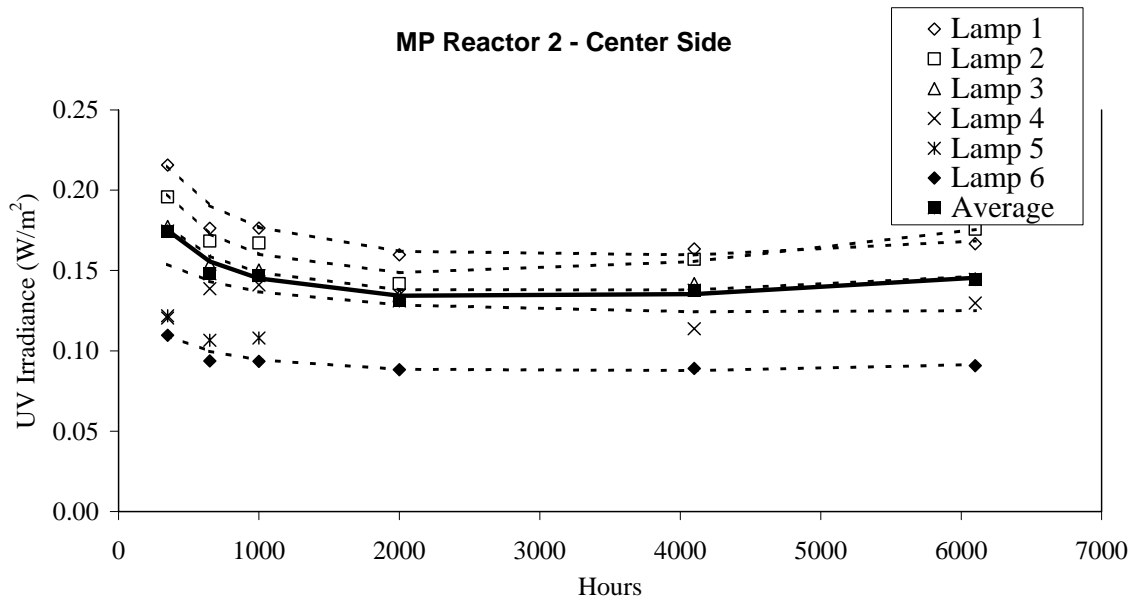


Figure 8.14 Lamp aging data for the UV reactor equipped with six 6.0-kW MP lamps - Lamps 1, 2, 3, 4, 5 and 6 were operated at 6.0, 6.0, 5.5, 5.0, 4.0, and 3.5 kW, respectively; Average excludes lamp 5

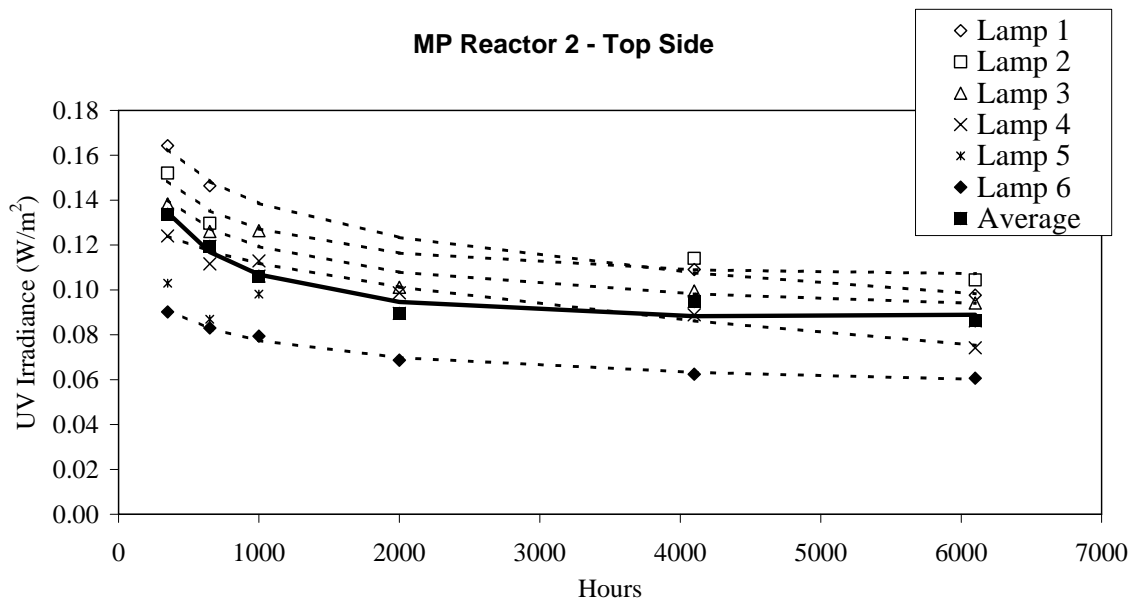
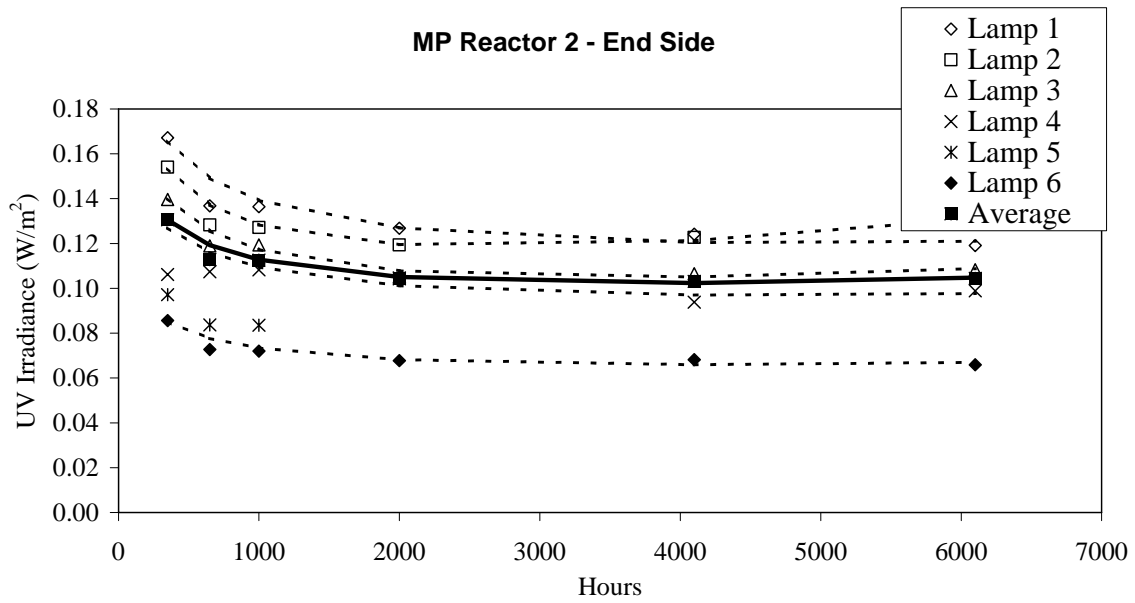


Figure 8.14 (Continued) Lamp aging data for the UV reactor equipped with six 6.0-kW MP lamps - Lamps 1, 2, 3, 4, 5 and 6 were operated at 6.0, 6.0, 5.5, 5.0, 4.0, and 3.5 kW, respectively; Average excludes lamp 5

Figure 8.14 also presents the average UV irradiance measured with five of the six lamps as a function of time. Lamp 5 was not included in the calculation because the lamp aging dataset for lamp 5 ended after 1,000 hrs. The data shows a reduction in UV irradiance as a function of time during the first 2,000 hours followed by an increase. The relation was best fit using the Hoerl function:

$$I = a \times b^t \times t^{-c} \quad (8.3)$$

where I is the UV irradiance, t is time, and a, b, and c are model coefficients. Table 8.4 presents the model coefficients obtained when the data was fitted to Equation 8.3 using non-linear regression. Like the 8-kW lamp data, the data at 350 hours was biased low and so was not used when fitting Equation 8.3 to the dataset.

Table 8.4
Coefficients for Equation 8.3 fitted to the lamp aging
data for the UV reactor equipped with six 6-kW MP lamps

Middle side position						
Coefficient	Lamp 1	Lamp 2	Lamp 3	Lamp 4	Lamp 6	Average
a	0.8144	0.9275	0.5999	0.3266	0.2955	0.6518
b	1.000073	1.000114	1.000072	1.000029	1.000055	1.000082
c	0.2315	0.2708	0.2122	0.1302	0.1732	0.2294

Quartile side position						
Coefficient	Lamp 1	Lamp 2	Lamp 3	Lamp 4	Lamp 6	Average
a	0.7630	0.8350	0.5840	0.7017	0.2808	0.4316
b	1.000064	1.000105	1.000067	1.000062	1.000052	1.000055
c	0.2242	0.2567	0.2108	0.2434	0.1691	0.1716

End side position						
Coefficient	Lamp 1	Lamp 2	Lamp 3	Lamp 4	Lamp 6	Average
a	0.5022	0.5494	0.4579	0.3294	0.2202	0.3406
b	1.000040	1.000083	1.000058	1.000036	1.000041	1.000045
c	0.1915	0.2226	0.2056	0.1648	0.1650	0.1665

End top position						
Coefficient	Lamp 1	Lamp 2	Lamp 3	Lamp 4	Lamp 6	Average
a	0.3803	0.3839	0.3544	0.1845	0.2289	0.5769
b	0.999984	1.000025	1.00001	0.999945	1.000006	1.000053
c	0.1438	0.1635	0.1589	0.06458	0.1579	0.2519

The Hoerl function involves the product of two functional relationships. The first expression is the power function term, t^c , where coefficient “c” is a positive number. The power function component accounts for the reduction in UV irradiance in the lamp aging data. The rate of reduction in UV irradiance increases as the coefficient “c” increases. The second expression is the term b^t , where coefficient “b” has a value slightly greater than one. The coefficient b accounts for the increase in UV irradiance that occurs after 2,000 hrs. As the coefficient “b” increases, the relation described by the Hoerl function has a greater tendency to curve upwards.

Figure 8.15 presents coefficients “a” and “b” as a function of ballast power. Unlike the lamp aging data on the 8-kW lamps described in the previous section, no significant relationships were identified between the fit coefficients and ballast power. Hence, the average relationship was used to describe lamp aging with the 6-kW MP lamps in subsequent sections of this report.

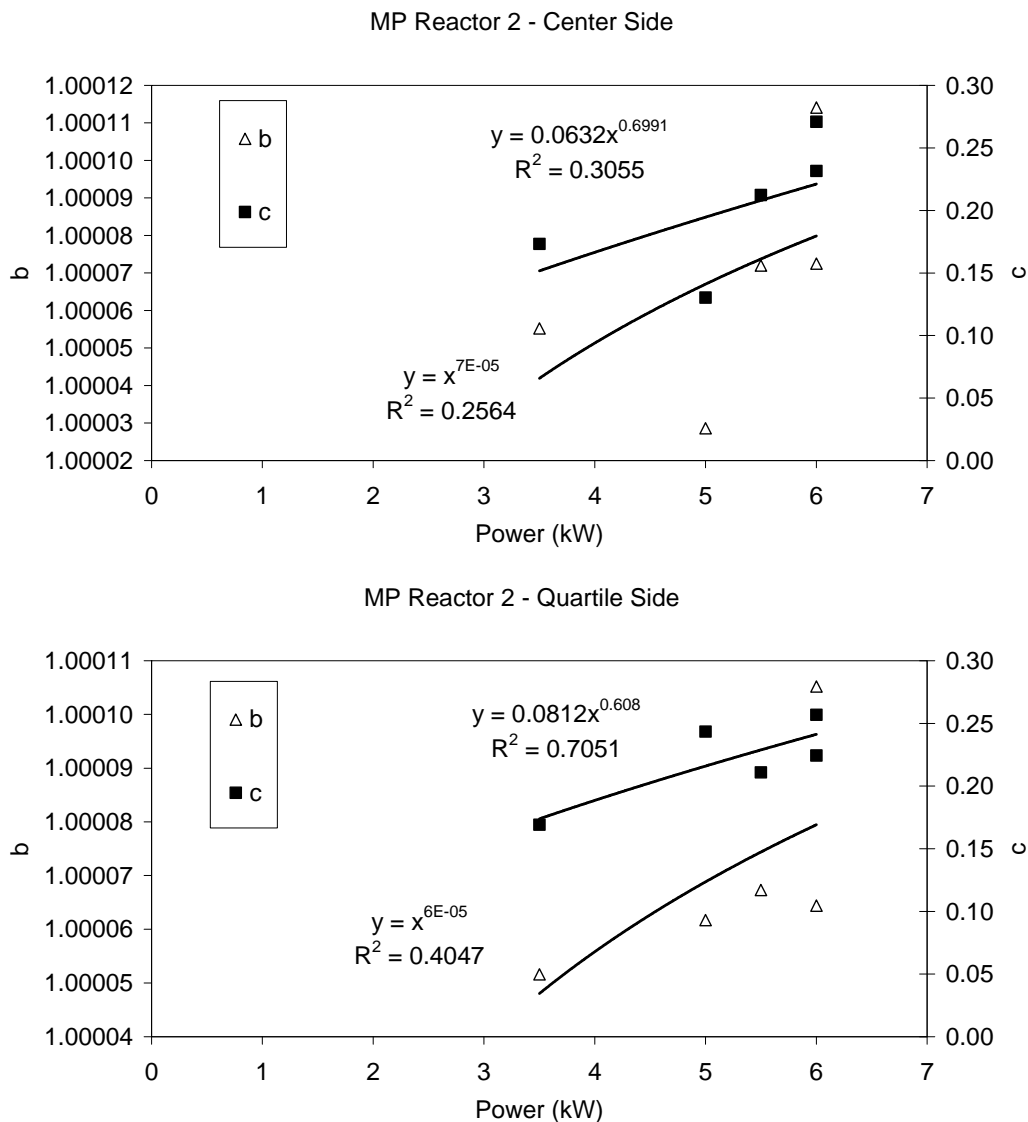


Figure 8.15 Coefficients b and c of Equation 8.3 as a function of ballast power for the UV reactor equipped with six 6.0-kW MP lamps

The spectral UV output of the lamp was examined to understand why the UV output initially went down for the first 2000 hours and then increased. [Figure 8.16](#) shows the spectral output of lamp 2 normalized for equal UV output from 200 to 350 nm. In the extreme short wavelength region (200 to 230 nm), the UV output decreases from 350 to 2000 hours and increases from 4100 to 6100 hours. While decreasing UV transmittance of the lamp envelope may explain the decrease in UV output during the first 2,000 hours, it does not explain the increase in UV output from 4100 to 6100 hours. The spectral UV output measured at 6100 hours also shows new spectral lines at 272, 300, 305, and 344 nm. This observation suggests the chemistry of the gas within the lamp changed over time.

[Figure 8.17](#) shows the spectral output in the region around the 254 Hg line. At high Hg vapor pressure, the 254 line shows up as an absorption line due to a phenomenon called imprisonment. As the Hg pressure increases, the mean free path length that a 254 nm photon travels before being absorbed by a mercury atom becomes shorter. As a result, the 254 photons are less likely to make it out of the arc and are more likely to be absorbed by a Hg atom and re-emitted at another wavelength. Since high pressure causes a broadening of the emission lines, an absorbed 254 photon is likely to be re-emitted at a slightly longer wavelength. Therefore, lower output at 254 compared to output at adjacent wavelengths indicates higher Hg operating pressure.

Comparing the 254 and 256 nm peaks in [Figure 8.17](#) shows that the Hg operating pressure followed the measured UV output over time. Hg pressure was highest at 350 hours, a minimum at 2000 hours, and then increased thereafter. The analysis suggests that the shape of the lamp-aging curve is a true reflection of the output of the lamp and not an artifact of the measurement system.

What would cause the Hg pressure to first decrease then increase? There is no certain answer available from this limited data, but certain scenarios are possible. One scenario is that initially Hg is removed from the arc by bonding with electrode contaminants causing the lamp-end blackening. Then, for some reason, the lamp envelope at the ends of the lamp becomes hotter (maybe due to absorbed radiation due to end blackening) which dissociates Hg from the molecular bonds that trap it, thereby increasing the Hg pressure in the lamp. The lamp ends must get hotter near end of life as evidenced by the observed bulging and devitrification of the quartz.

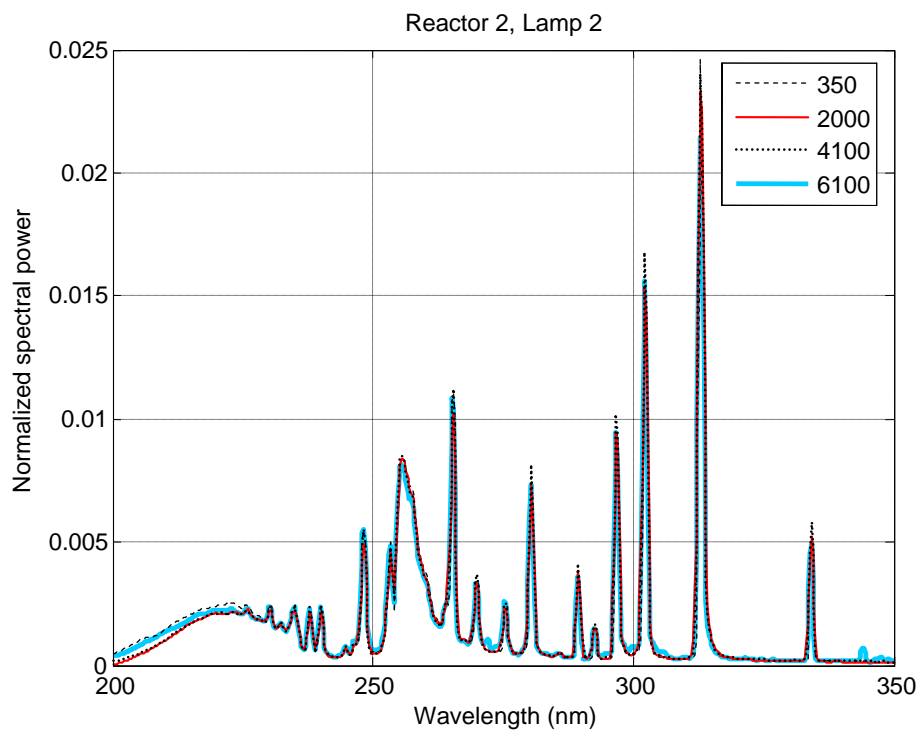


Figure 8.16 Spectral irradiance for medium pressure lamp #2, reactor #2 recorded at different operating times over the course of the study

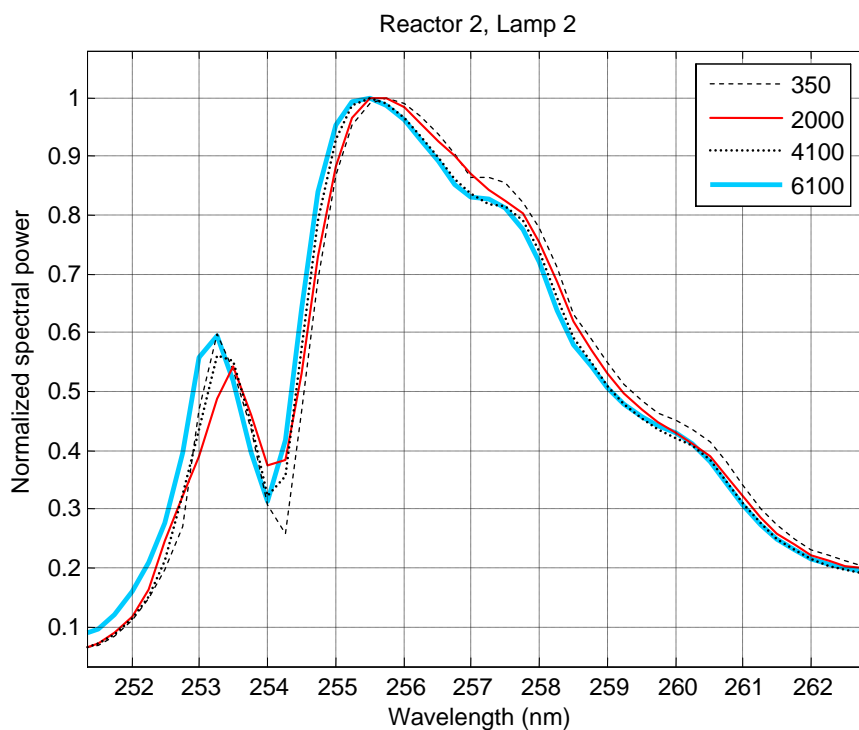


Figure 8.17 Expanded wavelength axis (zoom) of Figure 8.16 in the wavelength vicinity of the principle Hg emission line at 254 nm

Amalgam LPHO Lamps

Figure 8.18 presents UV irradiance as a function of lamp operating hours for the UV reactor equipped with eight 300-W amalgam LPHO lamps. Lamps 1 through 4 were operated at the 100 percent power setting both for the long-term aging and for the measurements of UV irradiance. Lamps 5 through 8 were operated at 80 percent power setting. Figure 8.18 also presents the average UV irradiance measured with the eight lamps as a function of time.

With the exception of some of data at 4000 hours, the data shows a reduction in UV irradiance as a function of time that can be modeled using a power function:

$$I = a \times t^{-b} \quad (8.4)$$

where I is the UV irradiance, t is time, and a and b are model coefficients. Table 8.5 presents the model coefficients obtained when the data was fitted to Equation 8.4 using non-linear regression. The data at 4000 hours was biased high and so was not used when fitting Equation 8.4 to the dataset.

The fit coefficients indicate the lamp-aging rate is greater with lamps operating at 100 percent power compared to the lamps operating at 80 percent power. However, a t-test comparing the b-coefficient of lamps 1 to 4 to lamps 5 to 8 shows this observation is only statistically significant (p < 0.05) with the quartile-side but not statistically significant with the center-side, end-side, and end-top positions.

Table 8.5
Empirical coefficients for Equation 8.4 fit to the lamp aging data for the
UV reactor equipped with eight 300-W amalgam LPHO lamps

Position	Center-side		Quartile-side		End-side		End-top	
Coefficient	a	b	a	b	a	b	a	b
Lamp 1	0.01059	0.05517	0.01316	0.09296	0.01047	0.09920	0.02398	0.2234
Lamp 2	0.01173	0.06419	0.01645	0.1220	0.01264	0.1236	0.01029	0.09330
Lamp 3	0.01072	0.05350	0.01086	0.05703	0.01032	0.08391	0.01462	0.1392
Lamp 4	0.01218	0.07163	0.01292	0.08469	0.01071	0.09694	0.03341	0.2700
Lamp 5	0.01038	0.05919	0.01111	0.06568	0.009240	0.08039	0.02014	0.2103
Lamp 6	0.008826	0.04562	0.008433	0.03757	0.008304	0.07915	0.009219	0.08928
Lamp 7	0.009599	0.05742	0.009040	0.04667	0.007764	0.06200	0.01601	0.1706
Lamp 8	0.009316	0.05109	0.009251	0.04977	0.009159	0.09043	0.01193	0.1238
Avg. 1 - 4	0.01129	0.06116	0.01316	0.08867	0.01097	0.1004	0.01861	0.1797
Avg. 5 - 8	0.009524	0.05342	0.009435	0.05023	0.008502	0.07618	0.01358	0.1468
Avg. 1 - 8	0.01040	0.05747	0.01117	0.06968	0.009695	0.08863	0.01595	0.1635
T-Test*	-	0.2		0.04		0.07		0.6

* T-test compares lamps 1 - 4 to lamps 5 - 8 using two-tailed distribution and assumes equal variance with samples.

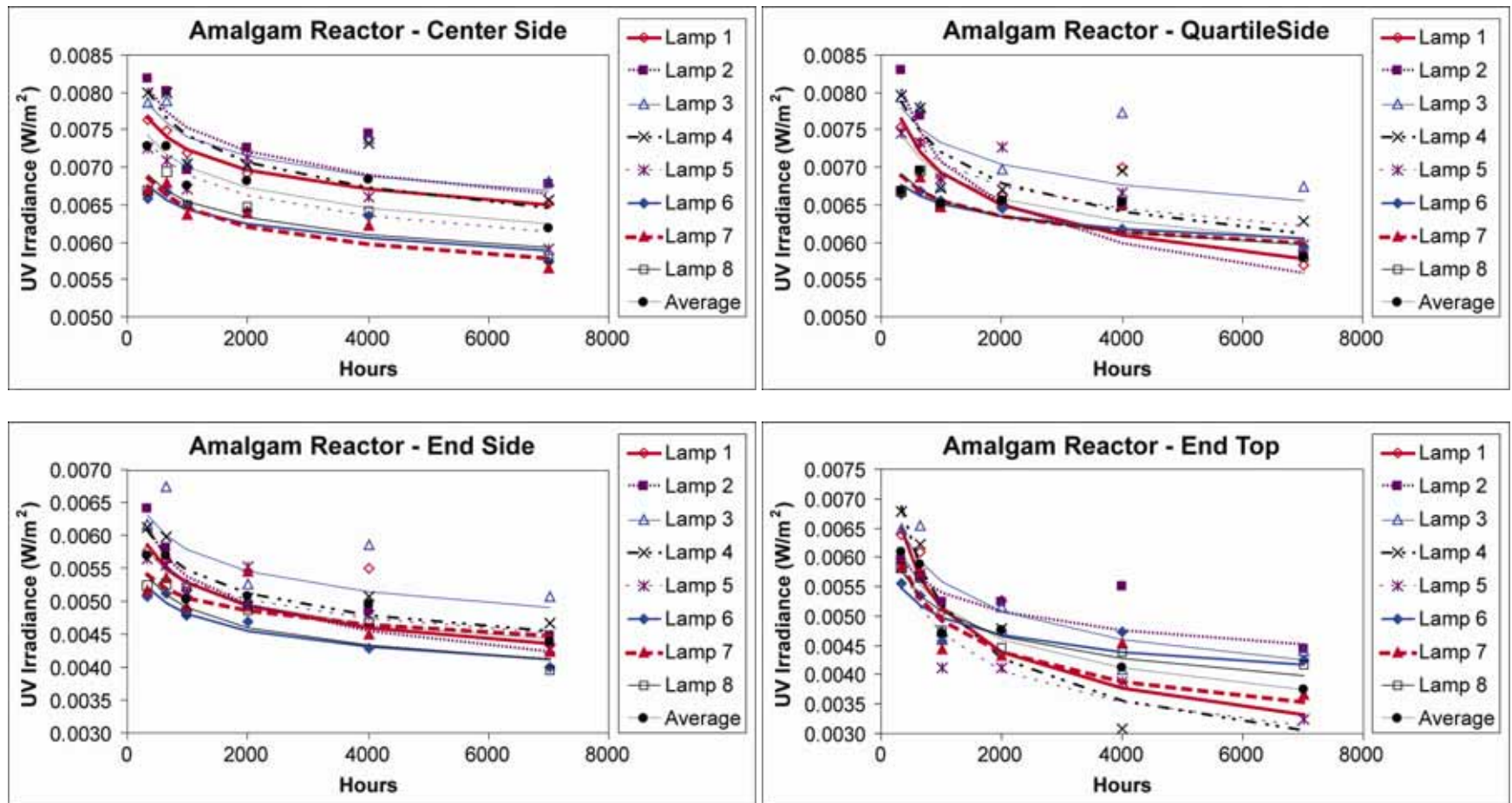


Figure 8.18 Lamp aging data for the UV reactor equipped with eight 300-W amalgam LPHO lamps. Lamps 1 through 4 operated at 100% power; Lamps 5 through 8 operated at 80% power

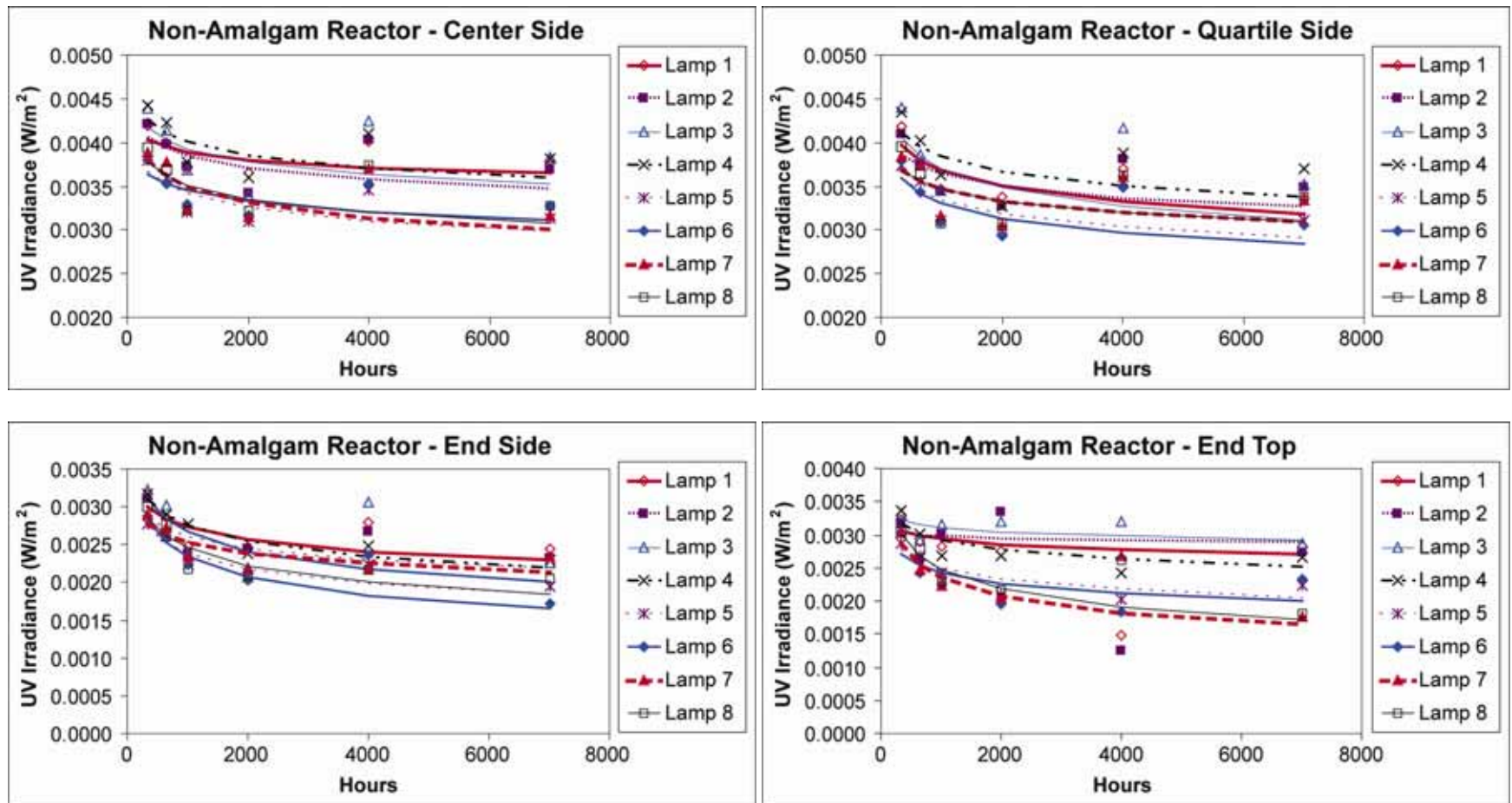


Figure 8.19 Lamp aging data for the UV reactor equipped with eight 130-W non-amalgam LPHO amps. Lamps 1 through 4 operated at 100% power; Lamps 5 through 8 operated at 80% power

Non-Amalgam LPHO Lamps

Figure 8.19 presents UV irradiance as a function of lamp operating hours for the UV reactor equipped with eight 130-W LPHO lamps. Lamps 1 through 4 were operated at the 100 percent power setting both for the long-term aging and for the measurements of UV irradiance. Lamps 5 through 8 were operated at the 80 percent power setting. Figure 8.19 also presents the average UV irradiance measured with the eight lamps as a function of time.

With the exception of some of the values measured at 4,000 hours, the data shows a reduction in UV irradiance as a function of time that can be modeled using a power function:

$$I = a \times t^{-b} \quad (8.5)$$

where I is the UV irradiance, t is time, and a and b are model coefficients. The data at 4000 hours was biased high and so was not used when fitting Equation 8.5 to the dataset.

Table 8.6 presents the model coefficients obtained when the data was fitted to Equation 8.5 using non-linear regression. A t-test comparing the b-coefficient of lamps 1 to 4 to Lamps 5 to 8 indicates the lamp-aging rate is greater ($p < 0.05$) with lamps operating at 80 percent power compared to the lamps operating at 100 percent power for the end-top position only. The t-test shows no statistical difference with the other locations.

Table 8.6
Empirical coefficients for Equation 8.5 fit to the lamp aging data for the
UV reactor equipped with eight 130-W non-amalgam LPHO high-output lamps

Position	Center-side		Quartile-side		End-side		End-top	
Coefficient	a	b	a	b	a	b	a	b
Lamp 1	0.004931	0.03415	0.006130	0.07406	0.005064	0.08960	0.003901	0.04128
Lamp 2	0.005529	0.05264	0.005365	0.05629	0.004825	0.0890	0.003302	0.01482
Lamp 3	0.005775	0.05571	0.006793	0.08825	0.007188	0.1437	0.003857	0.03111
Lamp 4	0.005918	0.05633	0.006007	0.06506	0.006144	0.1159	0.004967	0.07684
Lamp 5	0.005534	0.06990	0.005411	0.06983	0.005977	0.1333	0.005035	0.1010
Lamp 6	0.004958	0.05263	0.005660	0.07805	0.008178	0.1807	0.004833	0.09963
Lamp 7	0.005955	0.07720	0.005170	0.05820	0.004614	0.0866	0.008438	0.1847
Lamp 8	0.005574	0.06677	0.005162	0.05787	0.006714	0.1454	0.008947	0.1858
Avg. 1 - 4	0.005525	0.04968	0.006049	0.07077	0.005732	0.1094	0.003941	0.04007
Avg. 5 - 8	0.005495	0.06663	0.005342	0.06582	0.0062	0.1355	0.006531	0.14241
Avg. 1 - 8	0.005500	0.05762	0.005695	0.06840	0.005941	0.1218	0.004873	0.08434
T-Test*	-	0.06		0.6		0.3		0.01

* T-test compares lamps 1 - 4 to lamps 5 - 8 using two-tailed distribution and assumes equal variance with samples.

Sources of Error with Measurements of Lamp Output

It was not known whether the random error and bias in the lamp output measurements were due to real fluctuations in lamp output or to problems with measurement reproducibility. The data collected at 350 hours with the two MP reactors was biased low while the data collected at 4,000 hours with the LPHO reactors was biased high. These results suggested either a systematic error or the impact of a confounding factor.

Calibration inaccuracies of the spectrometer system were investigated, but nothing was found that could produce errors of more than a few percent. The instrument was calibrated every day that measurements were taken. Another source of error with the LPHO lamp measurements could be in the measurement procedure. Relying on the peaking output of the lamp might not have fully accounted for the temperature differences encountered at the different measurement times. It was thought that even though the lamps reached a peak in their UV output, light emission might not be uniform across the lamp, so the measured peak output might not have represented a repeatable operating condition. In addition, changes in the apparatus, such as fading and cracking of the black paint in the measurement chamber, could have influenced measurements, although these types of changes would have shown more systematic changes, but this did not occur.

Sleeve Transmittance Measurements

Quartz sleeves were taken from each reactor at the end of the lamp aging study for UV transmittance measurements. UV transmittance was measured to determine the effect of the fouling on UV transmittance and whether cleaning of the sleeves could recover the transmittance losses. The UV transmittance of unused quartz sleeves was measured for comparison.

The sleeves exhibited a wide range of visible fouling, from slight discoloration and haziness to being completely diffuse and rust-brown in color. Samples approximately 80 x 25 cm in size were cut from the sleeves using a diamond rotary saw. Samples were taken from positions equally spaced along the length of the sleeve.

Total diffuse spectral transmittance over the wavelength range from 240 to 300 nm was measured for each sample. Samples were placed against a 5 mm diameter flat aperture of a 20 cm-diameter integrating sphere. The sphere aperture was illuminated by a 30-watt deuterium lamp located approximately 6 cm away. Measurements of the source were recorded with no sample in place. Sample measurements were taken by placing the sample up against the sphere aperture. Because the samples were curved, the entire sample was not flat against the aperture. This caused a small amount of the diffusely transmitted UV flux to not be collected by the sphere. This amount was judged to be less than a few percent for a diffuse material. Spectral transmittance was calculated as the sample measurement divided by the source measurement (no sample in the UV beam) at each wavelength increment. The results are shown in [Figures 8.20](#) and [8.21](#).

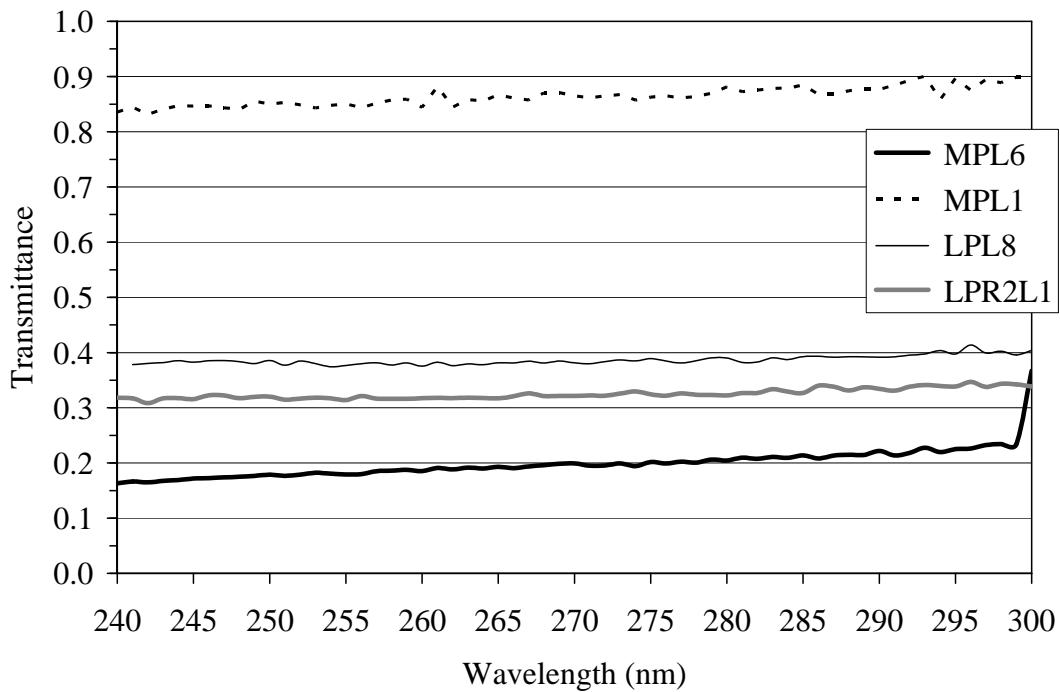


Figure 8.20 UV transmittance of quartz sleeve samples taken from the medium pressure reactors (MP) and the LPHO reactors (LP). The transmittance curves shown are the average of three samples

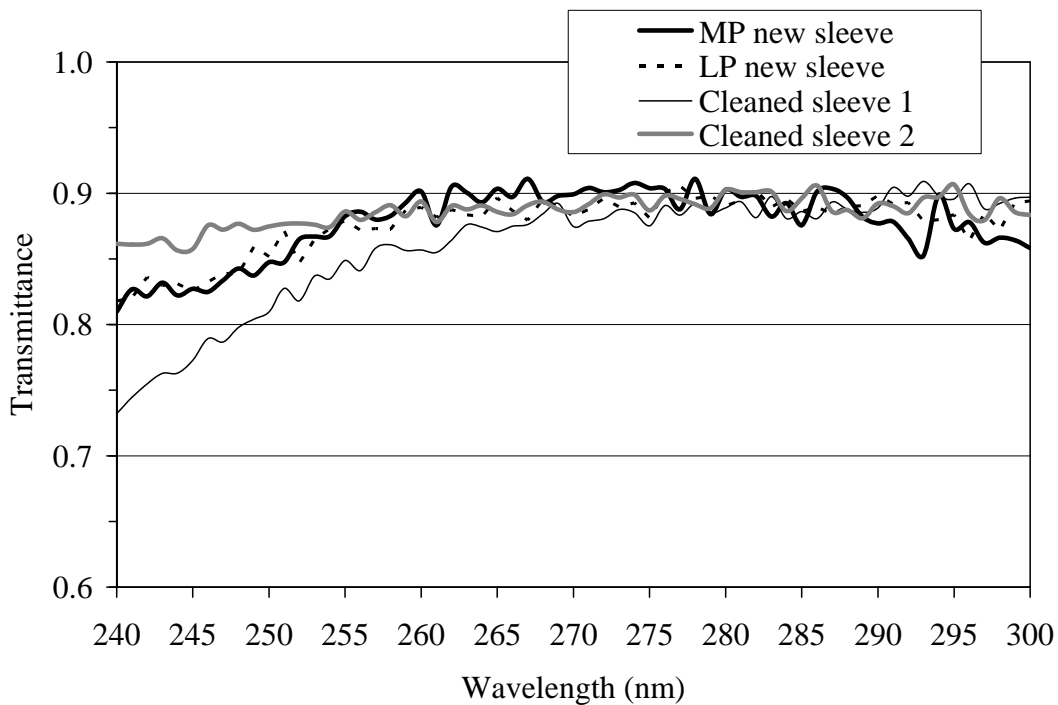


Figure 8.21 Transmittance of new quartz sleeve samples taken from replacement sleeves that were never used, and the transmittance of the two sleeve samples after cleaning with mild phosphoric acid bathroom cleaner

The following conclusions can be drawn from these data:

- Sleeve transmittance varied a lot (from less than 20 percent to over 85 percent) for the different reactors and also along the length of the sleeves.
- The UV transmittance appears to correlate well with the visible look of the sleeves, that is, the ones that look fouled do in fact have a low UV transmittance. Therefore the loss in UV transmittance is probably due to the foulant.
- When the outsides of the sleeves are cleaned with mild acid (bathroom cleaner with phosphoric acid in this case), the transmittance loss is recoverable as shown in [Figure 8.21](#).

UV Sensor Port Irradiance Measurements

While the LPHO reactors were equipped with UV sensor ports, the manufacturer did not provide UV sensors. Instead, UV irradiance was measured at these ports three times over the duration of the life tests using the double monochromator system with the integrating sphere and fiber-optic input. Data is provided in [Table 8.7](#).

Even though there are only a few measurements, it is clear that the UV irradiance at the sensor port locations decreased significantly over time, most likely due to fouling of the lamp sleeves and the sensor port window. Because the lowest measured lamp sleeve transmittance was approximately 18 percent, sensor port window fouling must have been significant.

As indicated by the two measurements taken at 650 hours with reactor 2, positioning of the fiber optic in front of the port windows caused some variability in the measurements. Unlike the UV sensors that are designed to be inserted into the port and mechanically fastened, the UV sensor used for these measurements had to remain outside the port where the irradiance is much more sensitive to positioning.

The MP reactors were equipped with UV sensors that also indicated significant fouling over the duration of the life tests.

Table 8.7
UV irradiance measured at the UV sensor ports of the LPHO reactors.

Hours of operation	UV irradiance	
	W/m ²	
	Reactor 1 (non-amalgam)	Reactor 2 (amalgam)
350	74.9	231.9
650	71.1	46.5
650 (trial 2)	--	30.3
7000	30.1	8.4

LPHO Ballast Starting Measurements

Electrical measurements were performed on a ballast supplied by the LPHO system manufacturer. The ballast evaluated was similar in appearance to the ballasts used on the LPHO reactors. However, instead of using an electrical signal to control the lamp power setting, the ballast was equipped with a knob that let the user adjust lamp current from 1.8 to 2.2 A. A center position on the knob indicated the appropriate setting for starting the lamp. Since labels on the ballast warned against starting the lamp with other settings, starting the lamp with other settings was not explored.

Figure 8.22 shows oscilloscope traces of the lamp current and electrode heating voltage when operating a UV lamp. The lamp current is approximately 1.56 A rms and the electrode heating voltage is 4.82 V rms. This value of heating voltage is similar to that found on other low pressure Hg discharge lamps, such as those used for lighting applications. Apparently, the ballast applies continuous electrode heating during operation of the lamp.

Figure 8.23 shows oscilloscope traces of the same quantities during the starting of the lamp. The time increment is 10 ms per division for a total trace length of 100 ms. Power is applied at the first 10-ms division marker from the left. The important feature to note is that both lamp current and electrode heating voltage are present at the same time.

This starting profile does not match any of the three major types of starting methods used by ballasts designed for commercial lighting: pre-heat/rapid start, instant start, or programmed start. Rather it is a combination of rapid start and instant start because the high voltage used to initiate the discharge is applied at the same time as the electrode heating voltage. Under these conditions, the electrode heating does little to prevent electrode damage during startup. Electrode damage due to sputtering occurs during the initial 10 to 30 ms when the lamp current is relatively high and the lamp electrodes have not reached their electron emissive temperature.

If UV lamps use electrode designs that are similar to those used with fluorescent lamps, then starting the lamp with this type of ballast has a considerable impact on lamp life. Operating a lamp on a three-hour per start cycle using instant start ballasts reduces lamp life by roughly one half compared to continuous operation. To maximize lamp life, a programmed-start ballast type should be used. With a programmed-start, the lamp electrodes are heated for approximately one second *before* the lamp voltage is applied, and then only a moderate lamp voltage is necessary (~300 volts) to start the lamps. Programmed-start ballasts allow lamps to be started frequently with no measurable impact on lamp life. They have been available for several years in the lighting industry and are recommended for use with UV lamps.

Power Measurements

The input power of each ballast and the lamp power consumption was measured at the end of the life test using a Xitron model 2503AH three-channel power meter. The medium pressure lamp ballasts had three-phase, 480 V power input, while the LPHO ballast had single-phase 120 V power input. The lamp input power was measured when the lamps were fully stabilized. The results are reported in Tables 8.8, 8.9, and 8.10. Results were used to calculate ballast efficiency, which ranged from 81 to 88 percent with the MP ballasts and 88 to 92 percent with the LPHO ballasts.

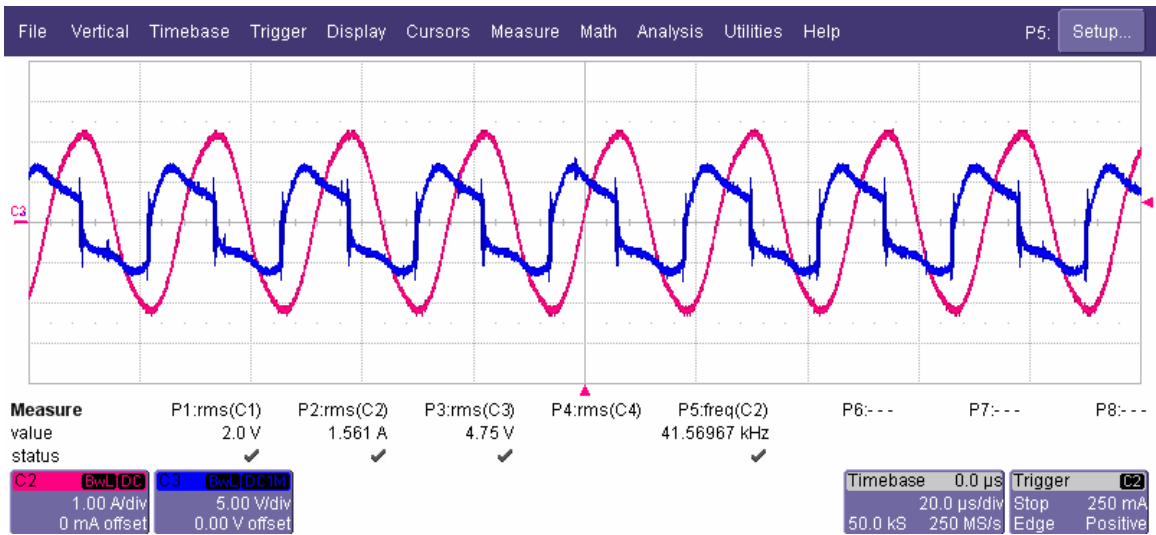


Figure 8.22 Oscilloscope traces of lamp current (C2, pink trace) and electrode heating voltage (C3, blue trace) for a stable operating lamp

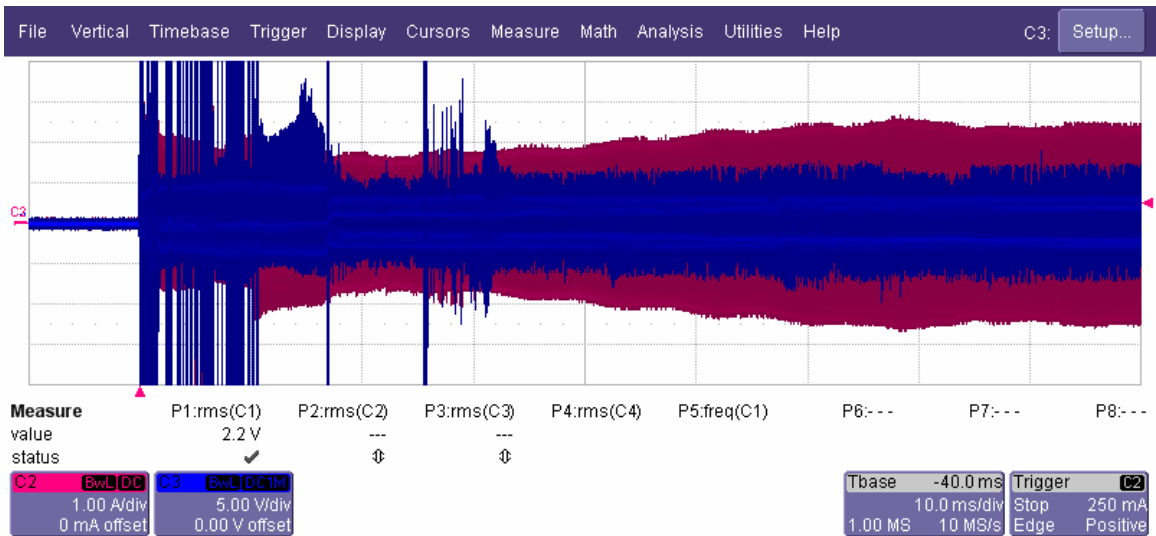


Figure 8.23 Oscilloscope traces of lamp current (C2, pink trace) and electrode heating voltage (C3, blue trace) during the starting of the lamp

Table 8.8
Electrical power measurements for medium pressure reactors

Lamp	Lamp power	Phase voltages	Phase currents	Power per phase	Ballast input power	Ballast efficiency
	W	V	A	W	W	
Medium pressure, reactor 1						
1	8000	480.9 479.1 478.4	10.98 10.932 10.96	3049 3024 3027	9100	87.9%
2	5010	479.2 478.4 477.9 478	7.171 7.118 7.148 7.815	1984 1966 1972 2157	5922	84.6%
3	5510	476.7 476.6 474.1	7.786 7.796 9.115	2143 2145 2495	6445	85.5%
4	6510	472.5 472.5	9.072 9.133	2475 2491	7461	87.3%
Medium pressure, reactor 2						
1	5510	477.2 479.2 481.6	8.002 8.042 8.044	2205 2225 2237	6666	82.7%
2	6000	478.2 480.3 482.8	8.598 8.634 8.635	2374 2394 2407	7175	83.6%
3	5010	480 481 484	7.388 7.436 7.434	2047 2065 2077	6190	80.9%
5	3500	479.5 480.8 483.3	5.532 5.569 5.575	1531 1546 1556	4633	75.5%
6	6000	478.9 479.5 482.6	8.61 8.651 8.643	2381 2395 2408	7184	83.5%

Table 8.9
Electrical power measurements for LPHO reactor 1

Lamp	Position	Voltage	Current	Power	Total power	Ballast eff.
		V	A	W	W	
Low pressure, reactor 1						
1	Center	171.4	0.7476	127.7	128.7	90.8%
	Left	172.5	0.7476	128.6		
	Left-end	173.2	0.7470	129.2		
	Top-right	173.7	0.7472	129.3		
	Ballast	204.7	0.6963	141.7	141.7	
2	Center	175.3	0.7512	131.2	131.4	90.8%
	Left	175.5	0.7513	131.4		
	Left-end	175.6	0.7512	131.3		
	Top-right	175.6	0.7513	131.5		
	Ballast	201.0	0.7239	144.7	144.7	
3	Center	175.4	0.7455	130.3	130.9	90.8%
	Left	176.4	0.7446	131.1		
	Left-end	176.5	0.7448	131.1		
	Top-right	176.6	0.7447	131.0		
	Ballast	204.6	0.7086	144.2	144.2	
4	Center	176.7	0.7657	134.9	135.5	92.8%
	Left	178.0	0.7656	135.8		
	Left-end	178.6	0.7659	136.4		
	Top-right	176.6	0.7656	134.8		
	Ballast	205.4	0.7150	146.0	146.0	
5	Center	188.8	0.5151	97.3	98.2	88.2%
	Left	191.1	0.5157	98.2		
	Left-end	192.6	0.5159	99.2		
	Top-right	190.8	0.5158	98.1		
	Ballast	204.3	0.5517	111.4	111.4	
6	Center	191.4	0.5294	101.1	101.4	91.2%
	Left	192.6	0.5293	101.7		
	Left-end	192.1	0.5292	101.5		
	Top-right	191.9	0.5291	101.4		
	Ballast	202.7	0.5554	111.2	111.2	
7	Center	182.8	0.5236	95.6	95.4	90.4%
	Left	184.0	0.5233	96.2		
	Left-end	182.0	0.5235	94.9		
	Top-right	181.5	0.5235	94.9		
	Ballast	202.9	0.5272	105.5	105.5	
8	Center	181.8	0.5200	94.7	94.8	89.2%
	Left	183.4	0.5199	95.1		
	Left-end	182.8	0.0520	94.9		
	Top-right	181.7	0.5203	94.4		
	Ballast	202.9	0.5310	106.3	106.3	

Table 8.10
Electrical power measurements for LPHO reactor 2

Lamp	Position	Voltage V	Current A	Power W	Total power W	Ballast eff.
Low pressure, reactor 2						
1	Center	152.2	1.953	296.6	296.4	90.8%
	Left	152.5	1.952	296.5		
	Left-end	152.0	1.953	296.3		
	Top-right	151.9	1.952	296.0		
	Ballast	203.2	1.610	326.3		
2	Center	150.6	2.086	312.4	315.0	90.9%
	Left	151.0	2.086	314.3		
	Left-end	151.0	2.086	314.7		
	Top-right	152.8	2.805	318.4		
	Ballast	203.1	1.707	346.3		
3	Center	155.3	2.001	309.9	310.6	90.7%
	Left	155.4	2.000	310.1		
	Left-end	156.1	2.000	310.3		
	Top-right	156.7	2.000	311.9		
	Ballast	203.1	1.690	342.5		
4	Center	150.1	2.002	299.6	302.2	91.6%
	Left	152.3	2.000	303.8		
	Left-end	153.2	2.000	304.8		
	Top-right	150.8	2.002	300.4		
	Ballast	203.9	1.620	329.9		
5	Center	164.7	1.479	242.6	243.4	90.7%
	Left	164.8	1.479	243.1		
	Left-end	165.5	1.478	243.9		
	Top-right	165.8	1.476	244.0		
	Ballast	205.6	1.307	268.3		
6	Center	162.6	1.494	242.1	243.6	90.6%
	Left	163.9	1.492	243.7		
	Left-end	164.4	1.492	244.4		
	Top-right	164.2	1.492	244.0		
	Ballast	204.9	1.314	268.9		
7	Center	164.7	1.491	244.6	244.2	91.0%
	Left	164.5	1.490	244.3		
	Left-end	164.4	1.490	244.2		
	Top-right	164.0	1.490	243.6		
	Ballast	204.7	1.312	268.3		
8	Center	162.6	1.479	239.8	239.4	90.8%
	Left	162.1	1.479	239.1		
	Left-end	162.3	1.479	239.3		
	Top-right	162.2	1.479	239.2		
	Ballast	205.2	1.286	263.6		

CONCLUSIONS AND RECOMMENDATIONS

A lamp aging study was conducted on four types of UV lamps – 300-W amalgam LPHO lamps, 130-W non-amalgam LPHO lamps, and 6.5 and 8-kW MP lamps. The following observations were made:

- Lamp aging observed with the 8-kW lamps depended on time and ballast power setting and could be modeled using:

$$I = A \times P^B \times \exp(-E \times P^F \times t) + C \times P^D \times (1 - \exp(-E \times P^F \times t)) \quad (8.6)$$

where I is the measured UV intensity, P is the ballast power setting, t is time, and A through F are model coefficients. Model coefficients depended on the location along the lamp length and about the circumference being modeled. The model predicts a faster lamp-aging rate with lower lamp power. The lamp-aging rate also depended on the lamp location, with faster rates at the lamp ends compared to the center.

- Lamp aging observed with the 6.5-kW lamps could be modeled using:

$$I = a \times b^t \times t^{-c} \quad (8.7)$$

where I is the measured UV intensity, t is time, and a , b and c are model coefficients. Lamp aging depended on time but no dependence on ballast power setting was observed. The lamp-aging rate also depended on the lamp location, with faster rates at the lamp ends compared to the center and at the top end compared to the side end. The lamp aging had an unusual profile as a function of time – the lamp output decreased for the first 3,000 to 4,000 hours and either stabilized or increased for the next 2,000 to 3,000 hours. The increase can be explained by changes in the amount of mercury available within the lamp to form the plasma.

- Lamp aging observed with the amalgam and non-amalgam lamps was modeled using:

$$I = a \times t^{-b} \quad (8.8)$$

where I is the measured UV intensity, t is time, and a and b are model coefficients. The rate of lamp aging was greater with the 300-W amalgam LPHO lamps compared to the 130-W non-amalgam LPHO lamps. The rate of lamp aging tended to be greater at the lamp ends and did not vary significantly with lamp power settings of 80 and 100 percent.

- Because the capital costs of a UV system depend on the lamp-aging factor used to size the UV system, a UV vendor with a lamp-aging factor higher than their competitors will realize a significant competitive advantage. Hence, UV vendors have a strong economic driver to base their lamp aging factors on the location about the lamp that gives the highest lamp-aging factor. Utilities need to ensure lamp-aging factors used to size a UV system are selected based on the most representative position along the length and about the circumference of the lamp.

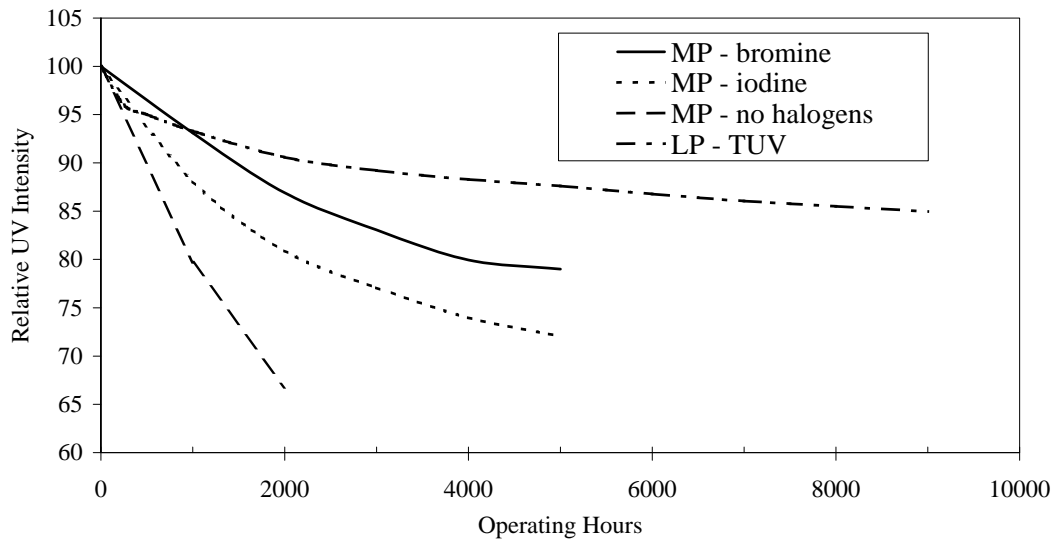
CHAPTER 9 LAMP AGING FACTOR ANALYSIS

This chapter describes the comparison of experimentally derived Lamp Aging Factors to typical industry rules-of-thumb. Specific objectives of this analysis were to:

- Collect UV system cost and lamp aging data for use in developing an engineering approach for determining the optimum Lamp Aging Factor for sizing UV systems.
- Compare industry lamp aging data with experimental lamp aging data presented in Chapter 8.
- Use UVCAT to analyze the cost impact of lamp replacement intervals in order to select the optimal Lamp Aging Factor for sizing UV systems

INDUSTRY UV SYSTEM COST AND LAMP AGING DATA

Data on lamp aging was collected from three sources - lamp manufacturers, UV reactor vendors, and utilities. The lamp manufacturers included Philips, General Electric, and Sylvania. Figure 9.1 provides the lamp-aging curves for LPHO and MP lamp technologies provided by Phillips. Figure 9.2 provides lamp-aging curves for LPHO, amalgam, and MP lamp technologies obtained from various bid documents for UV applications. Typically, most of the data reported by UV system and lamp manufacturers are curves without data. However, limited data indicates considerable variability from lamp-to-lamp can be expected with lamp aging data.



Source: Philips

Figure 9.1 Lamp aging curves for LPHO and MP lamp technologies

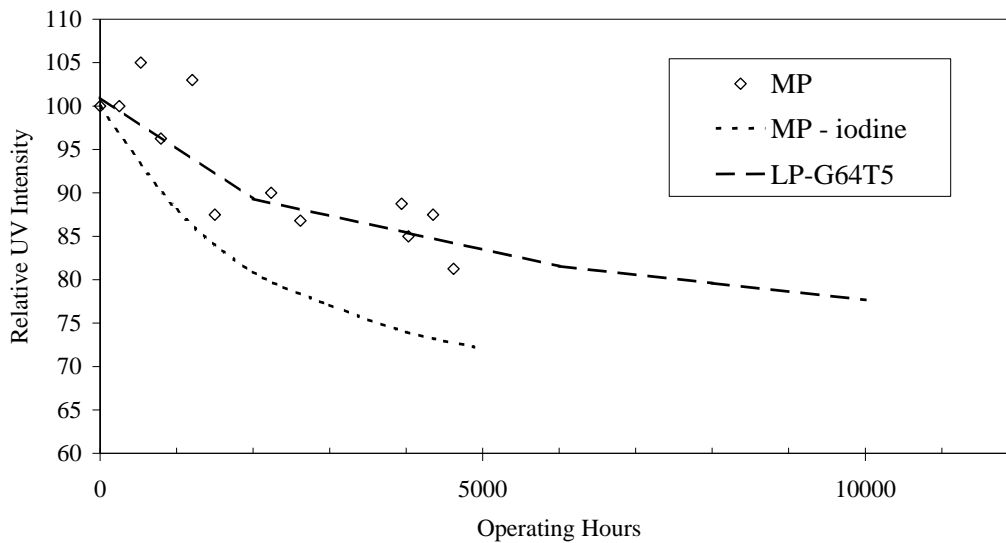


Figure 9.2 Lamp aging data for three lamp types

Phillips reported that the aging of LPHO lamps depends on three main factors - lamp current, on/off frequency, and fill gas and pressure. Migration of mercury into the lamp envelope is the main cause of a reduction in UV intensity. Lamp manufacturers coat the inside surface of the lamp envelope with compounds such as yttrium oxide to reduce the migration of mercury into the lamp envelope. Philips report that such coatings allow LPHO lamps to emit 80 to 90 percent of their original output after 9,000 hours of use at 8 on/off cycles per day. With only three on/off cycles per day, lamp life would be extended by approximately 40 percent. With one on/off cycle per hour, lamp life would be shortened by approximately 40 percent.

Phillips reported that aging of MP lamps is caused in part by the evaporation and condensation of tungsten from the electrodes to the internal surface of the lamp envelope. This process can be reversed by the addition of halogens.

Using non-linear regression, lamp-aging data were fitted to the following mathematical functions:

$$\text{Linear function:} \quad \text{Intensity} = A \times \text{Hours} + B \quad (9.1)$$

$$\text{Exponential function:} \quad \text{Intensity} = A \times \exp(B \times \text{Hours}) \quad (9.2)$$

$$\text{Modified exponential function:} \quad \text{Intensity} = A + B \times \exp(-C \times \text{Hours}) \quad (9.3)$$

$$\text{Shifted power function:} \quad \text{Intensity} = A \times (\text{Hours} - B)^C \quad (9.4)$$

$$\text{MMF function:} \quad \text{Intensity} = \frac{A \times B + C \times \text{Hours}^D}{B + \text{Hours}^D} \quad (9.5)$$

Figures 9.3a and 9.3b compares the model fits to the data from Figure 9.1. The models are extrapolated to 20,000 lamp hours. The linear and exponential models provide biased fits to the data, overestimating lamp aging at low and high lamp ages and underestimating lamp aging at intermediate lamp ages (Figure 9.3a). In contrast, the MMF, shifted power, and modified exponential functions provided unbiased fits to the data (Figure 9.3b). With extrapolation of the models to 20,000 lamp hours, the modified exponential function predicted less lamp aging than the MMF model, which predicted less lamp aging than the shifted power function. Notable is that the modified exponential function predicted a reduction of lamp output to a minimum constant value (coefficient A), beyond which no further reduction would occur. Clearly, any extrapolation of lamp aging data needs to be used with caution.

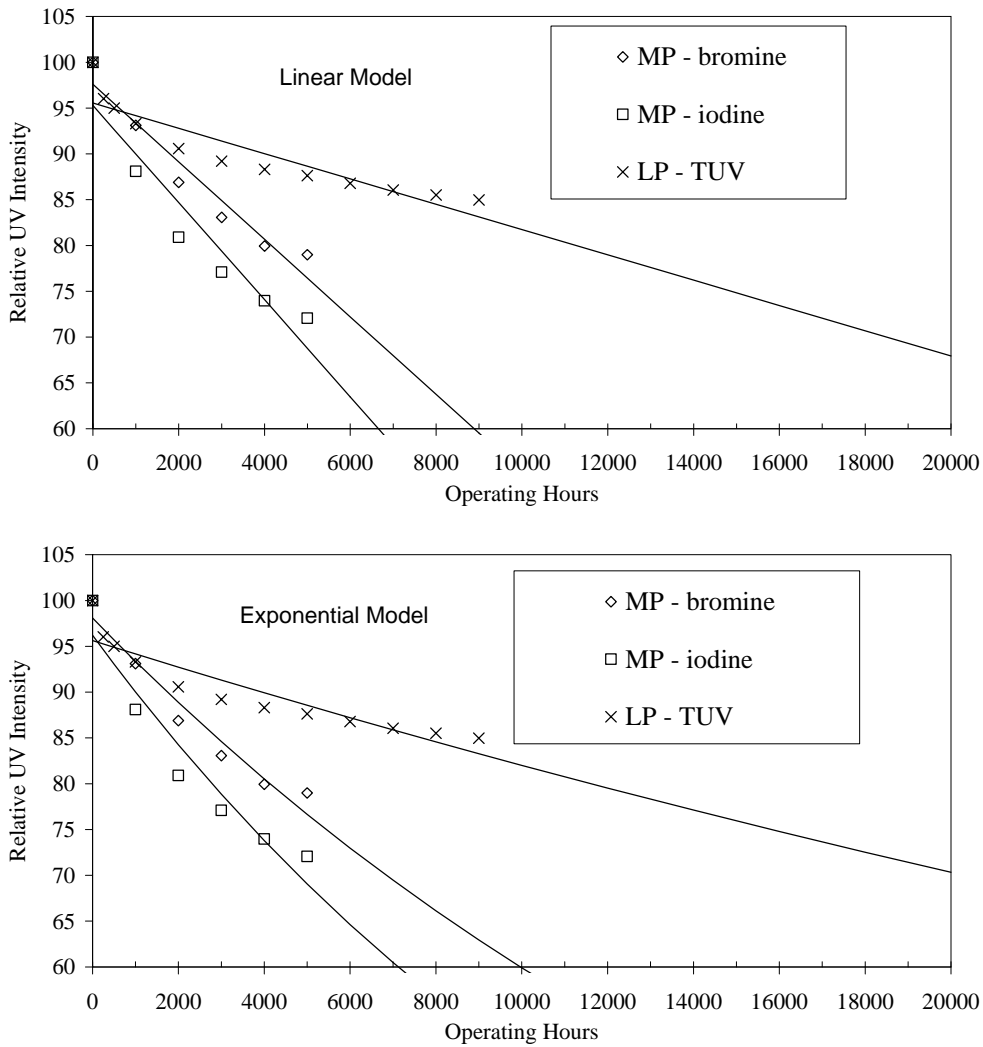


Figure 9.3 Model fits (curves) to lamp aging data (symbols)

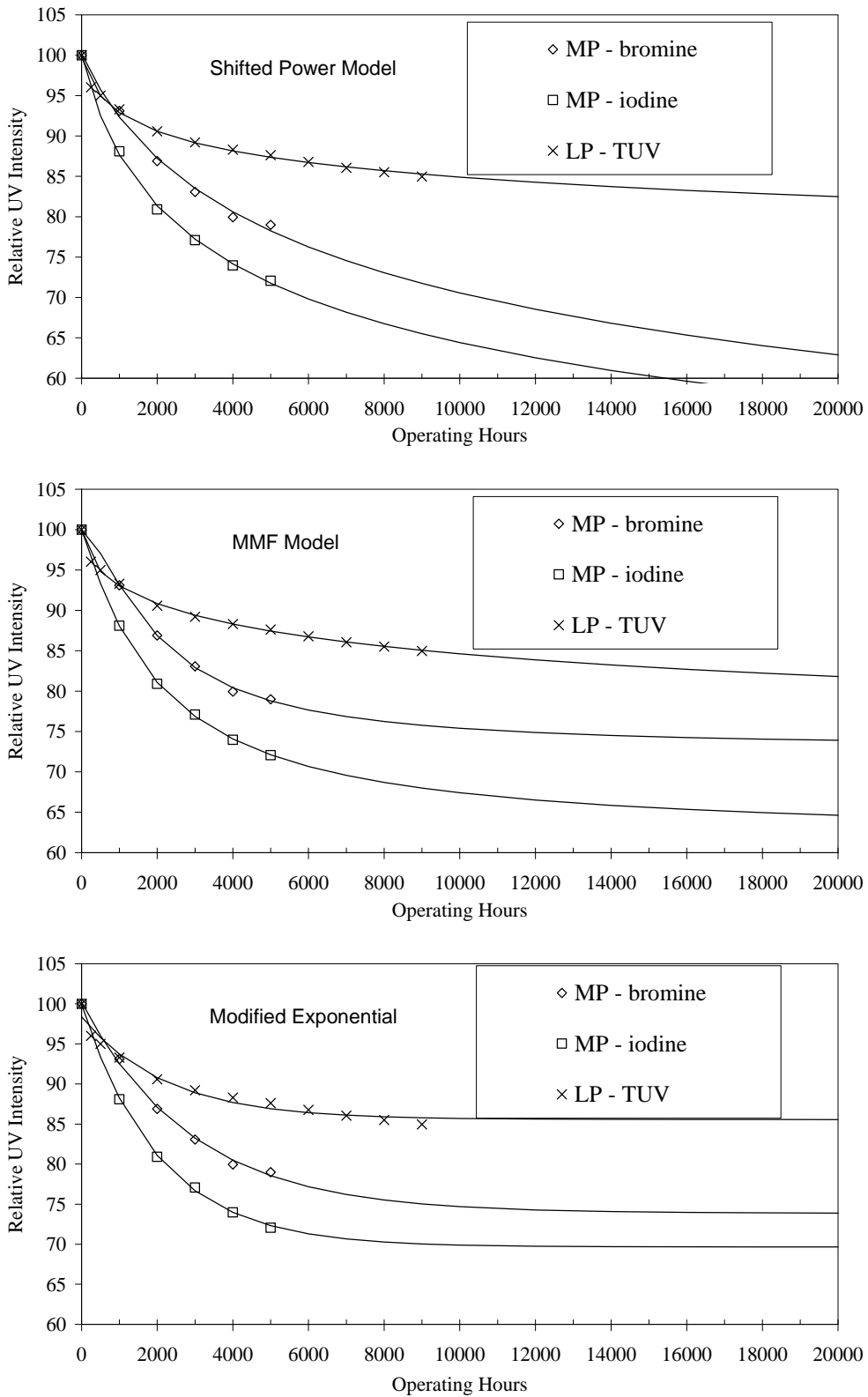


Figure 9.3 (Cont.) Model fits (curves) to lamp aging data (symbols)

Table 9.1 provides data provided by UV lamp manufacturers on lamp performance. Table 9.2 provides data for UV system components from various UV vendors. UV vendors claimed that the UV lamps used by their UV systems would operate for longer periods of time with less lamp aging than claimed by lamp manufacturers.

Table 9.1
Performance data on UV lamps provided by lamp manufacturers

Lamp manufacturer	A					B			C
Lamp characteristic	LP	LPHO	Amalgam	Long life amalgam	MP	LP	LPHO	MP	LP
Lamp power (W)	4 - 80	40 - 195	40 - 200	200 - 500	1,000 - 30,000	75	145	400 - 17,000	65
Lamp life (hrs)	8,000	8,000	8,000	12,000	2,000 - 5,000	9,000	9,000	5,000	7,500
Lamp aging factor (%)	75	70	65	80	75	85	80	80	80
Cool-down time (s)	<1	<1	<10	<10	<60	-	-	-	-
Warm-up time (min)	0.3 - 0.6	0.3 - 0.5	3 - 5	2 - 4	2 - 3	-	-	-	-
Max on/off cycles (#/day)	6	3	6	4	2 - 6	-	-	-	-
Mercury (mg/lamp)	<10	<30		<20	50 - 3,000	-	-	-	-
Arc length (cm)	5 - 150	5 - 150	20 - 150	80 - 150	10 - 150	147.3	147.3	-	-

Table 9.2
UV system component performance data

UV system	A	B	C	D	E	F	G	H
Lamp type	MP	MP	Amal-gam	MP	LP	LPHO	Amal-gam	MP
Lamp data								
Lamp 100% power (W)	10,000	10,600	300	8,000	65	155	300 - 400	4,000
Lamp life (hrs)	5,000	5,000	12,000	8,000	10,000	10,000	10,000	6,000
Lamp aging factor (%)	80	80	70	70	80	80	80	75
Lamp cost (\$)	575	317	190	700	-	-	-	-
Cool-down time (min)	5	7	0	5	-	-	-	-
Warm-up time (min)	5	5	4 - 10	2.5	0.5	-	-	-
Max on/off cycles (#/day)	3	3	4	4	7	7	7	12
Mercury/lamp	500	650	-	-	-	-	-	-
Arc length (cm)	65	61	135	89	147	142	142	70
Sleeve data								
Sleeve life (yrs)	5	10	10	6	-	-	-	-
Sleeve cost (\$)	535	145	95	400	-	-	-	-
Sleeve cleaning	Wiper	Wiper	Acid Rinse	Wiper	Wiper	Wiper	Wiper	Wiper
Fouling factor	90	95	90	100	-	-	-	-
UVT, new (%)	88	89	92	94	94	94	94	94
UVT, aged (%)	80	89	90	86	90	90	90	90
Ballast data								
Lamps per ballast	1	2	2	1	-	-	-	-
Ballast life (yrs)	10	10	5	5	5	5	5	5
Ballast costs (\$)	2,100	3,800	350	2,000	100	155	200	3,000
Ballast power setting	30 - 100	60, 80, 100	50 - 100	55, 79, 89, 100, 105	On/Off	-	-	50 - 100
Efficiency (%)	92	94	-	-	93.5	93.5	93.5	93.5
Duty UV sensor data								
UV sensor life (yrs)	5	3	10	10	-	-	-	-
UV sensor cost (\$)	1200	1200	1000	600	350	350	350	-
UV sensor calibration period (months)	-	18	12	-	14	14	14	14
UV sensor calibration cost (\$)	240	500	230	230	65	65	65	65

LAMP AGING FACTOR ANALYSIS USING UVCAT

Three hypothetical case studies were conducted using UVCAT to analyze the impact of lamp replacement intervals and lamp aging factors on UV system costs. UV systems were defined based on industry data on UV system components and performance and CFD-based predictions of UV dose delivery. [Table 9.3](#) describes the data inputs to UVCAT used to describe the UV system.

Table 9.3
Inputs to UVCAT for three UV system case studies

CASE STUDY		1	2	3
LAMP TYPE		MP	MP	LPHO
UV SYSTEM SIZING CRITERIA				
Maximum flow rate	mgd	47	47	47
Average flow rate	mgd	23	23	23
Average UVT	%	93	93	93
Design UVT	%	90	90	90
Design UV dose	mJ/cm ²	32	32	28
UV SYSTEM CONFIGURATION				
Max. flow rate per reactor	mgd	25.7	25.7	25.7
Number of trains	-	3	4	3
Number of reactors/train	-	1	1	1
Banks/reactor	-	2	1	8
Lamps/bank	-	3	8	12
Lamps/ballast	-	1	2	2
Duty UV sensors/bank	-	3	8	1
N ^o . of redundant trains	-	1	1	1
N ^o . of redundant reactors per train	-	0	0	0
LAMP DATA				
Lamp 100% power	kW	20	12	0.36
Lamp life	hrs.	5,000	5,000	12,000
Lamp aging factor	%	71.77	78.24	70.21
Lamp cost	\$	575	275	160
Lamp replacement time	min.	15	3	5
SLEEVE DATA				
Sleeve life	yrs.	5	10	10
Sleeve cost	\$	350	350	100
Sleeve replacement time	min.	25	10	5
Sleeve cleaning type	-	Wiper	Wiper	Rinse
Sleeve cleaning period	wks.	4	4	4
Sleeve cleaning time/reactor	min.	0	0	180
Fouling factor	%	85	95	85

(Continued)

Table 9.3 (Continued)
Inputs to UVCAT for three UV system case studies

CASE STUDY		1	2	3
LAMP TYPE	Units	MP	MP	LPHO
BALLAST DATA				
Ballast life	yrs.	10	5	5
Ballast costs	\$	1,800	6,000	300
Ballast replacement	min.	60	30	1
SENSOR DATA				
Sensor life	yrs.	5	3	10
Sensor cost	\$	1200	2100	650
Sensor replacement	min.	10	10	10
Sensor cal period	months	12	12	12
Sensor calibration cost	\$	70	550	230
UV DOSE PACING				
Peak UV Dose	mJ/cm ²	31.97	34.14	35.18
COST INPUTS				
Labor rate	\$/hr	60	60	60
Electricity cost	\$/kW-hr	0.05	0.05	0.05
Patent fees	\$/1,000 gal	0.015	0.015	0.015
Interest rate	%	4	4	4
Period	yrs.	15	15	15
UV reactor capital	\$	\$750,000	\$1,000,000	\$750,000
RELATIVE UV DOSE DELIVERY				
98% UVT	mJ/cm ²	124.7	95.0	131.7
95% UVT	mJ/cm ²	80.2	66.5	88.5
90% UVT	mJ/cm ²	45.1	41.7	52.7
85% UVT	mJ/cm ²	28.2	28.5	34.5
80% UVT	mJ/cm ²	18.9	20.6	24.1
75% UVT	mJ/cm ²	13.4	15.6	17.7
70% UVT	mJ/cm ²	10.0	12.3	13.5

All three UV systems were sized to treat a total flow rate (47 mgd) with a design UVT of 90 percent. The average flow rate and UVT were 23 mgd and 93 percent, respectively. The UV systems were sized to deliver a UV dose for 2.5-log *Cryptosporidium* inactivation credit based on the Tier 1 UV dose requirements of the 2003 USEPA *Ultraviolet Disinfection Guidance Manual*. Hence, the UV systems equipped with MP lamps were sized to deliver a UV dose, defined as an MS2 RED, of 32 mJ/cm² and the UV system equipped with LPHO lamps was sized to deliver a UV dose of 28 mJ/cm².

The first UV system consisted of three UV reactors in parallel, two duty reactors and one redundant. Each reactor consisted of two banks of three 20-kW MP lamps. A UV sensor monitored each lamp. The UV system was sized assuming a lamp life of 5,000 hours. The lamp-aging factor associated with this lamp age depended on the lamp-aging curve used with the model. The fouling factor used to size the UV system was 85 percent.

The second UV system consisted of four UV reactors in parallel, three duty reactors and one redundant. Each reactor consisted of one bank of eight 12-kW MP lamps. Each lamp was monitored by a UV sensor. The UV system was sized assuming a lamp life of 5,000 hours. The lamp-aging factor associated with this lamp age depended on the lamp-aging curve used with the model. The fouling factor used to size the UV system was 95 percent.

The third UV system consisted of three UV reactors in parallel, two duty reactors and one redundant. Each reactor consisted of eight banks of twelve 360 W LPHO lamps, each bank monitored by a UV sensor. The UV system was sized assuming a lamp life of 12,000 hours. The lamp-aging factor associated with this lamp age depended on the lamp-aging curve used with the model. The fouling factor used to size the UV system was 85 percent.

UV dose delivery by the UV systems was predicted using:

$$UV\ Dose = 10^A \times UVA^{B \times UVA} \times \left(\left(\frac{S}{S_o} \right) / Q_R \right)^C \times Banks^D \quad (9.6)$$

where UVA is the UV absorbance of the water adjusted for a 1-cm pathlength [UVA = -log(UVT)], S/S_o is the UV output from the lamps relative to a new lamp operating at 100 percent power in a new and unfouled sleeve, Q_R is the flow rate per UV reactor, banks is the number of operating banks of lamps per reactor, and A, B, C, and D are model coefficients. Under design conditions, S/S_o is set to the product of the lamp-aging and fouling factors (f_L × f_f).

The values for the model coefficients were obtained by fitting Equation 9.6 to UV dose data predicted by CFD-based modeling. Table 9.4 summarizes the coefficient values used in the model. The CFD-based UV dose predictions used to develop the model were obtained from data developed as part of the AwwaRF project 2977, *Design and Performance Guidelines for UV Sensor Systems* (2005).

Table 9.5 provides the equations for the lamp aging curves used in this analysis. The analysis included lamp aging curves based on industry data and data measured in this project. Figure 9.4 presents the curves predicted using those equations.

Table 9.4
UV dose model coefficients used to predict UV dose delivery for the three hypothetical UV system case studies

Coefficient	UV system 1	UV system 2	UV system 3
a	2.90326	2.36756	2.49874
b	10.2071	8.27457	9.19999
c	0.696709	0.673492	0.782147
d	1.09563	0.934112	0.948675

Table 9.5

Lamp aging equations used with the three hypothetical UV system case studies

UV system 1 Equations based on industry data	$I(\%) = A \times (t - B)^C$ $A = 330.86696, B = -891.62191, C = -0.17604356$			
UV system 2 Equations based on industry data	$I(\%) = A \times (t - B)^C$ $A = 411.28997, B = -1830.9318, C = -0.18795949$			
UV system 3 Equations based on industry data	$I(\%) = A \times (t - B)^C$ $A = 194.48957, B = -343.37802, C = -0.10815026$			
	If $t < 350$ hrs., then $I = 100\%$			
UV system 1 Lamp aging equation from this work	If $t \geq 350$ hrs., then $I = \frac{b^t \times t^{-c}}{b^{350} \times 350^{-c}} \times 100\%$			
	Center-Side $b = 1.000082$ $c = -0.2294$	Quartile-Side $b = 1.000055$ $c = 0.1716$	End-Side $b = 1.000045$ $c = 0.1665$	Top-Side $b = 1.000053$ $c = 0.2519$
UV system 2 Equations based on data measured in this work	$I = \left(\frac{A \times \left(P \times \frac{8}{12}\right)^B \times \exp\left(-E \times \left(P \times \frac{8}{12}\right)^F \times t\right)}{A \times \left(P \times \frac{8}{12}\right)^B} + \frac{C \times \left(P \times \frac{8}{12}\right)^D \times \left(1 - \exp\left(-E \times \left(P \times \frac{8}{12}\right)^F \times t\right)\right)}{A \times \left(P \times \frac{8}{12}\right)^B} \right) \times 100\%$			
	Center-Side $A = 0.0313$ $B = 0.8868$ $C = 0.038$ $D = 0.8842$ $E = 0.0872$ $F = -2.6733$	Quartile-Side $A = 0.0243$ $B = 1.0029$ $C = 0.0396$ $D = 0.8521$ $E = 0.0161$ $F = -1.7152$	End-Side $A = 0.0179$ $B = 1.0107$ $C = 0.0412$ $D = 0.7217$ $E = 0.0093$ $F = -1.3843$	Top-Side $A = 2.3784$ $B = -2.0993$ $C = 0.0237$ $D = 1.0582$ $E = 0.0045$ $F = -2.0043$
	If $t < 350$ hrs., then $I = 100\%$			
UV system 3 Lamp aging equation from this work	If $t \geq 350$ hrs., then $I = \frac{t^{-b}}{350^{-b}}$			
	Center-Side Amalgam $b = -0.05747$ Non-Amalgam $b = -0.05762$	Quartile-Side Amalgam $b = -0.06968$ Non-Amalgam $b = -0.06840$	End-Side Amalgam $b = -0.08863$ Non-Amalgam $b = -0.1218$	Top-Side Amalgam $b = -0.1635$ Non-Amalgam $b = -0.08434$

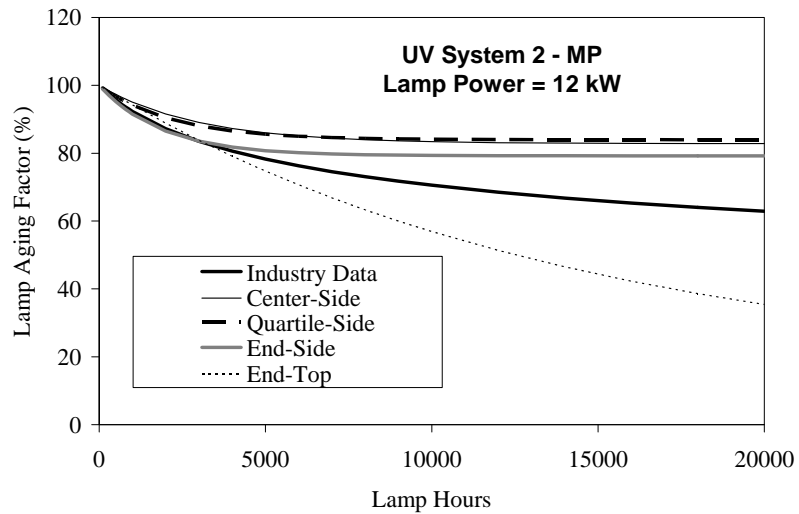
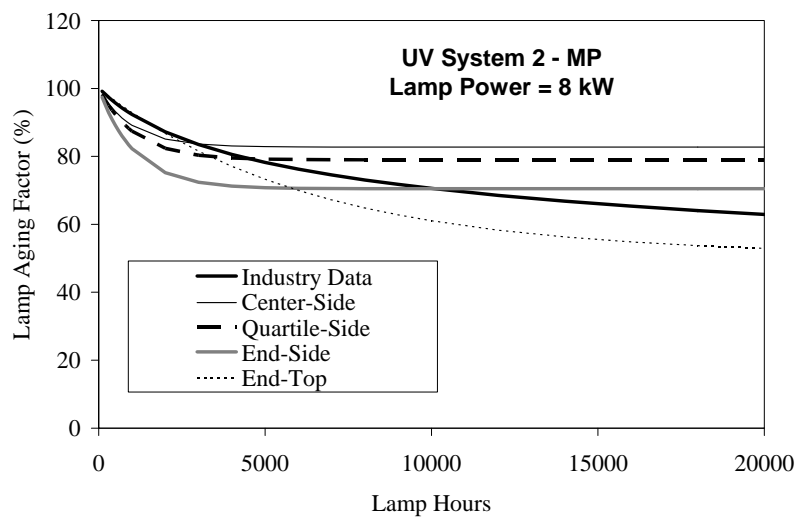
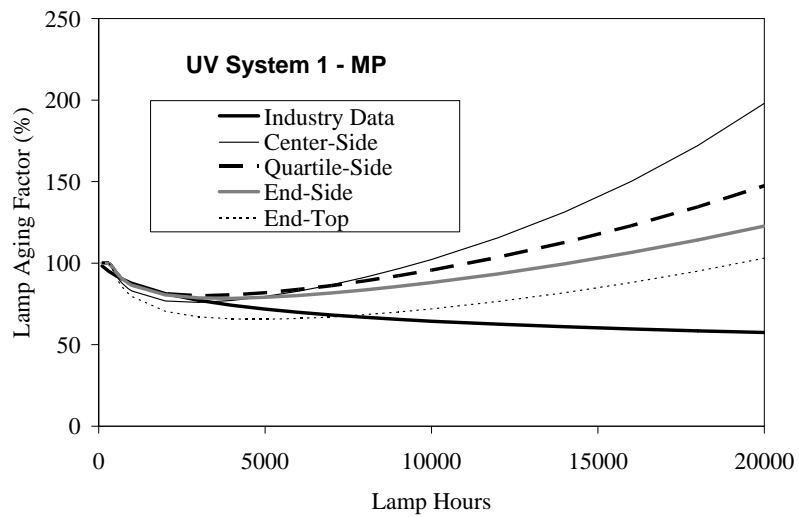


Figure 9.4 Lamp aging curves used in the UVCAT analysis of Lamp Aging Factors

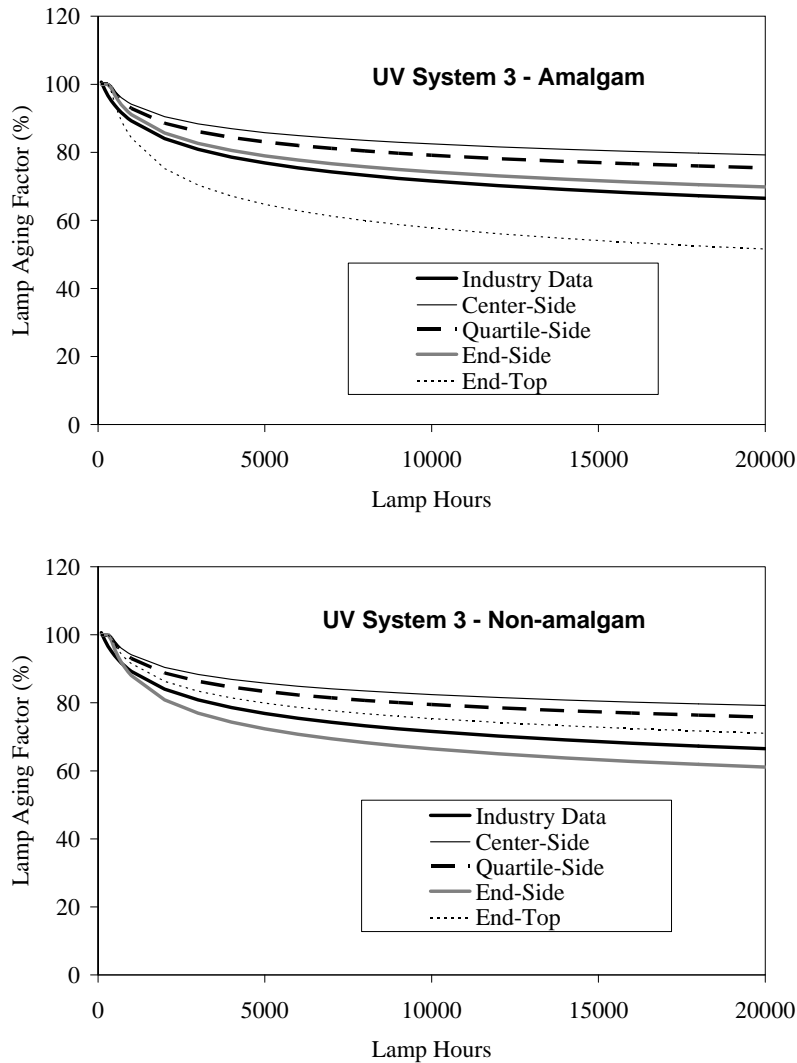


Figure 9.4 (Cont.) Lamp aging curves used in the UVCAT analysis of Lamp Aging Factors

For UV System 1, the lamp aging curves based on data measured in this project were derived from the Hoerl model defined by Equation 9.3. The Lamp Aging Factor is defined relative to the UV intensity predicted by Equation 9.3 at 350 hours. The Lamp Aging Factor is set to 100 percent for lamp aged less than 350 hours. As observed in Figure 9.3, the Hoerl model does not provide a realistic extrapolation of the lamp aging data beyond the range measured in this study (*i.e.*, 350 to 6,100 hours). Hence, UVCAT predictions beyond 6,100 hours for UV System 1 using the Hoerl model were not used.

For UV System 2, the lamp aging curves based on data measured in this project are derived from the Equation 9.2 with the exception that power is scaled by a factor of 8/12 to account for the difference between the power of the lamps used to develop the measured data and the power of the lamps used in the UVCAT simulation. Since Equation 9.2 provides reasonable extrapolation of the lamp aging data back to zero lamp hours, the Lamp Aging Factor is defined relative to the UV intensity predicted at zero hours.

For UV System 3, the lamp aging curves for the amalgam and non-amalgam lamps based on data measured in this project are based on the power functions defined by Equations 9.4 and 9.5. Since the power function does not provide reasonable extrapolation for lamp ages less than the lower bound of the range of lamp aging data measured in this study (*i.e.*, 350 hours), the Lamp Aging Factor is defined relative to the UV intensity predicted at 350 hours. The Lamp Aging Factor is set to 100 percent for a lamp aged less than 350 hours.

Using the industry lamp aging data, Figure 9.5 provides the present worth costs of the three UV systems predicted using the STANDARD LCA tool of UVCAT. The predictions assume no dose pacing by the UV system. In other words, the UV system operates with all duty reactor lamps on at a power setting that delivers the design UV dose assuming flow rate, UVT, and lamp aging and fouling are always at design conditions. The analysis also assumes lamp-aging curves based on industry data and a power cost of \$0.05 per kW-hr.

In Figure 9.5, the LPHO system had lower power and UPS costs due to the greater electrical efficiency of LPHO lamps. The MP systems had lower lamp replacement costs than the LPHO system primarily because the MP systems use many fewer lamps. While system MP1 had lower component costs than the LPHO system, system MP2 had significantly greater costs, primarily due to ballast and UV sensor replacement and calibration.

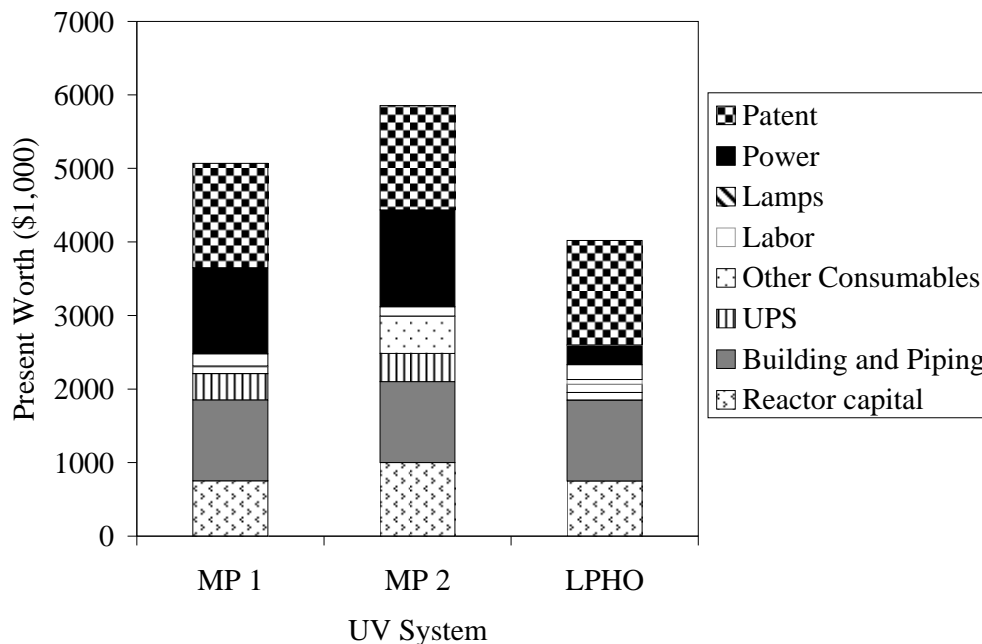


Figure 9.5 Present worth costs for the three hypothetical UV systems assuming no dose pacing and lamp aging curves based on industry data; Electricity assumed \$0.05/kW-hr

Figure 9.6 shows the impact of dose pacing strategies on O&M costs predicted by the STANDARD LCA tool of UVCAT. The analysis assumes lamp-aging curves based on industry data and a power cost of \$0.05/kW-hr. The dose-pacing strategies are defined as follows:

- Flow pacing - UV system operation assumes UVT, lamp aging, and fouling are always at design conditions. UV system turns on and off lamps and adjusts lamp power to deliver the design UV dose as the flow rate changes. STANDARD LCA tool calculates costs assuming the flow rate is always at average value.
- Flow and UVT pacing - UV system operation assumes lamp aging and fouling are always at design conditions. UV system turns on and off lamps and adjusts lamp power to deliver the design UV dose as flow rate and UVT change. STANDARD LCA tool calculates costs assuming flow rate and UVT are always at average values.
- Full dose pacing - UV system turns lamps on/off and adjusts lamp power to deliver the design UV dose as flow rate, UVT, and lamp aging and fouling change. STANDARD LCA tool calculates costs assuming flow rate, UVT, lamp aging, and fouling are always at average values.

As demonstrated in Figure 9.6, the O&M costs decrease as the extent of dose pacing increases. However, the magnitude of the cost savings obtained with dose pacing depends on the flow rate and UVT variability and the extent of lamp aging and sleeve fouling. In this example, significant cost savings were associated with flow pacing as compared to no dose pacing. However, the impact of flow and UVT pacing was incrementally smaller, in part because the average UVT (93%) was only somewhat greater than the design UVT (90%). The impact of full dose pacing was greater with MP1 and the LPHO UV systems compared to the MP2 system because MP2 used a 78 percent Lamp Aging Factor and a 95 percent Fouling Factor, while MP1 and LPHO used a 71 percent Lamp Aging Factor and a 85 percent Fouling Factor.

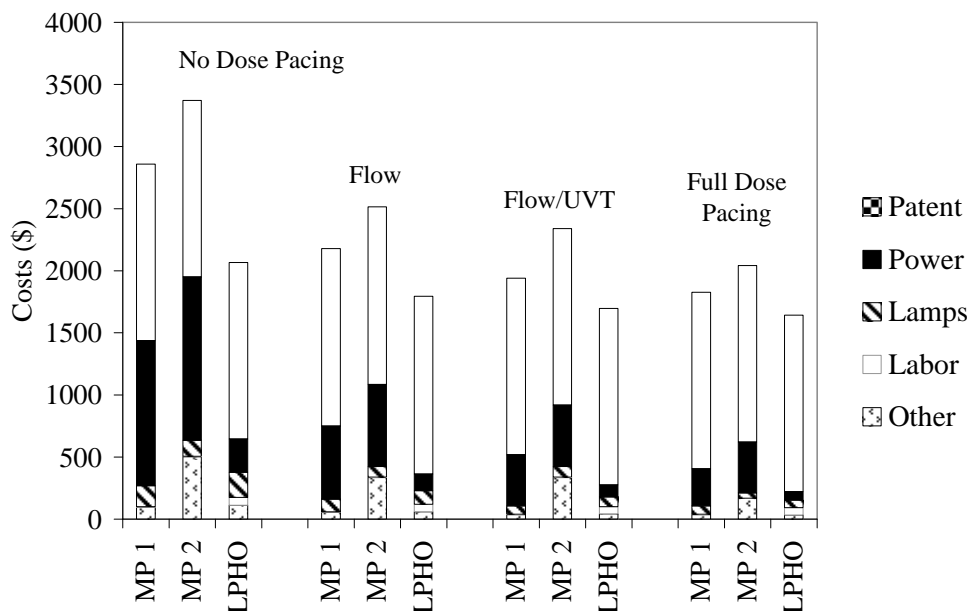


Figure 9.6 Impact of dose pacing strategies on O&M costs for the three hypothetical UV systems using lamp aging curves based on industry data; Electricity assumed \$0.05/kW-hr

Figure 9.7 shows the impact of power costs and dose pacing strategies on O&M costs predicted by the STANDARD LCA tool of UVCAT for UV System 1. Figure 9.8 shows a similar analysis for UV System 3 (amalgam lamps). The analysis assumes lamp-aging curves based on lamp aging data collected in this project and defined in Table 9.5. As expected, annual power costs increase proportional to the power cost. The absolute magnitude of the difference in the annual power costs between the MP reactors and those with LPHO lamps decreases with increased dose pacing. Since the power costs of MP reactors are greater than LPHO reactors, greater dose pacing improves the ability of MP systems to compete with LPHO systems.

Figure 9.9 shows the impact of the lamp replacement interval on life-cycle cost for the three hypothetical UV systems. The analysis uses lamp-aging curves based on industry lamp aging data, power costs of \$0.15/kW-hr, no dose pacing, and UV system sizing adjusted for different Lamp Aging Factors as a function of lamp replacement interval. With the MP UV systems (UV Systems 1 and 2), the life-cycle costs decrease with increased lamp replacement interval until a minimum is reached beyond which life-cycle costs increase. The minimum occurs at 1,000 hours with UV System 1, and 2,000 hours with UV System 2. This optimal replacement interval is notably less than the 5,000 to 6,000 hours given in Table 9.2 as the recommended replacement interval for commercial UV systems. The life-cycle cost savings associated with operating UV Systems 1 and 2 with 1,000- and 2,000-hour lamp replacement intervals instead of 5,000-hour replacement intervals are \$63,000 and \$48,000, respectively. Those savings increase to \$95,000 and \$107,000 when compared to a replacement interval of 8,000 hours. With the LPHO system (UV System 3), life-cycle costs decreased with increased lamp replacement intervals, asymptotically approaching a constant value at high lamp replacement intervals.

Figure 9.10 shows the impact of lamp replacement interval on life-cycle costs for the three UV systems where the lamp aging curves were developed using data measured in this project.

With UV System 1, the relation between life-cycle costs and lamp replacement interval depended on the lamp-aging curve. With the end-top lamp-aging curve, the life-cycle costs decreased to a minimum at 1,000 hours and then increased. However, with the center-side and end-side curves, the life-cycle costs decreased continuously as lamp replacement interval increased. The relationship between life-cycle costs and lamp replacement interval with this example is influenced by the shape of the lamp aging curve, which shows a decrease in UV output with increasing lamp age until ~3,000 hours, after which UV output increased. The decrease was notably greater with the end-top position compared to the center-side or end-side positions.

With UV System 2, the relationship between life-cycle costs and lamp replacement intervals depended on the lamp-aging curve and the ballast operating power. With lamp-aging curves that showed significant reduction in UV intensity over time (*e.g.*, top-side locations at low and high power, end-side location at low power), the life-cycle costs decreased with increasing lamp replacement intervals to a minimum at about 1,000 to 2,000 hours, after which costs increased. However, with lamp aging curves that showed less reduction in UV intensity over time, the life-cycle costs either showed a slight increase after the minima at 1,000 to 2,000 hours or continued to decrease, asymptotically approaching a plateau.

With the LPHO UV system equipped with either amalgam or non-amalgam lamps, life-cycle costs decreased with longer lamp replacement intervals until a plateau was reached at high lamp replacement intervals.

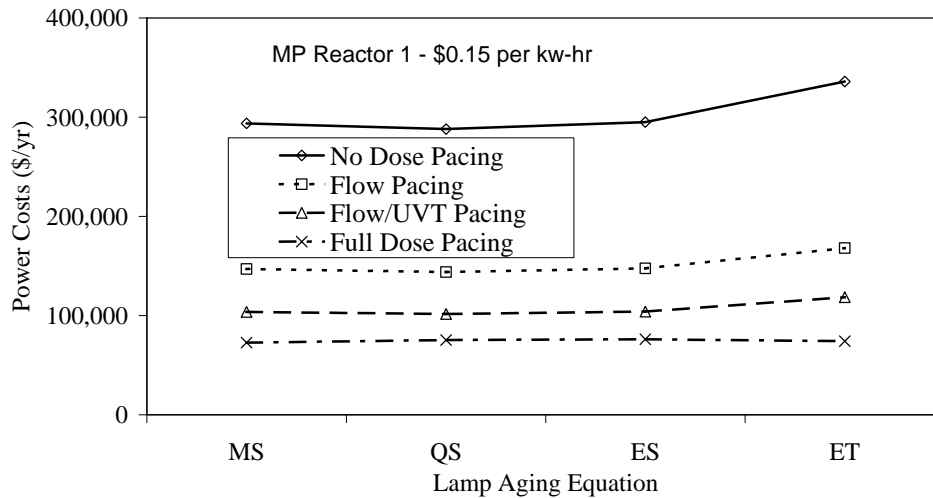
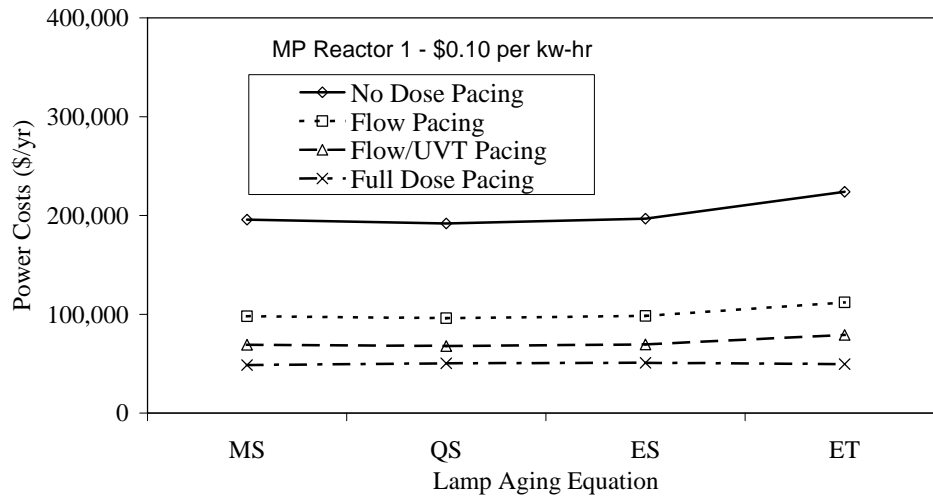
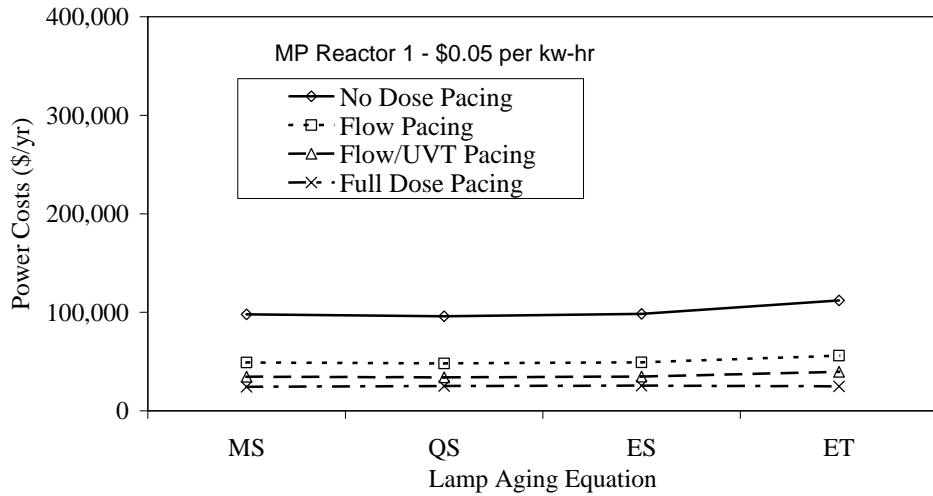


Figure 9.7 Impact of power costs and dose pacing strategies on O&M costs for UV System 1 using lamp aging curves based on MP lamp aging data measured in this project

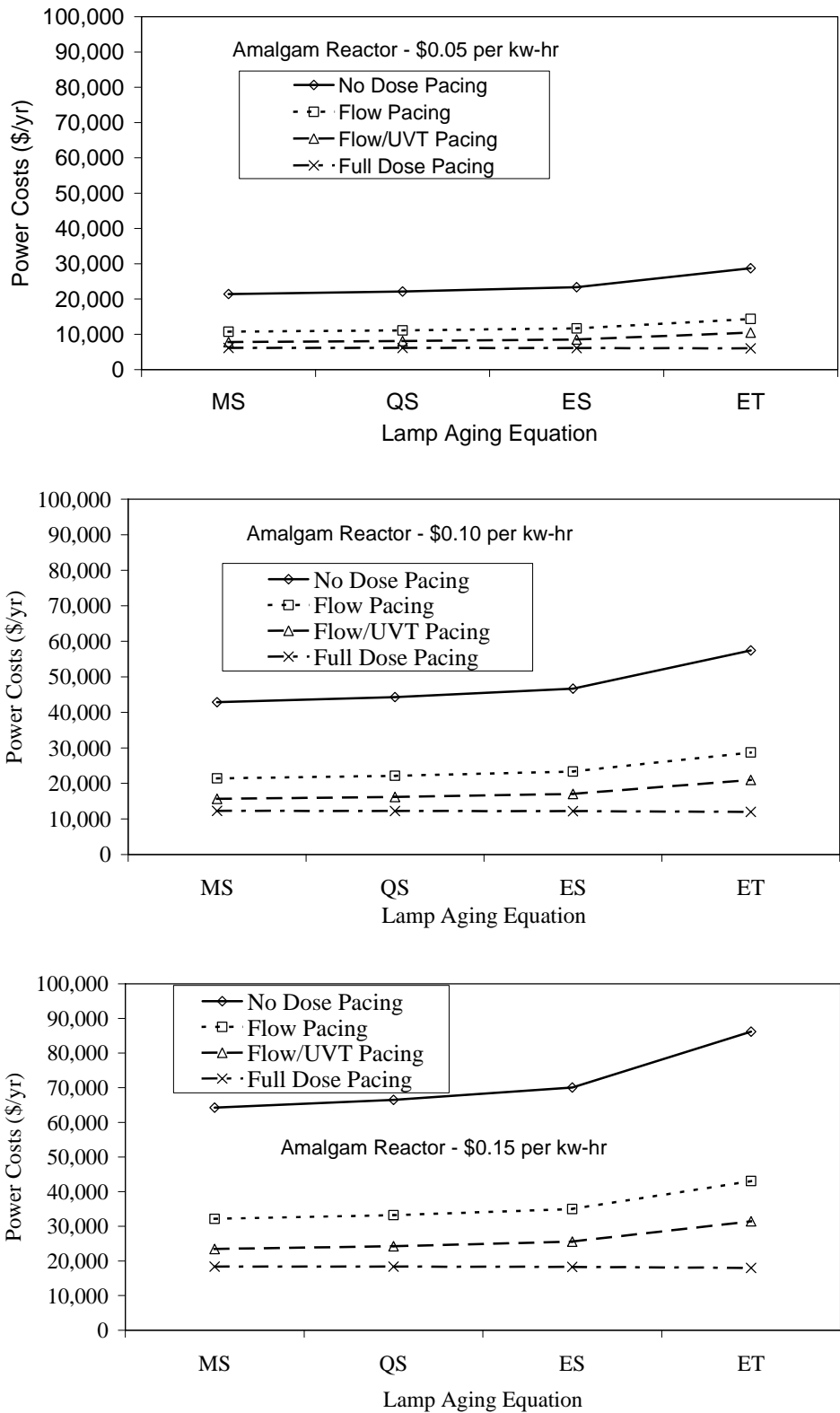


Figure 9.8 Impact of power costs and dose pacing strategies on O&M costs for UV System 3 using lamp aging curves based on amalgam lamp aging data measured in this project

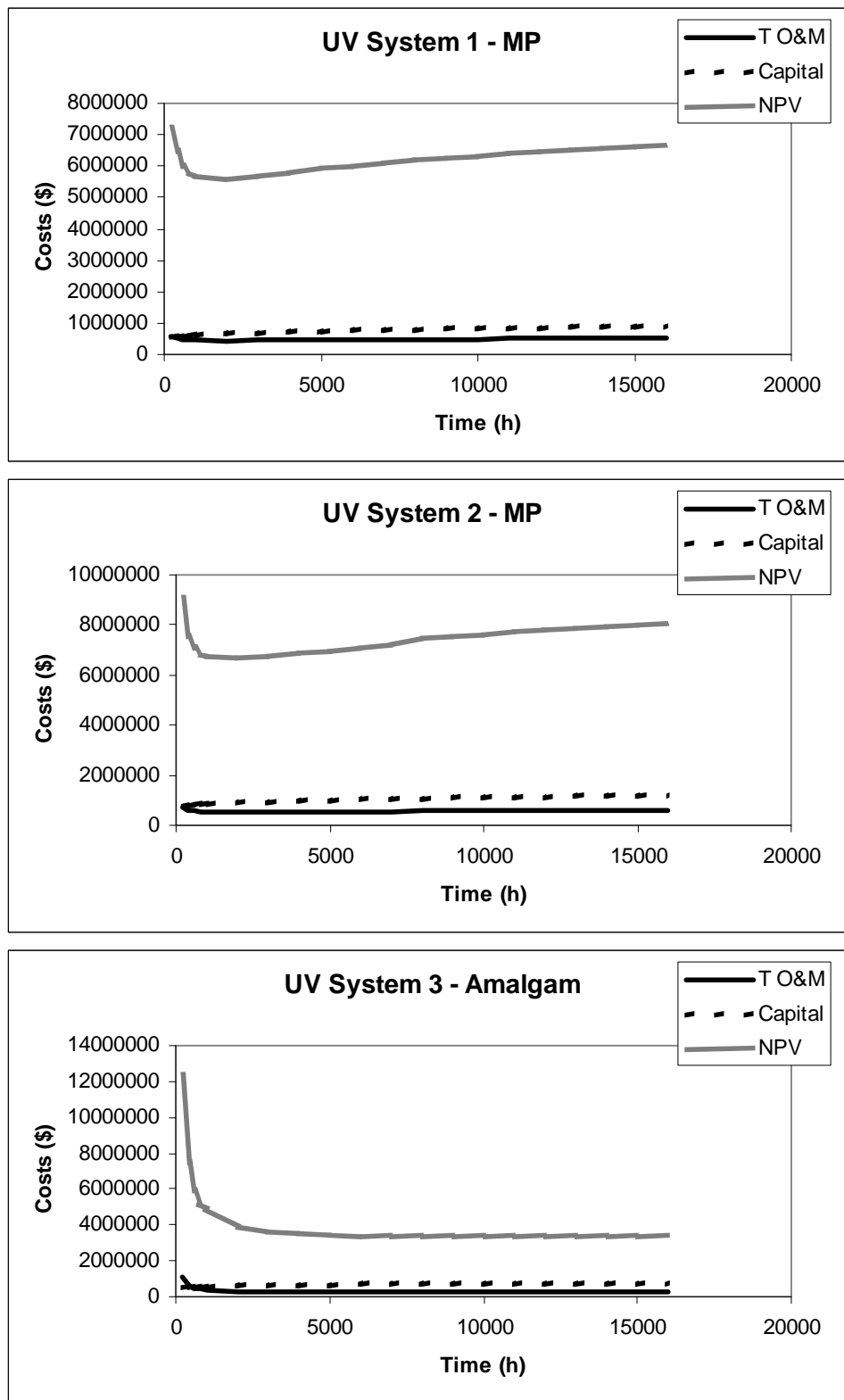


Figure 9.9 Impact of lamp replacement interval on life-cycle costs for the three hypothetical UV systems; Analysis uses lamp-aging curves from industry data, power costs of \$0.15/kW-hr, no dose pacing, and reactor capital costs varying with Lamp Aging Factor

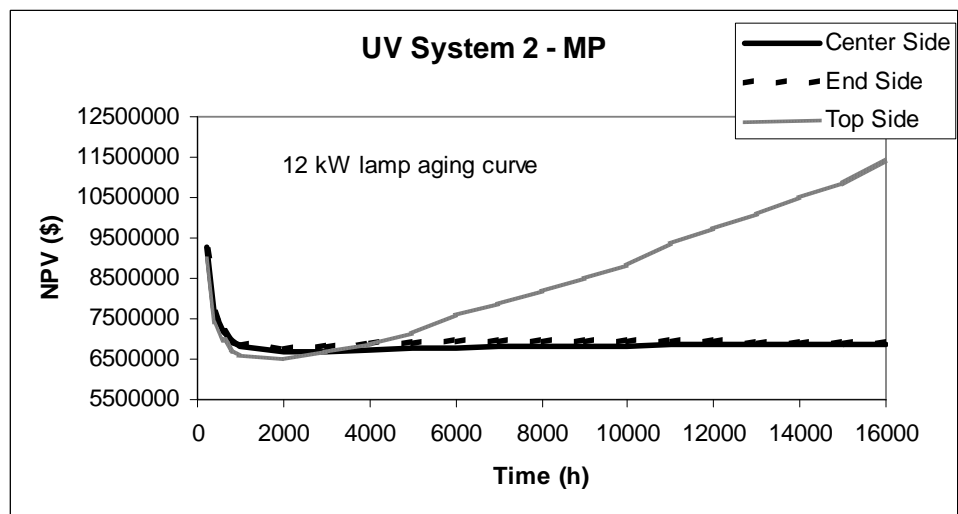
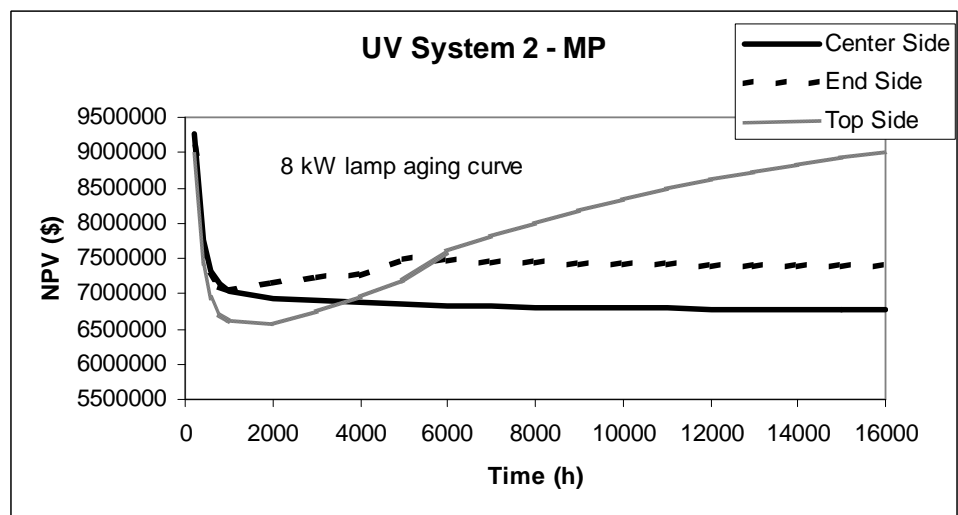
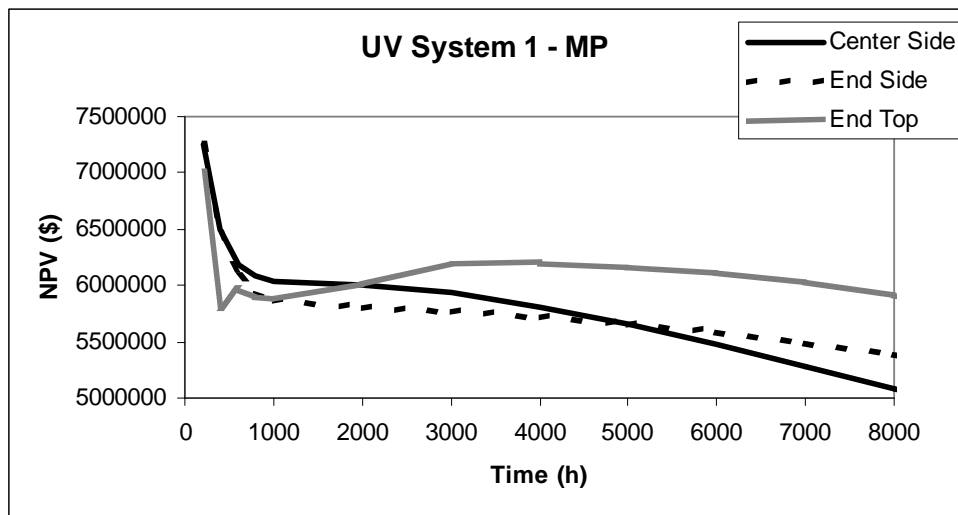


Figure 9.10 Impact of lamp replacement interval on life-cycle costs for the modeled UV systems, Analysis uses lamp-aging curves from data measured in this project, power costs of \$0.15/kW-hr, no dose pacing, and reactor capital costs varying with Lamp Aging Factor

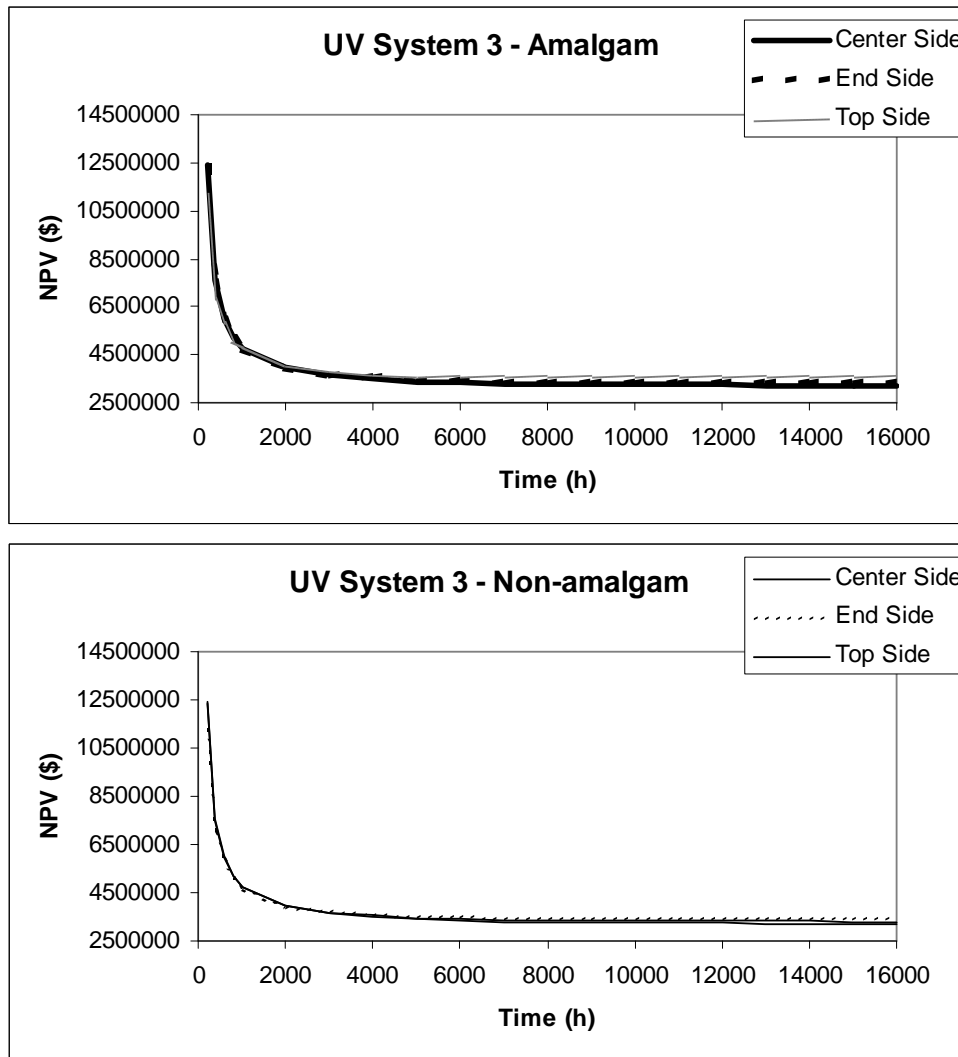


Figure 9.10 (Continued) Impact of lamp replacement interval on life-cycle costs for the modeled UV systems, Analysis uses lamp-aging curves from data measured in this project, power costs of \$0.15/kW-hr, no dose pacing, and reactor capital costs varying with Lamp Aging Factor

In summary, the analysis showed a reduction in life-cycle costs with increasing lamp replacement interval for UV systems using amalgam and non-amalgam lamps. However, the reduction occurred with diminishing returns and was not significant beyond 8,000 hours. The analysis also showed that an optimal lamp replacement interval can exist with UV systems using MP UV lamps. Optimal lamp replacement intervals between 1,000 to 2,000 hours were observed when the lamp-aging curve showed a significant reduction in UV intensity over time. However, if the lamp-aging curve does not show a significant reduction in UV intensity over time, the lamp replacement interval can be extended without an increase in life-cycle costs.

CHAPTER 10

UV DOSE MONITORING AND CONTROL ANALYSIS

This chapter provides an evaluation of UV dose monitoring and control strategies used by UV disinfection systems. Specific objectives of this analysis were to:

- Obtain industry data on UV dose monitoring and control strategies
- Obtain industry UVT and flow rate variability data
- Use UVCAT to assess and recommend approaches for UV dose monitoring and control as a function of UV system size, lamp and ballast technologies, configuration, and water flow rate and UVT

UV DOSE MONITORING AND CONTROL BY COMMERCIAL UV REACTORS

Conventional LP UV systems used in wastewater applications consist of one or more open-channel UV reactor trains in parallel. Each reactor train consists of one or more UV reactors with lamps oriented horizontal and parallel to flow (*e.g.*, Trojan UV3000¹) or vertical and perpendicular to flow (*e.g.*, IDI Aquaray 40²). One redundant reactor in series is often included in wastewater reuse applications but typically not for secondary effluent applications. Electronic ballasts that operate at one power setting typically drive the UV lamps. UV systems operate to deliver a target UV dose. The dose-control strategy often involves turning on and off banks of lamps in response to changing flow rate (termed flow pacing). In some cases, the dose-control strategy may also respond to measured UVT or predicted lamp aging. Because UV intensity sensors have a poor performance history in wastewater applications, they are typically not used in the dose-control algorithm. They are, however, used to indicate when the operator should initiate a manual sleeve cleaning either using an acid bath or manual wiping.

LPHO and amalgam systems used in wastewater applications are very similar to conventional LP systems with the following exceptions:

- LPHO and amalgam systems use electronic ballasts that adjust lamp power settings over some range and use automatic wipers to regularly clean foulants from the quartz sleeves housing the lamps. LPHO or amalgam systems with lamps oriented parallel to flow include the Trojan UV3000+ and the WEDECO TAK³ reactors, while systems with lamps oriented perpendicular to flow include the IDI Aquaray.
- Depending on the UV system manufacturer, the dose-control strategy involves turning on and off lamps and/or adjusting ballast power in response to a combination of changing flow rate, UVT, predicted lamp aging, and UV intensity sensor readings. Typically, UV sensors are not used for dose monitoring.

MP UV systems used in wastewater applications consist of one or more UV reactor trains in parallel. Each reactor train consists of one or more UV reactors with lamps oriented

¹ Trojan Technologies, Inc., Ont., Canada

² Infilco Degremont, Inc., Richmond, Va., USA

³ WEDECO UV Technologies, Charlotte, N.C., USA

horizontal and parallel to flow in an open channel reactor (*e.g.*, Trojan UV4000) or horizontal and perpendicular to flow in a closed vessel reactor (*e.g.*, Aquionics⁴). One redundant reactor in series is often included in wastewater reuse applications but typically not used in applications treating secondary effluent. Typically, lamp sleeves are cleaned using automatic wipers. Either electronic ballasts with many power settings (*e.g.*, 16) or electromagnetic ballasts with a few power settings (*e.g.*, 3) power the UV lamps. Depending on the UV system manufacturer, the dose-control strategy involves turning on and off banks of lamps and/or adjusting ballast power in response to a combination of changing flow rate, UVT, and predicted lamp aging. Typically, UV sensors are not used for UV dose monitoring.

LPHO and amalgam UV systems used in drinking water applications involved closed-vessel reactors with multiple rows of lamps oriented perpendicular to flow (*e.g.*, WEDECO K Series reactors) or a single bank of lamps oriented horizontal and parallel to flow (*e.g.*, Trojan UV Max or WEDECO BX Series reactors). One redundant reactor in parallel is often included with the UV system. Lamp sleeves are typically cleaned using off-line acid flush-and-rinse systems. Typically, electronic ballasts with many power settings power the UV lamps and a bank of lamps is monitored by one UV sensor. The dose-control strategy involves turning on and off banks of lamps and/or adjusting ballast power in response UV dose indicated using measurements of flow, UV sensor readings, and in some cases, UVT.

MP UV systems used in drinking water applications involved closed-vessel reactors with one or more banks of lamps oriented horizontal and perpendicular to flow (*e.g.*, Trojan SWIFT and Calgon Sentinel reactors). One redundant reactor in parallel is often included with the UV system. Lamp sleeves are typically cleaned using automatic wipers. Either electronic ballasts with many power settings or electromagnetic ballasts with a few power settings power the UV lamps. Typically, each lamp is monitoring by a dedicated UV sensor. The dose-control strategy involves turning on and off banks of lamps and adjusting ballast power in response to the UV dose indicated using measurements of flow rate, UV sensor readings, and in some cases, UVT.

LP, LPHO, amalgam, and MP UV systems used in drinking water applications use one of the following three approaches to indicate dose delivery:

UV Intensity Setpoint Approach

Measured flow rate and UV intensity are used to indicate UV dose. Ideally, the UV sensors are positioned within the UV reactor such that the delivered UV dose is proportional to the measured UV intensity as UVT and lamp output changes. Dose control involves adjusting lamp ballast power to produce a UV intensity above some target value defined as a function of flow rate or defined at the design flow rate. UV reactors validated under DVGW (2003) and ÖNORM (2003) standards use this approach.

UV Intensity and UVT Setpoint Approach

Measured flow rate, UV intensity, and UVT are used to indicate UV dose. UV intensity alarm setpoint values can be defined as a function of measured flow rate and UVT, design flow rate and UVT, or a combination of the two. Dose control involves adjusting the lamp ballast power to give UV intensity above some target value determined from the flow rate and UVT.

⁴ Erlanger, Ky., USA

Calculated Dose Approach

UV dose is calculated from the measured flow rate, UV intensity, and UVT. The UV dose calculation can be complex (based on CFD) or simple (based on empirical fits to performance data). Dose control involves adjusting the lamp ballast power and turning on and off lamps to give a calculated UV dose above the required value.

To obtain disinfection credit, USEPA requires all drinking water UV systems undergo UV reactor validation. UV validation involves microbial testing of UV reactors to determine UV dose delivery as a function of measured flow rate, UVT, and UV intensity. This data is used to show that the UV reactor is properly sized for a given UV application and to demonstrate the accuracy of the UV dose monitoring strategy used by the UV system.

UVT AND FLOW RATE VARIABILITY DATA

As mentioned, UV reactors employ dose-control strategies in response to changing flow rate and UVT. This section provides examples of flow rate and UVT profiles obtained from the following water and wastewater utilities:

- Poughkeepsie's Water Treatment Facility, Poughkeepsie, N.Y
- A large drinking water treatment plant located in the eastern U.S. (anonymous)
- City of Scott's Valley Reclamation Facility, Scott's Valley, Calif.
- Two wastewater treatment plants in California (anonymous)

Figure 10.1 shows the UV absorbance at 254 nm (UVA_{254}) of the combined filter effluent at the Poughkeepsie WTP. The data shows seasonal trends with higher UVA_{254} during the fall and winter and lower UVA_{254} during the spring and summer. There is also significant variability in the measured UVA_{254} around the seasonal trends. While part of that variability is due to measurement noise, a majority represents daily trends in UVA caused by changes in raw water UVA and water treatment efficiency.

Figures 10.2 and 10.3 give the flow rate and UVT data for a large WTP in the eastern United States. Both flow rate and UVT show significant trending over time. Like many drinking water treatment plants in the U.S., temporal trends in flow rate at this utility is strongly dependent upon construction and maintenance activities. Unlike Poughkeepsie, the UVT at this plant shows trending from year-to-year but does not show seasonal patterns. Like Poughkeepsie, there is significant variability in the UVT overlying this trend, some of which is likely measurement error and some caused by changes in raw water quality and treatment process efficiency.

Figures 10.4, 10.5, and 10.6 present flow rate and UVT data for two California wastewater treatment plant (WWTPs). The variability of flow rate at WWTPs depends on flow equalization, climate, storm events, and the daily, weekly, and seasonal trends in water use. The variability of UVT at WWTPs will depend on the impact of industry of the raw wastewater and the efficacy of upstream treatment. The UVTs of effluents from secondary WWTPs treating domestic wastewater can range from 65 to 80 percent. Effluents from treating wastewaters with a significant industrial component can be as low as 30 percent. Furthermore, effluents treated by physical-chemical processes also tend to be low (15 to 50 percent) and show diurnal cycling.

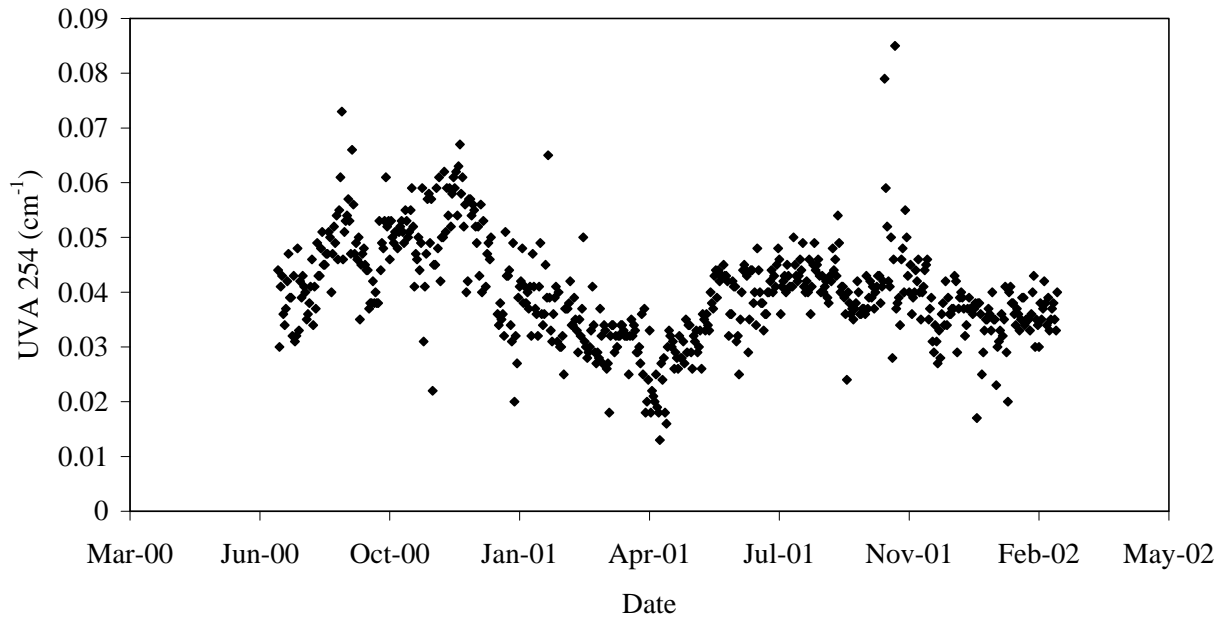


Figure 10.1 Poughkeepsie WTP filter effluent UV absorbance

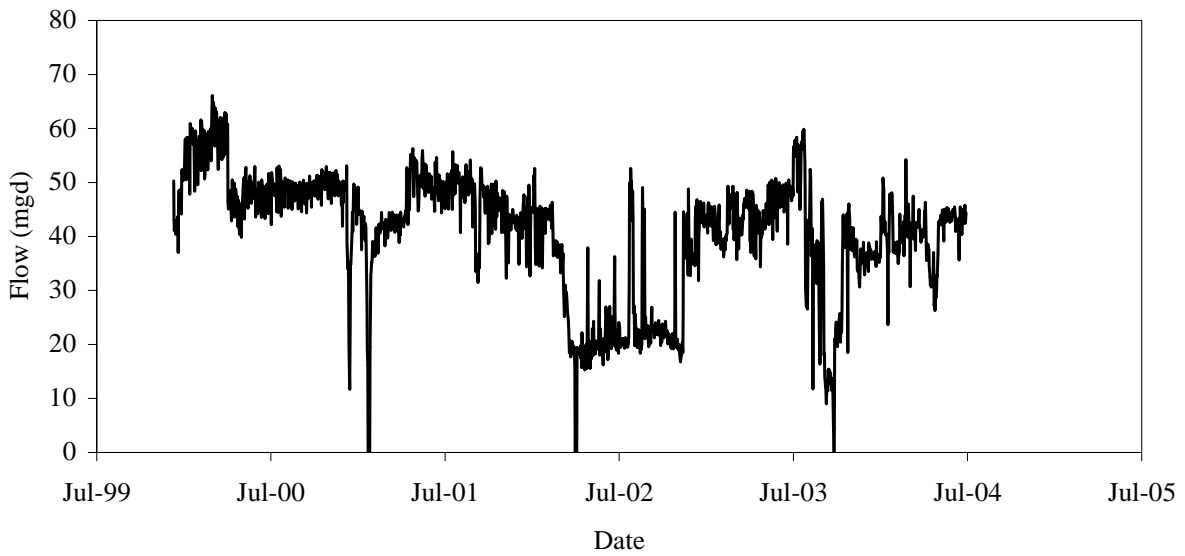


Figure 10.2 Flow rate data for an eastern U.S. WTP

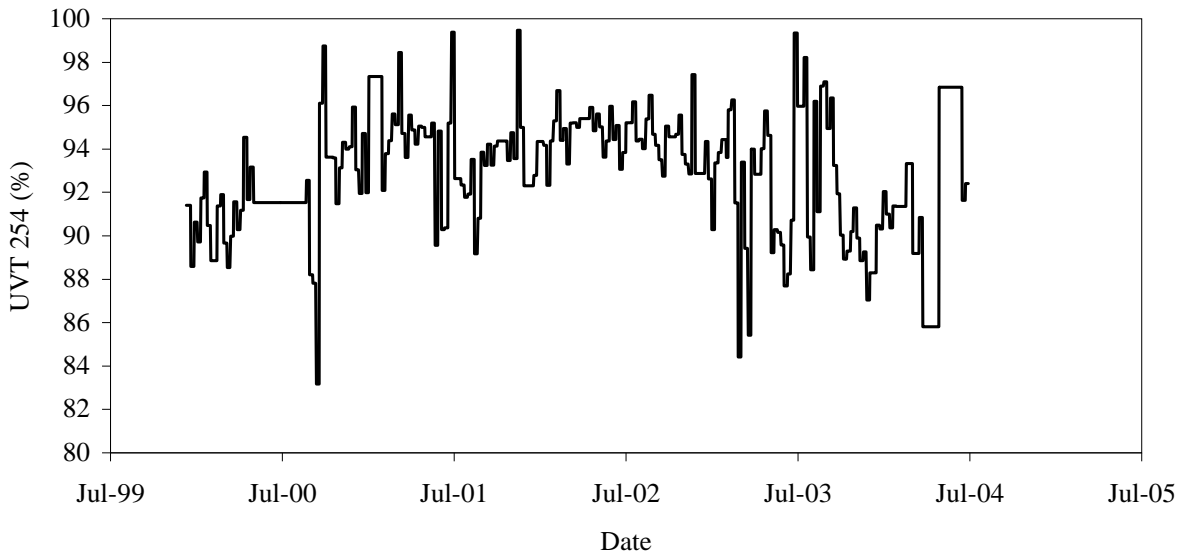


Figure 10.3 UVT data of an eastern U.S. WTP

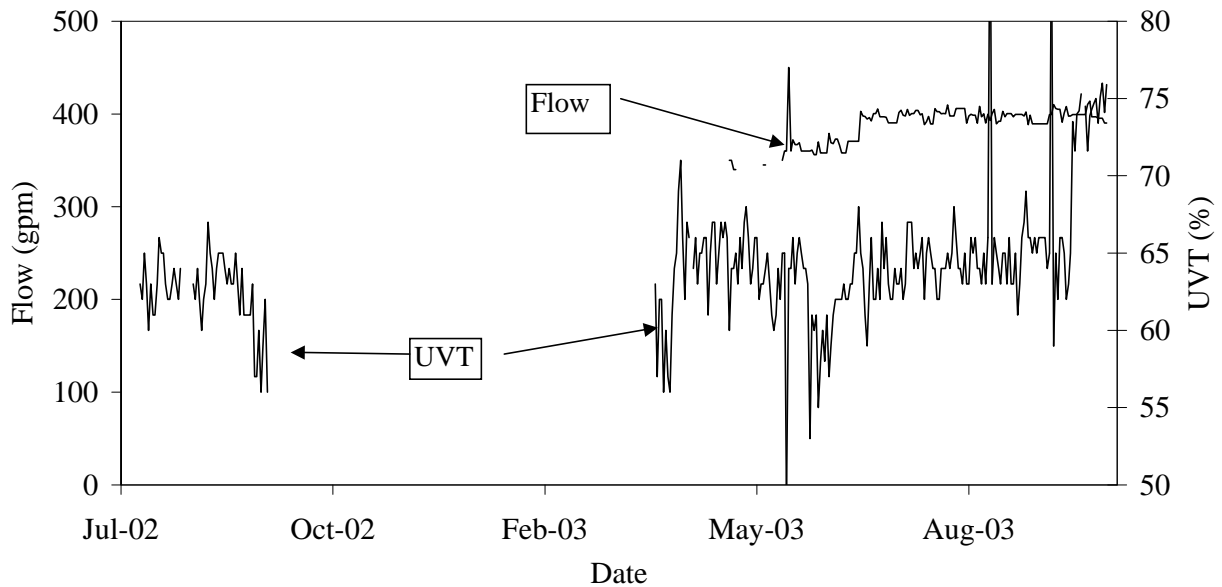


Figure 10.4 Scott's Valley effluent flow rate and UVT

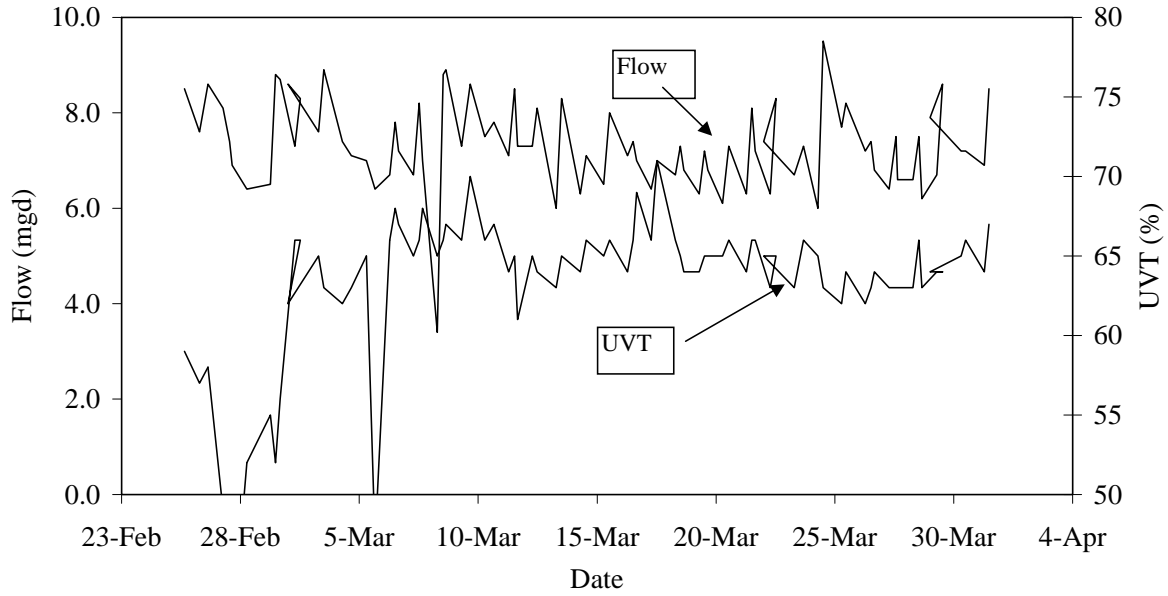


Figure 10.5 Flow rate and UVT at a California WWTP

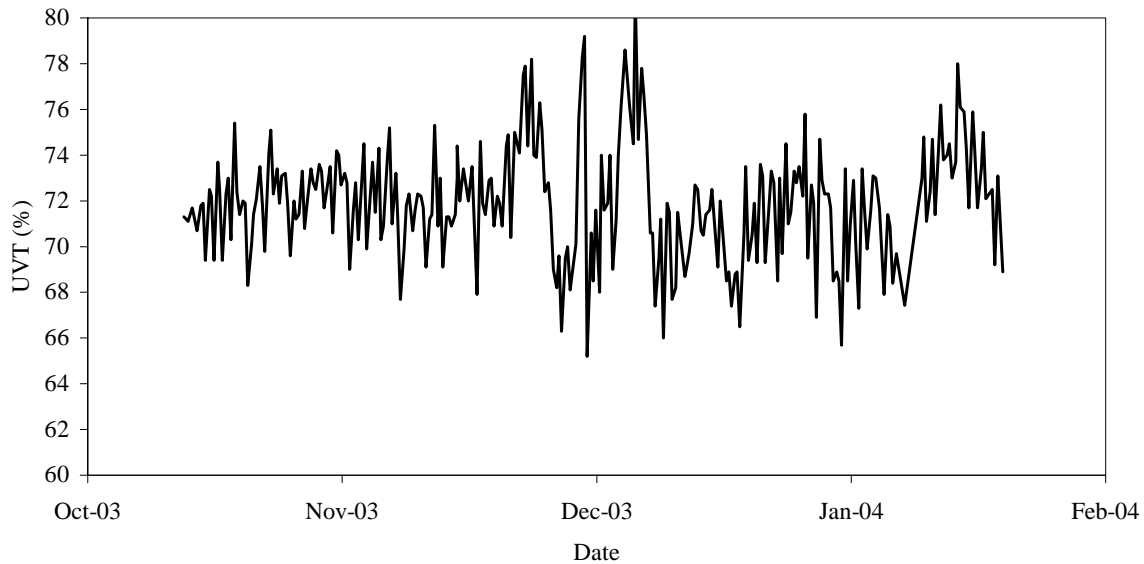


Figure 10.6 UVT at a California WWTP

While the effluent flow rate and UVT with Scott's Valley is relatively uniform over time, flow rates and UVT, WWTPs often experience significant variability in these parameters. For that reason, WWTPs should characterize their flow rate and UVT over time to determine data for sizing UV systems as opposed to relying on rule-of-thumb numbers. For example, while data shows that many secondary effluent systems have design UVTs ranging from 40 to 80 percent, 65 percent is often used as a rule-of-thumb design UVT. This inaccuracy can lead to significant under- or oversizing of the UV system for a given application.

DOSE-PACING ANALYSIS

This section presents UVCAT dose-pacing analysis for the following cases:

- Case 1. Using UVCAT to Evaluate UV System Sizing
- Case 2. Impact of Ballast Power Settings on Dose Pacing
- Case 3. Comparison of Dose Pacing Options
- Case 4. Impact of Lamp Orientation on Dose Pacing

With each analysis, the UV system uses a UPS to provide constant power and the probability of UV system component failure is set at zero, and the WTP serves a population of 10,000 persons.

Case 1. Using UVCAT to Evaluate UV System Sizing

Case 1 presents an example using UVCAT to size a UV system for the flow rate and UVT profile presented in [Figures 10.2](#) and [10.3](#). The UV system consisted of three reactors in parallel, two duty reactors plus one redundant reactor. Each reactor contained 1, 2, or 3 banks of 20-kW lamps. The reactors were operated to deliver a UV dose of 36 mJ/cm², defined as an MS2 RED, to achieve 3-log *Cryptosporidium* inactivation credit. UV dose delivery by the UV system was modeled using:

$$\text{RED} = 10^A \times \text{UVA}^{B \times \text{UVA}} \times \left(\frac{12 \times S/S_0}{Q} \right)^C \times \text{Banks}^D \quad (10.1)$$

where RED is Reduction Equivalent Dose, UVA is the UV absorbance at 254 nm in cm⁻¹, Q is flow in mgd, Banks is the number of operating banks, S is the UV sensor reading in W/m², and S₀ is the UV sensor readings that would occur with new lamps operating at 100 percent ballast power in clean quartz sleeves. The UV sensor reading, S was simulated using:

$$S = 10^a \times \exp(b \times \text{UVT}) \times P^c \times f_L \times f_f \quad (10.2)$$

where UVT is the UV transmittance of the water in %/cm, P is the power of the lamps in kW, f_L is the lamp aging factor, and f_f is the fouling factor. The value for S₀ was obtained from Equation 10.2 by setting P to 100 percent power, f_L to 1.0, and f_f to 1.0. The model coefficients for Equations 10.1 and 10.2 used with the simulation are given in [Table 10.1](#). The model coefficients were obtained from a CFD simulation of a hypothetical reactor.

Table 10.1
Model coefficients for Equations 10.1 and 10.2

Model coefficients for Case 1	Value
A	2.1513
B	10.207
C	0.69670
D	1.0956
a	-4
b	0.11
c	1.8

Cryptosporidium log inactivation was calculated from UV dose using Equation 12.2 and the coefficients in Table 12.11 described as “*Cryptosporidium* Tier 1 requirements for LP lamps”.

Figure 10.7 presents the UVCAT simulation of the UV system consisting of three 1-bank reactors. The analysis indicates the UV system is undersized as follows:

1. The UV system operates using the redundant third reactor
2. The ideal power is often greater than the actual power. The ratio of actual to ideal power is often less than one.
3. *Cryptosporidium* inactivation is often less than the target 3-log.
4. Significant off-specification performance occurs.

Figure 10.8 presents the UVCAT simulation of the UV system consisting of three 2-bank reactors. Similar to the UV system with three 1-bank reactors, the UV system with three 2-bank reactors still uses the redundant reactor to deliver the required UV dose. Hence, the UV system is still undersized. The ratio of actual-to-ideal power is typically equal to one and the log inactivation typically meets the 3-log requirement. However, there are three periods when the reactor cannot deliver the design UV dose (*i.e.*, ratio of actual-to-ideal power is less than one and the inactivation is less than 3-log). Because the reactor cannot deliver the design dose, the significant periods of off-specification performance occur. However, the analysis of public health protection shows that these off-specification periods do not significantly increase risk over the background level that occurs when dose delivery meets the 3-log requirement.

Figure 10.9 presents the UVCAT simulation of the UV system consisting of three 3-bank reactors. The analysis shows the UV system is appropriately sized for the application. Unlike the previous cases, the third redundant reactor is typically not required to deliver dose except for two periods when UVT spikes low. During those periods, the redundant reactor provides extra disinfection capacity to meet the dose delivery requirements. The proper sizing of the UV system is also indicated by the ratio of actual to ideal power being equal to or greater than one and the log *Cryptosporidium* inactivation being equal to or greater than 3. However, the analysis of public health showed a decrease in accumulated risk from 16.9 to 16.5 infections with the increase in reactor sizing from two to three banks. This result suggests that the increase in UV sizing did not provide significant advantages in terms of public health protection even though it significantly reduces the off-specification performance.

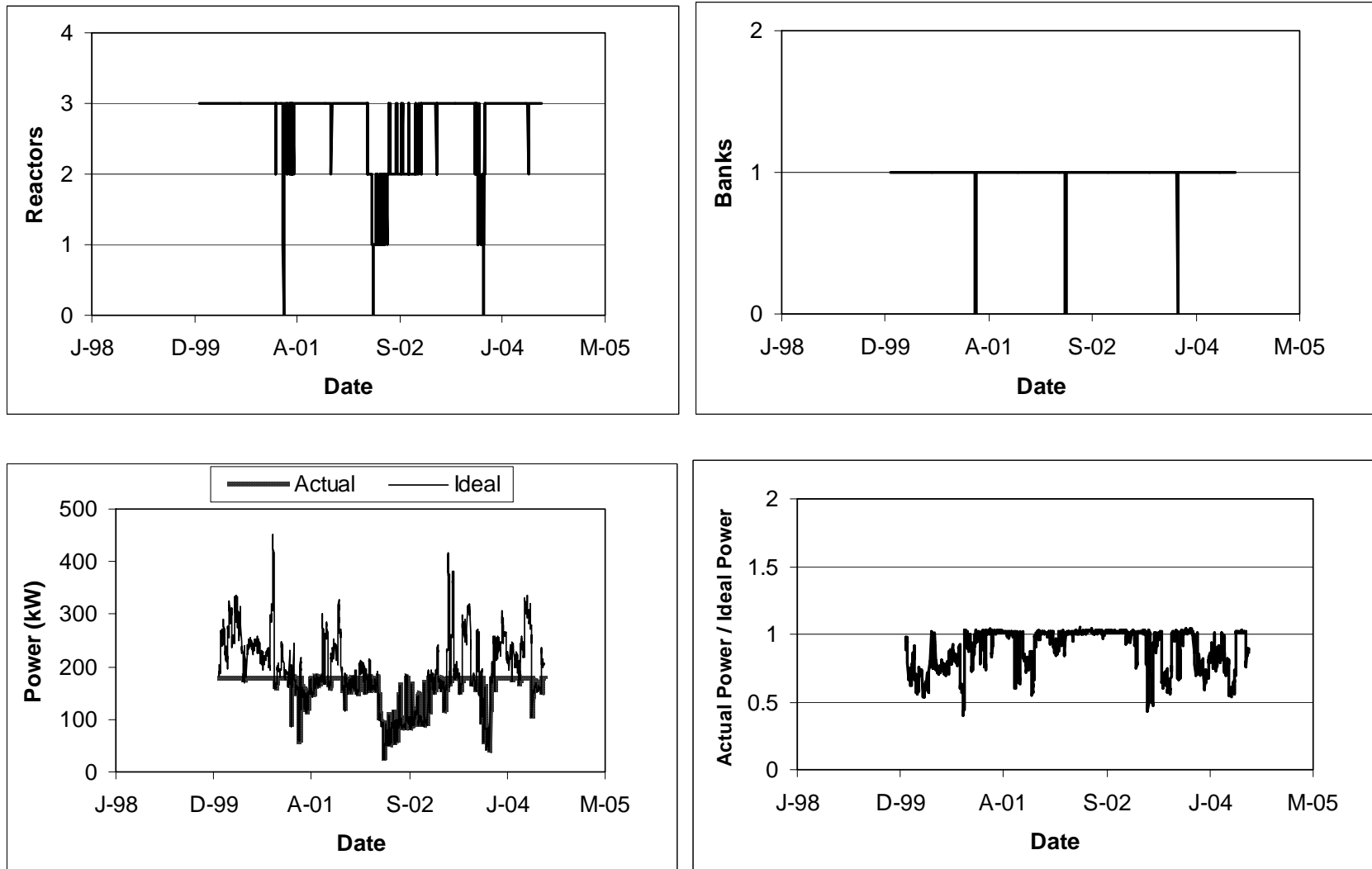


Figure 10.7 Case 1/three 1-bank reactors: reactors on (top left), banks on (top right), power consumption (bottom left), and ratio of ideal-to-actual power (bottom right)

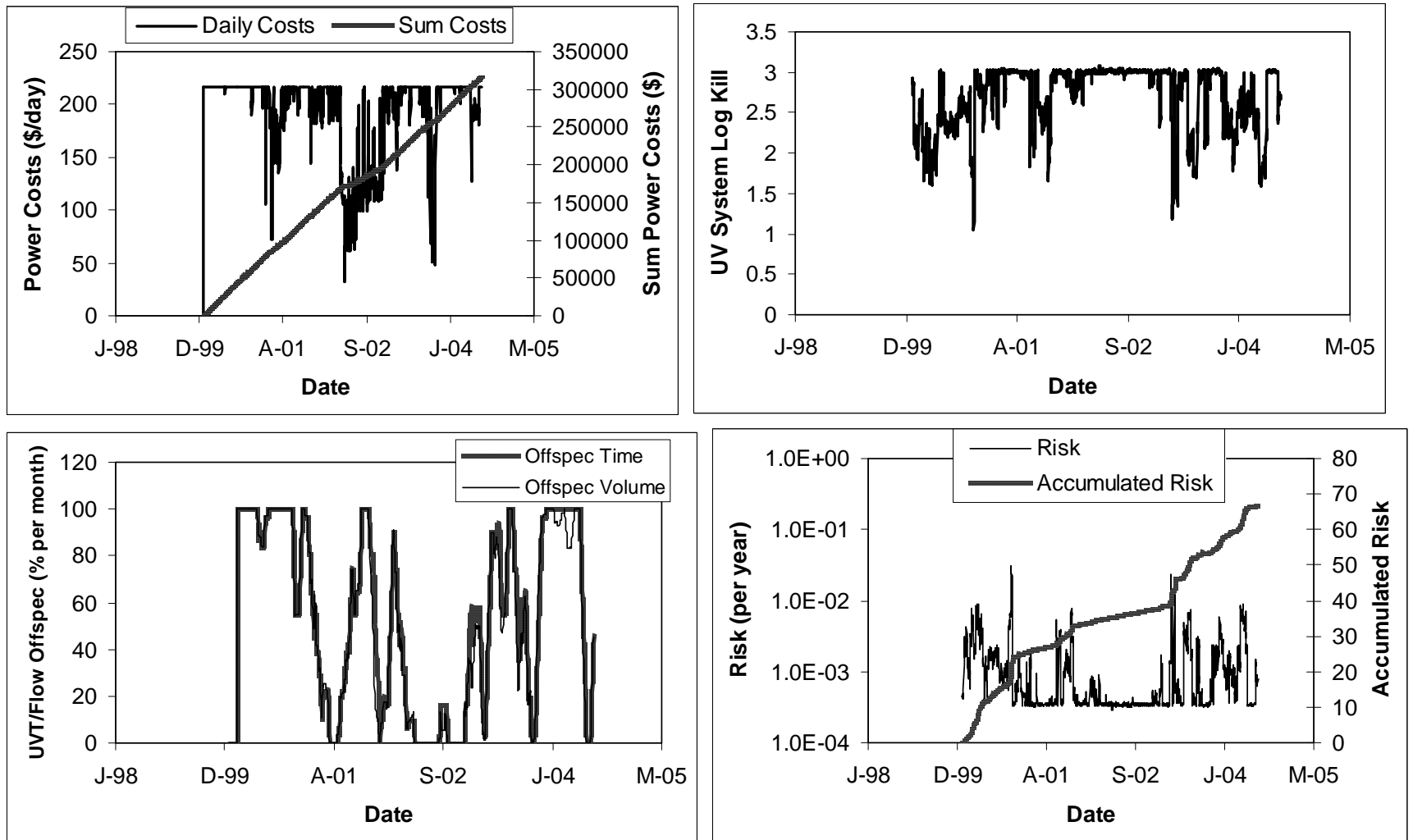


Figure 10.7 (Continued) Case 1/three 1-bank reactors: power costs (top left), UV system log kill (top right), off-specification performance (bottom left), health impact (bottom right)

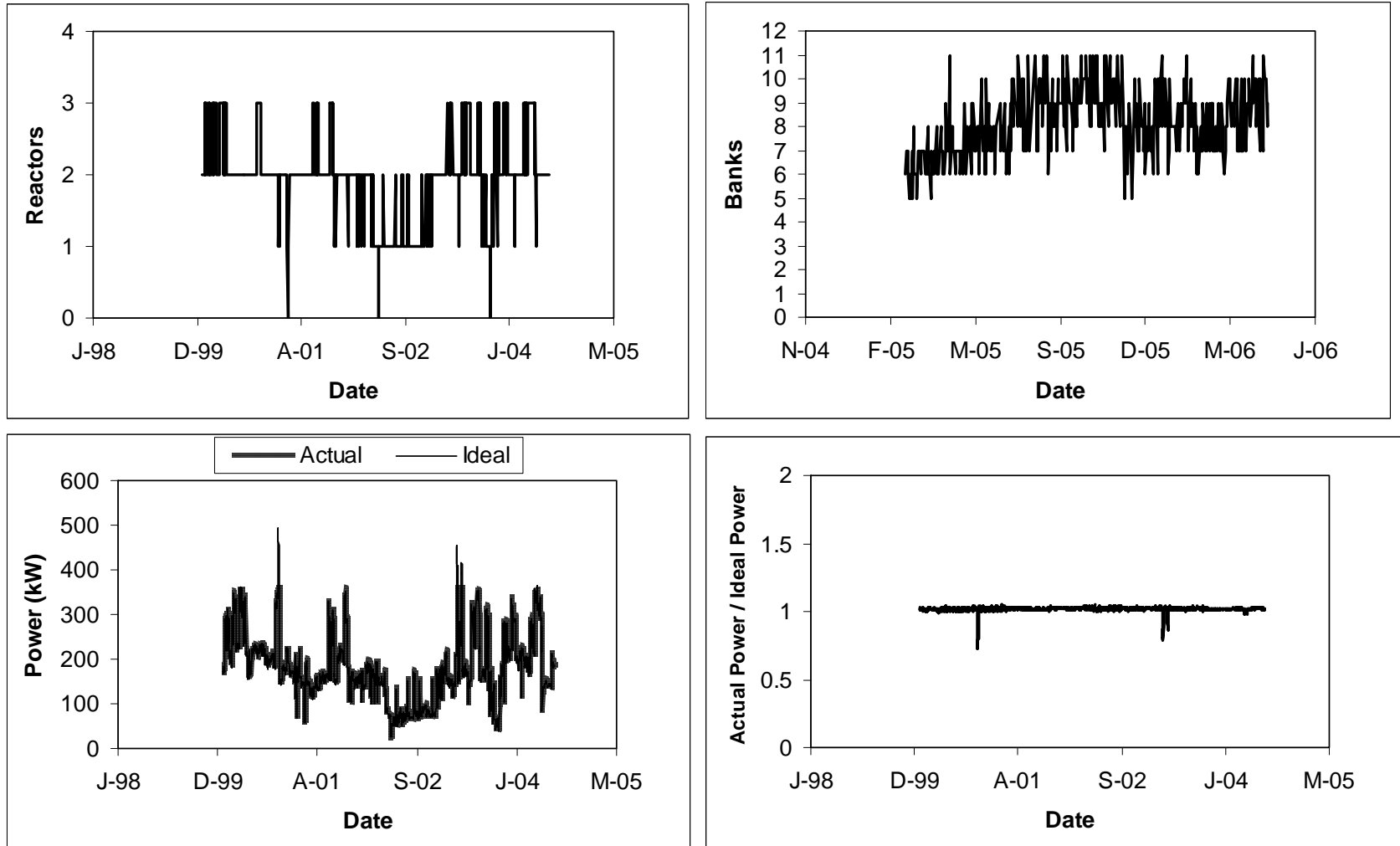


Figure 10.8 Case 1: UV system consisting of three 2-bank reactors: reactors on (top left), banks on (top right), power consumption (bottom left), and ratio of ideal-to-actual power (bottom right)

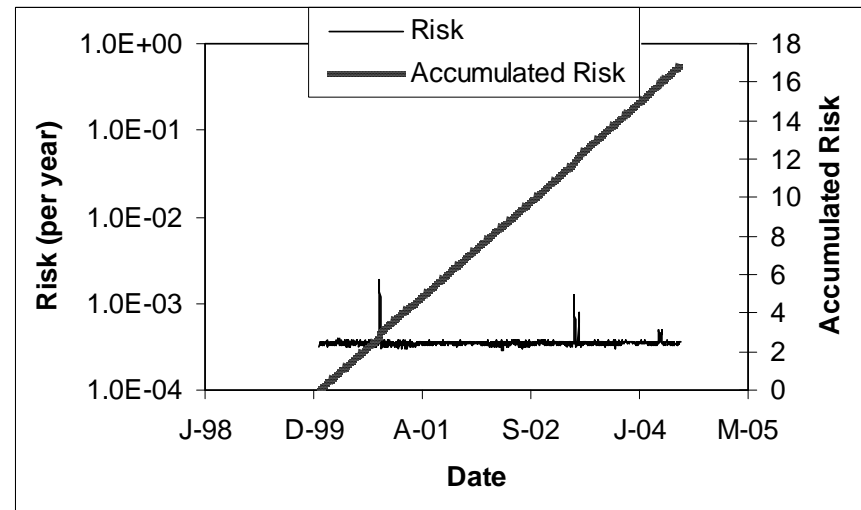
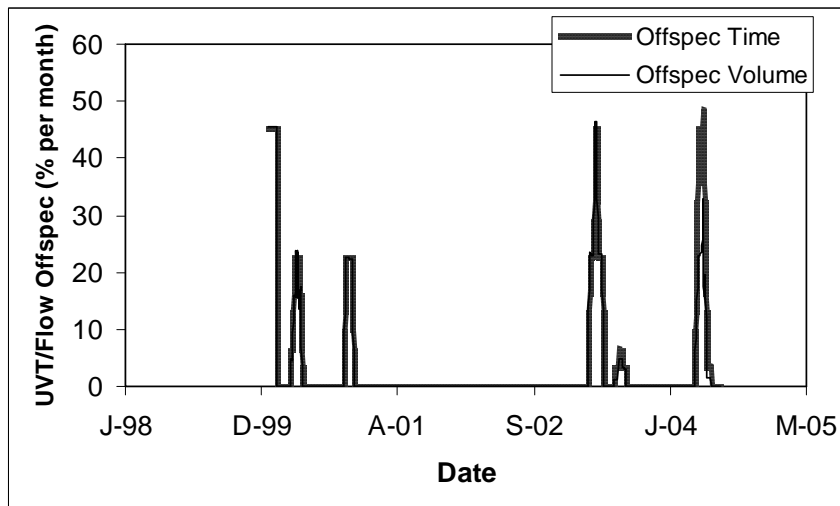
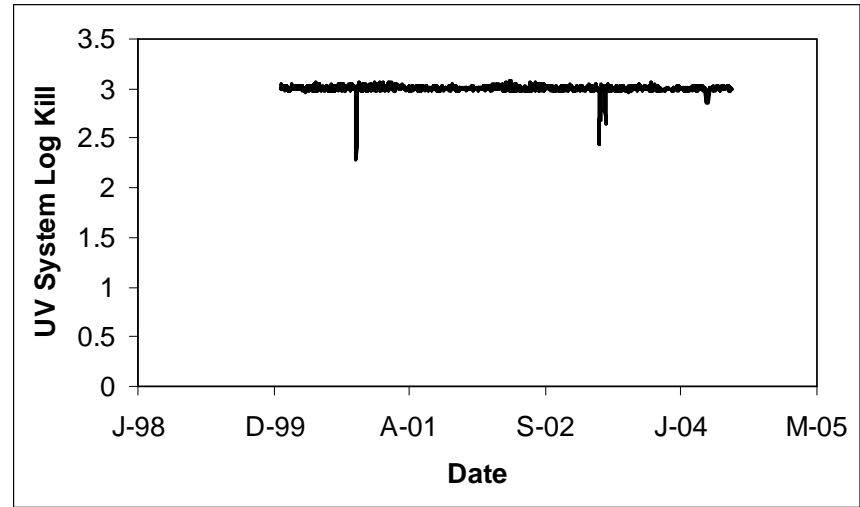
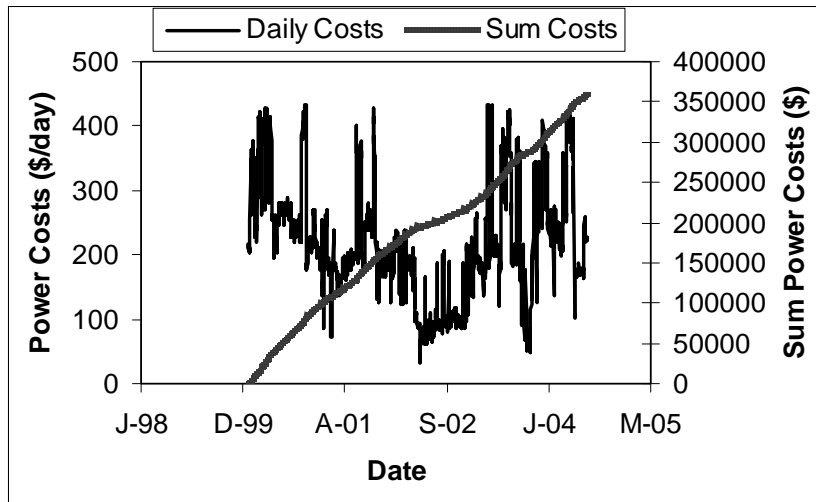


Figure 10.8 (Continued) Case 1/three 2-bank reactors: power costs (top left), UV system log kill (top right), off-specification performance (bottom left), health impact (bottom right)

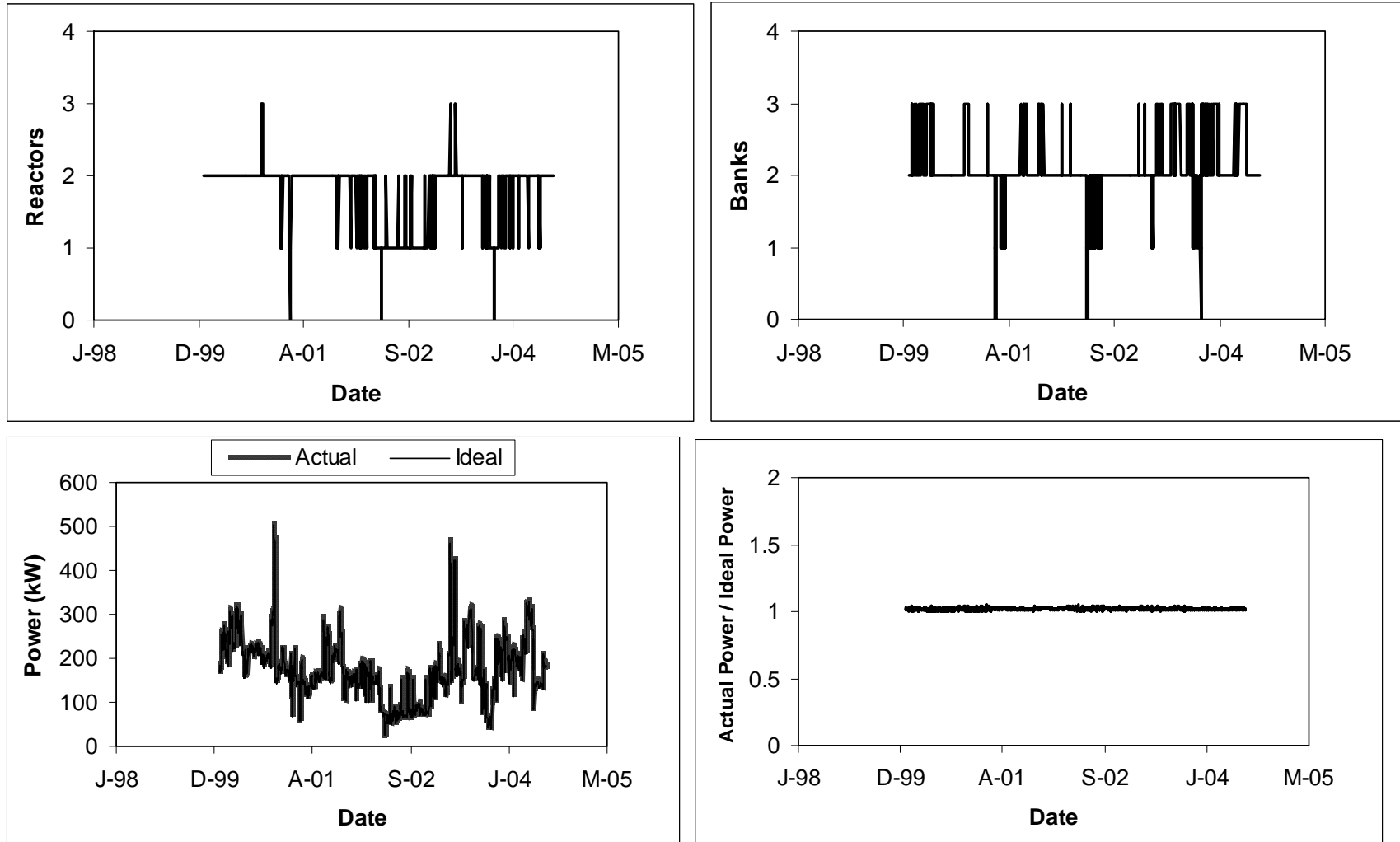


Figure 10.9 Case 1/three 3-bank reactors: reactors on (top left), banks on (top right), power consumption (bottom left), and ratio of ideal-to-actual power (bottom right)

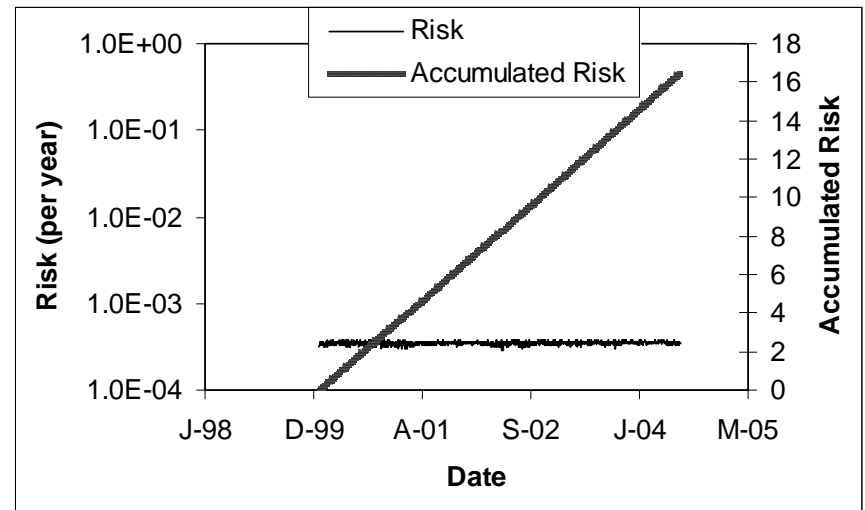
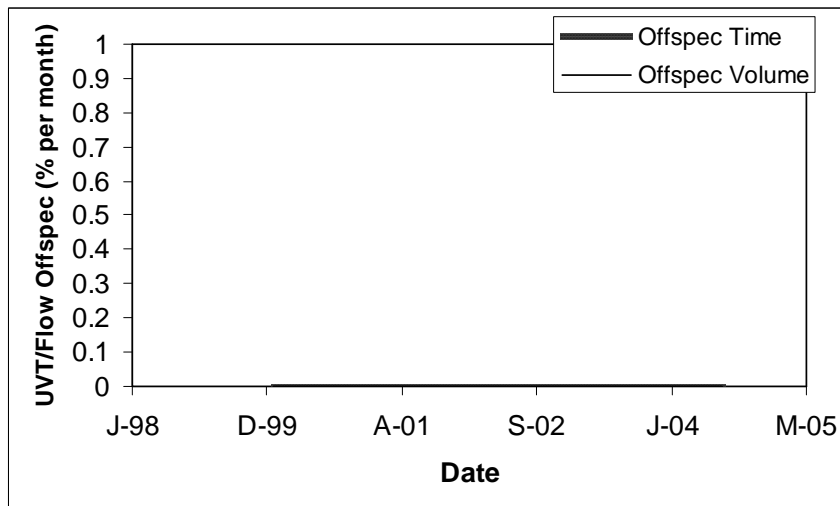
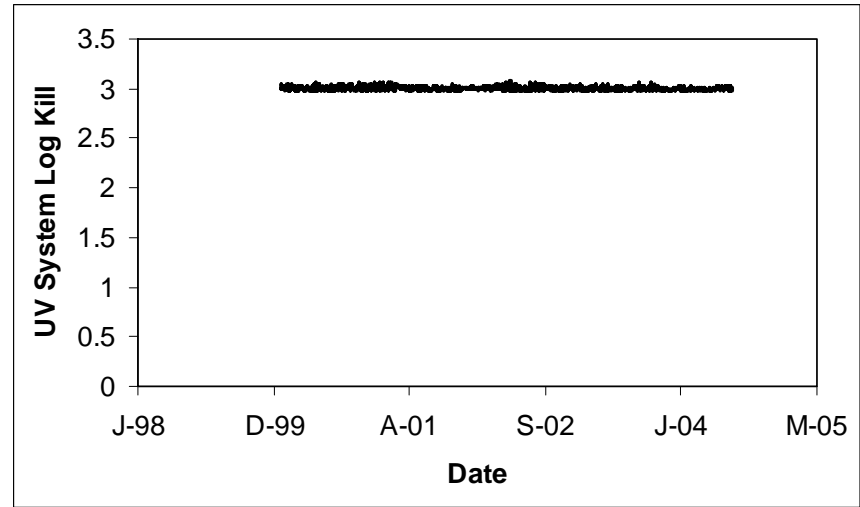
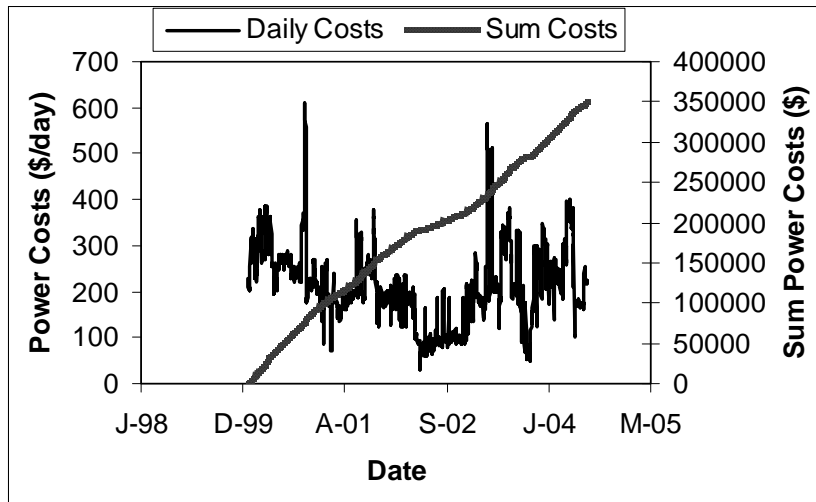


Figure 10.9 (Continued) Case 1/3 3-bank reactors: power costs (top left), UV system log kill (top right), off-specification performance (bottom left), health impact (bottom right)

Case 2. Impact of Ballast Power Settings on Dose Pacing

Case 2 presents an example of using UVCAT to evaluate the impact of ballast power settings on UV dose monitoring and control. The UV system consisted of four reactors in parallel – three duty reactors plus one redundant unit. Each reactor contained one bank of 12-kW lamps. The reactors were operated to deliver a UV dose of 36 mJ/cm², defined as an MS2 RED, for 3-log *Cryptosporidium* inactivation credit. UV dose delivery was modeled using:

$$RED = 10^A \times 8^D \times UVA^{B \times UVA} \times \left(\frac{P/100 \times f_f \times f_L}{Q} \right)^C \quad (10.3)$$

where RED is Reduction Equivalent Dose, UVA is the UV absorbance at 254 nm in cm⁻¹, Q is flow in mgd, and P is the relative power of the lamps in percent, f_L is the lamp aging factor, and f_f is the fouling factor. The model coefficients for Equation 10.3 are given in Table 10.1. Note that while the coefficient “D” was used in Equation 10.2 to define the impact of banks on RED for Case 1, the term “8^D” is used as a constant in Equation 10.3 and should not be interpreted as implying the Case 2 reactor has 8 banks.

Figure 10.10 presents the performance of the UV system equipped with electronic ballasts with power settings that range from 35 to 100 percent at 3-percent increments. The analysis of power consumption over time shows periods when the actual power is significantly greater than the ideal power. The ratio of actual power-to-ideal power over the simulated period had an average value of 1.11. The analysis shows that the reactor overdoses because it does not have sufficient turndown to provide efficient dose pacing with the flow rate and UVT profile used in the model. However, as indicated by the analysis of the log inactivation achieved, the overdosing does provide enhanced disinfection of the water beyond the 3-log target, so public health protection would be enhanced.

Figure 10.11 presents the performance of the UV system equipped with electromagnetic ballasts with power settings of 40, 60, 80, and 100 percent. Again, the analysis of power consumption over time shows periods when the actual power is significantly greater than the ideal power. The ratio of actual-to-ideal power consumption had an average value of 1.29, greater than for the electronic ballasts. The total accumulated power costs with the electromagnetic ballasts were \$183,694, also greater than the total accumulated power costs of the electronic ballasts (\$159,563). The benefit of this greater level of overdosing was a decrease in relative accumulated risk, from 12 to 9, over the simulated period.

Typically, the impact of ballast settings on UV reactor turndown is not considered when determining UV system O&M and life-cycle costs. As shown in this example, power costs are impacted by the range and increments between ballast power settings. Ballasts that provide continuous turndown over a wide range of settings are more energy-efficient and cost-effective in terms of O&M than electromagnetic ballasts with three or four power settings.

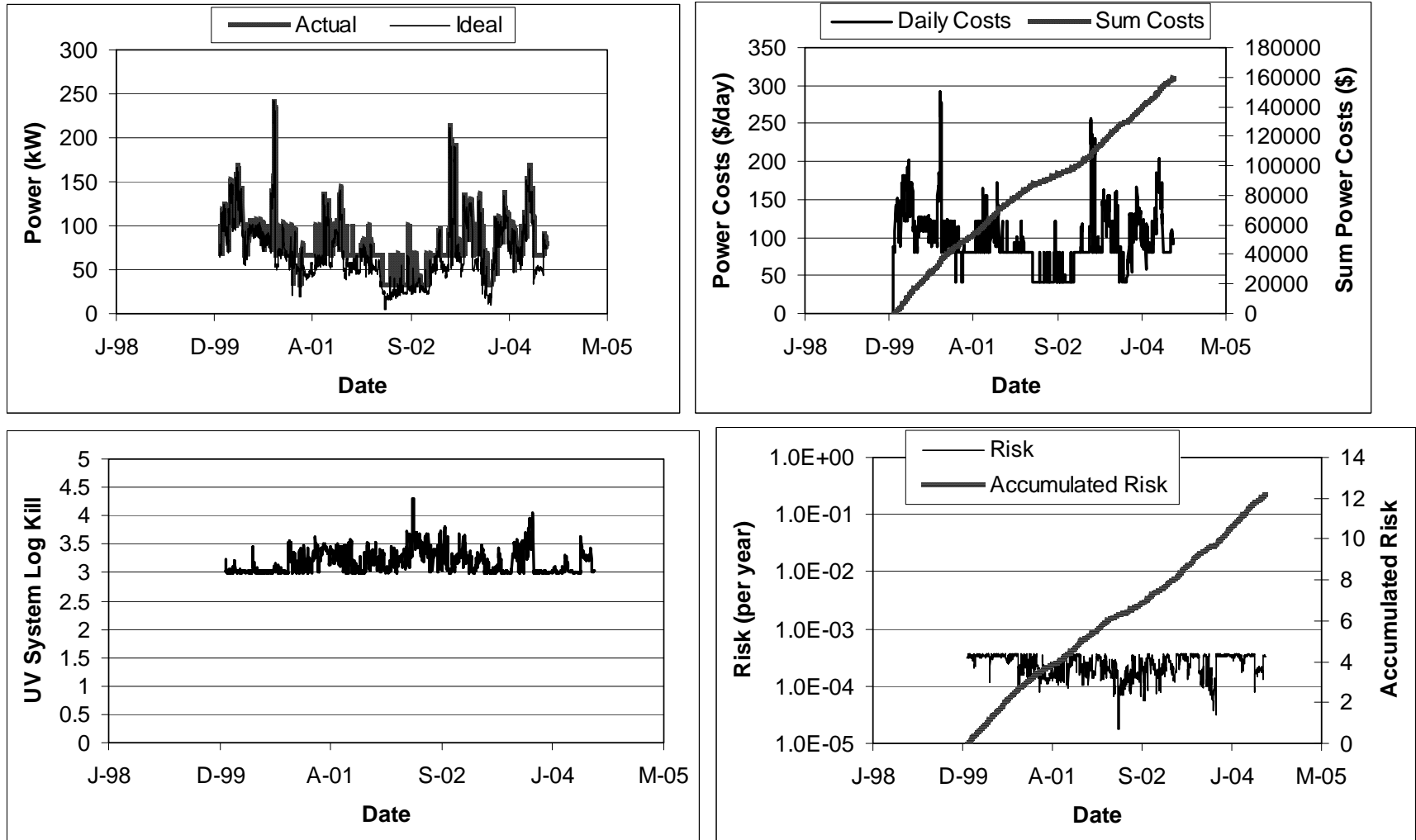


Figure 10.10 Case 2/four-train UV system with electronic ballasts: power consumption (top left), power costs (top right), log inactivation (bottom left), public health protection (bottom right)

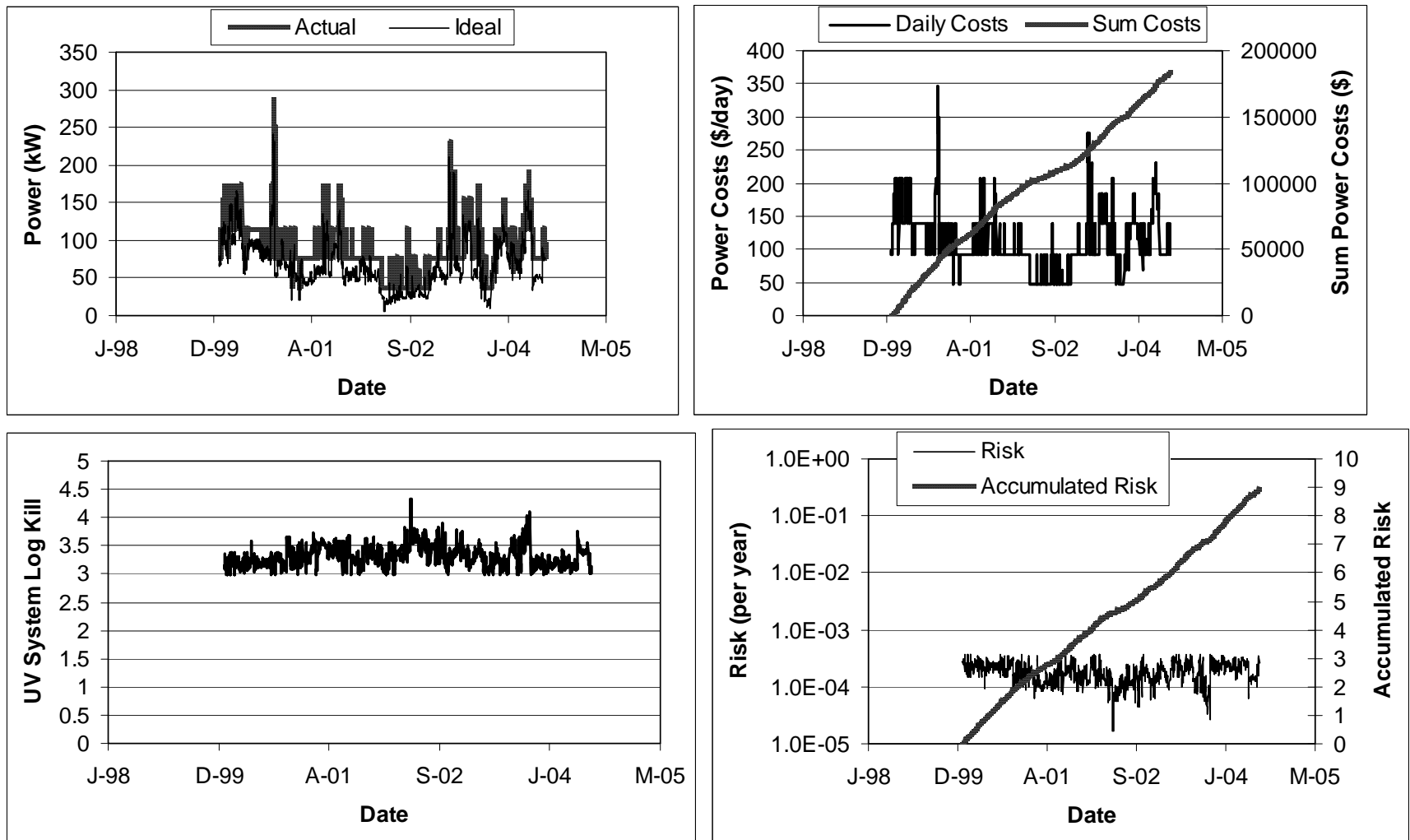


Figure 10.11 Case 2/four-train UV system with electromagnetic ballasts: power consumption (top left), power costs (top right), log inactivation (bottom left), public health protection (bottom right)

Case 3. Comparison of Dose Pacing Options

Case 3 presents an example of using UVCAT to evaluate the impact of dose pacing options on UV system performance, costs, and public health protection. The UV system consisted of four reactors in parallel, three duty reactors plus one redundant reactor. Each reactor contained ten banks of twelve 360-W lamps. The reactors were operated to deliver a UV dose of 36 mJ/cm², defined as an MS2 RED, to earn 3-log *Cryptosporidium* inactivation credit. UV dose delivery was modeled using:

$$RED = 10^A \times UVA^{B \times UVA} \times \left(\frac{S/S_o}{Q} \right)^C \times Banks^D \quad (10.4)$$

where RED is Reduction Equivalent Dose, UVA is the UV absorbance at 254 nm in cm⁻¹, Q is flow rate in mgd, Banks is the number of operating banks, S is the UV sensor reading in W/m², and S_o is the UV sensor readings that would occur with new lamps operating at 100 percent ballast power in clean quartz sleeves. The sensor reading, S was simulated using:

$$S = 10^a \times \exp(b \times UVT) \times \frac{P}{100} \times f_L \times f_f \quad (10.5)$$

where UVT is the UV transmittance of the water in %, P is the relative power of the lamps in %, f_L is the lamp aging factor, and f_f is the fouling factor. The value for S_o was obtained from Equation 10.2 by setting P equal to 100%, f_L to 1.0, and f_f to 1.0. The model coefficients for Equation 10.4 and 10.5 (Table 10.2) were obtained from a CFD simulation of a hypothetical reactor.

Table 10.2
Model coefficients for Equations 10.4 and 10.5

Model coefficients for Case 1	Value
A	2.4987
B	9.1999
C	0.78214
D	0.94867
a	-1.3829
b	0.056732

The UVCAT analysis evaluated the following dose-pacing strategies:

- No dose pacing - UV system operates with all lamps on all the time to deliver the design UV dose assuming flow, UVT, and relative lamp output are at design conditions
- Flow pacing - dose pacing only responds to changes in flow rate

- Flow and UVT dose pacing - dose pacing responds to changes in flow rate and UVT, but not UV sensor readings, worst-case lamp aging and fouling assumed
- Full dose pacing - dose pacing that responds to changes in flow rate, UVT, and UV sensor measurements

Figures 10.12 and 10.13 shows the number of reactors and banks of lamps operating with the four dose pacing options. Figure 10.14 shows the daily and accumulated power costs. Figures 10.15, 10.16, and 10.17 show the off spec performance, *Cryptosporidium* log inactivation, and associated public health protection, respectively.

With no dose pacing, except for when UVT fell below the validated range, all duty reactors and banks of lamps operate at a power setting that delivers the required UV dose assuming design conditions of flow, UVT, and relative lamp output. When UVT fell below the validated range used in the simulation, UVCAT assumed the UV system would operate with all available duty and redundant UV reactors on at 100 percent power. Because all lamps in the duty UV reactors were on at constant power, the power consumption and daily power costs were constant with time, except for no flow and off-specification periods. Because the UV system was overdosing, *Cryptosporidium* log inactivation significantly exceeded the 3-log target, resulting in enhanced public health protection.

With flow pacing, the UV system turns on and off reactors and lamps and adjusts lamp power as flow changes. However, the number of lamps and their power setting assumes UVT and relative lamp output are set to design values. As expected, the profile of power consumption and costs over time reflects the flow rate profile. UVCAT also predicted greater off-specification performance with the flow-pacing case compared to the no dose pacing case. The greater off-specification performance occurred because the water UVT fell below the design UVT value used as an input to the dose pacing strategy. Because the design UVT was higher than the actual UVT, the UV system operated with only nine banks of lamps and underdosed. If the reactor had operated with all ten banks on, the UV system would have delivered the required UV dose.

These results with flow pacing highlight the issues that can occur when the UVT falls below the default value used in the dose-monitoring algorithm. However, while off-specification performance associated with the low UV dose delivery was significant, the reactor still achieved greater than 2.5-log *Cryptosporidium* inactivation during those off-spec periods. Because flow pacing reduced overdosing, the accumulated public health protection was two times less than the case with no dose pacing. This comparison highlights the trade-off between costs and risk that can occur when different dose pacing strategies are compared.

With flow and UVT pacing, the UV system turns on and off reactors and lamps and adjusts lamp power as flow and UVT change but assumes the relative lamp output is set to the design value. With this case, the profile of power consumption and power costs over time reflects the combined impact of the flow rate and UVT profiles. Unlike the flow pacing case, UVCAT predicted the same off-specification performance as the no dose pacing case. Because UVCAT simulated flow and UVT pacing based on the UVT profile, as opposed to the design UVT value, the algorithm turned on the required number of banks when the UVT fell below the design value. With the flow and UVT pacing algorithm, *Cryptosporidium* log inactivation was always equal to or greater than the target, 3-log. However, because the degree of overdosing was less over time, the public health protection with flow and UVT dose pacing was not as great as with no dose pacing and flow pacing.

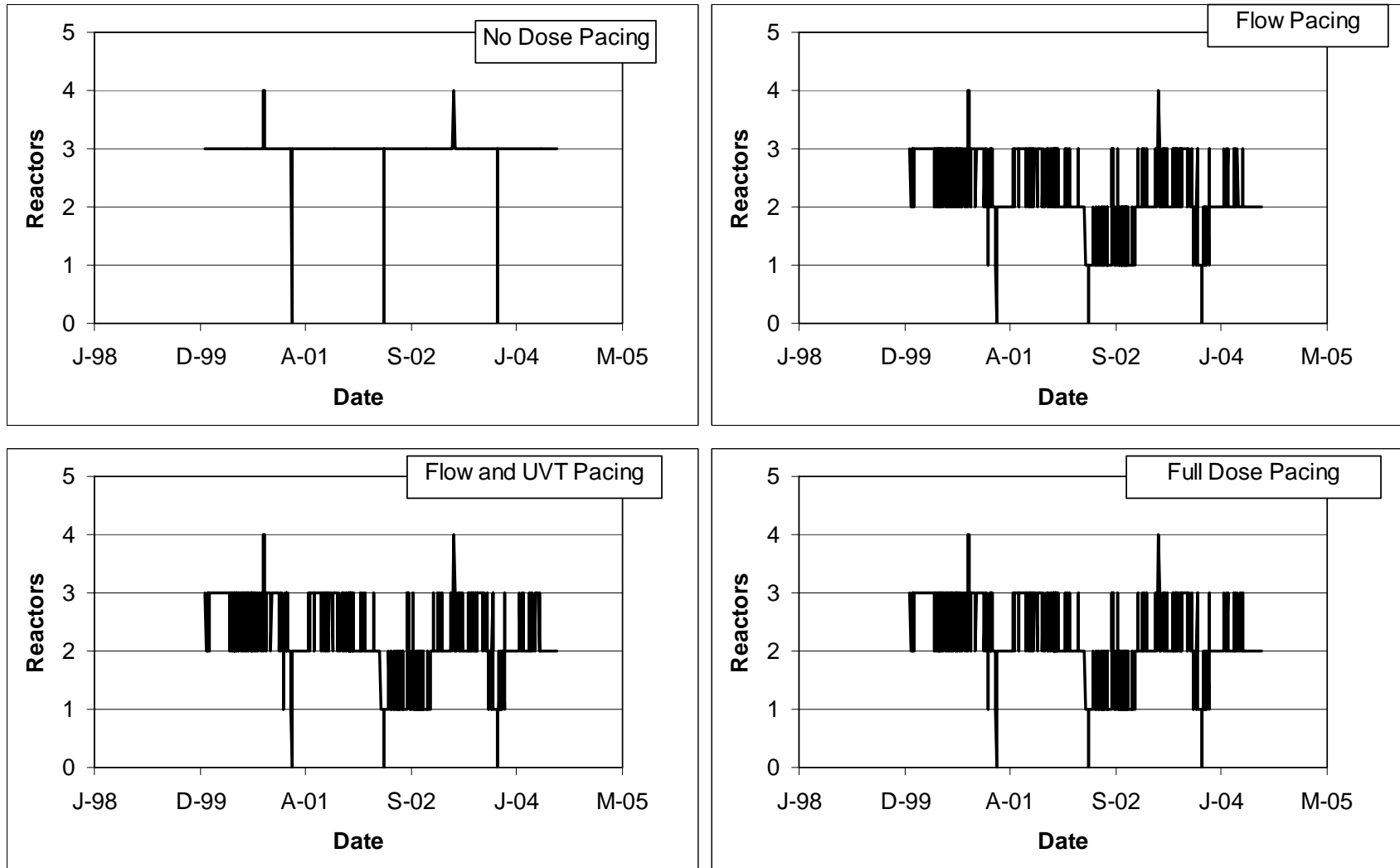


Figure 10.12 Case 3 reactors operating over time with no dose pacing (top left), flow pacing (top right), flow and UVT pacing (bottom left), and full dose pacing (bottom right)

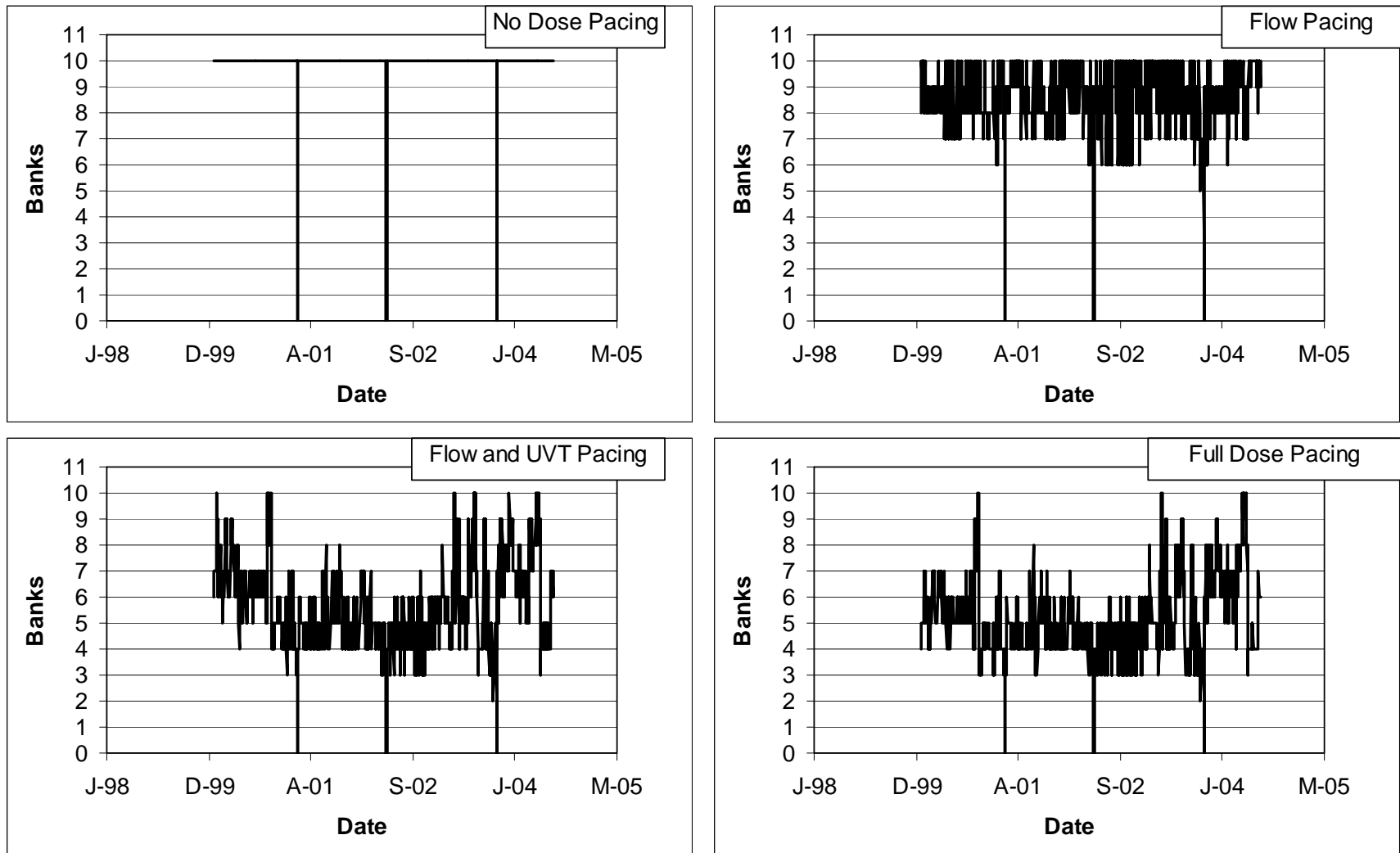


Figure 10.13 Case 3 banks operating over time with no dose pacing (top left), flow pacing (top right), flow and UVT pacing (bottom left), and full dose pacing (bottom right)

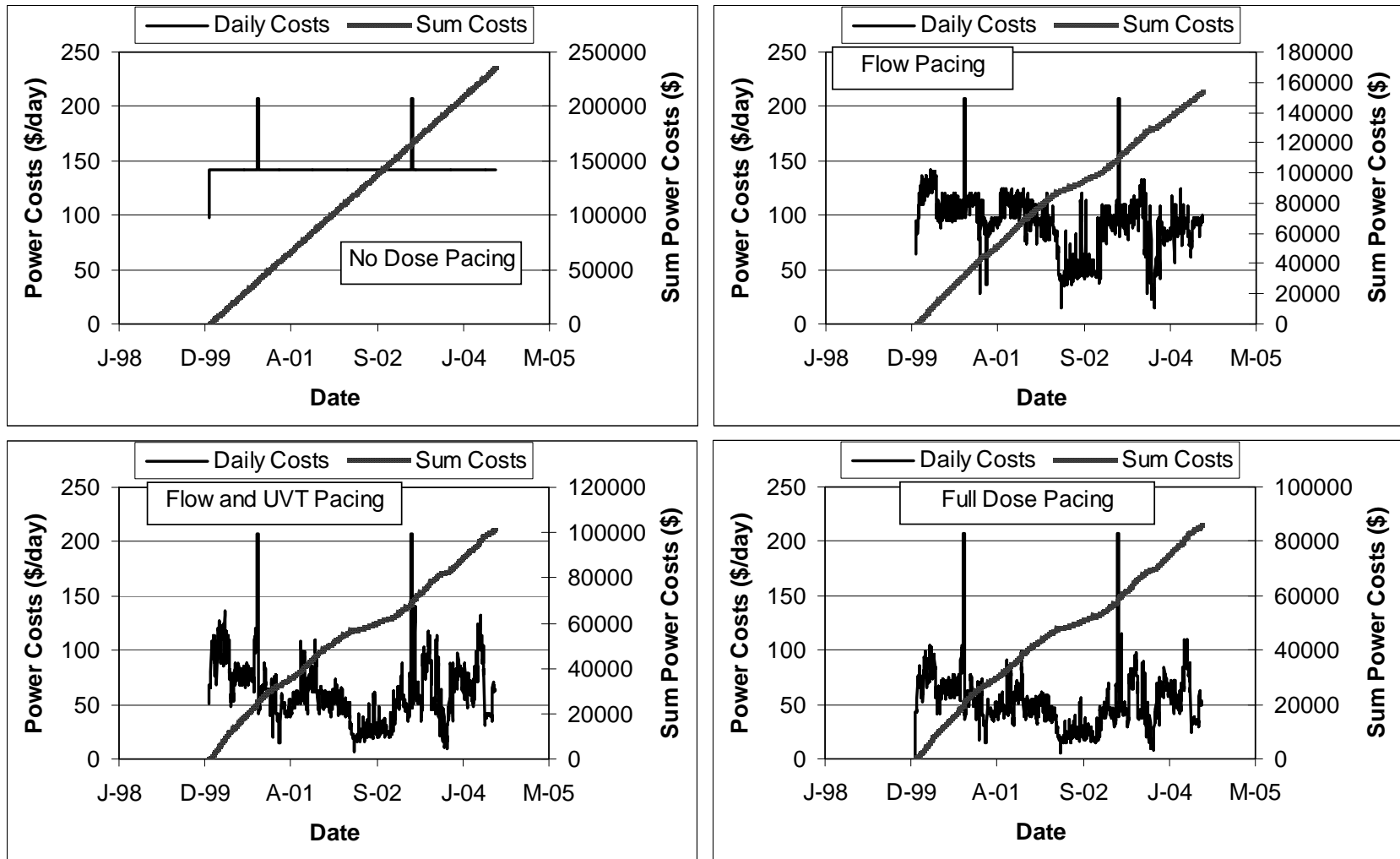


Figure 10.14 Case 3 power costs with no dose pacing (top left), flow pacing (top right), flow and UVT pacing (bottom left), and full dose pacing (bottom right)

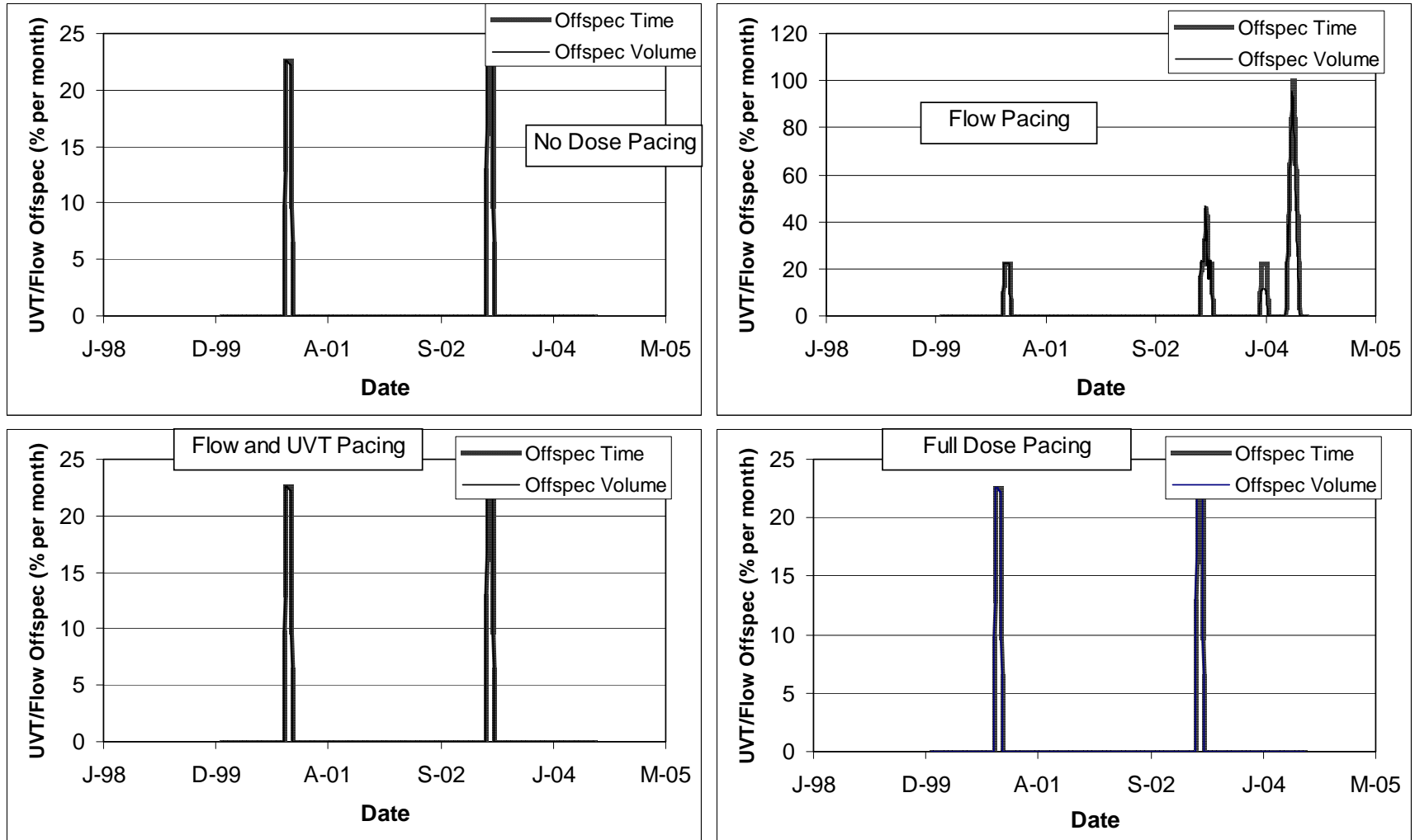


Figure 10.15 Case 3 off spec performance with no dose pacing (top left), flow pacing (top right), flow and UVT pacing (bottom left), and full dose pacing (bottom right)

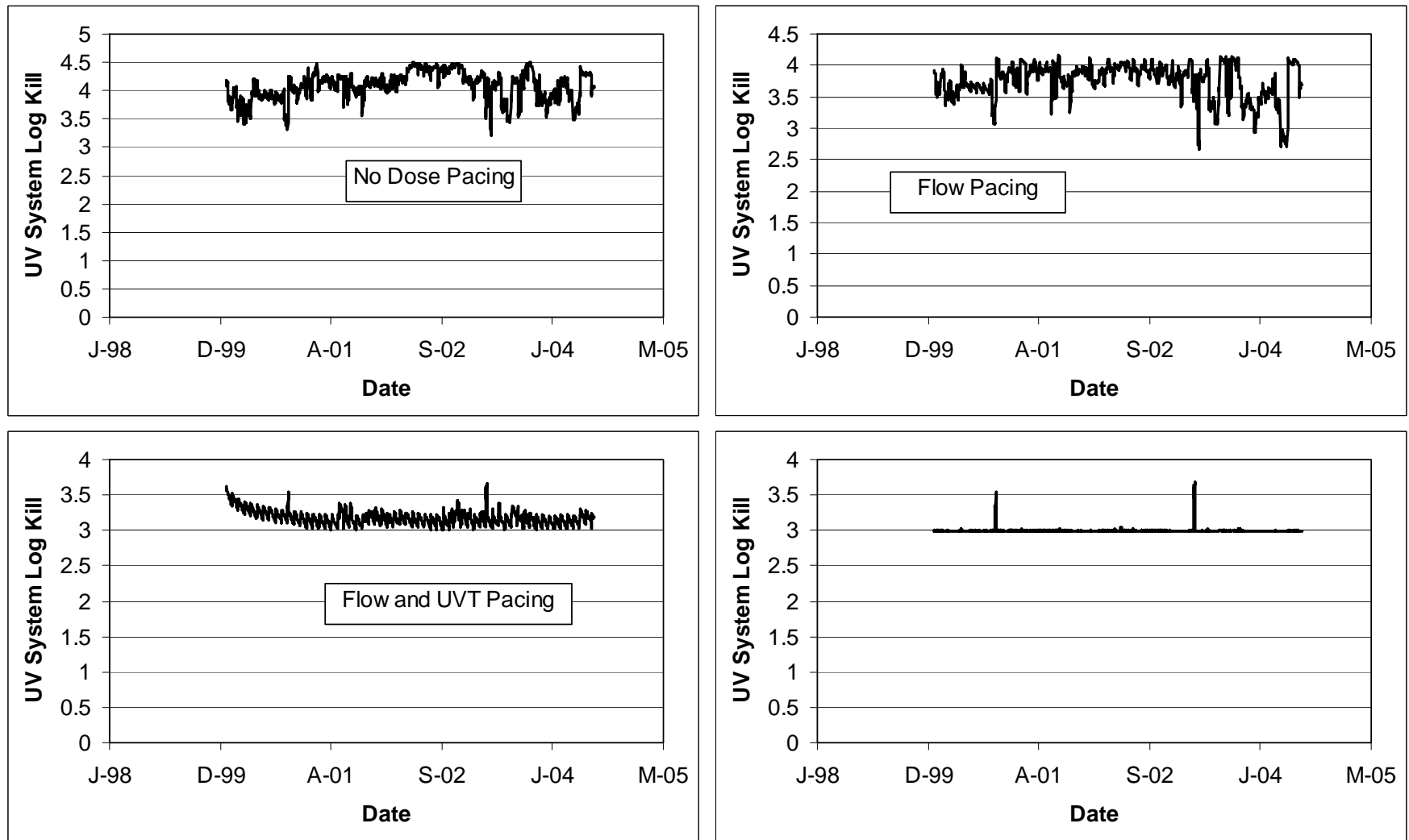


Figure 10.16 Case 3 *Cryptosporidium* inactivation with no dose pacing (top left), flow pacing (top right), flow and UVT pacing (bottom left), and full dose pacing (bottom right)

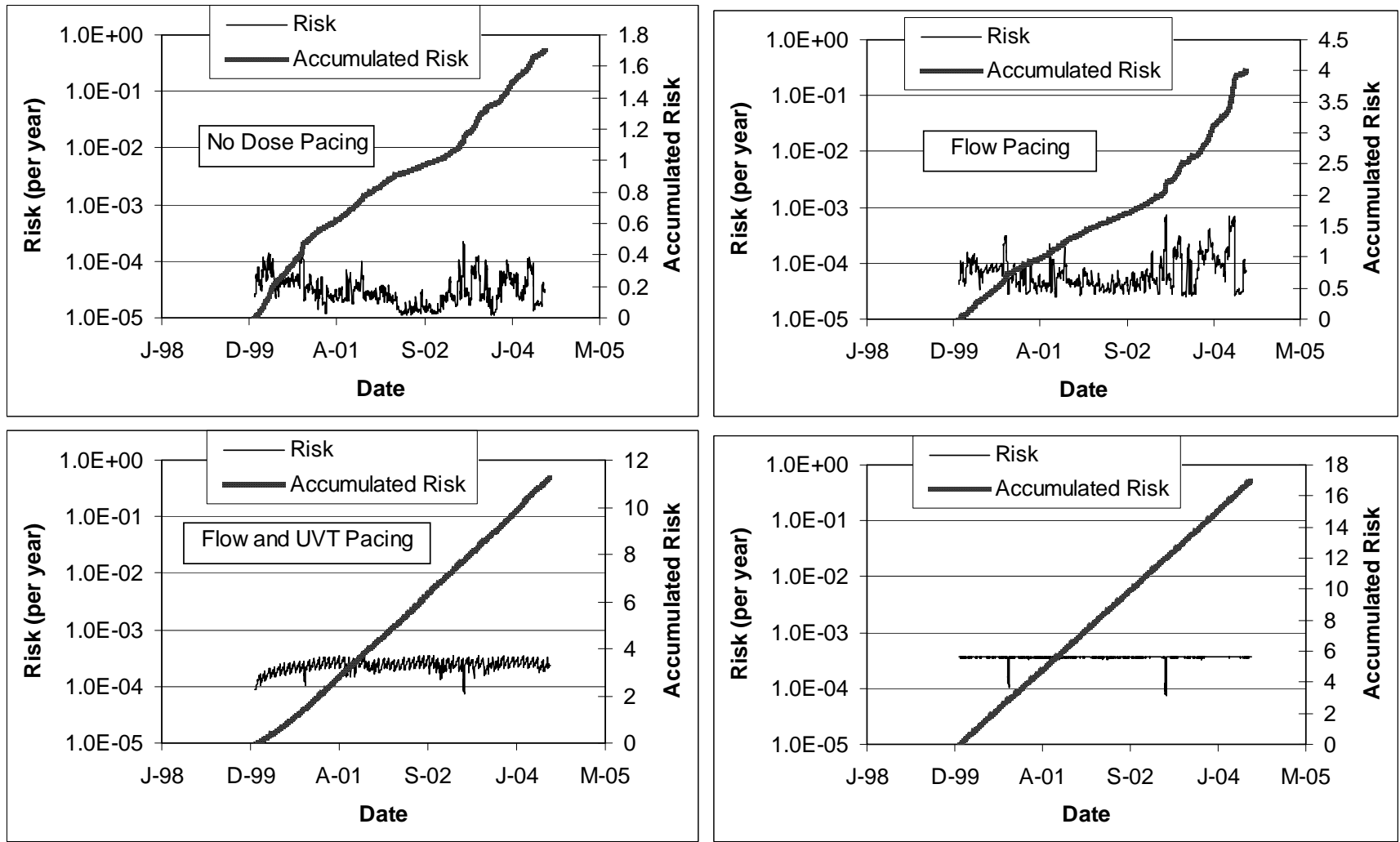


Figure 10.17 Case 3 public health protection with no dose pacing (top left), flow pacing (top right), flow and UVT pacing (bottom left), and full dose pacing (bottom right)

With full dose pacing, the UV system turns on and off reactors and lamps and adjusts lamp power as flow, UVT, and relative lamp output changes. The power consumption and cost profiles reflect the combined impact of flow rate, UVT, and lamp aging and fouling. Again, UVCAT predicts two off-specification periods that occur when UVT is below the lower limit of the validated range used in the simulation. With the full dose-pacing algorithm, *Cryptosporidium* log inactivation equaled but did not significantly exceed the 3-log target. As such, the public health protection was less than with the other dose pacing strategies.

Table 10.3 summarizes the power and UV O&M costs and public health risk with each of the four above-mentioned dose-pacing options. The results indicate that dose pacing can significantly reduce O&M costs. Compared to the case of no dose pacing, flow pacing reduced O&M costs by 36 percent, flow and UVT pacing reduced O&M costs by 60 percent, and full dose pacing reduced the O&M costs by 65 percent. However, dose pacing does reduce the level of public health protection provided by UV disinfection. Compared to the case of no dose pacing, flow pacing increased the overall public health risk 2.8-fold, flow and UVT pacing increased public health risk 6.8-fold, and full dose pacing increased public health risk 10-fold. Arguably, if the UV system delivers the required UV dose required to meet an approved public health objective, the increase in public health risk caused by implementing dose pacing is acceptable.

Case 4. Impact of Lamp Configuration on Dose Pacing

Case 4 presents an example of using UVCAT to evaluate the impact of the lamp configuration on UV system performance. This example compares two 4-reactor UV systems. The first UV system has the lamps in each reactor configured as 10 banks of 12 lamps, which is the Case 3/full dose-pacing scenario. The second UV system has each reactor configured with one bank of 120 lamps. Like the first UV system, the second uses full dose pacing and is operated to deliver a UV dose of 36 mJ/cm², defined as an MS2 RED, to achieve 3-log *Cryptosporidium* inactivation. UV dose delivery by the second UV system was modeled using:

Table 10.3
Comparison of O&M costs and public health risk with different dose pacing strategies

Dose pacing	None	Flow rate	Flow rate & UVT	Flow rate, UVT, lamp aging and fouling
Power (\$/yr)	\$51.7k	\$33.8k	\$22.3k	\$18.9k
O&M (\$/yr) (no patent)	\$126k	\$83.9k	\$58.6k	\$52.3k
Present worth O&M (15 yrs, 4%)	\$1,401k	\$933k	\$652k	\$582
Public health risk	0.37	0.88	2.5	3.8

$$\text{RED} = 10^A \times \text{UVA}^{B \times \text{UVA}} \times \left(\frac{S/S_o}{Q} \right)^C \times 10^D \quad (10.6)$$

where RED is Reduction Equivalent Dose, UVA is the UV absorbance at 254 nm in cm^{-1} , Q is flow in mgd, S is the UV sensor reading in W/m^2 , and S_o is the UV sensor readings that would occur with new lamps operating at 100 percent ballast power in clean quartz sleeves. The sensor reading, S was simulated using Equation 10.5. The model coefficients for Equation 10.4 were obtained from Table 10.3.

Figure 10.18 presents the performance of the one-bank UV system. The average ratio of actual-to-ideal power is 1.18, indicating the reactors were overdosing. The overdosing occurred because the turndown of the 1-bank reactors were limited to the existing range of ballast power settings. In comparison, the 10-bank reactor had an average actual-to-ideal power ratio of 1.01, indicating efficient dose pacing.

While dose pacing with the 1-bank UV system was less efficient than the 10-bank system, the annual power costs of the one-bank system were \$18,200/year, similar to the power costs of the 10-bank system (see Table 10.2). Power costs were similar because the 1-bank reactor typically operated with 269 lamps at a power setting of 43 percent ($269 \times 0.43 = 116$), while the 10-bank reactor typically operated with 139 lamps on at 86 percent power ($139 \times 0.86 = 120$). Because the coefficient d in Equations 10.4 and 10.6 is greater than 1.0, the reactors are more efficient at delivering dose with more lamps operating. Hence, the inefficiency of the dose-control strategy with the 1-bank reactor was offset by the increased efficiency of dose delivery (UV dose delivered per unit power). While power costs were similar with both systems, lamp replacement costs were twice as high with the one-bank reactors. Total O&M costs and present worth costs with the 1-bank system were \$69,600/year and \$773,000, respectively, notably higher than the 10-bank system (see Table 10.3). Public health risk with the 1-bank reactor was 2.8, slightly better than with the 10-bank system, reflecting the overdosing by the 1-bank reactor.

CONCLUSIONS AND RECOMMENDATIONS

The following conclusions and recommendations are made from this work:

- Dose pacing can provide significant cost benefits both in terms of power savings and component replacement. However, UV vendors offer different dose-pacing strategies.

UV systems used in wastewater applications typically do not use full dose pacing. Dose pacing is often not used if there are concerns about UV system reliability and indicator microbe inactivation. Flow pacing is commonly considered when engineers assess the life-cycle costs. Flow and UVT pacing is not very common, primarily because UVT monitors have a history of poor reliability. Full dose pacing would require a monitoring system that uses the measured UV intensity. This typically has not been done with wastewater UV systems. The UV intensity

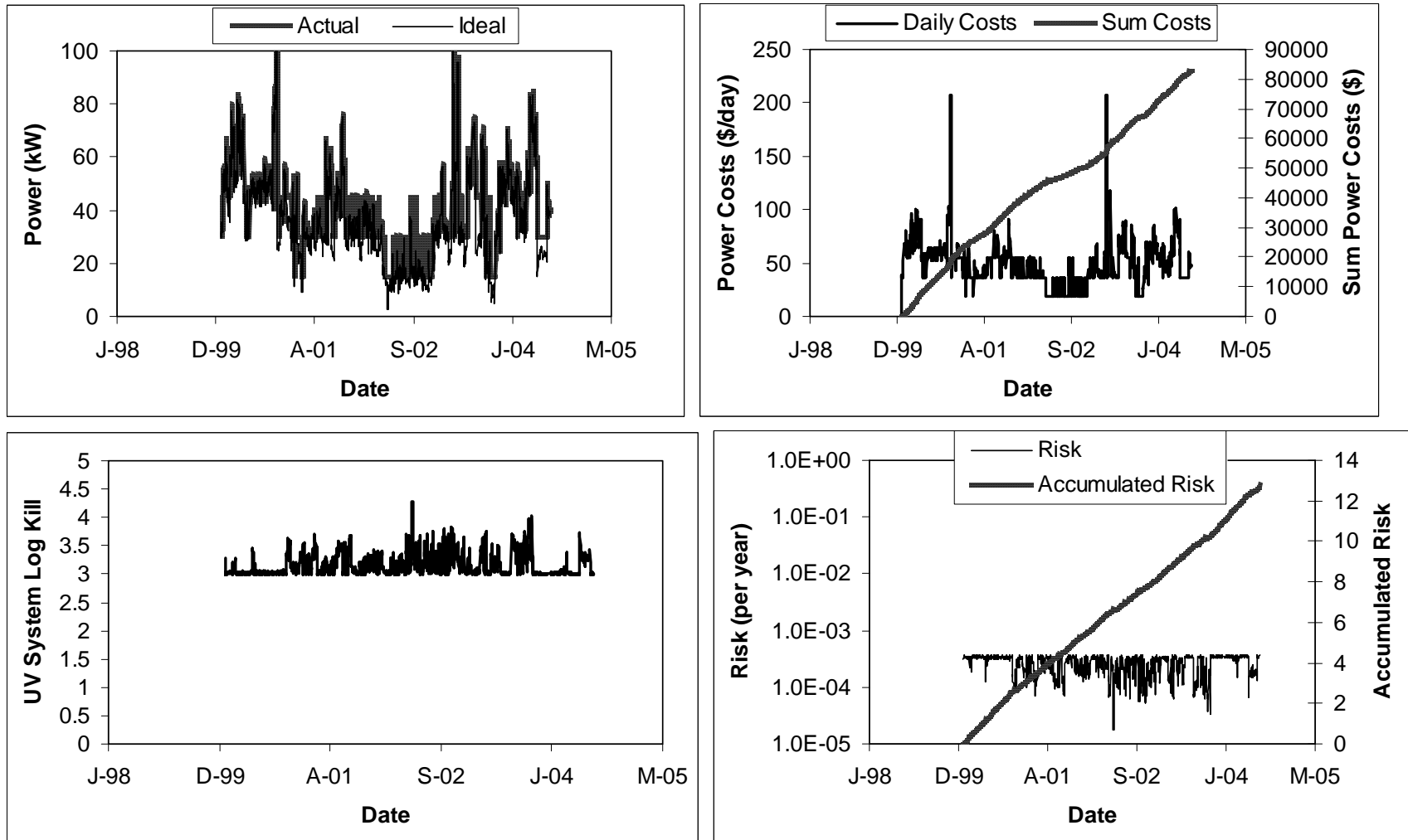


Figure 10.18 Case 4/1-bank UV system with full dose pacing: power consumption (top left), power costs (top right), UV system log kill (bottom left), health impact (bottom right)

setpoint approach might be the best approach of implementing full dose pacing because a UVT monitor would not be required.

With drinking water systems, regulations require that UV systems monitor flow rate, UV intensity, and if used in the dose-pacing strategy, UVT. While drinking water systems are capable of full dose pacing, some UV systems have not undergone validation testing that would enable its implementation. For example, many drinking water UV systems using the UV intensity setpoint approach are only validated at peak flow rate, thus, the control system cannot respond to changes in flow rate. As another example, with some UV systems, validation data is only obtained with a lamp power setting set to the product of the lamp aging and fouling factor used to size the UV system. Hence, the dose monitoring strategy must use a fixed value of S/S_0 equal to the design lamp output as a setpoint. In summary, while drinking water UV systems have the potential for full dose pacing because they monitor flow rate, UV intensity, and UVT, the lack of validation data may limit how dose pacing can be applied.

- UV systems using lamps oriented perpendicular to flow and configured as multiple banks of lamps in series will provide better dose pacing than UV reactors using lamps oriented parallel to flow and configured as one bank of lamps.

This is an issue both in drinking water and wastewater UV applications and should be considered when evaluating and selecting UV equipment for a given application. Another advantage of multiple banks in series is that the effective aging factor during operation of the UV system will be lower than the aging factor typically used to size the UV system provided banks of lamps are replaced as they reach their end-of-lamp-life and are not operated to provide uniform lamp aging with all banks. Thus, if a UV lamp has an aging factor of 85 percent after 5,000 hours, a 1- bank reactor should be sized using a lamp aging factor of 85 percent, while a multi-bank reactor should be sized using a higher value. UVCAT can be used to assess what that aging factor should be.

- The ballast settings used by UV reactors varies significantly both in drinking water and wastewater applications.

While some system use ballasts that only operate at 100 percent, others use ballast that operate at three or four different settings, and other provide continuous or near-continuous turndown. The power consumption of a UV system will be lower if dose pacing uses ballasts capable of continuous turndown. Currently, the increment between ballast power settings is typically not considered when determining the life-cycle costs of UV systems.

- The variability in flow rate and UVT has a large impact on the relative costs and benefits of the various dose-pacing strategies.

The variability in flow rate and UVT will be site specific with both drinking water and wastewater applications, the temporal variations in these parameters should be characterized early in the design process.

- The cost benefits of dose pacing are offset by an increase in public health risk. Utilities should consider the tradeoffs between cost and risk when assessing UV system operation alternatives.

CHAPTER 11

PEAK LOAD REDUCTION

In this chapter, peak load reduction during UV system operation is evaluated. Specific objectives of this analysis were to:

- Obtain industry data on energy pricing structures for New York State
- Investigate peak load reduction strategies for UV disinfection systems and recommend approaches to reduce energy costs at drinking water and wastewater utilities.

NEW YORK STATE ENERGY PRICING STRUCTURES

Energy deregulation in the State of New York began in the mid-1990s. This deregulation has allowed users to ‘shop around for electricity’; finding the energy supplier who best meets their needs at the most competitive prices.

In general, there are two approaches in energy rate structures - fixed rate and variable rate. With a fixed-rate structure, the cost of electricity includes a fixed rate for delivery and supply, which is agreed upon for a specified time, and a fixed rate for the cost of electricity, which would typically vary month-to-month based upon the electricity market price from the previous month. With a fixed rate pricing structure, the user’s electricity cost does not vary with on- and off-peak hour use.

With a variable-rate structure, the price of electricity fluctuates with the electricity demand. Price can vary seasonally, with higher prices in the summer and lower prices in the winter, or vary with the time-of-day, with higher prices during the day and lower during the night. If energy is primarily purchased during off-peak hours, a variable-rate structure can provide significant cost savings.

With both rate structures, the user incurs two basic charges: delivery and supply. The delivery charge is the charge the user incurs for utilizing power lines and infrastructure to the user’s site. This charge decreases when the required infrastructure decreases. The delivery charge can be subdivided into additional categories that may include a delivery service for the peak demand (*i.e.*, demand charge), power inefficiencies, purchase power adjustments, various credits, system benefits charges, and other miscellaneous energy delivery charges. The peak demand charge is based upon the user’s peak demand for energy. If the demand charge is based on energy use during on-peak hours, a user will significantly reduce their peak demand charge if their peak demand for energy occurs during off-peak hours.

The other basic charge that the user incurs is the supply charge, the charge for the total power used in a billing cycle. The supply charge rate may be fixed or variable, depending on the options available from the electric company. If the user is on a fixed-rate system, the supply charge is calculated as the total kilowatt-hours used during the billing cycle multiplied by a specified rate. If the user is on a variable-rate system, the supply charge is calculated using multiple rates, *e.g.*, different charges for on-peak and off-peak hours. In that situation, the user will significantly reduce power costs by using electricity during off-peak hours. In some instances the cost for electricity during on-peak hours may be twice that of off-peak hours.

Table 11.1
Example of New York State energy price structures

Price Structure	Period	Delivery charge (fixed) (¢/kWhr)	Supply charge (Varies daily) (¢/kWhr)	Transition charge (varies monthly) (¢/kWhr)	Total charge (¢/kWhr)
Non-residential regular	24 hrs	5.00	5.10	2.05	12.15
Non-residential day/night	Day	5.85	5.38	2.05	13.28
	Night	1.00	3.46	2.05	6.51

Source: <http://ebiz1.nyseg.com>

Table 11.1 presents examples of New York State power rates. These rates were used for the peak load reduction case study presented in the next section.

PEAK LOAD REDUCTION STRATEGIES FOR UV DISINFECTION

Many drinking water and wastewater utility managers across the U.S. are aware that they can reduce energy costs at their facilities using time-of-use or peak-load shaving strategies. Approaches for saving energy costs include:

- Using stand-by generators during peak electrical demand by the plant
- Using distribution system storage for supply during peak demand and turning down or turning off energy-intensive unit operations such as pumping
- Restricting water consumption practices like irrigation to reduce peak demand.

Factors impacting the use of off-site storage include:

- How much storage is available and how much is needed for emergency supply, fire supply, and peak demand
- Cost of adding new storage facilities.
- Impact of storage on water quality. Water cannot remain stagnant in the reservoir.

Many small utilities (10-mgd or less) operate during the day but not at night for operator convenience. Some utilities are uncomfortable if storage reservoirs are not kept filled to near capacity. For these and other similar reasons, politics, and not economics, often dictate whether a utility changes its water production patterns to take advantage of off-peak energy costs.

Because utilities are already evaluating peak load reduction strategies using the above-mentioned methods and implementing them when they are justified, this chapter focuses on identifying approaches for peak load reduction that would be unique to UV disinfection and new to the drinking water and wastewater treatment industry. A unique aspect of UV disinfection is the occasional need to use Uninterruptable Power Supplies (UPS systems). UV disinfection systems are sensitive to poor power quality such as voltage sags and cycle losses. UPS systems are used to provide constant power to the UV system, thereby ensuring continuous disinfection. Typical costs for UPS systems range from \$500 to 1,000/kW of capacity.

UPS systems could be used for peak load shaving. In particular, a new battery technology recently commercialized in Japan has been successfully used at wastewater treatment plants for reducing energy costs through peak load shaving.

NAS Battery Energy Storage Systems

A NAS Battery is a sodium-sulfur battery developed jointly by NGK Insulators, Ltd. (NGK) of Tokyo, Japan and the Tokyo Electrical Power Company. The sodium-sulfur battery stores energy more efficiently than lead batteries. It has been used in demonstration and pre-commercial projects for 10 years, and was made commercially available in April 2002. At the time of publication, a total of 88 projects had been installed, approximately 23 percent of which were at water and wastewater treatment plants. More recently, NGK has expanded operations by building a new commercial-scale manufacturing plant for the NAS battery.

The NAS battery can be used in three ways: 1) load leveling (LL) and peak shaving (PS), 2) emergency power supply (EPS), and 3) UPS. Load leveling and peak shaving take advantage of the on-peak and off-peak electric power demand. During off-peak hours the battery is charged using power purchased at a lower rate. During on-peak hours the battery is discharged to provide peak shaving, reducing the user's peak energy demand. Because the NAS battery has an efficiency of 75 percent, eight hours of peak shaving requires ten hours of charge time.

Storing energy at night and discharging energy during the day reduces costs in two ways. First, the utility can purchase power at a significantly reduced rate at night. Second, using the batteries during the day reduces the peak energy demand of the user. The peak demand is typically the maximum amount of energy in a billing cycle a user draws from the system during any 15-minute period. The 15-minute period is typically based upon the on-peak hours, but is company specific and should be researched before any assumptions are made. Utilizing the battery as a peak shaving method effectively reduces the peak demand of the utility, ultimately reducing the billed demand charges incurred by the user.

The remaining two uses of the NAS battery are EPS and UPS. Both of these are considered power quality issues. High power quality is essential for UV systems installed at water and wastewater treatment plants. Currently, it is becoming standard practice to install UPS systems for utilities to ensure that during a system outage, power is uninterrupted for the time necessary to make the required transitions to back-up power to prevent health and safety issues.

Overall, the NAS battery design is tailored to each individual application. To take full advantage of the NAS battery, the user needs to understand their power demands and energy pricing structures in detail. The NAS battery design can be optimized to provide a combination of UPS, emergency power supply, and peak shaving.

Peak Load Reduction Case Studies

Table 11.2 provides a cost benefit analysis of the NAS battery systems for five cases. The analysis assumed a 100-kW UV system. Case 1 represents a utility that pays a fixed rate throughout the day and uses a 5-minute UPS system. Case 2 represents a utility that pays different day and night time rates and uses a 5-minute UPS system. Cases 3 to 5 represent utilities paying different day and night time rates and use NAS systems during the day to power the UV system and using line power during the night to power the UV system and charge the NAS battery. The analysis in Case 3 uses current capital costs for the NAS batteries. The

analyses in Case 4 and 5 use NAS battery prices expected four and six years in the future, respectively, with the technology's efficiency improving over time. Power rates used in this analysis were taken from Table 11.1.

The analysis indicates that the NAS battery system has potential for providing a cost-effective alternative power supply for UV systems, especially if battery capital costs drop in the future due to more efficient production. The benefits of peak shaving were not considered here.

Table 11.2
Cost analysis comparing the NaS battery system to conventional
UPS for a 100 kW power consumption

		Case 1	Case 2	Case 3	Case 4	Case 5
Battery system	-	UPS	UPS	NAS	NAS	NAS
Electrical power						
Peak power	kW	100	100	100	100	100
Power use	hrs.	12	12	0	0	0
- Day						
- Night	hrs.	12	12	24	24	24
Energy cost	\$/kW-hr	0.1215	0.1328	0.1328	0.1328	0.1328
- Day						
- Night	\$/kW-hr	0.1215	0.0651	0.0651	0.0651	0.0651
Power costs	\$/yr	106,434	86,680	57,028	57,028	57,028
Period	yrs.	15	15	15	15	15
Interest	%	6	6	6	6	6
NPV	\$	\$1,534,419	\$1,249,636	\$822,146	\$822,146	\$822,146
UPS						
UPS period	min.	5	5	-	-	-
Electronics	\$/kW	300	300	-	-	-
Battery	\$/kW-hr	180	180	-	-	-
Total capital	\$	\$31,500	\$31,500	-	-	-
Battery replacement	\$/5 yrs.	180	180	-	-	-
Battery O&M	\$/kW-yr	15	15	-	-	-
Total NPV O&M	\$	\$8,650	\$8,650	-	-	-

(continued)

Table 11.2 (cont.)
Cost analysis comparing the NaS battery system to conventional
UPS for a 100 kW power consumption

		Case 1	Case 2	Case 3	Case 4	Case 5
NAS battery						
UPS period	hrs.	-	-	12	12	12
Modules		-	-	5.22	5.22	5.22
Module capital	\$/module	-	-	94,500	75,000	55,000
Power conversion system	\$/kW	-	-	280	280	280
End user balance of plant	\$/kW	-	-	100	100	100
Total capital	\$	-	-	\$531,043	\$429,304	\$324,957
Taxes/insurance	\$/kW-yr	-	-	46	46	46
Maintenance	\$/kW-yr	-	-	5	5	5
Heat losses	\$/kW-yr	-	-	22	22	22
Total O&M PV	\$	-	-	\$105,386	\$105,386	\$105,386
Total		\$1,574,569	\$1,289,786	\$1,458,575	\$1,356,835	\$1,252,488

CONCLUSIONS

Approaches for reducing peak electrical load reduction strategies for UV disinfection systems were investigated. The following observations were made:

- Utilities can purchase electrical power either at a fixed or variable rate. The cost of electricity purchased at night can be half the cost of electricity purchased during the day. For example, day and night time costs in New York State have been 13.3 and 6.5 ¢/kW-hr. If energy is purchased during off-peak hours, a variable-rate structure can provide significant cost savings.
- Advanced battery systems can be used to reduce UV disinfection power costs by storing energy at night when power costs are low and supplying energy during the day when power costs are high. Advanced battery systems also can be used as a UPS to ensure UV disinfection during short-term and sustained power interruptions.
- Sodium-sulfur batteries are a new battery technology recently commercialized in Japan. They have been successfully used at wastewater treatment plants for reducing energy costs through peak load shaving.
- Using the above-mentioned energy pricing structure for New York State, a UV system using a 12-hour sodium-sulfur battery system to take advantage of nighttime power costs has life-cycle costs comparable to a UV system using a 5-minute UPS. The analysis indicates that the sodium-sulfur battery system has potential for providing a cost-effective alternative power supply for UV systems, especially if battery capital costs drop in the future due to more efficient production or increased day time energy costs.

CHAPTER 12

UV SYSTEM FAILURE AND RISK ANALYSIS

This chapter describes the UV system failure and risk analysis using industry UV system failure data. Specific objectives of this analysis were to:

- Collect data of failure events that impact UV system performance including UV system component failure (lamps, ballast, UV sensors, UVT monitors) and power quality events
- Use UVCAT to conduct UV system risk analysis using the collected failure data.

INDUSTRY UV SYSTEM FAILURE DATA

Failure data were collected from four drinking water treatment plants, with UV systems from three different UV vendors, to determine the probability of key UV reactor component (lamps, ballasts, and UV sensors) failures. Failure probability was calculated using:

$$p = \frac{N_f / N_T}{t} \quad (12.1)$$

where p is the probability one unit will fail in one day, N_f is the total number of failure events, N_T is the total number of units in the UV system, and t is the time period in days. The calculated probabilities were used in the UVCAT risk analysis presented later in this chapter.

Utility 1, Vendor 1

Utility 1 is an unfiltered surface water supply with a 160-mgd UV system. [Table 12.1](#) describes the UV system. Eleven months of O&M data, from May 2004 to April 2005, was used to determine the typical failure rates for lamps, ballasts, UV sensors, lamp sleeves and UVT analyzers. [Table 12.2](#) summarizes the failure events and the failure probabilities.

The UV system uses an on-line UVT monitor for UV dose-delivery monitoring. The monitor is maintained and calibrated once every three months in accordance with manufacturer instructions. The WTP does not have a spectrophotometer on-site, but sends water samples to a lab located ten miles away. The UVT monitor is a sealed unit, and condensation can build up inside the unit. The WTP environment is not humid and the operators have considered modifying the UVT monitor by drilling holes into the unit and installing a fan. The UVT monitor is equipped with a wiping system that has failed twice. The cause of the failures were not known but appeared to go away after the unit was disconnected, cleaned, and brought back on-line.

Monthly reference UV sensor checks were conducted on two reactors for 18 months for AwwaRF Project 2977. The WTP plans to conduct reference sensors checks on all reactors once every three months in accordance with manufacturer recommendations. However, they currently do not have sufficient staff to do this task. Currently, they have two reference sensors on-site. During reference sensor checks, the optical window of the sensor is cleaned using alcohol wipes.

Table 12.1
UV system information for Utility 1, Vendor 1

Number of trains in parallel	17
Number of reactors per train	1
Number of duty trains	2 – 16 (flow dependant)
Number of stand-by trains	1
Number of lamps per reactor	8
Number of Banks per reactor	1
Number of lamps per bank	8
Number of lamps per ballast	2
Number of ballasts per reactor	4
Number of UV sensors per bank	8
Number of UV sensors per reactor	8
Number of UVT analyzers at the plant	1

Table 12.2
Summary of UV system component failure events for Utility 1, Vendor 1

System component	Total number in UV system	Failure events	Daily probability of failure
Lamps	136	11	2.45×10^{-4}
Ballasts	68	5	2.23×10^{-4}
UV sensors	136	0	0
UVT analyzers	1	2	6.06×10^{-3}
Sleeves	136	24	5.35×10^{-4}

Reactors have automatically shutdown for “low water level”, lamp failure, and high headloss alarms. The lamp failures were caused by a power spike, which caused the failure of two lamps in two reactors. Too few reactors being on-line at a given flow caused the high-headloss alarm. Flow stills passes through the UV system after shutdown until the operator manually closes the effluent valve. This was not considered a public health risk because chlorination is used downstream of the reactor. While the chlorination system has a back-up generator, the UV system does not have back-up power.

Overall, the operators found the UV system was reliable and easy to work on. However, they do report that approximately ten labor-hours are required to do maintenance on one reactor. As such, they found that they do not have enough manpower to keep up with scheduled maintenance. They feel that following scheduled maintenance would reduce problems they have experienced with the UV system.

Utility 2, Vendor 2

Utility 2 is a conventional water treatment plant designed to treat 63 mgd from a river supply. Table 12.3 describes the UV system. Fourteen months of O&M data, from September 2003 to December 2004, was used to determine failure rates for lamps, ballasts, UV sensors and lamp sleeves. Table 12.4 summarizes the failure events and the failure probabilities.

The UV system uses one magnetic flowmeter per reactor. The magnetic flowmeter is checked annually by passing all flow through each reactor and comparing measurements. The UV system does not use an on-line UVT analyzer because it is not needed for dose monitoring (UV intensity setpoint approach). However, UVT grab samples are sampled four times per day and analyzed using a spectrophotometer. Reference sensor checks of the duty UV sensors are required by the regulator to operate the UV system. They are performed monthly on all reactors using a hand-held reference sensor. Usually, no foulant or condensation is observed. UV sensor windows are cleaned with a Kim-wipe® after inspection. Two duty sensors have failed the reference sensor check, reading 50 percent below the reference sensor. No issues have been observed with the ballasts.

Table 12.3
UV system information for Utility 2, Vendor 2

Number of trains in parallel	3
Number of reactors per train	1
Number of duty trains	2
Number of stand-by trains	1
Number of lamps per reactor	6
Number of banks per reactor	3
Number of lamps per bank	2
Number of ballasts per lamps	2
Number of UV sensors per bank	2 (1 per lamp)
Number of UV sensors per reactor	6
Number of ballasts per reactor	12

Table 12.4
Summary of UV system component failure events for Utility 2, Vendor 2

System component	Total number in UV system	Failure events	Daily probability of failure
Lamps	18	13	1.72×10^{-3}
Ballasts	36	0	0
UV sensors	18	2	2.65×10^{-4}
Sleeves	18	7	9.26×10^{-4}

During initial start-up of the UV system operation, lamps were rupturing in their sleeves after ~500 lamp hours. The UV vendor changed the lamps and the new ones were performing well after 1,500 hours. Lamp replacement is expected every 5,000 hours. The Utility has also had two occasions of sleeve failure due to poor wiper alignment, which resulted in scoured lamp sleeves that required replacement. The problem was resolved by increasing the frequency of wiper maintenance to once every 1,500 hours. During inspection, wiper seals are replaced as needed and the reactor is cleaned. The process involves one day of work for two people. During each failure, the reactor leaked water and automatically shut down.

If a single reactor fails, the effluent valve shuts down in less than one minute and a second reactor comes on-line. If the whole UV system fails (*e.g.*, power failure), water is diverted to a storage area via an 84-inch by-pass valve.

Overall, operators state actual maintenance hours are greater than manufacturer claims. Nevertheless, they report that overall performance of the UV system was reliable once the lamp issue was resolved.

Utility 3, Vendor 1

Utility 3 is a conventional water treatment plant designed to treat 18 mgd from a river supply. [Table 12.5](#) describes the UV system. Twelve months of O&M data, from April 2004 to April 2005, was used to determine failure rates for lamps, ballasts and UV sensors. [Table 12.6](#) summarizes the failure events and the failure probabilities.

Table 12.5
UV system information for Utility 3, Vendor 1

Number of trains in parallel	6
Number of reactors per train	1
Number of duty trains	5
Number of stand-by trains	1
Number of lamps per reactor	4
Number of banks per reactor	1
Number of lamps per bank	4
Number of lamps per ballast	1
Number of UV sensors per bank	4
Number of UV sensors per reactor	4
Number of ballasts per reactor	4
Number of UVT analyzers at plant	1

Table 12.6
Summary of UV system component failure events for Utility 3, Vendor 1

System component	Total number in UV system	Failure events	Daily probability of failure
Lamps	24	2	2.31×10^{-4}
Ballasts	24	1	1.16×10^{-4}
UV sensors	24	4	4.63×10^{-4}
UVT analyzers	1	1	2.78×10^{-3}
Sleeves	24	1	1.16×10^{-4}

The UV system uses an on-line UVT monitor for monitoring UV dose delivery. It is maintained and calibrated once every six months in accordance with manufacturer instructions. The WTP does not have a spectrophotometer to double-check measurements made by the on-line monitor. Analysis of water samples obtained from the plant indicated that the on-line monitor was reading 3 to 4 percent higher UVT than measurements by a spectrophotometer.

The WTP conducted a year of monthly reference UV sensor checks on two reactors for the AwwaRF project 2977. The WTP has no plans to conduct regular reference sensor checks unless they indicate a measurement problem. The UV system is currently not being used for pathogen inactivation credit. Duty UV sensors are inspected during reference sensor checks and cleaned only if dirty. O-rings have been replaced to make it easier to insert the duty sensors into the sensor ports.

The plant has experienced three water leaks since system start-up in January 2004, each caused by a broken sleeve. The sleeves broke because the operator over-torqued the sleeve bolts. The motor driving the wiper has seized, causing a wiper failure with one reactor that was brought back into service. The motor seized because the drive shaft had rusted over the time the reactor was not being used.

Currently, the utility plans to replace the lamps after 5,000 hours but is considering waiting until lamp burnout to save money. At the time of investigation, aged lamps had been operating for 5,800 hours. While two reactor control systems have indicated lamp failures, the alarms were both due to a software glitch as opposed to a faulty lamp. However, four duty UV sensors have failed and were replaced under warranty.

The UV reactors have only had to shut down because of an upstream process failure. The SCADA system shut down the reactors and closed the effluent valves. Shutting the valves takes approximately one minute. In the rare occurrence of a power quality interruption, back-up generators would run the UV system.

Routine maintenance is done either annually or when lamps are replaced. While overall maintenance takes one day per reactor, three days are required to drain the filter, record observations, and refill the system and ensure there are no leaks. Dismantling the reactor and replacing components takes approximately six hours. At the time of investigation, the WTP was replacing lamps and doing routine maintenance. The lamp sleeves appeared spotless.

Overall, the operators are satisfied with the UV system reliability, finding the reactor to be easy to work on and well made overall.

Utility 4, Vendor 3

Utility 4 is a 19.5-mgd conventional surface water treatment plant. Table 12.7 describes the UV system. This utility had several major problems at start-up resulting in some significant retrofitting and redesigning of the installed UV reactors. Towards the beginning of 2005, the utility and State regulators agreed on an operating strategy that would enable the utility to obtain credit from the state for inactivation of their target microbe. Lamp failure rates for this 7-month period of operation is summarized in Table 12.8.

Table 12.7
UV system information for Utility 4, Vendor 3

Number of trains in parallel	6
Number of UV reactors per train	1
Number of duty trains	5
Number of stand-by trains	1
Number lamps per reactor	8
Number banks per reactor	1
Number lamps per bank	8
Number lamps per ballast	1
Number UV sensors per bank	8
Number UV sensors per reactor	8
Number ballast per reactor	8
Number of trains in parallel	6

Table 12.8
Summary of UV system component failure events for Utility 4, Vendor 3

System component	Total number in UV system	Failure events	Daily probability of failure
Lamps	48	17	1.57×10^{-3}

Power Quality Events

Power quality events occur when line voltage falls outside of the normal range of operation. As shown in Tables 12.9 and 12.10, power quality events are classified by voltage and duration.

Grebe *et al* (1996) studied the frequency of power quality events at 277 power distribution systems over a two-year period from June 1993 to June 1995. Power quality events were defined as episodes where the measured voltage was above 105 percent or below 95 percent for more than one cycle. They measured 107,834 power quality events corresponding to an average of 45 voltage sags and 5 interruptions/year. Power quality varied from site-to-site and seasonally. Voltage sags ranged from 1.5 to 7.2 events/month and interruptions ranged from 0.3 to 0.9 events/month with more frequent occurrences in the summer.

Power quality can be monitored over time using power analyzers. Various companies also sell specialized equipment for detecting, analyzing, and recording power quality events. In this work, SoftSwitching Technologies¹ provided representative power quality data for New York State for 2004 from their "i-grid" power quality monitoring system (www.i-grid.com). Ninety-eight power quality events were recorded over a 12-month period corresponding to 8.2 events/month, a daily probability of 0.27.

Table 12.9

IEEE classification of power quality events by voltage

<u>Voltage classification</u>	<u>Definition</u>
Voltage sag	10 to 90% of nominal voltage
Voltage surge	> 110% of nominal voltage
Voltage interruption	< 10% of nominal voltage

Table 12.10

IEEE classification of power quality events by duration

<u>Duration classification</u>	<u>Definition</u>
Instantaneous	0.5 - 30 cycles
Momentary	0.5 - 3 sec.
Temporary	3 - 60 sec.
Sustained	> 1 min.

¹ Middleton, Wis.

Figure 12.1 provides a monthly summary of the events, which shows a peak during the month of April. A majority of these events occurred from 11:26 pm on April 9th to 7:54 am on April 10th. Figure 12.2 provides a summary by days of the week, which shows a higher frequency on Friday and Saturday. However, those peaks are due to the events that occurred on April 9th and 10th. Figure 12.3 provides an hourly summary of events, which shows peaks at 7:00 am and 9:00 pm.

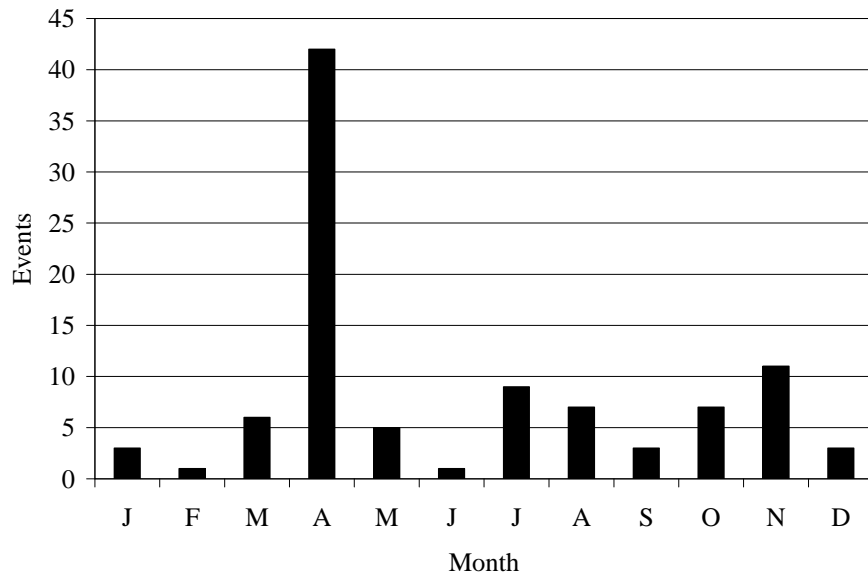


Figure 12.1 Monthly summary of power quality events from i-grid monitoring sites in New York State

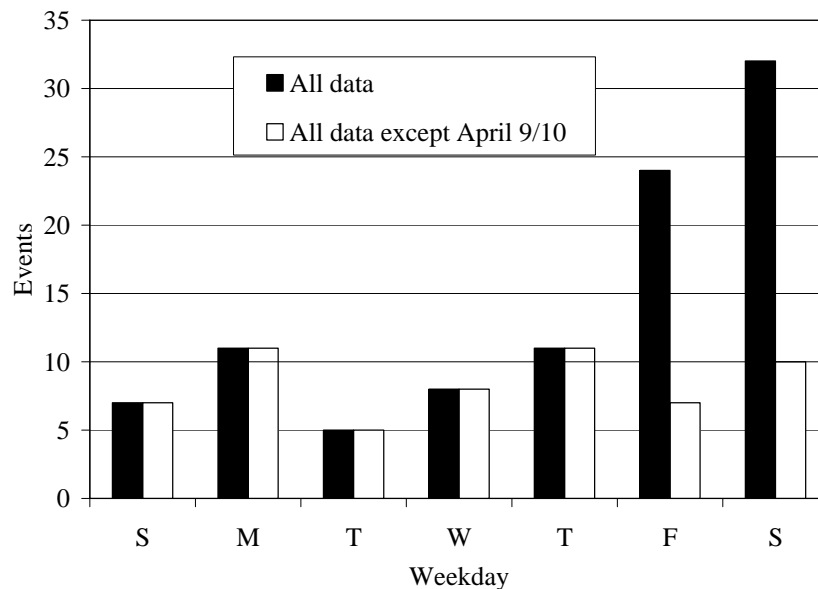


Figure 12.2 Summary of power quality events by weekday from i-grid monitoring sites in New York State

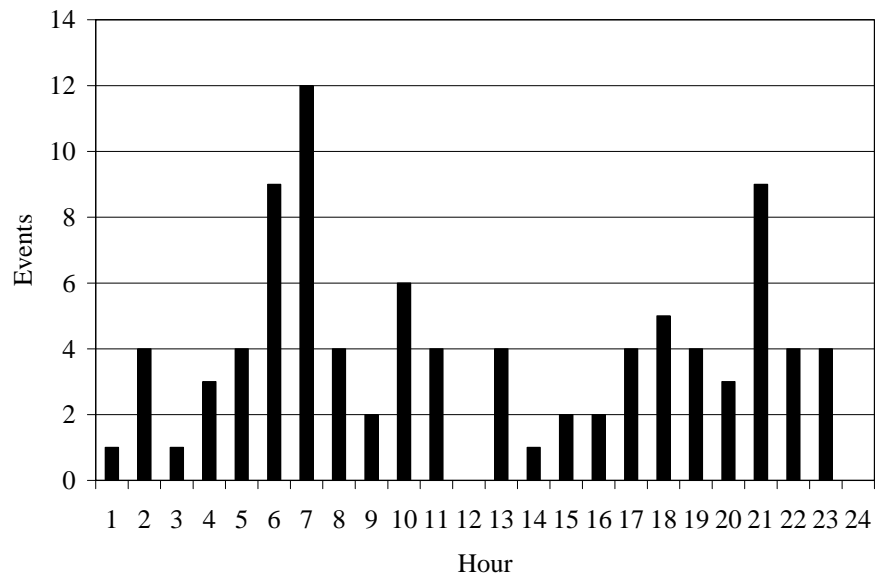


Figure 12.3 Hourly summary of power quality events from i-grid monitoring sites in New York State

UV SYSTEM FAILURE AND RISK ANALYSIS USING UVCAT

UVCAT allows the user to enter raw water pathogen concentration data and power quality data over time. Power quality data is entered as voltage and duration of power quality event. Other UVCAT risk data categories consist of back-up power, component reliability, and response to failure. This information includes:

- Voltage and duration of power quality event that causes UV system shutdown
- Use of UPS system
- Use of generators and generator start-up time
- Use of shutoff valves and valve closing time
- Lamp cool-down and warm-up times
- Daily probability of lamp, ballast, and UV sensor failure
- Population served by the WTP

The UVCAT RISK MODEL worksheet includes a UV dose-response model for the pathogen, a human infection dose-response model, and an infection risk model. The UV dose-response model for the pathogen includes a field for the entered UV dose and a field containing a formula for the resulting pathogen inactivation. A general model that fits a wide range of UV dose-response data containing tailing and shoulders is:

$$\log I = \frac{a \times b + c \times \text{UV Dose}^d}{b + \text{UV Dose}^d} \quad (12.2)$$

where a, b, c, and d are constants. Table 12.11 gives fit coefficients for *Cryptosporidium*, *Giardia*, rotavirus, and adenovirus based on requirements given in the 2003 Draft USEPA *Ultraviolet Disinfection Guidance Manual* (USEPA, 2003b).

The human infection dose-response model includes fields for the entered pathogen dose and a formula for the resulting probability of infection. LeChevallier *et al.* (2004) reported that number probability of infection with *Cryptosporidium* is 0.028 infections/oocyst. Other models have been published for *Giardia* and rotavirus (Regli *et al.* 1991) and adenovirus (Crabtree *et al.* 1997).

The infection risk model includes input fields for raw water pathogen concentration, the log removal by filtration, chemical disinfection, and UV disinfection, the volume of water consumed per day, the infections per pathogen dose, and the time period of interest. The model calculates the probability of infection during that time period using:

$$\text{Risk} = N_p \times 10^{-(\log I_{UV} + \log I_C + \log I_{\text{filt}})} \times V \times \text{DR} \times \Delta T \quad (12.3)$$

where N_p is the raw water pathogen concentration in microbes/L, $\log I_{UV}$ is the log inactivation by the UV system, $\log I_C$ is the log inactivation by chemical disinfection, $\log I_{\text{filt}}$ is the log inactivation by filtration, V is the volume of water consumed daily per person, DR is the probability of infection, and ΔT is the time period of interest. The model also calculates annual risk using:

Table 12.11
Coefficients for the pathogen UV dose-response model

Pathogen UV dose-response	Model coefficients			
	a	b	c	d
<i>Cryptosporidium</i> UV dose requirements	-0.00248	11.78	4.071	1.392
<i>Giardia</i> UV dose requirements	-0.02756	8.254	3.769	1.411
Adenovirus UV dose requirements	-0.0289	3964	14.34	1.404
<i>Cryptosporidium</i> Tier 1 requirements for LP lamps	-0.00878	157.8	4.586	1.584
<i>Giardia</i> Tier 1 requirements for LP lamps	-0.02009	120.1	4.384	1.567
Adenovirus Tier 1 requirements for LP lamps	-0.03953	6045	17.12	1.355

$$\text{AnnualRisk} = 1 - [1 - \text{Risk}]^{365/\Delta T} \quad (12.4)$$

The UVCAT risk outputs include UV dose delivery per reactor, pathogen inactivation by the UV system, risk, annual risk, and accumulated risk in the population over time.

UVCAT Risk Analysis Case Studies

The remainder of this chapter provides UVCAT risk analysis case studies for a LPHO UV system with varying levels of back-up power, lamp warm-up/cool-down times, voltage and cycle thresholds and component failure rates.

The UV system evaluated consisted of six reactors in parallel – five duty reactors and one redundant reactor. Each reactor contained 11 banks of twelve 360-W lamps. The reactors were sized to deliver a UV dose of 36 mJ/cm², defined as an MS2 RED, to achieve 3-log *Cryptosporidium* inactivation credit. UV dose delivery was modeled using:

$$\text{RED} = 10^A \times \text{UVA}^{B \times \text{UVA}} \times \left(\frac{S/S_o}{Q} \right)^C \times \text{Banks}^D \quad (12.5)$$

where RED is Reduction Equivalent Dose, UVA is the UV absorbance at 254 nm in cm⁻¹, Q is flow rate in mgd, Banks is the number of operating banks, S is the UV sensor reading in W/m², and S_o is the UV sensor readings that would occur with new lamps operating at 100 percent ballast power in clean quartz sleeves. The sensor reading, S was simulated using:

$$S = 10^a \times \exp(b \times \text{UVT}) \times \frac{P}{100} \times f_L \times f_f \quad (12.6)$$

where UVT is the percent UV transmittance of the water, P is the percent relative power of the lamps, f_L is the lamp aging factor, and f_f is the fouling factor. The value for S_o was obtained from Equation 12.6 by setting P equal to 100 percent, f_L to 1.0, and f_f to 1.0. The model coefficients for Equation 12.5 and 12.6 used with the simulation (Table 12.12) were obtained from a CFD simulation of a hypothetical reactor.

Table 12.12
Model coefficients for Equations 12.5 and 12.6

Model coefficients for Case 1	Value
A	2.4987
B	9.1999
C	0.78214
D	0.94867
a	-1.3829
b	0.056732

Table 12.13 summarizes the conditions for each risk analysis case study. Figure 12.4 gives the flow rates and UVT profiles for these case studies. Figure 12.5 gives the *Cryptosporidium* concentration profile of the raw water. Figure 12.6 gives the voltage overtime showing power quality events.

Table 12.13
Summary of conditions for risk analysis examples

Case		1	2	3	4	5	6
Operational UV dose	mJ/cm ²	36	36	36	36	36	50
UPS		Yes	No	No	No	Yes	No
Generator		No	No	Yes	Yes	No	Yes
Lamp cool-down time	(min)	4	4	4	2	4	4
Lamp warm-up time	(min)	5	5	5	2.5	5	5
Voltage threshold	(%)	90	90	90	80	90	90
Cycle threshold	(cycles)	1	1	1	10	1	1
Probability of lamp failure		0	0	0	0	0.1	0

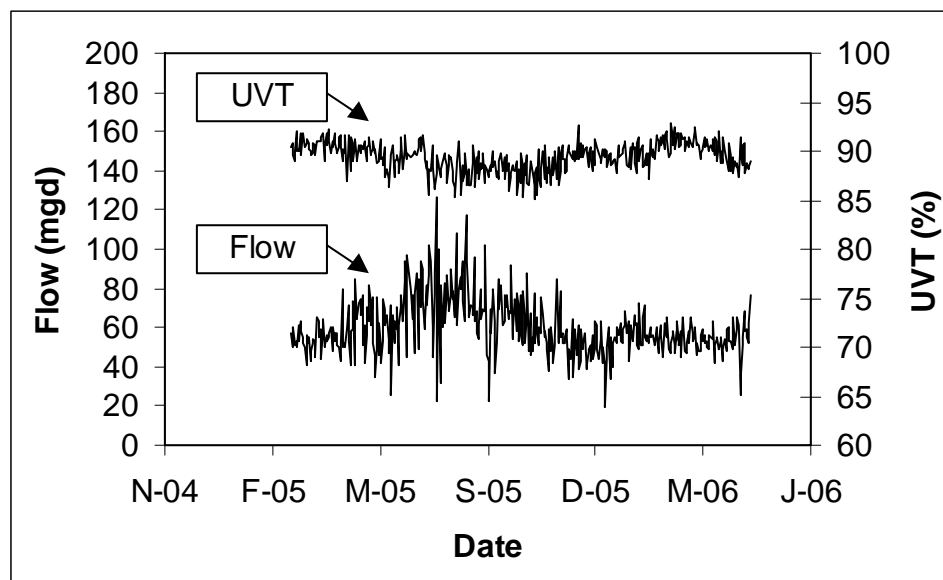


Figure 12.4 Flow rate and UVT profiles

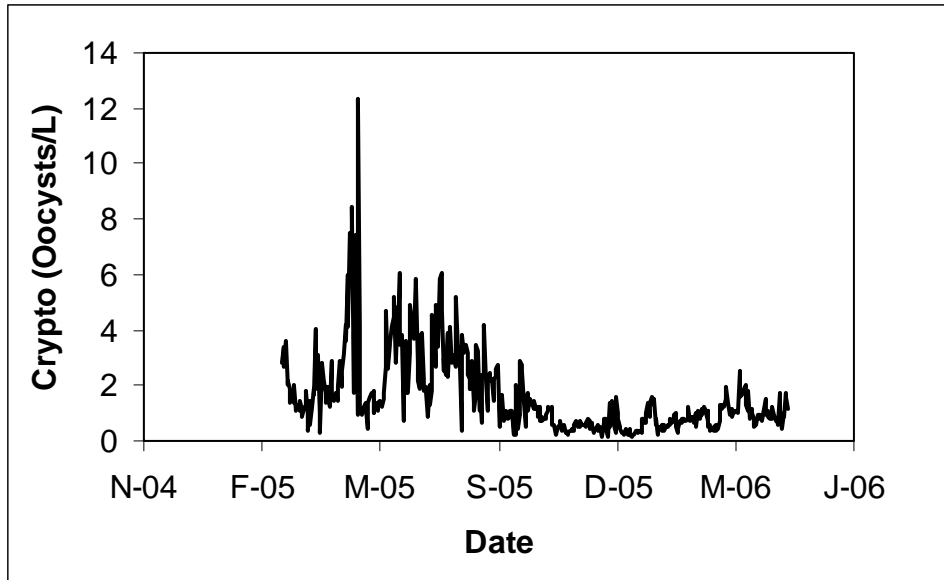


Figure 12.5 Raw water *Cryptosporidium* concentrations

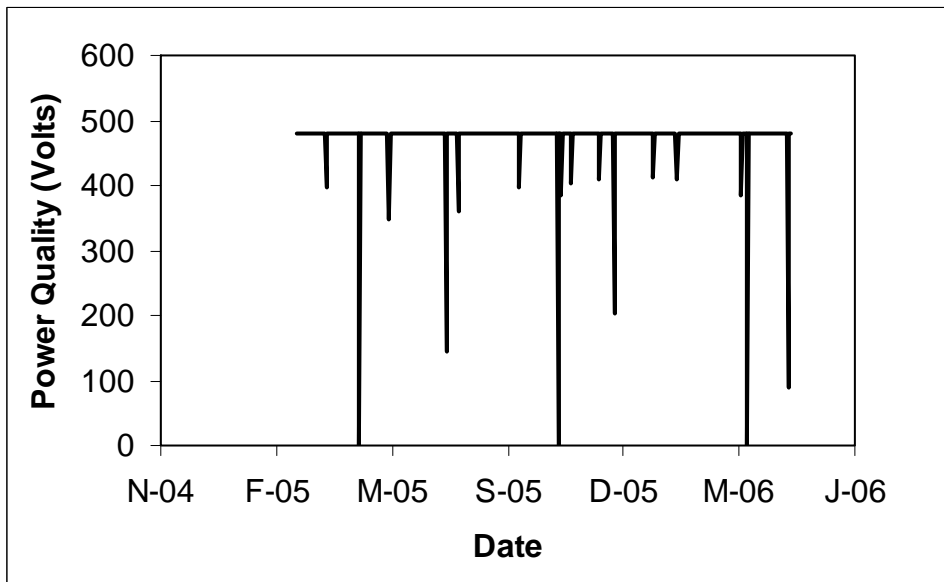


Figure 12.6 Line voltage data showing power quality events

Case Study 1

The UV system modeled in Case 1 uses a UPS to provide continuous power during power quality events. The analysis assumed no UV system component failures occurred during the simulated operating time. Figure 12.7 shows the number of LPHO reactor trains and banks needed over time to treat the water described in Figure 12.4. Figure 12.8 shows the power consumption and costs for the UV system. Figure 12.9 shows UV dose delivery by one of the UV reactors and log inactivation of *Cryptosporidium* achieved by the UV system. The analysis indicates the UV system was appropriately sized for the application. The slight overdosing was related to the discrete power settings used to power the ballast.

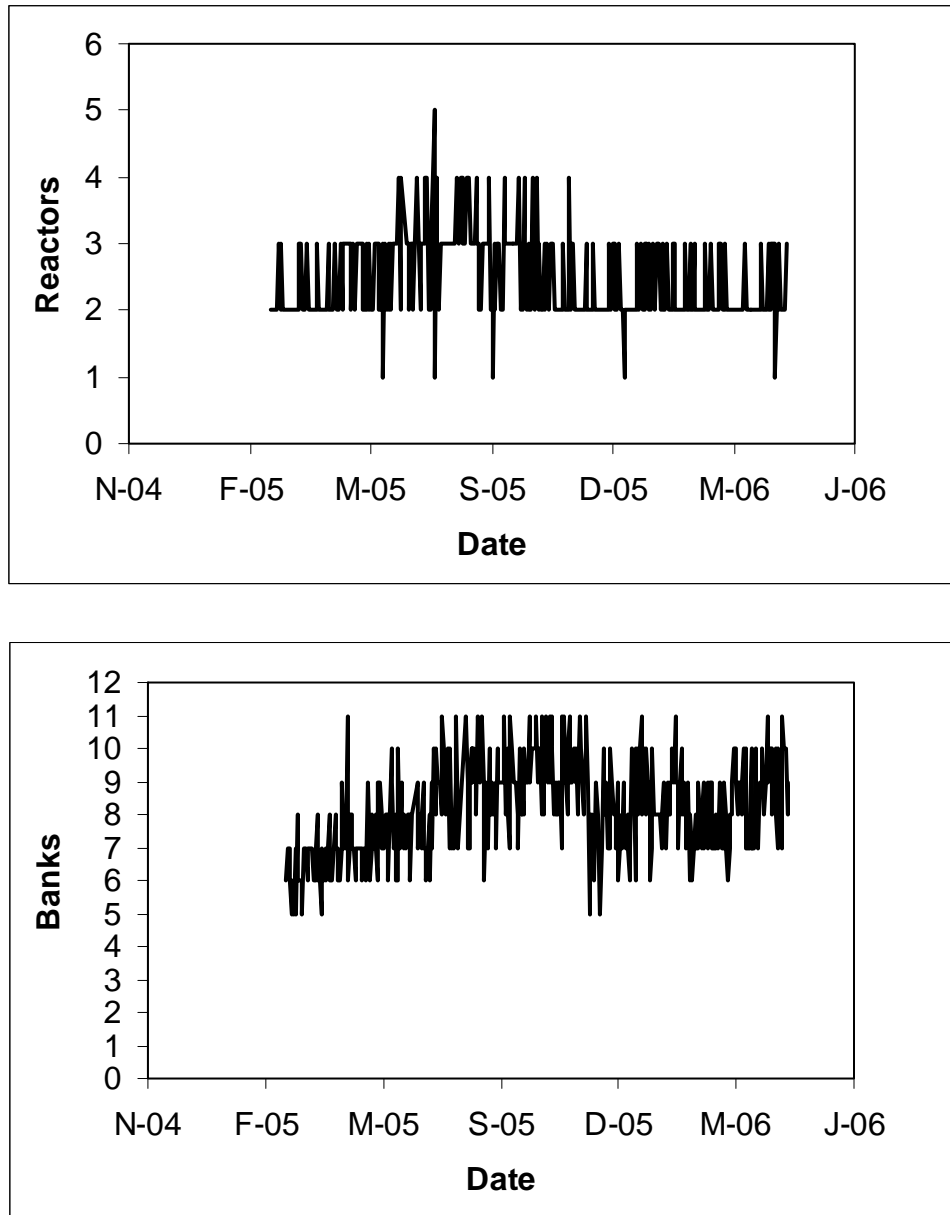


Figure 12.7 Number of reactors (top) and banks (bottom) of lamps predicted for the Case 1 LPHO system

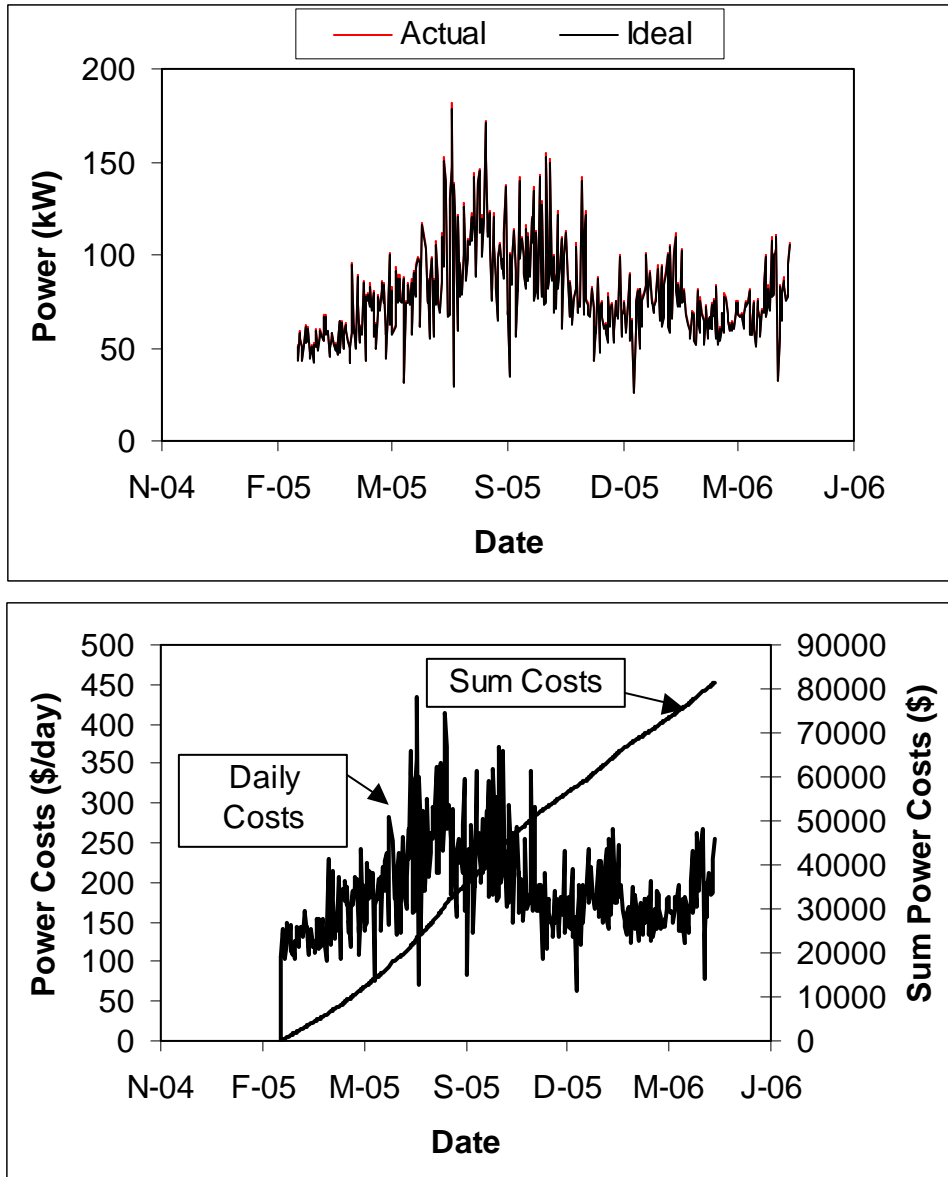


Figure 12.8 Power consumption (top) and costs (bottom) over time for the Case 1 LPHO system

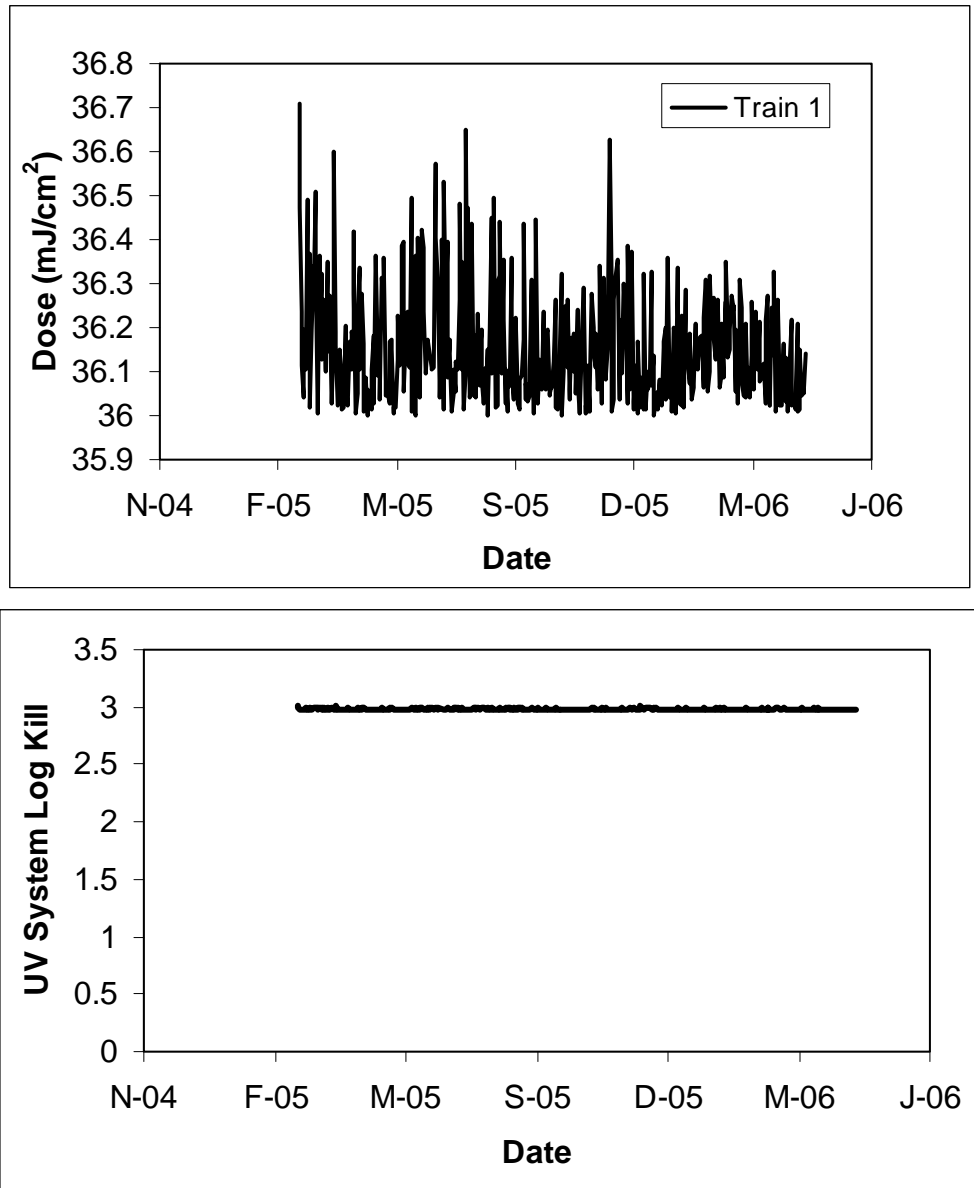


Figure 12.9 UV dose delivery by the first reactor (top) and UV system log inactivation (bottom) over time for the Case 1 LPHO system

Figure 12.10 shows public health risk assuming a population of 1,000,000 people and 2-log *Cryptosporidium* inactivation through the filters. The risk over time reflects the fluctuations raw water *Cryptosporidium* concentration and varies from 0.0015 to 0.000019 infections/year. The accumulated risk in the 1,000,000-person population was 240 infections over a 427-day period. This corresponds to an average annual risk of 2.0 infections/year per 10,000 persons.

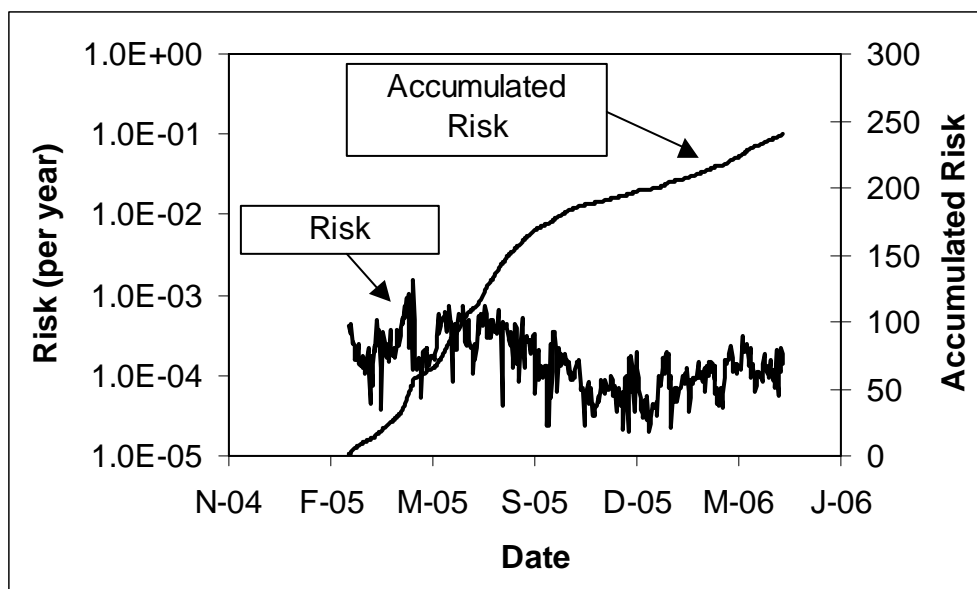


Figure 12.10 Annual health risk and accumulated *Cryptosporidium* infections in a population of 1,000,000 people for the Case 1 LPHO system

Case Study 2

Case Study 2 simulated the Case 1 UV system without a UPS. Figure 12.11 shows the log inactivation and the associated public health impact of providing no back-up power. The analysis assumed a 4-minute cool-down time and a 5-minute warm-up time. The analysis also assumed that the lamps extinguished during each power quality event (supply voltage dropped below 90 percent for periods of time longer than one cycle or 17 mS). Because the durations of the events were much shorter than the UV system restart time, the average log inactivation over the one-day time period when the events occurred was typically 2.2-log. However, one sustained interruption dropped the daily average log inactivation to 1.4-log. Compared to Case 1, not using any back-up power increased the number of infections from 240 to 350 infections per 1,000,000 people over a 427-day period. Seventy-two of those infections were associated with a sustained interruption on April 30, 2005. The average annual risk was 3.0 infections/year per 10,000 persons.

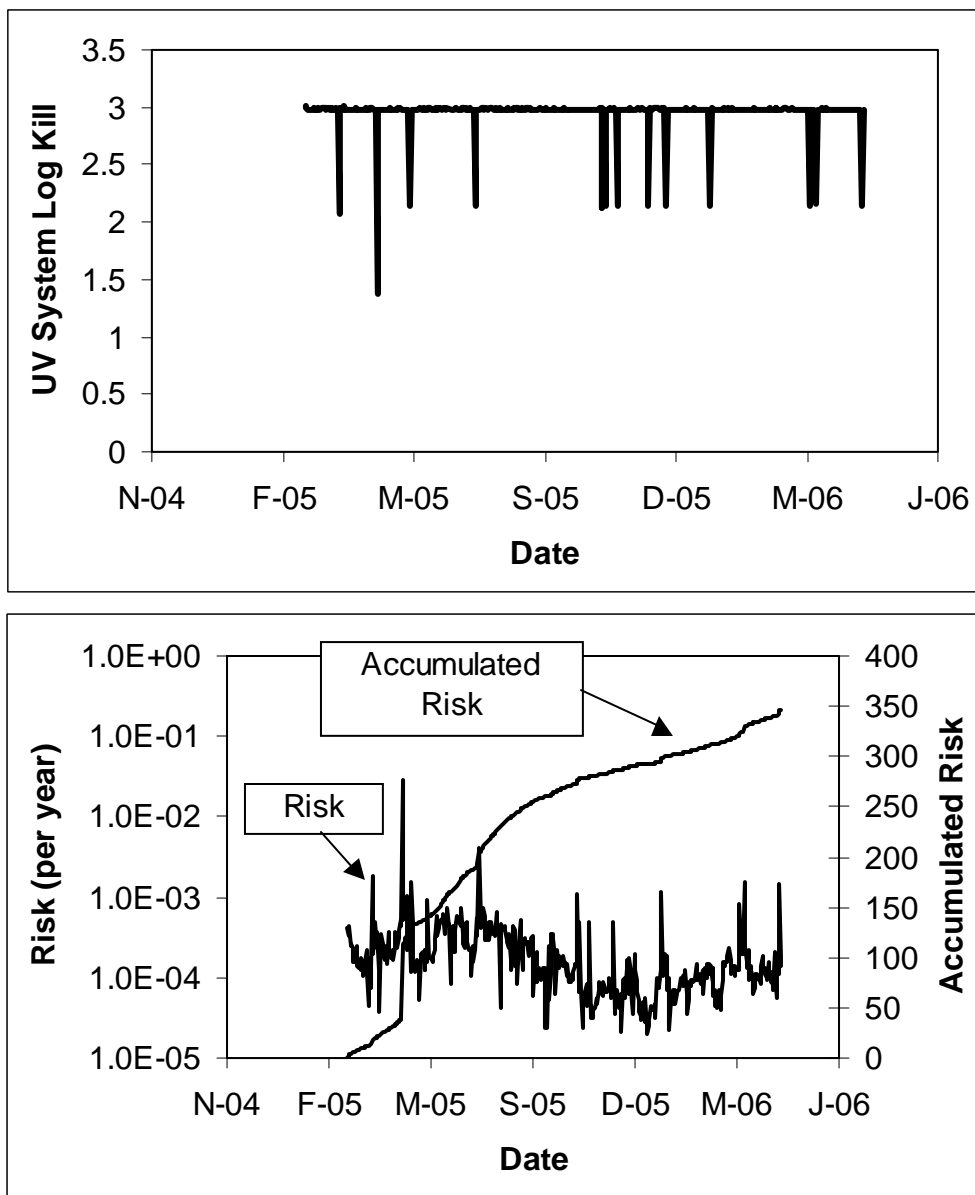


Figure 12.11 UV system log inactivation (top), and annual infection risk, and accumulated infection for the Case 2 LPHO system (bottom)

Case Study 3

In Case Study 3, the UPS system in Case 1 was replaced with a generator with a 2-minute start time. [Figure 12.12](#) shows the log inactivation and the associated public health impact. The main advantage of the generator is that it provided back-up power during sustained interruptions. The number of infections was 289 per million people, a value that is 20 percent greater than the number of infections with the UPS system. The average annual risk was 2.5 infections/year per 10,000 persons.

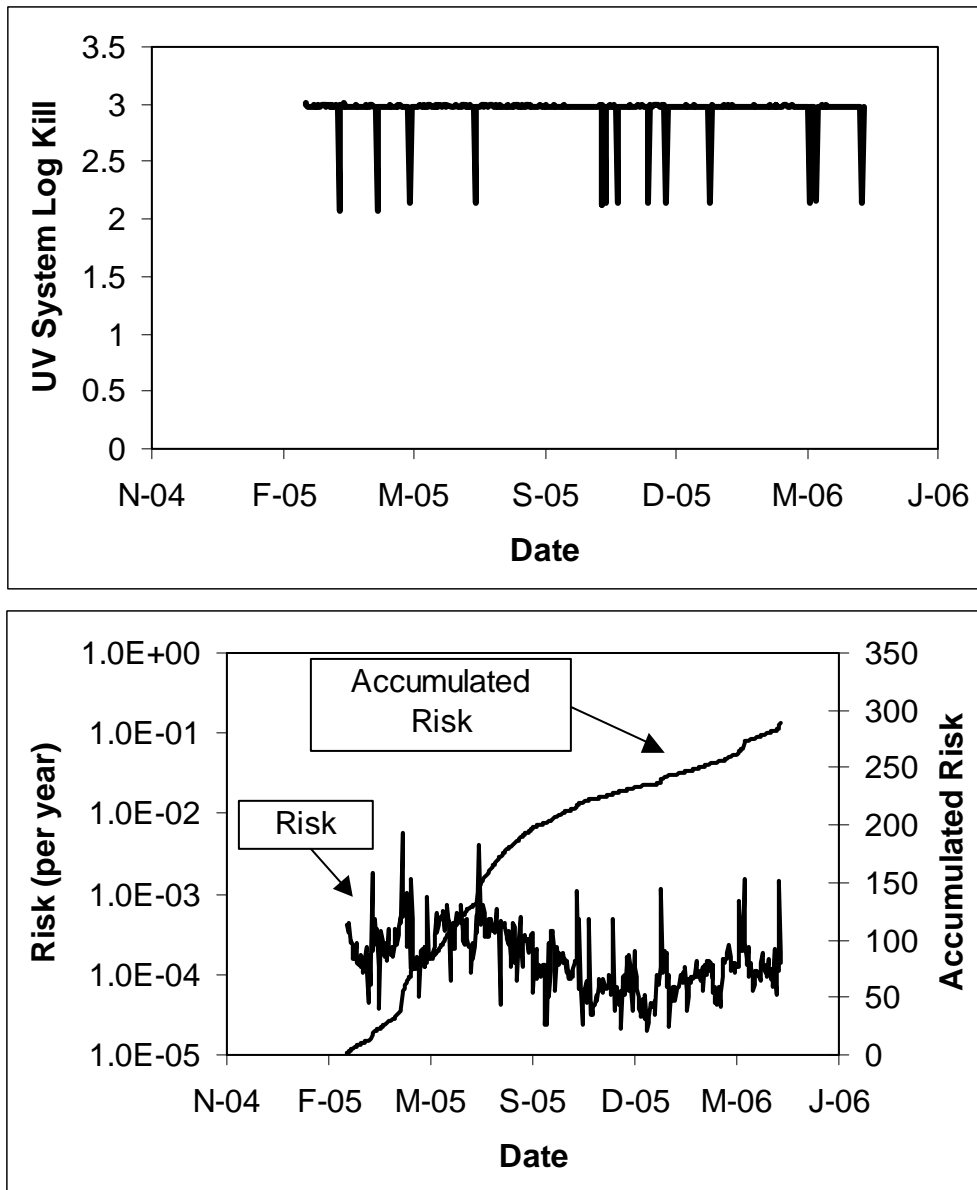


Figure 12.12 UV system log inactivation (top), and annual infection risk and accumulated infection (bottom) for the Case 3 LPHO system

Case Study 4

In Case Study 4, the UV system used a generator and the power quality thresholds were 80 percent nominal voltage and 10 cycles (in comparison to 90 percent nominal voltage and 1 cycle for Case Studies 1 to 3) and the lamp cool down and warm up times were shortened by a factor of 2 to 2.5 minutes, respectively. [Figure 12.13](#) shows the log inactivation and public health risk. Increasing the UV system's tolerance to power quality events and reducing the lamp restart times reduced the number of infections to 258 per million people, 7.5 percent above the number of infections with UPS.

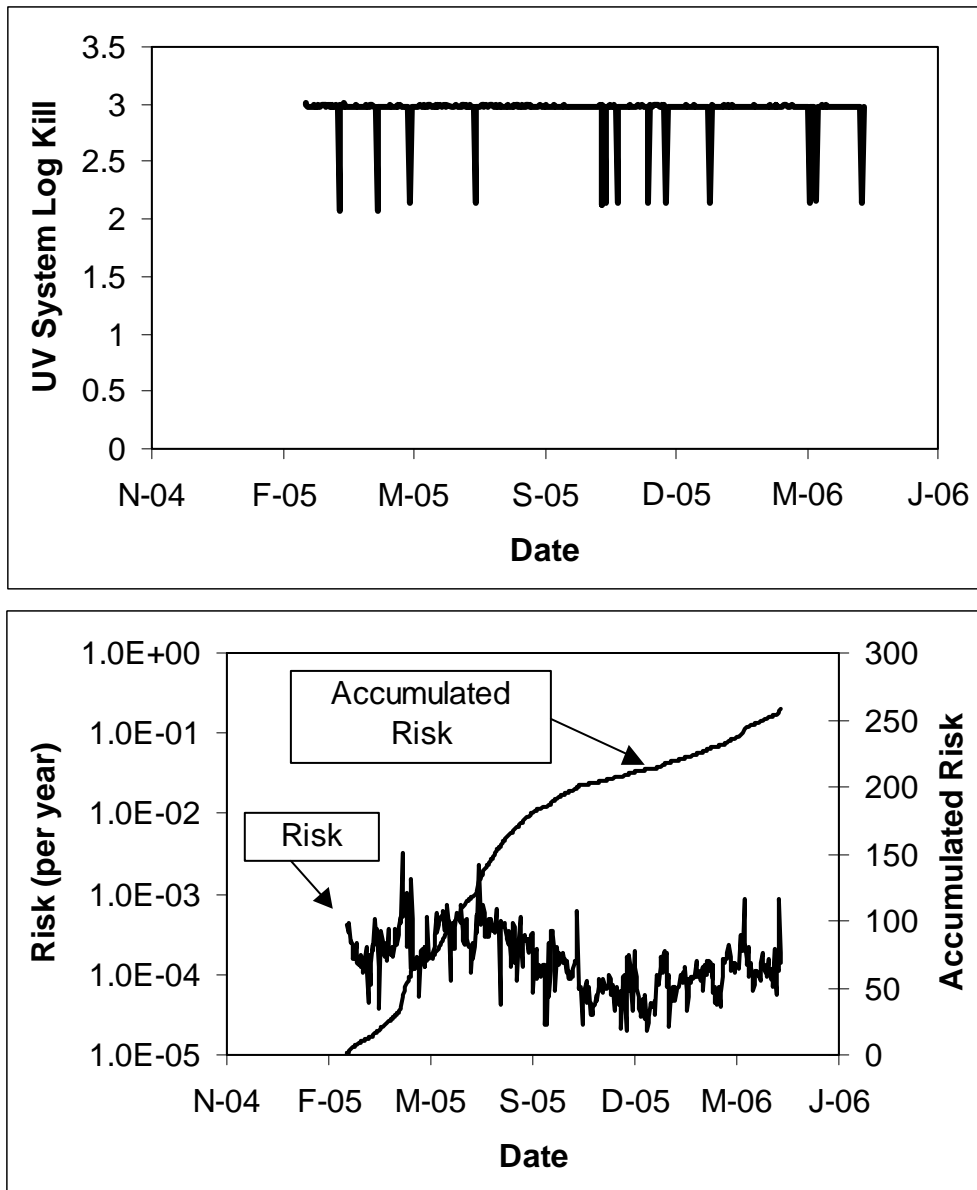


Figure 12.13 UV system log inactivation (top), and annual infection risk and accumulated infection (bottom) for the Case 4 LPHO system

If the annual risk of infection is considered on a log scale, it can be argued that if generators are used to provide backup power to the UV system and the UV system restart times are kept short the differences in public health protection of the UV system with and without UPS are negligible. In that case, arguments could be made to regulators that a UPS system does not provide significant improvement in public health protection.

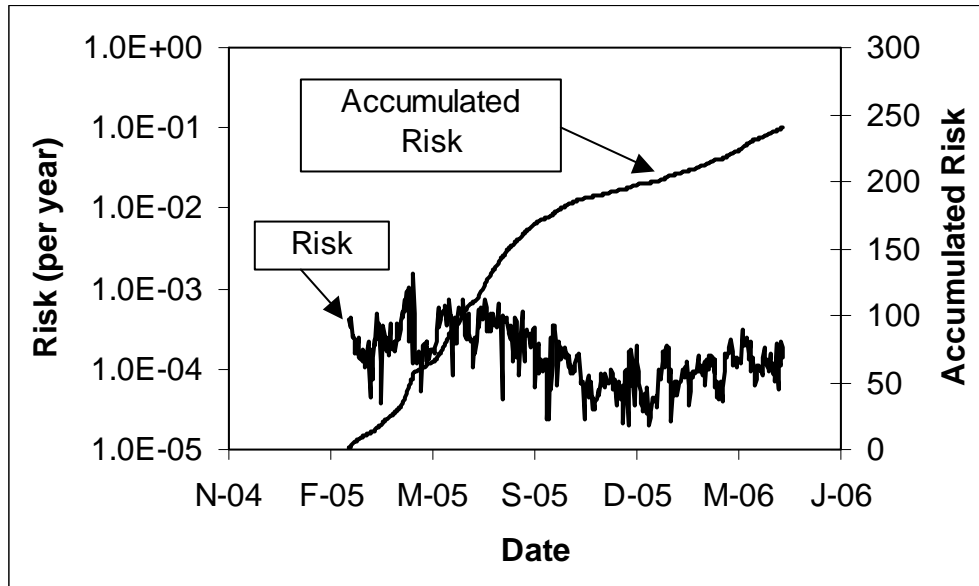


Figure 12.14 Annual infection risk and accumulated infection for the Case 5 LPHO system

Case Study 5

Case Study 5 assumes the Case 1 UV system with UPS had a daily probability of lamp failure of 0.1. Under lamp failure conditions, the UVCAT algorithm responds by turning all lamps on to 100 percent power. [Figure 12.14](#) shows the log inactivation and public health risk. In this scenario, the number of infections was 241 per million, equivalent to the number without any lamp failure. The results show that component failure with the UV system modeled does not pose a risk to public health protection.

Case Study 6

In Case Study 6, the Case 3 UV system (generator used for backup power) used a target UV dose of 50 mJ/cm² instead of 36 mJ/cm². [Figure 12.15](#) shows the log inactivation and the associated public health impact. With a UV dose target of 50 mJ/cm², the UV reactor achieved 3.5-log inactivation of *Cryptosporidium*, 0.5 log greater than the 3.0-log inactivation required. As such, the number of infections was only 125 infections per million persons, notably lower than the Case 1 UV system using UPS. These results show that operating at a higher UV dose can be used to offset the risk associated with power quality events. Operating at a higher operational UV dose should be considered as an alternate to providing UPS.

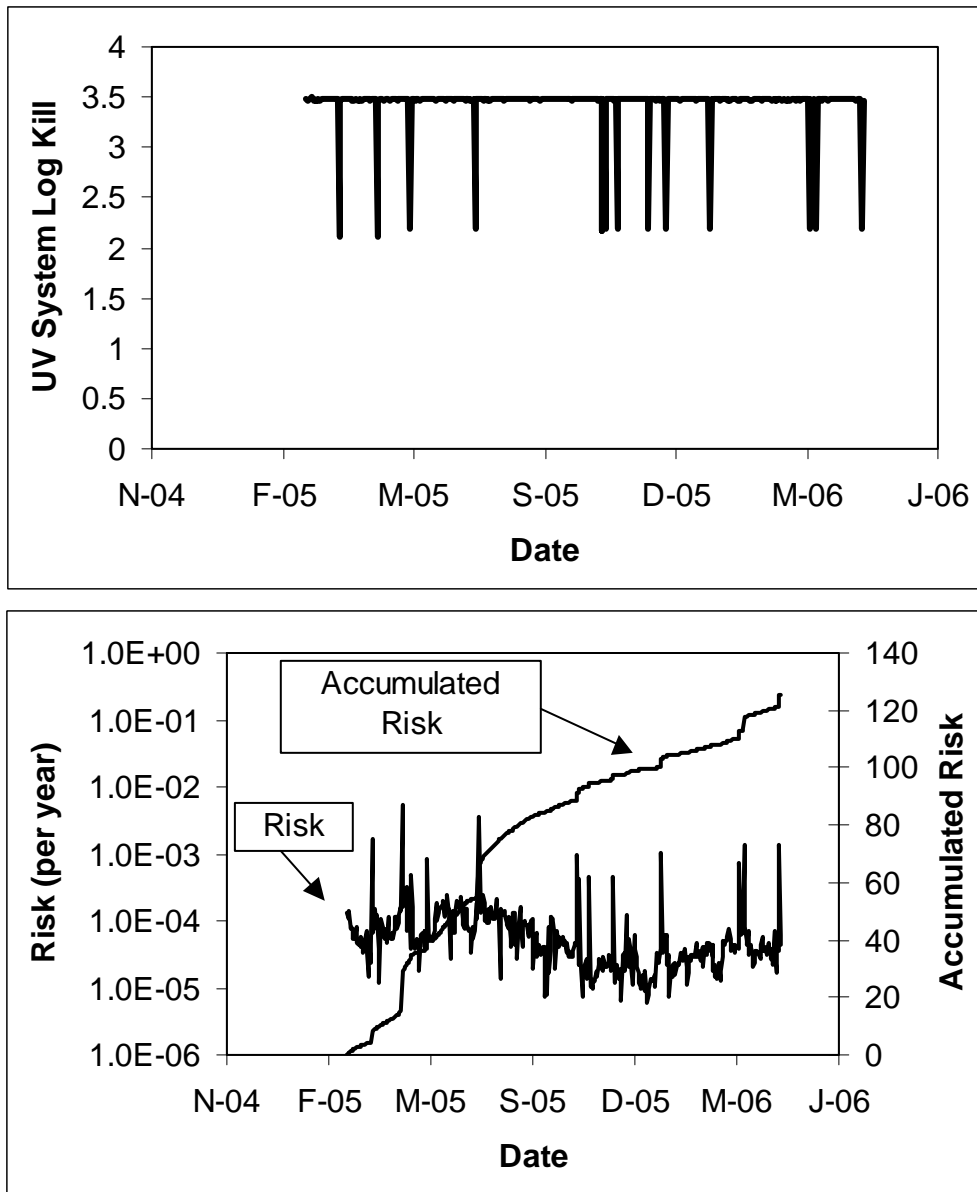


Figure 12.15 UV system log inactivation (top), and annual infection risk and accumulated infection (bottom) for the Case 6 LPHO system

CONCLUSIONS AND RECOMMENDATIONS

The Advanced Life Cycle Cost Analysis tool was used to evaluate the impact of dose-pacing strategies, operational dose, power quality events, and component failure on infection risk. The following observations were made:

- Risk analysis can provide a rational approach for sizing and operating a UV system to achieve a target level of public health protection.
- Regulators, utilities, and engineers should compare the risk associated with off-specification performance and UV system failure to a baseline level (USEPA's one infection per 10,000 persons per year risk target) in order to rank the importance of these events.
- Without back-up power, shutdown valves, or some other response measure, sustained voltage sags or power interruptions will have a significant adverse impact on public health protection.
- A UPS system is not always required with a UV disinfection system to provide adequate health protection. A UV system operating at a higher dose with a generator can provide better health protection than a UV system operating at the design dose with a UPS system.
- Component failure will have a minor impact on public health risk if the UV system always has one or more banks of lamps treating the flow. If the UV system operates as one-bank reactors and the number of lamps is low (*e.g.*, 2 or 4 lamps), lamp or ballast failure can lead to significant underdosing.
- There is poor correlation between UV system off-specification performance, as defined by the USEPA *UVDGM*, and public health risk. For example, low UVT events can easily cause off-specification operation that exceeds the 5-percent USEPA requirement, but has a negligible impact on public health risk. However, power quality events that cause UV system shutdown can lead to off-specification operation that meets the 5-percent requirement, but may have a serious adverse impact on public health protection.

APPENDIX A

UVCAT USER MANUAL

INTRODUCTION

The NYSERDA UV System Cost Analysis Tool (UVCAT) is an Excel[®] spreadsheet with embedded Visual Basic[®] software designed for analyzing UV system life-cycle costs and performance. UVCAT uses the spreadsheet as a user interface to enter data, initiate the software algorithms, and view the outputs. UVCAT is designed to conduct the following analyses:

- Standard Life-Cycle Cost (LCA) Analysis
- Lamp Replacement Interval Cost Analysis
- Advanced Life-Cycle Cost Analysis

Standard Life-Cycle Cost Analysis. The Standard Life-cycle Cost Analysis tool determines UV system O&M and present worth costs assuming the UV system operates under average conditions of flow rate, water UV transmittance (UVT), lamp aging, and fouling.

Lamp Replacement-Interval Cost Analysis. The Lamp Replacement Interval Cost Analysis tool estimates O&M and present worth costs for a UV system as a function of various lamp replacement intervals. The O&M costs are estimated assuming the UV system operates under average conditions of flow rate, UVT, lamp aging, and fouling.

Advanced Life-Cycle Cost Analysis. The Advanced Life-Cycle Cost Analysis tool simulates UV system operation over time as a function of flow rate, UVT, lamp aging, fouling, power quality, and UV system component failure. UV system operation is estimated using the UV dose monitoring and control algorithm specific to the UV system. The tool predicts the number of reactors and lamps, their power setting, UV dose delivery by each reactor, log inactivation of a target pathogen, and the associated public health protection. The tool predicts O&M costs by integrating power consumption, labor, and UV system component replacement over the time.

UVCAT INPUTS

Table A.1 lists the worksheets within UVCAT that are used to input data used by UVCAT. The following sections provides a description of the data entered into each worksheet.

Table A.1 UVCAT worksheets used for Input

Analysis	Input Worksheets
Standard life-cycle cost analysis	STANDARD LCA
Lamp replacement interval cost analysis	LAMP AGE LCA TOOL
Advanced life-cycle cost analysis	ADVANCED LCA WQ RED MODEL RISK MODEL

UV System Data Inputs

The UVCAT user enters data describing the UV system into the worksheets entitled STANDARD LCA, LAMP AGE LCA TOOL, and ADVANCED LCA. The user enters the UV system data as columns of data, where each column represents one UV system. Table A.2 summarizes the type of information entered in these worksheets.

The data inputs for each parameter in Table A.2 is described as follows:

UV System Sizing Criteria

This section is used to enter information on UV system sizing and operation as follows:

- Maximum flow - flow rate used to size the UV system.
- Average flow - average flow rate treated by the UV system.
- Average UVT - average UVT of the water passed through the UV system.
- Design UVT - water UVT (254 nm, 1-cm pathlength) used to size the UV system.
- Design UV Dose - required UV dose for treatment.
- Minimum Number of Trains - minimum number of UV reactor trains in operation.

Reactor Configuration

UV vendors and consultants often work together to define the configuration of the UV system for a given disinfection application. Often the engineer specifies the number of UV reactor trains in parallel and the number of UV reactors per train. The UV vendor often specifies the number of banks of UV lamps in each reactor and the number of UV lamps per bank. The UV vendor also defines the number of ballasts and UV sensors used per reactor. This section of the spreadsheet is used to enter the following information on the UV reactor configuration.

Table A.2 Data inputs into UVCAT

Parameter	Rows where data is entered:		
	STANDARD LCA	LAMP AGE LCA	ADVANCED LCA
Descriptive Information	15 - 18	19 - 21	15 - 18
UV System Sizing Criteria	41 - 45	25 - 29	42 - 47
Reactor Configuration	48 - 54	32 - 38	52 - 58
Redundancy	56 - 57	40 - 41	60 - 61
Lamp Data	59 - 72	43 - 56	63 - 76
Sleeve Data	74 - 80	58 - 64	78 - 84
Ballast Data	83 - 85	67 - 69	87 - 89
UV Sensor Data	87 - 92	71 - 76	91 - 96
Dose Model and Pacing	97 - 101	81 - 85	100 - 101
Failure Data	Not used	Not used	103 - 115
WTP Inputs	104 - 108	88 - 92	119 - 125
Capital Cost Inputs	113 - 141	97 - 125	128 - 160
Dose Delivery	149 - 165	133 - 149	Not used
Ballast Power Settings	Not used	Not used	164 - 187

- Max Flow per Reactor - the maximum flow per reactor as defined by headloss or validation limitations.
- Trains - number of UV reactor trains, including redundant reactor trains, installed in parallel and used to treat the flow through the UV system. As a special case, if one UV reactor is installed on each filter at a water treatment plant, the number of reactor trains is set to equal the number of filters. In this case, UV system redundancy is defined by the redundancy of the filters.
- Reactors/Train - number of UV reactors in series in each treatment train.
- Banks/Reactor - number of banks of UV lamps in each reactor. A bank of lamps can be defined as a group of lamps oriented across the reactor cross-section perpendicular to the flow through the UV reactor. In a multi-bank reactor, this configuration of lamps is repeated in the direction of flow. With the Advanced LCA tool, the banks per reactor are defined by the RED equation (see section 1.1.3).
- Lamps/Bank - number of lamps in each bank.
- Lamps/Ballast - number of lamps operated by each lamp ballast assembly. Ballast assemblies typically drive either one or two lamps.
- UV Sensors/Bank - number of duty UV sensors used per bank to monitor the UV lamps. LPHO and amalgam UV systems used in drinking water and wastewater reactors often use one UV sensor per bank of lamps. MP UV systems used in drinking water systems often use one UV sensor per lamp. MP UV systems used in wastewater systems use either one sensor per bank of lamps or do not use UV sensors.

Redundancy

Redundant UV reactors or trains are used to ensure the UV system provides the required UV dose when a UV reactor or train is out of service for maintenance or service. While UV systems used to treat secondary wastewaters typically do not use redundant reactors, UV systems used to treat re-use wastewaters (e.g. Title 22 applications) typically use one redundant reactor per train and UV systems used in drinking water applications typically use one redundant train. This section of the spreadsheet is used to enter the number of redundant trains and reactors per train used by the UV system.

Lamp Data

The most significant operating costs of a UV system are due to lamp replacement and power consumption. UV systems are sized to deliver the required UV dose with the degree of lamp aging that occurs when the lamps are replaced. Lamp aging data is typically provided by the UV vendors. This section of the spreadsheet is used to enter the following information on the lamps.

- Lamp 100% Power - electrical consumption of the UV lamp and ballast assembly when the UV lamp is operating at the 100% ballast power setting. The value can be estimated as the total power of the UV system operating at 100% power divided by the total number of UV lamps.

- Lamp Life - the average operating life of the lamp. In the UV literature, the life of LP, LPHO, and amalgam lamps is stated between 8,000 and 12,000 hours and the life of MP lamps is stated between 3,000 and 5,000 hours. Often, the UV vendor guarantees a lamp life and provides a pro-rata warranty. Typically, the guaranteed lamp life is used to assess operating costs.
- Lamp Aging Factor - the relative UV output of the lamp under end of Lamp Life conditions. Traditionally, an aging factor of 65 or 70% has been specified as design criteria for wastewater UV systems. However, the NWRI/AwwaRF UV Guidelines specify using a 50% aging factor for both drinking water and reuse applications. Recently, UV vendors have been reporting aging factors ranging from 80 to 95 % with both amalgam and MP lamp technologies used for drinking water and wastewater applications.
- Lamp Cost - purchase price of a new UV lamp.
- Lamp Replacement Time - operator time required to replace one lamp.
- Fit Type (MMF, EXP, LIN, CUSTOM) - the type of mathematical equation that describes lamp aging as a function of operating time. The equation must predict the lamp aging factor used for the design at the specified lamp replacement interval. The equations for each Fit Type are:

$$\text{MMF: Lamp Aging Factor} = \frac{A \times B + C \times \text{Hours}^D}{B + \text{Hours}^D}$$

$$\text{EXP: Lamp Aging Factor} = A \times \exp(B \times \text{Hours})$$

$$\text{LIN: Lamp Aging Factor} = A \times \text{Hours} + B$$

CUSTOM: The user enters a custom equation in the field “Lamp Aging Equation.”

- Coefficients A through F - the equation coefficients for the fit types MMF, EXP, LIN, and CUSTOM. If a coefficient is not used, enter “0”.
- Lamp Power - lamp aging equations can be defined as a function of the lamp operating power. The CUSTOM lamp aging model can use this field as a model coefficient.
- Lamp Aging Equation - the field contains an equation that calculates the lamp-aging factor for the lamp life entered in the Lamp Life field. The calculated value should equal the value entered into the Lamp Aging Factor field. If the two values are not equal, the equation predicting lamp aging factor as a function of lamp hours is not valid and must be corrected. If the fit type is MMF, EXP, or LIN, the contents of the column B cell contains an equation that can be copied and used. If the fit type is CUSTOM, the user must enter an equation. That equation must reference one or more of the coefficients A, B, C, D, E, F, and Lamp Power. For example, for the entered data in column C of the Standard LCA tool, the user could enter:

$$= C65 * \exp(C66 * C60) + C67$$

as a custom equation. The coefficients A, B, and C would be user defined and entered into cells C65, C66, and C67. Cells C68, C69, C70, and C71 would be set to zero since those coefficients are not used by the equation.

Sleeve Data

UV lamps used within UV reactors are housed within quartz sleeves. The quartz sleeves protect the lamp from the water flow through the reactor and control heat transfer from the lamp to the water. With operation of the UV system, the UV transmittance of the quartz sleeve will decrease due to external and internal fouling of the sleeve surfaces and aging of the quartz material. UV systems are equipped with cleaning mechanisms that remove foulant from the external surfaces of the sleeves. Typically, automatic wipers are used by MP and LPHO UV systems used in wastewater applications and MP UV systems used in drinking water applications. Manual or automatic off-line acid washes are used by LPHO used in drinking water applications. Manual wiping or off-line acid baths are used with LP systems used in both drinking water and wastewater applications. This section of the spreadsheet is used to enter the following information on the lamp sleeves.

- Sleeve Life - the average operating life of the lamp sleeves. UV vendors typically state sleeve lives that range from 5 to 10 years. Typically, the guaranteed sleeve life is used to assess operating costs.
- Sleeve Cost - purchase price of a new sleeve.
- Sleeve Replacement Time - operator time required to replace one sleeve.
- Sleeve Cleaning Type (Rinse, Wiper) - the type of cleaning mechanism used by the UV system.
- Sleeve Cleaning Period - the time period between sleeve cleaning.
- Sleeve Cleaning Time/Reactor - the operator time required to clean the sleeves of one UV reactor in the system.
- Fouling Factor - the ratio of the UV transmittance of an aged and fouled UV sleeve to the UV transmittance of a new and clean sleeve. This ratio is often termed the design fouling factor and is used to size the UV system.

Ballast Data

Many UV systems use electronic ballasts that power and control one or two UV lamps. Some UV systems use electromagnetic ballasts that consist of transformers to adjust the operating voltage and a network of capacitors to control lamp current. This section of the spreadsheet is used to enter the following information on the lamp ballasts.

- Ballast Life - the average operating life of the ballast. UV vendors typically state ballast life that ranges from 5 to 10 years. Typically, the guaranteed ballast life is used to assess operating costs.
- Ballast Cost - purchase price of a new ballast.
- Ballast Replacement - operator time required to replace a ballast.

UV Sensor Data

Drinking water UV systems are all equipped with UV sensors that are used for performance monitoring. Often the duty UV sensors used to monitor performance are regularly checked using an independent reference sensor. The duty sensors are either calibrated by a calibration lab or calibrated by the operator through comparison with a calibrated reference sensor. While many wastewater systems are equipped with UV sensors, they may or may not be used for performance monitoring and their readings are typically not checked with a reference sensor. This section of the spreadsheet is used to enter the following information on the UV sensors.

- Sensor Life - the average operating life of the duty UV sensor. UV vendors typically state UV sensor life that ranges from 3 to 5 years. Typically, the guaranteed sensor life is used to assess operating costs.
- Sensor Cost - purchase price of a new duty UV sensor.
- Sensor Replacement - operator time required to replace one duty UV sensor.
- Sensor Calibration Period - the time period between calibration of the duty UV sensor.
- Sensor Calibration Cost - cost to calibrate a new duty sensor excluding operator labor.
- Sensor Calibration - operator time required to calibrate one duty UV sensor. If the UV sensor is sent to the calibration lab, the cost is the time required to facilitate that.

Dose Pacing

While UV systems are sized to deliver the required UV dose under design conditions of flow rate, water UVT, lamp aging, and sleeve fouling, they typically operate at lower flow rate and higher water UVT with lamps and sleeves that are not as aged and fouled as the design conditions. Under these conditions, if the UV system operated with all lamps on at 100% power, the UV system would overdose. To prevent overdosing and minimize costs, UV systems turn on and off banks of lamps and reduce ballast power to ensure UV dose meets requirements without excessive overdosing. Dose-pacing strategies vary from UV reactor to reactor and from installation to installation. The UV system can turn on and off banks of lamps or adjust lamp power in response to one or more of the following measured parameters:

- Flow rate.
- Predicted lamp output based on lamp operating hours.
- UVT.
- UV intensity.

When measured intensity is used for dose pacing, it accounts for lamp aging and sleeve aging and fouling. In some cases, the measured intensity also accounts for UV transmittance and a UVT monitor is not required for monitoring UV system performance.

With the STANDARD LCA and LAMP AGE LCA tool, this section of the worksheet is used to indicate which factors impacting UV dose delivery are accounted for by the dose-pacing strategy used by the UV system. This section is also used to input the Peak UV Dose defined as

the UV dose delivered by the duty UV reactors operating under design conditions of flow rate, water UVT, lamp aging, and sleeve fouling with all lamps on at the 100% power setting. This value should be equal or greater than the required UV dose if the UV system is properly sized. For example, while seven UV lamps may be required to deliver the required UV dose for a given application, the UV system provided by the UV vendor is equipped with eight lamps configured as two banks of four lamps. Thus, the peak UV dose can be estimated as 8/7 of the required UV dose.

With the ADVANCED LCA tool, this section of the worksheet is used to indicate the UV dose monitoring and control algorithm used by the UV system. This is done by entering a numeric value into the field “Dose Model.” This numeric value provides a reference to a model for UV dose monitoring and control in the worksheet RED MODEL. The second line termed “Dose Model” is set to the name of the model referred to by the numeric value specifying the UV dose model. Details on how to define the UV dose monitoring and control model in the worksheet RED MODEL is provided in section 1.1.3.

Failure Data

UV dose delivery over time by a UV system is affected by power quality and UV system component reliability. Power quality events that cause the UV lamps to extinguish include voltage sags and interruptions. Typically, the lamps extinguish when the voltage drops below a threshold voltage value for some duration. A generator is often used to provide power to the UV system during a power interruption. However, a generator does not prevent the lamps from extinguishing during a power quality event. As an alternate, a UPS can be used to provide continuous power supply to the UV system during power quality events. The time required to startup a UV system following a power quality event will depend on the lamp cool-down and warm-up times, the duration of the power quality event, and the time required to startup a generator if used. UV dose delivery is also impacted by failure of UV lamps and ballasts. UV dose monitoring is impacted by failure of UV sensor and UVT monitors. This section of the worksheet is used to enter the following information on UV system failure and response to failure:

- Supply Voltage Lower Limit - the percentage of nominal voltage that causes lamps to extinguish.
- PQ Event Duration Lower Limit - the duration of power quality event that causes lamps to extinguish.
- UPS (y,n) - indicates if an uninterruptible power system used to provide backup power.
- Generator (y,n) - indicates if a generator used to provide backup power.
- Generator Start-up Time - time required to start up the generator following the power quality event.
- Lamp Cool-down Time - time required to cool down the lamps before they can be restarted.
- Lamp Warm-up Time - time required to startup a UV lamp after cool down.
- Lamp Failure Probability - probability a single UV lamp will fail over a one day period.

- Ballast Failure Probability - probability a single lamp ballast will fail over a one day period.
- UV Sensor Failure Probability - probability a single UV intensity sensor will fail over a one day period.
- UVT Monitor Failure Probability - probability a single UVT monitor will fail over a one day period.

WTP Inputs

This section of the spreadsheet is used to enter the following site-specific data that impacts UV system O&M costs and performance:

- Labor Rate - the average labor rate including overhead of the personnel operating and maintaining the UV system.
- Electricity Cost - the cost of electricity paid by the utility.
- Patent Fees - patent royalties paid by the utility for using the UV system. Currently, the Calgon Carbon Corporation has a patent for *Cryptosporidium* and *Giardia* inactivation and requests royalty payments of \$0.015 per 1000 gallons treated.
- Interest Rate - the annual interest rate on money borrowed by the utility.
- Period - the period over which the utility pays back money borrowed to pay for the UV system. The life-cycle cost assessment is conducted over that period.
- Supply Voltage - the nominal supply voltage to the UV system.
- Population - the population served by the UV system.

Capital Cost Inputs

This section of the spreadsheet is used to enter UV system capital cost information.

- Reactor - the total capital costs of the UV reactors including the control panels.
- Install factor - the cost of installing the UV equipment.
- Validation - the cost for validating the UV reactor.
- Inlet/Outlet Piping - the capital cost including installation of all inlet and outlet piping needed for the UV system including flowmeters, valves, pipes, and channels.
- Power Supply - capital cost of providing power to the UV system including switch gear, transformers, distribution panels, generators, and UPS systems.
- Other - other costs include yard piping, chlorine contactors, and low lift pumps.
- UV Building - capital costs for demolition, civil/site work, building, and HVAC.
- Instrumentation - capital cost of all instrumentation including SCADA and on-line UVT monitors.
- HVAC - an alternate field for entering HVAC.
- Miscellaneous Electrical - a field for entering cost of any miscellaneous electrical work.
- Civil/Site Work - an alternate field for entering civil site work.
- Contingency - capital cost contingency typically set as a percent of all capital costs.

- General Conditions - includes mobilization/demobilization, major equipment, site preparation such as fences, temporary facilities for contractors, bonds/insurance, permits, supervision and engineering salaries, support systems (e.g., water), and general expense items.
- Contractor O&P - contractor overhead and profit typically set as a percent of all the above costs.
- Engineering, Legal, and Administration - the engineering costs of the UV project typically set as a percent of all the above costs.
- Total - total of all capital costs.

UV Dose Delivery

If dose pacing accounts for water UVT, the Standard LCA and the Lamp Age LCA tools use data on dose delivery as a function of UVT to estimate O&M costs. This section of the Standard LCA and the Lamp Age LCA tools is used to enter data on dose delivery as a function of specified values of water UVT. UV dose delivery by the reactor should be entered for one UV reactor operating at the design flow rate with new lamps all on and operating at 100% power, and new clean sleeves.

Ballast Power Settings

The Advanced LCA tool allows the user to enter data on ballast power settings. The Advanced LCA tool uses this data to simulate UV system operation as a function of time. Ballast typically operate at discrete power settings. Enter the discrete power settings in ascending order starting with the minimum power setting. Enter “9999” if the indicated setting does not have a value. If the UV vendor states the ballast power settings are continuous, enter values from the minimum to maximum setting at increments equal to $(\text{Max}-\text{Min})/22$.

Water Quality Data

The Advanced LCA uses the worksheet entitled WQ to enter water quality data over time as follows:

Column	Data
A	Date/time
B	Flow rate
C	UVT
D	Raw water pathogen concentration
E	Supply Voltage
F	Power quality event duration

The last entry in column C should be “9999”. Up to 10,000 datasets of date/time, flow rate, and UVT can be entered.

RED Model

The worksheet entitled RED MODEL contains equations for UV dose monitoring and control for various UV systems. The information entered into cells A3 to C23 is used as an index to identify the various models in this worksheet. Cells A3 to A23 are used to enter the name of the UV system model. Cells B3 to B23 give the model identification number. Cells C3 to C23 define the column within this worksheet where the specified model is located.

The Advanced LCA algorithm programmed into UVCAT uses the models located in REDMODEL as a calculator to determine UV dose delivery and target ballast power settings given inputs on target UV dose, flow rate, UVT, number of banks of lamps, and ballast power setting. The structure of each referenced model is organized into five color-coded sections. The first section in rows 5 to 12, color-coded yellow, represents information that the Advanced LCA algorithm transfers into the model. This information includes:

- Target RED per reactor,
- Flow rate per reactor,
- Water UVT,
- Lamp aging factor,
- Fouling factor,
- Number of operating banks per reactor, and
- Actual Power Setting of type 1 and 2 lamps in each bank

The second section in rows 13 to 14, color-coded light blue, defines how many Type 1 and Type 2 lamps are in each bank and the model calculation cells. Type 1 and 2 lamps are defined as lamps within a bank that have a specified relationship between measured UV intensity and ballast power setting. With MP lamps, the relationship between measured UV intensity and ballast power setting may differ if the lamp is monitored from different directions because of a non-uniform UV intensity field around the lamp. With LPHO lamps, the relationship between measured UV intensity and ballast power setting may differ because one sensor monitors one lamp and another monitors multiple lamps. Note that the entered number of Type 1 and Type 2 lamps must add up to the total number of lamps in a bank. Furthermore, if the relationship between measured UV intensity and ballast power setting is the same for all lamps, the Type 1 lamps is set equal to the number of lamps in a bank and Type 2 lamps is set to zero.

The field termed Model Calc in row 15, color-coded light blue, is an alphanumeric string specifying the cells where the model equations are located. UVCAT uses this alphanumeric string to identify where the UV dose monitoring model equations are located in the worksheet for a given model. For example, for a model located in column G, Model Calc may be set to "G17:G34." This tells UVCAT that the equations used in the UV dose model are located in cells G17 to G34.

The third section in the model in rows 17 to 22, color-coded dark blue, contain equations for determining UV dose delivery, sensor readings, target ballast power settings, and target UV sensor values as follows:

- Row 17 - equation for the target ballast power for Type 1 lamps
- Row 18 - equation for the target ballast power for Type 2 lamps
- Row 19 - equation for the target UV sensor readings
- Row 20 - equation for the actual sensor reading
- Row 21 - equation for the actual UV dose delivered.

- Row 22 - equation indicating if the reactor is operating off spec

The UVCAT user defines these equations, either from the validation report for the UV system or from CFD-based modeling.

The target ballast power setting is defined as the ballast power setting predicted to deliver the target UV dose given the flow rate, UVT, lamp aging, fouling, trains, reactors, and banks entered in section 1 (color coded yellow). The target power setting calculated using the equations can be above, below, or within the range of ballast power settings used by the reactor. For example, the equation may determine that the UV reactor as defined in rows 5 to 12 would have to operate at a power setting of 200 percent to deliver the required UV dose. This outcome indicates to UVCAT that the UV system needs to operate with more reactors and banks of lamps.

The fourth section of the model in rows 24 and on, color-coded peach, contains other equations that can be referenced by the equations in rows 17 to 21. As many cells and equations as necessary can be used in this section to facilitate the calculation of target ballast power and delivered UV dose. However, the field Model Calc must include both the cell in rows 17 to 22 as well as the cells in this section.

The fifth and last section of the model occurs in rows below the fourth section and is color-coded light blue. These rows contain numeric constants used by the equations entered into sections 3 and 4. Ideally, the coefficients entered into section 5 and the equations entered into section 3 and 4 by the UVCAT user are based on validation data.

The example version of UVCAT provided with this report provides eight example RED models for drinking water reactors and three example RED models for wastewater reactors. These examples should be studied and understood by the UVCAT user before using UVCAT. These models can be used as a framework for defining models for commercial reactors.

IMPORTANT NOTE: The example drinking water models entered into UVCAT were developed based on models used by the industry but are not true models of commercial UV systems. UV vendors consider their models proprietary and do not want them published in the public domain. However, engineers and utilities can obtain validation reports from UV vendors that define the models or can work with UV vendors to develop a model.

Risk Model

The worksheet RISKMODEL is used to enter the UV dose-response of the target pathogen and the risk model for human infection. The Advanced LCA algorithm programmed into UVCAT uses these models as a calculator tool to determine log inactivation credit and public health impact of a given UV dose and a raw water pathogen concentration.

The pathogen UV dose-response is located in column C. Cell C7 contains the UV dose defined as the RED calculated using the UV dose model. Cell C8 contains an equation for the log inactivation expected with that UV dose. Cell C9 contains the maximum pathogen inactivation credit that a State will grant. Cell C10 contains the credited log inactivation based on the maximum pathogen credit and the calculated log inactivation.

The risk model for human infection is located in column G. Specific cells are as follows:

- Cell G7 - raw water pathogen concentration
- Cell G8 - log removal credit through the filter
- Cell G9 - UV log inactivation credit

- Cell G10 - Chemical disinfection log inactivation credit
- Cell G11 - Human water consumption per day
- Cell G12 - Number of infections per UV dose

UVCAT ALGORITHMS

The following sections describe the software algorithms used by UVCAT.

Standard Life-Cycle Cost Analysis

The Standard Life-Cycle Cost Analysis uses two subroutines. The first determines the operation status of the UV system under average conditions. The second determines O&M costs for those conditions and calculates the present worth costs factoring in capital costs.

Determining UV System Operating Status

The following steps are incorporated into a subroutine that determines the number of banks, lamps, ballasts, and UV sensors used for the UV reactor operating under average conditions of flow rate, UVT, lamp aging, and lamp fouling given the dose-pacing strategy used by the UV system.

Step 1. Calculate the total number of lamps in each reactor:

$$\text{Total lamps/reactor} = \text{Lamps/bank} \times \text{banks/reactor}$$

Step 2. Calculate the total number of lamps required under design conditions of UV dose, flow rate, UVT, lamp aging, and fouling.

$$\text{Total duty lamps} = (\text{Trains} - \text{Parallel Redundancy}) \times (\text{Reactors/Train} - \text{Series Redundancy}) \times \text{Total lamps/reactor} \times \text{Design UV Dose} / \text{Peak UV Dose}$$

This calculation factors in the specified redundancy of the UV system and the ratio of design to peak UV dose. The ratio accounts for the fact that the UV system may have the capacity to deliver a UV dose greater than the design UV dose under design conditions of flow rate, UVT, lamp aging, and fouling.

Step 3. If the UV system uses a dose-pacing strategy that responds to flow rate, adjust the total duty lamps by the ratio of average flow rate to peak flow rate.

$$\text{Total duty lamps} = \text{Total duty lamps} \times \text{Average flow rate} / \text{Peak flow rate}$$

Step 4. If the UV system uses a dose-pacing strategy that responds to UVT, adjust the total duty lamps by the ratio of UV dose delivered at design UVT to UV dose delivered at average UVT. Use interpolation of entered UV dose as a function of UVT to calculate the UV dose expected at average and design UVT.

$$\text{Total duty lamps} = \text{Total duty lamps} \times \text{UV Dose (Design UVT)} / \text{UV Dose (Average UVT)}$$

Step 5. If the UV system uses a dose-pacing strategy that responds to lamp aging, integrate the inverse of the lamp-aging curve over the lamp replacement interval. Determine the lamp age where the integrated value equals half the value over the lamp replacement interval. Adjust the total duty lamps by the lamp-aging factor that occurs at that lamp age. This approach

assumes that the increase in lamp power required to dose pace as a function of lamp aging is inversely proportional to the lamp-aging curve.

$$\text{Total duty lamps} = \text{Total duty lamps} \times \frac{\text{Output of new lamp}}{\text{Output of lamp at half of lamp-life}}$$

Step 6. If the UV system uses a dose-pacing strategy that responds to sleeve fouling, adjust the total duty lamps by the average fouling factor defined as $(1+f_f)/2$ where f_f is the design fouling factor.

$$\text{Total duty lamps} = \text{Total duty lamps} \times (1 + \text{Design fouling factor}) / 2$$

Step 7. Calculate the number of operating banks in the UV system.

$$\text{Duty Banks} = \text{Total duty lamps} / \text{Lamps/bank}$$

$$\text{If Duty Banks} > \text{Int}(\text{Duty Banks}) \text{ then Duty Banks} = \text{Duty Banks} + 1$$

The calculation assumes that the UV system always operates as multiples of a single bank.

Step 8. Calculate the power setting of the lamps in those banks.

$$\text{Power Setting} = \text{Total Duty lamps} / (\text{Duty Banks} \times \text{Lamps/bank})$$

Step 9. Calculate the number of operating lamps, ballast, and sensors in the duty banks.

$$\text{Duty Lamps} = \text{Duty Banks} \times \text{Lamps/Bank}$$

$$\text{Duty Ballasts} = \text{Duty Lamps} / \text{Lamps/Ballast}$$

$$\text{Duty UV Sensors} = \text{Duty Lamps} / \text{Lamps/Bank} \times \text{Duty UV Sensor/Bank}$$

Determining UV System Costs

The following steps are incorporated into a subroutine that determines the UV system O&M and life-cycle costs.

Step 1. Calculate the annual power costs.

$$\text{Power Costs} = \text{Power/Lamp} \times \text{Electricity Costs} \times \text{Duty Lamps} \times \text{Power Setting}$$

Step 2. Calculate the annual consumable costs.

$$\text{Lamp Costs} = \text{Duty Lamps} / \text{Lamp Life} \times \text{Lamp Cost}$$

$$\text{Sleeve Costs} = \text{Duty Lamps} / \text{Sleeve Life} \times \text{Sleeve Cost}$$

$$\text{Ballast Costs} = \text{Duty Ballasts} / \text{Ballast Life} \times \text{Ballast Cost}$$

$$\text{UV Duty Sensor Costs} = \text{Duty UV Sensors} / \text{UV Sensor Life} \times \text{UV Sensor Cost}$$

$$\text{UV Sensor Calibration Costs} = \text{Duty UV Sensors} / \text{UV Sensor Calibration Period} \times \text{Sensor Calibration Cost}$$

$$\text{Consumable Costs} = \text{Lamps Costs} + \text{Sleeve Costs} + \text{Ballast Costs} + \text{Duty UV Sensors Costs} + \text{Sensor Calibration Costs}$$

This calculation assumes that the sensor life is defined by operating time.

Step 3. Calculate annual labor costs.

$$\text{Lamp Replacement Labor} = \text{Duty Lamps} / \text{Lamp Life} \times \text{Lamp Replacement}$$

$$\text{Sleeve Replacement Labor} = \text{Duty Lamps} / \text{Duty UV Sensor Life} \times \text{Sensor Replacement}$$

If Sleeve Cleaning Type = "Rinse" then

$$\begin{aligned} \text{Cleaning Labor} &= (\text{Trains} - \text{Parallel Redundancy}) \times (\text{Reactors/Train} - \\ &\text{Series Redundancy}) / \text{Sleeve Cleaning Period} \\ &\times \text{Sleeve Cleaning Time/Reactor} \end{aligned}$$

$$\text{Ballast Replacement Labor} = \text{Duty Ballasts} / \text{Ballast Life} \times \text{Ballast Replacement}$$

$$\text{Sensor Replacement Labor} = \text{Duty Sensors} / \text{Sensor Life} \times \text{Sensor Replacement}$$

$$\text{Sensor Calibration Labor} = \text{Duty Sensors} / \text{Sensor Calibration Period} \times \text{Sensor Calibration}$$

$$\begin{aligned} \text{Labor Costs} &= \text{Lamp Replacement labor} + \text{Sleeve Replacement Labor} + \text{Cleaning Labor} \\ &+ \text{Ballast Replacement Labor} + \text{Sensor Replacement Labor} \\ &+ \text{Duty UV Sensor Calibration Labor} \end{aligned}$$

Step 4. Calculate Annual Patent Costs.

$$\text{Patent Costs} = \text{Total Flow} \times \text{Patent Cost}$$

Step 5. Calculate Total O&M Costs

$$\text{O\&M Costs} = \text{Power Costs} + \text{Consumable Costs} + \text{Labor Costs} + \text{Patent Costs}$$

Step 6. Calculate Reactor Capital Costs.

$$\text{Reactor Capital} = \text{Reactor Cost} \times \text{Reactors/Train} \times \text{Trains}$$

$$\begin{aligned} \text{Capital Costs} &= \text{Reactor Capital} + \text{Building Piping} + \text{Power Supply} + \text{Instrumentation} \\ &+ \text{Engineering} \end{aligned}$$

Step 7. Calculate Present Worth Costs.

$$\text{NPV} = 0$$

For $x = 1$ to Period

$$\text{NPV} = \text{NPV} + (1 + \text{Interest})^{-x}$$

Next x

$$\text{NPV} = \text{NPV} \times \text{O\&M Costs} + \text{Capital Costs}$$

Lamp Replacement Interval Cost Analysis

The Lamp Replacement Interval Cost Analysis determines the UV System Operating Status and UV System Costs for lamp replacement intervals from 1,000 to 20,000 hours in 1,000-hour increments. For each replacement interval, the algorithm adjusts the number of duty lamps by the ratio of the standard lamp aging factor to the lamp-aging factor associated with the interval. In other words, Step 2 of the subroutines that determines the UV System Operating Status includes:

$$\begin{aligned} \text{Total duty lamps} &= \text{Total duty lamps} \times \text{Lamp Aging Factor} \\ &/ \text{Lamp Aging Factor}(\text{Lamp Replacement Interval}) \end{aligned}$$

The Lamp Aging Factor for each interval is calculated using the entered Lamp Aging Equation.

If the Lamp Aging Flag is set to one, the algorithm also adjusts the capital costs by the ratio of the standard lamp aging factor to the lamp-aging factor associated with the interval.

$$\begin{aligned} \text{Capital Costs} &= \text{Capital Costs} \times \text{Lamp Aging Factor} / \\ &\text{Lamp Aging Factor}(\text{Lamp-Replacement Interval}) \end{aligned}$$

Advanced Life-Cycle Cost Analysis

The Advanced Life-Cycle Cost Analysis uses three subroutines. The first determines the operation status of the UV system for each data set of water quality data (date/time, flow rate, UVT). The second determines the impact of power quality and component failure events on UV dose delivery and provides an estimate of public health protection. The third estimate determines integrated O&M costs and calculates the present worth costs factoring in capital costs.

Determining UV System Operating Status

The following approach is used to determine the number of reactors and banks of lamps used by the UV system to deliver the target UV dose at various conditions of flow rate and UVT specified in the worksheet WQ.

Step 1. Define the first water quality data set (date/time, flow rate, UVT) as time zero data. Set lamp aging factors for each bank to 100 percent. Set fouling factors for the UV system to 100%.

Step 2. Set the number of operating reactors and operating banks equal to 1. Calculate the flow per reactor as:

$$\text{Flow per reactor} = \text{Flow} / \text{Number of Reactors}$$

Step 3. For each bank of lamps in the operating UV system, enter the flow per reactor, UVT, lamp aging factor, and fouling factor into the relevant model for UV dose monitoring and control in REDMODEL. Read the target ballast power setting needed to deliver the required UV dose. If the required ballast setting is greater than 100 percent with any bank or the UV system is off specification, increase the number of banks of lamps in the operating UV system and repeat this step. If the required ballast setting is less than 100% with all banks, then identify the ballast power setting that equals or just exceeds the target ballast power setting.

Step 4. Determine the minimum UV sensor reading per reactor accounting for ballast power setting, lamp aging, and fouling. The lamp aging factor and ballast power setting will vary from bank to bank depending on previous simulated operation. Using the model for UV dose monitoring referenced in REDMODEL, determine the UV dose delivered by each reactor using the minimum UV sensor reading.

Step 5. Read the next water quality dataset. Calculate the lamp hours with each bank of lamps based on the operation defined in Step 4. Determine the lamp age per bank using those updated numbers. Update the fouling factor based on the expected rate of fouling over that period.

Step 6. Repeat steps 3 to 5 for each combination of date/time, flow rate, UVT in the water quality dataset.

Determining the Impact of Power Quality and Component Failure Events

The following approach is used to determine the UV system response to power quality and UV system component failure.

Step 1. For each water quality dataset, if the Supply Voltage is less than the voltage threshold for a duration longer than the event duration threshold, then a power quality event has occurred that causes the lamps to extinguish.

Step 2. Determine the down time due to the power quality event as follows:

If UPS = yes then Downtime = 0

If UPS = No and Generator = Yes, Then

If PQ Event Duration > Generator Startup Time, Then

If Generator Startup Time > Lamp Cool Down Time, Then

Downtime = Generator Startup Time

Else

Downtime = Lamp Cool Down Time

End if

Else

If PQ Event Duration > Lamp Cool Down Time, Then

Downtime = PQ Event Duration

Else

Downtime = Lamp Cool Down Time

End if

End if

Downtime = Downtime + Lamp Warmup Time

End if

If UPS = No and Generator = No, then

If PQ Event Duration > Lamp Cool Down Time, Then

Downtime = PQ Event Duration

Else

Downtime = Lamp Cool Down Time

End if

Downtime = Downtime + Lamp Warmup Time

End If

If Automatic Flow Shutoff Valve = Yes and Shutoff Valve Response Time < Downtime,

Then

Downtime = Shutoff Valve Response Time

End if

Step 3. Assume zero UV dose delivery over the downtime duration.

Step 4. For each WQ dataset, determine if a lamp, ballast, or UV sensor has failed using a Monte Carlo approach. Calculate Delta Date/Time as the difference between the Date/Time of the current and previous WQ datasets:

Delta Date/Time = Date/Time (t) - Date/Time(t-1)

Determine the probability of lamp failure within that bank of lamps over the duration of Delta Date/Time:

Probability = 1 - (1 - Lamp Failure Probability per day) ^ (Lamps per Bank × Delta Date Time)

Generate a random number between 0 and 1. If the random number is less than the probability of failure for a lamp, then assume a lamp failure event has occurred:

If Probability < Random Number then Lamp Failure

Repeat these calculations using the probability of failure for ballasts and lamps.

Step 5. Assume the UV dose-monitoring algorithm cannot estimate dose delivery with a bank of lamps if a lamp, ballast, or UV sensor failure event has occurred. As such, UV dose delivery by that bank is assumed as zero. Calculate UV dose delivery by the UV reactor using the remaining number of banks of lamps. Use the minimum UV sensor reading with the various banks of lamps in the dose calculation.

Step 6. UV system will respond to the failure event by turning on a bank of lamps or a reactor. Calculate the time it takes to turn on the bank of lamps as:

$$\text{Failure time} = \text{Lamp Warmup Time}$$

Calculate the time it takes to turn on another reactor as:

$$\text{Failure Time} = \text{Automatic Valve Shut Off Time} + \text{Lamp Warmup Time}$$

Step 7. Using the pathogen UV dose response model in the worksheet RISKMODEL, determine dose delivery and log inactivation by each train of reactors for following cases:

1. Operation unaffected by power quality events or component failure,
2. Operation with zero UV dose delivery caused by the power quality event, and
3. Operation with reduced UV dose delivery caused by the component failure event.

Calculate log inactivation by the UV system over the Delta Date/Time period as follows:

$$\text{UV System Log Kill} = 0$$

For $x = 1$ to Trains

$$\text{UV System Log Kill} = \text{UV System Log Kill}$$

$$+ \text{Failure Time} / \text{Delta Date/Time} \times 10^{-(\text{Failure Log Kill})}$$

$$+ (\text{Delta Date/Time} - \text{Failure Time} - \text{Downtime}) / \text{Delta Date/Time} \times 10^{-(\text{Log Kill})}$$

Kill)

Next x

$$\text{UV System Log Kill} = -\log(\text{UV System Log Kill}/\text{Trains})$$

Step 8. Using the human infection UV dose response model in the worksheet RISKMODEL, calculate the risk of infection. Calculate the accumulated infections over time.

Step 9. Determine the monthly average off spec performance by time and by volume.

Determine Integrated O&M and Life-Cycle Costs

The following approach is used to determine the integrated O&M and life-cycle costs.

Step 1. After determining the operation of the UV system using the last WQ dataset, calculate the Total Bank Hours as the sum of the bank hours with each bank in each reactor:

$$\text{Total Bank Hours} = 0$$

For $x = 1$ to Trains

For $y = 1$ to Reactors

For $z = 1$ to Banks

$$\text{Total Bank Hours} = \text{Total Bank Hours} + \text{Bank Hours}(x,y,z)$$

Next z

Next y

Next x

Step 2. Calculate Total Delta Date/Time as the difference in the Date/Time of the first and last WQ datasets:

$$\text{Total Delta Date/Time} = \text{Date/Time}(\text{last}) - \text{Date/Time}(1)$$

Step 3. Calculate the average number of lamps, ballast, and UV sensors used by the UV system over the simulation as:

```

Total Power = 0
For x = 1 to Trains
  For y = 1 to Reactors
    For z = 1 to Banks
      Total Bank Hours = Total Bank Hours + Bank Hours (x,y,z)
    Next z
  Next y
Next x
Duty Lamps = Total Bank Hours × Lamps per Banks / Total Delta Date/Time
Duty Ballasts = Duty Lamps / Lamps/ballast
Duty UV Sensors = Duty Lamps / Lamps/bank × Sensors/Bank

```

Step 4. Calculate the integrated power consumed by each bank of lamps in each reactor:

```

Sum Power = 0
Do Until Last WQ Dataset
  For x = 1 to Trains
    For y = 1 to Reactors
      For z = 1 to Banks
        Sum Power = Sum Power + Power (x,y,z)
      Next z
    Next y
  Next x
Loop

```

Power Setting = Sum Power / Total Delta Date/Time / Power/Lamp / Duty lamps

Step 5. Determine O&M life-cycle costs using the Standard LCA subroutine for determining UV system costs.

UVCAT OUTPUTS

Table A.3 lists the worksheets within UVCAT that are used to output data generated by UVCAT.

Table A.3 UVCAT worksheets used for output

Analysis	Input worksheets
Standard life-cycle cost analysis	STANDARD LCA
Lamp Replacement Interval Cost Analysis	LAMP AGE LCA TOOL
Advanced life-cycle cost analysis	ADVANCED LCA WQ REACTOR DOSE TARGET POWER 1 TARGET POWER 2 POWER 1 POWER 2 LAMP HOURS LAMP AGING FACTOR

Standard Life-Cycle Cost Analysis

The outputs for the Standard Life-Cycle Cost Analysis are placed in the worksheet entitled INPUTS AND LCA in rows 19 through 30.

- Rows 19 and 20 provide the lamp life and aging factor used in the analysis. The data matches the data entered in Lamp Data and is provided for reference purposes.
- Rows 21 and 22 provide the number of duty lamps and power setting of those lamps with the UV system operating under average conditions of flow rate, UVT, lamp aging, and sleeve fouling given the dose-pacing strategy used by the UV system.
- Rows 23 through 33 provide annual O&M costs. Row 23 provides the annual power cost. Rows 25 through 29 provide annual consumables costs including lamp replacement, sleeve replacement, ballast replacement, sensor replacement, and sensor calibration, respectively. Row 30 provides the total annual consumable costs. Rows 31 and 32 provide the annual total labor and patent costs, respectively. Row 33 provides total annual O&M costs.
- Row 34 provides total capital costs. Rows 35 and 36 provides total present worth costs and present worth of O&M.
- Row 37 provides the ballast power setting the UV system operates at under design conditions. If the power setting is greater than 100%, the UV system is undersized for the design conditions of flow, UVT, lamp aging, and fouling. If the power setting is less than 100%, the UV system is oversized.

Lamp Replacement Interval Cost Analysis

The outputs for the Lamp Replacement Interval Cost Analysis are placed in the worksheet entitled LAMP AGE ANALYSIS.

Results for each case analyzed are placed in tables organized with the results for case 1 placed in rows 18 through 40, case 2 in rows 44 through 66, case 3 in rows 70 through 92, as so forth. The tables provide operating status and costs as a function of lamp replacement interval. Columns in each table are:

- Lamp Life - from 1,000 to 20,000 hours in 1,000 hour increments
- Age Factor - lamp aging factor associated with each lamp life
- Average Lamps - number of lamps that would operate under average conditions of flow rate, UVT, lamp age, and sleeve fouling.
- Power Setting - Power setting of those lamps
- Power - annual power costs
- Consumables - annual consumable costs
- Labor - annual labor costs
- Patent - annual patent costs
- Total O&M - total annual O&M costs
- Capital - total capital costs
- NPV - Net Present Value of O&M and capital costs

Information in each table can be graphed as a function of lamp replacement interval.

Advanced Life-Cycle Cost Analysis

The outputs from the advanced LCA tool are placed in the following worksheets:

- LAMP AGING FACTOR - relative output of the UV lamps in each banks of lamps as a function of time
- LAMP HOURS - number of operating hours accumulated by the lamps since lamp replacement in each bank of lamps as a function of time
- TARGET POWER 1 - target power predicted by the RED model for the type 1 lamps in each bank assuming ideal dose pacing with infinite turndown and turn up (ie, the target power could be 25 kW with lamps rated at 10 kW).
- TARGET POWER 2 - target power predicted by the RED model for the type 2 lamps in each bank
- POWER 1 - operating power setting of the type 1 lamps in each bank based the entered ballast power settings achievable
- POWER 2 - operating power setting of the type 2 lamps in each bank
- REACTOR DOSE - UV dose delivered by each reactor in the UV system as a function of time with operation not impacted by power quality events and component failure
- WQ - various measures of UV system performance as a function of time including:
 - Target RED - column I
 - Trains - column J
 - Reactors Per Train - column K
 - Banks per Reactor - column L
 - Flow rate per reactor - column M
 - Fouling Factor - column N
 - Total Power based on Power 1 and Power 2 data - column O
 - Ideal Total Power based on Target Power 1 and Target Power 2 data - column P
 - Ratio of Total Power and Ideal Total Power - column Q
 - Daily Power Costs - column R
 - Power Costs - column S
 - Sum Power Costs - column T
 - Ofspec Flag - column U
 - Percent Ofspec Time - column V
 - Percent Ofspec Volume - column W
 - UV System Log Kill - column X
 - Risk - column Y
 - Annual Risk - column Z
 - Accumulated Illness - column AA

The information placed into the above-mentioned worksheets is for the last column of analysis conducted by Advanced LCA Tool of UVCAT. Because UVCAT can conduct analysis of multiple sets of input data, the software also saves the worksheet WQ for each analysis to a user-defined file. The user can specify the filename and the directory where that file is saved in

cells B5 and B6 of the worksheet ADVANCED LCA. Examples of those output files are provided for the analysis conducted for this report.

Last, the CLEAR button in the worksheet ADVANCED LCA allows the UVCAT user to clear all output data in the above-mentioned spreadsheets. This feature is useful for removing output data from old files and minimizing the filesize of UVCAT EXCEL workbook. The example version of UVCAT provided with this report includes example output data.

QUALITY ASSURANCE/QUALITY CONTROL

The UVCAT software checks the inputs to the software and flags the user if those inputs do not meet the criteria given in Table A.4. The criteria provided in Table A.4 are broad and extend well beyond the typical range used with drinking water and wastewater reactors. The user should use Table A.4 as guidance for the values entered into UVCAT.

As discussed, UVCAT uses various models for lamp aging, UV dose delivery, pathogen UV dose-response, and risk analysis. Those models are defined by the user. UVCAT does not check the form of those models. If the form of those models gives results that make no sense, either the outputs from UVCAT will make no sense or the model could cause a software running error. For example, if the model used results in a divide by zero taking place, the software will stop and indicate an error with the following message:

“UVCAT encountered a running error”

The user should check their models for lamp aging, UV dose delivery, pathogen UV dose-response, and risk analysis to ensure they provide valid predictions over the range of conditions simulated using UVCAT. If UVCAT does encounter a mathematical error running the Advanced LCA, the user can investigate model predictions for the combination of WQ data that caused the software error by entering that data into the respective models.

Table A.4 UVCAT QA/QC Checks on Input Parameters.

Parameter	Units	UVCAT QA/QC Criteria
Maximum Flow rate	mgd	$0 < \text{Value} \leq 9999$
Average Flow rate	mgd	$0 < \text{Value} \leq 9999$
Average UVT	%	$0 < \text{Value} < 100$
Design UVT	%	$0 < \text{Value} < 100$
Design UV Dose	mJ/cm^2	$0 < \text{Value} \leq 9999$
Minimum Number of Trains	-	$0 \leq \text{Value} \leq 40$
Max. Flow rate per reactor	mgd	$0 < \text{Value} \leq 9999$
Number of Trains	-	$0 < \text{Value} \leq 40$
Number of Reactors/Train	-	$0 < \text{Value} \leq 8$
Banks/Reactor	-	$0 < \text{Value} \leq 30$
Lamps/Bank	-	$0 < \text{Value} \leq 9999$
Lamps/Ballast	-	$0 < \text{Value} \leq \text{Lamps/Bank}$

(Continued)

Table A.4 UVCAT QA/QC Checks on Input Parameters (cont.)

Parameter	Units	UVCAT QA/QC Criteria
Sensors/bank	-	$0 < \text{Value} \leq \text{Lamps/Bank}$
No. of Redundant Trains	-	$0 \leq \text{Value} < \text{Number of Trains}$
No. of Redundant Reactors per train	-	$0 \leq \text{Value} < \text{Number of Reactors/Train}$
Lamp 100% Power	kW	$0 < \text{Value} \leq 100$
Lamp Life	hrs	$0 < \text{Value} \leq 100,000$
Lamp Aging Factor	%	$0 < \text{Value} \leq 100$
Lamp Cost	\$	$0 < \text{Value} \leq 99,999$
Lamp Replacement Time	Min.	$0 < \text{Value} \leq 500$
Fit Type (MMF, EXP, LIN, CUSTOM)	-	Enter either MMF, EXP, LIN or CUSTOM
Coefficient A	-	Any numeric value, set to 0 if not used
Coefficient B	-	Any numeric value, set to 0 if not used
Coefficient C	-	Any numeric value, set to 0 if not used
Coefficient D	-	Any numeric value, set to 0 if not used
Sleeve Life	yrs	$0 < \text{Value} \leq 100$
Sleeve Cost	\$	$0 < \text{Value} \leq 20,000$
Sleeve Replacement Time	min	$0 < \text{Value} \leq 500$
Sleeve Cleaning Type (Rinse, Wiper)	-	Enter either "Rinse" or "Wiper"
Sleeve Cleaning Period	weeks	$0 < \text{Value} \leq 99$
Sleeve Cleaning Time/Reactor	min	If Sleeve Cleaning Type = Rinse, then $0 < \text{Value} \leq 1000$ If Sleeve Cleaning Type = Wiper, then $0 \leq \text{Value} \leq 100$
Fouling Factor	%	$0 < \text{Value} \leq 100$
Ballast Life	yrs	$0 < \text{Value} \leq 100$
Ballast Costs	\$	$0 < \text{Value} \leq 100,000$
Ballast replacement	min	$0 < \text{Value} \leq 600$
Sensor life	yrs	$0 < \text{Value} \leq 100$
Sensor cost	\$	$0 < \text{Value} \leq 20,000$
Sensor replacement	min	$0 < \text{Value} \leq 300$
Sensor cal period	months	$0 < \text{Value} \leq 60$
Sensor calibration cost	\$	$0 < \text{Value} \leq 9999$
Sensor calibration	min	$0 < \text{Value} \leq 600$
Dose Model	-	$0 < \text{Value} \leq 99$
Peak UV Dose	mJ/cm ²	$0 < \text{Value} \leq 9999$

(Continued)

Table A.4 UVCAT QA/QC Checks on Input Parameters (cont.)

Parameter	Units	UVCAT QA/QC Criteria
Flow (y/n)	-	Either “y” or “n”
Lamp Age (y/n)	-	Either “y” or “n”
Lamp Age (y/n)	-	Either “y” or “n”
UVT (y/n)	-	Either “y” or “n”
Fouling (y/n)	-	Either “y” or “n”
Supply Voltage Lower Limit	% nom	0 < Value < 100
PQ Event Duration Lower Limit	s	0 < Value ≤ 100
UPS (y/n)	-	Either “y” or “n”
Generator (y/n)	-	Either “y” or “n”
Generator Startup Time	s	0 < Value ≤ 1800
Automatic Flow Shutoff Valve (y/n)	-	Either “y” or “n”
Shut Off Valve Response Time	s	0 < Value ≤ 1800
Lamp Cool-down Time	min	0 < Value ≤ 30
Lamp Warmup Time	min	0 < Value ≤ 30
Lamp Failure Probability	per day	0 ≤ Value < 1
Ballast Failure Probability	per day	0 ≤ Value < 1
UV Sensor Failure Probability	per day	0 ≤ Value < 1
UVT Monitor Failure Probability	per day	0 ≤ Value < 1
Labor rate	\$/hr	0 < Value ≤ 999
Electricity Cost	\$/kWhr	0 < Value ≤ 99
Patent fees	\$/1000 gal	0 < Value ≤ 99
Interest rate	%	0 < Value ≤ 100
Period	yrs	0 < Value ≤ 99
Supply Voltage	volts	0 < Value ≤ 9999
Population	-	0 < Value ≤ 999,999,999
Dose Delivery vs UVT	mJ/cm ²	0 < Value ≤ 9999
Ballast Power Settings	%	0 < Value ≤ 150 9999
Starting Column	-	0 < Value < 254
Ending Column	-	0 < Value < 254
Lamp Aging Analysis Type	-	0 or 1
Save Directory	-	Valid MS Windows Directory Name
Save Directory	-	Valid MS Windows File Name
Date_Time	-	Valid Excel Date/Time Formatted Values
Flow rate	mgd	0 ≤ Value ≤ 9999
UVT	%	0 < Value < 100 or 9999
Pathogen Data	per L	0 < Value < 99,999,999
Supply Voltage	V	0 ≤ Value ≤ 9999

REFERENCES

- Blatchley, E.R. 1997. Numerical Modeling of UV Intensity: Application to Collimated-Beam Reactors and Continuous-Flow Systems. *Water Research*. 31(9):2205-2218.
- Bolton, J. 2000. Calculation of Ultraviolet Fluence Rate Distributions in an Annular Reactor: Significance of Refraction and Reflection. *Water Research*. 34(13):3315-3324.
- Cabaj, A., R. Sommer, and D. Schoenen. 1996. Biodosimetry: Model Calculations for U.V. Water Disinfection Devices with Regard to UV Dose Distributions. *Water Research*. 30(4):1003-1009.
- Chang, J.C.H., S.F. Osoff, D.C. Lobe, M.H. Dorfman, C.M. Dumais, R.G. Qualls, and J.D. Johnson. 1985. UV inactivation of pathogenic and indicator microorganisms. *Applied and Environmental Microbiology*, 49(6):1361-1365.
- Chiu, K., D.A. Lyn, and E.R. Blatchley. 1999. Integrated UV Disinfection Model Based on Particle Tracking. *Journal of Environmental Engineering*. 125(1):7-16.
- Clancy, J.L., Bukhari, Z.L., Hargy, T.M., Bolton, J.R., Dussert, B.W., Marshall, M.M. 2000. Using UV to inactivate *Cryptosporidium*. *Journal AWWA*, 92(9):97-104.
- Crabtree, K.D., C.P. Gerba, J.B. Rose and C.N. Haas. 1997. Waterborne adenovirus: a risk assessment. *Water Science and Technology*, Vol. 35, No. 11-12, pp. 1-6
- DVGW. 2003. UV Disinfection Devices for Drinking Water Supply—Requirements and Testing. DVGW W294. German Gas and Water Management Union (DVGW), Bonn, Germany.
- Gerba, C.P., D.M. Gramos, and N. Nwachuku. 2002. Comparative Inactivation of Enteroviruses and Adenovirus 2 by UV Light. *Applied and Environmental Microbiology*, 68(10): 5167-5169.
- Grebe, T.E., D.D. Sabin, and M.F. McGranaghan. 1996. *An Assessment of Distribution System Power Quality*. Electric Power Research Institute (EPRI) Project 3908 Final Report.
- Hargy, T., J. Clancy, K. Fallon, H.B. Wright, and K. Bircher. 2004. Stability of MS2 in Groundwaters. Proceedings of the AWWA Water Quality Technology Conference, San Antonio, Texas, November 14-18.
- Hyman, P. 1993. The Genetics of the Luria-Latarjet Effect in Bacteriophage T4: Evidence for the Involvement of Multiple DNA Repair Pathways. *Genetic Research*, 62:1-9.
- Kamiko, N., and S. Ohgaki. 1989. RNA Coliphages Q β as a Bioindicator of the UV Disinfection Efficiency. *Water Science and Technology*, 21:227-231.
- Kawar, K., J. Jenkins, B. Srikanth, and A. Shurtleff. 1998. Deterioration of the Light Transmittance Value of Quartz Sleeves Due to the Continuous Exposure to UV Radiation. *Ultrapure Water*, October.
- Lasobras, J. M. Muniesa, J. Frías, F. Lucena and J. Jofre. 1997. Relationship Between the Morphology of Bacteriophages and their Persistence in the Environment. *Water Science and Technology*, 35(11-12):129-132.
- LeChevallier, M.W., R.E. Hubel. 2004. *Cryptosporidium* Risk Analysis & UV Disinfection System Reliability. *IUVA News* 6 (2): 9-13
- Linden K.G., G. Shin, and M.D. Sobsey. 2000. Comparison of Monochromatic and Polychromatic UV Light for Disinfection Efficacy. In Proceedings of the AWWA Water Quality Technology Conference, Salt Lake City, Utah, November 5-8.

- Mackey, E.D., R.S. Cushing, M.L. Janex, N. Picard, J.M. Laine, and J.P. Malley. 2004. *Bridging Pilot-scale Testing to Full-scale Design of UV Disinfection Systems*. Awwa Research Foundation, Denver, CO.
- Meng, Q.S., and C.P. Gerba. 1996. Comparative Inactivation of Enteric Adenovirus, Poliovirus and Coliphages by Ultraviolet Irradiation. *Water Research*. 30(11):2665-2668.
- NWRI/AWWARF. 2003. *Ultraviolet Disinfection Guidelines for Drinking Water and Water Reuse, 2nd edition*. National Water Research Institute, Fountain Valley, California, in collaboration with Awwa Research Foundation.
- ÖNORM. 2001. Plants for the disinfection of water using ultraviolet radiation - Requirements and testing - Low pressure mercury lamp plants. ÖNORM M5973-1, A-1021. Österreichisches Normungsinstitut, Vienna, Austria.
- ÖNORM. 2003. Plants for the disinfection of water using ultraviolet radiation - Requirements and testing – Part 2: Medium pressure mercury lamp plants. ÖNORM M5873-2. Österreichisches Normungsinstitut, Vienna, Austria.
- Otaki, M. *et al.* 2003. Inactivation Differences of Microorganisms by Low Pressure UV and Pulsed Xenon Lamps. *Water Science and Technology*, 47:185-190.
- Phillips, R. 1983. *Sources and Applications of Ultraviolet Radiation*. Academic Press, NY.
- Qualls, R.G. and Johnson, J.D. 1983. Bioassay and UV dose Measurement in UV Disinfection. *Applied and Environmental Microbiology*, 45(3):872-877.
- Rauth, A.M. 1965. The Physical State of Viral Nucleic Acid and the Sensitivity of Viruses to Ultraviolet Light. *Biophysical Journal*, 5:257-273.
- Regli, S., J.B. Rose, C.N. Haas, and C.P. Gerba 1991. Modeling the Risk from Giardia and Viruses in Drinking Water. *Journal AWWA*, Vol. November, pp. 76-84
- Sommer, R., T. Haider, A. Cabaj, W. Pribil, and M. Lhotsky. 1998. Time UV dose Reciprocity in UV Disinfection of Water. *Water Science and Technology*, 38(12):145-150.
- Thurston-Enriquez, J.A. *et al.* 2003. Inactivation of Feline Calicivirus and Adenovirus Type 40 by UV Radiation. *AEM*, 69:577-582.
- USEPA 2002. USEPA UV Disinfection Guidance Manual Stakeholder Meeting, June 16, 2002.
- USEPA Office of Water. 2003a. UV Validation Protocol Calculator Tool. http://www.epa.gov/safewater/lt2/pdfs/guide_lt2_uvprotocoltool_draft.xls, USEPA, Washington, D.C.
- USEPA Office of Water. 2003b. Draft Ultraviolet Disinfection Guidance Manual, EPA 68-C-02-026, June 2003.
- USEPA Office of Water. 2006a. Long-Term 2 Enhanced Surface Water Treatment Rule, *Federal Register*, 71(3):654-786.
- USEPA Office of Water. 2006b. Stage 2 Disinfectants and Disinfection Byproducts Rule, *Federal Register*, 71(2):388-493.
- USEPA Office of Water. 2006c. *Ultraviolet Disinfection Guidance Manual*, EPA 815-R-06-007, November 2006.
- Wiedenmann, A., Fischer, B., Straub, U., Wang, C.H., Flehmig, B., Schoenen, D. 1993. Disinfection of HAV and MS2 Coliphage in Water by UV Irradiation: Comparison of UV-Susceptibility. *Water Science and Technology*, 27:335-338.
- Wilson, B.R. *et al.* 1992. Coliphage MS-2 as a UV Water Disinfection Efficacy Test Surrogate for Bacterial and Viral Pathogens. Proceedings of the AWWA Water Quality Technology Conference, Toronto, Ontario, November 15-19, pp. 219-235.

- Wright, H.B. and Lawryshyn, Y.A. 2000. An Assessment of the Bioassay Concept for UV Reactor Validation. In Proceedings of the 2000 Disinfection Specialty Conference. New Orleans, La.: WEF.
- Wright, H. and Cushing, R. 2002. Critical Aspects of UV dose Delivery Monitoring, Proceedings of the AWWA Annual Conference Conference & Exposition, New Orleans, LA., June 16-20.
- Wright, H.B., Mackey, E. and White, P. 2002. UV Disinfection Compliance Monitoring for Drinking Water Applications. Proceedings of the AWWA Water Quality Technology Conference, Seattle, WA., November 10-14.
- Wright, H.D., and S.P. Reddy. 2003. Factors Impacting the Precision of CFD-based Modeling of UV Reactor Performance. Proceedings of the AWWA Annual Conference & Exposition, Anaheim, CA, June 15-19.
- Wright, H.B., C. Schulz, A. Cabaj, T. Dzurny, and K. McCurdy. 2005. Field Performance of UV Sensor Systems Used with Drinking Water UV Disinfection Systems, Proceedings of the AWWA Annual Conference Conference & Exposition, San Francisco, CA, June 12-16.

ABBREVIATIONS

ATCC	American Type Culture Collection
AwwaRF	Awwa Research Foundation
BB	Boynton Beach Utilities, Fla.
CAF	combined aging and fouling
CCC	Calgon Carbon Corporation
CEC	Clancy Environmental Consultants
CFD	Computational Fluid Dynamics
cm	centimeter
°C	degrees celsius
DI	Deionized
DNA	Deoxyribonucleic acid
DPD	N,n-diethyl-p-phenylenediamine
DVGW	
E. Coli	<i>Escherichia coli</i>
ED	Electrodialysis
EPS	emergency power supply
g	gram
gal/day	gallons per day
HAV	Hepatitis A Virus
HVAC	heating, ventilation, and air conditioning
IX	Ion-exchange
J/m ²	Joules per square meter
L	liter
LAF	lamp aging factor
LCA	Life-Cycle Cost Analysis
LL	load leveling
L/min	liters per minute
LP	Low-pressure
LPHO	Low-pressure High-Output
LSA	lignin sulfonate
LT2ESWTR	Long-Term 2 Enhanced Surface Water Treatment Rule

M/DBP	Microbial/Disinfection By-products
Melb	City of Melbourne, Fla.
mgd	million gallons per day
mg/L	milligram per liter
MIEX [®]	Magnetic Ion Exchange
mJ/cm ²	millijoules per square centimeter
mL	milliliter
μL	microliter
mL/min	milliliter per minute
mm	millimeter
MP	Medium-pressure
MS2	Type 2 Male-Specific Coliphage
NF	Nanofiltration
NGK	NGK Insulators, Ltd.
NIST	National Institute of Standards and Technology
NL	New Lamp
nm	nanometer
NOM	Natural Organic Matter
NPDES	National Point Source Discharge Elimination System
O&M	Operations and Maintenance
OPPD	Omaha Public Power District, Neb.
pfu	plaque forming units
pfu/mL	plaque forming units per milliliter
PMT	photomultiplier tube
PS	peak shaving
PVC	polyvinyl chloride
RED	Reduction Equivalent UV Dose
RLA	relative lamp-aging
RNA	Ribonucleic Acid
RO	Reverse Osmosis
SiC	silicon carbide
TMDL	Total Maximum Daily Load

UPS	Uninterruptible Power Source
U.S.	United States
USEPA	United States Environmental Protection Agency
UV	Ultraviolet
UVA	UV Absorbance
UVA Range	The portion of the electromagnetic spectrum that ranges from approximately 315 to 400 nm
UVB Range	The portion of the electromagnetic spectrum that ranges from approximately 280 to 315 nm
UVC Range	The portion of the electromagnetic spectrum that ranges from approximately 200 to 280 nm
UVCAT	UV Cost Analysis Tool
UVDGM	UV Disinfection Guidance Manual
UVT	UV Transmittance
VF	Validation Factor
WTP	Water Treatment Plant
WWTP	Wastewater Treatment Plant



Advancing the Science of Water®

6666 West Quincy Avenue
Denver, CO 80235-3098 USA
P 303.347.6100
www.awwarf.org
email: info@awwarf.org



Sponsors Research
Develops Knowledge
Promotes Collaboration

The following organizations contributed financially to this Tailored Collaboration project:

- City of Phoenix
- City of Tacoma
- New York City Department of Environmental Protection

NYSERDA Report Number
07-07

1P-4C-91184-11/07-NH